DESIGN AND CONSTRUCTION OF A SMALL GAS TURBINE TO DRIVE A PERMANENT MAGNET HIGH SPEED GENERATOR

MUNZER SHEHADEH YOUSEF EBAID

A thesis submitted in partial fulfilment
of the requirements of the University of Hertfordshire
for the degree of Doctor of Philosophy

The programme of research was carried out in the Department of Aerospace, Automotive and Mechanical Engineering, University of Hertfordshire

in collaboration with

King Abdullah II Design & Development Bureau

August 2002

UNIVERSITY OF HERTFORDSHIRE
HATFIELD CAMPUS LRC
HATFIELD AL10 9AD
BIB 444970
CLASS 621.313 EBA
LOCATION Hat Thesis
BARCODE 4000075250

TO MY BELOVED PARENTS AND TO EVERY MEMBER OF MY FAMILY FOR THEIR PATIENCE, SUPPORT AND HELP THROUGHOUT MY STUDY

ABSTRACT

Radial gas turbines engines have established prominence in the field of small turbo-machinery because of their simplicity, relatively high performance and installation features. Thus they have been used in a variety of applications such as generator sets, small auxiliary power units (APU), air conditioning of aircraft cabins and hybrid electric vehicles turbines.

The current research describes the design, manufacturing, construction and testing a radial type small gas turbine. The aim was to design and build the engine to drive directly a high-speed permanent magnet alternator running at 60000 *rpm* and developing a maximum of 60 *kW*. This direct coupling arrangement produces a portable, light, compact, reliable and environment friendly power generator. These features make the generator set very attractive to use in many applications including emergency power generation for hospitals, in areas of natural disasters such as floods and earthquakes, in remote areas that cannot be served from the national grid, oil rigs, and in confined places of limited spaces.

It is important to recognize that the design of the main components, that is, the inward flow radial IFR turbines, the centrifugal compressor and the combustion chamber involve consideration of aero-dynamics, thermodynamics, fluid mechanics, stress analysis, vibration analysis, selection of bearings, selection of suitable materials and the requirements for manufacturing. These considerations are all inter-linked and a procedure has been followed to reach an optimum design.

This research was divided into three phases: **phase 1** dealt with the complete design of the inward radial turbine, the centrifugal compressor, the power transmission shaft, the selection of combustion chamber and the bearing housing including the selection of bearings. **Phase 2** dealt with mechanical consideration of the rotating components that is stress, thermal and vibration analyses of the turbine rotor, the impeller and the rotating shaft, respectively. Also it dealt with the selection of a suitable fuel and oil lubrication systems and a suitable starting system.

Phase 3 dealt with the manufacturing of the gas turbine components, balancing the rotating components, assembling the engine and finally commissioning and then testing the engine.

The current work in this thesis has put the light on a new design methodology on determining the optimum principal dimensions of the rotor and the impeller. This method, also, has defined the optimum number of blades and the axial length of the rotor and the impeller. Mathematical models linking the performance parameters and the design variables for the turbine and the compressor have been developed to assist in carrying out parametric studies to study the influence of the design parameters on the performance and on each other. Also, a new graphical matching procedure has been developed for the gas turbine components. This technique can serve as a valuable tool to determine the operating range and the engine running line. Furthermore, it would decide whether the gas turbine engine operates in a region of satisfactory compressor and turbine efficiencies.

ACKNOWLEDGEMENTS

I wish to express my deepest gratitude to my principal supervisor, **Professor F. S. Bhinder** for his advice, immense encouragement, guidance and trust throughout the period of this project. I would like to convey my special thanks to **Dr. Sami Nasser** for his helpful discussions, reviewing the work and providing valuable comments and support in putting this work together. His guidance and stimulation were indispensible for the completion of this thesis.

I would like to express my appreciation to King Abudulah II Design and Development Bureau and their staff for their continuous support and assistance throughout this project. Also, I would like to extend my deepest thanks to the CAD staff for their contribution and help. Special thanks to engineer **Nayef El-bdour** for his willingness, enthusiam and support to this project.

I would like also to express my deepest gratitude to the work force of the Al-azraq air base for their support . Special thanks to **Qusai Al-Hamdan** and **Omar El-Quran** for their help in the final stage of the research, their valuable suggestions and the support to the project. I would like to express my sincere appreciation to **Dr. Mahmood Hammad** of the University of Jordan for his continuous help and useful suggestions during this work

I would like to extend my gratitude to the staff of the administrative office at the Science Technology and Research Centre of the University of Hertfordshire for their continuous help. Special thanks and gratitude to **Mrs. Lorraine Nicholls** for her friendly assistance, patience and her continuous help with my research at the University. However, there are others, not just named, to whom I extend my thanks as well. I would like to thank the University of Hertfordshire, Aerospace, Automotive and Mechanical Engineering Department for their encouragements and resource support in several forms .

Most importantly, I wish to thank every member of my family for their continuous support, encouragement and patience during my research work.

LIST OF CONTENTS

NOMENCLATURE

NOTATION

SYMBOL	MEANING	UNIT
A	*Area*	m^2, cm^2, mm^2
A_d	*Area of solid turbine rotor*	m^2, cm^2, mm^2
A_x	*Flow area normal to mean streamline*	m^2, cm^2, mm^2
a	*Velocity of sound*	m/s
B_f	*Blockage factor*	----------
b	*Blade width*	m, cm, mm
c, C	*Absolute velocity of gas*	m/s
C_{pg}	*Specific heat at constant pressure for a turbine*	kJ/kgK
C_{pa}	*Specific heat at constant pressure for a compressor*	kJ/kgK
C_v	*Specific heat at constant volume*	kJ/kgK
C_f	*Coefficient of friction*	----------
d	*Diameter*	m, cm, mm
d_i	*Internal diameter of shaft*	m, cm, mm
d_o	*External diameter of shaft*	m, cm, mm
D_s	*Specific diameter*	----------
E	*Energy transfer*	kJ
F	*Force*	N
f	*Fuel to air ratio*	----------
f_c	*Friction factor*	----------
g_i	*Non-linear equality constraint*	----------
g_j	*Non-linear inequality constraint*	----------
G	*Shearing modulus*	N/m^2
H	*Stagnation enthalpy of the working fluid*	kJ/kg
h	*Static enthalpy of the working fluid*	kJ/kg
i	*Incidence angle*	*Radian, Degree*
J	*Dissipation factor*	----------
L	*Length*	m, cm, mm
L	*Loss term*	----------
M	*Mach number*	----------
$\dot{m}$	*Mass flow rate*	kg/s

...Continued

N	*Rotational speed*	$rev/\min$ *rpm*
n_b, N_b	*Blade number*	----------
N_s	*Specific speed*	rev/s , *rps*
P	*Stagnation pressure*	N/m^2 , *bar*
P_r	*Stagnation pressure ratio*	----------
p	*Static pressure*	N/m^2 , *bar*
$\dot{Q}, Q$	*Heat transfer per unit mass, heat transfer*	$kJ/kg/s, kJ$
R	*Gas constant*	kJ/kgK
R_e	*Reynolds number*	----------
R	*Degree of reaction*	----------
r_c	*Radius of curvature*	m, cm, mm
S	*Entropy*	kJ/kgK
T	*Stagnation temperature*	$^\circ K, ^\circ C$
t	*Static temperature*	$^\circ K, ^\circ C$
t	*Time*	sec
t	*Blade thickness*	m, cm, mm
u, U	*Peripheral velocity*	m/s
v, V	*Relative velocity*	m/s
$\dot{W}_s, W$	*Work output per unit mass, work output*	$kJ/kg/s, kJ$
$\overline{X}$	*Vector*	----------
z	*Distance from datum*	m
Z	*Rotor length*	m, cm, mm
$rpm, rev/\min$	*Revolution per minute*	----------

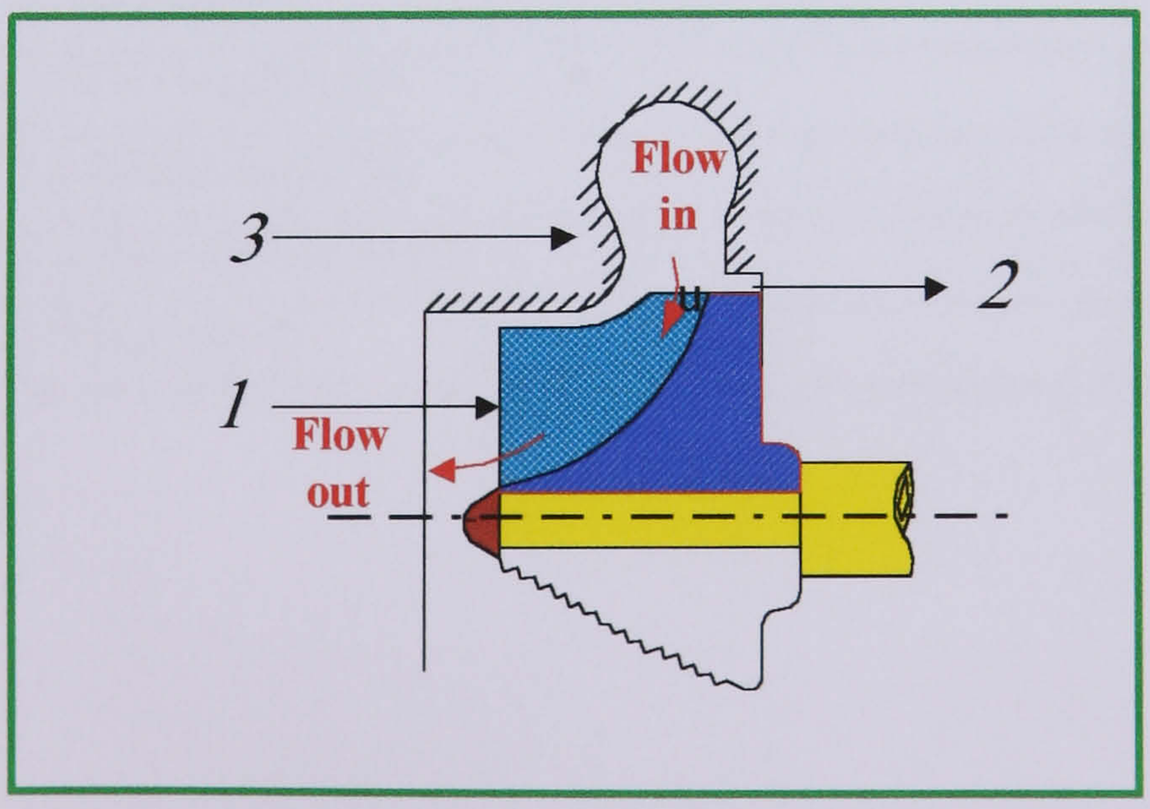

FIG. 1 SKETCH OF AN INWARD RADIAL TURBINE ROTOR

* Although, in general, the nomenclature is described in the text, the principal terms are also defined in the following. The diameters increase in accordance with the ascending order of the suffixes, e.g. $d_3 > d_2 > d_1$, as shown in **Fig. 1**. This approach has been followed because the same flow equations to be used for the compressor and the turbine.

GREEK SYMBOLS

SYMBOL	MEANING	UNITS
α	*Absolute flow angle relative to axial direction*	*radian, Degree*
β	*Relative flow angle relative to axial direction*	*radian, Degree*
β_b	*Blade angle relative to horizontal direction*	*radian, Degree*
γ	*Ratio of specific heats*	----------
ν	*Kinematic viscosity*	m^2/s
Δ	*Small increments of*	----------
λ	*Angular bend*	*radian, Degree*
Ω_s	*Specific speed parameter*	rad/s
η	*The efficiency of a process*	----------
ρ	*Density of the working fluid*	kg/m
τ	*Torque*	Nm
ξ	*Pressure loss in combustion chamber*	----------
φ	*Azimuth angle*	*Radian, Degree*
ψ_{BL}	*Blade loading coefficient*	----------
ϕ_{loss}	*Pressure loss coefficient*	----------
ϕ	*Absolute flow angle relative to vertical direction*	*Radian, Degree*
ϕ_{sf}	*Slip factor*	----------
ϕ_{fc}	*Flow coefficient*	----------
ω	*Angular velocity*	rad/s
σ_t	*Direct tensile stress*	N/m^2
σ_{shear}	*Shear stress*	N/m^2

SUBSCRIPTS

SYMBOL	MEANING	UNITS
0	*Stagnation condition*	----------
3	*Inlet turbine station **	----------
2	*Inlet rotor station **	----------
1	*Outlet mean rotor station **	----------
1*r*	*Relative flow at mean exit diameter*	----------
er	*Relative flow at exducer diameter*	----------
hr	*Relative flow at hub diameter*	----------
atm	*Atmospheric temperature*	----------
a	*Air, Axial*	----------
f	*Fuel*	----------
av	*Average*	----------
b	*Blade*	----------
c	*Compressor*	----------
cc	*Combustion chamber*	----------
e	*Exit condition, exducer*	----------
ex	*Exit*	----------
g	*Gas*	----------
h	*Hub*	----------
hydr	*Hydraulic*	----------
i	*Inlet, Number of equality constraint*	----------
incid	*Incidence*	----------
j	*Number of inequality constraint*	----------
mi	*Inlet meridional direction*	----------
m	*Meridional direction*	----------
m	*Mechanical*	----------
o	*Exit condition, External*	----------
p	*Ploytropic*	----------
s	*Spouting, shroud*	----------
SFL	*Skin friction loss*	----------
$t-s$	*Total to static*	----------
$t-t$	*Total to total*	----------
t, T	*Turbine, Tangential*	----------
R	*Rotor*	----------
rms	*Root mean square*	----------
w	*Tangential direction*	----------
wi	*Inlet tangential direction*	----------
v	*Volute*	----------
x, X	*Any section inside the rotor passage*	----------
ys	*Yield stress*	----------

SUPERSCRIPTS

SYMBOL	MEANING	UNITS
-	*Average*	----------
.	*Rate*	----------
o	*Degree*	----------

ABBREVIATIONS

SYMBOL	MEANING	UNITS
LCV	*Lower calorific value*	kJ/kgK
SFC	*Specific fuel consumption*	kg/kWh
Deg.	*Degree*	C, K
SGT	*Small gas turbine*	----------
HSTA	*High speed turbo-alternator*	
HSPMA	*High speed permanent magnet alternator*	----------
APU	*Auxiliary power unit*	----------
Cal.	*Calculated*	
OPRQP	*Optimisation Using Recursive Quadratic Programming*	
QP	*Quadratic Programming*	
w.r.t	*With respect to*	
ST	*Specific torque parameter*	----------
S_P	*Speed parameter*	----------
M_P	*Mass parameter*	----------
VR	*Velocity ratio parameter*	----------
Ref.	*Reference*	----------
No.	*Number*	----------
Fig.	*Figure*	----------
Sec.	*Section*	----------
K.E	*Kinetic energy*	

CHAPTER 1

1.1 INTRODUCTION

Portable power plants are needed urgently at the time of natural disasters caused by floods, earthquakes, famines etc. to supply electricity to aid the rescue work. If such power plants are designed specifically for this purpose, they would be very expensive because of the small numbers required by aid and rescue organisations; hence finding other applications is an economic necessity. Power plants in the similar power range would be very useful for hybrid vehicles, remote communities which may not have excess to the main grid, standby sets for hospitals, commercial buildings such as banks and stock exchanges, aircraft ground operations, oil rigs at sea, construction sites and defense applications.

Small power plants using reciprocating engines are currently available commercially **[1]**, but they are of speed 1500-3600 rpm, low power to weight ratio and high maintenance requirements. Therefore they are not easily transportable and occupy large space. Examples of these types are shown in **Table 1.1**.

Olympian Generator Set Models	Power (kW)	Speed (rpm)	Weight (Kg)	Length (m)	Width (m)	Height (m)	Volume (m^3)	Ref. No.
GEP 50	40	1500	813	2.000	0.710	1.331	1.890	[1]
GEP 65	52	1500	908	2.000	0.710	1.394	1.979	[1]
GEP 75	60	1500	955	2.000	0.710	1.331	1.890	[1]
GEP 100	80	1500	1200	2.400	0.750	1.437	2.587	[1]
Marine Generator Set Models	**Power (kW)**	**Speed (rpm)**	**Weight (Kg)**	**Length (m)**	**Width (m)**	**Height (m)**	**Volume (m^3)**	**Ref. No.**
EPJ5030M	30	1500	640	1.49	0.68	0.89	0.901	[1]
EPJ5045M	45	1500	780	1.68	0.78	0.96	1.258	[1]
EPJ5075M	75	1500	955	1.91	0.78	0.96	1.430	[1]

TABLE 1.1 MAIN DATA OF TWO TYPES OF GENERATING SETS

The alternative is a small gas turbine plant, which can overcome most of the drawbacks of the conventional power plants that use reciprocating engines. The gas turbine plant, **SGT** for short, would be based on the radial flow compressor and turbine;

and would drive the alternator directly, i.e. without a gearbox. The alternator, of necessity, would be a permanent magnet device and would run at the same speed as the gas turbine.

The problem presented for this research was to design a small gas turbine to match the load and speed dictated by the electrical generator. The proposed research programme comprised two projects: one dealing with the design of the gas turbine and the other with the design of the high-speed permanent magnet alternator. The former project is covered by the current work. The latter second project is the subject of a parallel research being carried out by another researcher.

1.2 DESCRIPTION OF THE TURBO-ALTERNATOR

A schematic view of the system comprising a small gas turbine connected to a permanent magnet alternator is shown in **Fig. 1.1**. The gas turbine comprises a compressor, a turbine and a combustion chamber. Additionally, the gas turbine engine includes fuel system, lubricating oil system, instrumentation and controls. These are not shown in the diagram; nevertheless they form an important part of the engine.

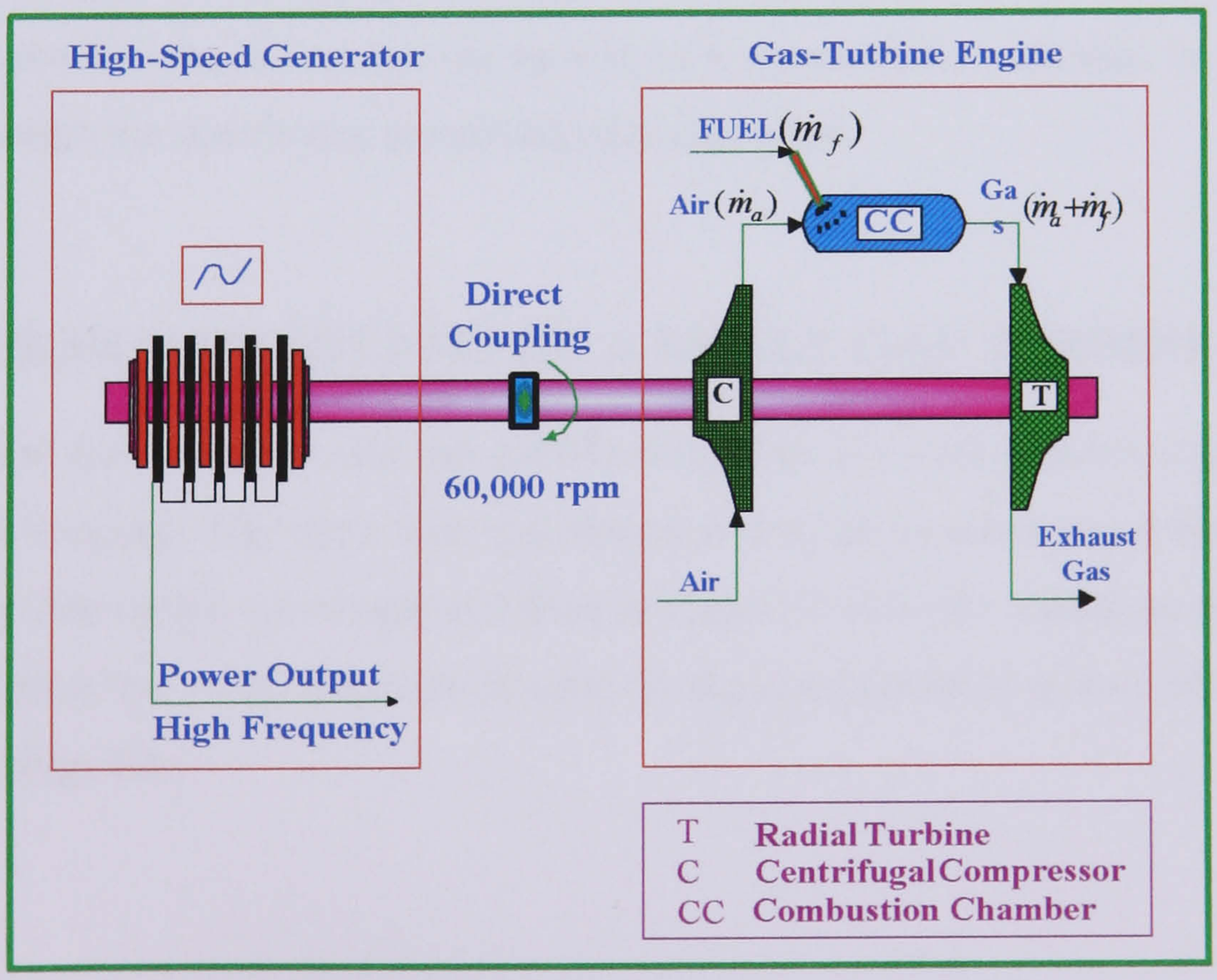

FIG. 1.1 SCHEMATIC DIAGRAM OF TURBO-ALTERNATOR

These systems were not part of the current design as they could be readily selected to fulfil the current requirements of this application. The task for this research was to design, manufacture and test the complete gas turbine engine, excluding the aforementioned systems, and working in combination with the alternator.

Before stating the aims of this research programme precisely, it is pertinent at this stage to provide an overview of the high-speed alternator since it had a major influence on the design of the turbine. This is described in the following section.

1.3 AN OVERVIEW OF THE HIGH SPEED ALTERNATOR

The high-speed alternator is simply an electrical power generation unit, which is coupled directly to a small gas turbine engine. Hence, the rotational speed of the alternator would be that of the turbine. A conventional alternator, which carries the windings on the armature, would be unsuitable for high-speed applications, as the windings would, almost certainly, dislocate due to the action of the centrifugal force. Hence, the rotor must be of solid construction; consequently it must carry permanent magnets, as it would not be possible to use electromagnets. Coupling the alternator to the gas turbine is another problematic area that would require perfect alignment between the two machines, but the benefit of a considerable reduction in weight and size outweigh the drawbacks associated with alignment.

1.4 DESIGN PROBLEMS OF A SMALL GAS TURBINE

The inward flow radial or IFR gas turbine comprises two aerodynamic components: a rotor and a casing. The rotor uses the change in angular momentum of the fluid from the inlet to the outlet into torque and thus produces shaft work. This is done by turning the flow from the radial direction at entry to the axial direction at exit of the rotor as shown in **Fig. 1.2**.

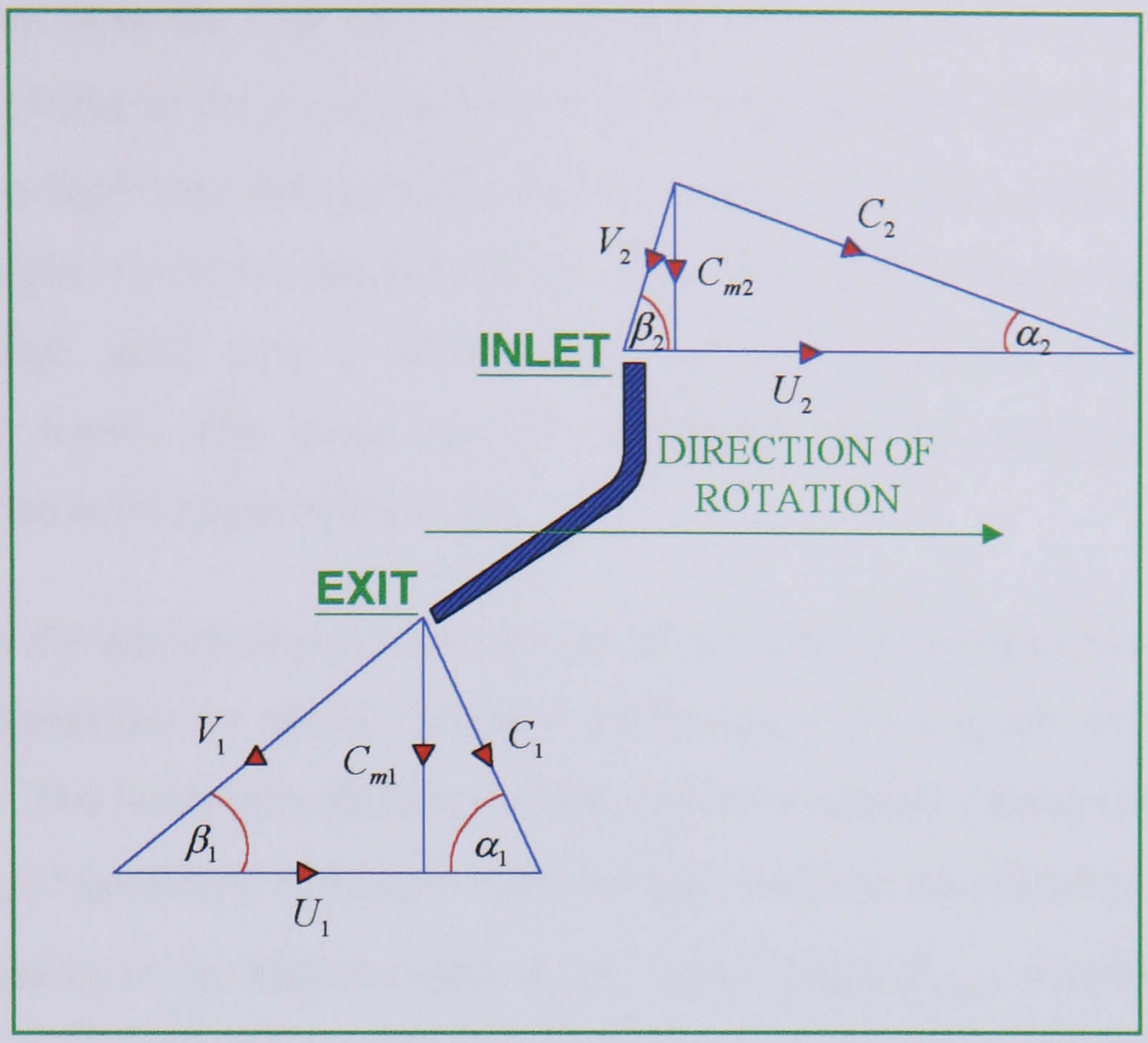

FIG. 1.2 TYPICAL VELOCITY TRIANGLES OF A RADIAL TURBINE

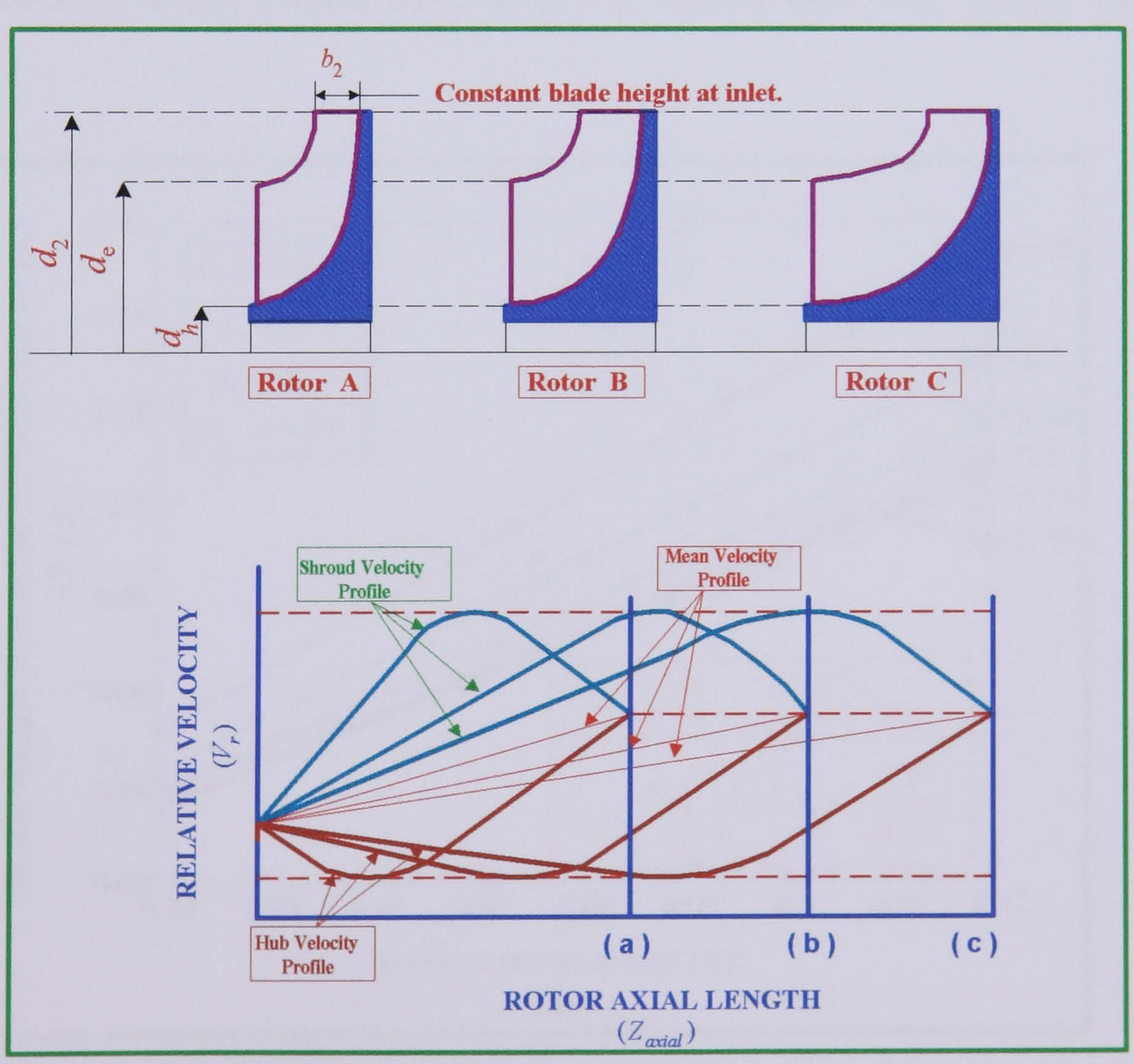

FIG. 1.3 QUALITATIVE DESCRIPTION OF THE EFFECT OF AN AXIAL LENGTH OF THE ROTOR ON VELOCITY DISTRIBUTION

It can be seen from the inlet and outlet velocity triangles, **Fig. 1.1** that although the mean flow relative to the rotor accelerates from velocity V_2 to velocity V_1, in certain region on the blade and hub surfaces, the flow experiences deceleration **Bhinder [2]** due to the highly three-dimensional nature of the flow. This is shown qualitatively in **Fig. 1.3**. High space rate of deceleration can lead to separation; consequently aerodynamic losses. The space rate of deceleration can be controlled by proper selection of the axial length of the rotor.

The purpose for aero-thermodynamic design of the rotor is to determine the principal geometric dimension to obtain optimum performance for a given set of operating conditions. The isentropic efficiency of the turbine is related, among other variables, to the ratios of geometric quantities such as blade width to tip diameter ratio b_2/d_2, exducer diameter to tip diameter ratio d_e/d_2, axial length Z_{axial}, absolute flow angle α_2 and the blade angle β_2. The applied load and the rotational speed, normally given as design specifications, also control the choice of the principal geometric ratios. Sometimes, as in the present case, these two requirements may conflict with each other.

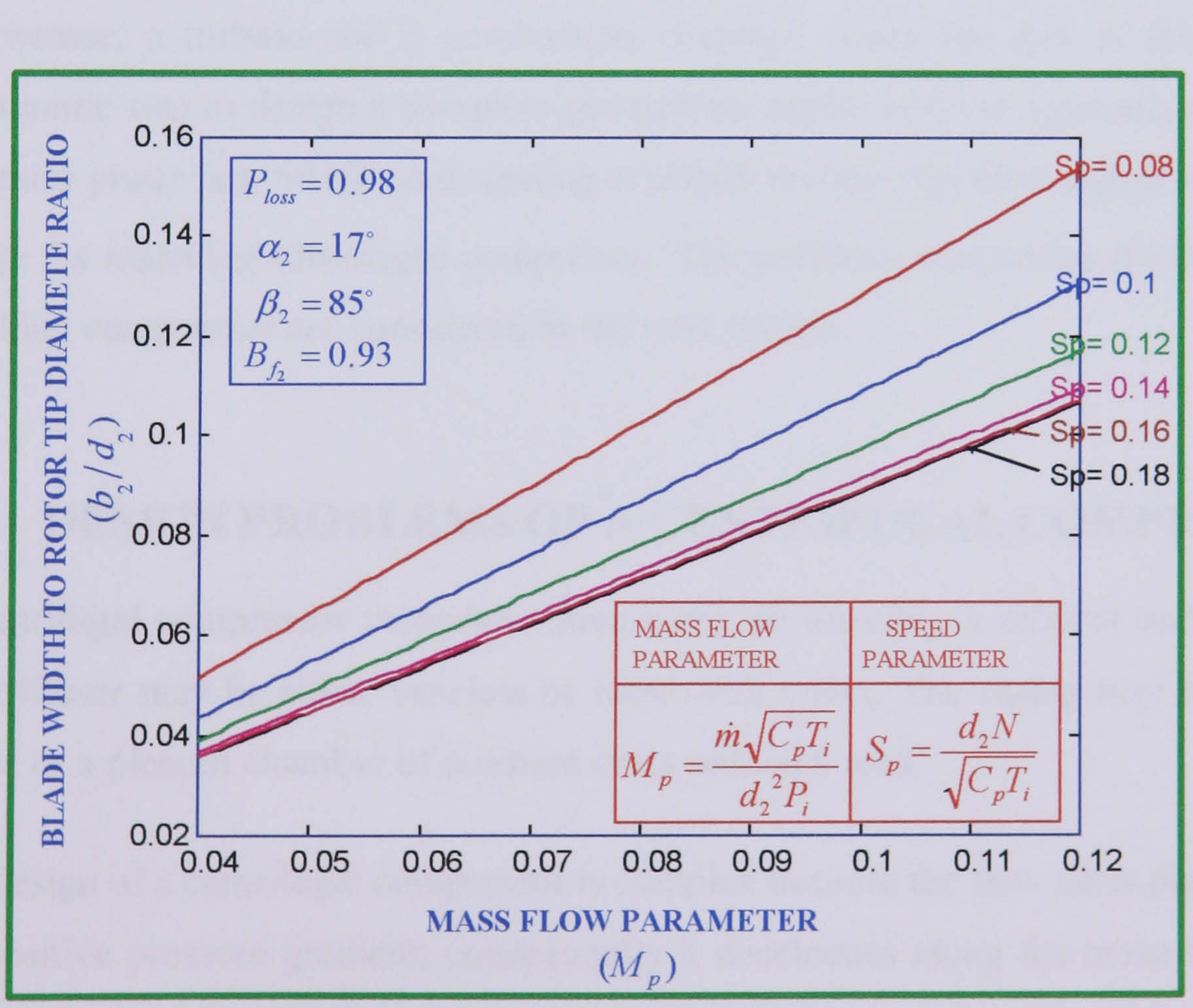

FIG. 1.4 **THE PLOT OF BLADE TIP WIDTH TO TIP DIAMETER RATIO *VS* MASS FLOW PARAMETER FOR A RANGE OF VALUES OF SPEED PARAMETER**

Figure. 1.4 above shows a plot of b_2/d_2 *vs.* mass flow parameter, $\dot{m}\sqrt{C_pT_i}/d_2^2P_i$ for a range of values of the speed parameter, $d_2N/\sqrt{C_pT_i}$. It is evident that if mass flow and speed are given to meet the design requirements, the choice of b_2/d_2 is very limited. Hence, achieving the optimum design of the rotor requires the use of parametric study to explore the influence of the full range of geometric ratios and the shape of the rotor on the performance of the gas turbine.

The casing may be either a nozzle-less volute or a constant cross section plenum chamber fitted with nozzles. The function of the casing is to accelerate flow and direct into the rotor uniformly around its periphery at a prescribed absolute flow angle. The former is comparatively low cost but requires a difficult design procedure to satisfy the aforementioned criteria and the latter is simpler to design because the nozzles take care the two of the aforementioned criteria. However, it is more expensive because of the need for an extra component, the nozzle ring. For the present research, it was decided to use a nozzle-less volute casing because of its lower cost.

It was stated earlier that a gas turbine engine has three principal components, a compressor, a turbine and a combustion chamber. Since the aim of this research programme was to design a complete gas turbine engine to drive a permanent magnet generator producing $60\,kW$ and running at 60000 rev/min, the next logical step was to design the matching centrifugal compressor. The problems concerning the design of a matching compressor are considered in the next section.

1.5 DESIGN PROBLEMS OF A CENTRIFUGAL COMPRESSOR

A centrifugal compressor comprises three parts: an impeller, a diffuser and a casing. The diffuser may be either vaneless or fitted with vanes. The casing may be either a volute or a plenum chamber of constant cross sectional area.

The design of a centrifugal compressor is complex because the flow takes place against the positive pressure gradient; consequently it decelerates along the mean flow path. Erroneous impeller design, for example, may lead to excessive space rates of deceleration in the inducer section, hence produce high losses. Another problem area

is the relative Mach number close to the inducer tip. In case of high-pressure ratio impellers, the inducer tip Mach number M_{er} may reach unity; consequently some part of the inlet area may be choked. Often this problem is addressed by cutting alternate blades back, resulting in splitter blades. However, it is not easy to ensure that flow rate in the resulting two channels would be equal because of the presence of jet and wake flows in the impeller flow passages.

The performance map of a compressor shown in **Fig. 1.5** is confined between two regions; **(a)** surge on the left and **(b)** choking on the right. Surge, choking and rotating stall are aerodynamic phenomena that have attracted much research and yet are not fully understood so that compressors may be designed to avoid them in order to increase the operating range.

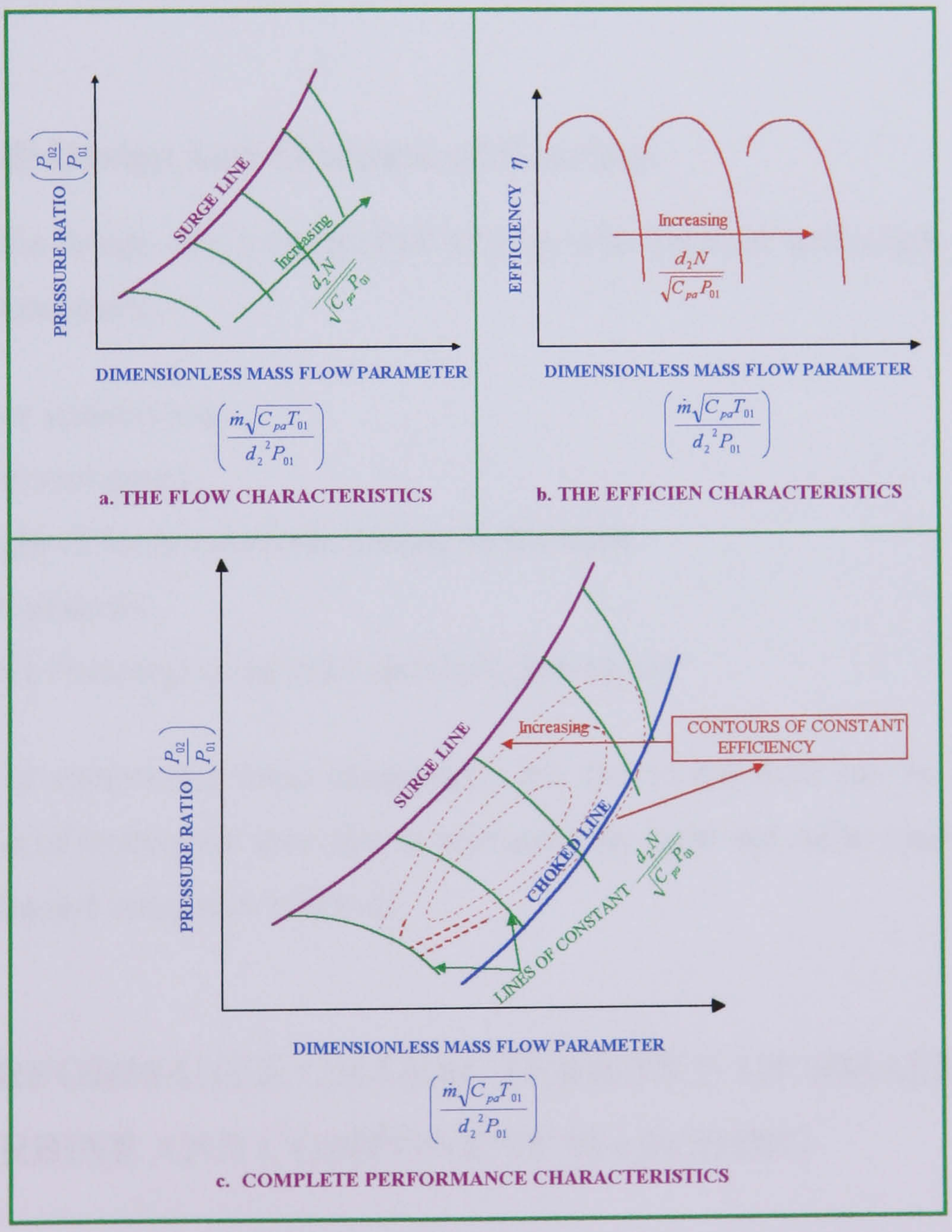

FIG. 1.5 TYPICAL PERFORMANCE CHARACTERISTICS OF A CENTRIFUGAL COMPRESSOR

1.6 THE MECHANICAL DESIGN PROBLEMS

The mechanical design of the rotating and operating systems covers two main areas as detailed bellow in **Sec. 1.6.1 to 1.6.2**.

1.6.1 Structural, Thermal and Vibration Analysis

Gas turbine components are subjected to high stresses due to centrifugal forces and elevated temperature. Therefore, structural, thermal and vibrational analyses must be carried out to ensure the safety under operating conditions. Proprietary finite element analyses programmes, such as **Nastran** and **Ansys**, are available for these analyses but the difficulty is that of modelling the components of radial flow turbo-machines because of their non-symmetry.

1.6.2 Shaft Design and Selection of Bearings

In general, the design of a rotating shaft of a specific diameter and length is based on following parameters: -

i. Power transmitted.

ii. Rotational speed.

iii. Weight of the components carried by the shaft.

iv. Shaft material

v. Type of bearings to be used and their dimensions.

Therefore, by considering these parameters, the size of the shaft can be determined. The selection of bearings is specified to withstand the axial and radial loads developed by the turbine and compressor wheels.

1.7 PERFORMANCE CHARACTERISTICS OF SMALL GAS TURBINE AND COMPONENT MATCHING

The mechanism of matching a turbine to a compressor at various loading conditions must satisfy the following criteria:

i. Gas total mass flow rate through turbine = Air plus fuel mass flow rate.

ii. Speed of compressor = Speed of turbine = Speed of Load.

iii. Torque of the compressor plus Torque of load = Torque of turbine.

iv. The pressure loss across the turbine is determined by the compressor pressure ratio and the pressure loss in the combustion chamber ξ_{cc}.

The only two conditions, which satisfy the matching criteria, are the load and speed, which are specified as design conditions, the others must be satisfied by design. This may be done with the help of the performance characteristics of the compressor and the turbine. Some either analytical or graphical method of achieving this goal will have to be developed.

1.8 AIMS OF PROJECT

The work arose initially from the need to develop a portable emergency electric power supply unit for natural disasters such as floods and earth quakes. The portability meant that the power unit must be a high-speed turbo-machine and the electrical alternator must be directly coupled.

The primary aim of this research programme is to design, manufacture and test a demonstration small gas turbine engine of 60 kW power shaft output, running at 60,000 rpm. The choice of load and speed was made by the design specifications of the electrical machine. The following steps were sequentially followed to achieve the current project's aim.

I. Comprehensive literature review.

ii. Mathematical modelling of the components parameters.

iii. Design of the turbine, compressor and the power transmission shaft.

iv. Selection of a combustion chamber and bearings.

v. Manufacturing and assembling the gas turbine components.

vi. Construction and commissioning of the experimental test facility.

vii. Experimental work.

viii. Validation of the results.

CHAPTER 2

REVIEW OF THE RELEVANT LITERATURE

2.1 INTRODUCTION

High-speed turbo-alternator machines of a power range of 10 to 100 kW become increasingly popular in recent years due to their attractive features for special applications as previously pointed out in **Chapter 1**. This chapter reviews studies related to the design, performance prediction and experimental work of the inward flow radial turbine, the centrifugal compressor and lastly the small gas turbine engine for high-speed turbo-alternator application. A summary of observations and concluding remarks are presented in the last section.

2.2 PREVIOUS WORK

Most of the published papers relating the design, performance prediction and experimental work of small gas turbine, which consists of an inward flow radial turbine, a combustion chamber and a centrifugal compressor, have been cited in the open literature as separate components. However, few papers have been found dealing with the design and performance of a small gas turbine as a complete engine. The design, performance prediction and experimental work of small gas turbine, would certainly involve reviewing the studies of the following as detailed in the respective sections.

Sec. 2.2.1 An inward flow radial turbine rotor and casing.

Sec. 2.2.2 Centrifugal compressor impeller, vaneless diffuser and the volute.

Sec. 2.2.3 Small gas turbine for high-speed turbo-alternator application.

2.2.1 The Inward Flow Radial Turbine

2.2.1.1 The turbine rotor

The aim of this research programme was to design a small gas turbine to drive an alternator mainly for emergency situations. Hence, the complete generator out of necessity was

required to be easily transportable. In order to meet this requirement it was necessary for the alternator to be directly coupled to the prime mover, which should be in this case, a small gas turbine. Because of the high rotational speed at which the gas turbine would operate most efficiently, the directly coupled alternator must be of permanent magnet solid rotor construction. The two principal design variables, i.e. load and rotational speed, of the small gas turbine would, in that case, be governed by the design of the alternator.

In the present research, the load and speed for the gas turbine were specified to be 60 kW and 60000 rev/min. This was a serious constraint on the design of the IFR turbine as explained in the following section.

For a limited turbine entry temperature T_{03}, the power output would be a function of cycle pressure ratio P_{02}/P_{01} and mass flow rate of air $\dot{m}_a$. The cycle pressure ratio, in turn, is a function of rotational speed N and tip diameter of the turbine rotor d_2. So if the rotational speed and power output were specified, these would then fix the tip diameter and blade width of the turbine rotor. The resulting design of blade width to tip diameter ratio b_2/d_2 might or might not be satisfactory for an optimum design configuration. This would affect the maximum achievable efficiency of the gas turbine. The relevant theory in support of these statements is given in **Chapter 3**.

The small gas turbine based on radial flow components has been used widely for a variety of applications, for example, turbochargers and auxiliary power units for aircraft for many years. Hence a large number of papers have been written on the aero-thermodynamic design, performance prediction, experimental investigations and manufacturing techniques. The papers dealing with the design problem subject to serious constraints as in the present case are scarce. Nevertheless, a list of papers is included in the references as bibliography. Papers that were considered relevant to the present work have been reviewed in some detail hereafter.

Wosika [3] undertook a research programme for developing an inward flow radial, IFR turbine for driving a fire pump. **Wosika** has suggested design parameters and values for $0.58 < d_e/d_2 < 0.71$, $\alpha_2 = 17^\circ$, $0.3 < c_{m1}/u_2 < 0.5$ etc. that would assist his design procedure.

The drawback of this work is that using these values tends to limit the progress in the development of better machines. However, his review of the available data has provided useful guidelines for preliminary design.

Wallace [4] proposed a one-dimensional method in which the independent variables $(P_r, T_i, R, u_2/c_s, d_h/d_2, d_2, \dot{m}, \alpha_2)$ and the dependent variables $(N, d_1, \beta_2, \beta_1, b_2, d_e, d_h)$ were identified. The method was used for calculating the design and off design point performance characteristics of **IFR** turbine. Flow in the nozzles and rotor passages was assumed to be isentropic. At the design point, **Wallace** assumed also the inlet and outlet velocity triangle to be right angles, therefore the performance could be readily calculated. At off-design point conditions, the direction of flow would no longer matched correctly with rotor, therefore the relative flow would make a finite angle with rotor blades.

A criterion for minimum number of blades was given in terms of the relative velocity in the rotor passage. Owing to the difference of pressure on the driving and trailing surfaces of a blade, the relative velocity on the latter surface would be less than that on the former surface. Blade spacing should be so arranged that the relative velocity at any point in the passage does not fall below a specified value. The transverse pressure difference between the passage centre line and the driving surface would be maximum at the outer radius. Therefore the estimate of the minimum number of blades for avoiding stagnation condition should be based on this radius.

Wallace's simple one-dimensional analysis makes a valuable contribution as it can be used with equal facility for calculating either the principal dimensions of the rotor for specific design requirements or the performance of a given turbine for designed operating conditions. The method may be refined by introducing suitable loss coefficients for the nozzles and the rotor. Also, it provided a method for calculating the minimum number of blades.

Ribaud and Mischel [5] described the work undertaken by Microturbo and Onera to design a 3.6 expansion ratio of **IFR** turbine to be applied to a small turbo-shaft engine of power between 40 and 70 kW . Microturbo experience had shown the losses in the nozzle guide vanes were estimated to be 3.6% of the inlet total pressure, the number of rotor blades was 13, the slip factor was chosen to be 0.886, and finally, the blade hub to tip ratio

at exducer exit d_h/d_e must be greater than 0.41 to reduce the trailing edge vibration. Onera design approach was based on $\alpha_2 = 15^\circ$ and $2.0 < v_1/v_2 < 2.5$.

The design specifications were given as follows; total pressure at turbine inlet = 3.81 bar, turbine inlet temperature = 953 K, mass flow rate = 0.67 kg/sec, and rotational speed = 59,200 rpm. By using the design data, the main geometry of the rotor and the aerodynamic parameters were calculated and listed in **Table 2.1**. The estimated turbine efficiency was claimed to be equal to 91%.

This research work has been considered to be important because it was addressed to the design of radial turbine for the lower range between $40\,kW$ to $70\,kW$ and provided reasonable data for a given inlet conditions. However, **Ribaud and Mischel** claimed that the stress level in the turbine was moderate without providing any stress calculations. In fact, this statement could be debatable unless a detailed stress analysis was carried out to justify their claim.

DESIGN PARAMETER	DESIGN VALUES
Rotor inlet diameter, d_2	17.02 cm
Exducer diameter, d_e	11.68 cm
Number of blades	13
Hub diameter, d_h	6.4 cm
Rotor inlet blade width, b_2	0.99 cm
Rotor axial length, z	5.42 cm
Rotor Inlet Mach No., M_2	0.8
Rotor exit Mach No. M_1	0.36
Exducer tip Mach No. M_{er}	0.78

TABLE 2.1 PRINCIPAL DIMENSIONS OF AN INWARD RADIAL FLOW TURBINE ROTOR DESIGNED BY MICRO-TURBO

Rohlik [6] has examined analytically the performance of **IFR** turbine in order to determine optimum design geometry for various applications as characterized by specific speed Ω_s. His procedure was used to determine the design point losses and corresponding efficiencies

for various combinations of α_2, d_1/d_2 and b_2/d_2. A mean flow path analysis was used and the main constraints in the analysis were as follows: $v_1/v_2 = 2.0$, $c_{w1} = 0$, $d_e/d_2 \leq 0.7$ and $d_h/d_e \geq 0.4$. The results of the analysis can be summarized as follows:

i. The flow conditions and the geometry parameters examined resulted in a range of specific speed Ω_s from 0.12 to 1.34 and maximum static and total efficiencies occurred at specific speed values of 0.58 and 0.93, respectively.

ii. Efficiency dropped rapidly with decreasing specific speed Ω_s in the low specific speed range. This drop resulted from the relatively high passage boundary layer, windage and clearance losses. At high Ω_s, the rotor exit loss was predominant because of the high volume flows.

iii. The ratio of b_2/d_2 increases with increasing Ω_s. The general rise of this ratio reflects the increase in nozzle flow area accompanying the larger flow rates of higher specific speed

Rohlik's method provided a good basis for the rapid selection of minimum loss, size and shape for any specific speed in the range used. The disadvantages of the analysis is in the assumptions made for the calculations, which have to be verified and for the same specific speed, several meridional configurations are possible. Therefore, specific speed is not entirely satisfactory as a parameter for the optimum choice of the principal design variables.

Bhinder [7] proposed a design method for **IFR** turbine rotor based on the assumption of one-dimensional steady flow. He specified the principal geometric variables of the turbine rotor as follows: d_h/d_2, d_e/d_2, d_1/d_2, b_2/d_2, β_{2b} and β_{1b}. The design method starts by applying a value for the ratio $d_h/d_2 = 0.2$, which is usually fixed by the shaft diameter and other mechanical requirements, a value of 90° for $\beta_{2b} = \beta_2$ to avoid bending stress in the rotor blades and assuming zero swirl at rotor exit, i.e. $\alpha_1 = 90°$.

Hence, the number of geometric variables is reduced to four, i.e. b_2/d_2, d_e/d_2, d_1/d_2, $\beta_{1b} = \beta_1$, in which a relationship between these variables, the performance parameters

such as total efficiency η_{t-t}, velocity ratio u_2/c_s and the degree of reaction R and operating conditions such as pressure ratio P_r, rotational speed N. mass flow rate $\dot{m}$ or specific work output $\dot{W}$ could be then established based on **Euler's** equation and velocity triangles at rotor inlet and outlet, respectively. **Bhinder** extended his analysis to include the flow in the rotor using the quasi method developed by **Katsanis [8]**. It can be concluded from this study that the systematic approach for the design of the turbine rotor would be useful for the designers, however, the draw back of this method was the assumption of the value for d_h/d_2 which may not produce the best achievable efficiency due to excessive blockage.

Benson [9] carried out a quantitative study of the turbine main variables at the design point. These variables were; b_2/d_2, d_1/d_2, d_e/d_2, α_2 and β_1. Also, the effect of rotor losses on the turbine performance was examined. The results of the work can be summarized as follows:

i. There is an optimum value for b_2/d_2 and this depending mainly on the nozzle outlet angle α_2. The optimum value increases with increase in α_2.

ii. The total-to-static efficiency decreases with increase in overall pressure ratio. In the region of maximum efficiency, the overall pressure ratio has only a marginal effect on the total-to-static efficiency.

iii. The design blade speed ratio u_2/c_s decreases with increase in rotor width; this produces an increase in the degree of reaction R across the rotor and the total-to-static efficiency is decreased.

iv. The rotor exit angle at mean diameter β_1 has a marginal effect on the performance as mass flow and torque are essentially controlled by inlet conditions. Normally, the exit angle controls the flow within the rotor and hence the rotor losses.

v. At low values of mean outlet diameter to inlet diameter d_1/d_2, the turbine operates with a high degree of reaction R, a low blade speed ratio u_2/c_s and a high positive exit swirl. There is an optimum value for d_1/d_2 for maximum total-to-static efficiency and this value depends on the rotor exit angle β_1 and the rotor losses.

The optimum value of d_1/d_2 for maximum efficiency increases with increase in the rotor loss coefficient but decreases with increase in outlet blade width to inlet blade width $(d_e - d_h)/b_2$.

vi. At maximum efficiency, the value of u_2/c_s is approximately 0.7 and is independent of the optimum value of d_1/d_2 .

viii. The trend observed by **Balje [10]** for the specific speed and specific diameter was confirmed in this work. The calculation showed that that the optimum efficiency for a radial turbine is obtained if the specific speed lies in the region of 50 to 97 with corresponding specific diameters of 2.65 to 1.34.

This work can be considered useful for design purposes as it provides some valuable data for inward flow radial turbine.

A comprehensive survey of literature relating to the components comprising a typical radial turbine was provided by **Baines [11]**. This focused mainly on published experimental information and the practical considerations for design, including loss predictions, secondary flows and special features such as partial, or splitter, blades and variable geometries. A very comprehensive text is due to **Whitfield and Baines [12]** with the emphasis on design, the book covers most of the topics relevant to both radial turbines and centrifugal compressors from basic one-dimensional theory to the mathematical specifications of three-dimensional geometries. These textbooks give general guidelines to the design theory of radial turbine and may be considered a very useful reference. However, they do not deal with design problems of radial turbines subjected to constraints such as power and speed.

Selecting the optimum number of rotor blades is a fundamental design requirement. **Watanabe and Ando [13]** conducted experimental work to study the influence of the number of rotor blades on the performance characteristics of IFR turbine. The results showed that the highest value of total efficiency η_{t-t} was obtained for the rotor with 32 blades at higher rotational speed above 11000 *rpm* when $\dot{m}$ was 0.108 Kg/s. For the second case where $\dot{m} = 0.1457$ Kg/s, i.e. larger mass flow, η_{t-t} was highest at rotor having 16 blades at higher rotational speed above 11000 *rpm*. This variation may be due to the

increase in frictional losses within the rotor passage in rotors with higher number of blades due to a larger mass flow rate used.

The results obtained by the authors can not be generalized because their experimental work was limited to a speed range between 40000-12000 *rpm* and only using two values of mass flow rate. However, their results showed the effect of mass flow rate and the speed on the optimum number of blades for best efficiency. This confirmed the trend at that time of using centrifugal compressors design guidelines, such as those due to **Stantiz [14]**, which tended towards higher blade numbers.

Further work was carried out by **Ariga *et al* [15]** regarding the effect of number of blades. They produced an early study of rotor flow patterns in the inlet region using purely radial bladed rotors. Initial results with only 8 blades found substantial flow separation due to excessive loading. The addition of splitter blades produced significant flow improvements. **Futral and Wasserbaur [16]** also studied the effect of splitter blades produced by measuring performance before and after their removal from a rotor with 11 full and 11 splitter blades. Surprisingly they found very little difference, which they attributed to the detrimental effect of increased loading being offset by a reduction in friction due to reduced wetted area.

Takamura and Nishiguchi [17] considered blade loading in more detail in their study of 12 rotors with varying blade numbers between 8 and 11 and blade shape. They concluded that blade loading depends greatly on blade shape as well as blade number. A similar study by **Chen *et al* [18]** found that reducing the blade number from 12 to 10 gave a drop in efficiency of about 2% and a flatter efficiency characteristic. They proposed that the blade-loading coefficient $\psi_{BL} = c_{w2}/u_2$ is a suitable parameter for judging loading and indicated that values in the range 0.95 to 1.0 coincided with optimum efficiency.

2.2.1.2 Turbine casing

The number of publications relating to volute design appears to have risen significantly since 1980s. **Chen [19]** proposed a quasi-three dimensional design method of volute casings for turbochargers turbine applications. Two volutes designs were developed, the first one is a trapezoidal cross-section with the depth of the volute Z is a function of radius

only and the second one where Z is a function of radius and azimuth angle. A tongue loss model was developed from the theory of the turbulence wake theory for incompressible flows. His findings can be summarized as:

i. The angular momentum is no longer conserved when the depth of the volute Z is a function of radius and azimuth angle, while the momentum is conserved when Z is a function of radius only.

ii. The tongue loss is little affected by pressure ratio compared with the friction loss. Their application to **Scrimshaw's [20]** turbine casings shows good agreement with experimental data.

Whitfield and Noor [21], proposed a non-dimensional analytical design procedure for nozzle-less volute casing by assuming the flow to be one-dimensional, compressible and based on the knowledge of the magnitude and direction of the absolute Mach number at rotor inlet, M_2. Basically, the authors adopted the following procedure:

i. Obtaining the overall size of the volute casing in the form of non-dimensional geometry, the radius ratio r_3/r_2 and the area ratio A_3/A_2, respectively.

ii. Calculating the geometry of the volute spiral flow path and cross-sectional area variation with azimuth angle in the form of non-dimensional geometry, the radius ratio r_ϕ/r_2 and area ratio A_ϕ/A_2 taken at the centriod relative to rotor inlet geometry.

iii. Specifying the passage cross-section shape and calculating the outer wall radius of the volute.

iv. Finally, the results obtained were then compared to the actual volute geometry used in a companion experimental investigation.

The flow characteristics such as Mach number M_ϕ and absolute flow angle α_ϕ at the centriod of the flow passage for every increment of azimuth angle ϕ were also derived and compared with experimental results in order to assess the validity of the empirical parameters used in the design procedure.

The results of their analysis can be summarized as follows:

i. The volute radius ratio r_3/r_2 measured from the volute centriod could be reduced by increasing the volute inlet Mach number M_3 and this will lead to increased volute passage losses. Therefore, a compromise between efficiency and size limitation must be considered.

ii. The volute area ratio A_3/A_2 is found to be less than one for all possible design conditions of M_2, α_2, α_3.

iii. The predicted results of centriod radius r_ϕ/r_2 and area ratio A_ϕ/A_2 as a function of azimuth angle have a significant effect on r_ϕ/r_2 and no detectable effect on A_ϕ/A_2.

In a later review of the method **Whitfield and Noor [22]** concluded that the energy dissipation had very little effect on the predicted geometry, dissipation of angular momentum was significant and required empirical correlation.

Owarish [23] carried out a similar work and developed a novel method of analysis and design of single entry nozzle-less casing. The method was based on two-dimensional flow and considering the shape of the volute. The results of his study can be summarized as follows:

i. Absolute flow angle $\alpha_{c\varphi}$ for a given cross section is independent of the azimuth angle near the centriod of cross section.

ii. Cross-sectional shape effect on $\alpha_{c\varphi}$ is significant, although the three casings start with the same value of $\alpha_{c\varphi}$ at rotor inlet. The rectangular shape, which has the minimum variation of width in the radial direction, shows the minimum variation of $\alpha_{c\varphi}$, whereas the elliptical shape, which has the maximum variation of width in the radial direction, shows the maximum variation of $\alpha_{c\varphi}$.

iii. The absolute flow angle α_2 varies from 11° to 16° around the periphery of the rotor inlet while the static pressure is almost small and equal to 1% and increases at an azimuth angle between 27° to 36°.

iv. The angular bend at the entry of the volute plays an important part in achieving the desired velocity profile and hence maximizing the tangential flow velocity c_{w2} at the rotor inlet. The author found 23° to be optimum.

Owarish reported that the rate at which sectional area changes in the radial direction, affects the value of $\alpha_{c\varphi}$. This would indicate that the ideal casing would be of variable shape, that is, the shape would change smoothly and gradually with azimuth angle.

This design method proposed has not been tested experimentally, in addition; it neglects the variation of the flow properties in the axial direction, which imposed a limitation on the theoretical results provided.

Gabarev and Fillipov [24] proposed a design method for a nozzle-less volute casing by considering the flow to be one-dimensional free vortex and disregarding the viscosity of the working fluid, secondary flows and leakages. His experimental investigations on a nozzle-less casing of a circular cross section showed similar results to **Owarish [23]**. Similar results were obtained from the experimental work carried out by **Hussian [25]** and **Rogo [26]**.

Wislicensus [27] proposed a design concept which states that a volute satisfies the law of constant angular momentum if the outer contour follows the logarithmic spiral and the flow proceeds between two parallel walls. These conditions will not be satisfied in practical design that favours sidewalls diverging towards the outer side.

Kastner and Bhinder [28] presented a method of predicting performance of a gas turbine fitted with a nozzle-less volute casing. The flow in the volute casing was treated to be one-dimensional and the total pressure loss occurring between the volute inlet and the rotor was determined by a simple loss factor.

The results in the first publication of this work show variations of flow quantities around the rotor periphery, whereas in the second publication assumes that the flow was uniform. It appears that the casing used in the second analysis was designed very carefully to reduce circumferential variations of flow observed in the first investigation. However, the authors have not given any details of the design of casing used in the second investigations.

Benson *et al* [29] carried out experimental investigations on the significance of the volute cross-sectional shape and its influence on the turbine efficiency. He tested volutes of both symmetrical and non-symmetrical types. Three volutes with equal inlet areas but different cross sectional shape and two volutes with similar shape but different inlet areas were studied. The main points observed were as follows:

i. The shape of volute had great influence on the turbine efficiency.

ii. Volute inlet area also influences the range and maximum efficiency obtained under the same operating conditions. Both volutes with rectangular cross-section but different areas gave efficiency curves different from the other.

Whitfield *et al* [30] reported a comprehensive measurement from a turbocharger volute. Their findings showed that a wide variation of α_2 (roughly 11° to 19°) and the assumption of free vortex was only felt to be valid over the first 180°.

Basset [31] carried out an experimental investigation on volute casing with rectangular cross-section in which its area reduced linearly with the azimuth angle. **Basset** reported the followings:

i. The total pressure loss across the nozzled and nozzle-less casing to be 15.2% and 4.9% of the dynamic pressure at casing inlet. He also found the reduction in the volute entry area gave higher-pressure loss. This was attributed high dynamic head in the duct.

ii. A negligible variation of the total pressure around the periphery of the rotor inlet occurred only when the total pressure profile at the inlet was uniform. Therefore, the piping upstream of the turbine should be arranged to achieve this objective.

iii. A significantly larger loss of total pressure and variation of the absolute flow angle occurred over the range of azimuth angle 120 to 170 degrees. This finding is similar to that of **Gabrev [24]** and was probably caused by secondary flows.

Japaski [32] conducted an experimental study of the flow mechanism in the turbine volute. The volute geometry was a rectangular cross-section. **Japaski's** main conclusions from the observations were that very strong secondary flow existed in the volute and large variations of flow angles were observed and total pressure loss was high. These results seemed unexpected and this may be attributed to the volute geometry as well as the poor manufacture of the volute.

Mizumachi *et al* [33] carried out an experimental work to verify the theoretical analysis based on the application of a five hole probe located in the centre of the volute passage and at series of azimuth angles around the discharge and the following results were reported.

i. The flow angle was dependent on the assumed rate of dissipation and on the swirl coefficient, which was found to lie between 0.85 and 0.9.

ii. The flow through the volute followed the free vortex pattern over the first 180 ° of azimuth angle and in the later part of the volute, the flow followed the 180° relation $c_w r^m = k$, where m was a function of azimuth angle ϕ and m approached zero as ϕ approaches 360°.

A performance comparison of a turbocharger turbine with both a vaned and vaneless volute was conducted By **Baines and Lavy [34]**. The vaned stator was designed with a throat area intended to give the same design point capacity as the original vaneless volute, assuming free vortex flow. A substantial reduction in peak efficiency resulted when using the vaneless volute. It was also noted that the efficiency at off design fell off less sharply in the vaneless case, suggesting a greater off-design incidence penalty when using guide vanes.

2.2.2 Centrifugal Compressor Impeller, Vaneless Diffuser and the Volute

The centrifugal compressor has attracted a great deal of attention during the last two or three decades. Hence, a large number of papers dealing with various aspects of radial and mixed flow centrifugal compressors were published. During the execution of this research programme, although an exhaustive study of the turbo-machinery literature was addressed to the IFR turbine engine as it was considered the core of the work in this thesis, the author was aware that a review of the most relevant papers regarding the design of centrifugal compressor should be included hereafter.

2.2.2.1 The impeller

Balje and Farmingdale [35] outlined a method for computing the characteristic values of a centrifugal compressor, such as work coefficients, loss coefficients and efficiency. These dimensionless quantities were presented as functions of Reynolds number $(R_e)_a = D_2 u_2 / \nu_1$, diameter ratio d_2/d_1, Mach number $M_a = u_2/a_1$ and flow factor c_{m1}/u_2, which refer to the size, the speed and the shape of the component. By combining the work and loss coefficients, the efficiency and pressure coefficients were calculated as function of the forgoing characteristics values.

The authors have produced a number of design diagrams for centrifugal compressor with radial blades impeller, which show the relationships of flow factor, pressure coefficient, efficiency and Mach number for specific values of Reynolds number $(R_e)_a = 2\times10^6\,(\mu = 1.3)$, slip factor $\phi_{sf} = 1.25$, diameter ratio $d_2/d_1 = 1.6$ and meridional velocity ratio $c_{m1}/c_{m2} = 1.0$. These diagrams highlight the following:

i. The optimum efficiency was obtained only over a narrow range of the flow factor c_{m1}/u_2, close to 0.3.

ii. At constant Mach number less than 1.2, both the pressure coefficient and the adiabatic efficiency drops only a little with increasing flow factor. At constant Mach number higher than 1.2, the drop of both parameters is quite noticeable.

iii. The pressure coefficient and adiabatic efficiency, at constant flow factor, increased considerably with decreasing Mach number.

The diagrams presented in this work could not be used as a general guide for the compressor design as they were produced for a special case. Moreover, the Mach number $M_a = u_2/a_1$ does not represent actual flow velocity.

Balje [10] pointed out that the maximum efficiency of the compressor is a unique function of the similarity parameters, specific speed N_s, Specific diameters D_s, Reynolds number R_e and Mach number M_1. His results indicate maximum efficiency would be expected when flow angle at impeller exit $\beta_2 \leq 90^\circ$, $130 \geq N_s \geq 90$ and $1.7 \geq D_s \geq 1.3$. Moreover, the peak value of the efficiency should increase with increasing Mach number for low specific speed. This is particularly noticeable in the case of radial compressors with large diameter ratio. **Balje's** work provided very useful guidelines and perhaps defines practical design boundaries. However, it did not deal with the methodology for the actual design.

Rodgers [36] presented a method of estimating the pressure-flow characteristics of radial compressors provided that the peak impeller and diffuser efficiencies and compressor geometries are prescribed. **Rodgers** employed this method to investigate the effects of the impeller tip diameter to inducer diameter ratio at mean streamline d_2/d_1, diffuser throat to impeller inlet area ratio A_d/A_1 and the inducer blade angle at mean streamline β_1 on the characteristics of 27 compressors of straight radial blades and zero prewhirl to the inducer inlet for design pressure ratio ranging from 3.0 to 6.0. His results are summarized as follows:

i. For impellers of pressure ratio exceeding 4.0, diameter ratios at mean inlet greater than 2.0 are desired for higher efficiency. Also, for adequate flow range between surge and choke at such pressure ratio, A_d/A_1 should probably be less than 0.2 and inducer blade angle β_1 not greater than 50 deg.

ii. The blade angle measured from the axial direction should be less than 60°. This is because of the high rate of turning could restrict the range of operation.

iii. It was found that the overall pressure-flow characteristics were primarily strong functions of the inducer and diffuser throat areas A_d/A_1 and. secondarily. were strong functions of the impeller diameter ratio d_2/d_1 .

Results given by **Ingham and Bhinder [37]**, which were obtained on a 6/1 pressure ratio compressor, also indicate that the space rate of turning of the fluid has a significant influence on the efficiency as well as the range of impellers.

Stahler [38] investigated the effect of inducer relative tip Mach number M_{er} on efficiency using several Boeings compressors. The results presented indicate the penalty that may be paid for the increase in M_{er}. Efficiency falls off rapidly for M_{er} greater than 0.8. Maximum efficiency η_{ad} of 79.5% occurred at M_{er} equal to 0.73. Since the design mass flow rate and the pressure ratio have not been given, it is therefore, difficult to deduce that the drop in efficiency is due to high Mach number effect or low speed effect.

Came [39] developed a computer-based centrifugal compressor design procedure for the impeller and the diffuser. The impeller design package includes a geometry modelling, aerodynamic analysis, stress analysis and the direct generation of data for manufacture by numerical control. The method of diffuser design incorporates analyses of the flow in the vaneless space and the diffuser channel geometry was selected based on pressure recovery data. These packages were used to design a centrifugal compressor of 6.5-pressure ratio and were tested experimentally to evaluate its performance. Then it was compared with that of an earlier compressor designed with less advanced techniques for the same aerodynamic duty. The experimental results showed that the performance of the compressor based on new technique gives better performance than the less advanced one. These results can be disputed on the basis that the two impellers were not similar as the new designed ones have a backswept blades while the less advanced one have radial blades.

Anderson *et al* [40] has investigated the effect of blade curvature of the impeller on centrifugal compressor performance. The three impellers used in this investigation have similar dimensions but different blade curvature, which is parabolic, elliptical and circular blade forms, respectively. This investigation has shown the following:

i. Impeller with elliptical blade curvature had highest peak adiabatic efficiency at all of the equivalent tip speeds except at 462 and 528 m/s. Impeller with the parabolic blade curvature had the highest peak efficiency at equivalent tip speeds of 462 and 528 m/s. Impeller with the circular blade curvature had the lowest peak adiabatic efficiency at equivalent tip speeds higher than 330 m/s. For the range of tip speeds investigated, all three impellers decreased in adiabatic efficiency with increasing tip speed.

ii. Impeller with the circular blade curvature had the highest slip factor of all three impellers.

iii. The variation of pressure ratio at peak adiabatic efficiencies with equivalent tip speed was more nearly the same for the three impellers than the variation of slip factor and peak adiabatic efficiency. Impeller with the circular blade curvature had the highest-pressure ratio at equivalent tip speeds as high as 396 m/s. Impeller with elliptical blade curvature had the highest at 429 and 495 m/s and impeller with the parabolic blade curvature had the highest peak at 462 m/s.

iv. Impeller with the circular blade curvature had the highest maximum specific capacity at all equivalent tip speeds up to 495 m/s. Impeller with elliptical blade curvature had nearly the same specific capacity as impeller with the circular blade curvature. Impeller with the parabolic blade curvature had a maximum specific capacity 6% to 11% smaller than that of impeller with the circular blade curvature.

v. Impeller with elliptical blade curvature had the largest useful operating range at a pressure ratio of 1.80. Impeller with the parabolic blade curvature had the largest useful operating range between pressure ratios of 2.20 to 3.00; and impeller with the circular blade curvature had smallest useful operating range at all pressure ratios.

iv. Impeller with elliptical blade curvature and impeller with the circular blade curvature exhibited an operational instability at high equivalent tip speeds near the maximum specific capacity.

This work is considered to be a valuable contribution and would help the designer to select the optimum blade shape for a specified application.

Ingham [41] carried out similar work to investigate the effect of an inducer design on the performance of a centrifugal compressor impeller. **Dean [42]** has produced experimental results from a low speed compressor showing a tip velocity profile, which he approximated to a square jet and wake flow. He suggested that for a centrifugal impeller, the theoretical maximum diffusion ratio v_2/v_1 is 0.5. He based his results on the work done by **Lieblein and Johnsen [43]** who achieved such diffusion in an axial stage. More modest design limits of $v_2/v_1 = 0.625$ were adopted by **Dallenbach *et al* [44] and Stiefel [45]**, but even these are seldom achieved due to the boundary layer separation, which occurs in most impellers.

2.2.2.2 Vaneless diffuser and the volute

The radial vaneless diffuser is a major source of inefficiency in centrifugal compressors; therefore, most of the work cited in the open literature was directed to study the flow and find methods to predict the losses in the vaneless diffuser in an attempt to increase its efficiency.

Polikovesky and Nevelson [46] calculated the loss for the incompressible flow and they found that the losses were predominantly at the diffuser entry. This was due to the high inlet loss, attributed to the impeller exit flow not completely filling the diffuser inlet cross section. **Brown [47]** obtained better results by varying the friction factor with radius and found that the highest value was at the entry.

Dean and Senoo [48] put forward a theory to explain the large total pressure losses at the diffuser inlet. Since the relative velocity distribution between the blades of an impeller in the circumferential direction is non-uniform, an unsteady flow is produced at the diffuser inlet. They proposed that this velocity profile can be considered as a jet and wake. In the diffuser these two flow regimes mix, producing a total pressure loss. An incompressible flow theory based on this model predicted that in most compressors, the jets and wakes would mix out to virtually uniform flow by a radius ratio (actual radius /diffuser inlet radius) of 1.05.

Johnston and Dean [49] presented a simplified version of jets and wakes theory. They developed their theory for incompressible flow and combined it with a one-dimensional treatment of the remainder of the diffuser. They suggested that separation caused by boundary layer, fluid tends to form regions of high and low energy, which they described as a jet and wake respectively.

A comparison of the losses by the two theories showed little difference provided that the swirl parameter c_w/c_r was greater than 2.0.

2.3 SMALL GAS TURBINE FOR HIGH-SPEED TURBO-ALTERNATOR APPLICATIONS

Because the use of high-speed turbo-alternator for power generation for a specific load and rotational speed is not common, relevant published literature is extremely limited. However, several papers were found in the open literature as described hereafter.

Anon [50] carried out an experimental work on a compound diesel engine for automotive use. A high-speed turbo-alternator, **HSTA** (10 kW at 100,000 rpm), with a radial turbine, was positioned downstream of the turbocharger to convert exhaust energy into electrical output. This was then used to improve overall engine efficiency by driving a high-speed motor positioned in the engine drive train. The ability to maintain **HSTA** turbine efficiency was claimed by controlling the **HSTA** speed independently of the engine condition; i.e. by allowing the turbine to operate within an acceptable range of isentropic velocity ratio. However, no mention was made of the implications of this for engine back pressure and the subsequent effect on engine performance, which could be considerable.

Cleland *et al* [51] developed a 1 to 3 kW **HSTA** for use in remote areas. The high-speed permanent alternator, **HSPMA** was designed to be directly driven by a radial turbine at 100,000 rpm via aerodynamic bearings. However, full test evaluation was prevented by problems with the bearing system. A similar system was described by **Barber and Boda [52]** for small community power supply. In this case the **HSPMA** was driven by an axial turbine to produce 20 kW at up to 60,000 rpm. It can be seen that research work on a complete integrated system combining a **SGT** and **HSPMA** was still scarce.

Rodgers [53] presented a re-appraisal of the small gas turbine turbo-alternator, two turbo-generator concepts were considered: the first concept was a SGT of radial type using an annular combustor while the second concept used a reverse annular combustor. Both would directly drive a high-speed generator.

Rodgers claimed that thermal efficiencies approaching 28% were attainable based upon current technology levels and with externally cooled metallic hot end components. Cost models indicated turbo-generators specific cost $\$/kW$ increases towards the lower range of its power output as a result of fixed cost assumptions for the controls and accessories costs. Capital cost increases towards the lower range of turbo-alternator. Small turbo-generators can play an important role and compete commercially if the manufacturing cost can be resolved.

Rodgers [54] extended his work and carried out a development programme to design, fabricate, and test a 10 kW high-speed alternator. The target of this work was to produce a gas turbine of 10 kW output with specific fuel consumption of 0.67 kg/kWh, without exceeding a turbine inlet temperature 1200 K. To achieve this goal, three-prototype turbo-generators package were tested. Detailed design work was initiated on three engine configurations with rotational speeds of 85,000, 100,000, and 110,000 rpm. This programme of work revealed the following results: -

i. The best design configuration to achieve the required objectives would incorporate a single stage centrifugal compressor and single stage radial turbine mounted back-to-back on a common rotor shaft. This arrangement being considered optimum from the standpoint of size, weight, simplicity and cost.

ii. It was estimated that the maximum allowable turbine inlet temperature at sea level conditions 15.5° C would be of the order of 944 K.

iii. The 85,000 rpm configurations appeared marginal from a performance standpoint, particularly if component clearances could not be strictly maintained.

iv. The 110,000 rpm configuration provided the best fuel economy 0.55 $kg/\sec$ but had the highest inducer tip relative Mach number and lowest flow range. The improvement in *SFC* at speeds above 100,000 rpm was relatively minor.

This study can be considered as a good reference for future research developments of turbo-alternator.

The primary aim of **Pullen's [55]** work was to design and develop a directly driven high-speed alternator and gas turbine as a portable generator with a power output of 50 kW . The motivation for producing such a device was the substantial reduction in weight and size of the generator in comparison to conventional low speed devices. The research area of his work was addressed to: -

i. The turbine performance and the aerodynamic design of the turbine volute.
ii. The mechanical designs aspects relating stress and vibration analysis.
iii. The design and development of the disc alternator.

His work showed the potential of turbo-alternator as a portable power plant.

Makey and Noe [56] carried out a research programme to develop a family of highly recuperated small gas turbine-driven generator sets rated from 3 to 30 kW . The proposed programme was to run the generator at the same speed of the compressor and the turbine, thus eliminating the need for a gearbox with no engine-driven accessories, hence no lubrication system as the rotor shaft will run on air bearings. The proposed system will offer an expected efficiency between 30% -35% and they claimed that the key issue to this high efficiency was the designing of a low cost circumferential recuperator of high effectiveness range of 90% - 95%.

The test results showed good performance, but were not as highly effective as those predicted by the computer programme. This may be due to higher heat losses than anticipated; therefore, better insulation techniques for circumferential recuperator will be required. A drawback of this work is the addition of an extra component that will add more weight to the unit.

Atkinson [57] carried out a research programme for the design and performance of radial turbines for small, low power applications. A design procedure was developed for the turbine rotor, inlet guide vanes and volute. The procedure was then evaluated through the design of $3.2\,kW$ turbine for an automotive turbo-alternator to be located in the exhaust of a small gasoline engine in a hybrid electric vehicle, to recover some of the waste energy. The turbine was designed to accept $27.1\ g/s$ of exhaust at $1073^{\circ}\ K$, with a total-to-static expansion ratio of 1.61:1 at 100000 rpm. The measured peak total-to-static efficiency was 80%, and the flow characteristic was within 2% of design. This was encouraging in the case of turbo-alternator turbine due to its very low power and size.

2.4 MAIN OBSERVATIONS FROM PREVIOUS WORK.

2.4.1 Inward Flow Radial Turbines and Centrifugal Compressors

i. Axial exit/tip velocity ratio c_{m1}/u_2, which has been referred to as the flow coefficient term was used by many designers in design calculations as a criterion factor for radial turbine efficiency. A recommended value for this factor for best efficiency should lie between 0.3 – 0.5. Another criterion factor for radial turbine performance is the velocity ratio u_2/c_s, in which a value between 0.67 to 0.7 would be optimum for best efficiency. Also, The blade-loading coefficient $\psi_{BL} = c_{w2}/u_2$ was recommended to be a good design criterion factor for radial turbines. On the basis of zero swirl assumption, ψ_{BL} should lie between values of 0.95 to 1.0 for best achievable efficiency.

ii. Specific speed N_s and specific diameter D_s were considered by some designers as performance parameters for radial turbines. Several charts were developed showing the relationship between the component's efficiency of radial flow machines and these parameters.

iii. Several experimental works revealed that higher blade numbers of **IFR** turbine were preferred for achieving best efficiency.

iv. Most of design methods of rotors and impellers of radial flow machines were based on one-dimensional approach.

v. It was observed that the shape of the impeller and hence blade curvature had a significant effect on the performance parameters such as the slip factor, efficiency, maximum flow capacity and the pressure ratio of centrifugal impellers.

vi. Design methods of the radial flow machine casing were based on the assumption of one-dimensional, free vortex and mass conservation. These methods produced satisfactory results in terms of performance and efficiency.

vii. Several experimental work results reported a wide variation of **IFR** volute discharge flow angle with azimuth angle around the volute, about 10° to 19°. Also, it was reported that most of the stagnation pressure loss occurred in the inlet region.

viii. The cross-sectional shape of the **IFR** volute had a great influence on the turbine efficiency. Also, it had an effect on the variation of the absolute flow angle α_2.

ix. The length of the angular bend at the entry of the **IFR** volute (known as the tongue) plays an important part in achieving the desired velocity profile, and hence maximizing the tangential flow velocity c_{w2} at the rotor inlet.

x. Mechanical considerations regarding stress analysis (centrifugal and thermal) and vibrations analysis of the radial components were not given the attention in the design approach of radial turbomachinery.

2.4.2 Small Gas Turbine For High Speed Turbo-Alternator Applications

i. Considerable attention has been paid to the development of small gas turbine engines for use in power generation to exploit their attractive features in terms of low cost, high power to weight ratio, and low emission.

ii. The best configuration of a small gas turbine for high-speed turbo-alternator applications would be a single stage centrifugal compressor, a combustion chamber and a single stage **IFR**. This arrangement being considered optimum from the

standpoint of size, weight, simplicity and cost. For $50kW$ turbo-alternator machine, the best thermal efficiency was achieved at a running speed of 93,000 rpm.

iii. High-speed turbo-alternator systems in which a small gas turbine coupled directly to high-speed permanent magnet alternator would be an optimum arrangement to reduce the system's cost, weight and size.

iv. Thermodynamic performance of small gas turbine engines are still primarily constrained by the temperature limit of the hot part of the engine, i.e. the turbine. Therefore, many research programmes have been carried out to study the feasibility of using ceramic materials to be used in the turbine industry as a replacement to the traditional metallic materials such as **Nimonic** and **Inconel** alloys.

v. All literature references agreed that small gas turbine engines, to be widely accepted over presently available units of the same power, must offer a substantial increase in efficiency, and a significant reduction in cost.

2.5 JUSTIFICATION OF THE AIMS.

i. Significant advances have been made in understanding the aero- thermodynamics design and performance of radial flow compressors and turbines, but published literature on system integration and design of the complete machine is still scarce. Therefore, this work represents a comprehensive design work of the complete system.

ii. For turbo-alternator systems, the driving speed of the gas turbine would be dictated by the speed of the directly-coupled alternator. For constant voltage and frequency output, the system speed must remain constant at the design and off design conditions. In the present research, the load and speed for the gas turbine were specified to be 60 kW and 60000 rev/min. This was a serious constraint on the design of the **IFR** turbine. Papers dealing with the design problem subject to serious constraints as in the present case are almost non-existent.

iii. An analytical method to determine the optimum number of blades and the axial length of the **IFR** turbine rotor was not cited in the open literature as far as the author is aware of. Therefore, developing a design method for calculating the optimum number of blades N_b and optimum axial length Z_{axial} for an **IFR** turbine rotor would offer a significant contribution. In addition to that, applying the method of prescribed meanstream velocity for the design of blade profile and flow channel of the **IFR** turbine does not appear to have been tackled in the published literature reviewed by the author.

iv. Complete analysis of the combined stresses (structural and thermal) and vibration of the rotating system due to the effect of centrifugal forces and elevated flow temperature were scarce and not given considerable attention. Therefore, detailed analysis of stresses due to combined centrifugal forces and thermal forces and vibration of the rotating system have been included in the current work using advanced computer software programmes.

v. Component matching between the turbine and the compressor is considered an important topic regarding the prediction of the performance of the system at the design and off-design conditions. Therefore, it is felt that some work is needed to cover this topic possibly with a new approach.

CHAPTER 3

TURBOMACHINERY THEORY, PERFORMANCE AND DESIGN MODELLING OF IFR TURBINE

3.1 THEORETICAL BACKGROUND

A full analysis of the performance parameters of the **IFR** turbine is presented in this Chapter. This entails complicated equations and parameters, which describe the design, performance and operation of **IFR** turbines.

3.1.1 Introduction

In general, gas turbines cover tremendous ranges of power, rates of mass flow and rotational speeds. For small power range $10-100\,kW$, the recommended configuration would be based on a simple gas turbine open system, which consists of a centrifugal compressor, a combustion chamber, a radial turbine and a power transmission shaft that connects the compressor and the turbine as shown in **Fig. 3.1**.

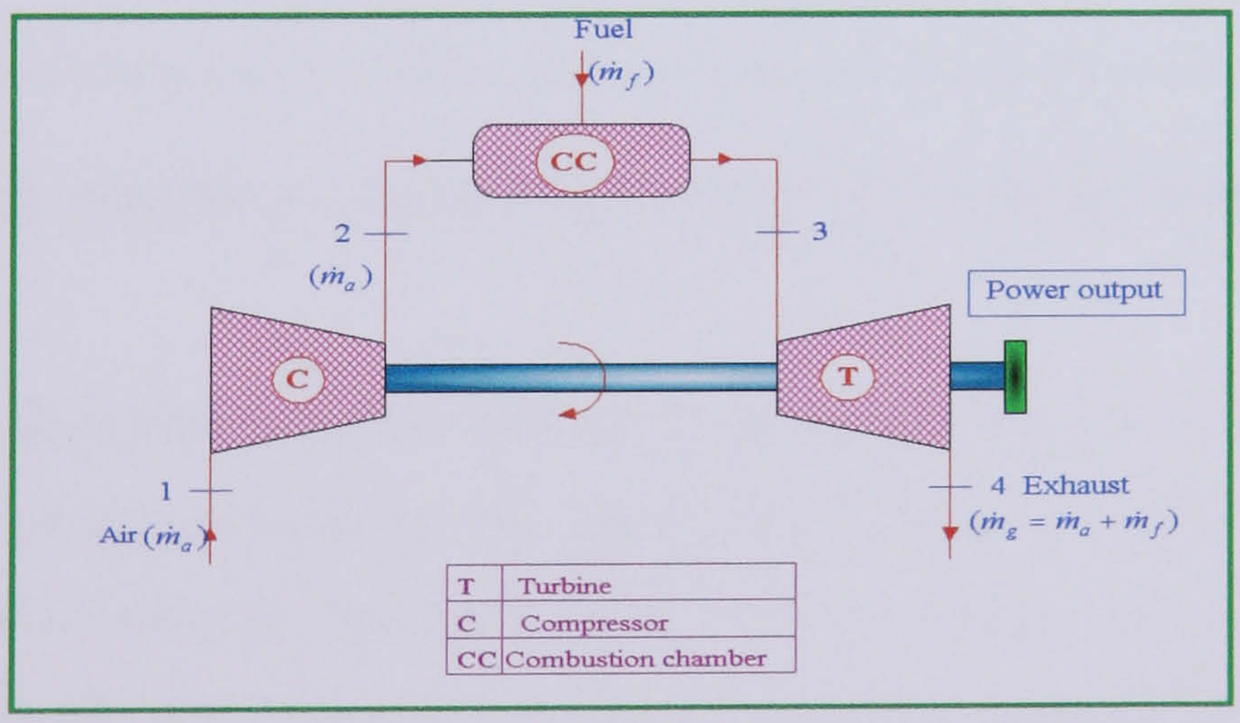

FIG. 3.1 AN OPEN SIMPLE GAS TURBINE CYCLE

In power generation applications, there are many arrangements of the compressor, turbine and the alternator on a single shaft. Only four arrangements are considered and the others hence omitted due to the alternator being close to the hot part of the engine.

Hence the alternator will be subjected to overheating. These four arrangements are shown in **Fig. 3.2** in which the alternator is always located at the compressor end.

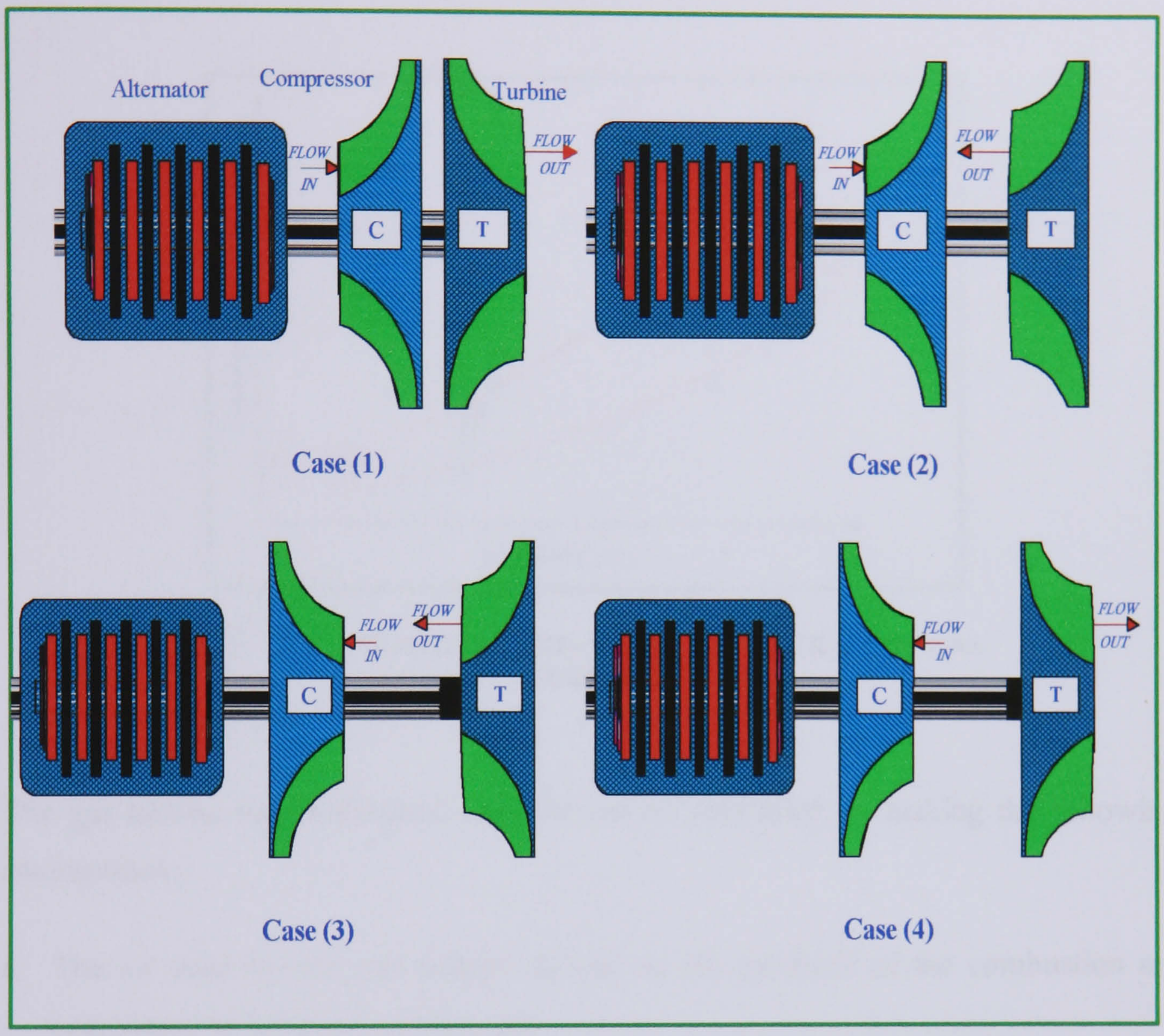

FIG. 3.2 POSSIBLE ARRANGEMENTS OF HIGH SPEED TURBO-ALTERNATOR

Another consideration was the end thrust developed due to aerodynamic pressure loading and pressure forces on the turbo-machinery rotors. For cases 1 and 3, the forces on the compressor and the turbine rotor act against each other. However, for cases 2 and 4, the net forces will not be zero and this may cause bearing problem in term of friction losses and instability. Therefore, cases 2 and 4 are dismissed. Ducting problems of the compressor inlet and turbine exhaust means dismissing case 3, leaving only case 1 as an available option.

3.1.2 Gas Turbine Cycle Analysis

For simple gas turbine, operates on Brayton cycle, is represented on T-S diagram as shown in **Fig. 3.3**.

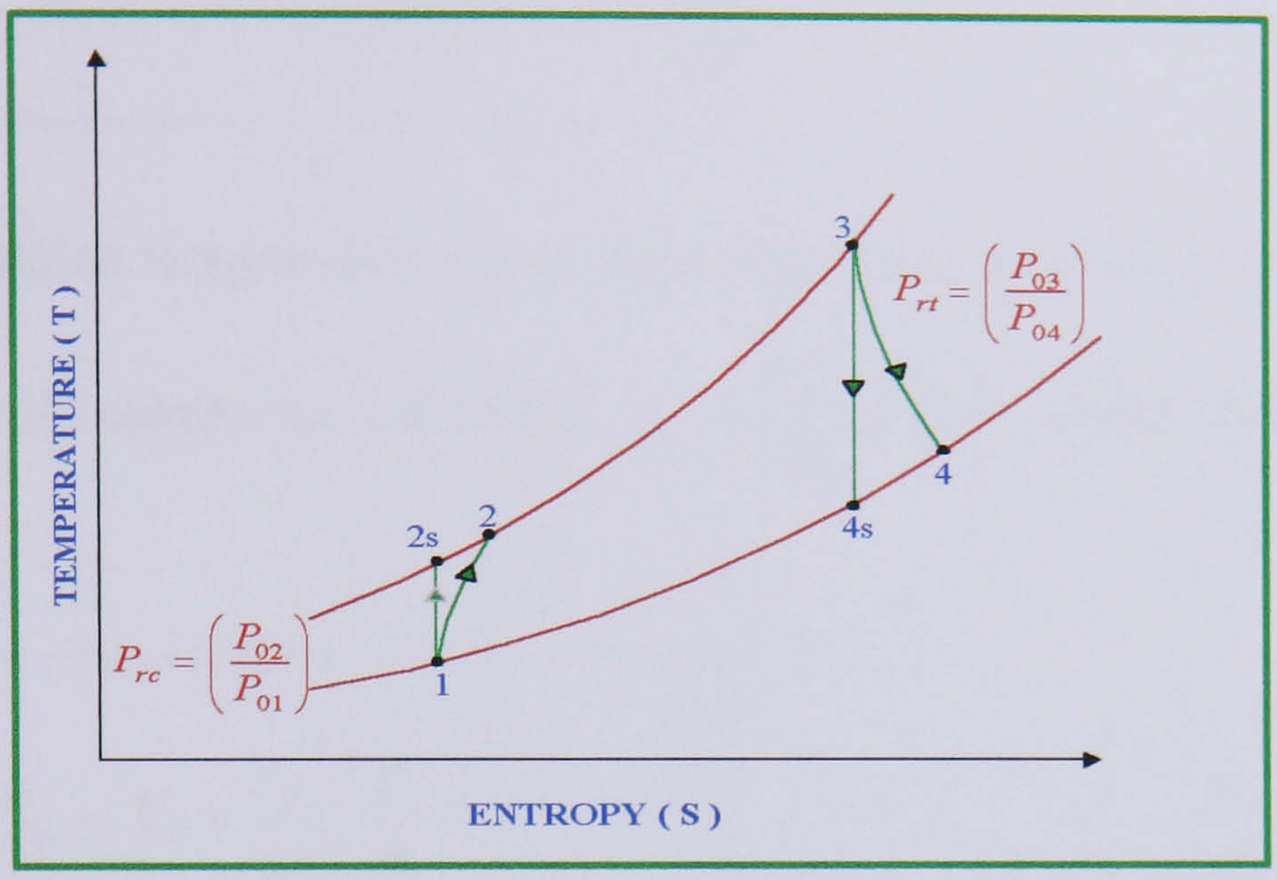

FIG. 3.3 TEMPERATURE- ENTROPY DIAGRAM OF GAS TURBINE CYCLE

The gas turbine thermodynamic analysis can be simplified by making the following assumptions:

i. The air used by the gas turbine as well as the products of the combustion are considered to behave as perfect gas.

ii. The specific heat capacities of the air and the combustion products are considered to be constant through the individual process and represented at the average temperature of that process.

iii. The loss of stagnation pressure in the combustion chamber is a constant percentage of combustion chamber inlet pressure.

The gas turbine cycle performance can be calculated in step-by-step analysis for each different component in the cycle as described hereafter.

Step 1 **Air compression in the compressor**

The compression power (W_c) is given by

$$W_c = \dot{m}_a C_{pa} \frac{T_{01}}{\eta_c}\left[\left(\frac{P_{02}}{P_{01}}\right)^{\frac{\gamma_a - 1}{\gamma_a}} - 1\right] \quad \textbf{(3.1)}$$

The final stagnation temperature T_{02} in the compression process can be derived from the definition of compressor efficiency, $\eta_c = \frac{(T_{02} - T_{01})_s}{(T_{02} - T_{01})}$ **(refer to Fig. 3.3)** to be expressed as:

$$T_{02} = T_{01} + \frac{T_{01}}{\eta_c}\left[\left(\frac{P_{02}}{P_{01}}\right)^{\frac{\gamma_a - 1}{\gamma_a}} - 1\right] \quad \textbf{(3.2)}$$

Step 2 **Combustion process**

The energy balance of the combustion chamber for a perfectly insulated chamber with no work transfer process can be expressed as:

$$\dot{m}_a H_{02} + \dot{m}_f H_f = \dot{m}_g H_{03} \quad (3.3)$$

Equation 3.3 can be transformed to give an expression for fuel/air ratio f

$$f = \frac{\dot{m}_f}{\dot{m}_a} = \frac{C_{pg}(T_{03} - T_{ref}) - C_{pa}(T_{02} - T_{ref})}{(LCV)(\eta_{cc}) - C_{pg}(T_{03} - T_{ref})} \quad \textbf{(3.4)}$$

Step 3 **Gas expansion in the turbine**

The turbine power W_t can be expressed as

$$W_t = (1 + f)\dot{m}_a C_{pg} \eta_t T_{03}\left[1 - \left(\frac{P_{04}}{P_{03}}\right)^{\frac{\gamma_g - 1}{\gamma_g}}\right] \quad \textbf{(3.5)}$$

The exhaust stagnation temperature T_{04} in the expansion process can be obtained from the definition of turbine efficiency, $\eta_t = \frac{(T_{03} - T_{04})}{(T_{03} - T_{04})_s}$, **(Fig. 3.3)** to be expressed as:

$$T_{04} = T_{03} - \eta_t T_{03}\left[1 - \left(\frac{P_{04}}{P_{03}}\right)^{\gamma_g - 1/\gamma_g}\right] \quad \textbf{(3.6)}$$

Step 4 **Thermal efficiency and specific fuel consumption of the cycle**

$$\eta_{th} = \frac{output\ power}{Input\ power} = \frac{W_{net}}{Q_{in}} = \frac{(W_t - W_c)}{f\dot{m}_a(LCV)} \quad \textbf{(3.7)}$$

$$SFC = \frac{3600f}{W_t - W_c} \quad \textbf{(3.8)}$$

Step 5 **Specific work output**

$$\dot{W}_s = \dot{W}_t - \dot{W}_c \quad (3.9)$$

From above, the efficiency of the gas turbine cycle can be increased by

i. Increasing the inlet turbine temperature T_{03}

ii. Increasing turbine inlet pressure P_{03}

iii. Increasing the component's efficiency $\eta_c, \eta_t, \eta_{cc}$.

3.1.3 Turbo-Machinery

Fluids machines are devices for either converting the energy held by a fluid into mechanical energy or visa versa. The mechanical energy is usually transmitted by a rotating shaft. A machine in which energy from the fluid is converted directly to the mechanical energy of a rotating member is known as a **turbine**. If the primary object is to increase the pressure of the gas, the machine is termed a **compressor**.

3.1.3.1 Turbo-machinery classification

A classification of types of turbo-machines is summarized in the **Table 3.1**

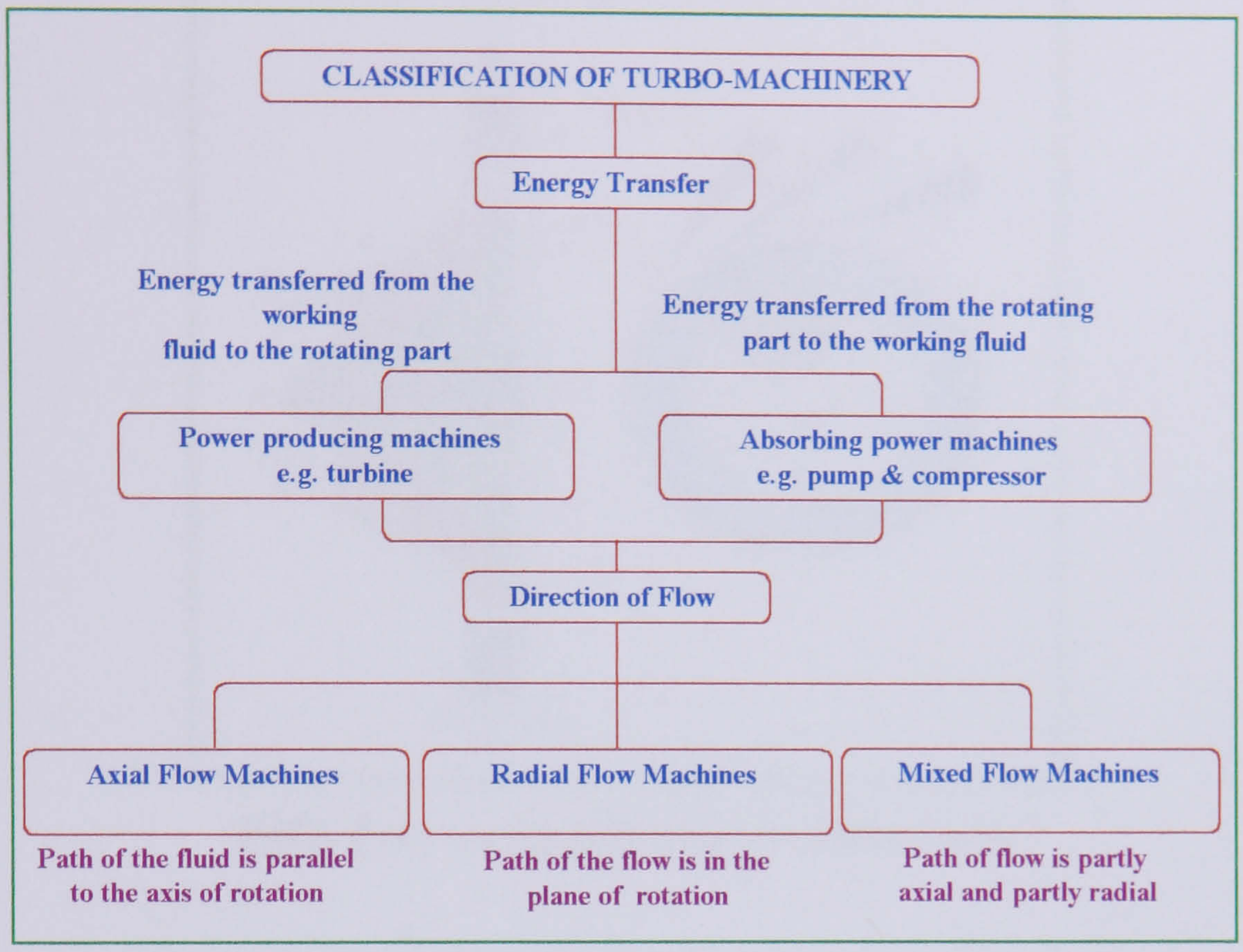

TABLE 3.1 CLASSIFICATION OF TURBO-MACHINERY

3.1.3.2 Radial turbo-machinery

For radial turbo-machinery, there are two main types, which are:

i. The centrifugal compressor

ii. The radial turbine

Both types consist of two main parts as shown in **Figs. 3.4, 3.5**. The stator part is referred to as the casing or the volute. The rotating part is referred to as either the rotor for the turbine or the impeller for the compressor. Detailed description of these parts will be given in later Chapters.

3.1.4 Basic Equations For Radial Turbo-Machinery

The basic equations that are required to analysis the flow through radial turbo-machinery are the equation of continuity, equation of momentum, and the general energy equation. The derivation of momentum and steady flow energy equations can

be found in any thermodynamics and turbomachinery textbooks; hence they are not referenced hereafter.

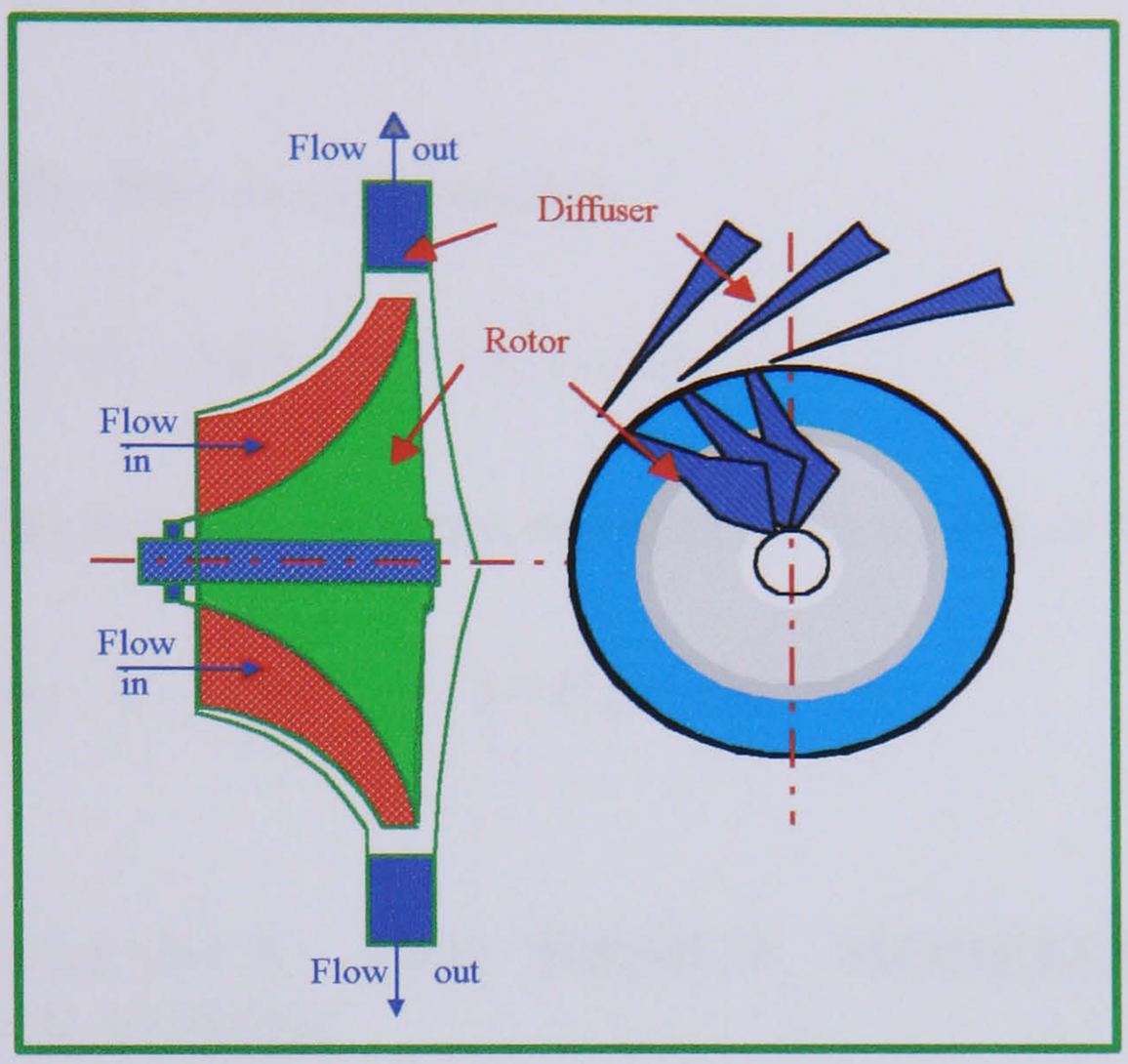

FIG. 3.4 A CENTRIFUGAL COMPRESSOR

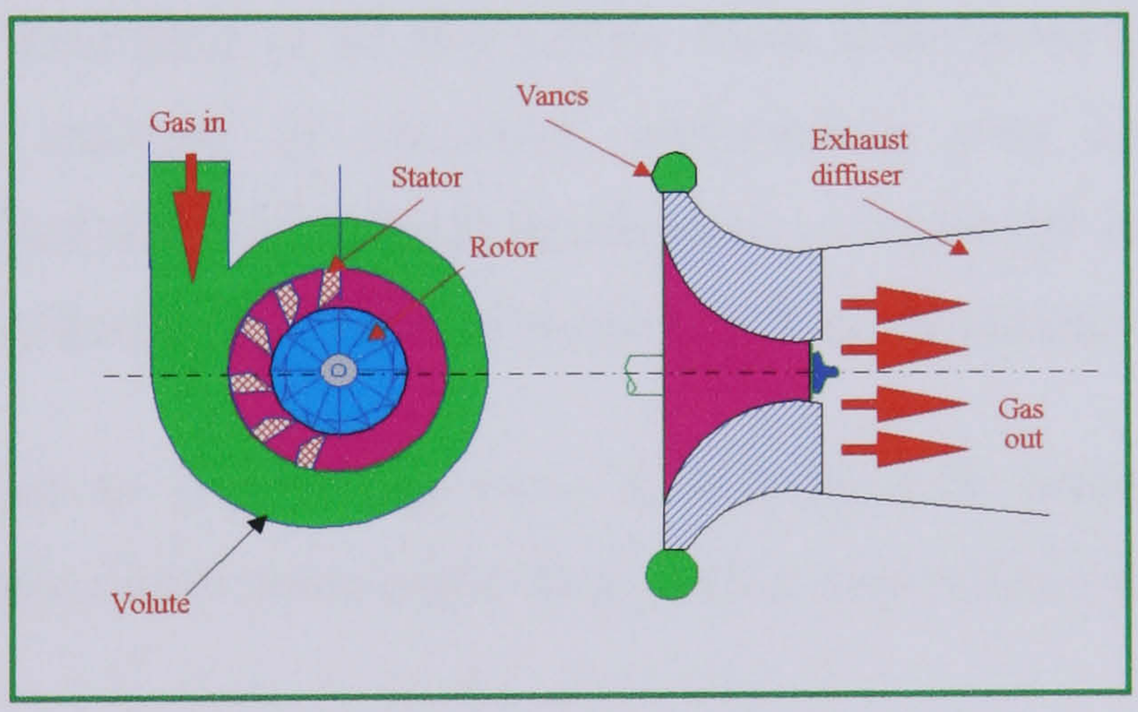

FIG. 3.5 AN INWARD FLOW RADIAL TURBINE

3.1.4.1 Equation of continuity

Mass flow rate: $$\dot{m} = \rho_1 A_1 c_1 = \rho_2 A_2 c_2 \tag{3.10}$$

3.1.4.2 The momentum equation (Euler's equation)

Specific Work output: $$\dot{W}_s = (c_{w2} u_2 - c_{w1} u_1) \tag{3.11a}$$

Equation 3.11a can be expanded to give

$$\dot{W}_s = (c_{w2}u_2 - c_{w1}u_1) = \frac{1}{2}\left[(u_2{}^2 - u_1{}^2) - (v_2{}^2 - v_1{}^2) + (c_2{}^2 - c_1{}^2)\right] \qquad (3.11b)$$

3.1.4.3 The steady- flow energy equation

$$\dot{Q} - \dot{W} = (h_2 - h_1) + \frac{1}{2}(c_2{}^2 - c_1{}^2) + g(z_2 - z_1) \qquad (3.12a)$$

Assuming no change in potential energy, equation 3.16a is reduced to give

$$\dot{W} = (h_2 - h_1) + \frac{1}{2}(c_2{}^2 - c_1{}^2) = H_{02} - H_{01} \qquad (3.12b)$$

3.2 PERFORMANCE AND DESIGN MODELLING OF IFR TURBINE ROTOR

3.2.1 Introduction

The mathematical modelling of an **IFR** turbine rotor is desirable for many purposes including design, analysis of measured performance data and estimation of performance. The mathematical models developed and employed in the present work are essentially one-dimensional, which is implicit in **Euler's** equation

The performance of an **IFR** turbine rotor is controlled by several dependent and independent variables which come under three main categorizes as shown in **Table 3.2**

CONTROL VARIABLES	DESIGN VARIABLES	PERFORMANCE PARAMETERS
Inlet pressure	Tip diameter, Blade width	Mass flow rate
Inlet temperature	Exducer and Hub diameter	Isentropic efficiency
Rotational speed	Axial length, Blade angles	Torque developed
Properties of working fluids	Inlet and outlet Mach numbers	Degree of reaction, Flow coefficient and blade loading coefficient

TABLE 3.2 MAIN PARAMETERS OF AN INWARD FLOW RADIAL TURBINE

The interaction between the three categories can be studied, without referring to the flow in a turbo-machine, by combining the main variables involved into a relatively smaller number of dimensionless groups and expressed them in terms of design variables as described hereafter.

3.2.2 Development of Non-Dimensional Performance Parameters of IFR Turbine Rotor

Applying the steady flow energy equation for the **IFR** turbine between inlet **(i)** and outlet **(e)** conditions, i.e. the work transfer from the turbine can be described as:

$$-W = \dot{m}\Delta(h + \frac{c^2}{2})_{i-e} \tag{3.13}$$

Further assuming the working fluid behaves as a perfect gas, and its specific heat C_p is independent of T for the range of temperatures considered, equation 3.13 for the ideal and the actual power produced by the turbine can be converted to equation 3.14 as shown below:

$$(W)_{actual} = \dot{m}C_p\eta_{t-t}(T_i - T_e)_s = \dot{m}C_p\eta_{t-t}T_i\left[1 - \left(\frac{P_e}{P_i}\right)^{\gamma-1/\gamma}\right] \tag{3.14}$$

Where,

H, T, P, η_{t-t} are total enthalpy, total temperature, total pressure and total-to-total isentropic efficiency respectively, of the working fluid.

From mechanical considerations

$$(W)_{actual} = \tau 2\pi N \tag{3.15}$$

Hence, equating 3.14 and 3.15 and dividing by $d_2{}^3 P_i$, it can be shown that:

$$\frac{\tau}{d_2{}^3 P_i} = \frac{\eta_{t-t}}{2\pi}\left(\frac{\dot{m}\sqrt{C_p T_i}}{d_2{}^2 P_i}\right)\left(\frac{d_2 N}{\sqrt{C_p T_i}}\right)^{-1}\left[1 - \left(\frac{P_e}{P_i}\right)^{\gamma-1/\gamma}\right] \tag{3.16}$$

or

$$\boxed{\frac{\tau}{d_2\dot{m}\sqrt{C_pT_i}} = \frac{\eta_{t-t}}{2\pi}\left(\frac{d_2N}{\sqrt{C_pT_i}}\right)^{-1}\left[1-\left(\frac{P_e}{P_i}\right)^{\frac{\gamma-1}{\gamma}}\right]} \quad \textbf{(3.17)}$$

By definition, the spouting velocity c_s is given as:

$$c_s = \sqrt{2C_pT_i\left[1-\left(\frac{P_e}{P_i}\right)^{\frac{\gamma-1}{\gamma}}\right]} \quad (3.18)$$

and the blade tip speed u_2 as

$$u_2 = \pi d_2 N \quad (3.19)$$

By combining equations 3.18 and 3.19 and re-arranging, an expression for the velocity speed ratio is obtained:

$$\boxed{\frac{u_2}{c_s} = \frac{\pi}{\sqrt{2}}\left[\left(\frac{\frac{d_2N}{\sqrt{C_pT_i}}}{\sqrt{1-\left(\frac{P_e}{P_i}\right)^{\frac{\gamma-1}{\gamma}}}}\right)\right]} \quad \textbf{(3.20)}$$

The non-dimensional parameter u_2/c_s is referred to as the isentropic velocity ratio or spouting velocity ratio.

Also, substituting equation 3.20 in equation 3.17, the following expression for specific torque is obtained:

$$\boxed{\frac{\tau}{d_2\dot{m}\sqrt{C_pT_i}} = \frac{\sqrt{2}}{4}\left(\frac{\eta_{t-t}}{u_2/c_s}\right)\left[1-\left(\frac{P_e}{P_i}\right)^{\frac{\gamma-1}{\gamma}}\right]^{\frac{1}{2}}} \quad \textbf{(3.21)}$$

Where:

$\frac{\dot{m}\sqrt{C_pT_i}}{d_2{}^2P_i}$ = Dimensionless mass flow parameter (M_p)

$\frac{d_2 N}{\sqrt{C_p T_i}}$ = Dimensionless speed parameter (S_P)

$\frac{\tau}{d_2 \dot{m} \sqrt{C_p T_i}}$ = Dimensionless specific torque parameter, dimensionless torque per unit mass flow rate (ST)

$\frac{\tau}{d_2^{\,3} P_i}$ = Dimensionless torque parameter

$\frac{P_i}{P_e}$ = Total to total pressure ratio (P_r)

$\frac{u_2}{c_s}$ = Isentropic velocity ratio (VR)

η_{t-t} = Adiabatic efficiency from total inlet to total outlet conditions

3.2.3 Relationship Between Turbine Performance Parameters and Geometric Design Variables

The geometrical shape of a typical **IFR** turbine is shown in **Fig. 3.6** and the principal dimensions are defined in **Table 3.3**.

PARAMETER	NOTATION	PARAMETER	NOTATION
Rotor tip diameter	d_2	Blade angle at rotor inlet	β_{b2}
Rotor blade width at tip	b_2	Blade angle at exducer	β_{be}
Rotor exducer diameter	d_e	Blade angle at hub	β_{bh}
Rotor hub diameter	d_h	Blade angle at exit mean diameter	β_{b1}
Rotor mean diameter at exit	d_1	Axial length	Z_{axial}

TABLE 3.3 PRINCIPAL DIMENSIONS OF A TURBINE ROTOR

The design variables include the ratios of the geometric dimensions such as b_2/d_2 d_1/d_2, d_e/d_2, d_h/d_2. Furthermore, it is assumed that the blade angles and the flow angles are the same under certain conditions, i.e. $\beta_{b2} = \beta_2$, etc.

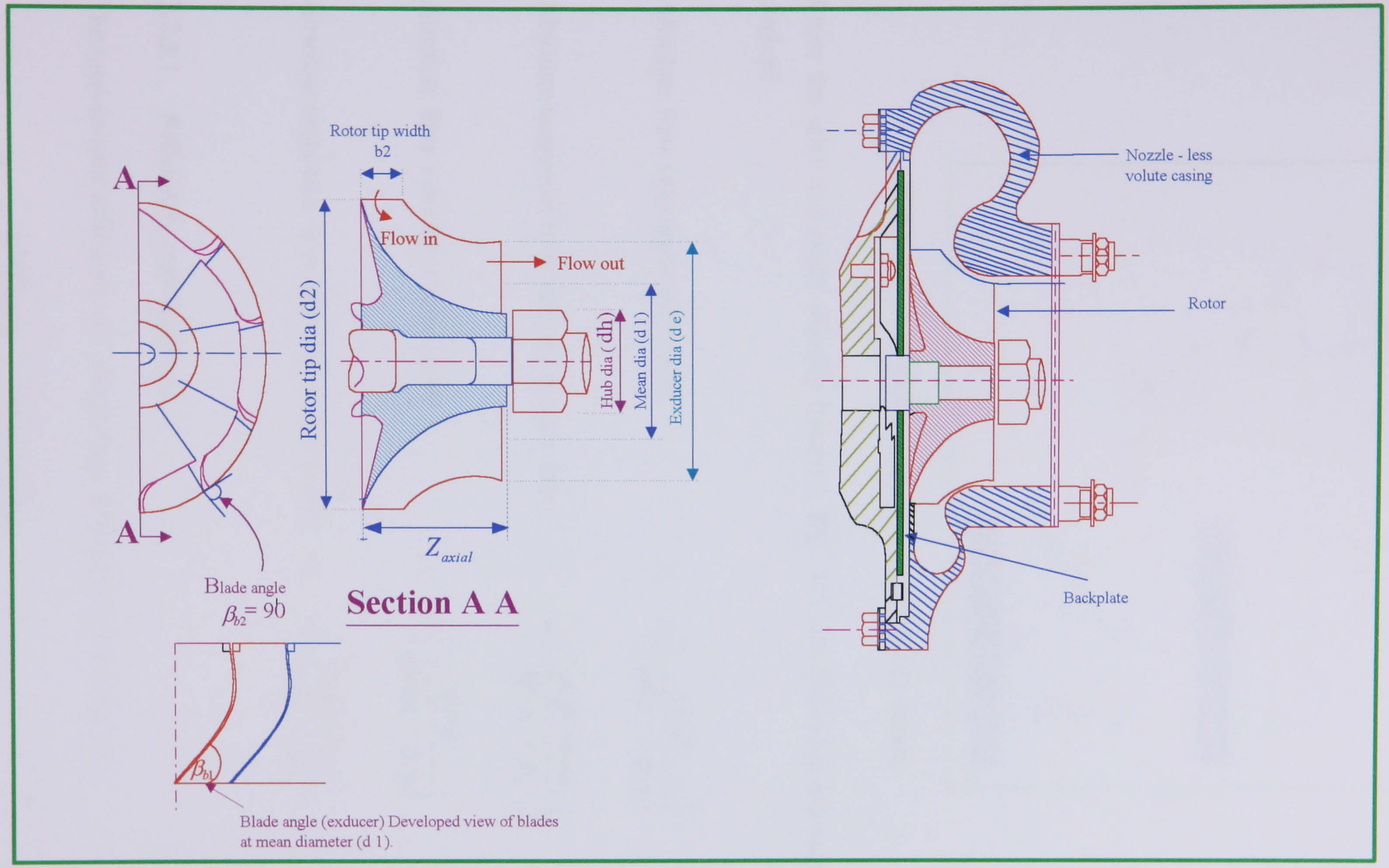

FIG. 3.6 THE GEOMETRICAL SHAPE AND THE PRINCIPAL DIMENSIONS OF THE TURBINE

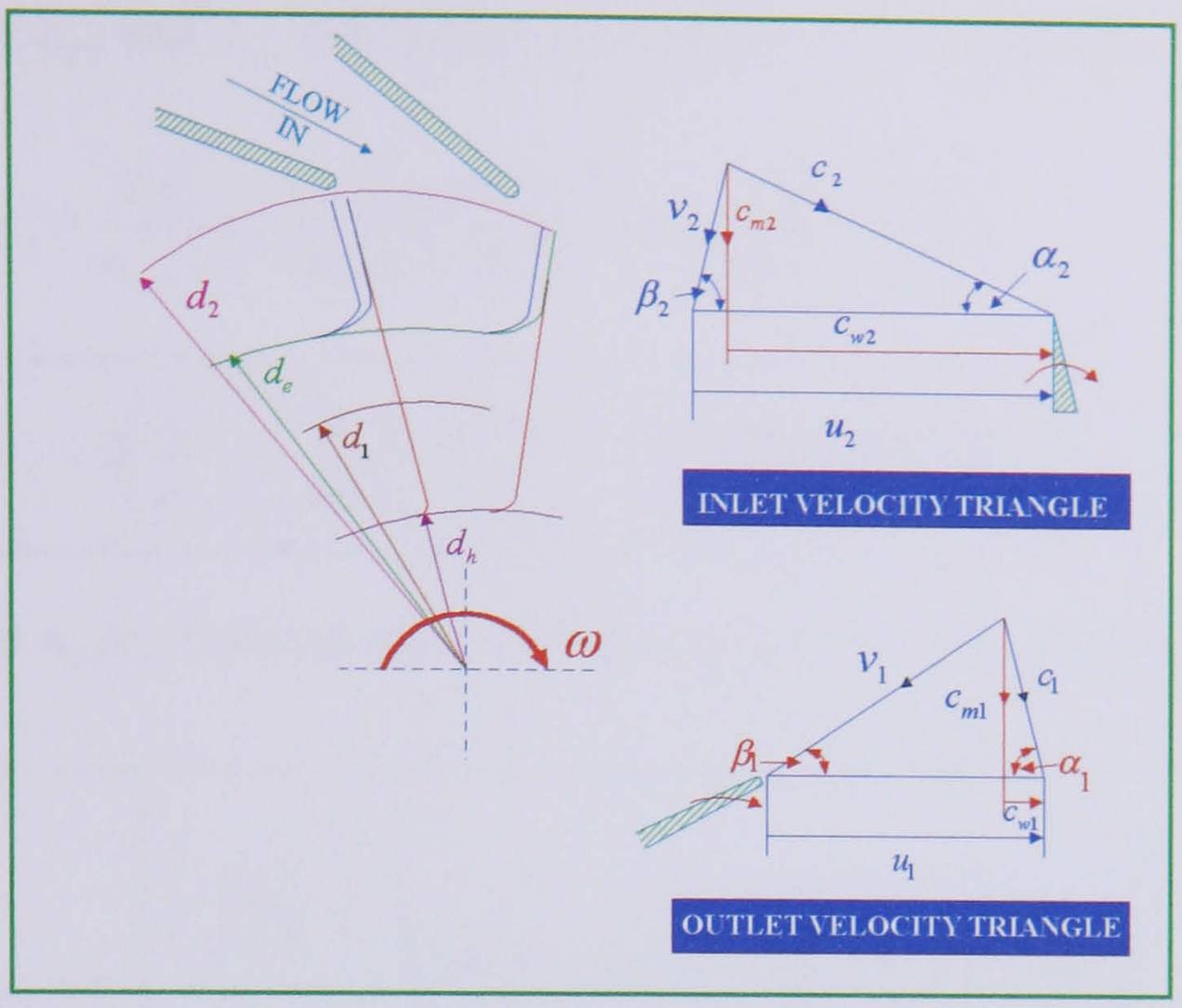

FIG. 3.7 VELOCITY TRIANGLES OF IFR TURBINE

From the inlet and outlet velocity triangles, **Fig. 3.7**, the following expressions are derived

Absolute flow velocity at rotor inlet: $$c_2 = u_2\left(\frac{\sin\beta_2}{\sin(\alpha_2+\beta_2)}\right) \quad (3.22)$$

Absolute tangential flow velocity at rotor inlet: $$c_{w2} = u_2\left(\frac{\sin\beta_2\cos\alpha_2}{\sin(\alpha_2+\beta_2)}\right) \quad (3.23)$$

Absolute flow velocity at rotor outlet $$c_1 = u_1\left(\frac{\sin\beta_1}{\sin(\alpha_1+\beta_1)}\right) \quad (3.24)$$

Absolute tangential flow velocity at rotor outlet: $$c_{w1} = u_1\left(\frac{\sin\beta_1\cos\alpha_1}{\sin(\alpha_1+\beta_1)}\right) \quad (3.25)$$

3.2.3.1 Efficiency expression (η_{t-t})

The total-to-total efficiency of a single stage **IFR** turbine is defined as:

$$\eta_{t-t} = \frac{(\Delta H)_{actual}}{(\Delta H)_{isentropic}} = \frac{u_2c_{w2} - u_1c_{w1}}{{c_s}^2/2} \quad (3.26)$$

Substituting for c_{w2} and c_{w1} from equations 3.23 and 3.25 in equation 3.26 gives

$$\eta_{t-t} = \frac{2}{c_s^{\,2}}\left[\left(u_2^{\,2}\frac{\sin\beta_2\cos\alpha_2}{\sin(\alpha_2+\beta_2)}\right)-\left(u_1^{\,2}\frac{\sin\beta_1\cos\alpha_1}{\sin(\alpha_1+\beta_1)}\right)\right]$$

$$\boxed{\eta_{t-t} = 2\left(\frac{u_2}{c_s}\right)^2\left[\left(\frac{\sin\beta_2\cos\alpha_2}{\sin(\alpha_2+\beta_2)}\right)-\left(\frac{(d_1^{\,2})}{(d_2^{\,2})}\frac{\sin\beta_1\cos\alpha_1}{\sin(\alpha_1+\beta_1)}\right)\right]} \quad \textbf{(3.27)}$$

Substituting for u_2/c_s from equation 3.20 in equation 3.27, η_{t-t} can be expressed as:

$$\boxed{\eta_{t-t} = \pi^2\left[\frac{\left(\frac{d_2N}{\sqrt{C_pT_i}}\right)^2}{1-\left(\frac{P_e}{P_i}\right)^{\frac{\gamma-1}{\gamma}}}\right]\left[\left(\frac{\sin\beta_2\cos\alpha_2}{\sin(\alpha_2+\beta_2)}\right)-\left(\frac{(d_1^{\,2})}{(d_2^{\,2})}\frac{\sin\beta_1\cos\alpha_1}{\sin(\alpha_1+\beta_1)}\right)\right]} \quad \textbf{(3.28)}$$

Equation 3.28 showed that $\eta_{t-t} = f(P_r, S_p, \alpha_1, \beta_1, \alpha_2, \beta_2, d_1/d_2)$

3.2.3.2 Degree of reaction expression (R)

By definition, the degree of reaction is described as the ratio between static enthalpy drop across the rotor to the total enthalpy drop across the turbine stage as:

$$R = \frac{h_2 - h_1}{H_i - H_e}$$

$$R = \frac{h_2 - h_1}{H_i - H_e} = \left[\left(\frac{(H_{02} - \frac{c_2^{\,2}}{2}) - (H_{01} - \frac{c_1^{\,2}}{2})}{H_i - H_e}\right)\right]$$

Since the total enthalpy drop in the rotor is equal to the total enthalpy drop in the stage and by considering the flow is adiabatic as shown in **Fig. 3.8**

i.e. $H_i = H_{02}$ and $H_e = H_{01}$, therefore the above expression can be expressed as:

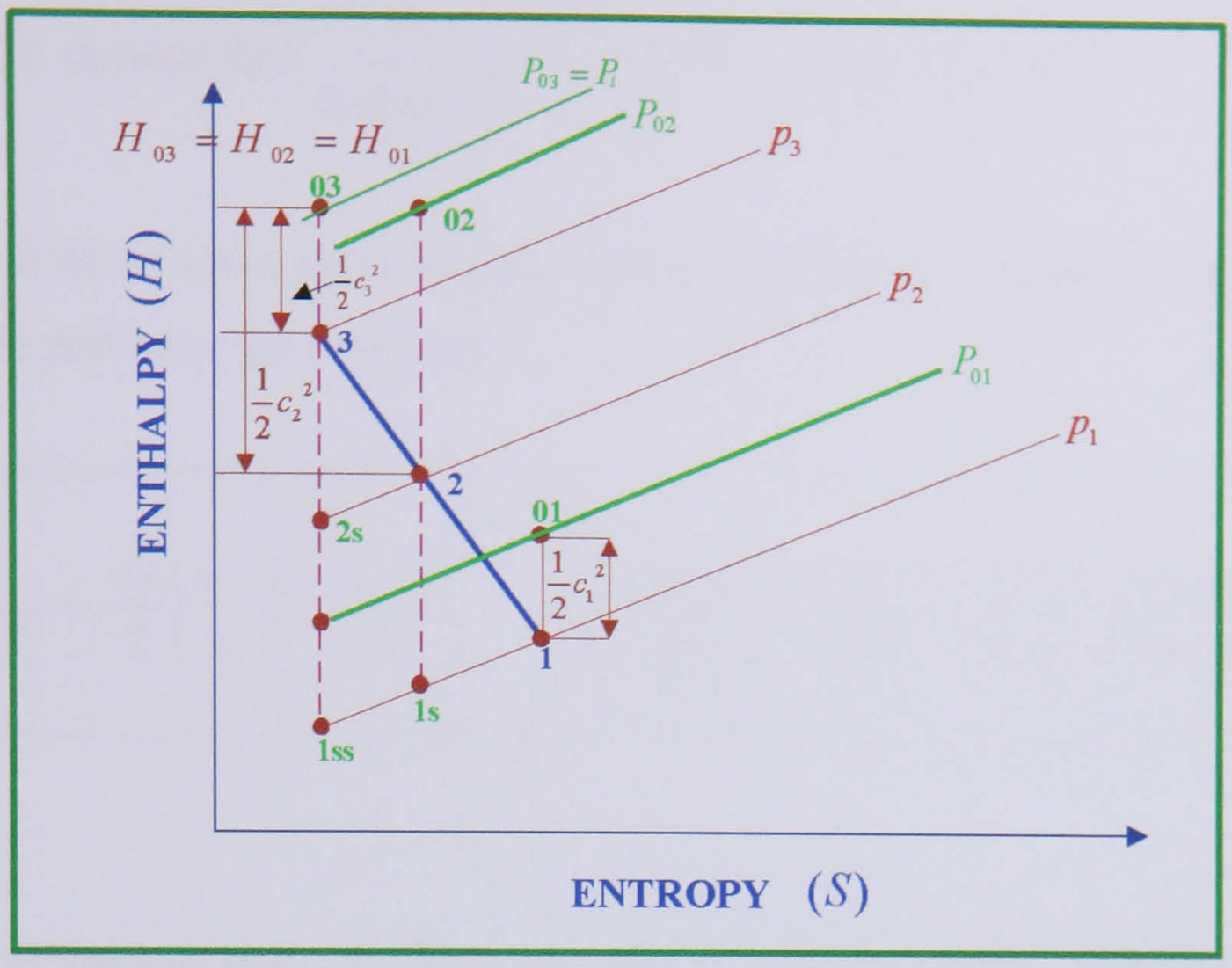

FIG. 3.8 ENTHALPY – ENTROPY DIAGRAM FOR A TURBINE STAGE

$$R = 1 - \frac{1}{2}\left(\frac{c_2^2 - c_1^2}{c_{w2}u_2 - c_{w1}u_1}\right)$$

$$R = 1 - \frac{1}{2}\left[\frac{\left(\frac{\sin\beta_2}{\sin(\alpha_2+\beta_2)}\right)^2 - \left(\frac{d_1}{d_2}\right)^2\left(\frac{\sin\beta_1}{\sin(\alpha_1+\beta_1)}\right)^2}{\left(\frac{\sin\beta_2\cos\alpha_2}{\sin(\alpha_2+\beta_2)}\right) - \left(\frac{d_1}{d_2}\right)^2\left(\frac{\sin\beta_1\cos\alpha_1}{\sin(\alpha_1+\beta_1)}\right)}\right] \quad \textbf{(3.29)}$$

Equation 3.29 showed that $R = f(\alpha_1, \beta_1, \alpha_2, \beta_2, d_1/d_2)$

3.2.3.3 Specific torque expression $(\tau/d_2\dot{m}\sqrt{C_pT_i})$

Substituting for η_{t-t} from equation 3.28 in equation 3.17, an expression for specific torque is obtained:

$$\frac{\tau}{d_2\dot{m}\sqrt{C_pT_i}} = \frac{\pi}{2}\left(\frac{d_2N}{\sqrt{C_pT_i}}\right)\left[\left(\frac{\sin\beta_2\cos\alpha_2}{\sin(\alpha_2+\beta_2)}\right) - \left(\frac{d_1}{d_2}\right)^2\left(\frac{\sin\beta_1\cos\alpha_1}{\sin(\alpha_1+\beta_1)}\right)\right] \quad \textbf{(3.30)}$$

Equation 3.30 showed that $\frac{\tau}{d_2 \dot{m} \sqrt{C_p T_i}} = f(S_p, \alpha_2, \beta_2, \alpha_1, \beta_1, d_1/d_2)$

Another form of dimensionless specific torque is obtained in terms of velocity ratio, pressure ratio and rotor geometry as:

$$\frac{\tau}{d_2 \dot{m} \sqrt{C_p T_i}} = \frac{\sqrt{2}}{2}\left(\frac{u_2}{c_s}\right)\left[1-\left(\frac{P_e}{P_i}\right)^{\gamma-1}{}_{\gamma}\right]^{1/2}\left[\left(\frac{\sin\beta_2 \cos\alpha_2}{\sin(\alpha_2+\beta_2)}\right)-\left(\frac{d_1}{d_2}\right)^2\left(\frac{\sin\alpha_1 \cos\beta_1}{\sin(\alpha_1+\beta_1)}\right)\right] \quad \textbf{(3.31)}$$

Equation 3.31 showed that $\frac{\tau}{d_2 \dot{m} \sqrt{C_p T_i}} = f(u_2/c_s, P_e/P_i, \alpha_2, \beta_2, \alpha_1, \beta_1, d_1/d_2)$

3.2.3.4 Flow coefficient expression (c_{m1}/u_2)

Flow coefficients are commonly used in axial turbine efficiency correlations. In the case of radial turbines, a modified form is often used based on the exit meridional velocity:

$$\phi_{fc} = c_{m1}/u_2 \quad (3.32)$$

Flow coefficient can be expressed in terms of geometric dimensions of the **IFR** rotor as shown below:

From exit velocity diagram, **Fig. 3.7**

$$c_{m1} = c_1 \sin\alpha_1 = \left[u_1\left(\frac{\sin\beta_1}{\sin(\alpha_1+\beta_1)}\right)\right]\sin\alpha_1 \quad (3.33)$$

Substituting for c_{m1} into equation 3.32 and re-arranging will give:

$$\phi_{fc} = \left(\frac{u_1}{u_2}\right)\left(\frac{\sin\alpha_1 \sin\beta_1}{\sin(\alpha_1+\beta_1)}\right) \quad (3.34)$$

$$\phi_{fc} = \left(\frac{d_1}{d_2}\right)\left(\frac{\sin\alpha_1 \sin\beta_1}{\sin(\alpha_1 + \beta_1)}\right) \tag{3.35}$$

Equation 3.35 showed that $\phi_{fc} = f(\alpha_1, \beta_1, d_1/d_2)$

3.2.3.5 Blade loading coefficient (c_{w2}/u_2)

Blade loading coefficients ψ_{BL} are used extensively in axial turbine efficiency correlations. However, **Baines [58]** has suggested that the blade-loading coefficient may be valuable parameters in radial turbine performance correlations. It is based on the actual total enthalpy change through the turbine and is usually defined using the rotor tip speed parameter:

$$\psi_{BL} = \frac{(\Delta H_{i-e})_{actual}}{u_2^{\,2}} = \frac{H_{02} - H_{01}}{u_2^{\,2}} = \frac{c_{w2}u_2 - c_{w1}u_1}{u_2^{\,2}} = \frac{c_{w2}}{u_2} - \left(\frac{u_1}{u_2}\right)\left(\frac{c_{w1}}{u_2}\right) \tag{3.36}$$

Equation 3.36 can be expressed in terms of geometric dimensions of the rotor by using equations 3.23 and 3.25 to develop into:

$$\psi_{BL} = \left(\frac{\sin\beta_2 \cos\alpha_2}{\sin(\alpha_2 + \beta_2)}\right) - \left(\frac{d_1}{d_2}\right)^2 \left(\frac{\sin\beta_1 \cos\alpha_1}{\sin(\alpha_1 + \beta_1)}\right) \tag{3.37}$$

Equation 3.37 shows that blade loading $\psi_{BL} = f(\alpha_2, \beta_2, \alpha_1, \beta_1, d_1/d_2)$

Equations (3.27, 3.29, 3.30, 3.31, 3.35, 3.37) provide general relationships between the geometric variables, which include $(d_1/d_2\ , \beta_2, \alpha_2, \beta_1, \alpha_1)$ and the performance parameters such as the total-to-total efficiency η_{tt}, specific torque parameter $\tau/d_2\dot{m}\sqrt{C_pT_i}$, degree of reaction R, flow coefficient ϕ_{fc} and blade loading coefficient ψ_{BL}.

It should be emphasized at this point that the angles β_1, β_2 are relative flow angles respectively, and should not be confused with the blade angles β_{1b} and β_{2b} of the IFR turbine. Under certain conditions however, the flow and blade angles may be equal.

In order to study the relative influence of all the geometric variables involved on the performance characteristics, large number of solutions would be obtained. Therefore, in view of the magnitude of the task, the design condition will be considered here where $\beta_2 = 85^\circ$ for minimum incidence loss based on flat plate model data **Bhinder [2]** and $\alpha_1 = 90^\circ$ (zero swirl at rotor exit). Therefore, equations (3.27, 3.29, 3.30, 3.31, 3.35, 3.37) can now be re-written based on these assumptions as follows: -

$$(\eta_{t-t})_{design} = 2\left[\left(\frac{u_2}{c_s}\right)^2\right]_{design}\left[\left(\frac{\sin\beta_2\cos\alpha_2}{\sin(\alpha_2+\beta_2)}\right)\right]_{design} \quad \textbf{(3.38)}$$

$$(R)_{design} = 1-\frac{1}{2}\left[\frac{\left(\frac{\sin\beta_2}{\sin(\alpha_2+\beta_2)}\right)^2-\left(\frac{d_1}{d_2}\right)^2\left(\tan^2\beta_1\right)}{\left(\frac{\sin\beta_2\cos\alpha_2}{\sin(\alpha_2+\beta_2)}\right)}\right]_{design} \quad \textbf{(3.39)}$$

$$\left(\frac{\tau}{d_2\dot{m}\sqrt{C_pT_i}}\right)_{design} = \frac{\pi}{2}\left(\frac{d_2N}{\sqrt{C_pT_i}}\right)_{design}\left(\frac{\sin\beta_2\cos\alpha_2}{\sin(\alpha_2+\beta_2)}\right)_{design} \quad \textbf{(3.40)}$$

or

$$\left(\frac{\tau}{d_2{}^3P_i}\right)_{design} = \frac{\pi}{2}\left(\frac{\dot{m}\sqrt{C_pT_i}}{d_2{}^2P_i}\right)_{design}\left(\frac{d_2N}{\sqrt{C_pT_i}}\right)_{design}\left(\frac{\sin\beta_2\cos\alpha_2}{\sin(\alpha_2+\beta_2)}\right)_{design} \quad \textbf{(3.41)}$$

$$(\phi_{fc})_{design} = \frac{c_{m1}}{u_2} = \left(\frac{d_1}{d_2}\right)_{design}(\tan\beta_1)_{design} \quad \textbf{(3.42)}$$

$$(\psi_{BL})_{design} = \frac{c_{w2}}{u_2} = \left(\frac{\sin\beta_2\cos\alpha_2}{\sin(\alpha_2+\beta_2)}\right)_{design} \quad \textbf{(3.43)}$$

3.2.4 Development of Rotor Aerodynamics Parameters

3.2.4.1 Absolute flow Mach number at rotor inlet (M_2)

The absolute Mach number at rotor inlet is given as:

$$M_2 = \frac{c_2}{a_2} \tag{3.44}$$

From inlet velocity triangle shown in **Fig. 3.7**, and using sine rule:

$$\frac{c_2}{\sin\beta_2} = \frac{u_2}{\sin(180-(\alpha_2+\beta_2))} = \frac{u_2}{\sin(\alpha_2+\beta_2)} \tag{3.45}$$

Substituting equation 3.45 for c_2 into equation 3.44 gives:

$$M_2 = \left(\frac{u_2}{a_2}\right)\left(\frac{\sin\beta_2}{\sin(\alpha_2+\beta_2)}\right) \tag{3.46}$$

The velocity of sound can be expressed as:

$$a_2 = a_i\left(\frac{t_2}{T_i}\right)^{\frac{1}{2}} \tag{3.47}$$

and $$\frac{t_2}{T_{02}} = 1 - \frac{{c_2}^2}{2C_pT_{02}}$$

For adiabatic flow, $T_{02} = T_i$, the above expression can be re-arranged as follows:

$$\frac{t_2}{T_i} = 1 - \frac{{c_2}^2}{2C_pT_i} \tag{3.48}$$

Combining equations 3.45 and 3.48 and substituting into equation 3.47 and re-arranging gives:

$$a_2 = a_i\left[1 - \frac{{u_2}^2}{2C_pT_i}\left(\frac{\sin\beta_2}{\sin(\alpha_2+\beta_2)}\right)^2\right]^{\frac{1}{2}} \tag{3.49}$$

By definition $$a_i = \sqrt{\gamma RT_i} \tag{3.50}$$

Substituting equation 3.50 into 3.49 gives:

$$a_2 = a_i\left[1-\frac{\gamma-1}{2}\left(\frac{u_2}{a_i}\right)^2\left(\frac{\sin\beta_2}{\sin(\alpha_2+\beta_2)}\right)^2\right]^{1/2} \tag{3.51}$$

Hence, by substituting equation 3.51 into 3.46, the following expression can be obtained:

$$M_2 = \frac{\left(\frac{u_2}{a_i}\right)\left(\frac{\sin\beta_2}{\sin(\alpha_2+\beta_2)}\right)}{\left[1-\frac{\gamma-1}{2}\left(\frac{u_2}{a_i}\right)^2\left(\frac{\sin\beta_2}{\sin(\alpha_2+\beta_2)}\right)^2\right]^{1/2}} \tag{3.52}$$

The expression u_2/a_i can be written as:

$$\frac{u_2}{a_i} = (u_2/c_s)(c_s/a_i) \tag{3.53}$$

Where c_s is the spouting (isentropic) velocity across the IFR turbine stage and can be expressed in the following form:

$$c_s = \left[2C_pT_i\left\{1-\left(\frac{P_e}{P_i}\right)^{\gamma-1/\gamma}\right\}\right]^{1/2}$$

Substitute the above expression in equation 3.53 to develop equation 3.54 as:

$$\frac{u_2}{a_i} = \frac{u_2}{c_s}\left[\frac{2}{\gamma-1}\left\{1-\left(\frac{P_e}{P_i}\right)^{\gamma-1/\gamma}\right\}\right]^{1/2} \tag{3.54}$$

Substituting equation 3.54 into 3.52 and re-arranging, an equation for Mach number M_2 at the rotor inlet can be obtained as:

$$M_2 = \frac{\frac{u_2}{c_s}\left[\frac{2}{\gamma-1}\left\{1-\left(\frac{P_e}{P_i}\right)^{\gamma-1/\gamma}\right\}\right]^{1/2}}{\left[\left(\frac{\sin(\alpha_2+\beta_2)}{\sin\beta_2}\right)^2-\left(\frac{u_2}{c_s}\right)^2\left\{1-\left(\frac{P_e}{P_i}\right)^{\gamma-1/\gamma}\right\}\right]^{1/2}} \tag{3.55}$$

3.2.4.2 Velocity ratio (u_2/c_s)

An expression for u_2/c_s can be obtained by re- arranging equation 3.55.

$$\frac{u_2}{c_s} = \frac{\left[\frac{\sin(\alpha_2+\beta_2)}{\sin\beta_2}\right]\left[\frac{(\gamma-1)M_2^{\,2}}{1+(\frac{\gamma-1}{2})M_2^{\,2}}\right]^{\frac{1}{2}}}{\sqrt{2}\left[1-\left(\frac{P_e}{P_i}\right)^{\frac{\gamma-1}{\gamma}}\right]^{\frac{1}{2}}} \qquad (3.56)$$

3.2.4.3 Relative Mach number at the exducer tip diameter (M_{er})

The velocity profile considered at the rotor outlet is of the free vortex type with constant axial component of the absolute velocity. This free vortex type of discharge will follow the well-known relationship, $c_w r = \text{constant}$.

The relative velocity at exducer tip diameter expression v_e can be written from the outlet velocity triangle diagram, displayed in **Fig. 3.9**

$$v_e^{\,2} = c_{me}^{\,2} + (u_e - c_{we})^2$$

$$v_e^{\,2} = c_{me}^{\,2} + u_2^{\,2}\left(\frac{u_e}{u_2} - \frac{c_{we}}{u_2}\right)^2 \qquad (3.57)$$

For simplicity, let $\frac{u_e}{u_2} = k_1$, $\frac{c_{we}}{u_2} = k_2$, and divide equation 3.57 by $\gamma R t_1$:

$$\frac{v_e^{\,2}}{\gamma R t_1} = \frac{c_{me}^{\,2}}{\gamma R t_1} + \frac{u_2^{\,2}}{\gamma R t_1}(k_1 - k_2)^2$$

As $c_{me} = c_{m1} = c_1 \sin\alpha_1$, and multiplying the second term of **RHS** of the expression above by $\frac{T_i}{T_e} = \frac{T_{03}}{T_{01}}$ and re-arranging, the above expression can be written as :

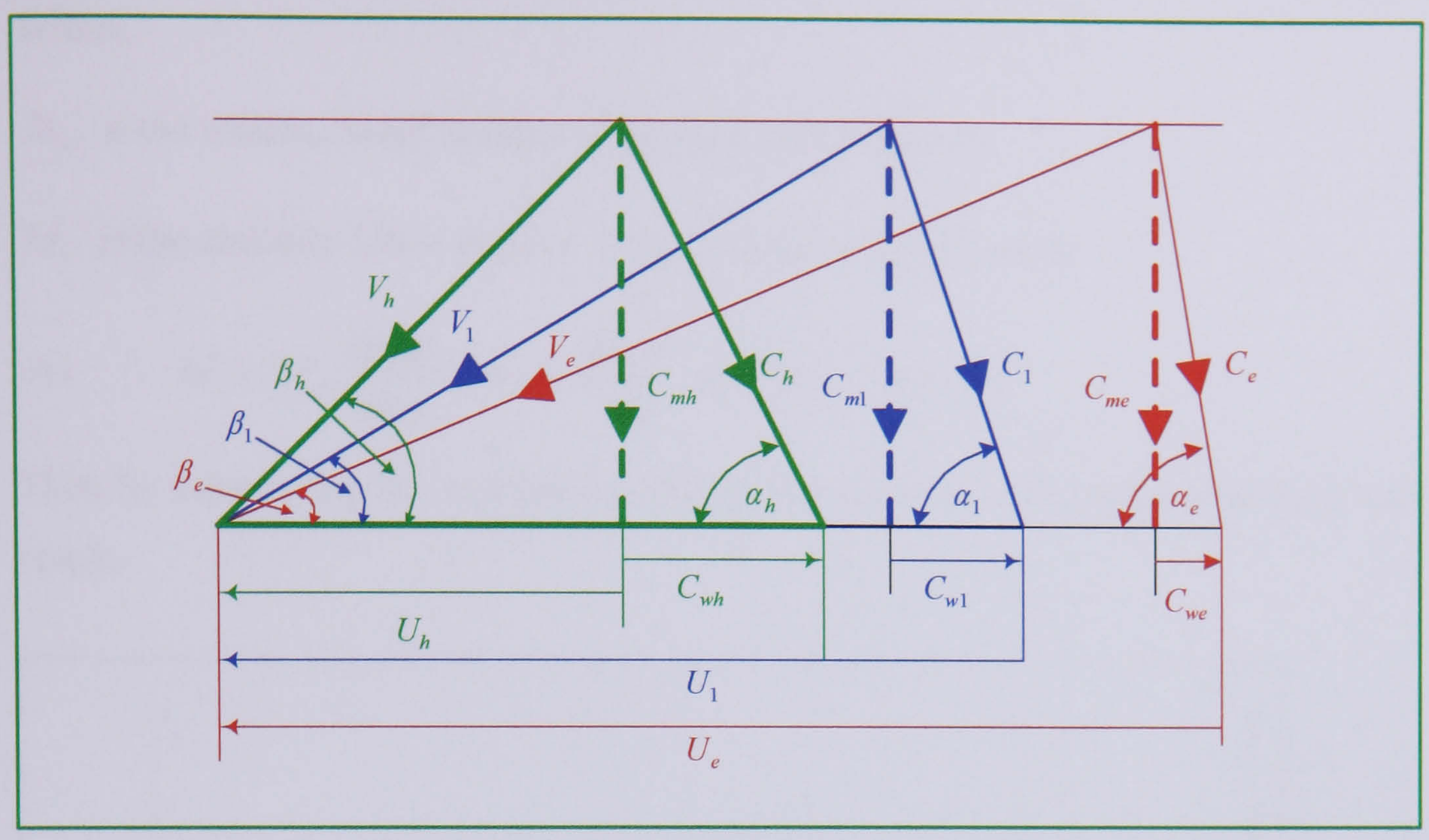

FIG. 3.9 VELOCITY TRIANGLES REPRESENTATION OF A FREE VORTEX FLOW AT THE EXDUCER OF AN IFR TURBINE ROTOR WITH CONSTANT AXIAL COMPONENT OF THE ABSOLUTE VELOCITY

$$M_{er}^{\ 2} = M_1^{\ 2}(\sin\alpha_1)^2 + \left(\frac{\left(\frac{u_2^{\ 2}T_i}{T_e}\right)}{\left(\frac{\gamma R t_1 T_i}{T_e}\right)}\right)(k_1 - k_2)^2 \qquad (3.58)$$

As $$M_1 = M_{er}\frac{\sin\beta_e}{\sin\alpha_1},$$

$$\frac{T_{01}}{T_{03}} = \frac{T_e}{T_i} = 1 - \eta_{t-t}\left(1 - \left(\frac{P_e}{P_i}\right)^{\gamma-1/\gamma}\right)$$

$$\frac{t_1}{T_{01}} = \frac{t_1}{T_e} = \frac{1}{1 + \frac{\gamma-1}{2}M_1^{\ 2}}$$

Substituting the expressions above into equation 3.58 results:

$$M_{er}^{\ 2} = \left(M_{er}\ \sin\beta_e\right)^2 + \left[\left(\frac{u_2^{\ 2}}{\gamma R T_i}\right)\left\{\frac{1 + \frac{\gamma-1}{2}M_1^{\ 2}}{1 - \eta_{tt}\left(1 - (\frac{P_e}{P_i})^{\gamma-1/\gamma}\right)}\right\}\right](k_1 - k_2)^2 \qquad (3.59)$$

Where,

M_{er} is the relative Mach number at exducer tip diameter.

M_1 is the absolute Mach number at rotor outlet mean diameter.

As $M_1 = M_{er}\dfrac{\sin\beta_e}{\sin\alpha_1}$, $u_2 = \dfrac{\pi d_2 N}{60}$ and $\gamma R = C_p(\gamma - 1)$

Then by substituting the expressions above into equation 3.59 and re-arranging would result:

$$M_{er}^{\,2} = \left[\frac{\left(\frac{\pi}{60}\right)^2\left(\frac{d_2 N}{\sqrt{C_p T_i}}\right)^2\left(\frac{u_e}{u_2}\right)-\left(\frac{c_{we}}{u_2}\right)^2}{(\gamma-1)\left\{1-\eta_{tt}\left(1-\left(\frac{P_e}{P_i}\right)^{\gamma-1/\gamma}\right)\right\}\left\{1-\sin^2\beta_e\left(1+\frac{\left(\left(\frac{\pi}{60}\right)\left(\frac{d_2 N}{\sqrt{C_p T_i}}\right)\right)^2\left(\left(\frac{u_e}{u_2}\right)-\left(\frac{c_{we}}{u_2}\right)\right)^2}{2\left(1-\eta_{tt}\left(1-\left(\frac{P_e}{P_i}\right)^{\gamma-1}{}_{\gamma}\right)\right)\left(\sin^2\alpha_1\right)}\right)_e\right\}}\right] \quad \textbf{(3.60a)}$$

Substituting for $\dfrac{u_e}{u_2} = \dfrac{d_e}{d_2}$ and $c_{we} = 0$ (assuming zero swirl at rotor exit), then equation 3.60a is transformed to the form as displayed below:

$$M_{er} = \left[\frac{\left(\frac{\pi}{60}\right)^2\left(\frac{d_2 N}{\sqrt{C_p T_i}}\right)^2\left(\frac{d_e}{d_2}\right)^2}{(\gamma-1)\left\{1-\eta_{tt}\left(1-\left(\frac{P_e}{P_i}\right)^{\gamma-1}{}_{\gamma}\right)\right\}\left\{1-\sin^2\beta_e\left(1+\frac{\left(\left(\frac{\pi}{60}\right)\left(\frac{d_2 N}{\sqrt{C_p T_i}}\right)\right)^2\left(\left(\frac{d_e}{d_2}\right)^2\right)}{2\left(1-\eta_{tt}\left(1-\left(\frac{P_e}{P_i}\right)^{\gamma-1}{}_{\gamma}\right)\right)}\right)\right\}}\right]^{1}{}_{2} \quad \textbf{(3.60b)}$$

3.2.4.4 Absolute inlet flow angle (α_2) and relative flow angle (β_2)

An expression for α_2 can be developed in terms of speed parameter $d_2N/\sqrt{C_pT_i}$. inlet Mach number M_2 and blade-loading factor $(\psi_2)_{BL}$ as follows:

By definition, $$M_2{}^2 = \frac{c_2{}^2}{\gamma R t_2} = \left(\frac{c_2{}^2}{\gamma R T_{02}}\right)\left(\frac{T_{02}}{t_2}\right)$$

$$M_2{}^2 = \left(\frac{c_2{}^2}{(\gamma-1)C_pT_{02}}\right)\left(1+\frac{\gamma-1}{2}M_2{}^2\right) \tag{3.61}$$

Re-arranging equation 3.61 for $c_2/\sqrt{C_pT_{02}}$ would result to

$$\frac{c_2}{\sqrt{C_pT_{02}}} = \left(\frac{\sqrt{\gamma-1)M_2{}^2}}{\sqrt{1+\frac{\gamma-1}{2}M_2{}^2}}\right) \tag{3.62}$$

From inlet velocity triangle, **Fig. 3.7**

$$\cos\alpha_2 = \frac{c_{w2}}{c_2} = \left(\frac{c_{w2}}{u_2}\right)\left(\frac{u_2}{c_2}\right) \tag{3.63a}$$

Substituting for c_2 from equation 3.62 and for $u_2 = \pi d_2N/60$ into equation 3.63a and re-arranging would give:

$$\boxed{\alpha_2 = \cos^{-1}\left[\left(\frac{c_{w2}}{u_2}\right)\left(\frac{\pi}{60}\right)\left(\frac{d_2N}{\sqrt{C_pT_i}}\right)\left(\frac{\sqrt{\frac{1}{\gamma-1}+\frac{1}{2}M_2{}^2}}{M_2}\right)\right]} \tag{3.63b}$$

Similarly an expression for β_2 can be obtained as:

$$\boxed{\beta_2 = \tan^{-1}\left[\left(\frac{1}{1-(\psi_2)_{BL}}\right)\left(\frac{1}{\frac{\pi}{60}\left(\frac{d_2N}{\sqrt{C_pT_i}}\right)}\right)\left(\frac{M_2}{\sqrt{\frac{1}{\gamma-1}+\frac{1}{2}M_2{}^2}}\right)(\sin\alpha_2)\right]} \tag{3.64}$$

3.2.4.5 Relative flow velocity ratio (v_2/v_1)

An expression for v_2/v_1 in terms of inlet blade loading factor $(\psi_2)_{BL}$, pressure ratio P_i/P_e, speed parameter $d_2N/\sqrt{C_pT_i}$, and relative inlet and outlet flow angles β_2, β_1 is developed as follows:

Consider the inlet velocity triangle **Fig. 3.7** and using the sine rule, it can be written:

$$\frac{v_2}{\sin\alpha_2} = \frac{u_2}{\sin(\alpha_2+\beta_2)} \tag{3.65}$$

$$\frac{v_2}{u_2} = \frac{\sin\alpha_2}{\sin(\alpha_2+\beta_2)} \tag{3.66}$$

Multiply **LHS** of equation 3.66 by v_1/v_1 and divide both sides by $1/\sqrt{C_pT_{01}}$ and by putting $u_2 = \pi d_2 N/60$, then equation 3.66 becomes:

$$\frac{v_1}{\sqrt{C_pT_{01}}}\cdot\frac{v_2}{v_1} = \left(\frac{\pi}{60}\right)\left(\frac{d_2N}{\sqrt{C_pT_{01}}}\right)\left(\frac{\sin\alpha_2}{\sin(\alpha_2+\beta_2)}\right) \tag{3.67}$$

Multiply and divide **RHS** of equation 3.67 by $c_1/\sqrt{\gamma Rt_1}$ and re-arranging resulted into:

$$\frac{v_2}{v_1} = \left(\frac{\pi}{60}\right)\left(\frac{d_2N}{\sqrt{C_pT_{01}}}\right)\left(\frac{c_1}{v_1}\right)\left(\frac{\sqrt{\gamma Rt_1}}{c_1}\right)\left(\sqrt{\frac{C_pT_{01}}{\gamma Rt_1}}\right)\left(\frac{\sin\alpha_2}{\sin(\alpha_2+\beta_2)}\right) \tag{3.68}$$

But $\dfrac{c_1}{v_1} = \dfrac{\sin\beta_1}{\sin\alpha_1}$, $M_1 = \dfrac{c_1}{\sqrt{\gamma Rt_1}}$

and $\sqrt{\dfrac{C_pT_{01}}{\gamma Rt_1}} = \sqrt{\dfrac{1+\dfrac{\gamma-1}{2}M_1^{\,2}}{\gamma-1}} = \sqrt{\dfrac{1}{\gamma-1}+\dfrac{M_1^{\,2}}{2}}$

Substituting the above three expressions into equation 3.68 would give:

$$\frac{v_2}{v_1} = \left(\frac{\pi}{60}\right)\left(\frac{d_2N}{\sqrt{C_pT_{01}}}\right)\left(\frac{\sin\beta_1}{\sin\alpha_1}\right)\left(\frac{\sqrt{\dfrac{1}{\gamma-1}+\dfrac{M_1^{\,2}}{2}}}{M_1}\right)\left(\frac{\sin\alpha_2}{\sin(\alpha_2+\beta_2)}\right) \tag{3.69}$$

Multiply and divide **LHS** of equation 3.66 by $(u_2 - c_{w2})$ resulted into:

$$\frac{v_2}{u_2} = \left(\frac{v_2}{u_2}\right)\left(\frac{u_2 - c_{w2}}{u_2 - c_{w2}}\right) = \left(\frac{v_2}{u_2}\right)\left(\frac{u_2(1 - \frac{c_{w2}}{u_2})}{v_{w2}}\right) = \left(\frac{1 - (c_{w2}\ u_2}{\cos\beta_2}\right) = \frac{\sin\alpha_2}{\sin(\alpha_2 + \beta_2)} \qquad (3.70)$$

Since $$\frac{d_2 N}{\sqrt{C_p T_{01}}} = \left(\frac{d_2 N}{\sqrt{C_p T_{03}}}\right)\left(\sqrt{\frac{T_{03}}{T_{01}}}\right)$$

and $$M_1 = M_{er}\left(\frac{\sin\beta_e}{\sin\alpha_1}\right)$$

Then by substituting for $\frac{\sin\alpha_2}{\sin(\alpha_2 + \beta_2)}$, $\frac{d_2 N}{\sqrt{C_p T_{01}}}$ and M_1 into equation 3.69 would give:

$$\frac{v_2}{v_1} = \left(\frac{\pi(1 - (c_{w2}/u_2)}{60}\right)\left(\frac{d_2 N}{\sqrt{C_p T_{03}}}\right)\left(\frac{\sin\beta_1}{(\cos\beta_2)(\sin\alpha_1)}\right)\left(\sqrt{\frac{T_{03}}{T_{01}}}\right)\left(\frac{\sqrt{\frac{1}{\gamma - 1} + \frac{M_{er}{}^2 \sin^2\beta_e}{2\sin^2\alpha_1}}}{M_{er}(\frac{\sin\beta_e}{\sin\alpha_1})}\right) \qquad (3.71)$$

For zero swirl at the outlet, i.e. $\alpha_1 = 90^\circ$, equation 3.71 in the general form becomes:

$$\boxed{\frac{v_2}{v_1} = \left(\frac{\pi(1 - (c_{w2}\ u_2)}{60}\right)\left(\frac{d_2 N}{\sqrt{C_p T_i}}\right)\left(\frac{\sin\beta_1}{\cos\beta_2}\right)\left(\sqrt{\frac{T_i}{T_e}}\right)\left(\frac{\sqrt{\frac{1}{\gamma - 1} + \frac{M_{er}{}^2 \sin^2\beta_e}{2}}}{M_{er}\sin\beta_e}\right)} \qquad (3.72)$$

3.2.5 Development of Mass Flow Parameter $\left(\frac{\dot{m}\sqrt{C_p T_i}}{d_2{}^2 P_i}\right)$

Two models for the mass flow parameter were developed. These are termed as model (1) and model (2).

3.2.5.1 Mass flow parameter in terms of rotor outlet design variables, model (1)

Using the continuity equation at rotor outlet for mass flow rate gives:

$$\dot{m} = \rho_1 A_1 c_1 \sin\alpha_1$$

Assuming zero- swirl at rotor outlet, i.e. $\alpha_1 = 90^\circ$

$$\dot{m} = \left(\frac{\rho_1}{\rho_{01}}\rho_{01}\right) A_1 c_1 \tag{3.73}$$

But $$\frac{\rho_1}{\rho_{01}} = \left(\frac{t_1}{T_{01}}\right)^{\frac{1}{\gamma-1}} \text{ and } \rho_{01} = \frac{P_{01}}{RT_{01}}$$

Substituting the two expressions above and introducing blockage factor β_{f_1} at rotor exit in equation 3.73 would result into

$$\frac{\dot{m}\sqrt{C_p T_{01}}}{d_2^{\,2} P_{01}} = \left(\frac{t_1}{T_{01}}\right)^{\frac{1}{\gamma-1}} \left(\frac{C_p}{R}\right) \left(\frac{c_1}{\sqrt{C_p T_{01}}}\right) \left(\pi B_{f_1} \left(\frac{d_e^{\,2}}{d_2^{\,2}} - \frac{d_h^{\,2}}{d_2^{\,2}}\right)\right) \tag{3.74}$$

But $$\frac{\dot{m}\sqrt{C_p T_{01}}}{d_2^{\,2} P_{01}} = \left(\frac{\dot{m}\sqrt{C_p T_{02}}}{d_2^{\,2} P_{02}}\right) \left(\frac{P_{02}}{P_{01}}\right) \left(\frac{T_{01}}{T_{02}}\right)^{\frac{1}{2}} \tag{3.75}$$

Substituting equation 3.75 into equation 3.74 and re-arranging would develop into:

$$\frac{\dot{m}\sqrt{C_p T_{02}}}{d_2^{\,2} P_{02}} = \left(\frac{P_{01}}{P_{02}}\right) \left(\frac{T_{02}}{T_{01}}\right)^{\frac{1}{2}} \left(\frac{t_1}{T_{01}}\right)^{\frac{1}{\gamma-1}} \left(\frac{C_p}{R}\right) \left(\frac{c_1}{\sqrt{C_p T_{01}}}\right) \left[\pi B_{f_1} \left(\left(\frac{d_e}{d_2}\right)^2 - \left(\frac{d_h}{d_2}\right)^2\right)\right] \tag{3.76}$$

But $$\frac{C_p}{R} = \frac{\gamma}{\gamma-1}, \quad \left(\frac{t_1}{T_{01}}\right)^{\frac{1}{\gamma-1}} = \left(1 - \frac{c_1^{\,2}}{2C_p T_{01}}\right)^{\frac{1}{\gamma-1}} \text{ and } \frac{T_{02}}{T_{01}} = \left[\frac{1}{1 - \eta_{tt}\left(1 - \frac{P_{01}}{P_{02}}\right)^{\frac{\gamma-1}{\gamma}}}\right]$$

UNIVERSITY OF HERTFORDSHIRE LRC

Then by substituting for C_p/R, T_{02}/T_{01} and $(t_1/T_{01})^{1/(\gamma-1)}$ expressions into equation 3.76 yield to:

$$\frac{\dot{m}\sqrt{C_pT_{02}}}{{d_2}^2P_{02}}=\left(\frac{\gamma}{\gamma-1}\right)\left(\frac{P_{01}}{P_{02}}\right)\left(1-\frac{{c_1}^2}{2C_pT_{01}}\right)^{1/(\gamma-1)}\left(\frac{c_1}{\sqrt{C_pT_{01}}}\right)\left[\pi B_{f_1}\left((\frac{d_e}{d_2})-(\frac{d_h}{d_2})^2\right)\right]$$
$$\times\left[1-\eta_{tt}\left(1-(\frac{P_{01}}{P_{02}})^{(\gamma-1)/\gamma}\right)\right]^{-1/2} \qquad (3.77)$$

As $$\frac{c_1}{\sqrt{C_pT_{01}}}=\frac{c_1}{\sqrt{C_pT_{01}(\frac{t_1}{t_1})}}=\frac{c_1}{\sqrt{\frac{\gamma Rt_1}{\gamma-1}(1+\frac{{c_1}^2}{2C_pt_1})}}=\frac{c_1}{\sqrt{\frac{\gamma Rt_1}{\gamma-1}(1+(\frac{\gamma-1}{2})(\frac{{c_1}^2}{\gamma Rt_1})}}$$

In terms of Mach number M_1, the above expression can be developed into

$$\frac{c_1}{\sqrt{C_pT_{01}}}=\left(\frac{\sqrt{\gamma-1}M_1}{\sqrt{1+\frac{\gamma-1}{2}{M_1}^2}}\right)$$

Substituting for $c_1/\sqrt{C_pT_{01}}$ above into equation 3.77 and re-arranging would result into:

$$\frac{\dot{m}\sqrt{C_pT_{02}}}{{d_2}^2P_{02}}=\left(\frac{\gamma}{\sqrt{\gamma-1}}\right)\left(\frac{P_{01}}{P_{02}}\right)\left[B_{f_1}\left(\frac{\pi}{4}\right)\left((\frac{d_e}{d_2})^2-(\frac{d_h}{d_2})^2\right)\right]\left[\frac{M_1}{\left(1+\frac{\gamma-1}{2}{M_1}^2\right)^{(\gamma+1)/2(\gamma-1)}}\right]$$
$$\times\left[\frac{1}{1-\eta_{tt}\left(1-(\frac{P_{01}}{P_{02}})^{(\gamma-1)/\gamma}\right)}\right]^{1/2} \qquad (3.78)$$

But $P_{02}=\phi_{pl}P_{03}=\phi_{pl}P_i$ where ϕ_{pl} is the pressure loss across the stator

Hence, mass flow parameter above can be expressed in terms of stagnation pressure ratio across the turbine stage and rotor exit conditions as:

$$\frac{\dot{m}\sqrt{C_p T_i}}{{d_2}^2 P_i} = \left(\frac{\gamma}{\sqrt{\gamma-1}}\right)\left(\frac{P_e}{P_i}\right)\left[B_{f_1}\left(\frac{\pi}{4}\right)\left(\left(\frac{d_e}{d_2}\right)^2 - \left(\frac{d_h}{d_2}\right)^2\right)\right]\left[\frac{M_{er}\sin\beta_e}{\left(1+\frac{\gamma-1}{2}(M_{er}\sin\beta_e)^2\right)^{\gamma+1/2(\gamma-1)}}\right] \times \left[\frac{1}{1-\eta_{tt}\left(1-\left(\frac{P_e}{\phi_{pl}P_i}\right)^{\gamma-1/\gamma}\right)}\right]^{1/2} \quad \textbf{(3.79a)}$$

Where $\beta_{f_1} = 1 - \frac{2}{\pi}\left[\frac{(t_2/d_2)}{(d_e/d_2)+(d_h/d_2)}\right]$

3.2.5.2 Mass flow parameter in terms of rotor inlet design variables, model (2)

Similarly, an expression for the mass flow parameter in terms of rotor inlet design variables can be developed as:

$$\frac{\dot{m}\sqrt{C_p T_i}}{{d_2}^2 P_i} = \left(\frac{\phi_{pl}\gamma}{\sqrt{\gamma-1}}\right)\left(\pi B_{f_2}\frac{b_2}{d_2}\right)\left[\frac{M_2}{\left(1+\frac{\gamma-1}{2}{M_2}^2\right)^{\gamma+1/2(\gamma-1)}}\right](\sin\alpha_2) \quad \textbf{(3.79b)}$$

3.2.6 Development of Blade Tip Width to Tip Diameter Ratio Parameter (b_2/d_2)

At inlet to turbine rotor, using the continuity equation and velocity triangle at inlet, the mass flow rate is given by:

$$\dot{m} = \rho_2 A_2 c_{m2} = (\frac{p_2}{Rt_2})(\pi d_2 b_2)(c_2 \sin\alpha_2) \tag{3.80}$$

As $$p_2 = P_{02}\left(\frac{t_2}{T_{02}}\right)^{\gamma/\gamma-1}$$

$$t_2 = T_{02}(1 - \frac{{c_2}^2}{2C_p T_{02}})$$

$$c_2 = u_2 \frac{\sin\beta_2}{\sin(\alpha_2 + \beta_2)}$$

Substituting for p_2, t_2 and c_2 expressions in equation 3.80, and rearranging would give:

$$\dot{m} = \frac{P_{02}}{RT_{02}}\left(1 - \frac{{c_2}^2}{2C_p T_{02}}\right)^{1/\gamma-1}\left(\pi {d_2}^2 \frac{b_2}{d_2}\right)\left(u_2 \frac{\sin\alpha_2 \sin\beta_2}{\sin(\alpha_2 + \beta_2)}\right) \tag{3.81}$$

Introducing rotor inlet blockage factor B_{f_2}, pressure loss coefficient ϕ_{pl} at rotor inlet would imply the following:

$$P_{02} = \phi_{pl}(P_{03}) = \phi_{pl}(P_i),\ T_{02} = T_{03} = T_i,\ R = C_p \frac{\gamma - 1}{\gamma}$$

Substituting for P_{02}, T_{02}, and R in equation 3.81 would give:

$$\dot{m} = \frac{\phi_{pl}(P_i)}{C_p \frac{\gamma - 1}{\gamma} T_i}\left(1 - \frac{{c_2}^2}{2C_p T_i}\right)^{1/\gamma-1}\left(B_{f_2}\pi {d_2}^2 \frac{b_2}{d_2}\right)\left(u_2 \frac{\sin\alpha_2 \sin\beta_2}{\sin(\alpha_2 + \beta_2)}\right) \tag{3.82}$$

Finally, substituting for u_2, c_2 in equation 3.82 and re-arranging, an expression for b_2/d_2 is obtained as:

$$\frac{b_2}{d_2} = \frac{\left(\frac{\gamma - 1/\gamma}{\pi^2 \phi_{pl} B_{f_2}}\right)\left(\frac{\dot{m}\sqrt{C_p T_i}}{{d_2}^2 P_i}\right)\left(\frac{\sin(\alpha_2 + \beta_2)}{\sin\alpha_2 \sin\beta_2}\right)}{\left(\frac{d_2 N}{\sqrt{C_p T_i}}\right)\left[1 - \frac{\pi^2}{2}\left(\left(\frac{d_2 N}{\sqrt{C_p T_i}}\right)\left(\frac{\sin\beta_2}{\sin(\alpha_2 + \beta_2)}\right)\right)^2\right]^{1/\gamma - 1}} \quad \textbf{(3.83)}$$

3.2.7 Blade Tip Velocity at Rotor Inlet (u_2)

From $$c_s = \sqrt{2C_p T_i\left[1 - \left(\frac{P_e}{P_i}\right)^{\gamma - 1/\gamma}\right]} \quad (3.84)$$

and $$u_2 = \left(\frac{u_2}{c_s}\right)(c_s) \quad (3.85)$$

Substituting equation 3.85 into equation 3.84, would give:

$$u_2 = \left(\frac{u_2}{c_s}\right)\left\{\sqrt{2C_p T_i\left[1 - \left(\frac{P_e}{P_i}\right)^{\gamma - 1/\gamma}\right]}\right\} \quad \textbf{(3.86)}$$

3.2.8 Development of a Specific Speed (Ω_s) Model for IFR Turbine

The concept of specific speed has been used in the literature to classify turbomachinery types. Specific speed is a similarity parameter and it is sometimes referred to as a shape factor and is given by the following equation:

$$N_s = \frac{N(\dot{Q}_e)^{1/2}}{(\Delta H_{i-e})_s} = \frac{N(\dot{Q}_1)^{1/2}}{(\Delta H_{3-1})_s^{3/4}} \quad (3.87)$$

This equation can be developed and expressed in terms of the design variables of the turbine as follows:

$$\dot{Q}_1 = \frac{\dot{m}Rt_1}{p_1} \tag{3.88}$$

Equation 3.88 can be modified to include other dimensionless parameters, as follows:

$$\dot{Q}_1 = \frac{\dot{m}Rt_1}{p_1} = \left(\frac{\dot{m}Rt_1}{p_1}\right)\left(\frac{d_2^{\,2}}{d_2^{\,2}}\right)\left(\frac{T_{01}}{T_{01}}\right)\left(\frac{P_{01}}{P_{01}}\right)\left(\frac{C_p}{C_p}\right)$$

$$= \left(\frac{\dot{m}C_pT_{01}}{d_2^{\,2}P_{01}}\right)\left(\frac{R}{C_p}\right)\left(\frac{t_1}{T_{01}}\right)\left(\frac{P_{01}}{p_1}\right)\left(d_2^{\,2}\right) \tag{3.89}$$

Substituting for $\frac{R}{C_p} = \frac{\gamma - 1}{\gamma}$ and $\left(\frac{t_1}{T_{01}}\right)\left(\frac{P_{01}}{p_1}\right) = \left[1 + \frac{\gamma - 1}{2}M_1^{\,2}\right]^{\frac{1}{\gamma - 1}}$ into equation 3.89 gives:

$$\dot{Q}_1 = \left(\frac{\dot{m}C_pT_{01}}{d_2^{\,2}P_{01}}\right)\left(\frac{\gamma - 1}{\gamma}\right)\left(1 + \frac{\gamma - 1}{2}M_1^{\,2}\right)^{\frac{1}{\gamma - 1}}\left(d_2^{\,2}\right) \tag{3.90}$$

Equation 3.90 can be further modified to give:

$$\dot{Q}_1 = \left(\frac{\dot{m}\sqrt{C_pT_{03}}}{d_2^{\,2}P_{03}}\right)\left(\sqrt{\frac{T_{01}}{T_{03}}}\right)\left(\frac{P_{03}}{P_{01}}\right)\left(\frac{\gamma - 1}{\gamma}\right)\left(1 + \frac{\gamma - 1}{2}M_1^{\,2}\right)^{\frac{1}{\gamma - 1}}\left(\sqrt{C_pT_{01}}\right)\left(d_2^{\,2}\right) \tag{3.91}$$

But $$\Delta(H_{3-1})_s = C_pT_{03}\left[1 - \left(\frac{P_{01}}{P_{03}}\right)^{\frac{\gamma - 1}{\gamma}}\right] \tag{3.92}$$

Substituting equations 3.91 and 3.92 into equation 3.87 would give:

$$\frac{N(\dot{Q}_1)^{1/2}}{\Delta(H_{3-1})_s^{3/4}} = \frac{\left[\left(\frac{\gamma-1}{\gamma}\right)\left(\frac{P_{03}}{P_{01}}\right)\left(\frac{\dot{m}\sqrt{C_pT_{03}}}{d_2{}^2P_{03}}\right)\left(1+\frac{\gamma-1}{2}M_1{}^2\right)^{1/\gamma-1}\right]^{1/2}\left(\frac{T_{01}}{T_{03}}\right)^{1/4}(C_pT_{01})^{1/4}(d_2N)}{\left[C_pT_{03}\left\{1-\left(\frac{P_{01}}{P_{03}}\right)^{\gamma-1/\gamma}\right\}\right]^{3/4}} \quad (3.93a)$$

Equation 3.93a can be further modified to give

$$\frac{N(\dot{Q}_1)^{1/2}}{\Delta(H_{3-1})_s^{3/4}} = \frac{\left[\left(\frac{\gamma-1}{\gamma}\right)\left(\frac{P_{03}}{P_{01}}\right)\left(\frac{\dot{m}\sqrt{C_pT_{03}}}{d_2{}^2P_{03}}\right)\left(1+\frac{\gamma-1}{2}M_1{}^2\right)^{1/\gamma-1}\right]^{1/2}\left(\frac{T_{01}}{T_{03}}\right)^{1/4}\left(\frac{d_2N}{\sqrt{C_pT_{03}}}\right)}{\left[\left\{1-\left(\frac{P_{01}}{P_{03}}\right)^{\gamma-1/\gamma}\right\}\right]^{3/4}} \quad (3.93b)$$

Substituting for $\frac{T_{01}}{T_{03}} = 1-\eta_{tt}\left[1-\left(\frac{P_{01}}{P_{03}}\right)^{\gamma-1/\gamma}\right]$ into equation 3.93b, resulted into

$$N_s = \frac{N(\dot{Q}_1)^{1/2}}{\Delta(H_{3-1})_s^{3/4}} = \frac{\left[\left(\frac{\gamma-1}{\gamma}\right)\left(\frac{P_{03}}{P_{01}}\right)\left(\frac{\dot{m}\sqrt{C_pT_{03}}}{d_2{}^2P_{03}}\right)\left(1+\frac{\gamma-1}{2}M_1{}^2\right)^{1/\gamma-1}\right]^{1/2}\left[1-\eta_{tt}\left\{1-\left(\frac{P_{01}}{P_{03}}\right)^{\gamma-1/\gamma}\right\}\right]^{1/2}\left(\frac{d_2N}{\sqrt{C_pT_{03}}}\right)}{\left[\left\{1-\left(\frac{P_{01}}{P_{03}}\right)^{\gamma-1/\gamma}\right\}\right]^{3/4}} \quad \mathbf{(3.94)}$$

The N_s term above is given in *rps* and can be expressed in rad/s by substituting $\Omega_s = 2\pi N_s$, hence equation 3.94 in the general form notation becomes:

$$\Omega_s = (2\pi)\frac{\left[\left(\frac{\gamma-1}{\gamma}\right)\left(\frac{P_i}{P_e}\right)\left(\frac{\dot{m}\sqrt{C_pT_i}}{d_2{}^2P_i}\right)\left(1+\frac{\gamma-1}{2}M_1{}^2\right)^{1/\gamma-1}\right]^{1/2}\left[1-\eta_{tt}\left\{1-\left(\frac{P_e}{P_i}\right)^{\gamma-1/\gamma}\right\}\right]^{1/2}\left(\frac{d_2N}{\sqrt{C_pT_i}}\right)}{\left[\left\{1-\left(\frac{P_e}{P_i}\right)^{\gamma-1/\gamma}\right\}\right]^{3/4}}$$

(3.95)

Specific speed Ω_s is referred to as a shape factor; therefore it would be appropriate to express equation 3.95 in terms of the geometric dimensions of the rotor. This can be done by substituting equations $M_1 = M_{er}\sin\beta_e$ and 3.79a into equation 3.95 and re-arranging would develop into:

$$\Omega_s = 2\pi\frac{\left[\left(\sqrt{\gamma-1}\right)\left(\frac{\pi B_{f_1}}{4}\right)\left\{\left(\frac{d_e}{d_2}\right)^2-\left(\frac{d_h}{d_2}\right)^2\right\}\left\{\frac{M_{er}\sin\beta_e}{\left[1+\frac{\gamma-1}{2}(M_{er}\sin\beta_e)^2\right]^{1/2}}\right\}\right]^{1/2}\left[1-\eta_{tt}\left(\frac{P_e}{P_i}\right)^{\gamma-1/\gamma}\right]^{1/4}\left(\frac{d_2N}{\sqrt{C_pT_i}}\right)}{\left[1-\left(\frac{P_e}{P_i}\right)^{\gamma-1/\gamma}\right]^{3/4}}$$

(3.96)

3.2.9 Development of a Specific Diameter (D_s) Model of IFR Turbine

By definition, specific diameter in non-dimensional form is given as

$$D_s = \frac{d_2(\Delta H_{3-1})_s{}^{1/4}}{(\dot{Q}_1)^{1/2}} \tag{3.97}$$

Substituting equations 3.91 and 3.92 into equation 3.97 would give

$$D_s = \frac{d_2(\Delta H_{3-1})_s^{1/4}}{(\dot{Q}_1)^{1/2}} = \frac{\left[C_p T_{03}\left\{1-\left(\frac{P_{01}}{P_{03}}\right)^{\gamma-1/\gamma}\right\}\right]^{1/4}}{\left[\left(\frac{\gamma-1}{\gamma}\right)\left(\frac{P_{03}}{P_{01}}\right)\left(\frac{\dot{m}\sqrt{C_p T_{03}}}{d_2{}^2 P_{03}}\right)\left(1+\frac{\gamma-1}{2}M_1{}^2\right)^{1/\gamma-1}\right]^{1/2}\left(\frac{T_{01}}{T_{03}}\right)^{1/4}(C_p T_{03})^{1/4}} \quad (3.98a)$$

Equation 3.98a can be further modified to give

$$D_s = \frac{d_2(\Delta H_{3-1})^{1/4}}{(\dot{Q}_1)^{1/2}} = \frac{\left[\left\{1-\left(\frac{P_{01}}{P_{03}}\right)^{\gamma-1/\gamma}\right\}\right]^{1/4}}{\left[\left(\frac{\gamma-1}{\gamma}\right)\left(\frac{P_{03}}{P_{01}}\right)\left(\frac{\dot{m}\sqrt{C_p T_{03}}}{d_2{}^2 P_{03}}\right)\left(1+\frac{\gamma-1}{2}M_1{}^2\right)^{1/\gamma-1}\right]^{1/2}\left[1-\eta_{tt}\left\{1-\left(\frac{P_{01}}{P_{03}}\right)^{\gamma-1/\gamma}\right\}\right]^{1/4}} \quad (3.98b)$$

Equation 3.98b for the specific diameter can be expressed in terms of the geometric dimensions of the rotor in the general form as:

$$D_s = \frac{\left[\left\{1-\left(\frac{P_e}{P_i}\right)^{\gamma-1/\gamma}\right\}\right]^{1/4}}{\left[\left(\sqrt{\gamma-1}\right)\left(\frac{\pi B_{f_1}}{4}\right)\left\{\left(\frac{d_e}{d_2}\right)^2-\left(\frac{d_h}{d_2}\right)^2\right\}\left\{\frac{M_{er}\sin\beta_e}{\left(1+\frac{\gamma-1}{2}(M_{er}\sin\beta_e)^2\right)^{1/2}}\right\}\right]^{1/2}} \quad (3.99)$$

Balje [10] reported that the predicted region of achievable best efficiency for specific diameters would be in the range 3.0 to 5.0.

3.3 DESIGN MODELLING OF NOZZLE-LESS VOLUTE CASING

The theory and modelling of a nozzle-less volute casing is based on the assumptions of steady, step by step one-dimensional and adiabatic flow conditions in which the mass is changing as linear function of the azimuth angle while the energy and momentum are conserved. The complete design modelling of the main parameters of the casing is described hereafter.

3.3.1 Principal design variables of nozzle-less volute casing

3.3.1.1 Volute parameters

i. The cross-sectional area A_φ of the volute and the variation of this area as a function of the azimuth angle φ.

ii. The radial distance of the centriod $\bar{r}_\varphi$ of the cross-sectional area from the axis of rotation.

iii. The shape of the volute cross-section.

3.3.1.2 Rotor parameters

i. Rotor tip diameter d_2 and blade tip width b_2.

ii. Effective peripheral flow area A_2 or the number of blades and blade thickness at d_2.

3.3.1.3 Operating conditions

i. Rotational speed, N

ii. Mass flow rate, $\dot{m}$

iii. Stagnation temperature, T_i and stagnation pressure P_i of the working gas at the entry flange of the turbine.

3.3.2 Development of Main Design Parameters

For any angular station of the nozzle-less volute at azimuth angle φ, the cross-sectional area is A_φ and the distance of its centriod from the axis of rotation is r_φ as shown in **Fig. 3.10**.

The tangential mass flow through any cross-section plane at azimuth angle φ is:

$$\dot{m}_{w\varphi} = \rho_\varphi A_\varphi c_{w\varphi} = \dot{m}\left(\frac{\varphi}{360}\right) \tag{3.100}$$

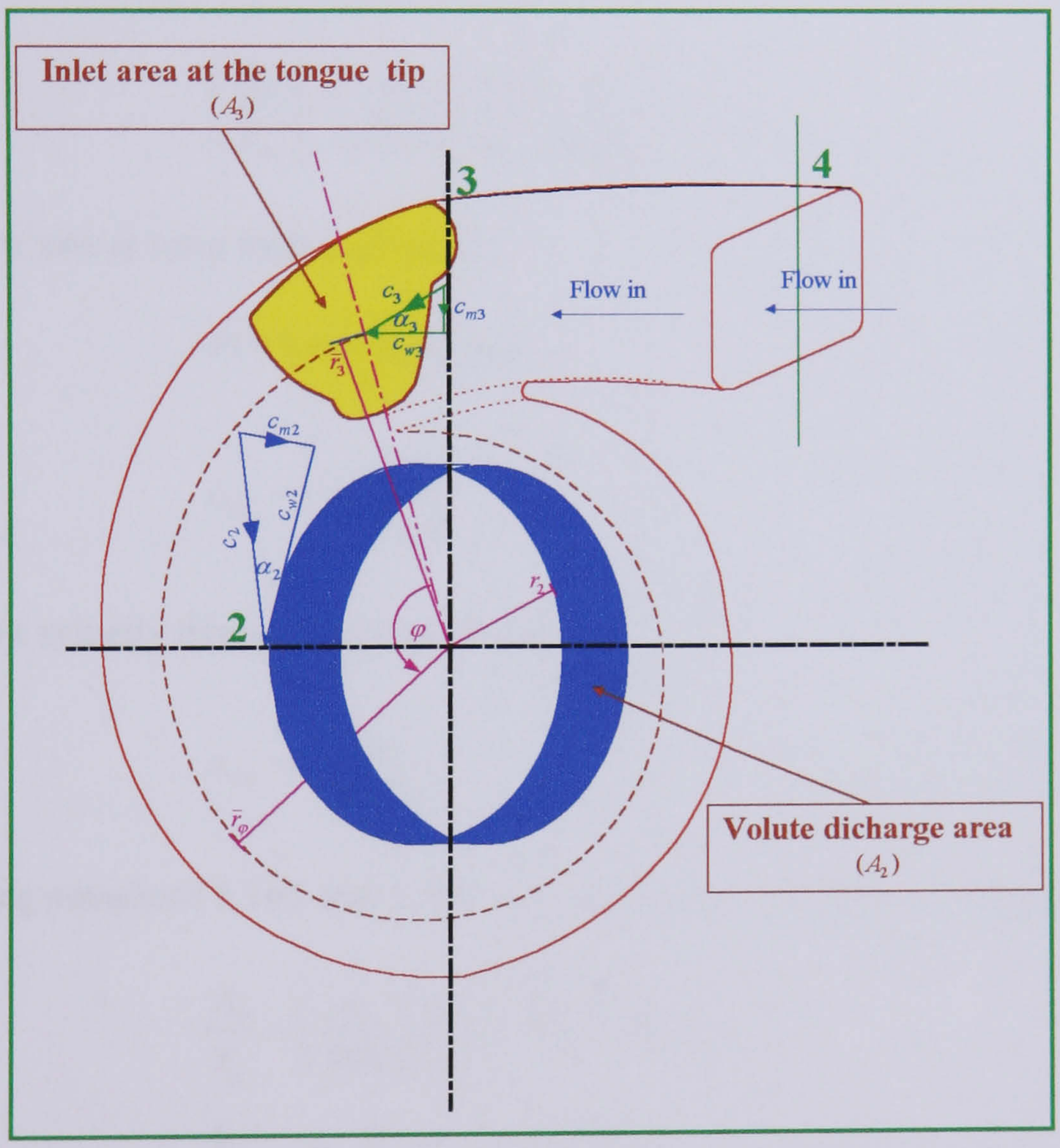

FIG. 3.10 SCHEMATIC DIAGRAM OF NOZZLE-LESS VOLUTE CASING

Re-arranging for $c_{w\varphi}$ will give:

$$c_{w\varphi} = \left(\frac{\varphi}{360}\right)\left(\frac{\dot{m}}{\rho_\varphi A_\varphi}\right) \tag{3.101}$$

Using the equation of free vortex flow $C_w r = k$, the relationship given below follows the conservation of mass, energy and of angular momentum

$$c_{w\varphi}\bar{r}_{\varphi} = c_{w2}r_2 = k \tag{3.102}$$

Substituting equation 3.102 into equation 3.101 would give:

$$(c_{w2})\left(\frac{r_2}{\bar{r}_{\varphi}}\right) = \left(\frac{\varphi}{360}\right)\left(\frac{\dot{m}}{\rho_{\varphi}A_{\varphi}}\right) \tag{3.103}$$

Re-arranging equation 3.103 gives:

$$\left(\frac{A_{\varphi}}{\bar{r}_{\varphi}}\right) = \left(\frac{\varphi}{360}\right)\left(\frac{\dot{m}}{\rho_{\varphi}}\right)\left(\frac{1}{r_2 c_{w2}}\right) \tag{3.104}$$

Mass flow rate at rotor inlet is given by:

$$\dot{m} = (\rho_2)(B_{f_2}A_2)c_{m2}$$

i.e.
$$c_{m2} = \left(\frac{\dot{m}}{\rho_2 B_{f_2} A_2}\right) \tag{3.105}$$

From inlet velocity triangle depicted in **Fig. 3.7**

$$c_{w2} = \left(\frac{c_{m2}}{\tan\alpha_2}\right) \tag{3.106}$$

Combining equations 3.105 and 3.106 with equation 3.104 and re-arranging yield to

$$\frac{A_{\varphi}}{\bar{r}_{\varphi}} = \left(\frac{\varphi}{360}\right)\left(\frac{\rho_2}{\rho_{\varphi}}\right)\left(\frac{B_{f_2}A_2}{r_2}\right)(\tan\alpha_2) \tag{3.107}$$

$$\frac{A_{\varphi}}{A_2} = (B_{f_2})\left(\frac{\varphi}{360}\right)\left(\frac{\rho_2}{\rho_{\varphi}}\right)\left(\frac{\bar{r}_{\varphi}}{r_2}\right)(\tan\alpha_2) \tag{3.108}$$

But
$$\frac{\rho_2}{\rho_{\varphi}} = \left(\frac{T_2}{T_{\varphi}}\right)^{\frac{1}{\gamma-1}} = \left[\frac{T_{02} - \left(\frac{c_2^{\,2}}{2C_p}\right)}{T_{0\varphi} - \left(\frac{c_{w\varphi}^{\,2}}{2C_p}\right)}\right]^{\frac{1}{\gamma-1}} = \left[\frac{1 - \left(\frac{c_2^{\,2}}{2C_pT_{02}}\right)}{\left(\frac{T_{0\varphi}}{T_{02}}\right) - \left(\frac{c_{w\varphi}^{\,2}}{2C_pT_{0\varphi}}\right)}\right]^{\frac{1}{\gamma-1}} \tag{3.109}$$

Since adiabatic conditions in the volute is assumed, then

$$T_{02} = T_{0\varphi} = T_{03} = T_i$$

i.e. equation 3.106 becomes

$$\frac{\rho_2}{\rho_\varphi} = \left[\frac{1-\left(\frac{c_2^{\,2}}{2C_pT_i}\right)}{1-\left(\frac{c_{w\varphi}^{\,2}}{2C_pT_i}\right)}\right]^{1/\gamma-1} \tag{3.110}$$

From inlet velocity triangle depicted in **Fig. 3.7**

$$c_{w2} = u_2\left(\frac{\sin\beta_2\cos\alpha_2}{\sin(\alpha_2+\beta_2)}\right) \text{ and } c_2 = u_2\left(\frac{\sin\beta_2}{\sin(\alpha_2+\beta_2)}\right)$$

Substituting for c_{w2} into equation 3.102 would give:

$$c_{w\varphi} = u_2\left(\frac{r_2}{r_\varphi}\right)\left(\frac{\sin\beta_2\cos\alpha_2}{\sin(\alpha_2+\beta_2)}\right) \tag{3.111}$$

Substituting the expressions c_2 and $c_{w\phi}$ into equation 3.111 and re-arranging **yield to:**

$$\frac{\rho_2}{\rho_\varphi} = \left[\frac{1-\left(\frac{\pi}{\sqrt{2}}\cdot\frac{d_2N}{\sqrt{C_pT_i}}\cdot\frac{\sin\beta_2}{\sin(\alpha_2+\beta_2)}\right)^2}{1-\left(\frac{\pi}{\sqrt{2}}\cdot\frac{r_2}{\bar{r}_\varphi}\cdot\frac{d_2N}{\sqrt{C_pT_i}}\cdot\frac{\sin\beta_2\cos\alpha_2}{\sin(\alpha_2+\beta_2)}\right)^2}\right]^{1/\gamma-1} \tag{3.112}$$

Finally by substituting for ρ_2/ρ_φ in equation 3.108 and re-arranging, the following expression is obtained:

$$\frac{A_\varphi}{A_2} = (B_{f_2})(\tan\alpha_2)\left(\frac{\varphi}{360}\right)\left(\frac{\bar{r}_\varphi}{r_2}\right)\left[\frac{1-\left(\frac{\pi}{\sqrt{2}}\cdot\frac{d_2N}{\sqrt{C_pT_i}}\cdot\frac{\sin\beta_2}{\sin(\alpha_2+\beta_2)}\right)^2}{1-\left(\frac{\pi}{\sqrt{2}}\cdot\frac{r_2}{\bar{r}_\varphi}\frac{d_2N}{\sqrt{C_pT_i}}\cdot\frac{\sin\beta_2\cos\alpha_2}{\sin(\alpha_2+\beta_2)}\right)^2}\right]^{1/\gamma-1} \tag{3.113}$$

Where B_{f_2} is the blockage factor corresponding to rotor entry and is given as:

$$B_{f_2} = 1 - \left(\frac{N_b t_2 b_2}{\pi d_2 b_2} \right) \tag{3.114}$$

Where N_b : Number of blades

t_2 : Thickness of inlet rotor blades

Equation 3.114 can be re-arranged to give the volute design parameter $A_\varphi / \bar{r}_\varphi$ at any azimuth angle as:

$$\frac{A_\varphi}{\bar{r}_\varphi} = (B_{f_2})(\tan \alpha_2) \left(\frac{\varphi}{360} \right) \left(\frac{A_2}{r_2} \right) \left[\frac{1 - \left(\frac{\pi}{\sqrt{2}} \cdot \frac{d_2 N}{\sqrt{C_p T_i}} \cdot \frac{\sin \beta_2}{\sin(\alpha_2 + \beta_2)} \right)^2}{1 - \left(\frac{\pi}{\sqrt{2}} \cdot \frac{r_2}{\bar{r}_\varphi} \frac{d_2 N}{\sqrt{C_p T_i}} \cdot \frac{\sin \beta_2 \cos \alpha_2}{\sin(\alpha_2 + \beta_2)} \right)^2} \right]^{1/\gamma - 1} \tag{3.115}$$

Equation 3.115 represents a fundamental design equation linking the main design parameter $A_\varphi / \bar{r}_\varphi$ of the nozzle-less volute casing with relevant principal dimensions of the rotor and the operating conditions.

3.4 SUMMARY

A complete analysis of the performance parameters of the IFR turbine has been presented in this Chapter. The developed modelling equations have been employed to investigate the influence of the individual parameter on the overall performance of turbine and on each other. The equations have also been used to design of various parts of the IFR turbine as described in the following Chapter.

CHAPTER 4

DESIGN OF INWARD FLOW RADIAL TURBINE

4.1 INTRODUCTION

A complete theoretical analysis and design modelling of radial turbine was described in **Chapter 3**. An integrated approach for the overall design of a single stage inward flow radial turbine comprising a rotor and the casing based on this analysis will be described in this Chapter. The current **IFR** turbine is designed to drive a directly-coupled permanent magnet high- speed alternator running at 60000 *rpm* and developing a maximum $60\,kW$ electrical power.

4.2 DESIGN OF INWARD FLOW RADIAL TURBINE ROTOR

The complete design of the **IFR** turbine rotor requires the aero-thermodynamic, structural and manufacturing criteria to be satisfied simultaneously. The design specifications normally include the mass flow rate of the working fluid, pressure ratio, and in some cases, rotational speed. In the current work, the task is to determine:

i. The pricipal dimensions of the rotor including the number of blades to meet the overall performance requirements within the known constraints.

ii. The optimum axial length of the rotor.

iii. The design of the flow channel.

4.2.1 Choice of Principal Dimensions of an IFR Turbine Rotor and Number of Blades

The choice of the principal dimensions of a turbine rotor for a given set of inlet design specifications as shown in **Table 4.1**, can be found by solving equations (3.20, 3.60b, 3.63, 3.72, 3.79a, 3.83) that were derived in **Chapter 3**. An analytical method is

indeed difficult and can be very time consuming, especially if the complete procedure has to be repeated for different design cases.

DESIGN SPECIFICATION	DESIGN VALUE
Mass flow, $\dot{m}$	$0.572\ kg/s$
Pressure ratio, P_i/P_e	3.6
Inlet stagnation temperature, T_i	$1000^{\circ}K$
Rotational speed, N	$60000\ rev/\min$

TABLE 4.1 INPUT DATA AT DESIGN POINT OF IFR TURBINE

In view of this, numerical optimisation techniques can be a useful tool to problems involving a large number of variables. Many algorithms have been developed by **Biggs [59,60,61]**. In this section, an adaption of this numerical optimisation technique to the design of the **IFR** turbine rotor is applied and described in the following section.

The optimisation programme started by assigning different values to a set of parameters $X_1, X_2, X_3, \ldots\ldots\ldots X_n$. Therefore, an objective function denoted by $F(\overline{X})$, where $\overline{X}$ is a vector with elements, $X_1, X_2, X_3, \ldots\ldots\ldots X_n$ must be formulated and the aim is to determine the values of the vector $\overline{X}$, which will find the optimum value of the function $F(\overline{X})$. This function may be subjected to possible linear or non- linear equality and inequality constraints, i.e.

$$g_i = 0 \qquad i = 1, 2, 3, \ldots\ldots\ldots\ldots\ldots\ldots\ldots m_e$$

$$g_j \geq 0 \qquad j = m_e + 1, m_e + 2, \ldots\ldots\ldots\ldots\ldots m$$

Where:

g_i and g_j represent non-linear equality and inequality constraints, respectively. The subscripts i and j refer to the number of constraints.

4.2.1.1 Constraint optimisation technique procedure

The frame size and weight of an **IFR** turbine is often an important parameter consideration, in view of this, the size of the turbine rotor plays an important rule in

determining the overall size of such a turbine. Therefore. the aim is to minimise the rotor tip diameter d_2 and this can be considered a constraint optimisation problem. The procedure to solve such a problem is described below:

i. Selection of main principal parameters of a turbine rotor

The choice of selecting the principal parameters of a turbine rotor to solve this optimisation problem is given by the matrix:

$$\overline{X} = \begin{bmatrix} d_2 & = X(1) \\ u_2/c_s & = X(2) \\ \alpha_2 & = X(3) \\ (\psi_2)_{BL} & = X(4) \\ M_2 & = X(5) \\ b_2/d_2 & = X(6) \\ M_{er} & = X(7) \\ B_e & = X(8) \\ d_e/d_2 & = X(9) \\ d_h/d_2 & = X(10) \end{bmatrix}$$

ii. Formulation of the objective function

The objective function is to optimise the rotor tip diameter and it can be formulated as follows:

$$F(X) = d_2 = X(1)$$

iii. Formulation of equality and inequality constraints

A. *Equality constraints*

A.1 $$g(1) = \frac{d_2 N}{\sqrt{C_p T_i}} - \left(\frac{60\sqrt{2}}{\pi}\right)\left(\frac{u_2}{c_s}\right)\left[\sqrt{1-\left(\frac{P_e}{P_i}\right)^{\gamma-1/\gamma}}\right] = 0 \qquad (4.1)$$

A.2 $$g(2)=\cos\alpha_2-\left(\frac{c_{w2}}{u_2}\right)\left(\frac{\pi}{60}\right)\left(\frac{d_2N}{\sqrt{C_pT_i}}\right)\left(\sqrt{\frac{1+\frac{\gamma-1}{2}M_2{}^2}{(\gamma-1)M_2{}^2}}\right)=0 \qquad (4.2)$$

A.3 $$g(3)=\left(\frac{b_2}{d_2}\right)-\frac{\dot{m}\sqrt{C_pT_i}}{d_2{}^2P_i}\left[\frac{1}{\phi\pi B_{f_2}}\left(\frac{\sqrt{\gamma-1}}{\gamma}\right)\right]\left[\frac{\left(1+\frac{\gamma-1}{2}M_2{}^2\right)^{\gamma+1/2(\gamma-1)}}{M_2\sin\alpha_2}\right]=0 \qquad (4.3)$$

A.4

$$g(4)=\frac{\dot{m}\sqrt{C_pT_i}}{d_2{}^2P_i}-\left(\frac{P_e}{P_i}\right)\left[\frac{1}{\left\{1-\eta_{tt}\left(1-(\frac{P_e}{P_i})^{\gamma-1/\gamma}\right)\right\}}\right]^{1/2}\left[B_{f_1}\left(\frac{\pi}{4}\right)\left(\frac{\gamma}{\sqrt{\gamma-1}}\right)\left((\frac{d_e}{d_2})^2-(\frac{d_h}{d_2})^2\right)\right]$$

$$\times\left[\frac{M_{er}\sin\beta_e}{\left(1+(\frac{\gamma-1}{2})(M_{er}\sin\beta_e)^2\right)^{\gamma+1/2(\gamma-1)}}\right]=0 \qquad (4.4)$$

A.5

$$g(5)=M_{er}-\left[\frac{\left(\frac{\pi}{60}\right)^2\left(\frac{d_2N}{\sqrt{C_pT_i}}\right)^2(\frac{d_e}{d_2})^2}{(\gamma-1)\left\{1-\eta_{tt}\left(1-(\frac{P_e}{P_i})^{\gamma-1/\gamma}\right)\right\}\left\{1-\sin^2\beta_e\left(1+\frac{(\frac{\pi}{60})(\frac{d_2N}{\sqrt{C_pT_i}})^2(\frac{d_e}{d_2})^2}{2\left(1-\eta_{tt}(1-(\frac{P_e}{P_i})^{\gamma-1/\gamma}\right)(\sin^2\alpha_1)}\right)\right\}}\right]^{1/2}=0 \qquad (4.5)$$

B. *Inequality constraints*

B.1 $u_2/c_s \leq 0.707$: Velocity ratio is governed by permissible maximum efficiency.

$$g(6) = u_2/c_s - 0.707 \tag{4.6}$$

B.2 $\alpha_2 \leq 21^\circ$: Absolute flow angle at rotor inlet is fixed by turbine efficiency.

$$g(7) = \alpha_2 - 21^\circ \tag{4.7}$$

B.3 $c_{w2}/u_2 \leq 1.0$: Specified by minimum incidence loss considartion.

$$g(8) = c_{w2}/u_2 - 1.0 \tag{4.8}$$

B.4 $M_2 \leq 1.0$: Mach number at rotor inlet specified by shock at rotor entry.

$$g(9) = M_2 - 1.0 \tag{4.9}$$

B.5 $b_2/d_2 \leq 0.15$: Blade width to tip diameter ratio governed by leakage loss.

$$g(10) = b_2/d_2 - 0.15 \tag{4.10}$$

B.6 $M_{er} \leq 1.0$: Mach number at exducer tip diameter governed by choking condition.

$$g(11) = M_{er} - 1.0 \tag{4.11}$$

B.7 $\beta_e \geq 25^\circ$: Relative flow angle at exducer tip diameter fixed by the rotor machining requirements and the relative Mach number M_{er} at exducer tip.

$$g(12) = 25 - \beta_e \tag{4.12}$$

B.8 $d_e/d_2 \leq 0.75$: Exducer to tip diameter ratio fixed by permissible relative Mach number M_{er} to keep the exducer tip Mach number subsonic.

$$g(13) = d_e/d_2 - 0.75 \tag{4.13}$$

B.9 $d_h/d_2 \geq 0.25$: Hub to tip diameter ratio specified by stress limitation and blockage factor.

$$g(15) = 0.25 - d_h/d_2 \tag{4.14}$$

B.10 $d_2 \leq 20.0$: This is controlled by the size of the turbine, rotor tip speed and stress limitation.

$$g(16) = d_2 - 20.0 \tag{4.15}$$

B.11 $v_2/v_1 \geq 2.0$: This is specified by the axial length of the rotor

$$g(17) = v_2/v_1 - 2.0 \tag{4.16}$$

4.2.1.2 Optimisation programme

OPRQP Fortran programme (double precision), short for optimisation using recursive quadratic programming is used to solve a general non-linear programming problem using the successive quadratic programming algorithm and a user- supplied gradient. The description of the **OPRQP** programme is found in **Refs. [57,58,59]**.

The only unusual feature is the use of the rotor tip diameter d_2 as an optimisation variable and an objective function. However, such a choice should not affect the working of the programme.

The objective function and the equality and inequality constraints with their first derivatives are inserted into the programme into two sub-routines called, **call function** and **call gradient**.

4.2.1.3 Optimisation results

The optimisation computer programme was run for several number of blades. The final output results for each run gives the numerical values of the matrix $\overline{X}$ and the corresponding number of blades for each run.

Optimisation results reveal that the changes in the values of the objective function for the number of blades ranging from 12-20 blades is relatively small. Consequently, any blade number chosen in this range is quite satisfactory. For the present research, the optimum number of blades which gives the best values of the objective function is 12.

4.2.2 Design Calculations Based on Data Obtained by Numerical Optimisation Technique.

4.2.2.1 Design data

The optimum design data of the turbine rotor obtained using the optimisation technique is shown in **Table 4.2**. A schematic drawing of the turbine rotor including the main dimensions is shown in **Fig. 4.1**.

DESIGN PARAMETER	DESIGN VALUE
N_b	12 *Blades*
d_2	16.91 *cm*
u_2/c_s	0.67
α_2	17.0°
c_{w2}/u_2	0.97
M_2	0.93
b_2/d_2	0.051
M_{er}	0.80
β_e	27.0°
d_e/d_2	0.70
d_h/d_2	0.36

TABLE 4.2 DESIGN DATA OF A TURBINE ROTOR OBTAINED USING OPTIMISATION TECHNIQUE

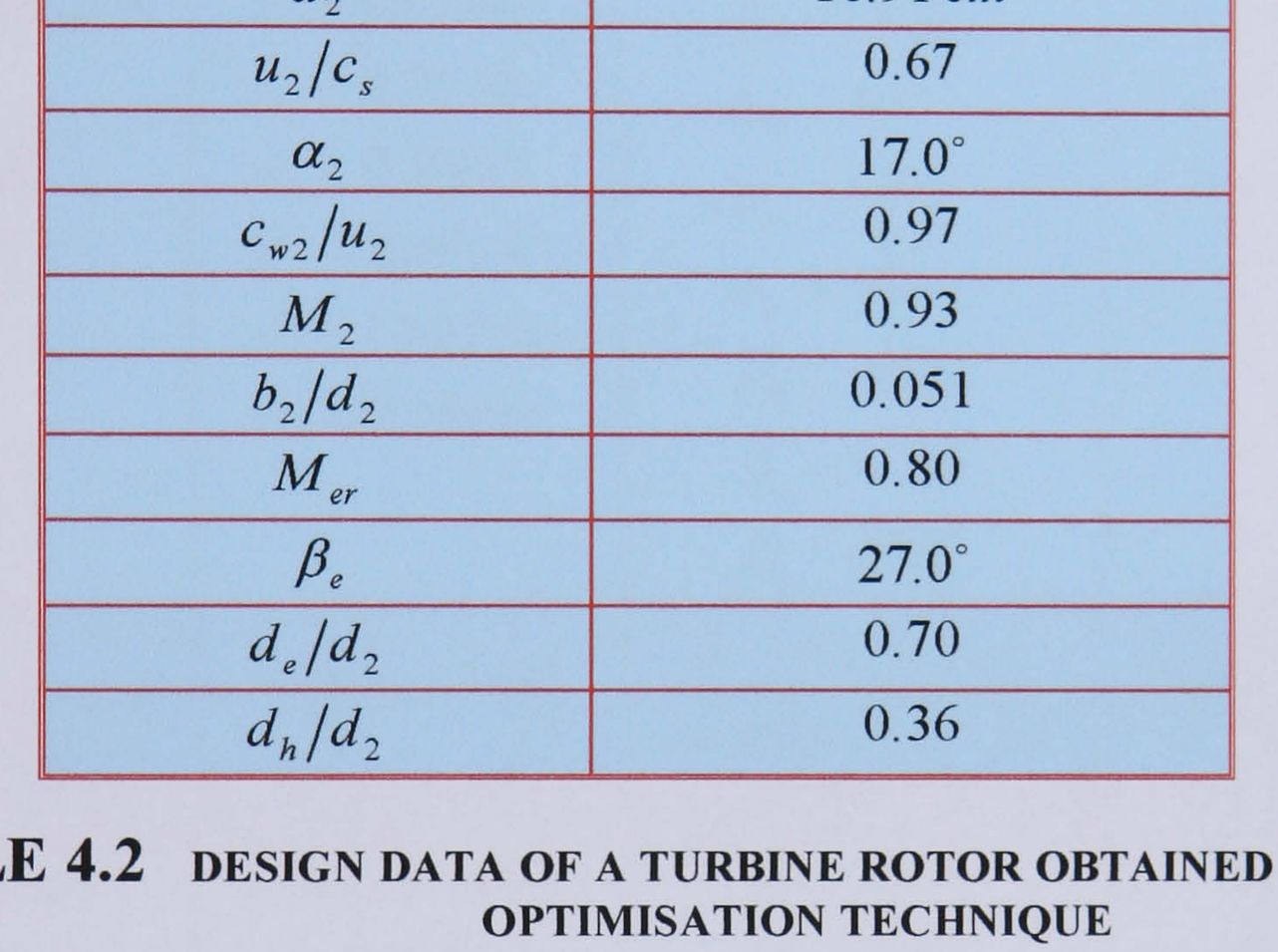

FIG. 4.1 THE DESIGN GEOMETRY OF AN IFR TURBINE ROTOR BASED ON NUMERICAL OPTIMISATION

4.2.2.2 Rotor design

Using the design data from **Table 4.2**, the design calculations for the aerodynamics and performance parameters were carried out based on the equations derived in **Chapter 3**. Consequently, a complete summary of the output results is obtained and listed in **Tables 4.3**.

DESIGN SPECIFICATIONS	GEOMETRICAL DIMENSIONS	FLOW ANGLES AT ROTOR INLET AND EXIT	FLOW VELOCTIES AT ROTOR INLET
$W_{net} = 60\,kW$ $N = 60000\,r.p.m$ $P_i/P_e = 4.0$ $T_i = 1000\,K$ $\dot{m}_g = 0.574$	$d_2 = 16.91\,cm$ $b_2 = 0.87\,cm$ $\bar{t}_2 = 0.25\,cm$ $d_1 = 9.30\,cm$ $d_h = 6.09\,cm$ $d_e = 11.67\,cm$ $\bar{t}_1 = 0.15\,cm$	$\alpha_2 = 17.0^\circ$ $\beta_2 = 84.2^\circ$ $\alpha_1 = 90^\circ$ $\alpha_h = 90^\circ$ $\alpha_e = 90^\circ$ $\beta_h = 44.32^\circ$ $\beta_1 = 32.59^\circ$ $\beta_e = 27.0^\circ$	$c_2 = 538.82\,m/s$ $v_2 = 158.13\,m/s$ $c_{m2} = 157.34\,m/s$ $c_{w2} = 515.11\,m/s$
FLOW VELOCITIES AT ROTOR EXIT	**ROTOR SPEED**	**MACH NUMBER AT ROTOR INLET AND EXIT**	**PERFORMANCE PARAMETERS**
$c_1 = 186.77\,m/s$ $c_{w2} = 0.0\,m/s$ $c_h = 186.77\,m/s$ $c_e = 186.77\,m/s$ $v_1 = 346.77\,m/s$ $v_h = 267.32\,m/s$ $v_e = 411.39\,m/s$	$u_2 = 531.24\,m/s$ $u_1 = 292.18\,m/s$ $u_h = 191.25\,m/s$ $u_e = 366.55\,m/s$	$M_2 = 0.93$ $M_1 = 0.35$ $M_{hr} = 0.50$ $M_{1r} = 0.65$ $M_{er} = 0.8$	$S_P = 0.157$ $S_T = 0.24$ $\eta_{tt} = 0.87$ $R = 0.56$ $\Omega_s = 0.55$ $D_s = 3.46$

TABLE 4.3 DESIGN DATA FOR AN IFR TURBINE ROTOR BASED ON THE RESULTS OF NUMERICAL OPTIMISATION

4.2.3 The Choice of Axial Length

Referring to **Fig. 1.3 of Chapter 1**, it was argued although the mean flow relative to the rotor accelerates from inlet to outlet, in certain regions on the blade and hub surfaces, the flow experiences deceleration. High space rate of deceleration can be lead

to separation, consequently aerodynamic losses. The space rate of deceleration can be controlled by proper selection of axial length.

As far as could be ascertained from the published literature, there was little information available to the designer to help him in the choice of axial length of **IFR** turbine. In the following, a systematic procedure for obtaining the axial length for a prescribed meanstream velocity profile is described.

4.2.3.1 The theory of the prescribed mean stream velocity distribution method

The total relative velocity V corresponding to the root mean square diameter at entry may be resolved into three components in the axial V_z, radial V_r and tangential direction V_w. In most designs, the radial component at rotor inlet is maximum, and the axial component is zero. At the rotor outlet, in the case of an **IFR** turbine rotor, the radial component becomes zero and the axial component attains a maximum value.

The tangential component increases, but its boundary values are not known. A mean streamline is defined as a locus of points joining the *rms* radius r_1 with a point at r_2 which bisects b_2. The exact location of this point can be found by applying the continuity equation at the rotor inlet, and hence, defining the streamline boundaries. The constraints on the choice of this line are that the radial and tangential components must not accelerate to such an extent that the value of total relative velocity V exceeds the choking conditions.

The relative velocity vector $\overline{V}$ at any point inside the turbine rotor passage, as shown in **Fig. 4.2**, may be resolved into three basic components along the axial, radial and tangential directions, $\overline{V}_z$, $\overline{V}_r$, $\overline{V}_w$ respectively. $\overline{V}_m$ is the velocity vector along the mean streamline in the hub-to-shroud plane. From **Fig. 4.2**, the total velocity vector $\overline{V}$ could be expressed in terms of its three vector components as:

$$\overline{V} = \overline{V}_z + \overline{V}_r + \overline{V}_w \tag{4.17}$$

But
$$\overline{V}_m = \overline{V}_z + \overline{V}_r \tag{4.18}$$

Substituting equation 4.18 into equation 4.17 would give

$$\overline{V} = \overline{V}_w + \overline{V}_m \tag{4.19a}$$

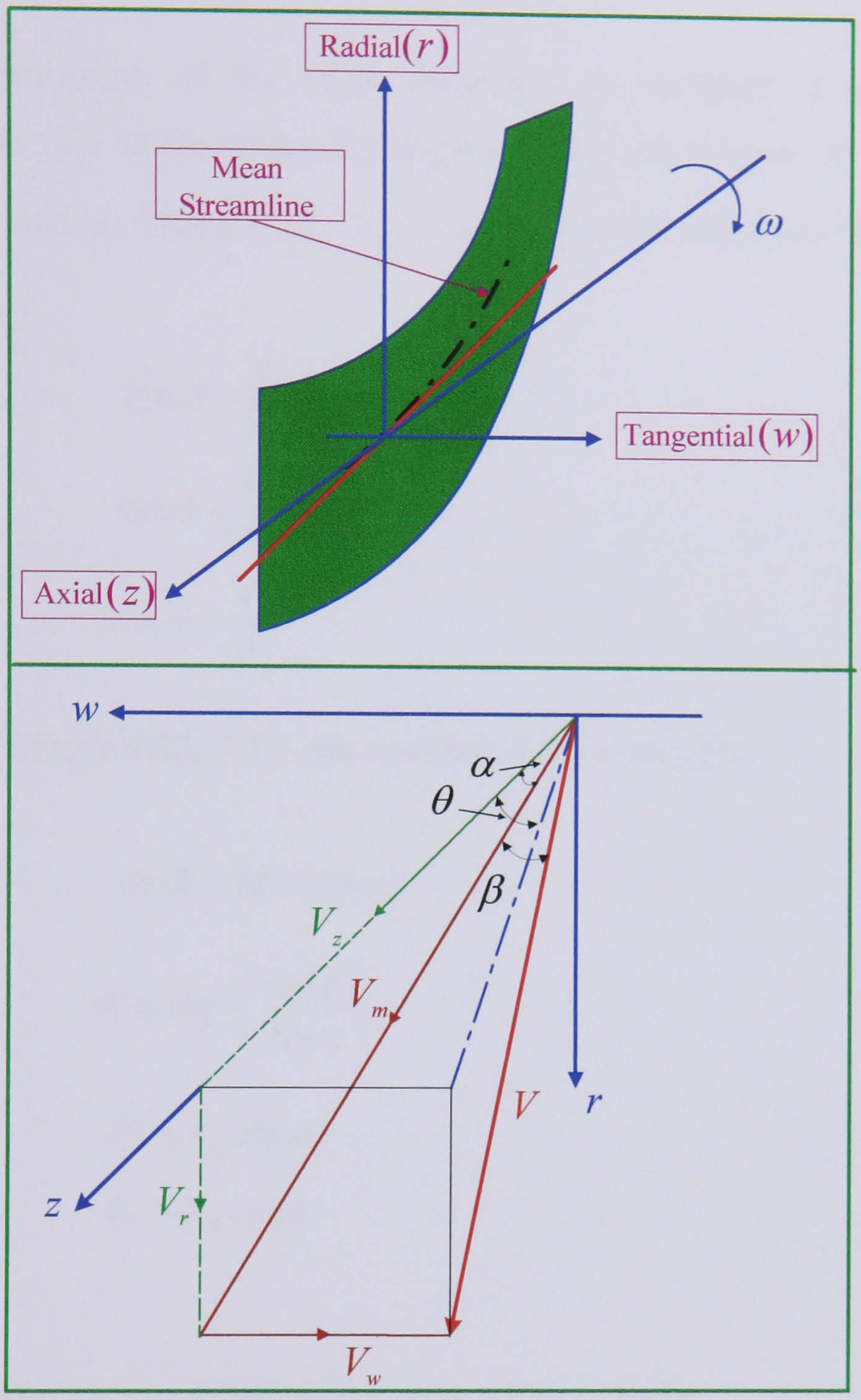

FIG. 4.2 NOTATION FOR RELATIVE VELOCITY VECTOR AND ITS COMPONENTS

or

$$V^2 = V_w^{\ 2} + V_m^{\ 2} \tag{4.19b}$$

Where $V_w = V \sin\beta$

Substituting for $\overline{V}_w$ in equation 4.19b and re-arranging, the flow angle could be expressed as a function of V and V_m as follows:

$$\beta = \sin^{-1}\sqrt{1 - V_m{}^2 / V} \tag{4.20}$$

The spatial description of the mean streamline is specified if any two-velocity components and one of the following angles α, β, θ are known. It is convenient to assume V_m, V and α, hence V_r, V_z, V_w, β and θ can be written as functions of these quantities as:

$$\tan\beta = \frac{V_w}{V_m} \tag{4.21}$$

But

$$\tan\theta = \frac{V_w}{V_z} \tag{4.22}$$

and

$$\cos\alpha = \frac{V_z}{V_m} \tag{4.23}$$

Substituting equations 4.22, 4.23 into equation 4.21 would give

$$\tan\beta = \tan\theta\cos\alpha \tag{4.24}$$

or

$$\theta = \tan^{-1}\left(\frac{\tan\beta}{\cos\alpha}\right) \tag{4.25}$$

Where

$$V_r = V_m \sin\alpha \tag{4.26}$$

and

$$V_z = V_m \cos\alpha \tag{4.27}$$

4.2.3.2 Procedure for obtaining mean streamline velocity

The spatial description of the mean streamline can be found iteratively by assuming a starting value for the meridional length z_m, and describing the component velocities and angles mentioned in the preceding section. **Fig. 4.3** shows three meridional lengths 0.02, 0.04, 0.06 in m of a turbine rotor. **Fig. 4.4** describes the velocity components V_r. V_z and V_w for one value of Z and **Fig. 4.5** describes the angle α between the meridional and the axial velocity. At the start, all these figures are based on the assumption that the velocity and the angle α variation are linear.

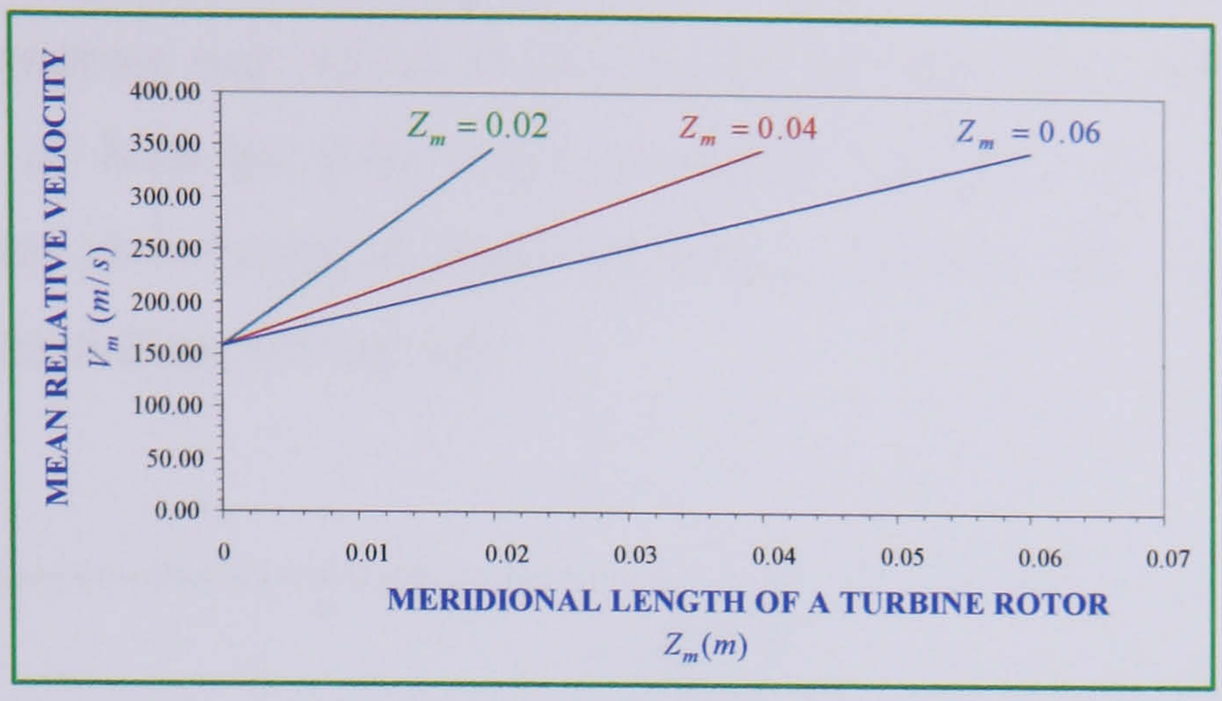

FIG. 4.3 ASSUMED LINEAR RELATIONSHIP OF TOTAL RELATIVE VELOCITY ALONG MEAN STREAMLINE OF VARIOUS MERIDIONAL LENGTHS WITH THE SAME BOUNDARY CONDITIONS

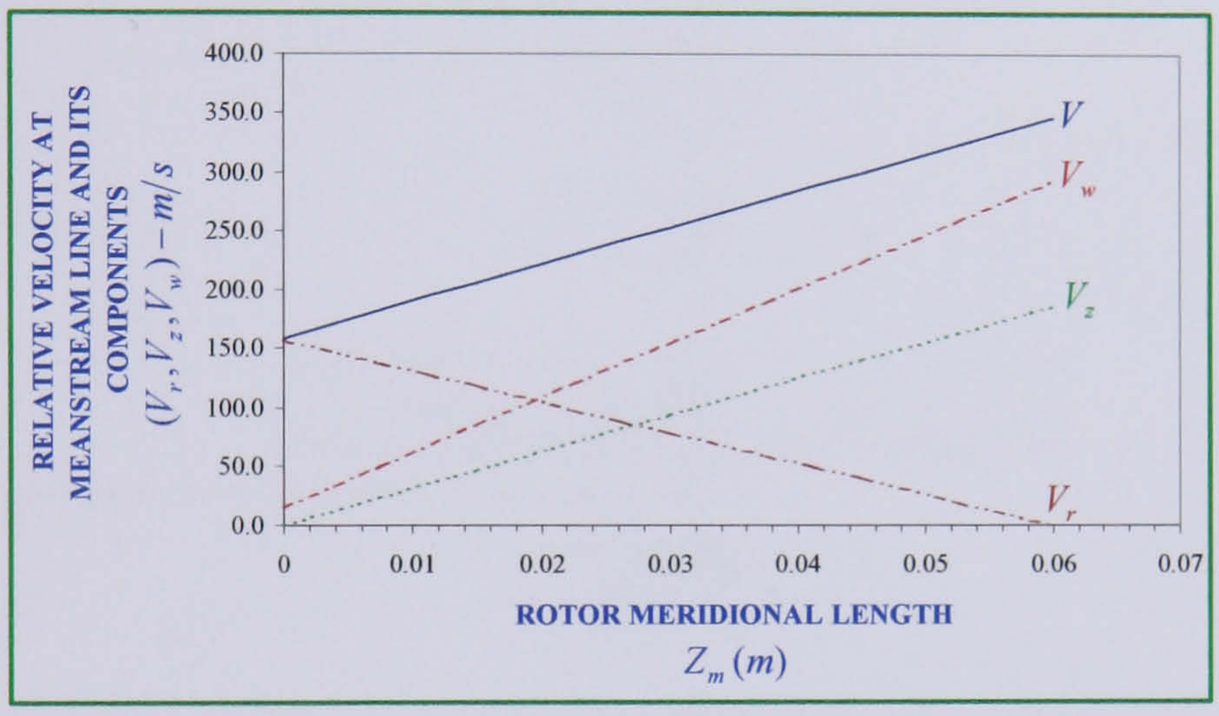

FIG. 4.4 ASSUMED LINEAR RELATIONSHIP OF TOTAL RELATIVE VELOCITY AND ITS COMPONENTS FOR A TURBINE ROTOR OF MERIDIONAL LENGTH OF $0.06\,m$

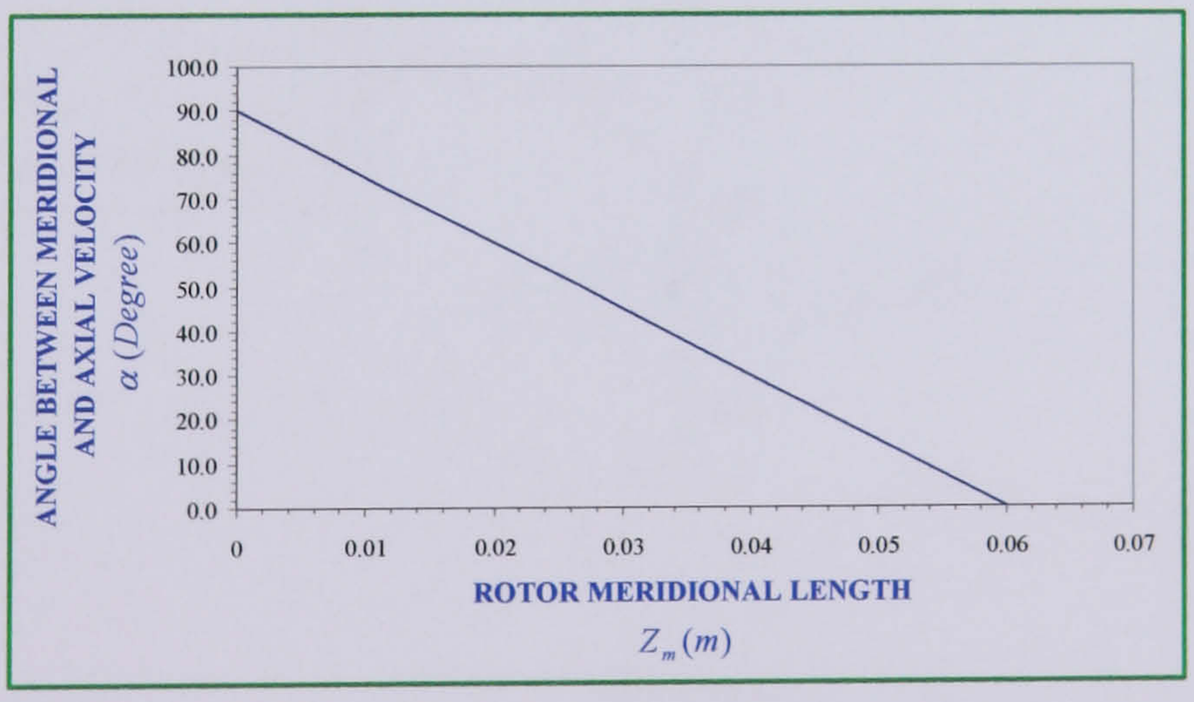

FIG. 4.5 ASSUMED LINEAR RELATIONSHIP OF THE ANGLE BETWEEN MERIDIONAL VELOCITY AND AXIAL PLANE ALONG MEAN STREAMLINE FOR A TURBINE ROTOR OF A MERIDIONAL LENGTH OF $0.06\,m$

A computer programme was written to perform the iterative calculations to check this linear variation of both the total relative velocity and the angle α along mean streamline. A flow chart based on this programme is shown in **Fig. 4.6** and the output results are plotted in **Figs. 4.7** and **4.8**.

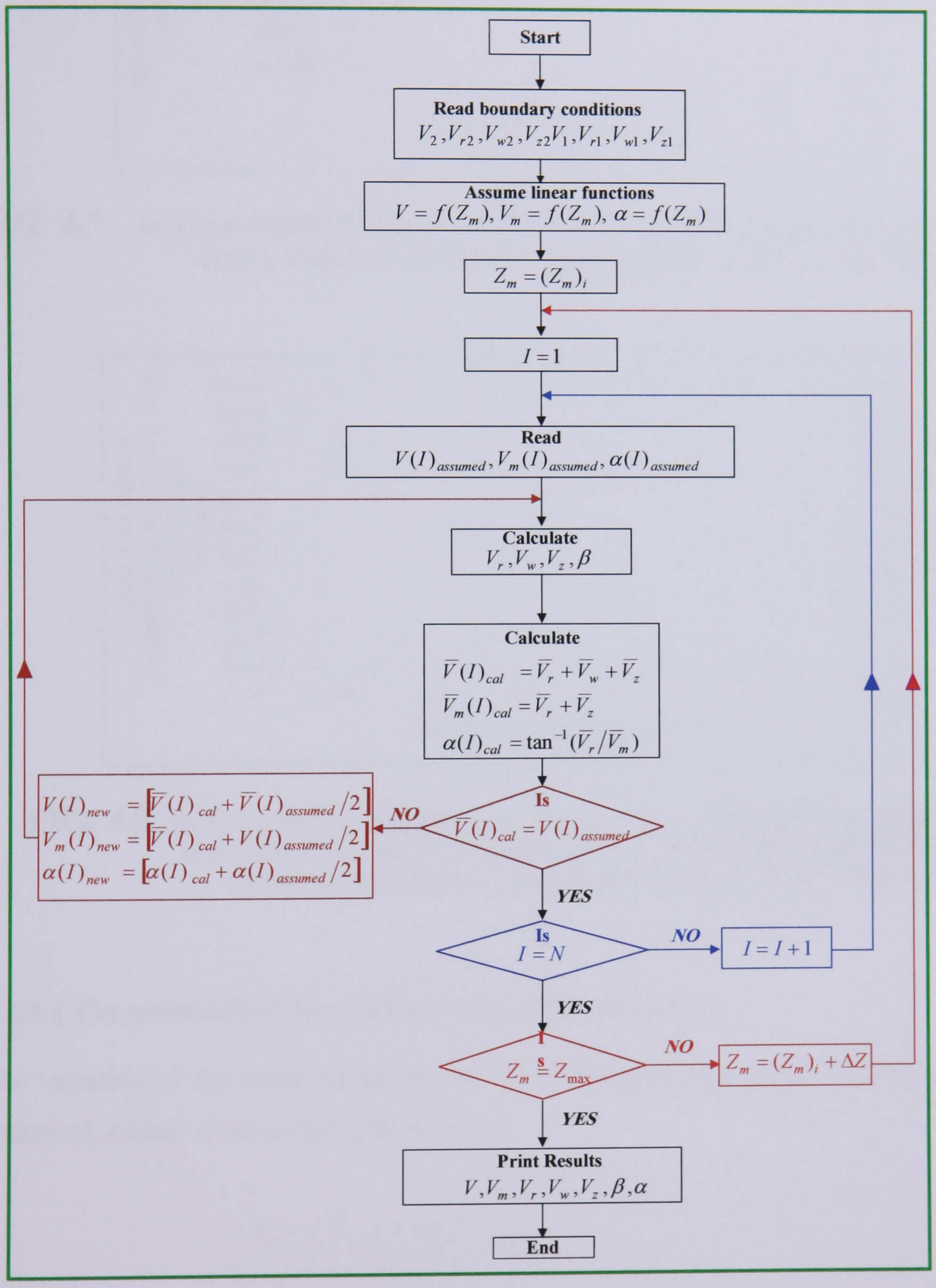

FIG. 4.6 FLOW CHART TO CALCULATE VELOCITIES AND FLOW ANGLES BASED ON EQUATIONS 4.17 TO 4.27

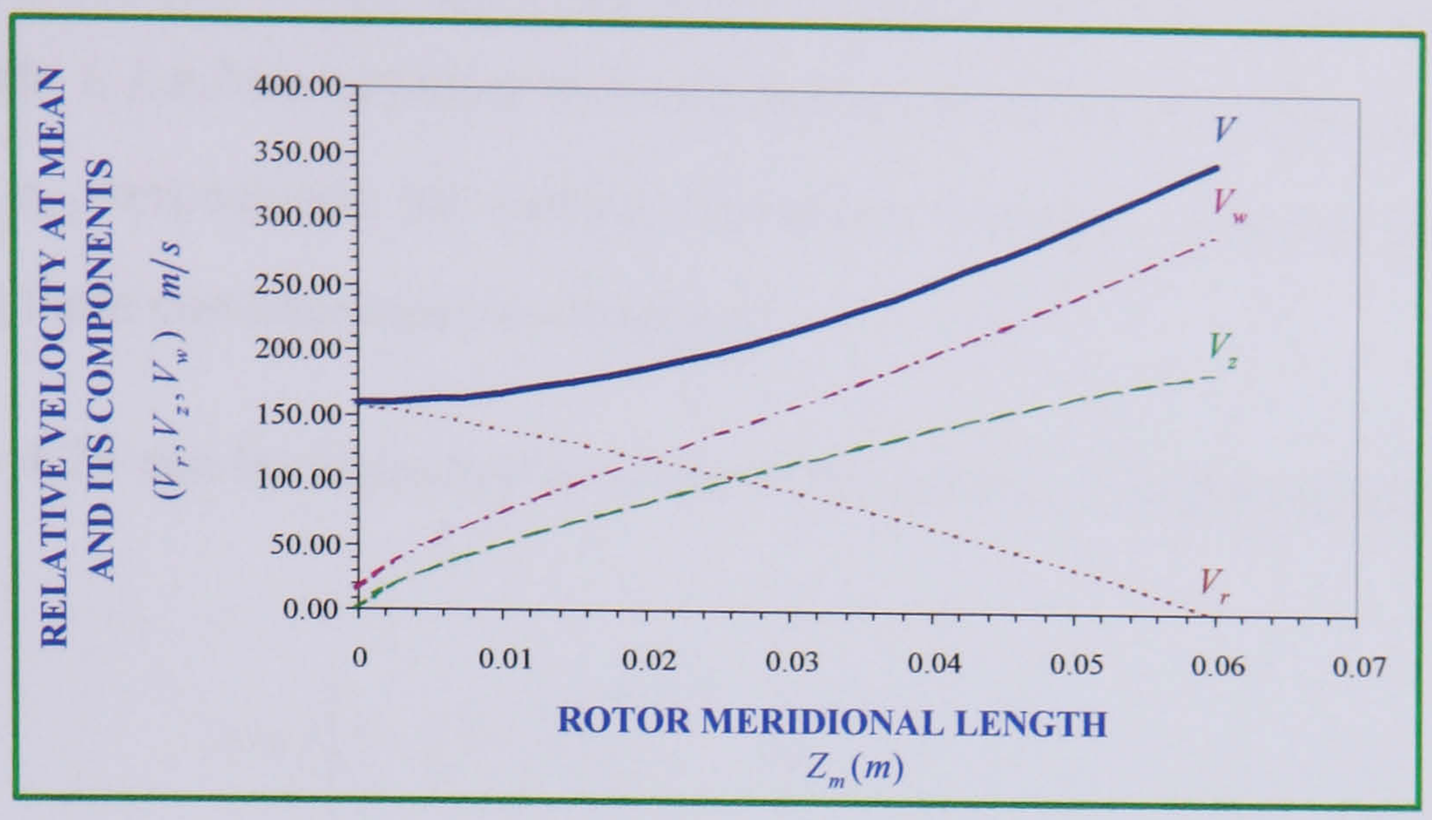

FIG. 4.7 ACTUAL PRESENTATION OF VELOCITIES ALONG MEAN STREAMLINE FOR A TURBINE ROTOR OF A MERIDIONAL LENGTH OF $0.06\,m$

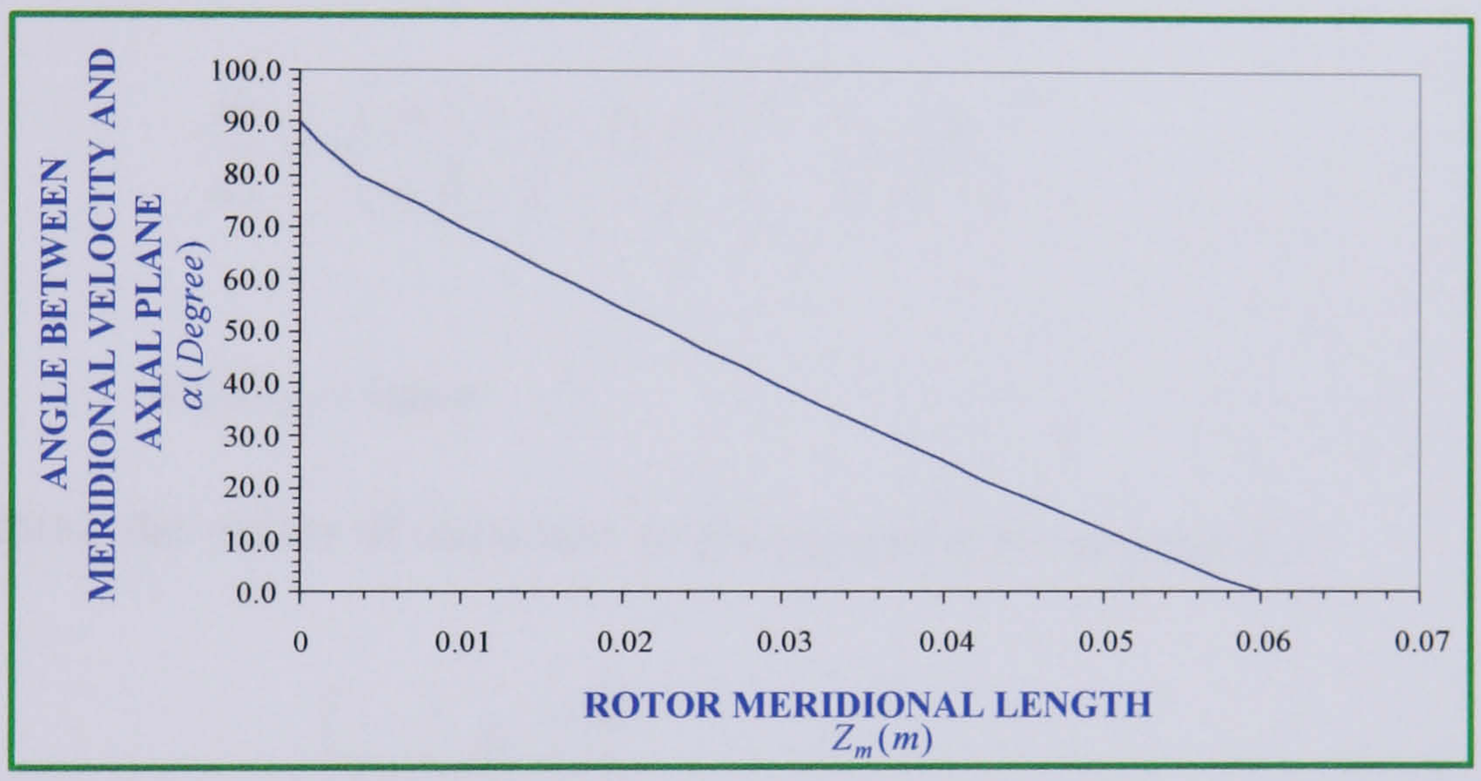

FIG. 4.8 ACTUAL PRESENTATION OF THE ANGLE α BETWEEN MERIDIONAL AND AXIAL PLANE VARIATION ALONG MEAN STREAMLINE FOR A TURBINE ROTOR OF A MERIDIONAL LENGTH OF $0.06\,m$

4.2.3.3 The geometrical description of the meanstream line

The variation of the mean streamline in the meridional plane can be represented by means of **Lame'** ovals of the general form:

$$\left(\frac{z_m + i}{j}\right)^p + \left(\frac{r + k}{l}\right)^q = 1 \tag{4.28}$$

where the radius, r represents the mean streamline in the meridional plane. The coefficients i, j, k, l are obtained from the end conditions $r_1, r_2, (dr/dz_m)_1, (dr/dz_m)_2$ at z_{m1} and z_{m2} respectively. By varying the indices p and q, a series of analytic curves satisfying these conditions can be obtained.

Equation 4.28 can be expressed in terms of the radius, r in the meridional plane as follows:

$$r = l\left[1-\left(\frac{z_m+i}{j}\right)^p\right]^{1/q} - k \tag{4.29}$$

The slope variation of the equation 4.29 can be obtained by differentiating with respect to z_m as follows:

$$\frac{dr}{dz} = -\left(\frac{p}{q}\right)\left(\frac{l}{j}\right)\left(\frac{z_m+i}{j}\right)^{p-1}\left(\frac{r+k}{l}\right)^{1-q} \tag{4.30}$$

Where: $dr/dz_m = \tan\alpha$

By definition, the radius of curvature in the general form is given by:

$$r_c = \frac{\left[1+\left(\frac{dr}{dz_m}\right)^2\right]^{3}{}^{2}}{\frac{d^2r}{dz_m{}^2}} \tag{4.31}$$

Hence, $d^2r/dz_m{}^2$ can be expressed as

$$\frac{d^2r}{dz_m{}^2} = \left(\frac{dr}{dz_m}\right)\frac{dr}{dz_m}\left[\left(\frac{p-1}{z_m+i}\right)+\left(\frac{1-q}{r+k}\right)\frac{dr}{dz_m}\right] \tag{4.32}$$

The solution of equation 4.30 depends particularly on the slopes of the two ends of the curve. The simplest case corresponds to, for example, streamlines of a radial inlet, and axial outlet of an **IFR** turbine rotor, for which the two slopes at the inlet and outlet are

$(dr/dz_m)_2 = \infty$ and $(dr/dz_m)_1 = 0$, respectively. Therefore, using these boundary conditions, the solution of the coefficients is as follows:

$$i = -z_{m2}, \quad j = z_{m2} - z_{m1}, \quad k = -r_2, \quad l = r_1 - r_2$$

The values to evaluate the coefficients above are obtained from the design values obtained by numerical optimisation.

The length of the streamline is given by:

$$L = \int_{z_{m1}}^{z_{m2}} \left(1 + \frac{d^2 r}{dz_m^{\,2}}\right)^{1/2} dz_m \tag{4.33}$$

4.2.4 Design of The Rotor Flow Channel

In the preceding sections, the factors governing the choice of the principal dimensions of the rotor were obtained. Also, it was shown how numerical optimisation techniques might be used to arrive at the best values obtainable within specified constraints. Also, the path of the mean streamline in the hub to shroud and blade-to-blade planes were defined. In this section, the design of the flow channels is considered. The final shape of the flow channels may be obtained by using a direct design approach as described hereafter.

4.2.4.1 The design approach

The number of blades has already been decided from **Sec. 4.2**, therefore, the number of channels Y can be determined. The shape of the meridional streamline in the hub to shroud, blade-to-blade planes and the values of the meridional components of the relative velocity v_m have also been determined. The aim now is to calculate channel areas normal to the mean streamline.

The flow area A_x normal to the mean streamline at any section X as shown in **Fig. 4.9** is given by the continuity relationship as:

$$A_x = \frac{\dot{m}}{Y \rho_x v_{mx}} \tag{4.34}$$

The values of $\dot{m}$, v_{mx} and Y are already determined. In order to calculate the density ρ_x of the working fluid at any section, it is necessary to know the losses as a function of the geometrical parameters of the rotor.

A. loss models and their formulation

The losses in a turbine rotor can be divided into external losses, such as windage and disc friction and internal losses, such as fluid friction, shock losses, etc. The internal losses will lead to a drop in stagnation pressure of the working fluid, and the external losses will result in producing less shaft work. The external losses do not affect the properties of the working fluid. Hence, in this section, the internal losses only will be considered.

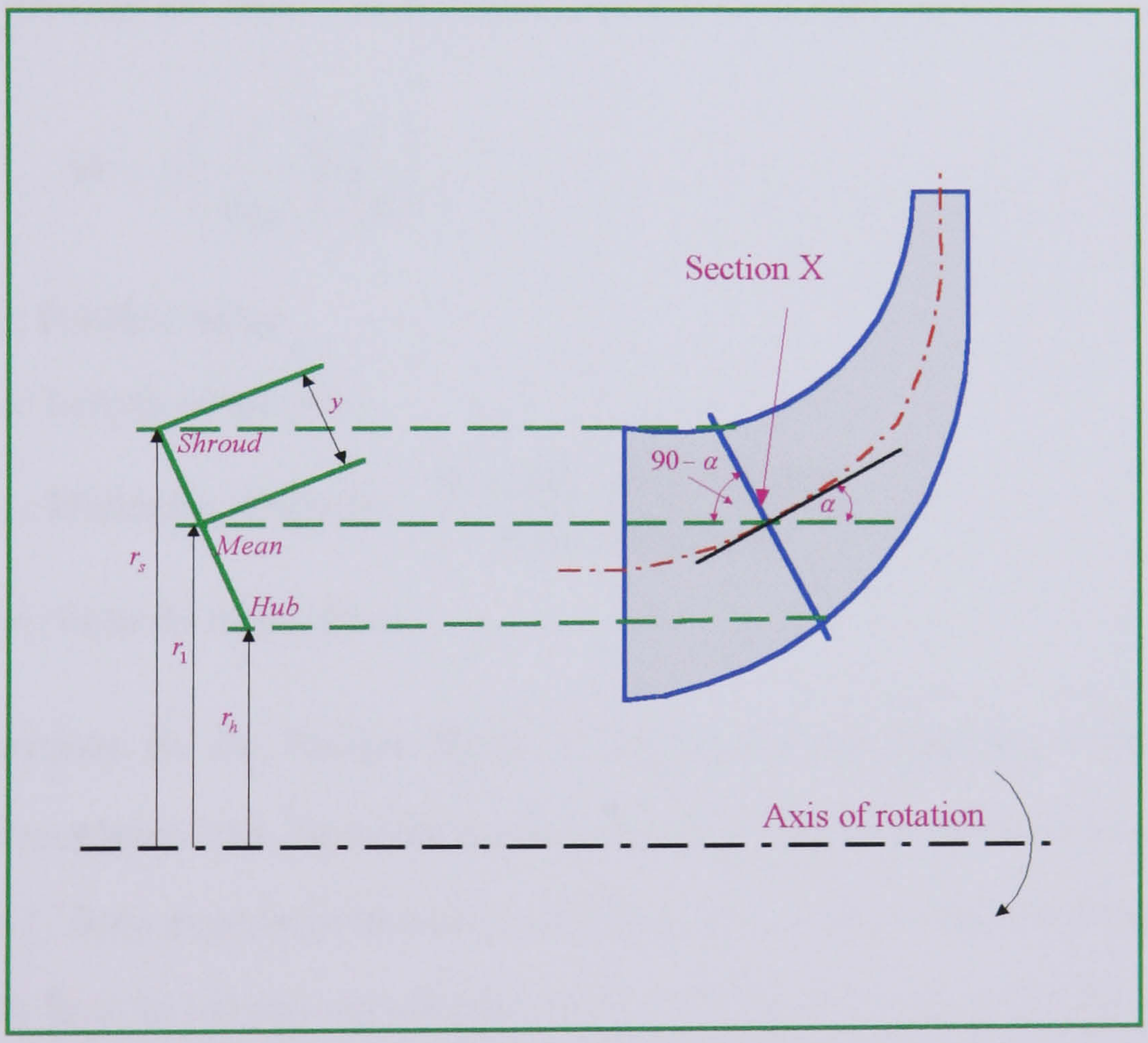

FIG. 4.9 FLOW AREA A_x AT SECTION X PERPENDICULAR TO MEAN STREAMLINE

Losses are represented here as loss coefficients related to the kinetic energy. Therefore, at any station X, losses are given by the following relation,

i.e. $$(\Delta q)_x = (\frac{\Delta h}{u^2\ 2g})_x = (\frac{1}{2}\frac{\Delta P}{\rho u^2})_x \quad (4.35)$$

The internal losses in an **IFR** turbine rotor are given as follows:

A.1 Skin friction losses

These losses are due to the shear force exerted on the working fluid in the boundary layer. The shift of the flow in the rotor from radial to axial direction, and similar shift from the inlet to the outlet in the blade-to-blade plane make an accurate estimation of the friction effects in the rotor passage extremely difficult and sometimes doubtful. Different loss models were derived by **Balje [62]** and **Johnston [63]** and on the basis of the results available in the published literature, it is difficult to choose one method in preference to another. For the design proposed in the current work, a simple friction model was used for the sake of convenience, described in equation 4.36:

$$\Delta h = f_c\left(\frac{l}{d_{hydr}}\right)\left(\frac{v^2}{2g}\right) \quad (4.36)$$

Where f_c : Friction factor

l : Length of the pipe

h_{hyd} : Hydraulic diameter $= \dfrac{4 \times \text{cross - sectional area}}{\text{wetted perimeter}}$

v : Velocity of the flow

Many expressions for the friction factor f_c reported in the literature define it as a function of roughness and Reynolds number R_e only. **Ito [64]** deduced an empirical formula for f_c from experimental results and backed by some theoretical consideration for turbulent flow in smooth curved pipe. This formula seems to define the influence of the curvature upon the resistance with satisfactory accuracy. Equation 4.37 derived from **Ito's** experimental results describes f_c as a function of R_e and curvature parameter:

$$f_c = \frac{(0.029) + 0.304\left[R_e\left(\frac{b_{av}}{r_c}\right)^2\right]^{-\frac{1}{4}}}{\left(\frac{r_c}{b_{av}}\right)^{\frac{1}{2}}} \tag{4.37}$$

Where: r_c : Radius of curvature

b_{av} : Average passage blade height is assumed constant and is taken as the average between blade inlet and outlet and is given by the relation:

$$b_{av} = 0.25\left[b_2 + \left(\frac{d_e - d_h}{2}\right)\right]$$

R_e : Reynolds number and is given as: $R_e = \frac{2b_{av}\mathrm{v}}{\nu}$

ν : Kinematic viscosity (μ/ρ)

The application of equation 4.37 provides good agreement with the experimental results in the range of $R_e(b_{av}/r_c)^2 \leq 300$. Similar formula was proposed for calculating f_c for turbulent flow with R_e higher than 300, this is given by the equation:

$$f_c = 0.136\,(R_e)^{-1}{}_4\left[R_e\left(\frac{b_{av}}{r_c}\right)^2\right]^{\frac{1}{20}} \tag{4.38}$$

Where: $f_s = 0.136\,(R_e)^{-1}{}_4$ Blasius law, **Walshaw and Jobson [65]**

Dallenbach *et al* [44] calculated the friction losses based on equation 4.36 and suggested the use of an empirical constant. The value of this constant was 1.4. Therefore, equation 4.36 becomes:

$$\Delta h = (1.4)(f_c)\left(\frac{\Delta l}{d_{hydr}}\right)\left(\frac{v^2}{2g}\right) \tag{4.39}$$

Substituting equation 4.38 into 4.39 would give:

$$\Delta h = (1.4)(0.316)\left[(R_e)^{-\frac{1}{4}} \left\{ R_e \left(\frac{b_{av}}{r_c} \right)^2 \right\}^{\frac{1}{20}} \right] \left(\frac{\Delta l}{d_{hydr}} \right) \left(\frac{v^2}{2g} \right) \tag{4.40}$$

Using **Balje [62]** notation, and making the losses dimensionless by dividing equation 4.40 by the $u^2/2g$, equation 4.40 at any section X can be developed into:

$$\boxed{\left(\frac{\Delta h}{u^2/2g} \right)_x = \left[(\Delta q)_{SFL} \right]_x = (0.4424) \left[(R_e)^{-\frac{1}{4}} \left\{ R_e \left(\frac{b_{av}}{r_c} \right)^2 \right\}^{\frac{1}{20}} \right]_x \left(\frac{\Delta l}{d_{hydr}} \right)_x \left(\frac{v^2}{u^2} \right)_x} \tag{4.41}$$

A.2 Blade loading losses

Blade loading losses occur due to recalculation produced by the pressure gradients within the flow channels from the pressure side to the section side of the blades. A model proposed by **Dallenbach *et al* [44]** for the combined diffusion and blade-loading losses at any section X of radial component is given by:

$$\boxed{(\Delta q_{DBL})_x = 1 - \left(\frac{v_x}{v_2} \right) \left[1 + \left(\frac{\pi d \sin \beta}{2 \Delta l_x} \right)_x \right] + \left(\frac{\pi du}{2 \Delta l v_2} \right)_x} \tag{4.42}$$

A.3 Incidence loss

The incidence loss refer to any work in turning the working fluid from its direction of approach to the rotor to the direction required by the blade passage. It can be argued that since incidence is a mechanism, which creates passage disturbances. A large part of the incidence loss is, in fact, a passage loss. Whether such argument assists or hinders the process of turbine performance modelling is debatable.

A.4 Shock losses

These losses are due to shock waves in supersonic flow, but, since the relative flow in **IFR** turbine rotor is generally subsonic almost everywhere. Therefore, the shock losses can be justifiably ignored.

B. Density expression

The density of the working fluid changes as it proceeds from the inlet to the outlet of the **IFR** rotor and its value at any section X, ρ_x can be calculated from the following relationship:

$$\rho_x = \left(1 - \frac{v_x^{\,2}}{2C_pT_x}\right)^{1/\gamma-1}\left(\frac{P_x}{RT_x}\right) \tag{4.43}$$

Where T_x, P_x and v_x are local values of stagnation temperature, stagnation pressure and relative velocity.

B.1 Temperature expression at any section inside the passage (T_x)

Using **Euler** equation between inlet and exit condition of a turbine rotor

$$H_i - H_e = (c_{wi}u_i) - (c_{we}u_e) \tag{4.44}$$

Equation 4.44 can be expressed between inlet and any section X inside the rotor passage as:

$$H_i - H_x = (c_{wi}u_i) - (c_{wx}u_x) \tag{4.45}$$

Equation 4.45 can be expressed in terms of static conditions as:

$$(h_i + \frac{1}{2}c_i^{\,2} - c_{wi}u_i) = (h_x + \frac{1}{2}c_x^{\,2} - c_{wx}u_x) \tag{4.46}$$

In general, the absolute flow velocity c can be written in terms of its three components as:

$$c^2 = c_w^{\,2} + c_m^{\,2} + c_z^{\,2}$$

Substituting the above expression in equation 4.46 gives:

$$h_i + \frac{1}{2}(c_{wi}^{\,2} + c_{mi}^{\,2} + c_{zi}^{\,2}) - c_{wi}u_i = h_x + \frac{1}{2}(c_{wx}^{\,2} + c_{mx}^{\,2} + c_{zx}^{\,2}) - c_{wx}u_x \tag{4.47}$$

Taking the **RHS** of equation 4.47, adding and subtracting $u_x^2/2$ results:

$$\textbf{RHS} = h_x + \frac{1}{2}\left[(u_x - c_{wx})^2 + (c_{mx}^2 + c_{zx}^2 - u_x^2)\right] \tag{4.48}$$

From the velocity vector diagram at any section X

$$\bar{v}_x = \bar{u}_x - \bar{c}_x$$

Where:

$$\bar{v}_{wx} = \bar{u}_x - \bar{c}_{wx}, \quad \bar{v}_{mx} = 0 - \bar{c}_{mx}, \quad \bar{v}_{zx} = 0 - \bar{c}_{zx}$$

Substituting for $u_x - c_{wx}$, c_{mx}, c_{zx} in equation 4.48 and re-arranging, resulted into:

$$\textbf{RHS} = h_x + \frac{1}{2}(v_x^2 - u_x^2) \tag{4.49}$$

Applying the same procedure to the **LHS** of equation 4.47, yield to:

$$\textbf{LHS} = h_i + \frac{1}{2}(v_i^2 - u_i^2) \tag{4.50}$$

Equation 4.46 can be expressed in the form using equations 4.49 and 4.50 as:

$$h_i + \frac{1}{2}(v_i^2 - u_i^2) = h_x + \frac{1}{2}(v_x^2 - u_x^2) \tag{4.51}$$

From velocity triangle, it can be seen that:

$$c_{mx}^2 = c_x^2 - c_{wx}^2$$

and $$v_{mx}^2 = v_x^2 - v_{wx}^2$$

Since $$c_{mx} = v_{mx}$$

Hence $$(c_x^2 - c_{wx}^2) = (v_x^2 - v_{wx}^2) = v_x^2 - (u_x - c_{wx})^2 \tag{4.52}$$

Re-arranging equation 4.52 will give:

$$c_x^2 = v_x^2 + 2c_{wx}u_x - u_x^2 \tag{4.53}$$

At inlet condition, equation 4.53 becomes:

$$c_i^2 = v_i^2 + 2c_{wi}u_x - u_i^2 \tag{4.54}$$

By definition, the total enthalpy is given by:

$$H = h + \frac{1}{2}c^2$$

Then, at inlet condition

$$h_i = H_i - \frac{1}{2}c_i^{\,2} = H_i - \frac{1}{2}(v_i^{\,2} + 2c_{wi}u_i - u_i^{\,2})$$

$$h_i = H_i - c_{wi} + \frac{1}{2}(v_i^{\,2} - u_i^{\,2}) \qquad (4.55)$$

Substituting for h_i from equation 4.55 in equation 4.51 and re-arranging would give:

$$h_x = H_i - c_{wi}u_i - \frac{1}{2}(v_x^{\,2} - u_x^{\,2}) \qquad (4.56)$$

Dividing by H_i and re-arranging equation 4.56 results:

$$\frac{h_x + \frac{1}{2}v_x^{\,2}}{H_i} = 1 - \left(\frac{c_{wi}u_i}{H_i}\right) + \frac{1}{2}\left(\frac{u_x^{\,2}}{H_i}\right) \qquad (4.57)$$

Assuming the working fluid to behave as a perfect gas and from the definition of $H = C_p T$. Then equation 4.57 becomes:

$$\boxed{\frac{T_x}{T_i} = 1 + \frac{1}{2}\left(\frac{u_x^{\,2} - 2c_{wi}u_i}{C_p T_i}\right)} \qquad \textbf{(4.58)}$$

Using equation 4.58, the stagnation temperature at any section X inside the rotor passage can be calculated, provided that inlet conditions and the blade velocity $u_x = \pi d_x N/60$ are already known or calculated.

B.2 Pressure expression at any section inside the passage (P_x)

The stagnation pressure between each step is initially assumed to vary isentropically. subsequently, the drop in pressure due to the internal losses is calculated using the loss models discussed previously and then subtracted from the isentropic pressure.

Hence, it can be written the actual stagnation pressure P_x at any step J is given by:

$$\boxed{[P_x]_J = [P_{xs}]_J - [\Delta P_x]_{J-1}^{J}} \tag{4.59}$$

C. Flow channel area, shroud and hub contours at any section X inside the rotor passage A_x

C.1 Flow channel area at any section inside the passage (A_x)

The flow is normal to the mean streamline, hence, the hub and shroud contours can now be calculated as follows:

From **Fig. 4.10**, it can be written

$$\sin(90-\alpha) = \frac{r_s - r_{rms}}{y} \quad \text{or} \quad y = (r_s - r_{rms})/\cos\alpha \tag{4.60}$$

The area of the cone generated by the rotation of the line y around the axis of rotation could be written in general as:

$$A_x = \pi\, y(r_s + r_{rms}) \tag{4.61}$$

Substituting equation 4.61 in equation 4.60 results:

$$\boxed{A_x = \frac{\pi(r_s^{\,2} - r_{rms}^{\,2})}{\cos\alpha}} \tag{4.62}$$

From continuity equation:

$$\boxed{A_x = \frac{1}{2}\frac{\dot{m}}{\rho_x v_m B_f}} \tag{4.63}$$

Either equation 4.62 or 4.63 can be used to calculate the flow area channel.

C.2 Shroud contours at any section inside the passage (r_s)

Equating equation 4.62 and 4.63, the radius of the shroud contour at any section X can be expressed as:

$$r_{sx} = \sqrt{(r_{rms}{}^2)_x + \frac{1}{2}\frac{\dot{m}\cos\alpha_x}{\pi\,\rho_x v_{mx} B_f}} \qquad \textbf{(4.64)}$$

C.3 Hub contours at any section inside the passage (r_h)

By definition:

$$r = r_{rms} = \sqrt{\frac{r_s{}^2 + r_h{}^2}{2}}$$

From which r_{hx} at any section X can be calculated as:

$$r_{hx} = \sqrt{(2r_{rms}{}^2)_x - r_{sx}{}^2} \qquad \textbf{(4.65)}$$

4.2.5 Rotor model and Optimisation of Meridional Length

A computer programme was written to optimise the meridional length for minimum losses and to calculate hub and shroud contours. The output results are presented in **Fig. 4.11**, which provides a plot of total stagnation pressure loss inside the passage vs. meridional length of the **IFR** turbine rotor. It showed that the optimum meridional length was found to be equal to $40.0\,mm$ for minimum pressure loss in the passage.

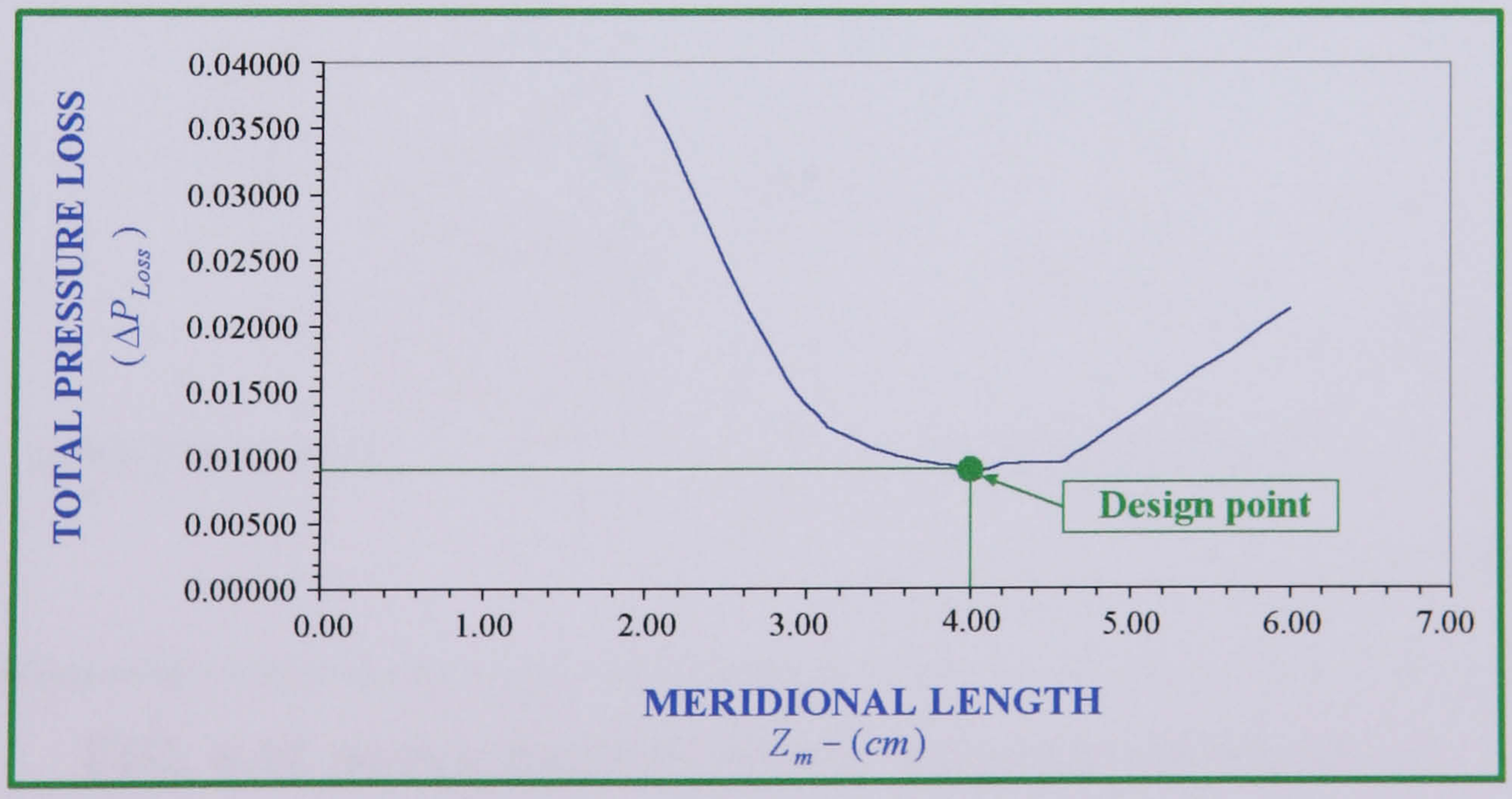

FIG. 4.11 TOTAL PRESSURE LOSS VS. MERIDIONAL LENGTH

Figure 4.12 shows the detailed drawings of the turbine rotor

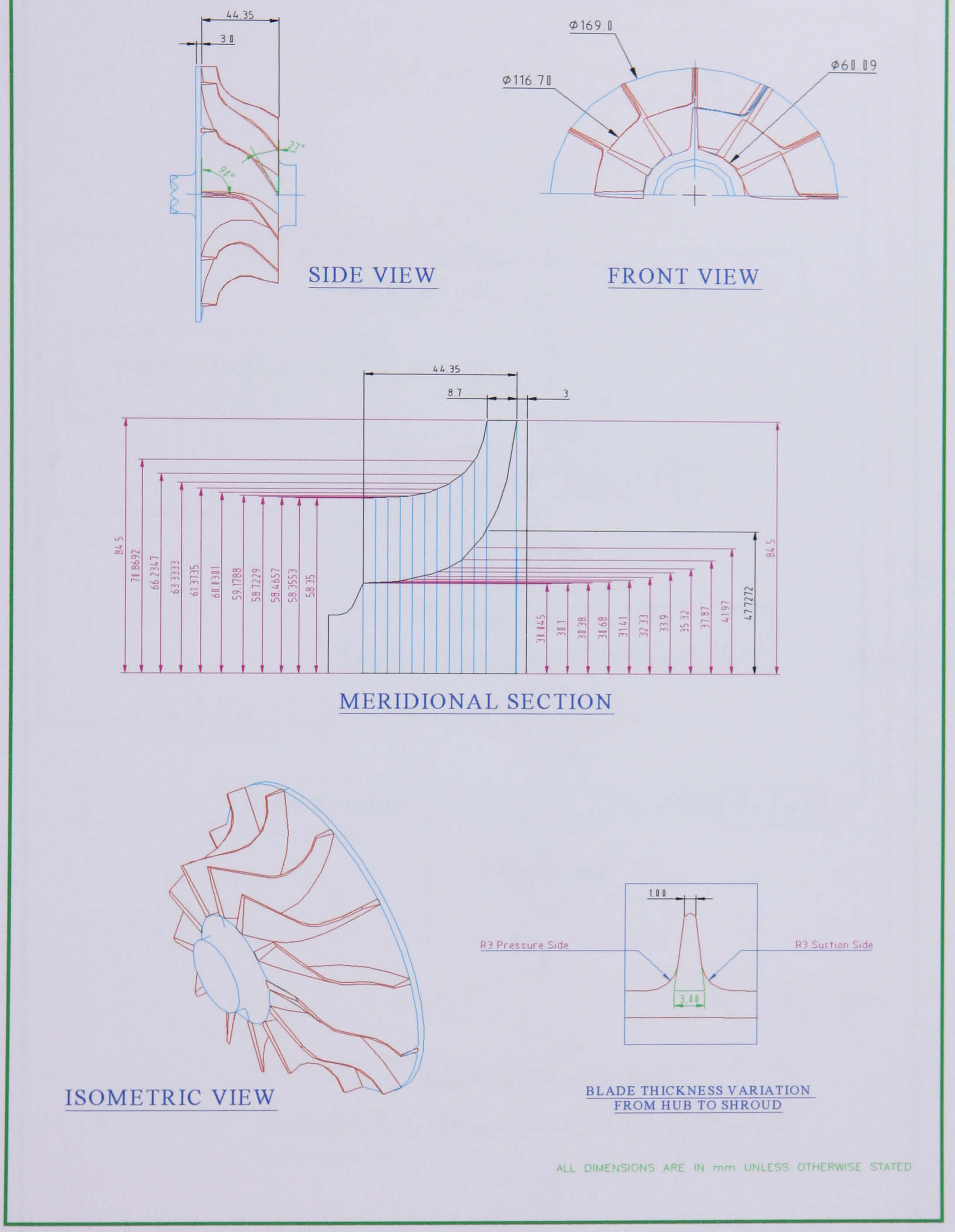

FIG. 4.12 DETAIL DRAWING OF THE DESIGNED TURBINE ROTOR

The flow chart given in **Fig. 4.13** shows the sequence of operation based on the written computer programme aforementioned.

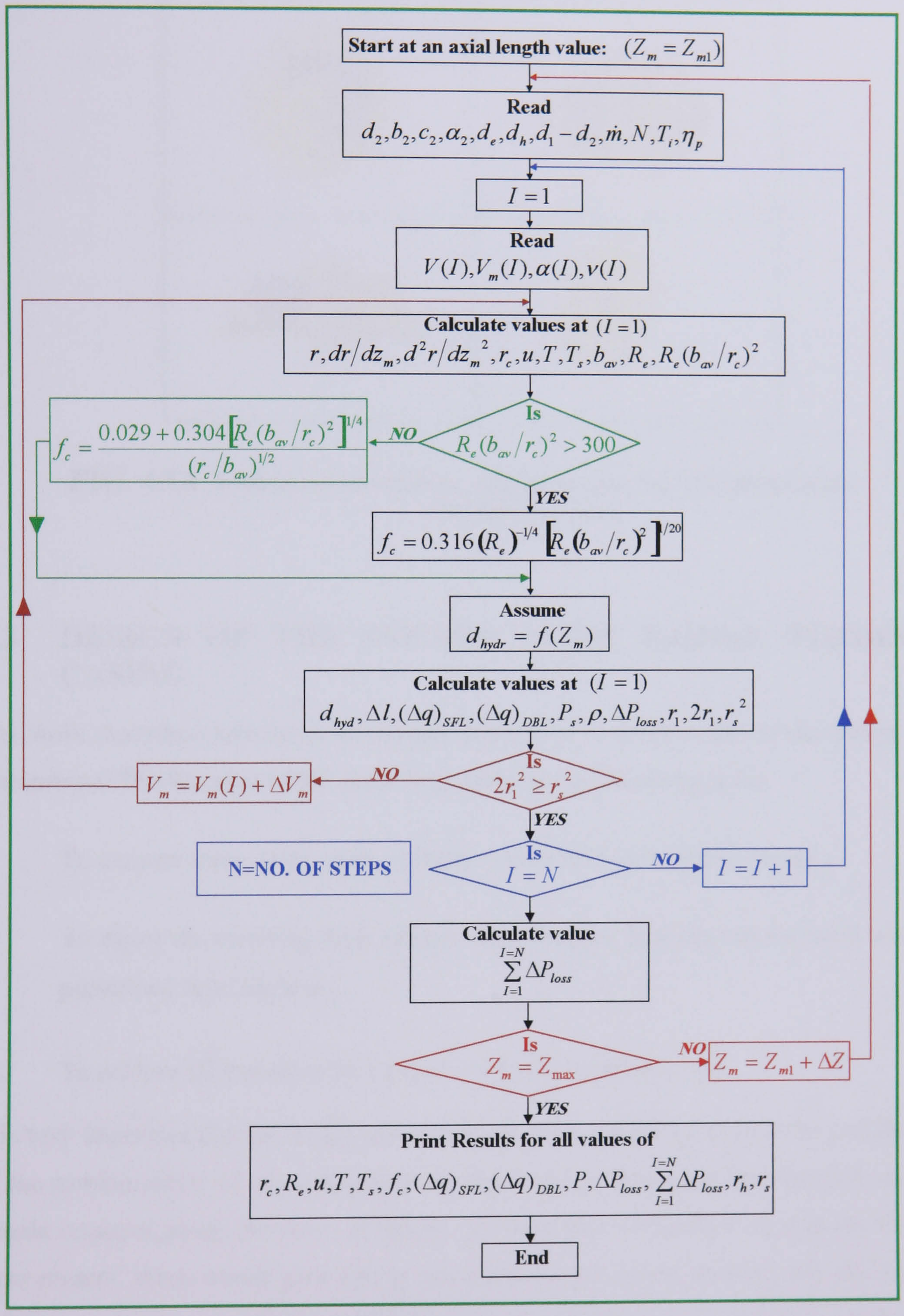

FIG. 4.13 FLOW CHART FOR THE OPTIMISATION OF THE MERIDIONAL LENGTH AND THE DESIGN OF THE FLOW PASSAGE

The final design representation of the **IFR** turbine rotor as s three-dimensional solid model is shown in **Fig. 4.14**.

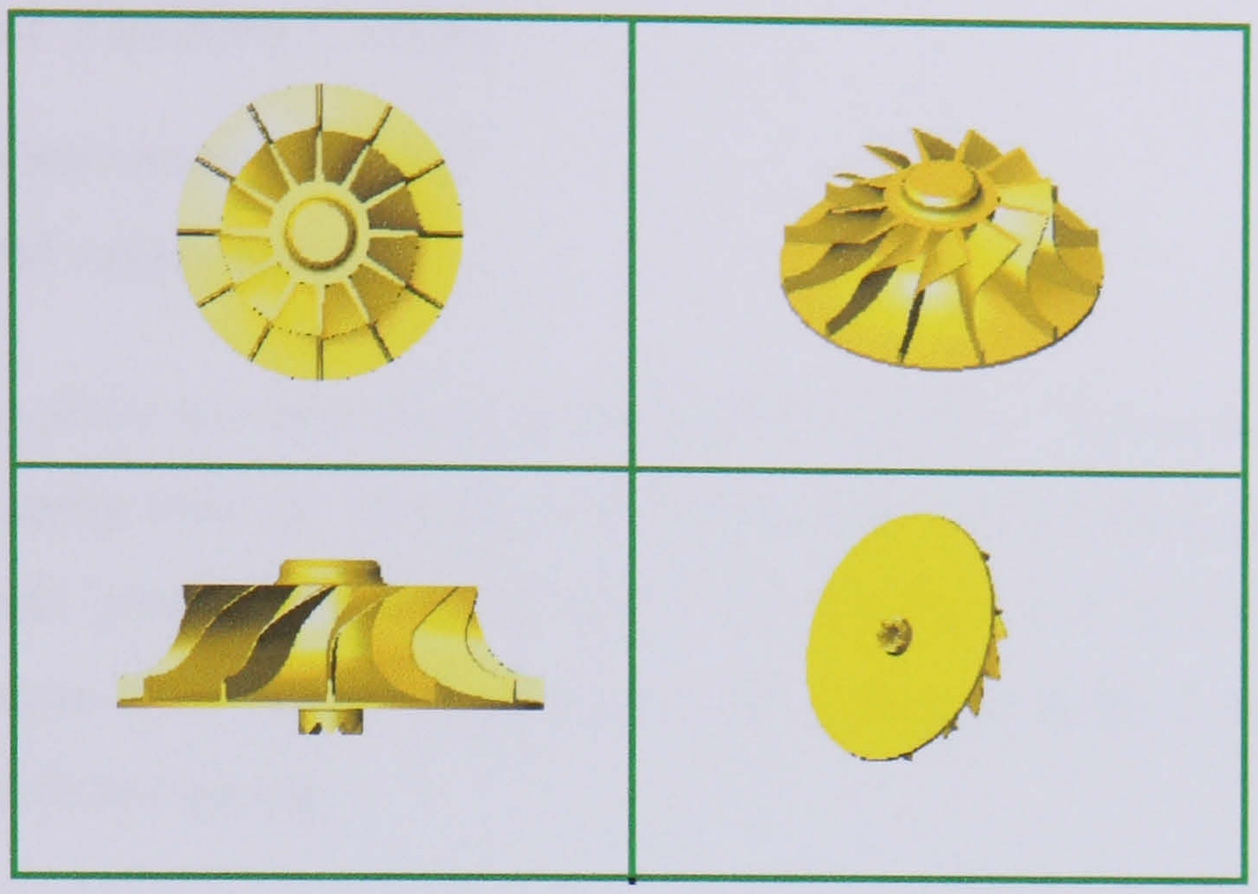

FIG. 4.14 THREE DIMENSIONAL SOLID MODEL OF THE DESIGNED TURBINE ROTOR

4.3 DESIGN OF THE INWARD FLOW RADIAL TURBINE CASING

The work described here form an integral part of the research work on the design of **IFR** turbine. The function of the stator is to perform the following tasks:

i. To convert some of the static enthalpy of the flow into kinetic energy.

ii. To direct the resulting high velocity fluid streams into the turbine rotor at the prescribed flow angle α_2.

iii. To achieve **(i)** and **(ii)** with a minimum loss of total pressure.

It is very important that the casing gives uniform flow conditions around the periphery of the turbine rotor, i.e. the magnitude of the velocity vector and the direction must remain constant along the rotor periphery. If variations of the flow around the rotor were present, these would give rise to non-uniform mass flux entering into the rotor and the varying magnitude of tangential velocity component. As the torque is produced by the change in angular momentum of the fluid, variations of torque around the rotor

would occur, thus causing non-uniformity of pressure distribution and hence rotor blade vibration.

4.3.1 Types of Turbine Casing

i. The plenum chamber stator

ii. The spiral volute stator

The spiral volute stator incorporates nozzles or be nozzle-less. The main advantages of the nozzle-less casing over the nozzled type can because it is cheaper and the nozzle-less casing permits greater flexibility to the flow and allows it to adjust it self over a wider range of mass flow rates. Therefore, for the present research, it was decided to use a nozzle-less volute casing.

4.3.2 The Design of Nozzle-Less Casing

4.3.2.1 Introduction

The flow in the nozzle-less volute casing is complex and not readily amenable to a simple analytical model. However, despite this difficulty, it may be interesting to note that turbines, which were designed by using relatively simple approaches, are known to have produced very good performance.

4.3.2.2 Basic design requirements

i. Accelerate the working fluid to the leading edge of the rotor and generate the desired rotor inlet conditions in terms of the magnitude and direction of the absolute velocity vector.

ii. Distribute the working fluid uniformly around the rotor periphery.

iii. Achieve these requirements as efficiently as possible that is with minimum loss in stagnation pressure.

The required inlet conditions must be derived from the desired turbine performance, e.g. the desired power output. The nozzle-less volute must be designed to provide these

rotor inlet conditions. The preliminary design of the volute is often based on the assumptions of an adiabatic flow, together with a free vortex distribution about the rotor.

4.3.2.3 Design assumptions

i. Steady one-dimensional isentropic flow, constant angular momentum, energy and conservation of mass along the volute length.

ii. Vortex motion is fully established before the commencement of any outer flow from the volute in the radial direction. This is a necessary condition for the flow angles α_2 and β_2 to be independent of the azimuth angle and the flow into the rotor to be uniform.

iii. The flow near the outer wall profile is assumed to follow the same contour as the outer profile of the casing, the boundary layer thickness being negligible.

A diagrammatic sketch of an **IFR** turbine fitted with a nozzle-less casing is shown in **Fig. 4.15**.

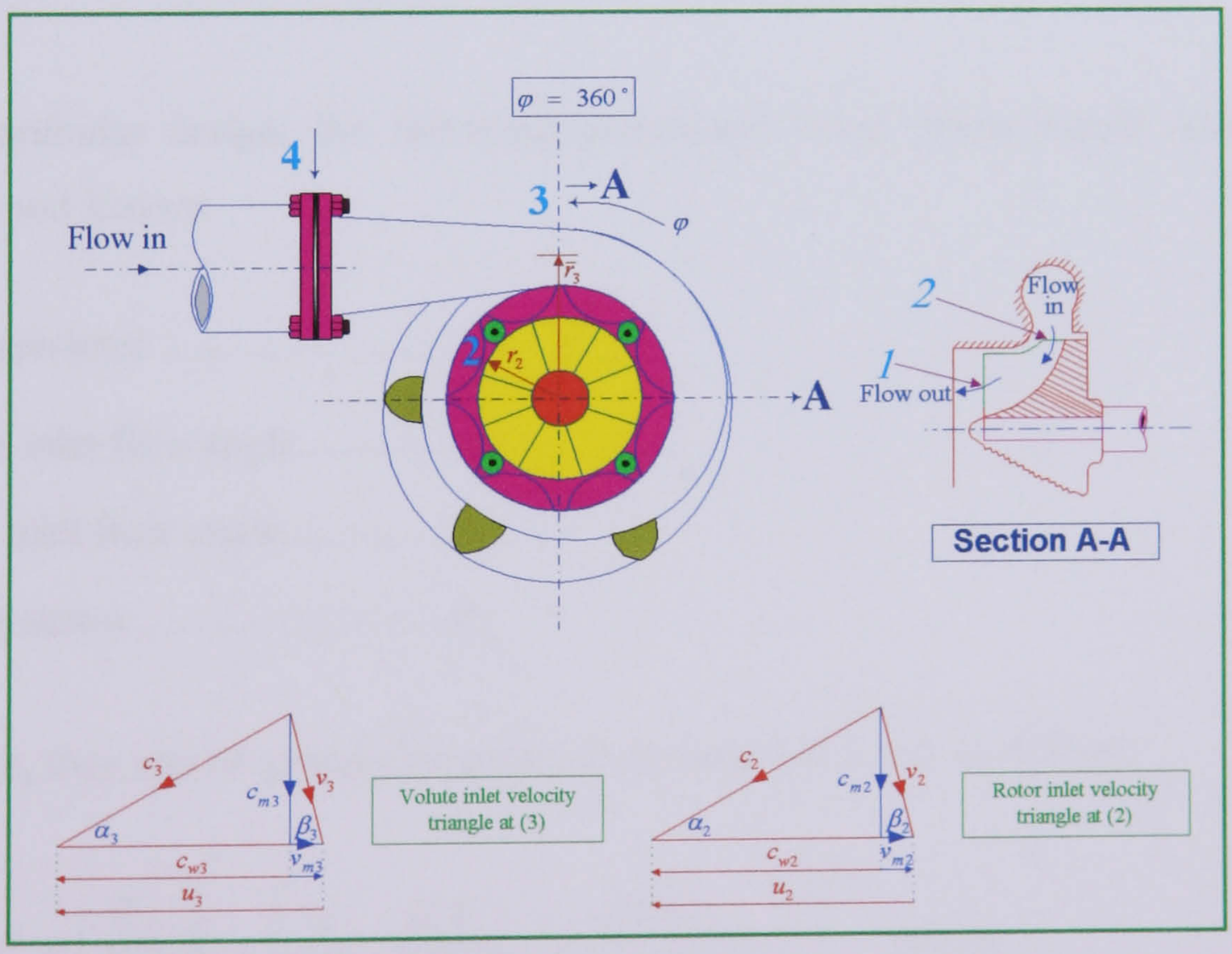

FIG. 4.15 INWARD RADIAL TURBINE FITTED WITH A SINGLE NOZZLE-LESS VOLUTE CASING

4.3.2.4 Design calculations

The actual design calculation of the volute geometry is based on equation 3.113 derived in **Chapter 3** and on the following design data given in **Table 4.4**

SPECIFICATIONS	RATING
Design volute inlet stagnation temperature, T_{03}	1000 K
Design volute inlet Mach number, M_3	0.54
Design volute inlet absolute flow angle, α_3	15°
Design volute discharge stagnation temperature, T_{02} (rotor inlet design condition)	1000 K
Design volute discharge Mach number, M_2	0.95
Design volute discharge absolute flow angle, α_2	17°
Design relative flow angle at rotor inlet, β_2	85°
Design speed parameter, $d_2N/\sqrt{C_pT_{03}}$	0.157
Rotor inlet blade width, b_2	0.87 cm
Rotor inlet tip diameter, d_2	16.9 cm
Blockage factor at rotor inlet, B_{f_2}	0.93

TABLE 4.4 DESIGN VALUES FOR NOZZLE-LESS VOLUTE CASING

For a particular design, the following parameters listed below would normally be constant and known

Speed parameter ..... $d_2N/\sqrt{C_pT_i}$

Absolute inlet flow angle ..... α_2

Relative inlet flow angle..... β_2

Blockage factor..... B_{f_2}

Therefore, they can be grouped together from equation 3.113 as follows:

$$F_1 = \left(\frac{B_{f_2}}{360}\right)\left[1-\left(\frac{\pi}{\sqrt{2}}\cdot\frac{d_2N}{\sqrt{C_pT_i}}\cdot\frac{\sin\beta_2}{\sin(\alpha_2+\beta)_2}\right)^2\right]^{1/\gamma-1}(\tan\alpha_2) \qquad (4.66)$$

and,

$$F_2 = \left[\left(\frac{\pi}{\sqrt{2}} \cdot \frac{d_2 N}{\sqrt{C_p T_i}} \cdot \frac{\sin\beta_2 \cos\alpha_2}{\sin(\alpha_2+\beta)_2}\right)\right]^2 \tag{4.67}$$

Substituting the expressions F_1 and F_2 into equation 3.113 from **Chapter 3** would give an area ratio at any azimuth angle as:

$$\frac{A_\varphi}{A_2} = \varphi\left(\frac{\bar{r}_\varphi}{r_2}\right)\left[\frac{F_1}{\left(1-\frac{F_2}{(\bar{r}_\varphi/r_2)^2}\right)^{1/\gamma-1}}\right] = \left[\frac{\varphi \cdot F_1\left(\frac{\bar{r}_\varphi}{r_2}\right)}{\left(\frac{\bar{r}_\varphi}{r_2}\right)^{-2/\gamma-1}\left\{\left(\frac{\bar{r}_\varphi}{r_2}\right)^2 - F_2\right\}^{1/\gamma-1}}\right] \tag{4.68}$$

Re-arranging equation 4.68 resulted into

$$\boxed{\frac{A_\varphi}{A_2} = \frac{\left[(\varphi \cdot F_1)\left(\frac{r_\varphi}{r_2}\right)^{\frac{\gamma+1}{\gamma-1}}\right]}{\left[\left(\frac{\bar{r}_\varphi}{r_2}\right)^2 - F_2\right]^{1/\gamma-1}}} \tag{4.69}$$

Similarly, substituting the expressions F_1 and F_2 into equation 3.115 would give an area to radius ratio at any azimuth angle as shown below:

$$\boxed{\frac{A_\varphi}{\bar{r}_\varphi} = \left[\frac{\varphi \cdot F_1\left(\frac{A_2}{r_2}\right)}{\left(\frac{\bar{r}_\varphi}{r_2}\right)^{-2/\gamma-1}\left\{\left(\frac{\bar{r}_\varphi}{r_2}\right)^2 - F_2\right\}^{1/\gamma-1}}\right]} \tag{4.70}$$

In general, the solution of equation 4.69 is based on the graphical representation as shown in **Fig. 4.13**. The choice of $(\bar{r}_\varphi/r_2)_{\min}$ and $(\bar{r}_\varphi/r_2)_{\max}$ would normally dictated

by the tip diameter of the rotor and the allowable overall dimensions of the volute casing. In the current work, the design values of $(\bar{r}_\varphi / r_2)_{\min}$ and $(\bar{r}_\varphi / r_2)_{\max}$ were chosen to be 1.013 and 1.668, respectively.

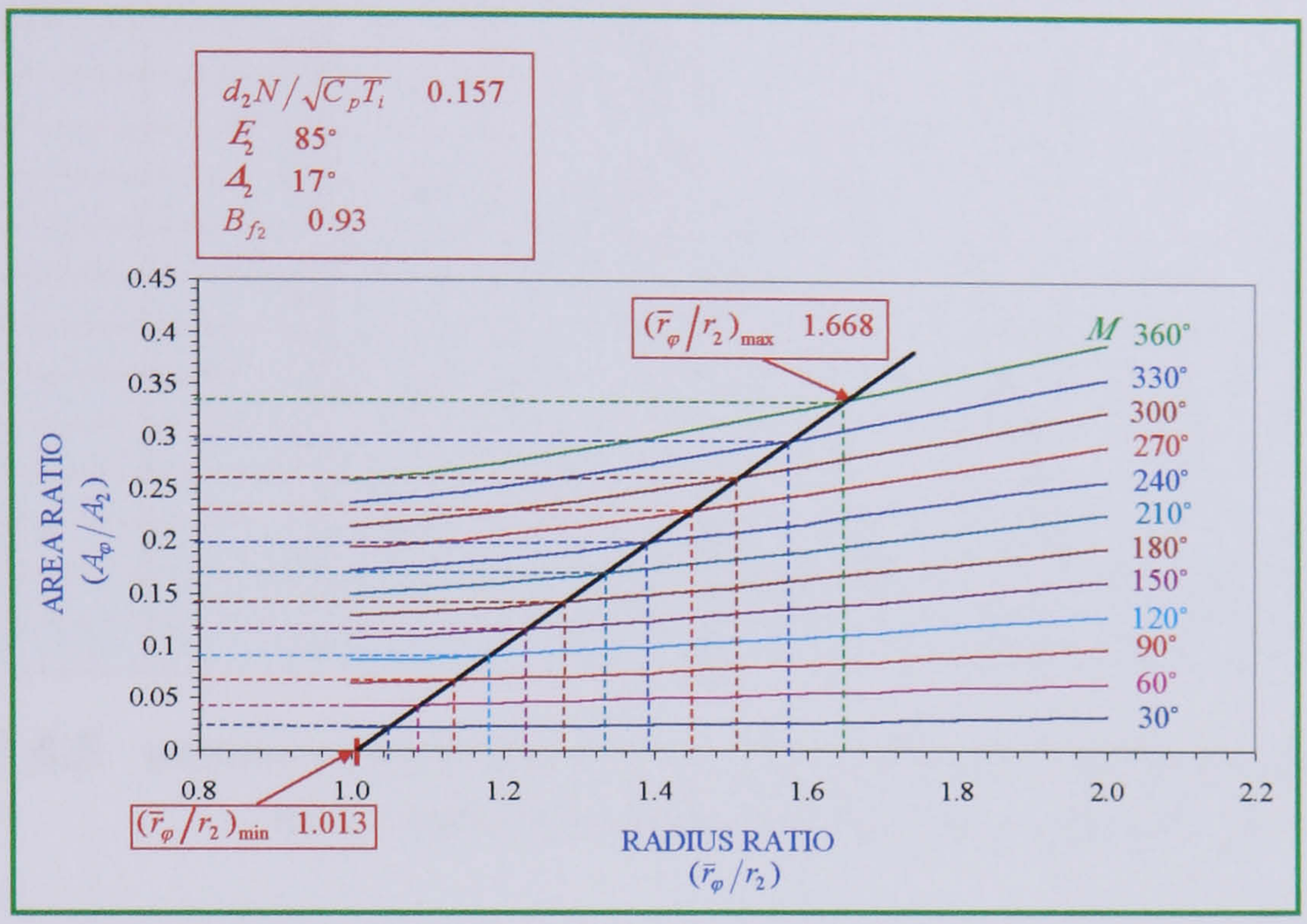

FIG. 4.13 DESIGN GRAPH SHOWING THE RELATIONSHIP BETWEEN AREA RATIO, RADIUS RATIO AND AZIMUTH ANGLE AT $(\bar{r}_\varphi / r_2)_{\max} = 1.668$

The final design results of $A_\varphi / \bar{r}_\varphi$ versus φ can be obtained from the corresponding values of A_φ / A_2 , $\bar{r}_\varphi / r_2$ and φ of **Fig. 4.13** or read directly from **Figs. 4.14**.

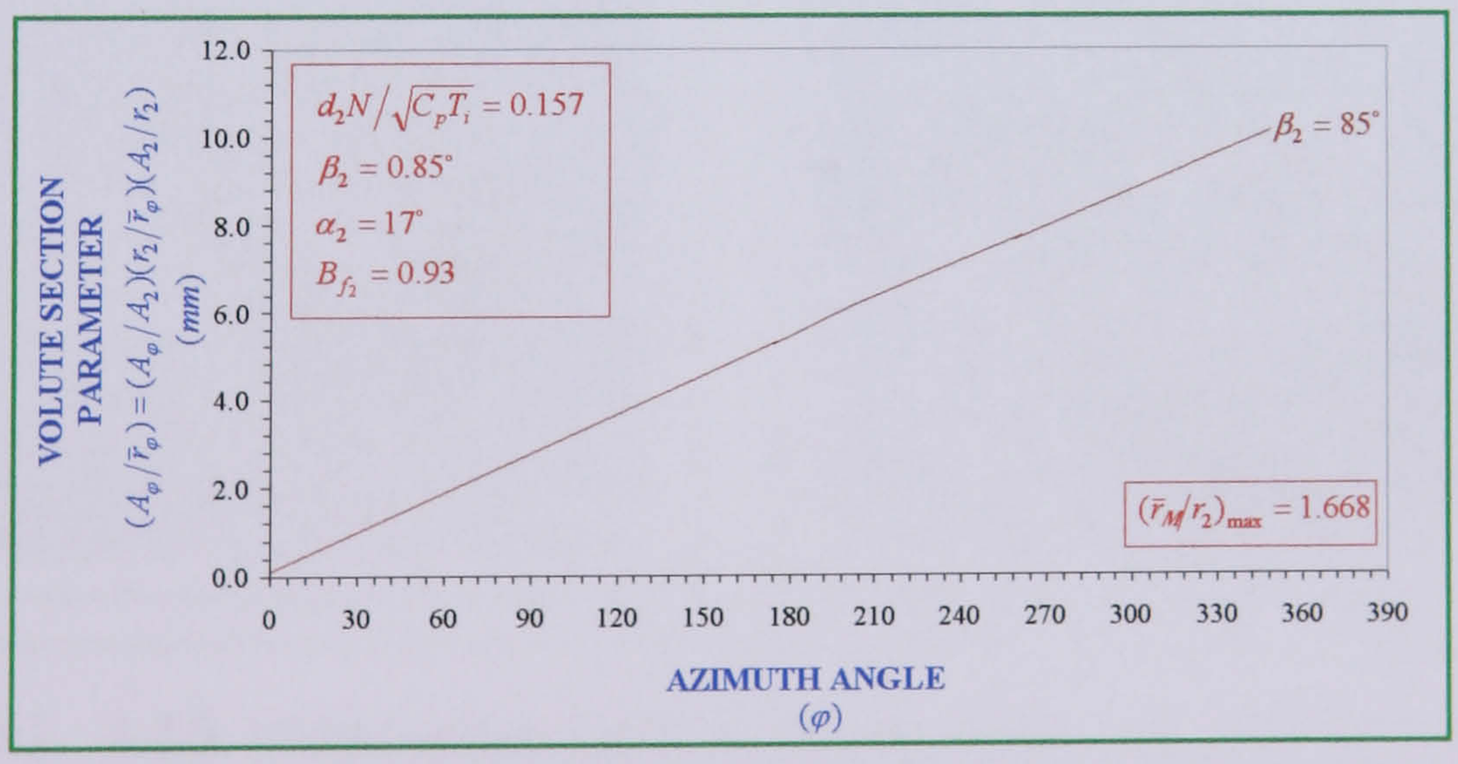

FIG. 4.14 DESIGN GRAPH FOR A SINGLE ENTRY NOZZLE-LESS VOLUTE CASING

The final design values are shown in **Table 4.5**

POSITION OF POINTS	AZIMUTH ANGLE (deg .)	RADIUS OF CENTRIOD	ELEVATION-Z (*mm*)	RADIUS OF CASING CROSS SECTION (*mm*)
1	0	85.45	-53	3.00
2	30	90.24	-51.53	4.47
3	40	94.87	-50.93	5.07
4	90	99.49	-48.23	7.77
5	120	104.10	-44.42	11.38
4	150	108.71	-40.4	15.40
7	180	113.32	-34.27	19.73
8	210	117.94	-31.47	24.29
9	240	122.55	-24.91	29.09
10	270	127.14	-21.89	34.11
11	300	131.77	-14.44	39.34
12	330	134.39	-11.14	44.84
13	340	141.00	-5.43	50.57
14	383	144.54	-5.43	50.57

TABLE 4.5 DESIGN GEOMETRICAL VALUES OF TURBINE NOZZLE-LESS CASING OF A CIRCULAR CROSS-SECTIONAL AREA FOR $\beta_2 = 85^\circ$

4.3.2.5 Turbine casing developed model

A complete three-dimensional solid model assembly of the nozzle-less casing is depicted in **Fig 4.15**.

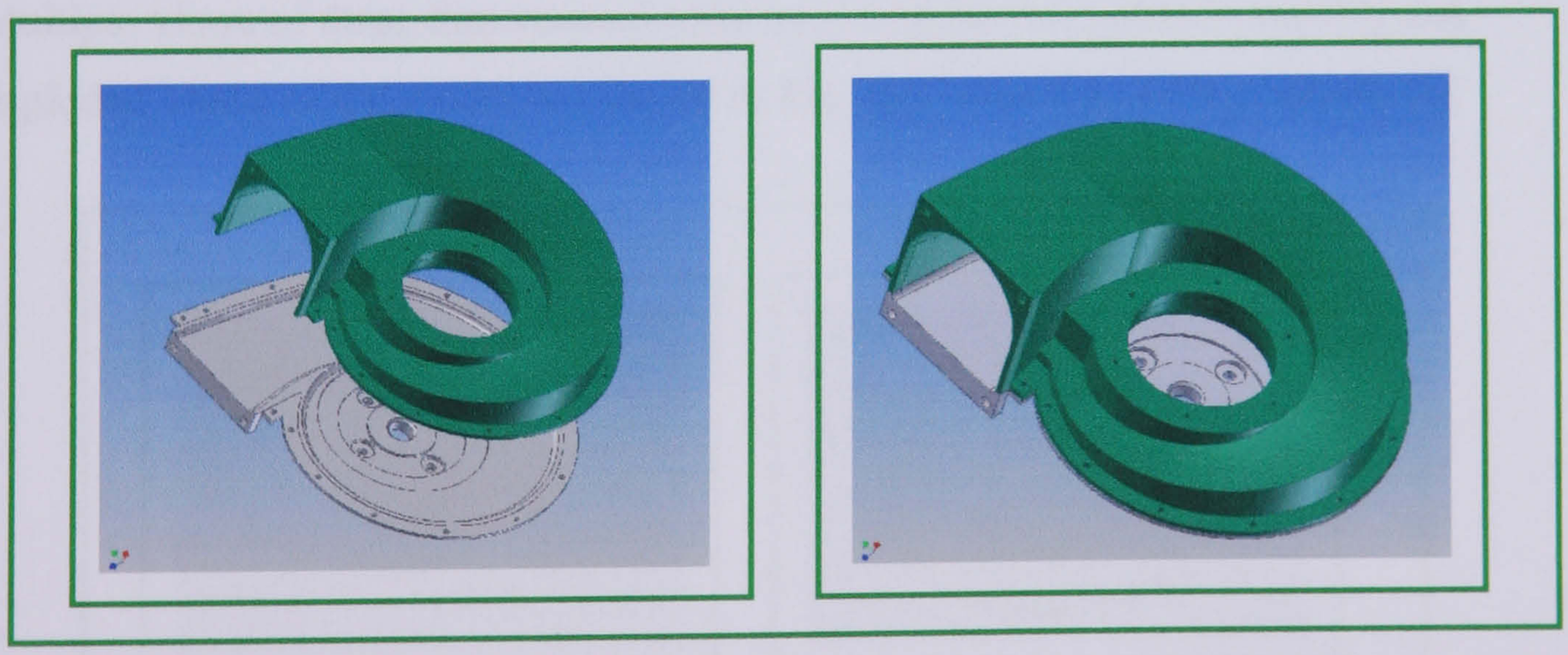

FIG. 4.15 THREE-DIMENSIONAL SOLID MODEL ASSEMBLY OF THE NOZZLE-LESS VOLUTE CASING

The final design drawing of turbine nozzle-less casing is given **Fig. 4.16**.

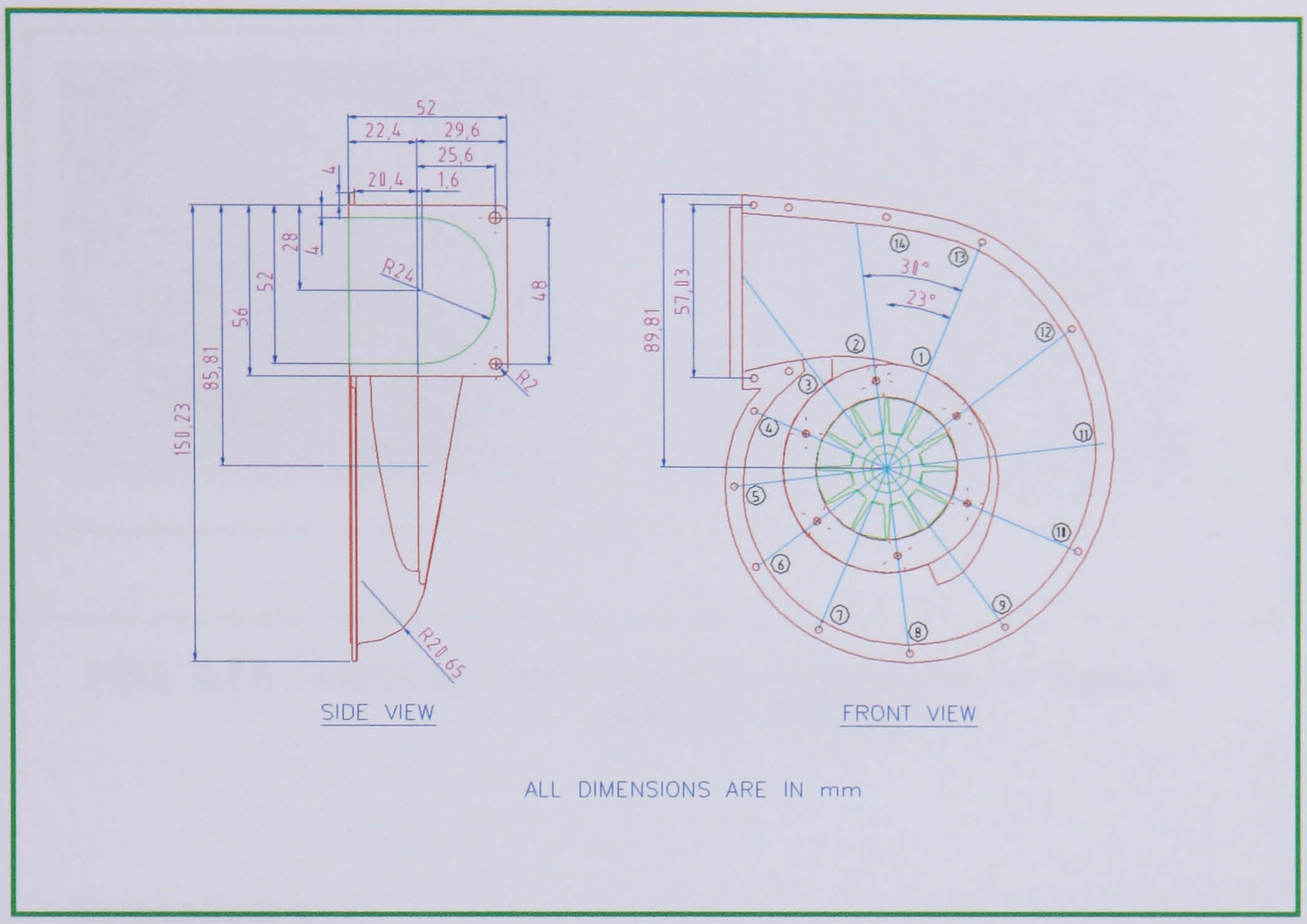

FIG. 4.16 DESIGN SCHEMATIC DRAWING OF THE OF IFR TURBINE ASSEMBLY

4.4 AN INWARD FLOW RADIAL TURBINE FINAL MODEL

Multiple views of three-dimensional solid model of the IFR turbine assembly and exploded views of the model are shown in **Fig. 4.17 and Fig. 4.18**, respectively.

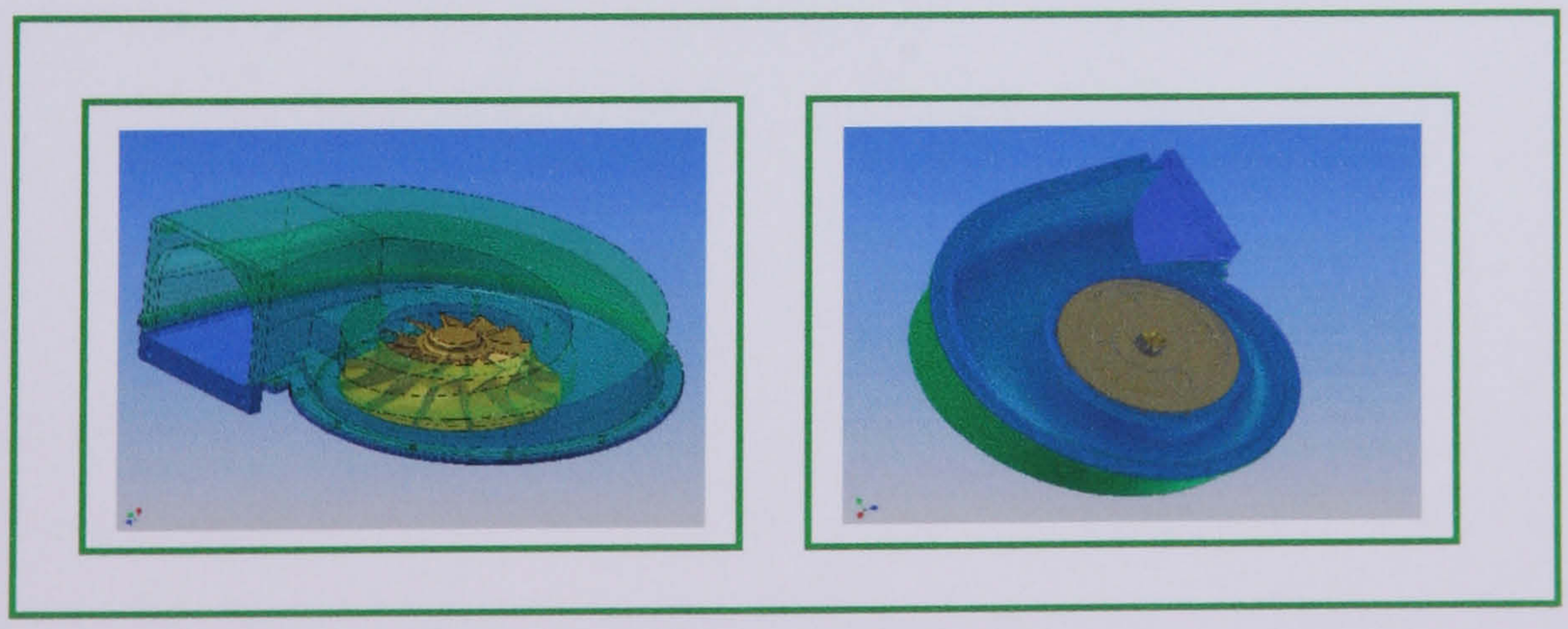

FIG. 4.17 THREE DIMENSIONAL SOLID MODEL OF THE IFR TURBINE ASSEMBLY

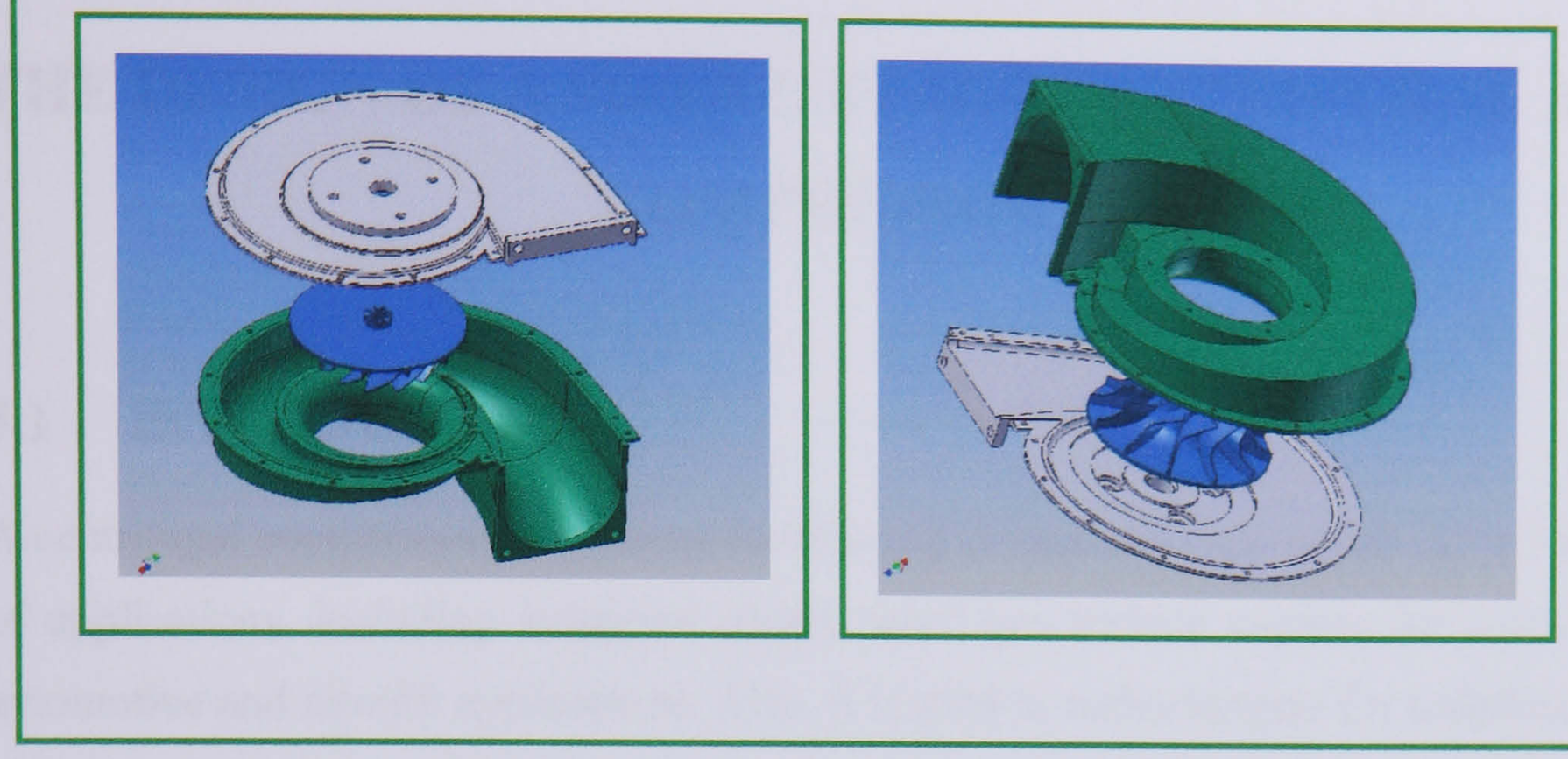

FIG. 4.18 EXPLODED VIEWS OF THE SOLID MODEL OF THE IFR TURBINE ASSEMBLY

4.5 SUMMARY

A complete design of the rotor and the casing of the **IFR** turbine, based on the design parameters evaluated in the analysis of Chapter 3 have been presented in this Chapter. Basic dimensions for the rotor and the casing have been determined using rules, equations, optimisation methods and design requirements. A complete three-dimensional model of the **IFR** turbine was developed.

CHAPTER 5

THE DESIGN OF A SINGLE STAGE CENTRIFUGAL AIR COMPRESSOR

5.1 INTRODUCTION

A centrifugal compressor is a pressure-producing device and used widely for a variety of applications, including industrial plants, small gas turbine engines for industrial, automotive and aircraft applications. Also, it is used in turbochargers for reciprocating internal combustion engines.

The air compressor occupies a position of importance in a gas turbine engine equal in every respect to that of the turbine. Since the net useful output power of the turbine engine is the difference between turbine output and compressor input, then an inefficient compressor can largely eliminate the gain from a highly efficient turbine. Furthermore, for efficient overall performance, it is essential that the turbine characteristics match those of the compressor.

The main advantages of centrifugal compressors are:

i. Simplicity and ruggedness of construction.

ii. High stage pressure ratio capability.

iii. Its ability to operate more efficiently over a wider range of mass flow rate than a comparable axial flow compressor.

iv. Wider range of stable operation between surging and choking limits at a given rotational speed.

This Chapter details the parameters employed in the current work to design the single stage centrifugal compressor associated with the turbine design of **Chapter 4**.

5.2 CENTRIFUGAL COMPRESSOR COMPONENTS

The terminology used to define the components of a centrifugal compressor is shown in **Fig. 5.1**. In general, a centrifugal compressor comprises inlet air intake, inlet guide vanes, the impeller, the diffuser and the volute.

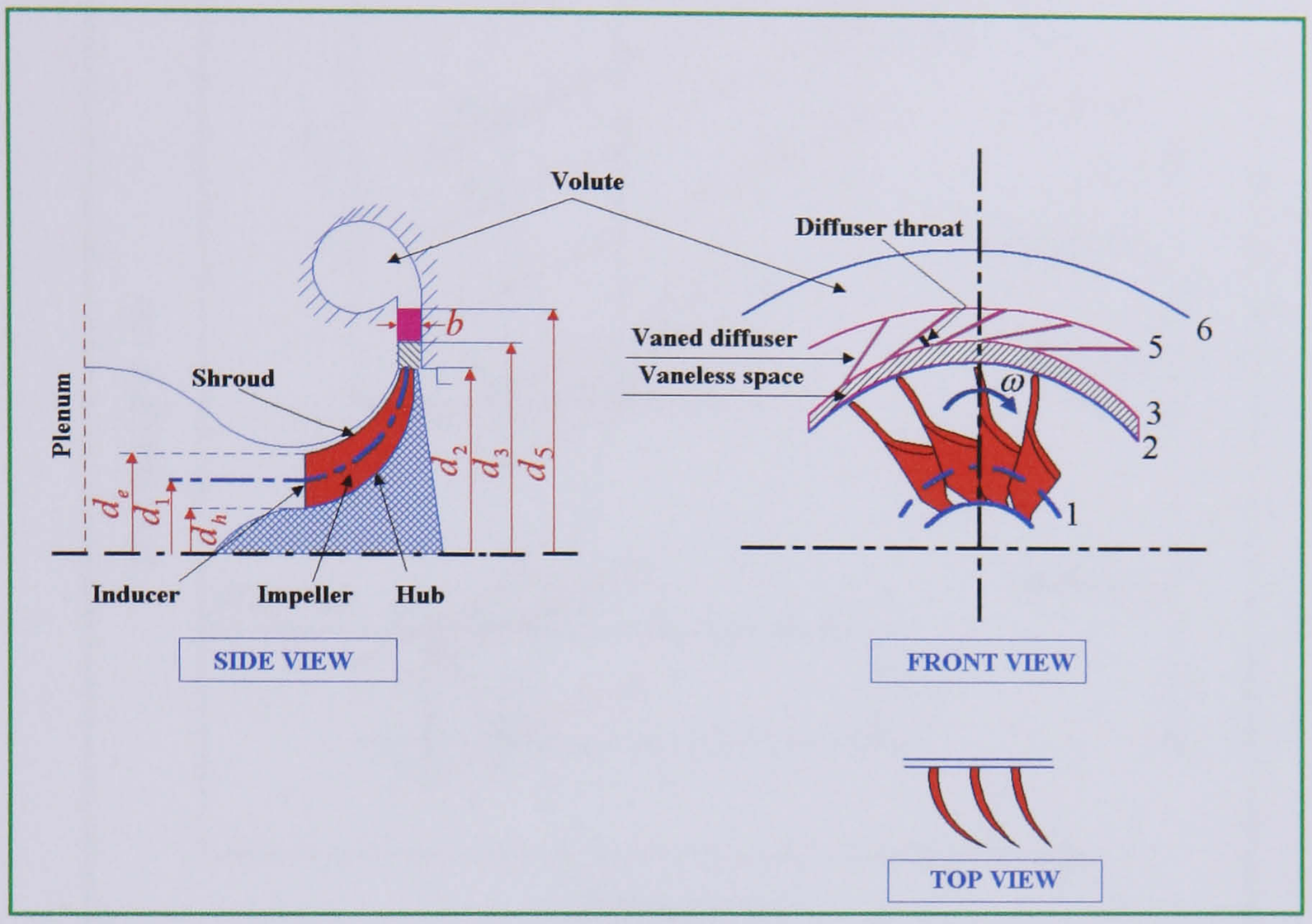

FIG. 5.1 COMPONENTS OF CENTRIFUGAL COMPRESSOR

5.3 ENTHALPY-ENTROPY DIAGRAM OF A CENTRIFUGAL COMPRESSOR

An enthalpy – entropy diagram is presented to show the compression process progression in the compressor stage as shown in **Fig. 5.2**. It should be noted that the process departs from isentropic compression due to losses caused by friction, viscous drag and others.

5.4 SLIP FACTOR

Many attempts in predicting the amount of slip have been cited in the open literature and several slip factor correlations have been given as follows:

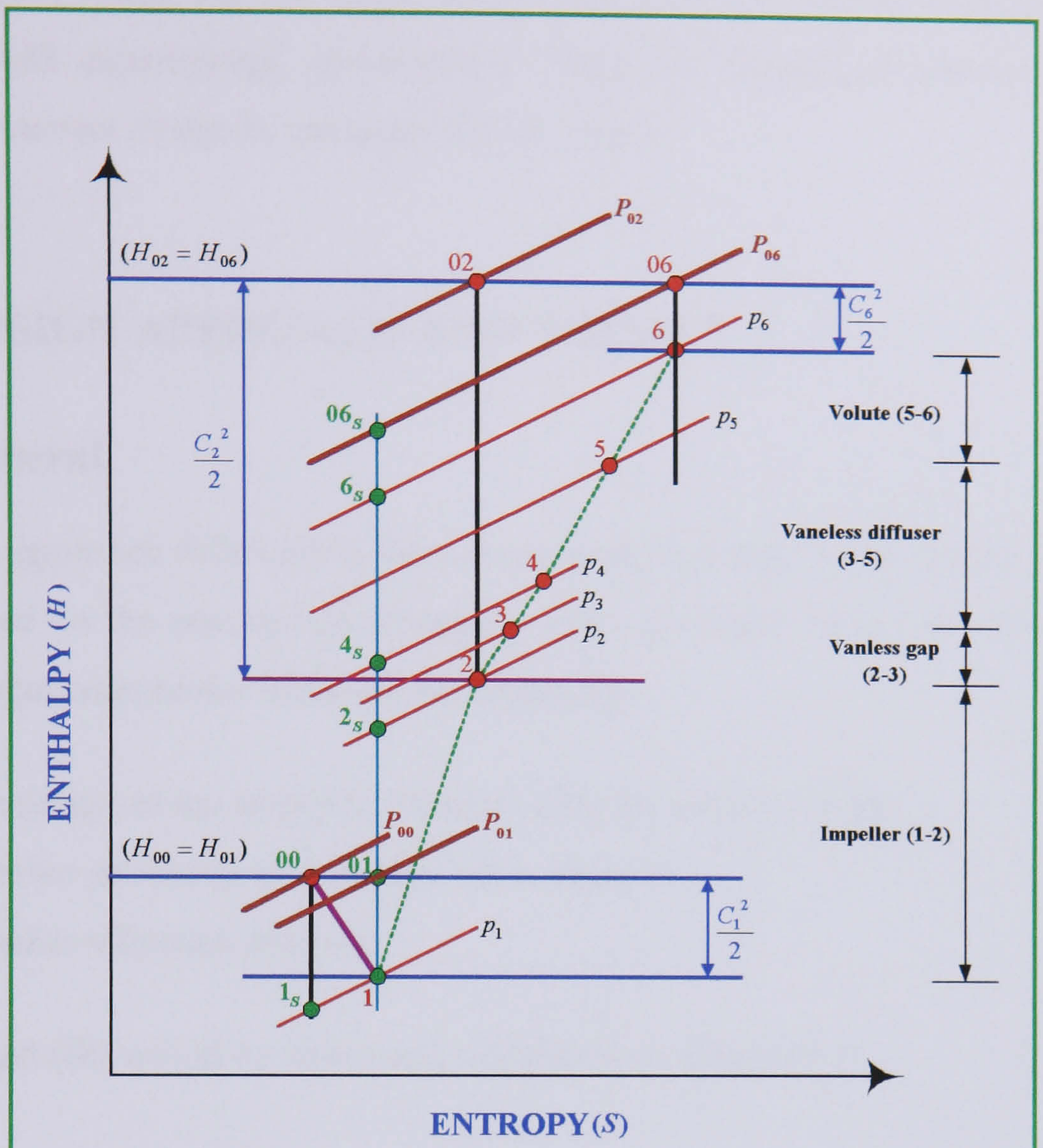

FIG. 5.2 GENERALIZED H-S DIAGRAM FOR A CENTRIFUGAL COMPRESSOR

i. **Stodola [66]** slip factor formula

$$\phi_{sf} = 1 - \frac{\pi}{N_b} \sin \beta_{b2} \tag{5.3}$$

ii. **Wiesner [67]** slip factor formula

$$\phi_{sf} = 1 - \frac{\sqrt{\cos \beta_{b2}}}{(N_b)^{0.7}} \tag{5.4}$$

iii. **Stanitz [68]** slip factor formula

$$\phi_{sf} = 1 - \frac{0.63}{N_b} \tag{5.5}$$

Ferguson [69] found that for radial vaned impellers, the **Stantiz** expression agreed very well with experimental observations. Therefore**, Stantiz** correlation formula is used in the current design to calculate the slip factor.

5.5 DESIGN APPROACH AND THEORY

5.5.1 General

The design approach followed in the current work is similar to the **IFR** turbine design that is, based on the assumption of step-by-step one-dimensional flow. The design of the centrifugal compressor included the following:

i. The design of the Impeller, vaneless diffuser and the volute.

ii. Impeller structural and thermal stress analysis.

iii. Impeller vibration analysis.

Items **(ii)** and **(iii)** would be addressed, separately, in **Chapter** 7.

5.5.2 Impeller Design

5.5.2.1 Impeller geometry

The impeller of a centrifugal compressor may be considered as generalized fluid handling system and the variables which will completely describe the design and performance of this system may be divided into three groups as shown in **Table 5.1**. For a given set of performance requirements, the design approach entails the calculation of complete geometrical parameters of the impeller, in addition, it is necessary to identify the constraints such as inducer Mach number, temperature and stress limits.

The geometric shape of a typical radial flow impeller including the velocity triangles, assuming zero swirl at impeller inlet, are shown in **Fig. 5**.7. Note that the designation used for the principal dimensions for the impeller is the same as for the turbine rotor.

CONTROL VARIABLES	DESIGN VARIABLES	PERFORMANCE REQUIREMENTS
Inlet pressure	Tip diameter, blade width	Mass flow rate
Inlet temperature	Inducer and hub diameters	Isentropic efficiency
Rotational speed	Axial length, blade angles	Pressure ratio
Properties of working fluids	Mach numbers, Reynolds number	Diffusion ratio, Specific speed, Specific diameter, Flow coefficient.

TABLE 5.1 MAIN PARAMETERS OF A CENTRIFUGAL COMPRESSOR IMPELLER

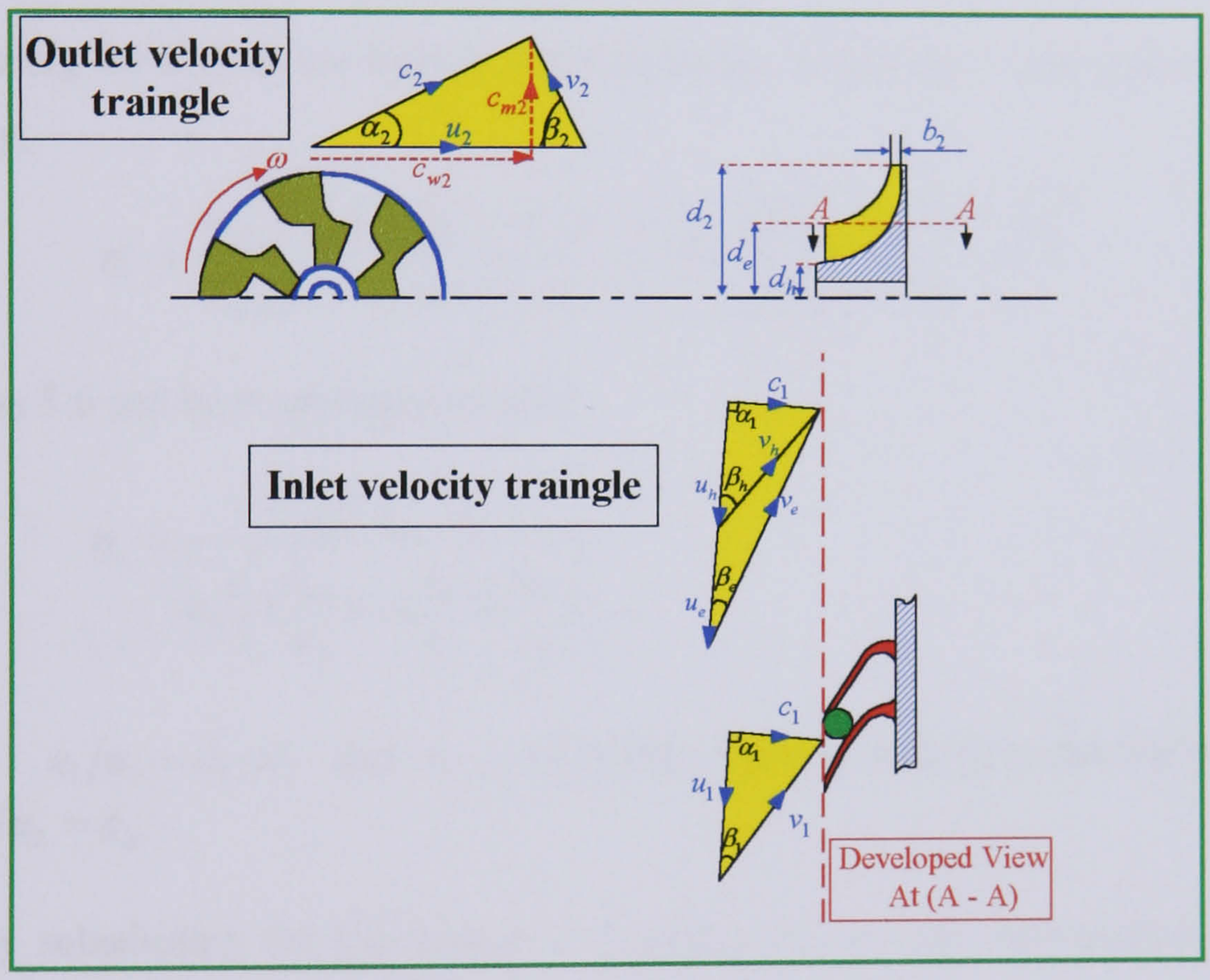

FIG. 5.3 THREE VIEWS OF THE RADIAL FLOW CENTRIFUGAL IMPELLER WITH THE INLET AND OUTLET VELOCITY TRIANGLES

5.5.2.2 Impeller inlet design parameters

Before commencing any design procedure, prior knowledge of some parameters must be available, whilst others must be assumed. For an inducer design, prior knowledge of the following parameters is usually available:

i. The inlet stagnation pressure and temperature; the standard atmospheric conditions are often applicable.

ii. The degree of pre-whirl; here it will be assumed that the flow enters the inducer with zero pre-whirl.

iii. The mass flow rate of the working fluid.

In addition several aerodynamic and geometrical expressions of the flow must be derived to evaluate the principal dimensions for the inducer and these are:

A. <u>Speed parameter</u> $\left(\frac{d_2 N}{\sqrt{C_{pa} T_{01}}}\right)$

Considering the flow at the inducer mean diameter, compressor isentropic efficiency is given by:

$$\eta_c = \frac{W_{ideal}}{W_{actual}} = \frac{C_{pa}(T_{02} - T_{01})}{c_{w2}u_2 - c_{w1}u_1} = \frac{C_{pa}T_{01}\left[(P_{02}/P_{01})^{\gamma-1/\gamma} - 1\right]}{c_{w2}u_2 - c_{w1}u_1} \tag{5.6}$$

Equation 5.6 can be re-arranged to give

$$\eta_c = \frac{C_{pa}(T_{02} - T_{01})}{u_2^{\,2}\left(\left(\frac{c_{w2}}{u_2}\right) - \left(\frac{c_{w1}}{u_2}\right)\left(\frac{u_1}{u_2}\right)\right)} \tag{5.7}$$

But $u_1/u_2 = d_1/d_2$ and $u_2 = \pi d_2 N/60$, Also by definition, the slip factor equal to $c_{w2}/u_2 = \phi_{sf}$

Then by substituting the expressions for u_1/u_2, u_2, c_{w2}/u_2 in equation 5.7 would result:

$$\frac{d_2 N}{\sqrt{C_{pa} T_{01}}} = \frac{60}{\pi}\sqrt{\frac{1}{\eta_c}\left[\frac{(P_{02}/P_{01})^{\gamma-1/\gamma} - 1}{\phi_{sf} - (c_{w1}/u_2)(d_1/d_2)}\right]} \tag{5.8}$$

Considering the flow at the inducer tip and hub, respectively, equation 5.8 at the inducer tip and hub would be as:

$$\frac{d_2 N}{\sqrt{C_{pa} T_{01}}} = \frac{60}{\pi}\sqrt{\frac{1}{\eta_c}\left[\frac{(P_{02}/P_{01})^{\gamma-1/\gamma} - 1}{\phi_{sf} - (c_{we}/u_2)(d_e/d_2)}\right]} \tag{5.9}$$

$$\frac{d_2 N}{\sqrt{C_{pa} T_{01}}} = \frac{601}{\pi} \sqrt{\frac{1}{\eta_c} \left[\frac{\left(P_{02}/P_{01}\right)^{\gamma-1/\gamma} - 1}{\phi_{sf} - (c_{wh}/u_2)(d_h/d_2)} \right]} \qquad \textbf{(5.10)}$$

B. Relative flow Mach number at inducer tip diameter (M_{er})

Reference to inlet velocity diagram at inducer tip, **Fig. 5.3** and by following the same procedure given in **Sec. 3.2.4.3** of **Chapter 3**. The following expression for M_{er} can be written as:

$$M_{er}{}^2 = \frac{\left(\frac{\pi d_2 N}{60\sqrt{C_{pa} T_{01}}} \right)^2 \left(\frac{d_e}{d_2} \right)^2}{(\gamma - 1)\left[1 - \sin^2 \beta_e \left\{ 1 + \frac{1}{2} \left(\frac{\pi d_2 N}{60\sqrt{C_{pa} T_{01}}} \right)^2 \left(\frac{d_e}{d_2} \right)^2 \right\} \right]} \qquad \textbf{(5.11)}$$

C. Mass flow parameter $\left(\frac{\dot{m}\sqrt{C_{pa} T_{01}}}{d_2{}^2 P_{01}} \right)$

An expression for the mass flow parameter can be derived by following the same steps given in **Sec. 3.2.5** of **Chapter 3**. The final expression is given as:

$$\frac{\dot{m}\sqrt{C_{pa} T_{01}}}{d_2{}^2 P_{01}} = \left(\frac{\gamma}{\sqrt{\gamma - 1}} \right) \left[B_{f_1} \left(\frac{\pi}{4} \right) \left(\left(\frac{d_e}{d_2} \right)^2 - \left(\frac{d_h}{d_2} \right)^2 \right) \right] \left[\frac{M_{er} \sin \beta_e}{\left(1 + \frac{\gamma - 1}{2} (M_{er} \sin \beta_e)^2 \right)^{\frac{\gamma+1}{2(\gamma-1)}}} \right] \qquad \textbf{(5.12)}$$

For simplicity

Let $k_1 = \left(\frac{\gamma}{\sqrt{\gamma - 1}} \right) \left(\frac{\pi B_{f_1}}{4} \right)$ and $k_2 = 1 - \left(\frac{d_h}{d_e} \right)^2$

Also, $$(\frac{d_e}{d_2})^2 = (\frac{u_e}{u_2})^2 = \frac{(v_e \cos\beta_e)^2}{(\pi d_2 N/60)^2} = \frac{(\gamma R t_1)(M_{er}{}^2 \cos^2\beta_e)}{(\pi d_2 N)^2}$$

Substitute for k_1 , k_2 and d_e/d_2 in equation 5.12 and re-arranging resulted into

$$\frac{\left(\frac{\dot{m}\sqrt{C_{pa}T_{01}}}{d_2{}^2 P_{01}}\right)(\pi d_2 N)^2}{k_1 k_2 (\gamma R t_1)} = \left[\frac{M_{er}{}^3 \sin\beta_e \cos^2\beta_e}{\left(1+\frac{\gamma-1}{2}(M_{er}\sin\beta_e)^2\right)^{\frac{\gamma+1}{2(\gamma-1)}}}\right] \quad (5.13)$$

But $$t_1 = \frac{T_{01}}{1+\frac{\gamma-1}{2}(M_{er}\sin\beta_e)^2}$$

Substitute for t_1 in equation 5.13 and rearrange would give:

$$\frac{\frac{\dot{m}N}{1-(d_h/d_e)^2}}{(P_{01}\sqrt{\gamma R T_{01}})k_3} = \frac{\dot{m}N^2}{(P_{01}\sqrt{\gamma R T_{01}})k_2 k_3} = \left[\frac{M_{er}{}^3 \sin\beta_e \cos^2\beta_e}{\left(1+\frac{\gamma-1}{2}(M_{er}\sin\beta_e)^2\right)^{\frac{3\gamma-1)}{2(\gamma-1)}}}\right] \quad \textbf{(5.14)}$$

Where: $k_2 = 1-(d_h/d_e)^2$ and $k_3 = (4\pi/\beta_{f_1})$

D. <u>Inducer tip to impeller tip diameter ratio</u> (d_e/d_2) <u>and hub to impeller tip diameter ratio</u> (d_h/d_2)

Equation 5.11 can be re-arranged to develop an expression for d_e/d_2 as:

$$\frac{d_e}{d_2} = \left(\frac{M_{er}}{\frac{\pi d_2 N}{60\sqrt{C_{pa}T_{01}}}}\right)\left[\sqrt{\frac{(\gamma-1)\cos^2\beta_e}{1+\frac{\gamma-1}{2}M_{er}{}^2\sin^2\beta_e}}\right] \quad \textbf{(5.15)}$$

Equation 5.12 can be re-arranged to develop an expression for d_h/d_2 as:

$$\frac{d_h}{d_2}=\left(\frac{d_e}{d_2}\right)\sqrt{1-\left[\frac{\left(\frac{\dot{m}\sqrt{C_{pa}T_{01}}}{d_2{}^2P_{01}}\right)\left\{1+\frac{\gamma-1}{2}\left(M_{er}\sin\beta_e\right)^2\right\}^{\frac{\gamma+1}{2(\gamma-1)}}}{\left(B_{f_1}\right)\left(\frac{\pi}{4}\right)\left(\frac{\gamma}{\sqrt{\gamma-1}}\right)\left(\frac{d_e}{d_2}\right)^2\left(M_{er}\sin\beta_e\right)}\right]} \qquad \textbf{(5.16)}$$

5.5.2.3 Impeller outlet design parameters

A. <u>Diffusion ratio parameter</u> (v_2/v_1)

Following the same derivation procedure given in **Sec. 3.2.4.6** of **Chapter 3**, an expression for (v_2/v_1) can be written as

$$\frac{v_2}{v_1}=\pi\left(1-\phi_{sf}\right)\left(\frac{\sin\beta_1}{\cos\beta_2}\right)\left(\frac{\sqrt{\frac{1}{\gamma-1}+\frac{M_{er}{}^2\sin^2\beta_e}{2}}}{M_{er}\sin\beta_e}\right)\left(\frac{1}{\pi}\sqrt{\frac{1}{\eta_c}\left(\frac{(P_{02}/P_{01})^{\gamma-1\,\gamma}-1}{\phi_{sf}}\right)}\right) \qquad \textbf{(5.17)}$$

B. <u>Blade tip width to impeller tip diameter ratio expression</u> (b_2/d_2)

Two models for calculating blade tip width to tip diameter ratio will be developed. These are termed **model (1)** and **model (2)**. The former is expressed in terms of mass flow parameter $\dot{m}\sqrt{C_pT_i}/d_2{}^2P_i$, speed parameter $d_2N/\sqrt{C_pT_i}$, flow angles α_2 and M_2 at rotor inlet. The latter is expressed in terms of inlet blade loading factor $(\psi_2)_{BL}$, number of blades N_b, $d_2N/\sqrt{C_pT_i}$ and angle α_2

B.1 Model (1)

The derivation of model (1) is similar to that given in **Sec. 3.26** of **Chapter 3** and it can be written as:

$$\frac{b_2}{d_2} = \left(\frac{1}{\pi B_{f_2}}\right)\left(\frac{\sqrt{\gamma-1}}{\gamma}\right)\left[\frac{\left(\frac{\dot{m}\sqrt{C_{pa}T_{01}}}{{d_2}^2 P_{01}}\right)\left(1+\frac{1}{\eta_c}\left(\frac{P_{02}}{P_{01}}\right)^{\gamma-1\ \gamma}-1\right)^{1\ 2}}{\left(\frac{P_{02}}{P_{01}}\right)}\right]\left[\frac{\left(1+\frac{\gamma-1}{2}{M_2}^2\right)^{\frac{\gamma+1}{2(\gamma-1)}}}{M_2\sin\alpha_2}\right] \tag{5.18}$$

B.2 Model (2)

Using **Stahler [38]** for slip factor $\phi_{sf} = c_{w2}/u_2$ of an impeller having 19 blades:

$$\phi_{sf} = \frac{c_{w2}}{u_2} = 1 - 1.25\left(\frac{Q}{N{d_2}^3}\right) \tag{5.19}$$

Applying the above expression for the impeller of N_b blades

$$\phi_{sf} = \frac{c_{w2}}{u_2} = 1 - \left(\frac{1.25\times 19}{N_b}\right)\left(\frac{Q}{N{d_2}^3}\right) = 1 - \left(\frac{23.75}{N_b}\right)\left(\frac{\pi b_2 d_2 c_{m2}}{N{d_2}^3}\right) \tag{5.20}$$

Re-arranging equation 5.20 would give:

$$\phi_{sf} = 1 - \left(\frac{23.75}{N_b}\right)\left(\frac{\pi^2}{\pi N d_2\ 60}\right)\left(\frac{b_2}{d_2}\right)(c_{m2}) \tag{5.21}$$

Equation 5.21 can be developed into:

$$\frac{b_2}{d_2} = \left[1-\phi_{sf}\right]\left(\frac{N_b}{234.4}\right)\left(\frac{u_2}{c_{m2}}\frac{c_{w2}}{c_{w2}}\right) \tag{5.22}$$

$$\frac{b_2}{d_2} = \left(\frac{N_b}{234.4}\right)\left(\frac{1-\phi_{sf}}{\phi_{sf}}\right)\left(\frac{1}{\tan\alpha_2}\right) \tag{5.23}$$

5.5.3 Choice of Principal Dimensions of the Impeller by Numerical Optimisation

5.5.3.1 Objective function

The procedure followed here is similar to that used for the turbine rotor described in **Chapter 4**. The objective function of the matrix $\overline{X}$ is formulated as:

$$\overline{X} = \begin{bmatrix} d_2 & = X(1) \\ M_{er} & = X(2) \\ \beta_e & = X(3) \\ d_e/d_2 & = X(4) \\ d_h/d_2 & = X(5) \\ \alpha_2 & = X(6) \\ b_2 & = X(7) \\ v_2/v_1 & = X(8) \\ \beta_2 & = X(9) \\ M_2 & = X(10) \\ \beta_1 & = X(11) \end{bmatrix}$$

5.5.3.2 Equality and inequality constraints

A. ***Equality constraints***

.

i.

$$g(1) = \frac{\dot{m}\sqrt{C_{pa}T_{01}}}{d_2{}^2 P_{01}} - \left(\frac{\gamma}{\sqrt{\gamma-1}}\right)\left[B_{f_1}\left(\frac{\pi}{4}\right)\left(\left(\frac{d_e}{d_2}\right)^2 - \left(\frac{d_h}{d_2}\right)^2\right)\right]\left[\frac{M_{er}\sin\beta_e}{\left(1+\frac{\gamma-1}{2}(M_{er}\sin\beta_e)^2\right)^{\frac{\gamma+1}{2(\gamma-1)}}}\right] \quad (5.24)$$

ii.

$$g(2) = \frac{b_2}{d_2} - \left(\frac{1}{\pi B_{f_2}}\right)\left(\frac{\sqrt{\gamma-1}}{\gamma}\right)\left[\frac{\left(\frac{\dot{m}\sqrt{C_{pa}T_{01}}}{d_2{}^2 P_{01}}\right)\left(1+\frac{1}{\eta_c}\left(\frac{P_{02}}{P_{01}}\right)^{\gamma-1/\gamma}-1\right)^{1/2}}{\left(\frac{P_{02}}{P_{01}}\right)}\right]\left[\frac{\left(1+\frac{\gamma-1}{2}M_2{}^2\right)^{\frac{\gamma+1}{2(\gamma-1)}}}{M_2\sin\alpha_2}\right] \quad (5.25)$$

$$g(3)=\frac{v_2}{v_1}-\pi\left(1-\phi_{sf}\right)\left(\frac{\sin\beta_1}{\cos\beta_2}\right)\left(\frac{\sqrt{\frac{1}{\gamma-1}+\frac{M_{er}{}^2\sin^2\beta_e}{2}}}{M_{er}\sin\beta_e}\right)\left(\frac{1}{\pi}\sqrt{\frac{1}{\eta_c}\left(\frac{(P_{02}/P_{01})^{\gamma-1/\gamma}-1}{\phi_{sf}}\right)}\right) \tag{5.26}$$

iv. $$g(4)=\frac{b_2}{d_2}-\left(\frac{N_b}{234.4}\right)\left(\frac{1/\phi_{sf}-1}{\tan\alpha_2}\right) \tag{5.27}$$

B. ***Inequality constraints***

i. $d_2 \le 20.0\,cm$: This is governed by the size of the compressor

$$g(5)=20.0-d_2 \tag{5.28}$$

ii. $M_{er} \le 1.0$: Specified by the subsonic flow requirements

$$g(6)=1.0-M_{er} \tag{5.29}$$

iii. $\beta_e \ge 25^\circ$: Specified by maximum flow at inducer inlet

$$g(7)=\beta_e-25^\circ \tag{5.30}$$

iv. $d_e/d_2 \ge 0.55$: Governed by the relative Mach number

$$g(8)=d_e/d_2-0.55 \tag{5.31}$$

v. $d_h/d_2 \le 0.40$: Specified by stress limitation and number of blades.

$$g(9)=0.40-d_h/d_2 \tag{5.32}$$

vi. $\alpha_2 \ge 17^\circ$: Controlled by diffusion ratio

$$g(10)=\alpha_2-17^\circ \tag{5.33}$$

vii. $b_2 \ge 0.004$: Governed by leakage loss and diffusion ratio

$$g(11)=b_2-0.004 \tag{5.34}$$

viii. $v_2/v_1 \ge 0.55$: Governed by flow separation in the impeller passage

$$g(12)=v_2/v_1-0.55 \tag{5.35}$$

ix. $\beta_2 \geq 60^\circ$: Specified by diffusion ratio requirements

$$g(13) = \beta_2 - 60^\circ \tag{5.36}$$

x. $M_2 \geq 0.95$: fixed by relative flow angle at impeller exit

$$g(14) = M_2 - 0.95 \tag{5.37}$$

xi. $\beta_1 \geq 35^\circ$: Governed by inducer and hub diameter

$$g(15) = \beta_1 - 35^\circ \tag{5.38}$$

5.5.3.3 Optimisation solution

The required input data used to solve this optimisation problem is listed in **Table 5.2**

DESIGN SPECIFICATION	DESIGN VALUE
Mass flow, $\dot{m}_a$	0.566
Pressure ratio, P_{02}/P_{01}	4.0
Inlet stagnation temperature, T_{01}	$300^\circ K$
Rotational speed, N	60000 *rpm*

TABLE 5.2 INPUT DATA AT DESIGN POINT

The same **OPRQP** programme was used to solve this optimisation problem and was run for several numbers of blades. The optimum solution of the matrix $\overline{X}$ obtained from the optimisation technique is listed in **Table 5.3**.

DESIGN PARAMETERS	DESIGN VALUES	DESIGN PARAMETERS	DESIGN VALUES
N_b	15 *Blades*	d_h/d_2	0.20
d_2	15.19*cm*	b_2	6.4*mm*
M_{er}	0.90	v_2/v_1	0.65
β_e	30°	β_2	68.0°
d_e/d_2	0.56	M_2	1.14

TABLE 5.3 DESIGN DATA OBTAINED USING AN OPTIMIZATION TECHNIQUE

5.5.3.5 Design data obtained by numerical optimisation

The complete calculated design data for the impeller based on the output results of the numerical optimisation are listed in **Table 5.4**.

DESIGN SPECIFICATIONS	GEOMETRICAL DIMENSIONS	FLOW ANGLES AT IMPELLER INLET AND EXIT	FLOW VELOCITIES AT IMPELLER EXIT
$\dot{m}_a = 0.566\,kg/s$ $N = 60000\,rpm$ $\frac{P_{02}}{P_{01}} = 4.0$ $T_{01} = 300\,K$ $t_1 = 288.16\,K$ $p_1 = 0.87\,bar$ $\rho_1 = 1.05\,kg/m^3$	$d_2 = 15.19\,cm$ $b_2 = 0.64\,cm$ $\bar{t}_{th2} = 0.2\,cm$ $d_1 = 6.387\,cm$ $d_h = 3.038\,cm$ $d_e = 8.506\,cm$ $\bar{t}_{th1} = 0.2\,cm$	$\alpha_2 = 21.0^\circ$ $\beta_2 = 68^\circ$ $\alpha_1 = 90^\circ$ $\alpha_h = 90^\circ$ $\alpha_e = 90^\circ$ $\beta_h = 58.53^\circ$ $\beta_1 = 37.56^\circ$ $\beta_e = 30^\circ$	$c_2 = 441.66\,m/s$ $c_{m2} = 158.28\,m/s$ $c_{w2} = 412.32\,m/s$ $v_2 = 170.71\,m/s$ $v_{m2} = 158.28\,m/s$ $v_{w2} = 63.95\,m/s$
FLOW VELOCITIES AT IMPELLER EXIT	**IMPELLER SPEED AT INLET AND OUTLET**	**MACH NUMBER AT IMPELLER INLET AND EXIT**	**PERFORMANCE PARAMETERS**
$c_1 = 154.29\,m/s$ $c_{w1} = 0.0\,m/s$ $c_h = 154.29\,m/s$ $c_e = 154.29\,m/s$ $v_1 = 253.10\,m/s$ $v_{w1} = 200.65\,m/s$ $v_h = 180.89\,m/s$ $v_e = 308.58\,m/s$	$u_2 = 476.27\,m/s$ $u_1 = 200.65\,m/s$ $u_h = 95.44\,m/s$ $u_e = 267.24\,m/s$	$M_2 = 1.14$ $M_1 = 0.453$ $M_{hr} = 0.532$ $M_{1r} = 0.743$ $M_{er} = 0.90$	$S_P = 0.277$ $M_p = 0.134$ $\eta_c = 0.83$ $c_{m1}/u_2 = 0.33$ $v_2/v_1 = 0.67$

TABLE 5.4 COMPLETE SET OF CALCULATED DESIGN DATA OF A CENTRIFUGAL IMPELLER BASED ON NUMERICAL OPTIMISATION

5.6 DESIGN OF THE IMPELLER FLOW CHANNEL

5.6.1 Prescribed Meanstream Velocity

The method of prescribed meanstream velocity for the design of the impeller flow channel followed here is similar to that used for the turbine rotor described in **Chapter 4**. The main figures of the output results are presented hereafter.

Figures 5.4 and **5.5** show the actual values of the relative velocity and the components along the mean streamline of the impeller.

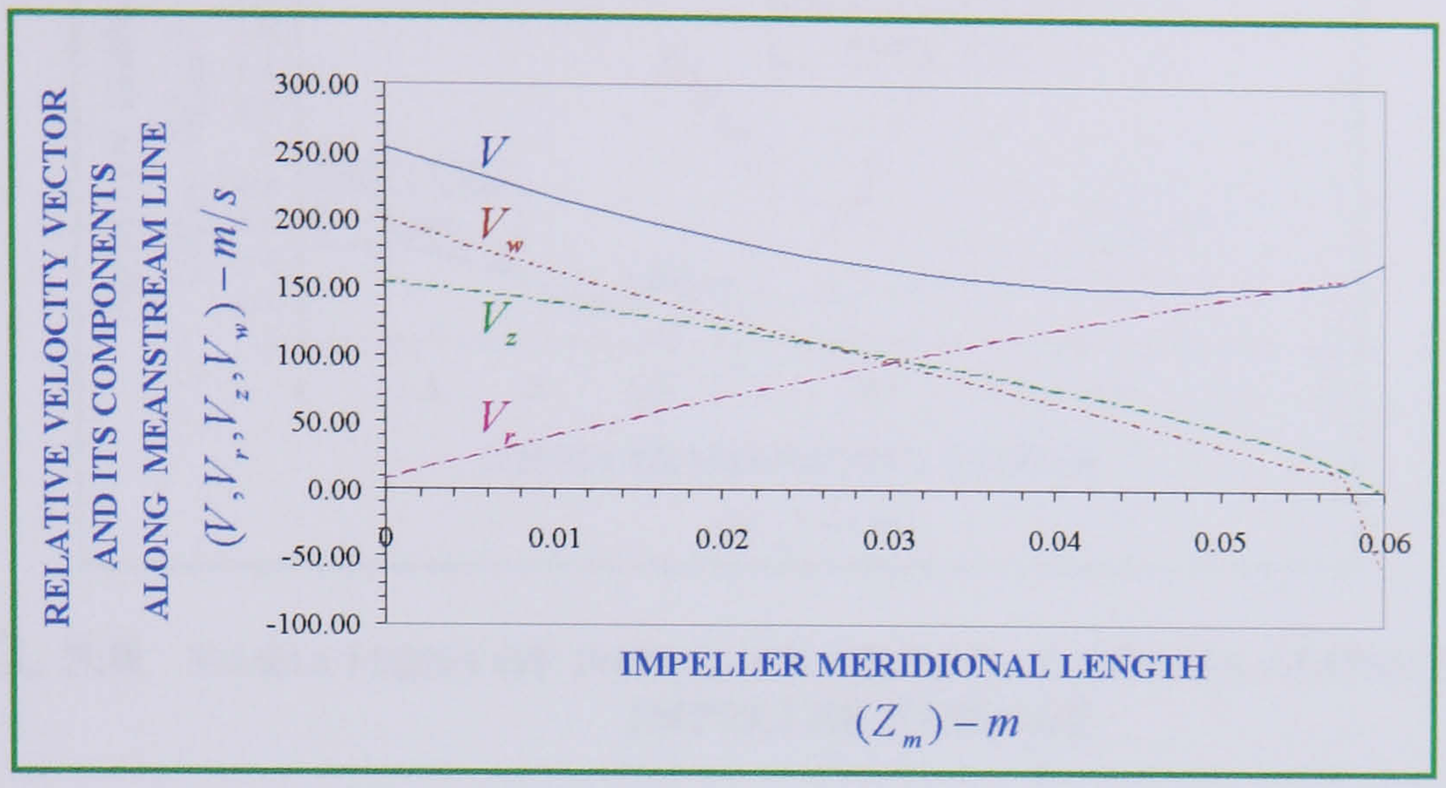

FIG. 5.4 ACTUAL VALUES OF TOTAL RELATIVE VELOCITY AND ITS COMPONENTS ALONG MEAN STREAMLINE OF A MERIDIONAL LENGTH OF $z_m = 0.06m$

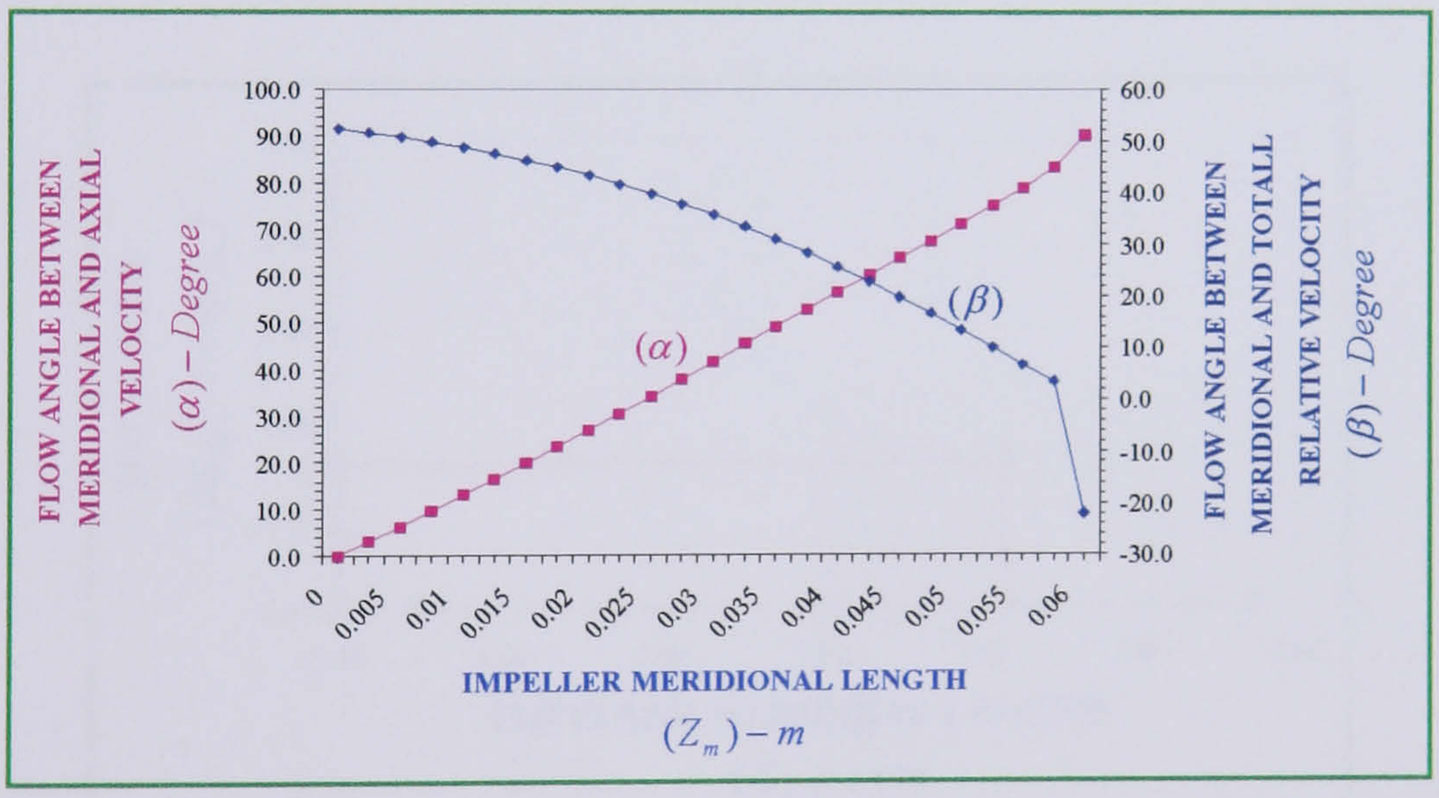

FIG. 5.5 ACTUAL VALUES OF THE FLOW ANGLES α AND β ALONG MEAN STREAMLINE OF A MERIDIONAL LENGTH OF $z_m = 0.06m$

Figure 5.6 shows a plot of impeller internal losses, that is, skin friction losses Δq_{SFL} and diffusion and blading losses Δq_{DBL} vs. meridional length of a centrifugal impeller. It can be seen that Δq_{SFL} is lowest for the smallest axial length and increases

as the axial length is increased while Δq_{DBL} is highest for the smallest axial length and decreases as the axial length is increased.

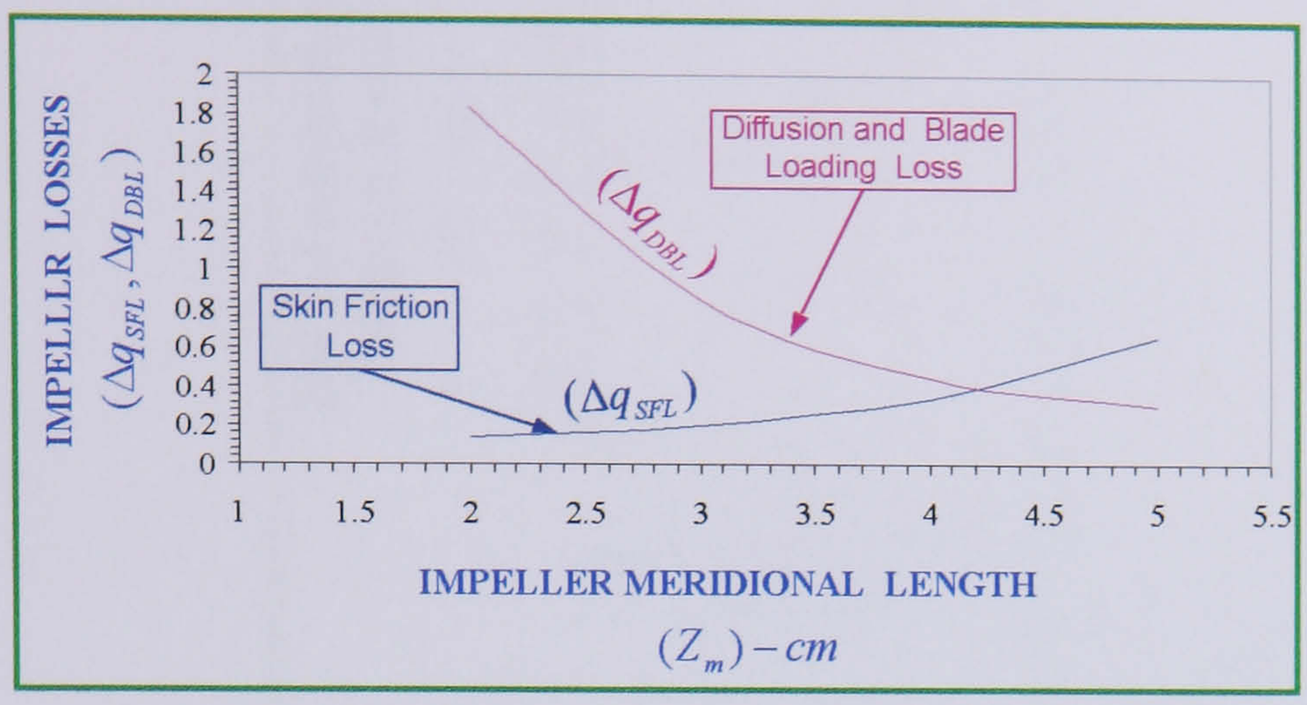

FIG. 5.6 VARIATIONS OF IMPELLER INTERNAL LOSSES ALONG THE IMPELLER PASSAGE

Figure 5.7 shows a plot of total pressure loss inside the passage vs. meridional length of a centrifugal impeller. It can be seen that the optimum meridional length was found to be $41.5\,mm$ for minimum pressure loss in the passage.

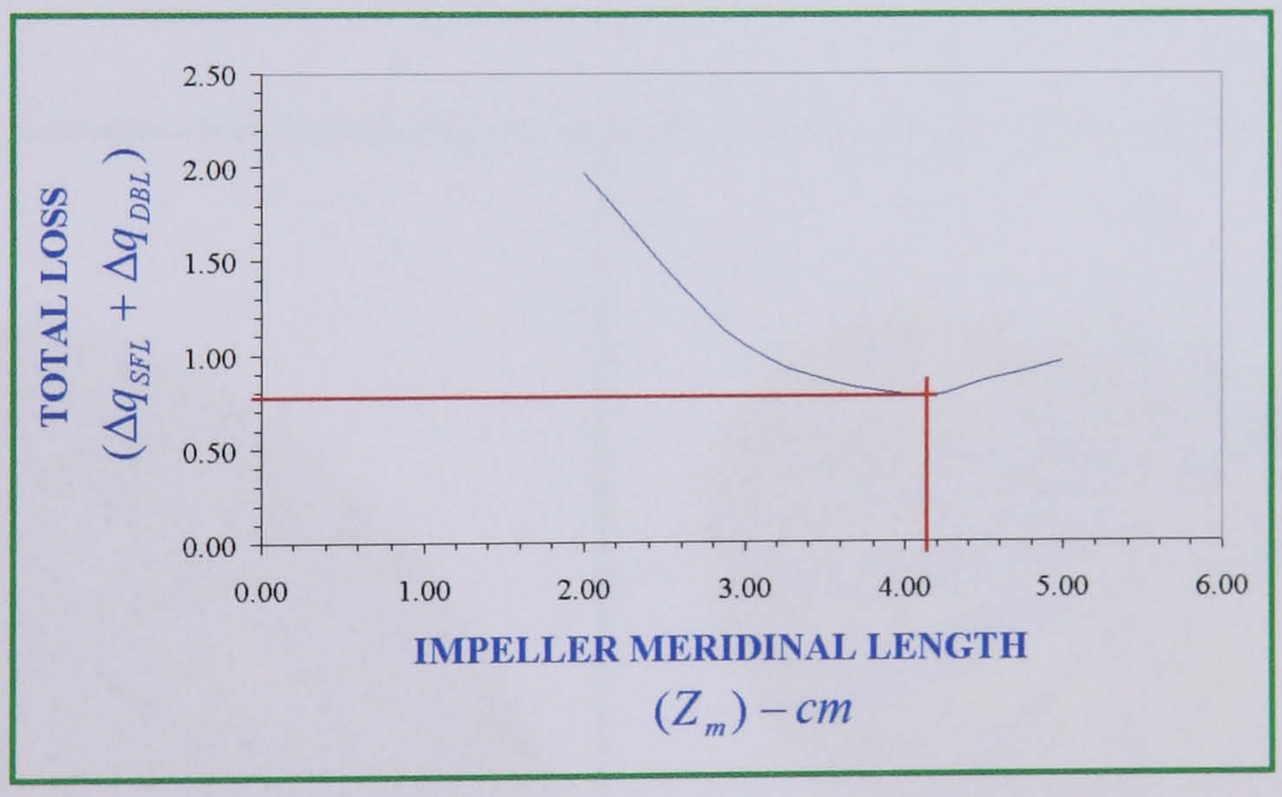

FIG. 5.7 OVERALL IMPELLER INTERNAL LOSSES ALONG THE IMPELLER PASSAGE

5.6.2 Blade Shape

The resulting blade shape obtained by using the prescribed mean stream velocity theory is shown in **Fig. 5.8**.

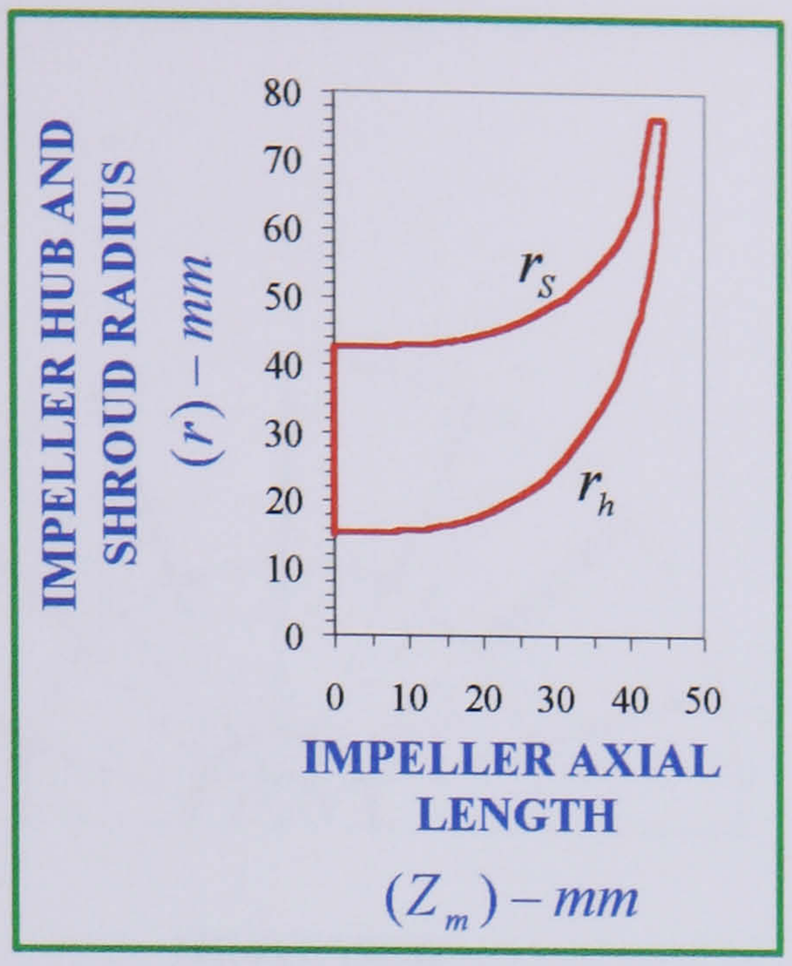

FIG. 5.8 BLADE SHAPE BASED ON PRESCRIBED MEAN STREAM VELOCITY

5.6.3 Impeller Solid Model

A three-dimensional solid model of the impeller was developed as shown in **Fig. 5.9** and the final design drawing of the impeller is shown **Fig. 5.10**.

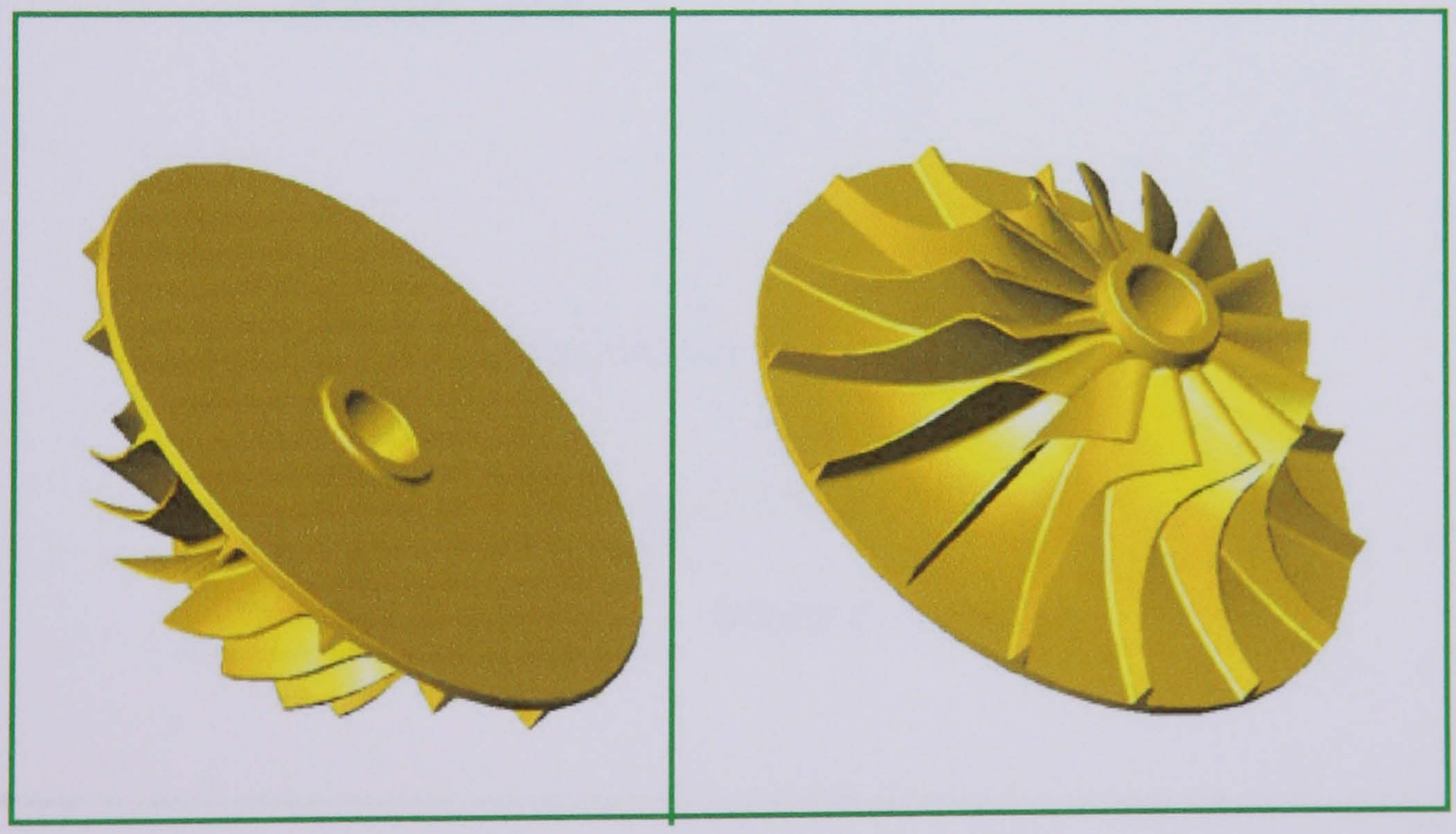

FIG. 5.9 THREE-DIMENSIONAL SOLID MODEL OF THE IMPELLER

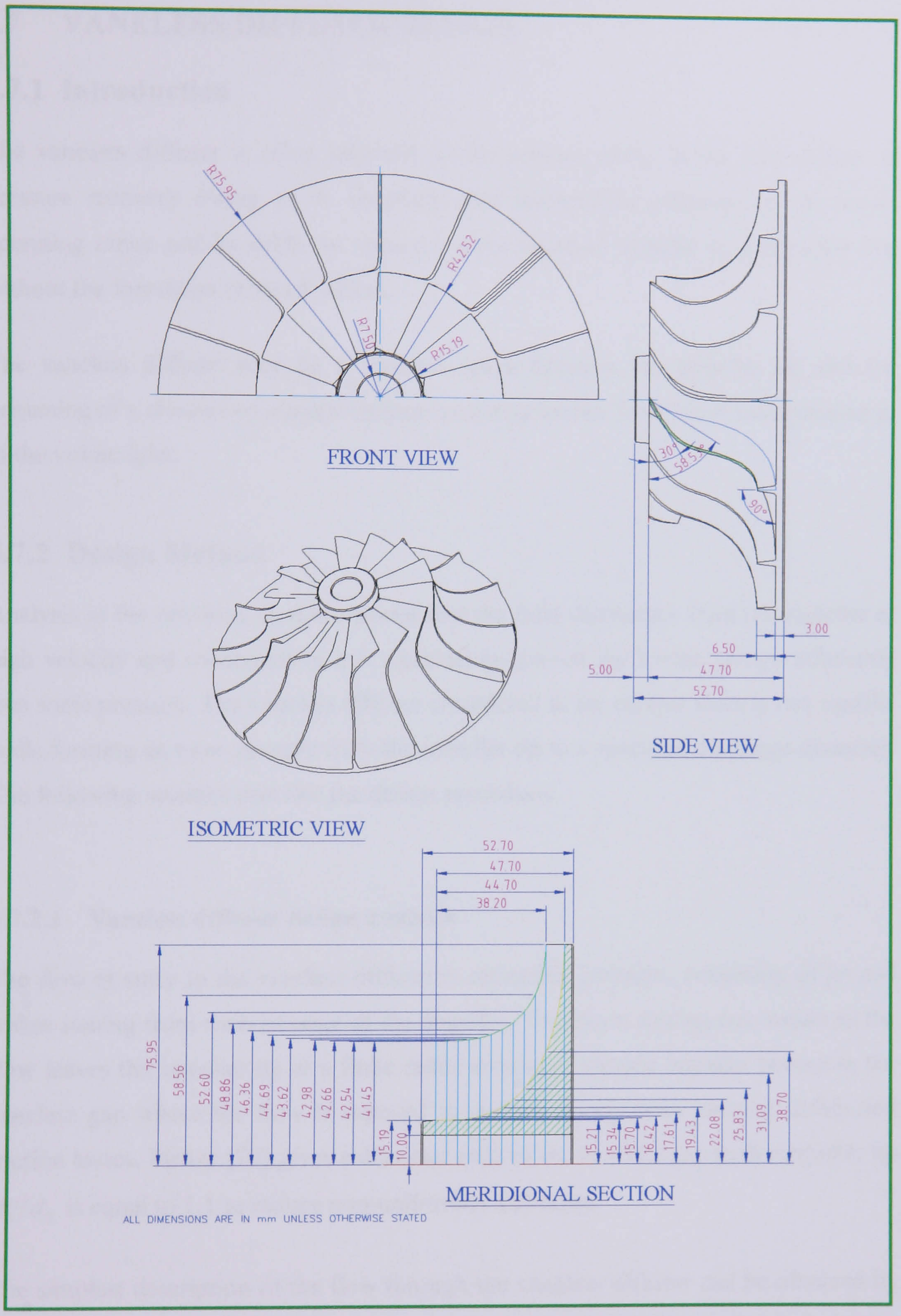

FIG. 5.10 DETAIL DRAWING OF THE IMPELLER

5.7 VANELESS DIFFUSER DESIGN

5.7.1 Introduction

The vaneless diffuser is often adopted, in the present work, as the sole means of pressure recovery owing to its simplicity and inexpensive construction, its broad operating range and its ability to reduce a sonic absolute velocity to a subsonic one without the formation of shock waves.

The vaneless diffuser may be a vaneless space between the impeller tip and the beginning of a channel or cascade diffuser or it may be run from the impeller discharge to the volute inlet.

5.7.2 Design Method

Analysis in the previous section showed that the fluid discharges from the impeller at high velocity and consequently it is essential to convert the kinetic energy efficiently into static pressure. The vaneless diffuser considered in the current work is two parallel walls forming an open passage from the impeller tip to a specified discharge diameter. The following sections describe the design procedure.

5.7.2.1 Vaneless diffuser design analysis

The flow at entry to the vaneless diffuser is extremely complex, consisting of jet and wakes issuing from each passage of the impeller. Therefore, mixing out occurs as the flow leaves the impeller tip at a finite radial increment outside impeller known as the vaneless gap where the flow is exposed to sudden enlargement forming eddies and friction losses. **Fisher [70]** gives a diameter ratio of the vaneless gap to the impeller tip d_3/d_2 is equal to 1.1 to reduce non-uniformity and noise.

The simplest description of the flow through the vaneless diffuser can be obtained by considering the angular momentum equation used for the impeller applied between the impeller exit (2) and the vaneless diffuser exit (5), **(refer to Fig. 5.1)**

$$\tau = \dot{m}(c_{\omega 5} r_5 - c_{\omega 2} r_2)$$

For the case of an open passage where the flow is only retained by the side walls and in the absence of any wall friction force, the torque τ exerted on the fluid is zero and the angular momentum equation above reduces to free vortex relationship

i.e. $$c_{\omega 5} r_5 = c_{\omega 2} r_2 \tag{5.39}$$

At any station along the diffuser in relation to impeller exit, the above equation is written as:

$$c_\omega r = c_{\omega 2} r_2$$

$$c_\omega / c_{\omega 2} = d_2 / d \tag{5.40}$$

Applying mass continuity at any station along the diffuser in relation to impeller exit would give:

$$\dot{m} = \rho_2 A_2 c_{m2} = \rho A c_m$$

$$\dot{m} = \rho_2 A_2 c_{\omega 2} \tan\alpha_2 = \rho A c_\omega \tan\alpha$$

$$\frac{\rho}{\rho_2} = \left(\frac{A_2}{A}\right)\left(\frac{c_{\omega 2}}{c_\omega}\right)\left(\frac{\tan\alpha_2}{\tan\alpha}\right) \tag{5.41}$$

Combining equations 5.40 and 5.41 and re-arranging would give:

$$\frac{\rho}{\rho_2} = \left(\frac{d}{d_2}\right)\left(\frac{A_2}{A}\right)\left(\frac{\tan\alpha_2}{\tan\alpha}\right) \tag{5.42}$$

From equation of state

$$\frac{\rho}{\rho_2} = \left(\frac{p}{p_2}\right)\left(\frac{t_2}{t}\right)$$

and $$\frac{A_2}{A} = \frac{\pi b_2 d_2}{\pi d b}$$

Substitute the expressions $\frac{\rho}{\rho_2}, \frac{A_2}{A}$ in equation 5.42 gives:

$$\frac{p}{p_2} = \left(\frac{t}{t_2}\right)\left(\frac{b_2}{b}\right)\left(\frac{\tan\alpha_2}{\tan\alpha}\right) \tag{5.43}$$

For adiabatic condition in the vaneless diffuser,

$$\frac{t}{t_2} = \frac{1 - \dfrac{c^2}{2C_{pa}T_{02}}}{1 - \dfrac{c_2^{\,2}}{2C_{pa}T_{02}}} \tag{5.44}$$

and from velocity triangle, the velocities c and c_2 can be expressed as

$$c = \frac{c_\omega}{\cos\alpha} = \frac{c_{\omega 2}(r_2/r)}{\cos\alpha}$$

and $$c_2 = \frac{c_{\omega 2}}{\cos\alpha_2}$$

Substituting for c_2 and c expressions in equation 5.44 and combining with equation 5.43 will give an expression for static pressure rise ratio within the vaneless diffuser as:

$$\frac{p}{p_2} = \left[\frac{1 - \dfrac{\left(\dfrac{c_{\omega 2}}{\cos\alpha}\right)^2\left(\dfrac{r_2}{r}\right)^2}{2C_{pa}T_{02}}}{1 - \dfrac{\left(\dfrac{c_{\omega 2}}{\cos\alpha_2}\right)^2}{2C_{pa}T_{02}}}\right]\left[\frac{b_2}{b}\right]\left[\frac{\tan\alpha_2}{\tan\alpha}\right] \tag{5.45}$$

For parallel wall vaneless diffuser, the width $b = b_3 = b_5$

Hence equation 5.45 becomes

$$\frac{p}{p_2} = \left[\frac{1 - \dfrac{\left(\dfrac{c_{\omega 2}}{\cos\alpha}\right)^2\left(\dfrac{r_2}{r}\right)^2}{2C_{pa}T_{02}}}{1 - \dfrac{\left(\dfrac{c_{\omega 2}}{\cos\alpha_2}\right)^2}{2C_{pa}T_{02}}}\right]\left[\frac{b_2}{b_5}\right]\left[\frac{\tan\alpha_2}{\tan\alpha}\right] \tag{5.46}$$

Equation 5.46 showed that the static pressure rise in the vaneless diffuser is a function of radius ratio r/r_2 and the absolute flow angle α . For an efficient diffusion, the flow angle α must be reduced with increasing radius ratio.

Equation 5.46 is plotted as shown in **Fig. 5.11** to show the variation of pressure recovery in the vaneless diffuser.

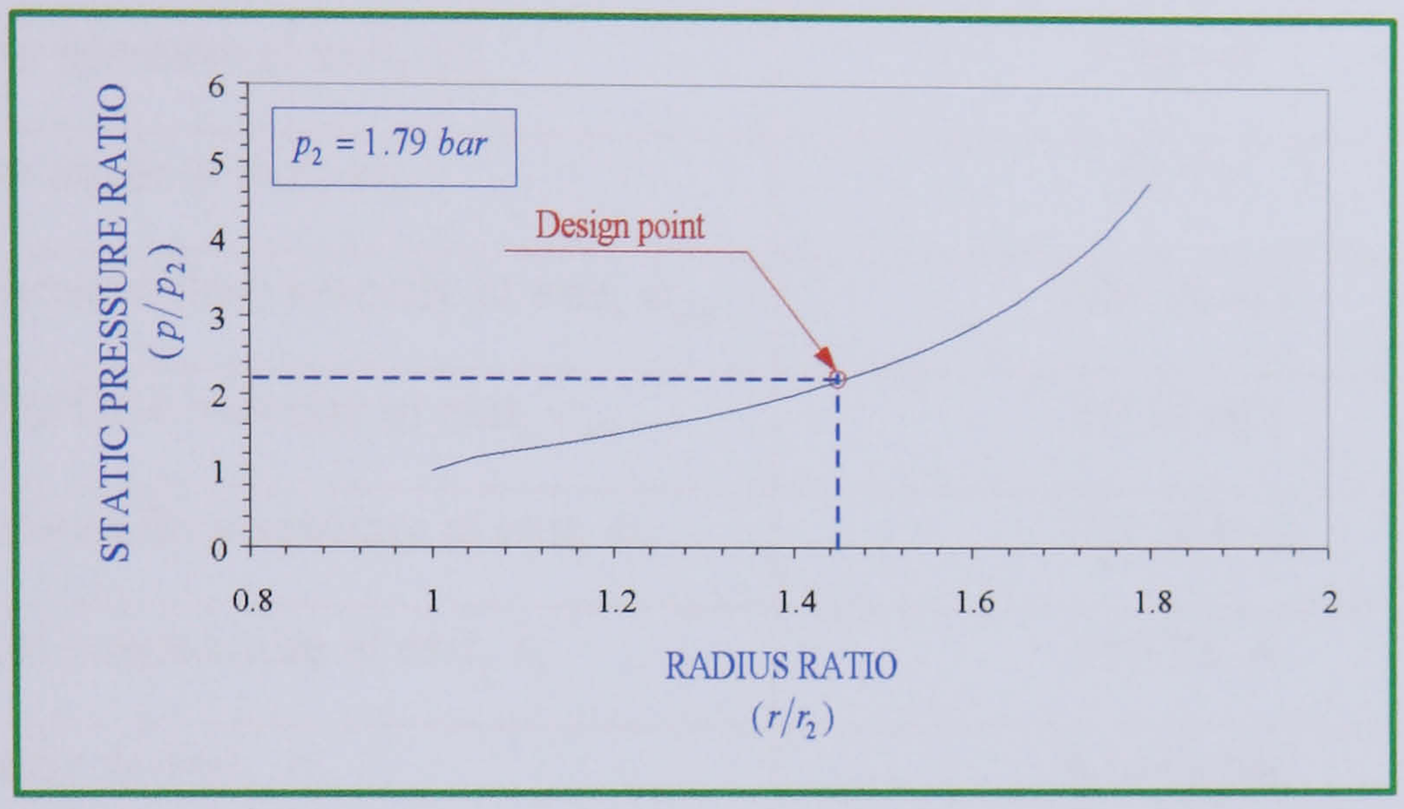

FIG. 5.11 PRESSURE RISE IN THE VANELESS DIFFUSER

Figure 5.12 shows the variation of both the tangential and radial velocities with radius ratio in the vaneless diffuser. It showed that both velocities are decreasing with increasing radius ratio.

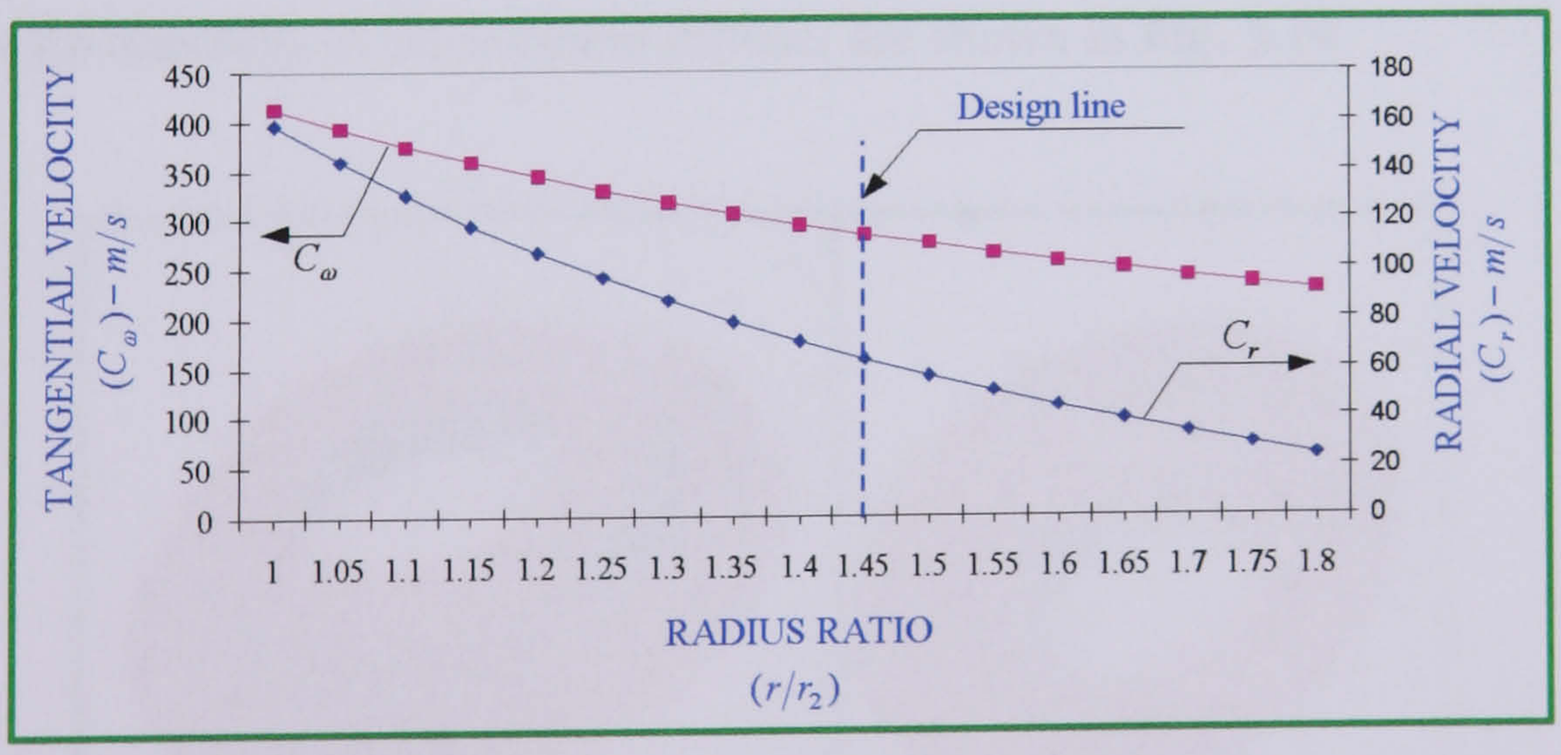

FIG. 5.12 VARIATION OF TANGENTIAL AND RADIAL VELOCITIES WITH RADIUS RATIO IN THE VANELESS DIFFUSER

5.7.2.2 Vaneless diffuser design data

The final design data of the vaneless diffuser parameters at exit are given in **Table 5.5**.

DESIGN PARAMETER	DESIGN VALUES
Vaneless diffuser diameter, d_5	$22.026\,cm$
Vaneless diffuser width, b_5	$0.582\,cm$
Static pressure at exit, p_5	$3.88\,bar$
Flow angle at exit, α_5	12.55°
Tangential flow velocity at exit, $c_{\omega 5}$	$284.36\,m/s$
Radial flow velocity at exit, c_{r5}	$63.37\,m/s$
Absolute flow velocity at exit, c_5	$291.33\,m/s$
Static temperature at exit, t_5	$430.28^{\circ}\,K$
Density at exit, ρ_5	$3.14\,kg/m^3$

TABLE 5.5 COMPLETE DESIGN DATA OF VANELESS DIFFUSER

5.7.2.3 Vaneless diffuser final model

A three-dimensional solid model of the vaneless diffuser is shown in **Fig. 5.13** and the final design drawings of the vaneless diffuser are shown in **Fig. 5.14**.

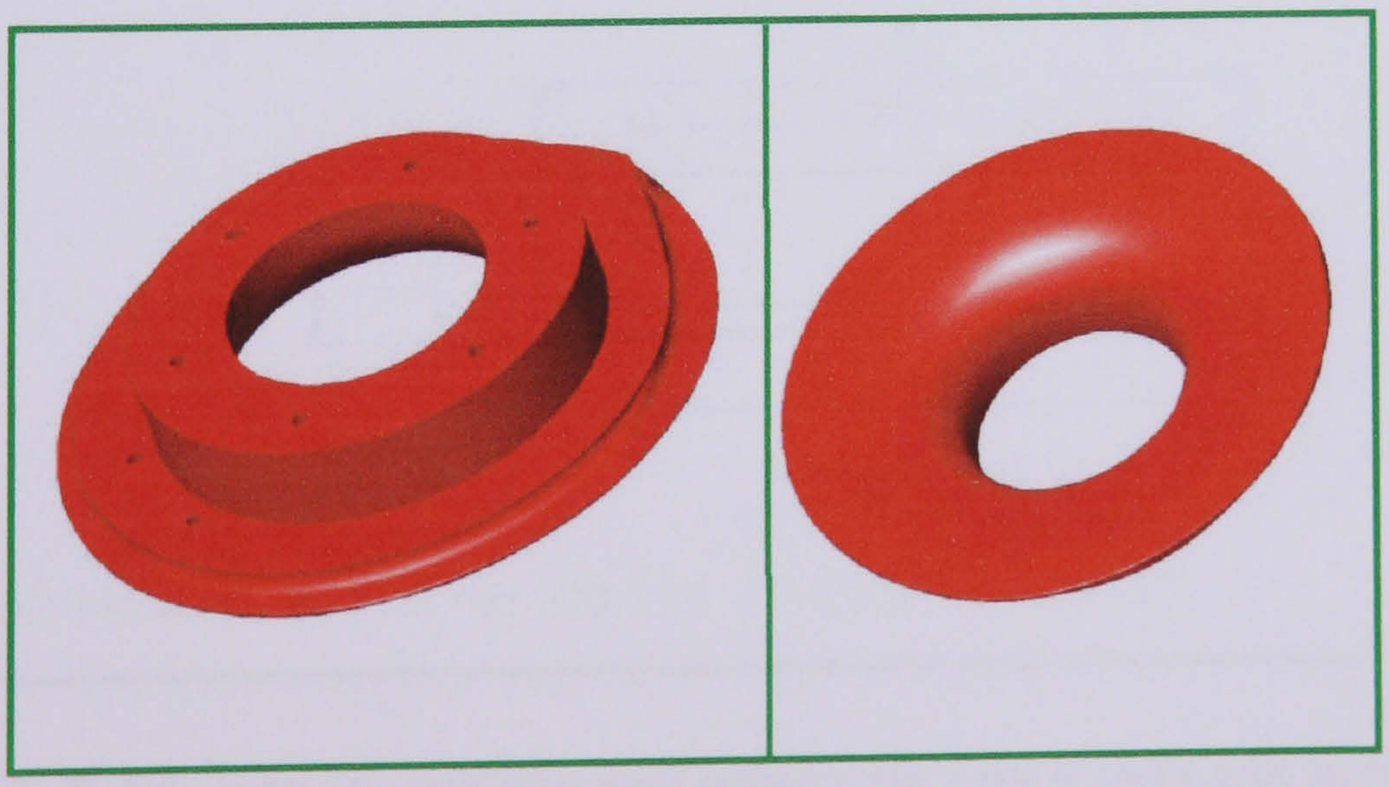

FIG. 5.13 THREE DIMENSIONAL SOLID MODEL OF THE VANELESS DIFFUSER

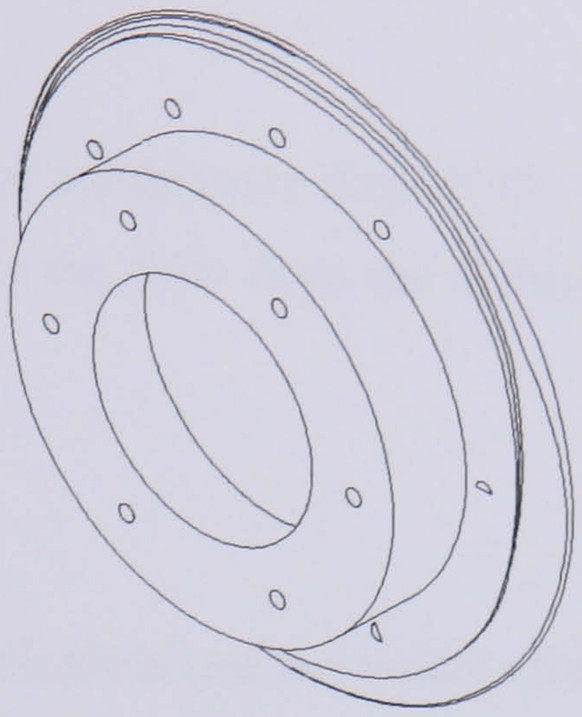

ISOMETRIC VIEW

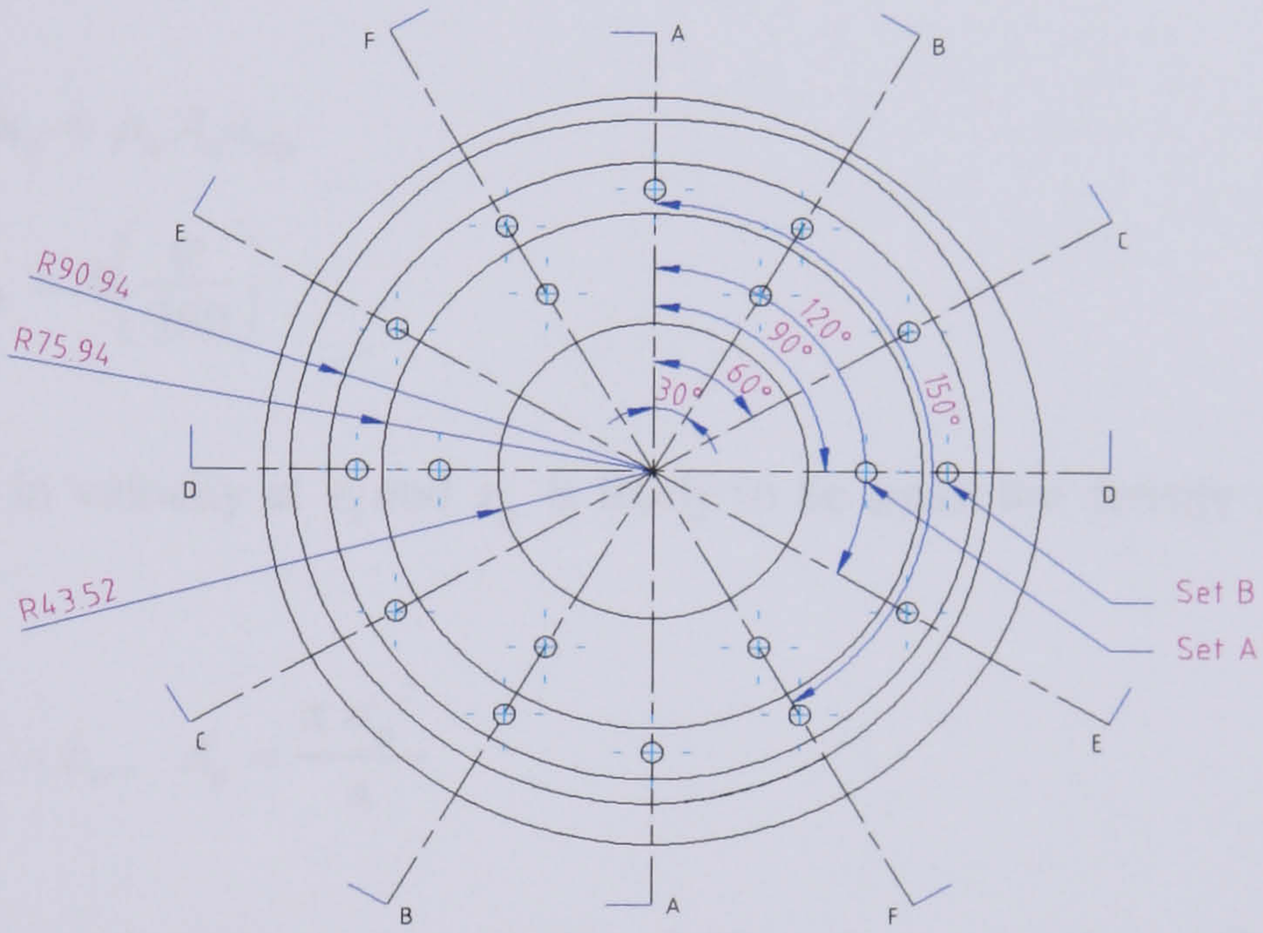

TOP VIEW

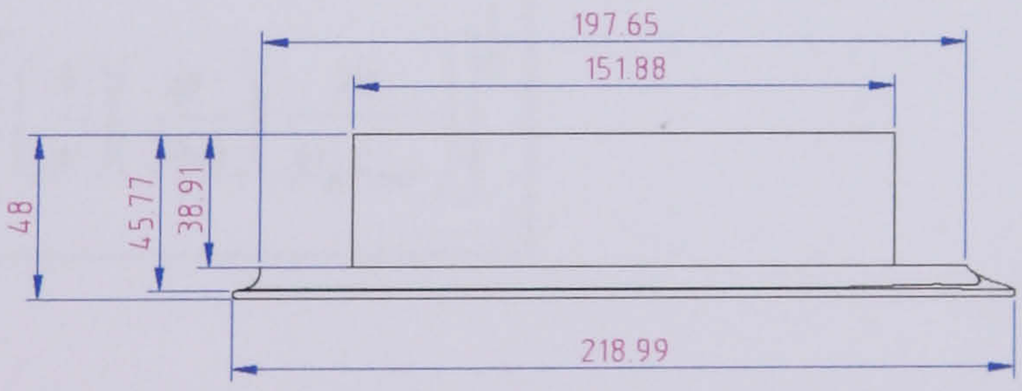

FRONT VIEW

ALL DIMENSIONS ARE IN mm UNLESS OTHERWISE STATED

FIG. 5.14 DETAIL DESIGN DRAWINGS OF THE VANELESS DIFFUSER

5.8 VOLUTE DESIGN

5.8.1 Introduction

The last basic component of a centrifugal compressor stage is the volute or scroll. It is a spiral – shaped housing which collects the flow from the diffuser and passes it to a pipe at the exit.

5.8.2 Design Method

Considering the flow in the volute is frictionless and the volute cross-section is circular for simplicity and ease of manufacture. Therefore, by applying the mass continuity at the centroid and at any azimuth angle φ of the volute will give:

$$\dot{m}_{\varphi} = \rho_{\varphi} A_{\varphi} c_{\omega\varphi} \tag{5.47}$$

But $$\dot{m}_{\varphi} = \dot{m}\left(\frac{\varphi}{360}\right)$$

Since the difference in velocity at r_5 and r_{φ} is likely to be small the density ratio will be nearly one, then

$$\rho_{\varphi} = \rho_5, \quad c_{\omega\varphi} = c_{\omega}, \quad A_{\varphi} = \frac{\pi d_{\varphi}^{\,2}}{4}$$

Substituting the above expressions in equation 5.47 and re-arranging will give an expression for volute cross-section diameter at any azimuth angle as:

$$\boxed{d_{\varphi} = \left[\left(\frac{4}{\pi}\right)\left(\frac{\varphi}{360}\right)\left(\frac{\dot{m}}{\rho_{\varphi} c_{\omega\varphi}}\right)\right]^{\frac{1}{2}}} \tag{5.48}$$

5.8.3 Final Design Model of the Volute

Final design model drawings of the volute and three-dimensional solid model of the volute are shown **Fig. 5.15** and **Fig. 5.16**, respectively.

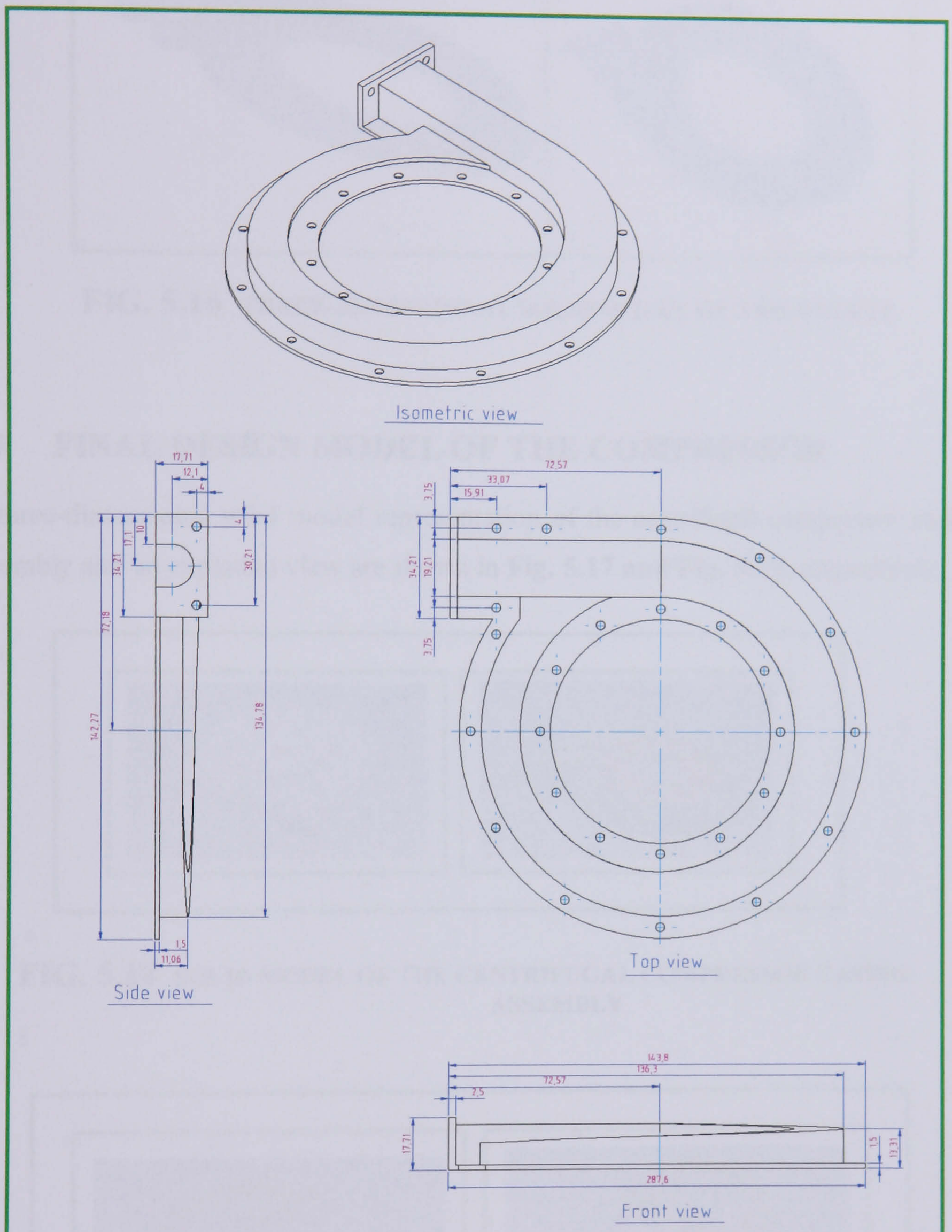

FIG. 5.15 DETAIL DESIGN DRAWING OF THE VOLUTE

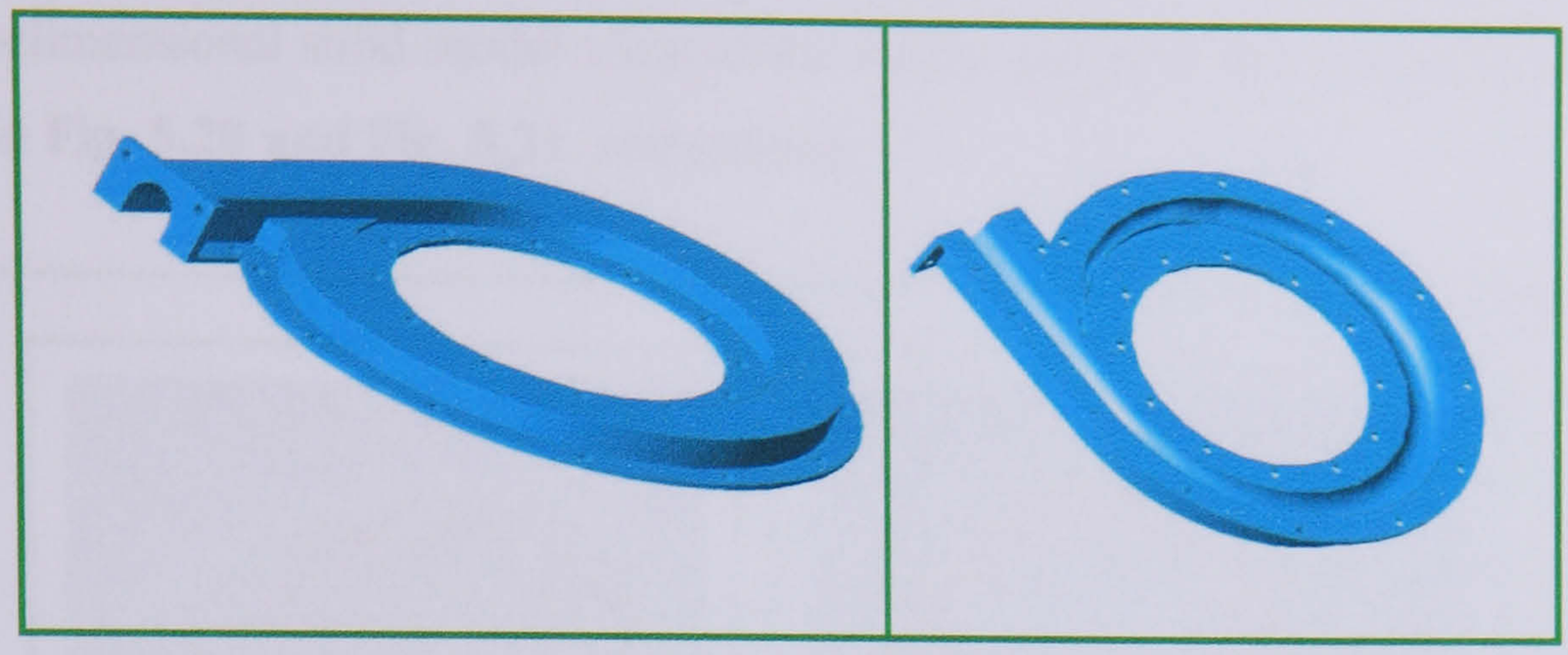

FIG. 5.16 THREE-DIMENSIONAL SOLID MODEL OF THE VOLUTE

5.9 FINAL DESIGN MODEL OF THE COMPRESSOR

A three-dimensional solid model representation of the centrifugal compressor casing assembly and an exploded view are shown in **Fig. 5.17 and Fig. 5.18**, respectively.

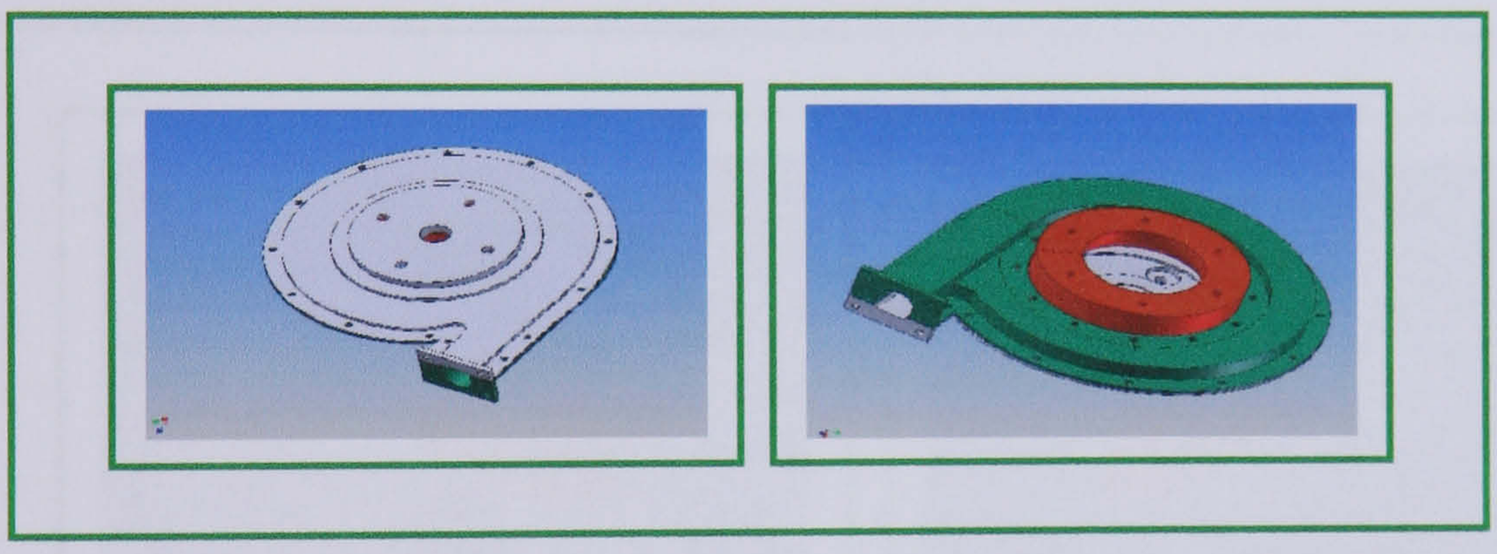

FIG. 5.18 SOLID MODEL OF THE CENTRIFUGAL COMPRESSOR CASING ASSEMBLY

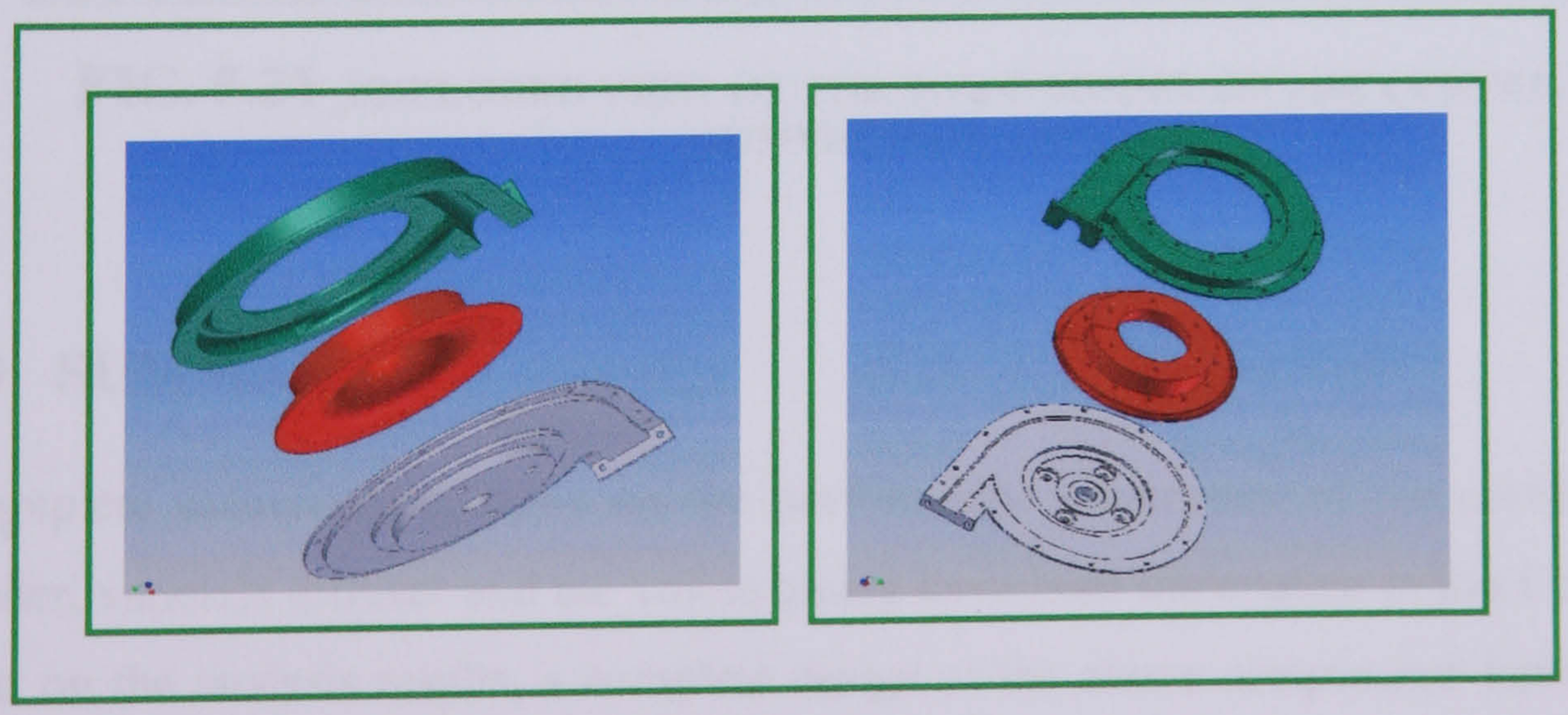

FIG. 5.19 EXPLODED VIEW OF SOLID MODEL OF THE CENTRIFUGAL COMPRESSOR CASING ASSEMBLY

A three-dimensional solid model view of the whole assembly and exploded view are shown in **Fig. 5.20 and Fig. 5.21**, respectively.

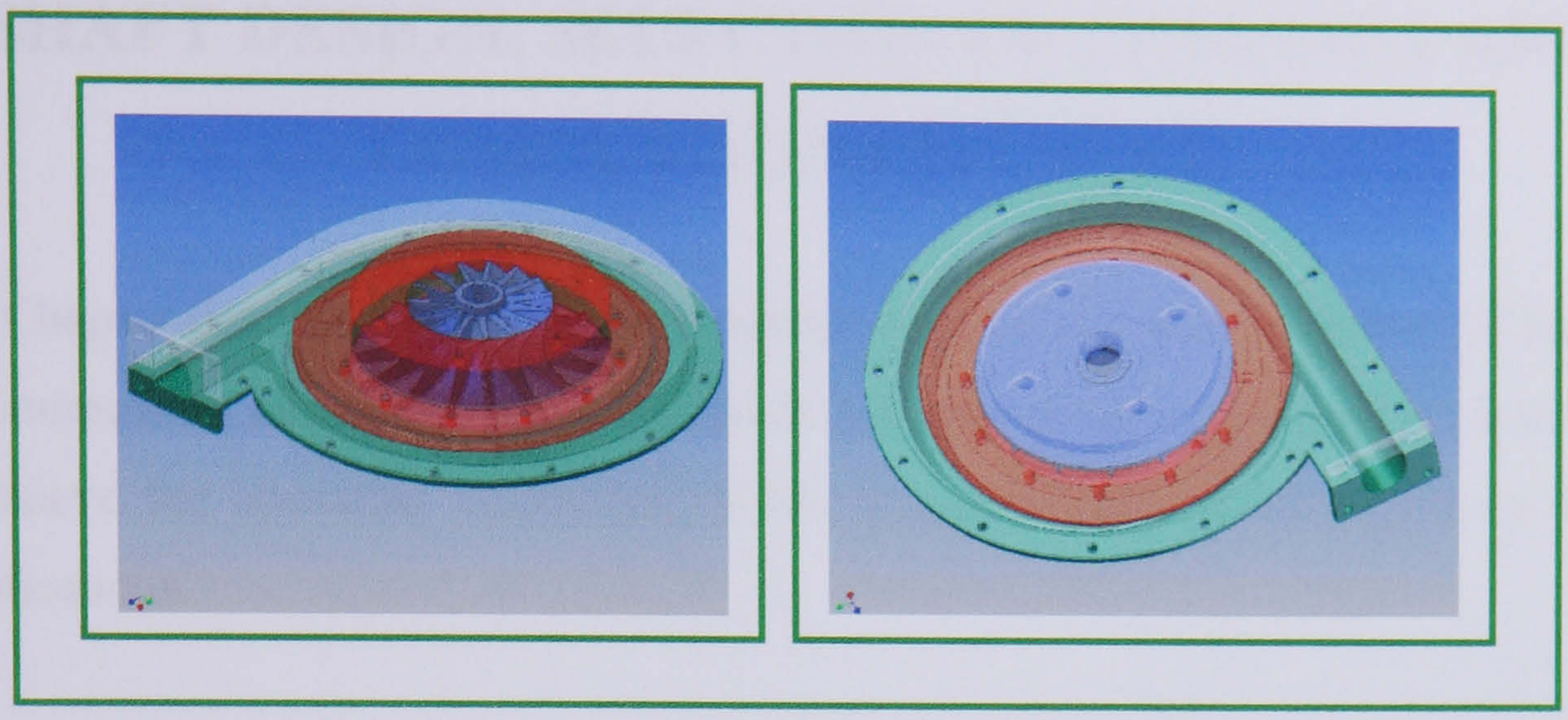

FIG. 5.20 THREE-DIMENSIONAL SOLID MODEL OF THE CENTRIFUGAL COMPRESSOR ASSEMBLY

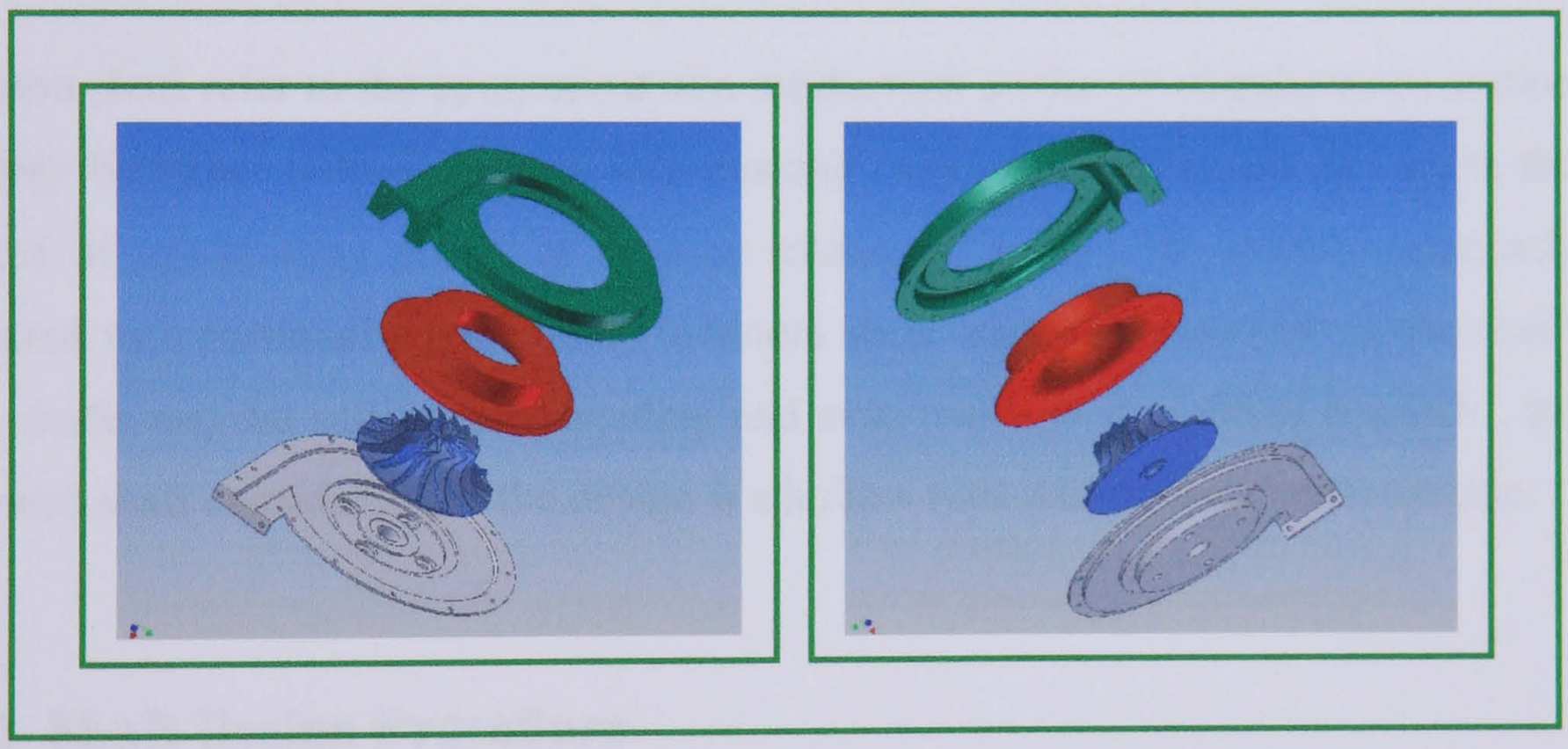

FIG. 5.21 EXPLODED VIEW OF THE SOLID MODEL OF THE CENTRIFUGAL COMPRESSOR ASSEMBLY

5.10 SUMMARY

A complete theoretical analysis on the performance parameters of the compressor impeller, vaneless diffuser and the volute casing have been undertaken in this Chapter. Based on the analysis results, a complete design of the above components have been presented and finalised.

CHAPTER 6

SHAFT DESIGN, SELECTION OF BEARINGS AND COMBUSTION CHAMBER

This Chapter details the design of the turbine-compressor shaft, selection of bearings and combustion chamber. Proper design or selection of these components is required to achieve the operating conditions of the complete gas turbine engine to the set specifications.

6.1 SHAFT DESIGN

6.1.1 Introduction

The term shaft refer to the component of a mechanical device of circular cross section and may be either hollow or solid that transmit rotational motion and power. In the process of transmitting power at a given rotational speed , the shaft is inherently subjected to a torsional stress. Thus, torsional shear stress is developed in the shaft. Also, shafts may be subjected to bending and axial loads. In the current research , the proposed shaft considered for the design is a hollow type with stepped cross-section.

6.1.2 Shaft Design Procedure

Shaft design consists primarily of the determination of the correct shaft diameter and length to ensure satisfactory strength and rigidity, when the shaft is transmitting power under various operating and loading conditions. Design of shafts of ductile materials based on strength is controlled by the maximum shear theory. Shafting is usually subjected to torsion, bending and axial loads. In small gas turbines, bending loads due to the weight of the rotor and impeller are considered very small and can be neglected. Therefore, the only loads considered here are those due to torque and axial loads.

6.1.2.1 Main design equations of a hollow shaft

i. Torsional loads

The torsional stress σ_{shear} developed due to torsional loads is given as:

$$(\sigma_{shear})_{d=d_0} = k_t \frac{16\tau d_0}{\pi(d_0^{\,4} - d_i^{\,4})} \qquad \text{(At outer diameter)} \qquad (6.1)$$

$$(\sigma_{shear})_{d=d_i} = k_t \frac{16\tau d_i}{\pi(d_0^{\,4} - d_i^{\,4})} \qquad \text{(At inner diameter)} \qquad (6.2)$$

Where:

k_t = The combined shock and fatigue factor applied to torsional moment, normal range between (1.0-1.5) .

ii. Axial loads

The tensile σ_t or compressive stress σ_c developed due to axial loads is given as:

$$\sigma_t = \sigma_c = \frac{4F_a}{\pi(d_0^{\,4} - d_i^{\,4})} \qquad (6.3)$$

6.1.2.2 Shaft design requirements

i. Shaft-bolt assembly

In the current work, it is required to design a rotating hollow stepped shaft of a specfied length L and various outer diameters d_1, d_2 and d_3. Also, to design a main bolt to pass through the hollow shaft and its function is to connect the turbine rotor and the centrifugal impeller together. The design objective of the shaft-bolt assembly is to be able to support safely both the rotor and the impeller. Schematic diagrams of the proposed shaft and the bolt are shown in **Figs. 6.1** and **6.2** respectively.

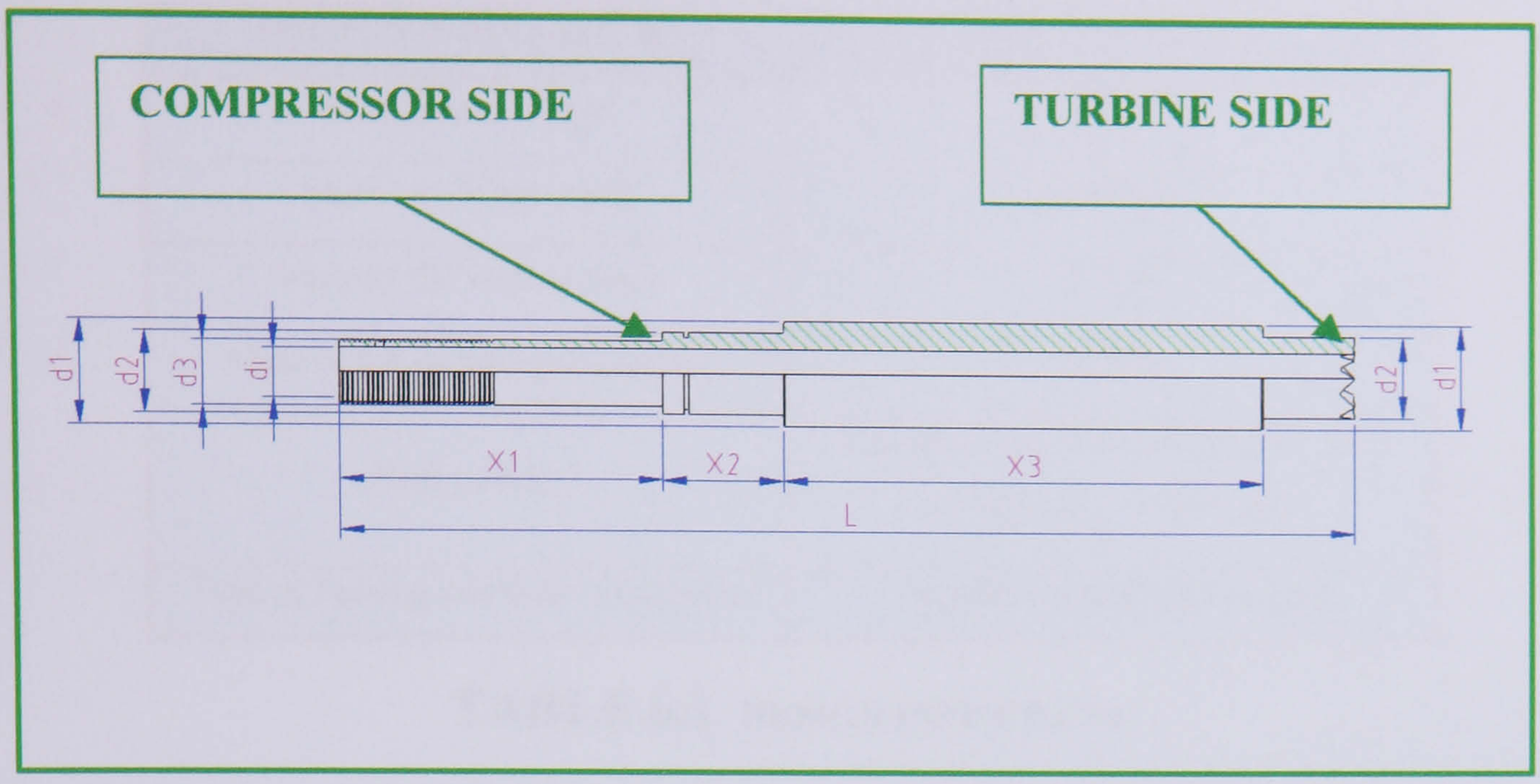

FIG. 6.1 SCHEMATIC DIAGRAM OF PROPOSED HOLLOW SHAFT

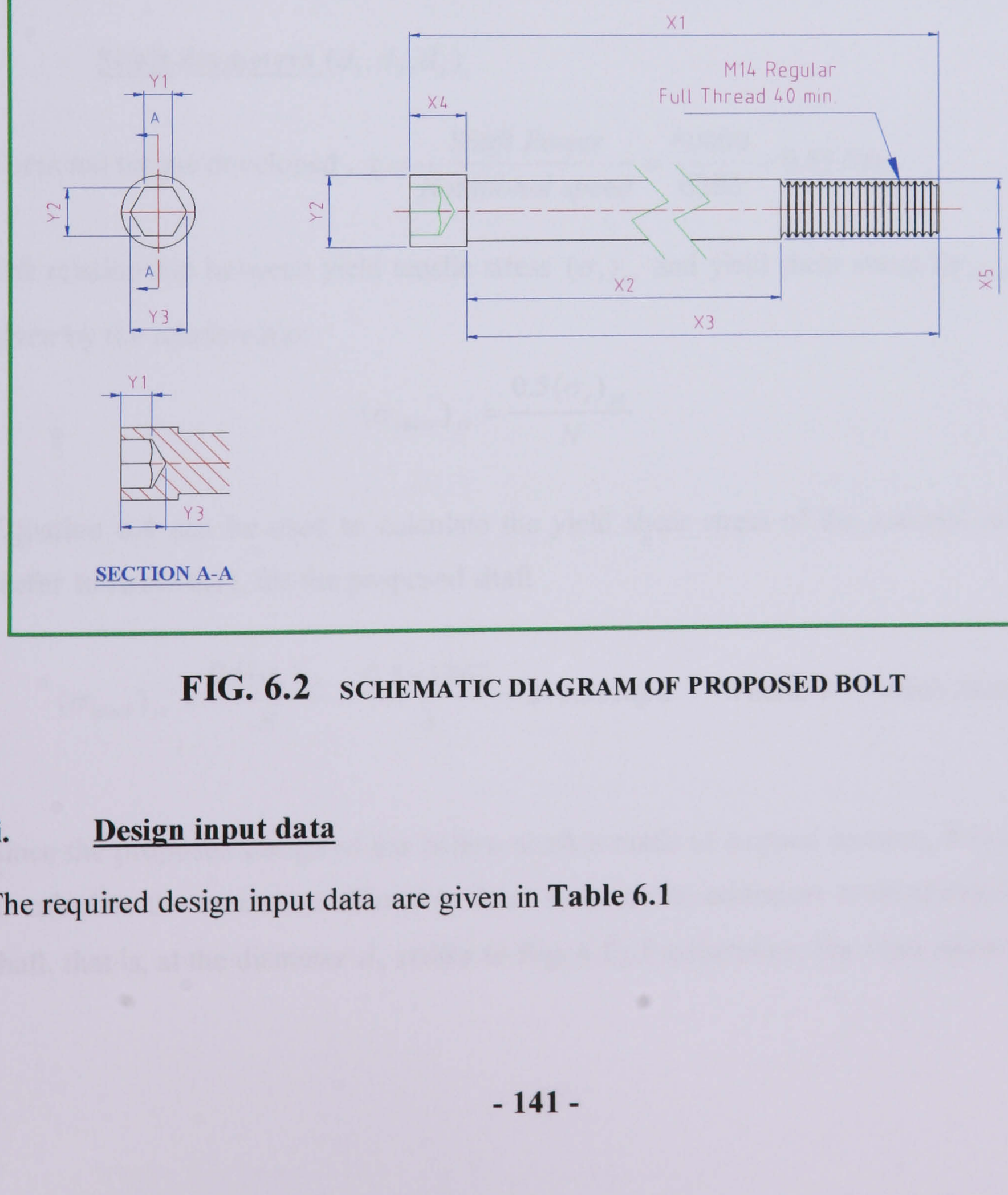

FIG. 6.2 SCHEMATIC DIAGRAM OF PROPOSED BOLT

ii. Design input data

The required design input data are given in **Table 6.1**

DESIGN PARAMETER	DESIGN VALUE
Shaft power output	$60kW$
Shaft rotational speed	$60000rpm$
Mass of the turbine rotor	$2.94kg$
Mass of the centrifugal impeller	$0.85kg$
Shaft material	Stainless steel, Type ASIA 630,UNS S17400, $\sigma_{ys} = 1262Mpa$
Type of bearing and their dimensions	Angular contact ball bearings

TABLE 6.1 DESIGN INPUT DATA

6.1.2.3 Shaft design calculations

The calculation procedure for the main dimensions of the hollow shaft is carried as follows:

i. **Shaft diameters** (d_1, d_2, d_3)

Torsional torque developed , $\tau = \dfrac{Shaft\ Power}{Rotational\ speed} = \dfrac{60000}{6283} = 9.55\ Nm$

The relationship between yield tensile stress $(\sigma_t)_{ys}$ and yield shear stress $(\sigma_{shear})_{ys}$ is given by the relationship:

$$(\sigma_{shear})_{ys} = \frac{0.5(\sigma_t)_{ys}}{N} \tag{6.4}$$

Equation 6.4 can be used to calculate the yield shear stress of the material selected **(refer toTable 6.1)**, for the proposed shaft

$(\sigma_{shear})_{ys} = \dfrac{0.5(\sigma_t)_{ys}}{N} = \dfrac{0.5 \times 1262}{3} = 210.33\,Mpa$ Where, N = safety factor = 3

Since the proposed design of the hollow shaft is made of stepped sections, it is a must to calculate the maximum allowable shear stress at the minimum cross-section of the shaft, that is, at the diameter d_3 (**refer to Fig. 6.1**). Furthermore, the shear stress at this

diameter d_3 must be less than the allowable shear stress of the material for a safe design. In the current research work, the minimum outer diameter d_3 of the hollow shaft is specified by the size of the impeller bore diameter which is equal to $20\,mm$ and the internal diameter of the hollow shaft is specified by the size of the hearth coupling of the rotor which is equal to $15\,mm$.

i.e $d_{\min} = d_3 = 20\,mm$, $d_i = 15\,mm$ and by using equation 6.2, then the maximum allowable shear stress at this local section is calculated as follows:

$$\left[(\sigma_{shear})_{\max}\right]_{d_3=d_1} = k_t \frac{16\tau d_3}{\pi(d_3^{\,4} - d_i^{\,4})} = (1.5)\frac{(16)(9.55)(0.02)}{\pi(0.02^4 - 0.015^4)} = 0.833MPa$$

Where: $k_t\ (range) = 1.0 - 1.5$, in this case k_t is selected to be equal to 1.5

It can be deduced that the calculated maximum shear stress $(\sigma_{shear})_{\max}$ at d_3 is below the value of the allowable shear stress of the material. Once this minimum diameter of the stepped hollow shaft is determind, then the diameter of other sections d_2 and d_1 can be determind and their values are based on the size of the selected bearings which satisfies the design requirements. In this case, calculations showed that the size of the required bearing is $25\,mm$ **(refer to Sec. 6.2)**.

ii. <u>Shaft length</u> (L)

The total length of the shaft L and the best location of the bearings on the shaft can be determind by considering the rotating system assembly. The design requirements of the shaft L are based on the following criteria:

i. The shaft length should be kept as short as possible for a good design to reduce bending effects.

ii. The selected bearing should be attached as close as possible to the main components attached to the shaft, that is, the rotor and the impeller.

iii. The axial length of the rotor, the impeller and the bearings.

iv. The position of the centre of gravity of the rotating system asembly. For a good design, it should lie between the two bearings for a stable design.

With the aid of the **CAD** software, the masses and their centre of gravity **(C.G)** of the rotor, impeller, main shaft , the bolt and the holding nut can be known, hence the **(C.G)** of the rotating system would be determind. If the position of system **(C.G)** doesnot satisfy the design requirements, the shaft length is changed until a satisfied design value is obtained. In this case L was found to be equal to 304.4 mm. Also, the best location of the bearings was determined. The final dimensions of the rotating assembly and bearings location are shown in **Fig. 6.3**.

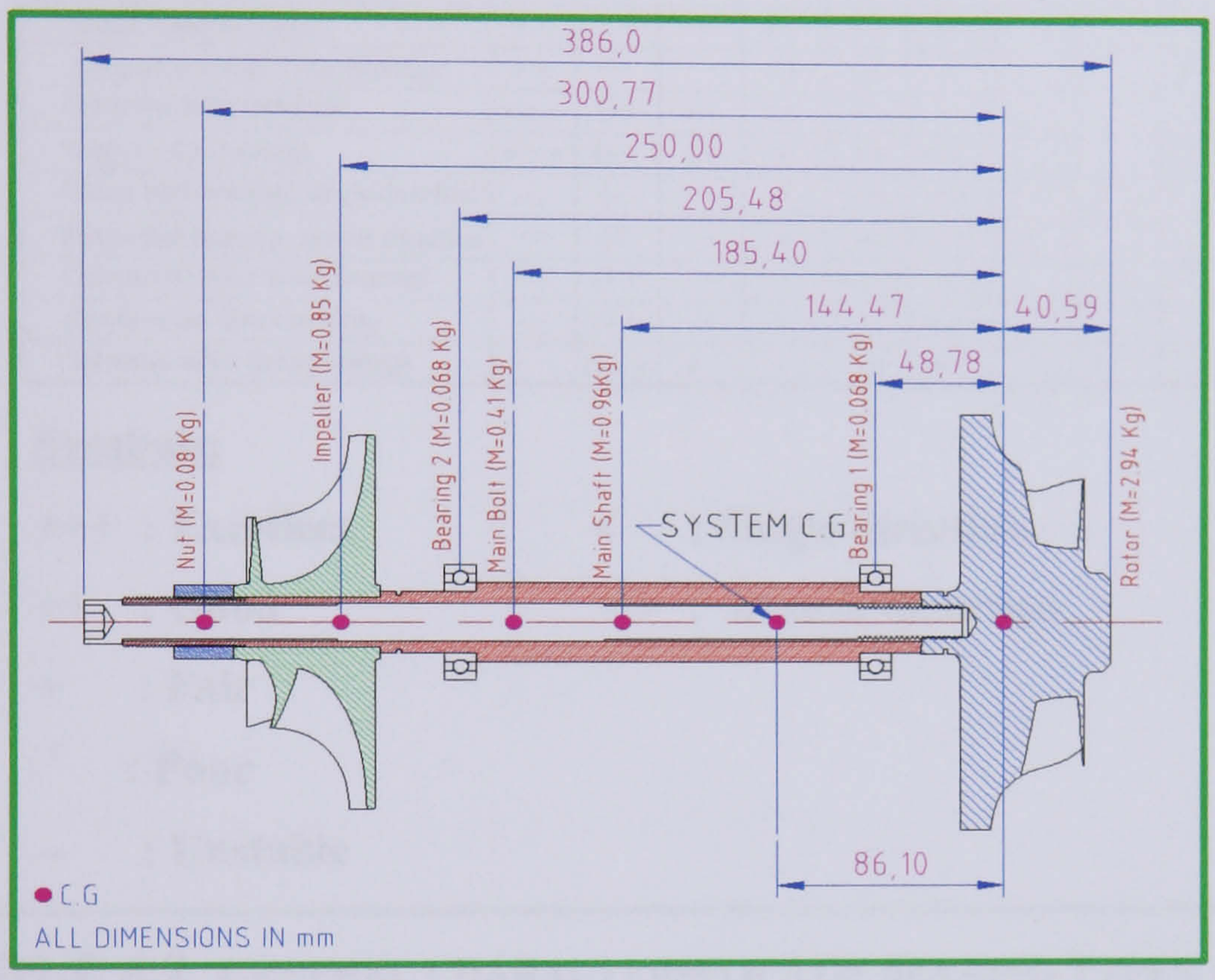

FIG. 6.3 SCHEMATIC DIAGRAM OF THE PROPOSED ROTATING SYSTEM SHOWING C.G OF THE SYSTEM AND THE COMPONENTS

6.2 SELECTION OF BEARINGS

6.2.1 Type Selection

In general, Ball and roller bearings are usually recommended for small gas turbines. Ball bearings are used to withstand loads parallel to shaft axis (thrust loads) sometimes in conjunction with radial loads transverse to the axis, while roller bearings are usually used for direct radial loads. Selection of bearing type to use in a given application can be aided by referring to **Table 6.2**, provided by **Ref. [71]**.

Characteristics / Bearing type	Load carrying capacity: radial	Load carrying capacity: Axial	Load carrying capacity: combined	Speed capability	Running accuracy	Stiffness	Quiet operation	Low torque	Suitable as locating bearing	Suitable as non locating bearing
Deep groove ball bearing	+	⟨+⟩		+++	+++	+	+++	+++	++	+
Self-aligning ball bearing	+	⟨–⟩	–	++	++	+			+	+
Angular contact ball bearing	++	⟨++	++		+++	++	++		++	
Four-point contact ball bearings	+	⟨++⟩	++	+	+	++			++	
Cylindrical roller bearings with cage	++	– –		+++	+++	++	+	++	– –	++
Cylindrical roller bearings full complement	+++	⟨–	–		++	+++			–	
Needle roller bearings	++	– –	– –	++	++	++			– –	++
Allignment needle roller bearings	++	– –	– –	++	+	+			– –	++
Spherical roller bearings	+++	⟨+⟩	++	++	++	++			++	+
Tapper roller bearings	+++	⟨++	++	+	++	++			+++	
Thrust Ball bearings, single direction	– –	⟨+	– –	+	++	++				
Thrust Ball bearings, double direction	– –	⟨+	– –	+	++	++				
Cylindrical roller thrust bearings	– –	⟨++	– –	–	+++	+++				
Needle roller thrust bearings	– –	⟨++	– –	–	+	+++				
Spherical roller thrust bearings	– –	⟨+++	+	–	++	++				

Symbols:

+++ : Excellent **< : Single direction**

++ : Good **<> : Double direction**

+ : Fair

- : Poor

-- : Unstable

TABLE 6.2 GENERAL CHARACTERISTICS OF BEARING TYPES, REF. [89]

For small gas turbine applications, Bearings are subjected to combined radial and axial loadings. Therefore, the type suited to the present work application is the angular contact ball bearings, **Table 6.2**.

6.2.2 Bearing Size

The selection of the approriate bearing size depends on the following criteria:

i. The magnitudes of applied static and dynamic loads respectively.

ii. Rotoational speed

iii. Fatigue life.

Based on satisfying the above criteria, the selection of the required bearing can be determind. The final dimensions of the bearing are: Inner bore = $25\,mm$, Outer bore = $47\,mm$. Once these dimensions are known, then the outer diameters d_2 and d_3 of the hollow shaft can be determind. In this case they are $25\,mm$ and $32.2\,mm$, respectively.

6.2.3 Bearing Material

The most important feature of the bearing material is the ball bearings. Ceramic ball bearings **(Silicon Nitride Si3N4)** was chosen and bought from **SNFA Bearing Limited [72]** for the current application. The choice was made based on the following advantages compared to steel ball bearings :

i. Longer life, even at high loads.
ii. Higher resistance to seizure in critical lubrication situations.
iii. Lower power dissipation.
iv. Higher speed both with oil and grease lubrication.
v. Higher acceleration and deceleration limits.
vi. Greater static and dynamic rigidity.
vii. Lower wear.
viii. Reduced mass (40% of steel), high hardness and good fatigue resistance.

6.3 BEARING HOUSING

The bearing housing was designed to accommodate the bearings and to provide oil lubrication. Detail drawing and of the bearing housing is shown in in **Fig. 6.4** and **Fig. 6.5**, respectively.

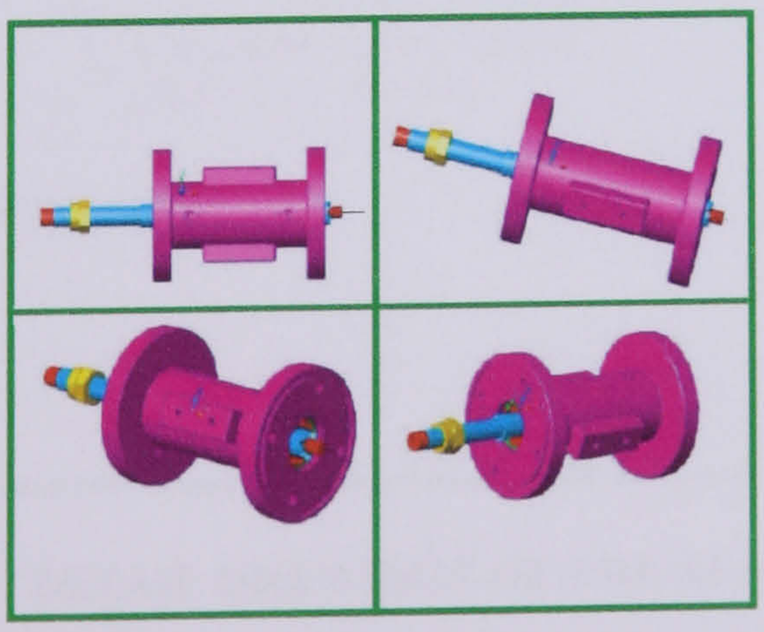

FIG. 6.4 THREE DIMENSIONAL SOLID MODEL DIAGRAM OF BEARING HOUSING

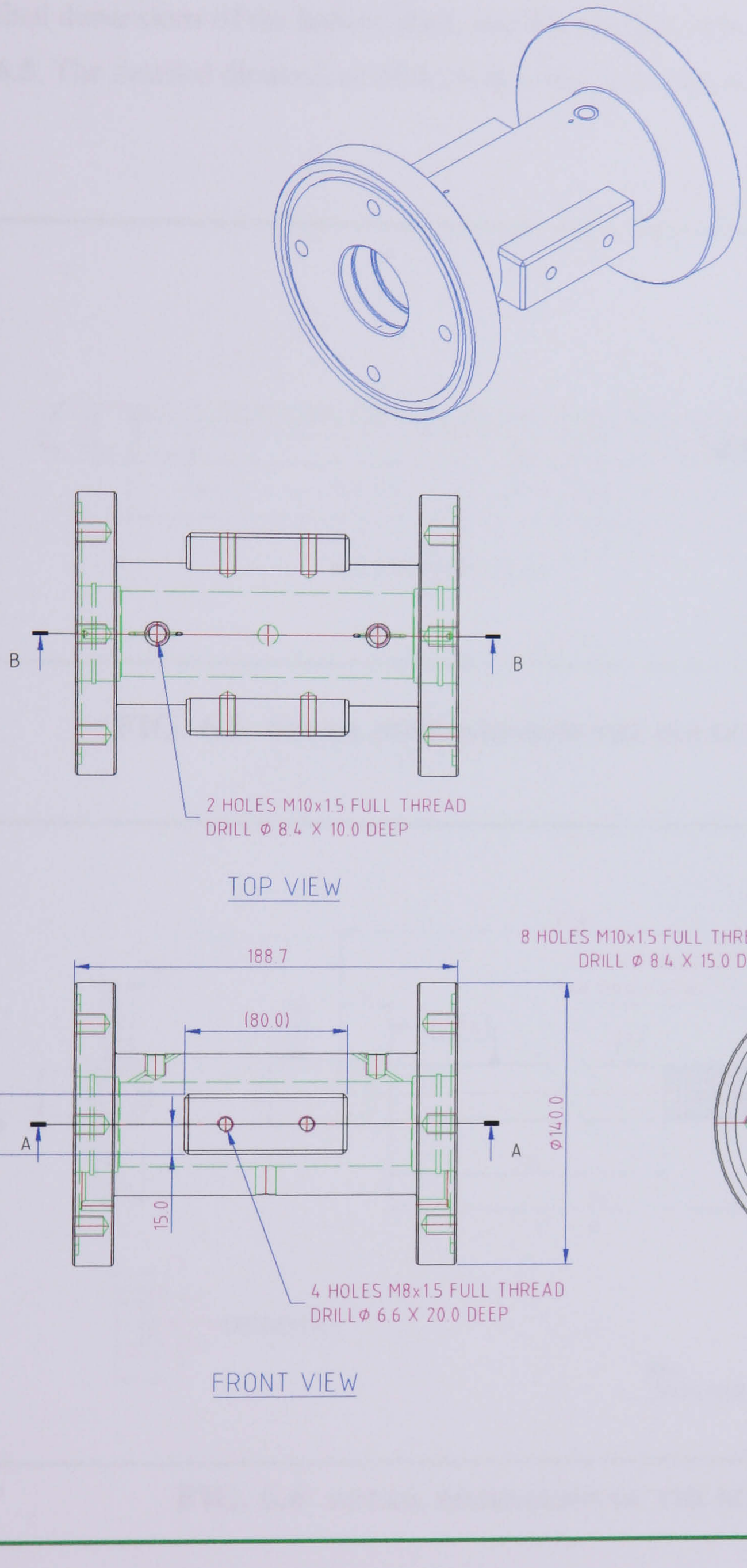

FIG. 6.4 DETAIL DRAWINGS OF THE BEARING HOUSING

6.4 FINAL MODEL OF THE SHAFT-BOLT ASSEMBLY

The final dimensions of the hollow shaft, and the position of the bearings are shown in **Fig. 6.5**. The detailed dimensions of the bolt is shown in **Fig. 6.6**.

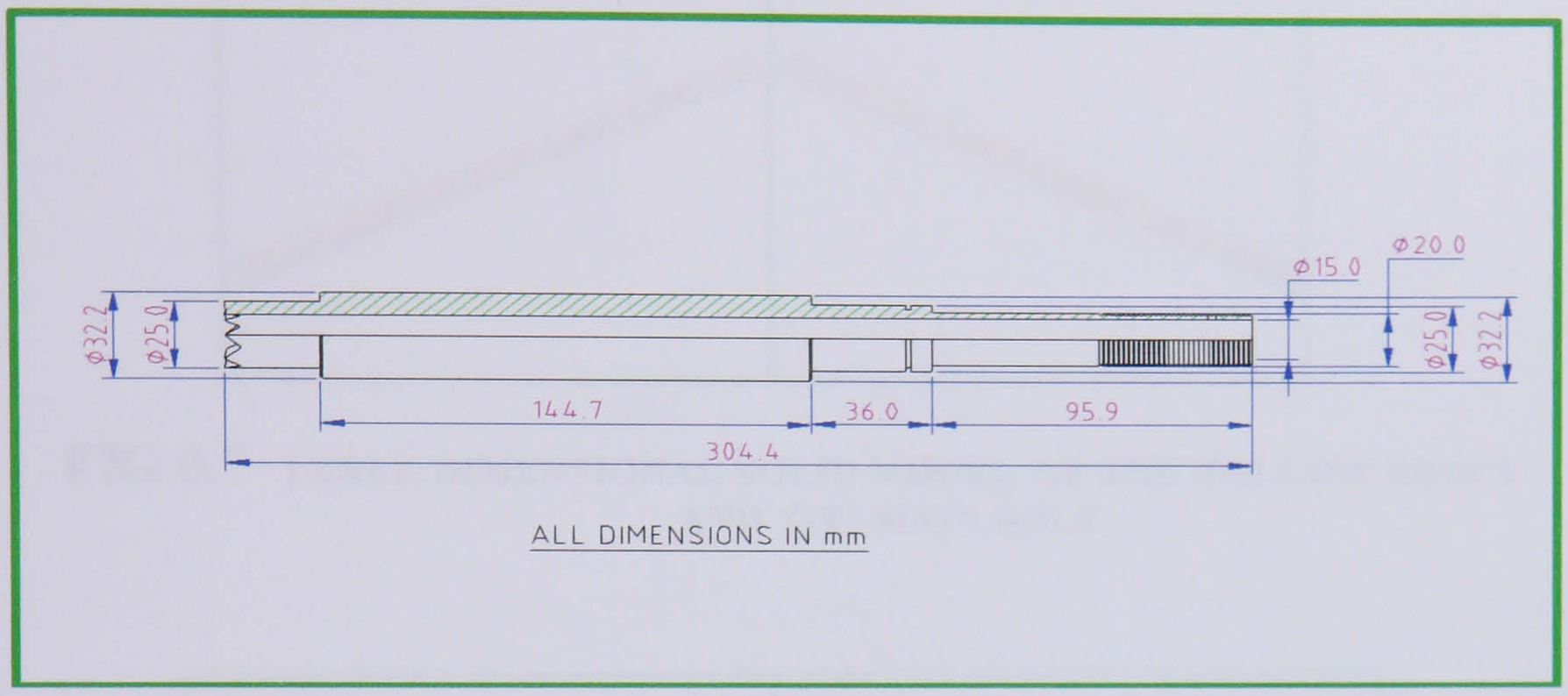

FIG. 6.5 DETAIL DIMENSIONS OF THE HOLLOW SHAFT

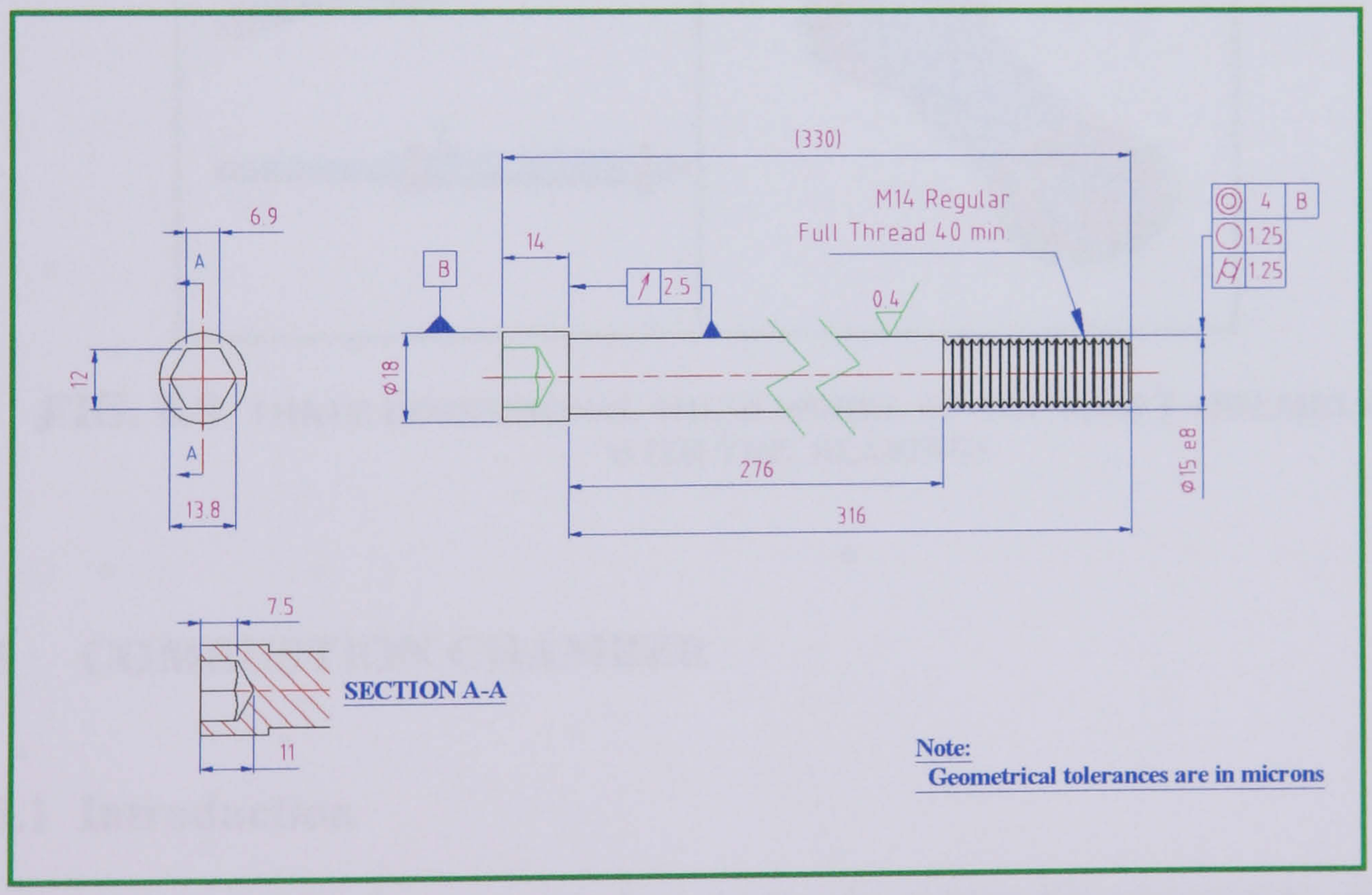

FIG. 6.6 DETAIL DIMENSIONS OF THE BOLT

A three-dimensional solid model of the hollow shaft, the main bolt and the shaft –bolt assembly including the bearings are shown in **Figs. 6.7** and **6.8**, respectively.

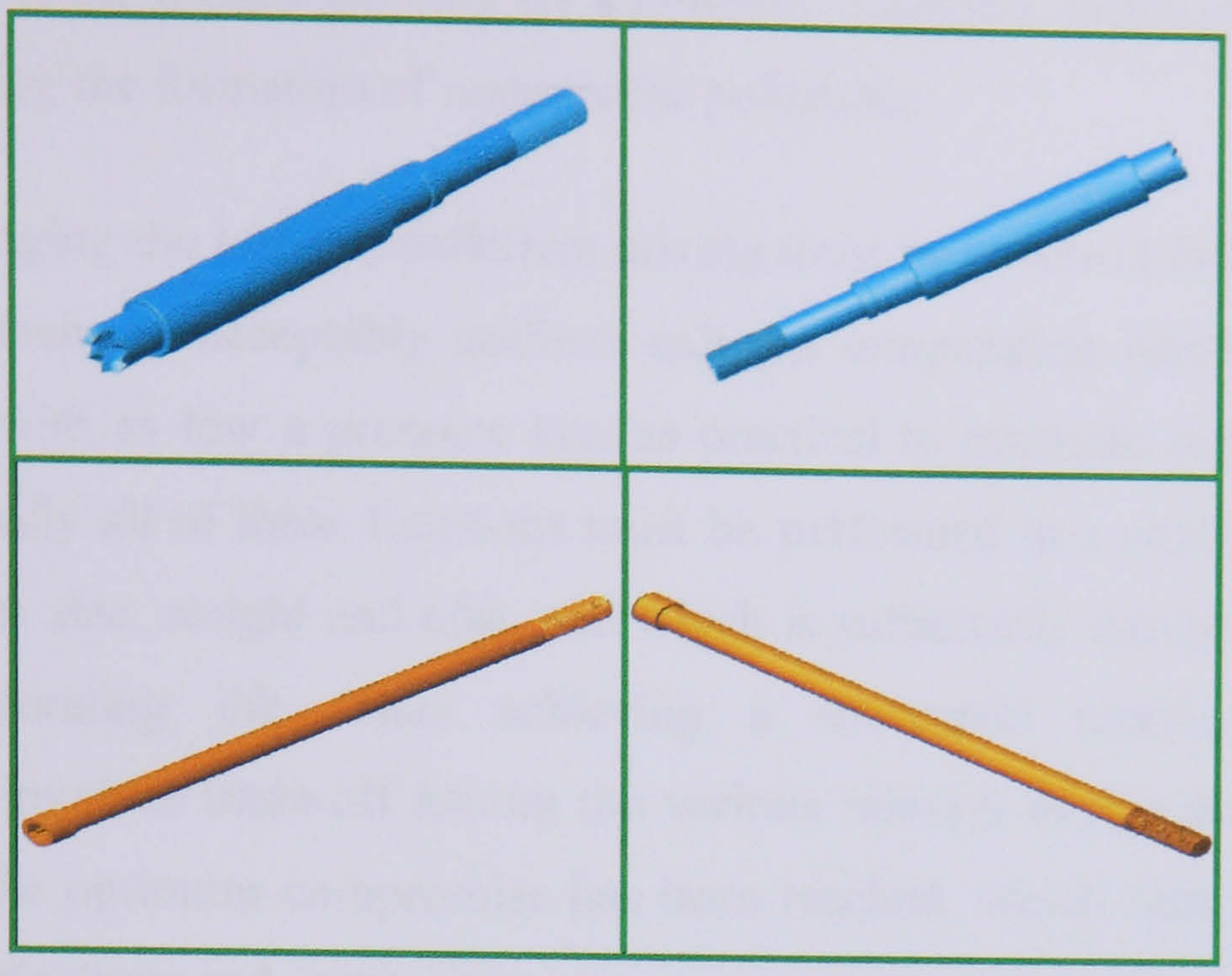

FIG 6.7 THREE DIMENSIONAL SOLID MODEL OF THE HOLLOW SHAFT AND THE MAIN BOLT

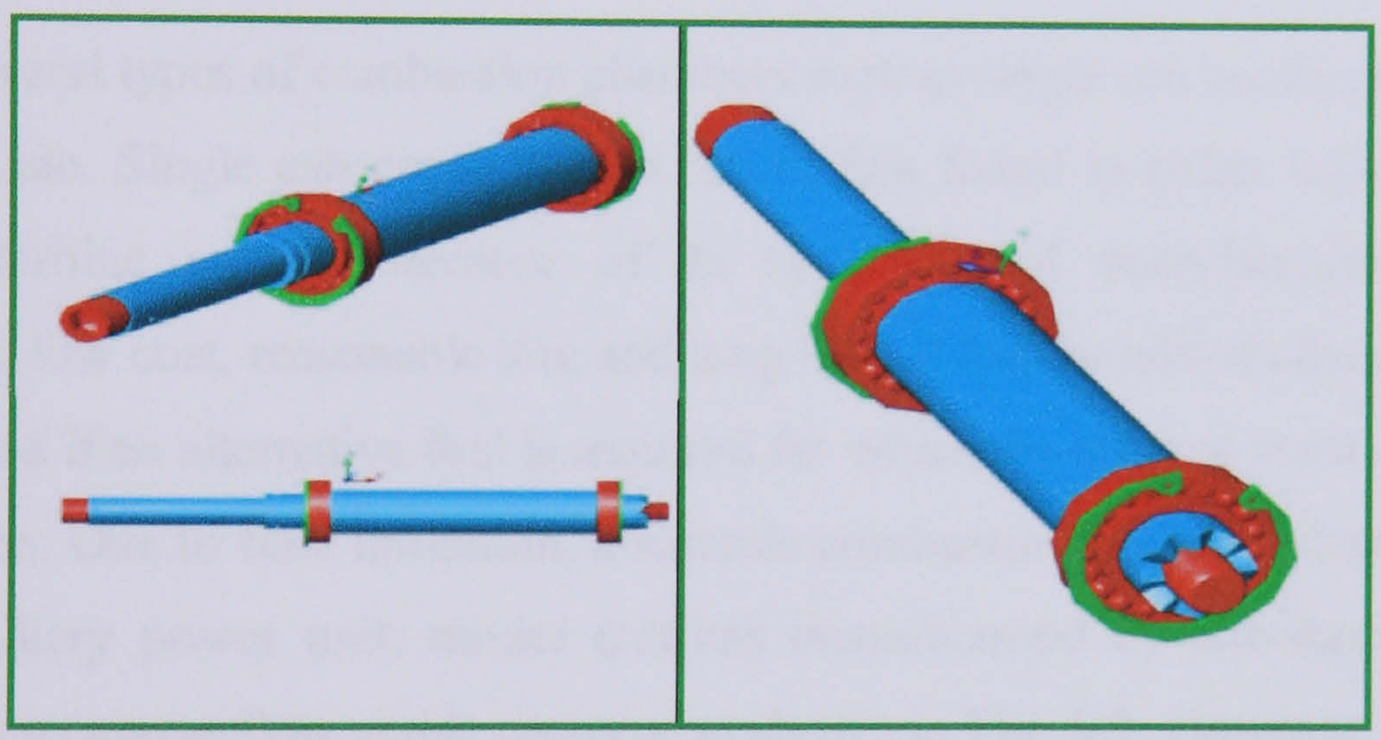

FIG. 6.8 THREE DIMENSIONAL SOLID MODEL OF THE SHAFT ASSEMBLY WITH THE BEARINGS

6.5 COMBUSTION CHAMBER

6.5.1 Introduction

A gas turbine combustion chamber is a device for raising the temperature of the incoming air stream by the addition and combustion of fuel. In serving this purpose, the combustion chamber must satisfy many different requirements. It must be capable of initiating ignition easily and must operate stably over a wide range of conditions. At

all operating points, it must provide for essentially complete combustion of the fuel while minimising the formation of undesiarble pollutants.

To avoid damaging the turbine, sufficient mixing must be achieved in the combustion chamber to obtain an acceptably uniform exit gas temperature distribution. Also it must operate with as low a pressure loss as practical to maintain high overall cycle efficiency. Finally all of these functions must be performed in a configuration which has a minimum size, weight and cost, and which is sufficiently durable to achieve an acceptable operating life. Thus achieving a successful combustion chamber configuration involves trade-off among the various relavent design and performance criteria until the optimum compromise has been reached, which best satisfies all the imposed specifications and constraints.

6.5.2 Selection of Combustion Chamber

There are several types of combustion chambers such as single can combustor, Annular combustors, etc. Single can combustor is most often found in either industrial, or in small gas turbine engines because of its simplicity of manufacturing, ease of maintenance, low cost, reasonable size and long life . It has the added advantage that is easily replaced if an alternative fuel is required for which the original combustor would not be suitabe. Due to time limitation, a suitable combustor liner was adapted from an existing auxiliary power unit, model **GTCP85** manufactured by **Air-Research**. This combustor is a reverse flow single can type as shown in **Fig. 6.9**. However, The reason for excluding out the existing combustor casing because it was too large and found quiet difficult to modify it to fit the turbine inlet port. Therefore, a new combustor casing was designed to fit both the combustion liner and the turbine inlet assembly.

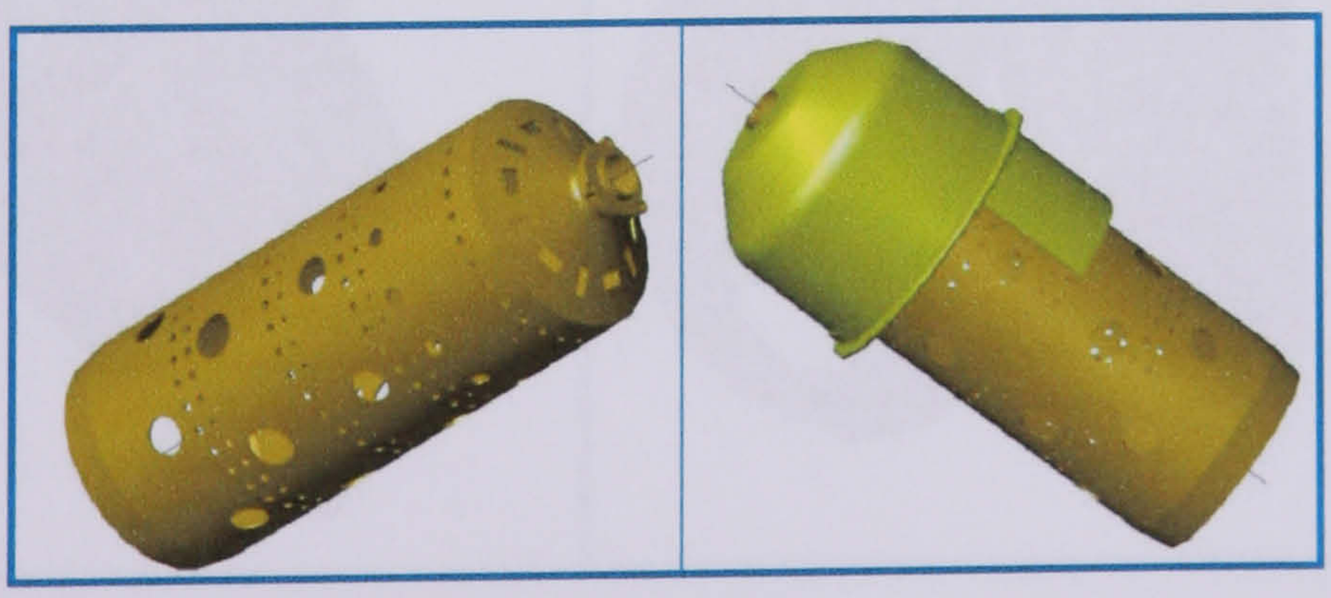

FIG. 6.9 SOLID MODEL OF A SINGLE CAN COMBUSTOR LINER ADAPTED FROM AN AUXILIARY POWER UNIT, MODEL GTCP85

Detailed dimensions of the selected combustion chamber liner are given in **Fig. 6.10**.

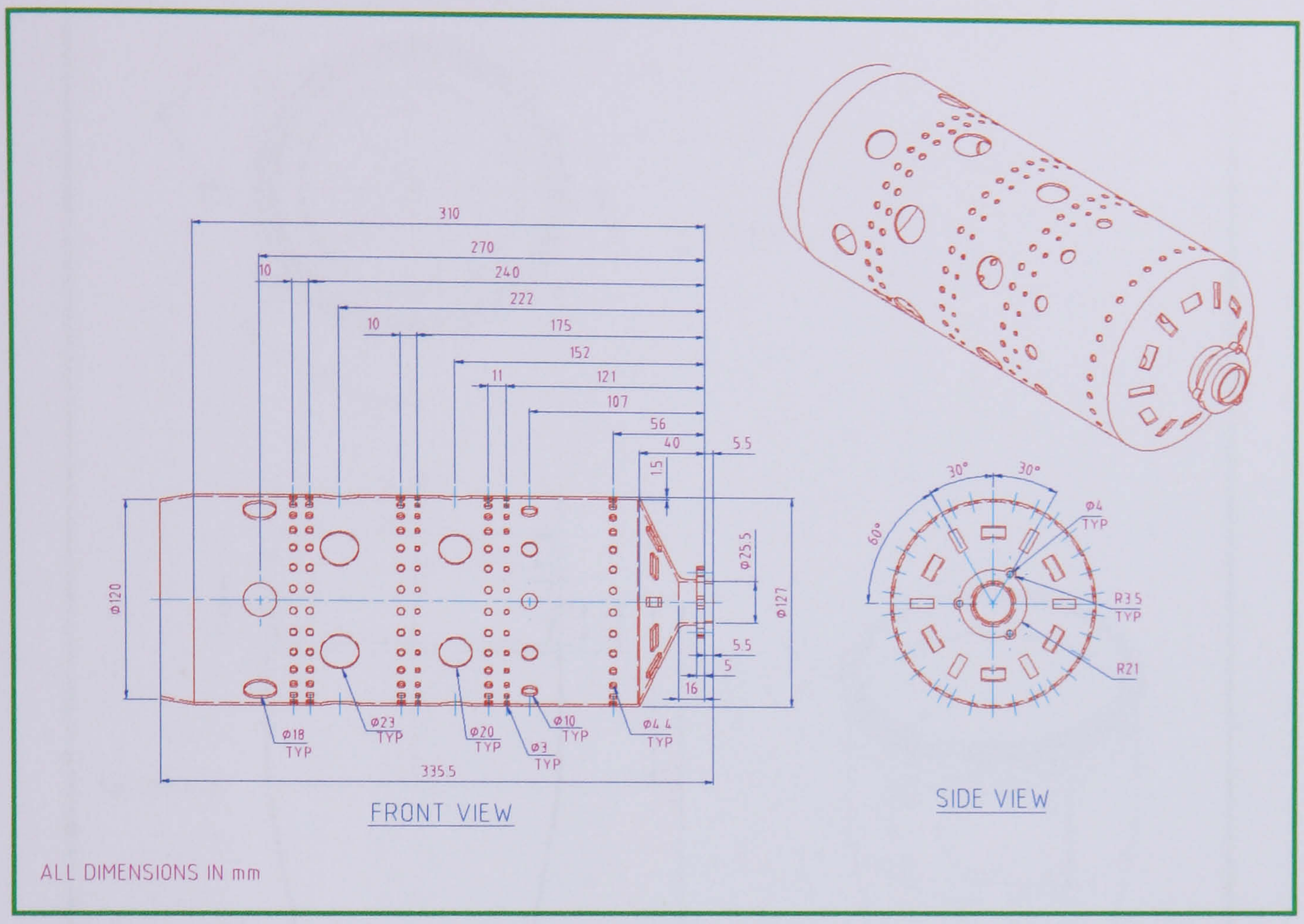

FIG. 6.10 DETAILED DRAWING OF A SINGLE CAN COMBUSTOR LINER ADAPTED FROM AN AUXILIARY POWER UNIT MODEL GTCP85

A three dimensional solid model and detailed dimensions of the combustor casing are shown in **Fig. 6.11** and **Fig. 6.12**, respectively.

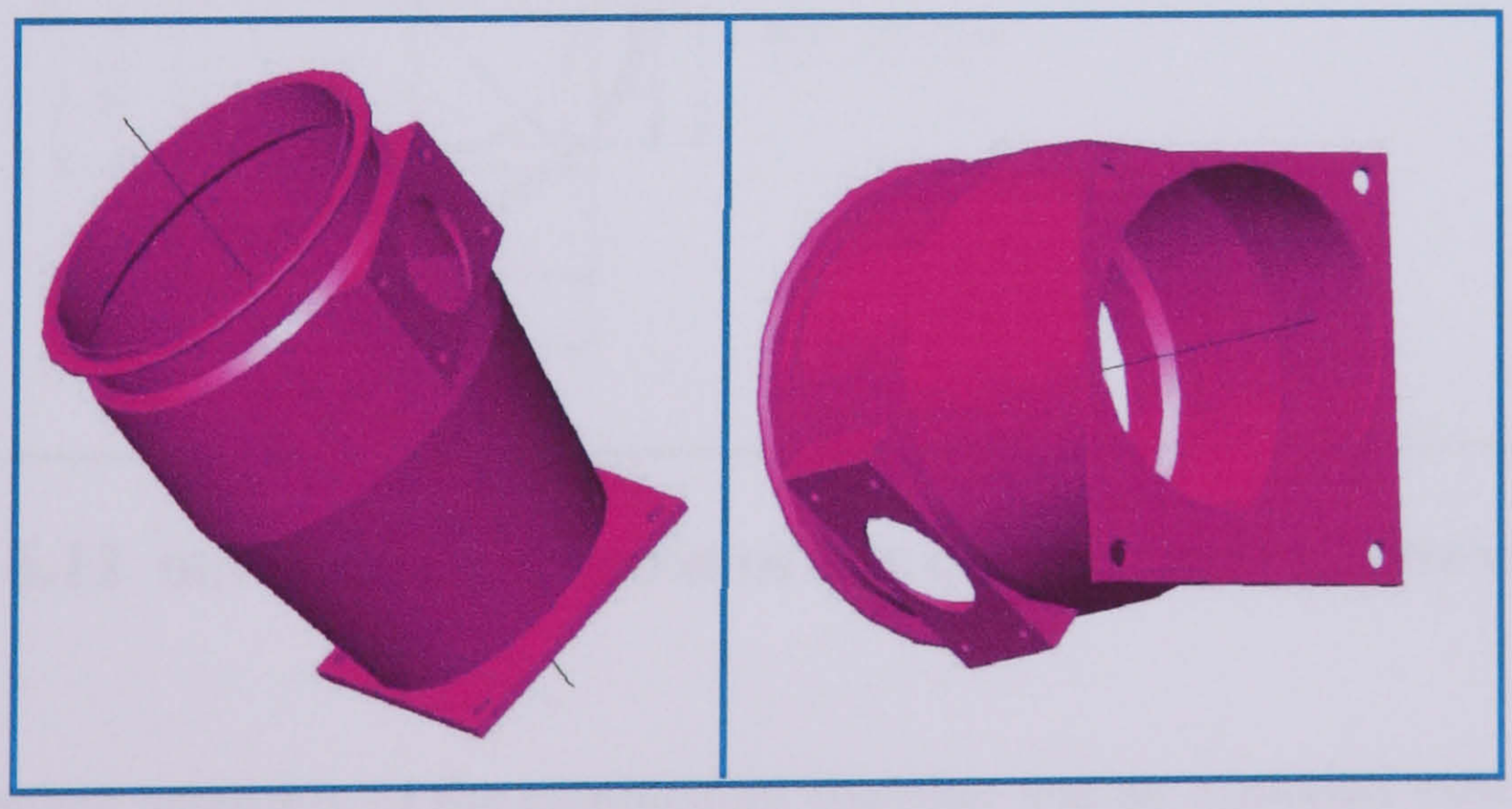

FIG. 6.11 THREE DIMENSIONAL SOLID MODEL OF COMBUSTOR CASING

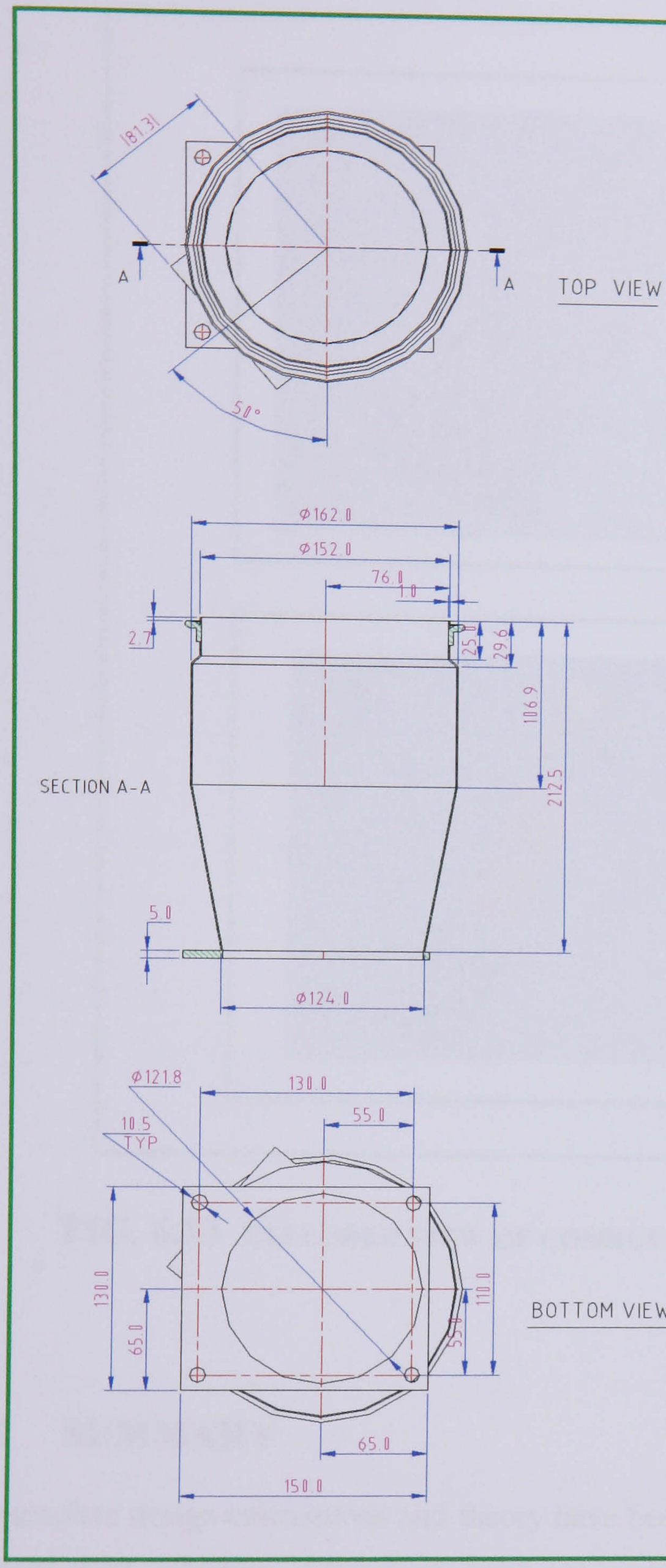

FIG. 6.12 DETAILED DIMENSIONS OF THE COMBUSTION CHAMBER CASING

The complete assembly of the combustion chamber and an exploded view is depicted in **Fig. 6.13**.

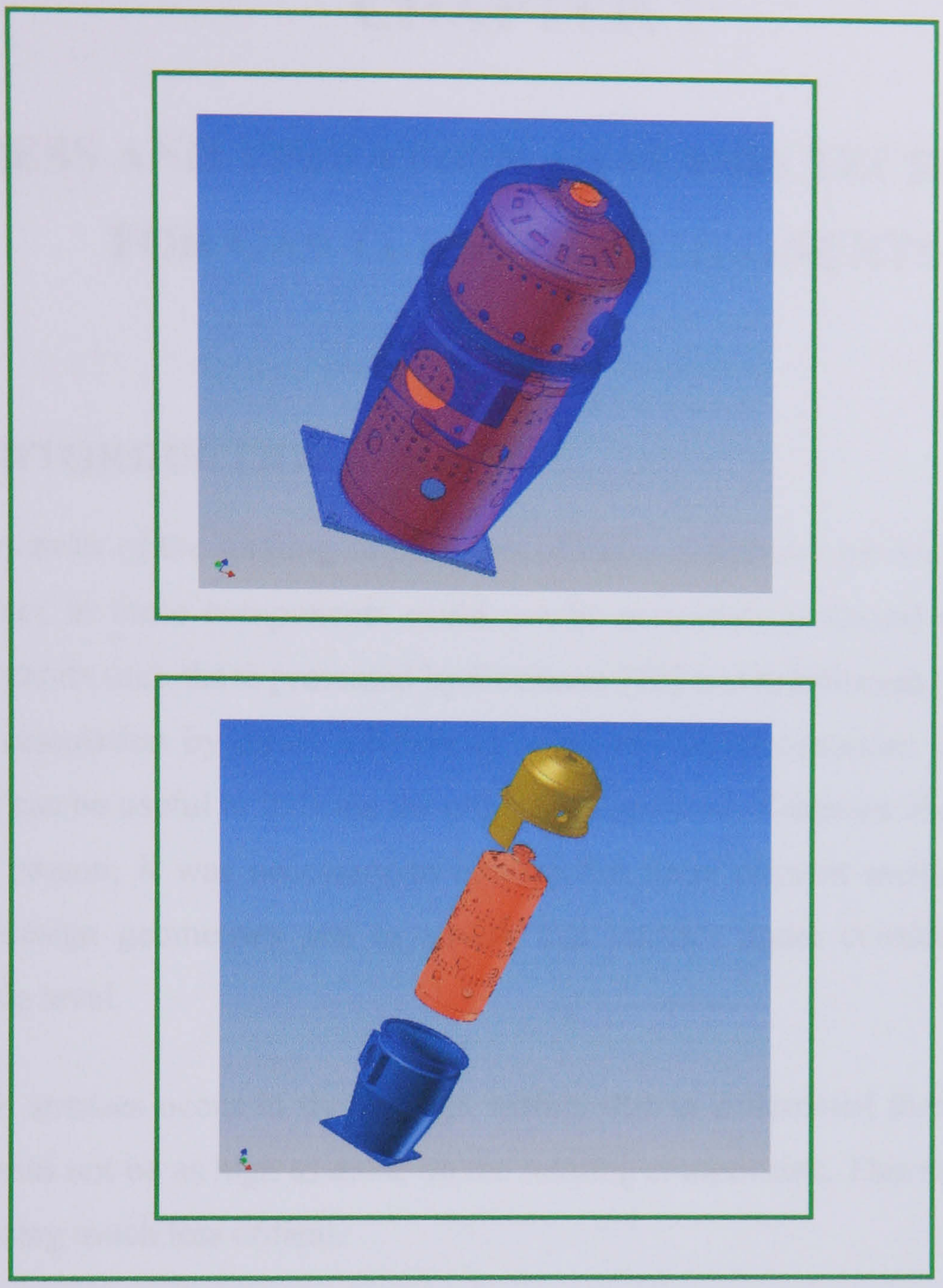

FIG. 6.13 EXPLODED VIEW OF COMBUSTION CHAMBER ASSEMBLY

6.6 SUMMARY

A complete design calculations and theory have been presented in this Chapter for the turbine shaft, selection of bearings, combustion chamber casing. Detailed design and drawings and three-dimensional models of the above components have been produced as a result of the calculations given in the current Chapter.

CHAPTER 7

STRESS AND VIBRATION ANALYSIS TECHNIQUES FOR GAS TURBINE COMPONENTS

7.1 INTORDUCTION

The geometries of the rotating components of turbo-machinery are complex and hence the stresses in these components could not be accurately predicted using analytical stress methods such those presented by **Swanson [73]** and **Schilhansh [74]** and usually refer to calculation by direct solution of stress and strain equations. However, these methods can be useful to indicate the order of magnitude of stresses likely to be found. For this reason, it was necessary to employ the finite element method as a tool to analyse design geometries and to ensure that stresses under consideration were at acceptable level.

Although stresses occur in the casings, mainly due to differential thermal expansion, these would not be as high as those on the rotating components. This makes the design of the casing much less critical.

Thermal stresses present another topic for consideration. The effect of flow of high temperature gas especially in the rotor necessitates the need to analyse this effect and must be considered in combination with the centrifugal effect to find the overall combined stress effect on these rotating component, as it is shown later in the analysis.

Another important area of consideration is the effect of vibration of the rotating shaft and its components. Destructive shaft vibrations can occur in any rotating system. As the shaft rotates, there are periodic forces on the shaft due to the residual out of balance masses, forces originating from the rolling elements in the bearings and aerodynamic forces on the compressor and turbine rotors. If the frequency of these forces matches the natural frequency of either the shaft or shaft components, the result may be a failure, either from instability or high cycle fatigue.

It is impossible to ensure all the natural frequencies never coincide with the frequency of the forces but precautions must be taken to avoid obvious problems. Again classical vibration analysis methods are incapable to deal with the complex rotating assembly and so finite element method has to be employed.

7.2 FINITE ELEMENT PACKAGE – ANSYS SOFTWARE

ANSYS is a computer programme for finite element analysis and design. **ANSYS** programme has many finite element analysis capabilities ranging from a simple linear static to a complex, non-linear dynamic analysis. The procedure for a typical **ANSYS** analysis can be divided into three distinct steps, namely:

i. Building the model.
ii. Apply loads and obtain the solution.
iii. Review the results.

7.3 TYPES OF ANALYSIS

ANSYS programme was used in this research work to analyse the following stresses:

i. Structural analysis due to centrifugal forces.
ii. Thermal analysis due to high temperature of the flowing fluid
iii. Combined analysis of structural and thermal effects.
iv. Model (vibration) analysis due to high rotational speed.

These analysis were carried out on the rotor, impeller and the rotating shaft as it will be shown later.

7.4 ANSYS ANALYSIS OF THE ROTOR, IMPELLER AND ROTATING SHAFT

As mentioned earlier, the analysis carried out on these components includes structural, thermal and vibration. Material properties (physical and thermal) of the components under study, that is, the turbine rotor and compressor impeller must be defined and

specified as input data. The results of the analysis on these components are described hereafter:

7.4.1 Structure and Thermal Stress Analysis of a Turbine Rotor

The material selected for turbine rotor is an Inconel alloy-718 because of its high tensile strength and its ability to withstand high temperatures. **Fig. 7.1** shows a graphical plot of the mechanical properties of this alloy under various temperatures extracted from **Ref. [75]**.

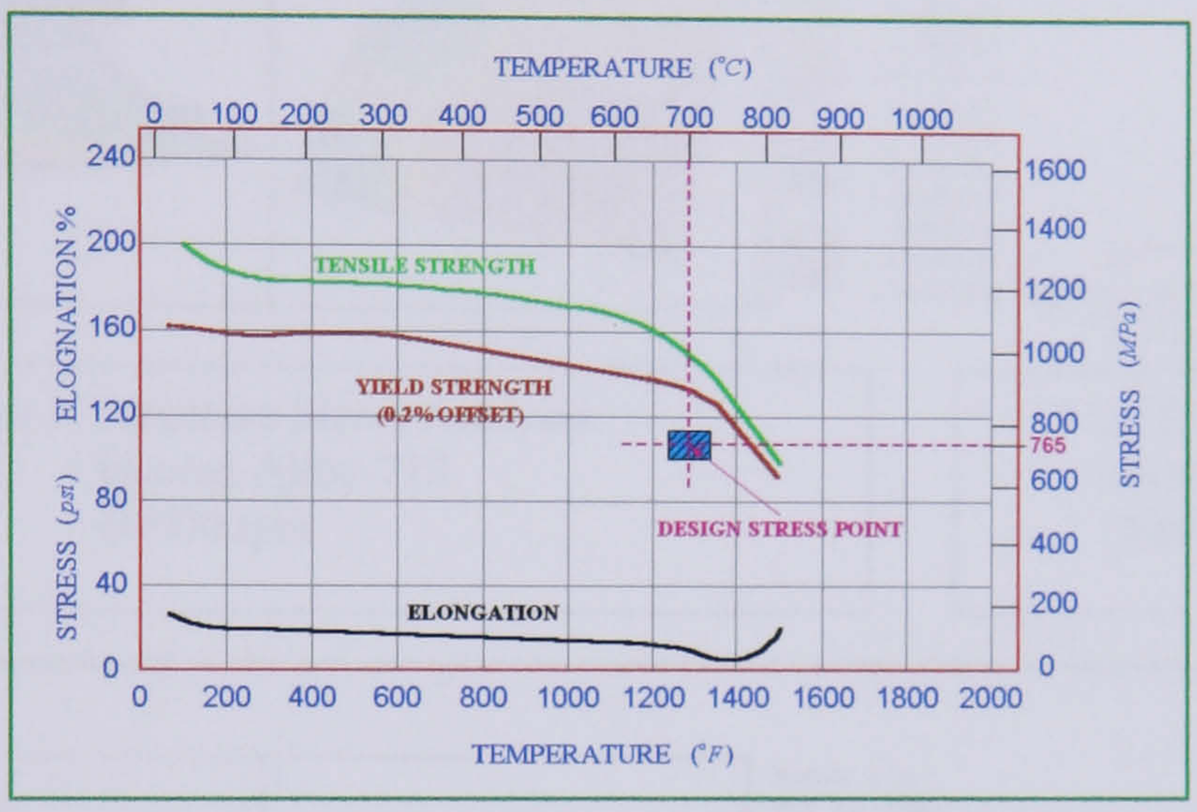

FIG. 7.1 PHYSICAL PROPERTIES OF INCONEL ALLOY-718 (PRECIPITATION HARDENED)

A complete structrural and thermal stresse analysis and displacements for the turbine rotor running at the design speed of $60000\,rpm$ was carried out. The output results were expressed in Von Mises equivalent stress (N/m^2) and the displacements in (m) as shown in **Figs. 7.2** to **7.4**. **Fig. 7.4** gives the range of combined stress values in the turbine section and also shows that the maximum and minimum stresse values are equal to $0.765\times10^9\ N/m^2$ $(765\,MPa)$ and $0.119\times10^7\ N/m^2\ (1.19\,Mpa)$, respectively. The maximum stresses occur at the rotor centre while the minimum stresses occur at the rotor tip diameter d_2. Displcement analysis showed that the maximum and mininmum dispalcements are equal to $1.77\,mm$ and $0.13\,mm$ and both occured at the rotor tip and centre, respectively. These results indicate that the selected material for the turbine rotor, which is the Inconel alloy-718, is satisfactory and can withstand the combined stresses exerted on the rotor at the design conditions.

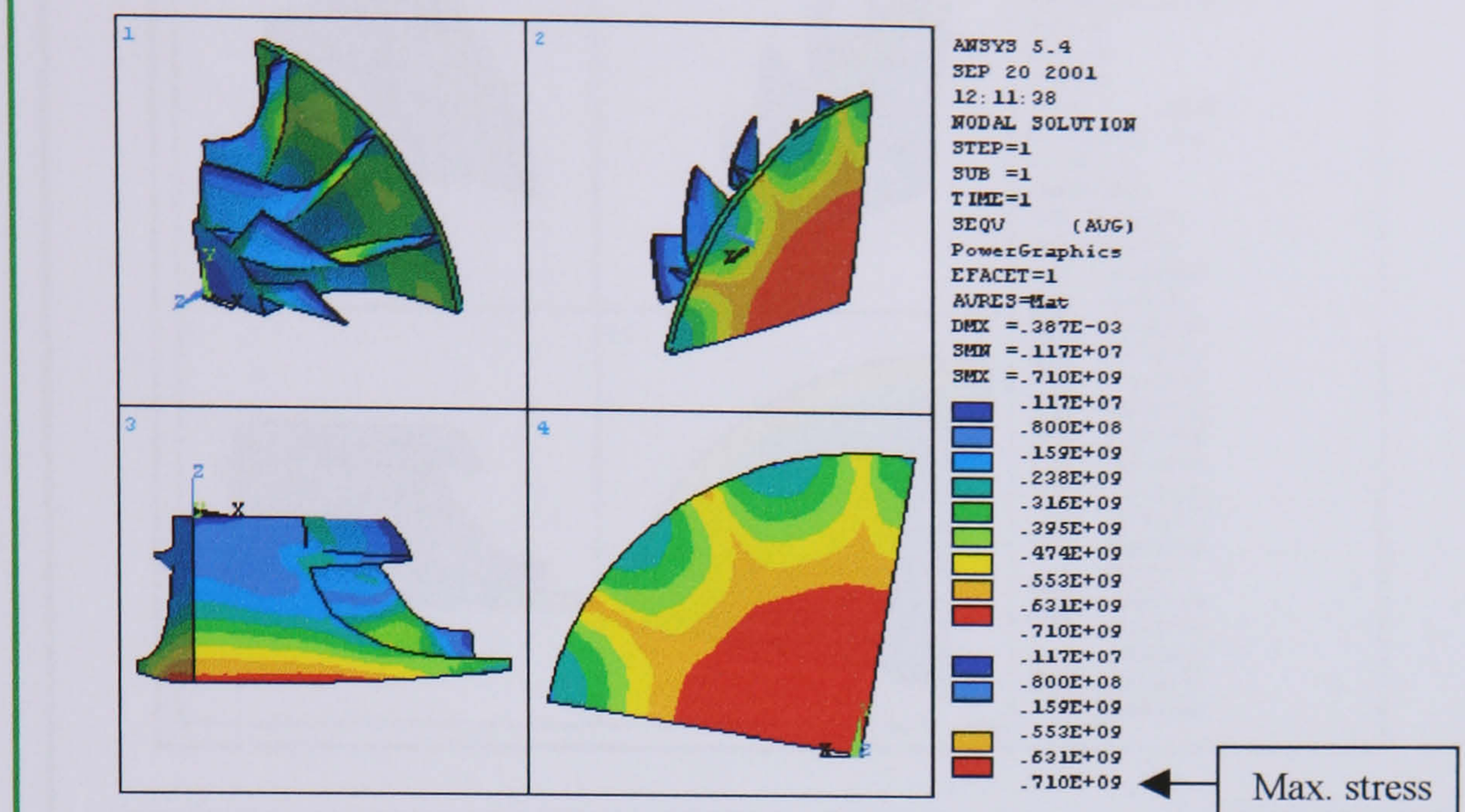

Load case 1: Structure Stress Analysis
Material : Inconel Alloy-718
Speed : 60000 rpm

Von Mises stresses (N/m^2)

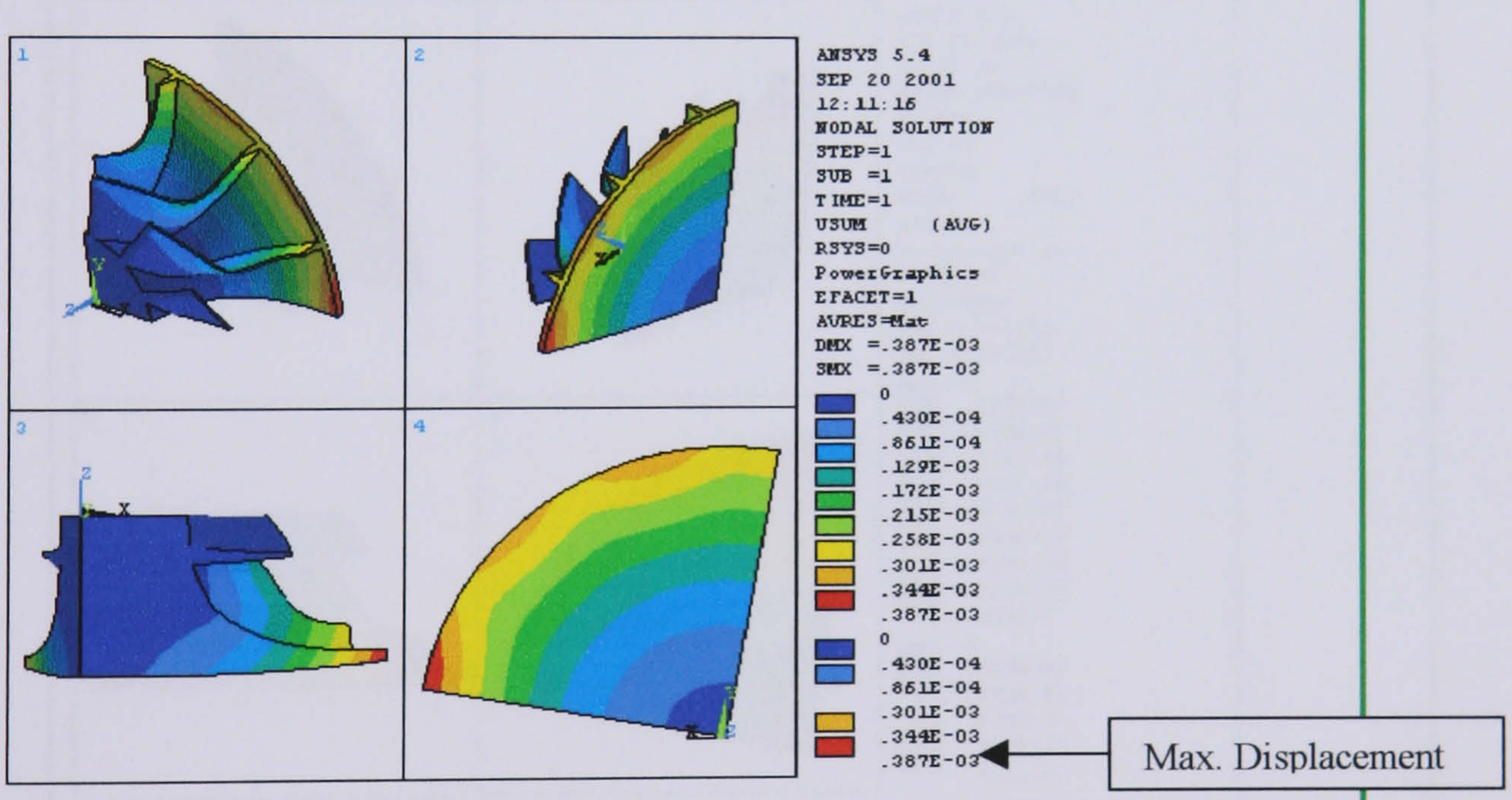

Load case 1: Structure Displacement Analysis
Material : Inconel Alloy -718
Speed : 60000 rpm

Displacement unit (m)

FIG. 7.2 STRUCTURE ANALYSIS OF A SECTION OF A TURBINE ROTOR

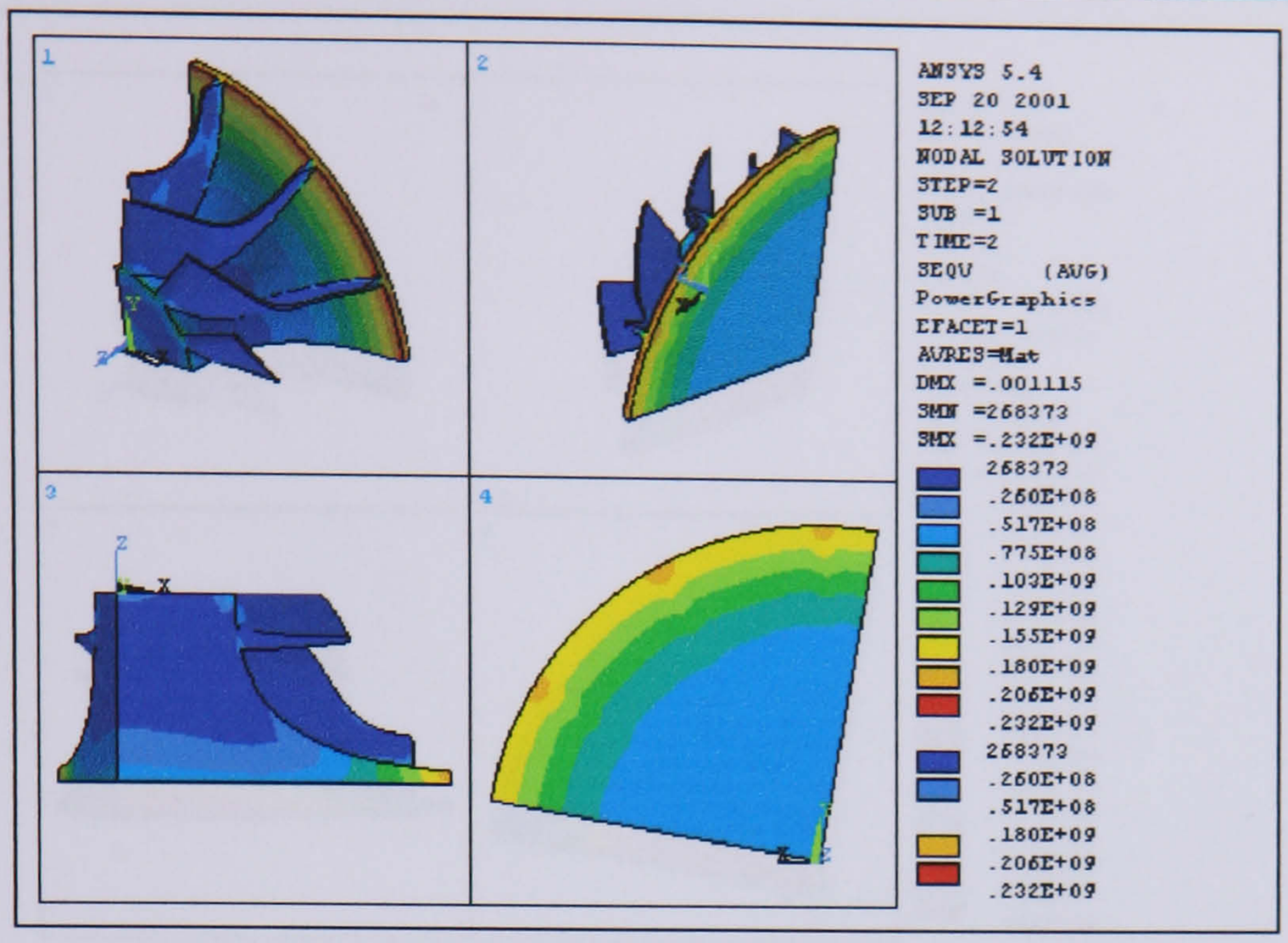

Load case 2: Thermal Stress Analysis
Material : Inconel Alloy-718
Speed : 60000 rpm

Von Mises stresses (N/m^2)

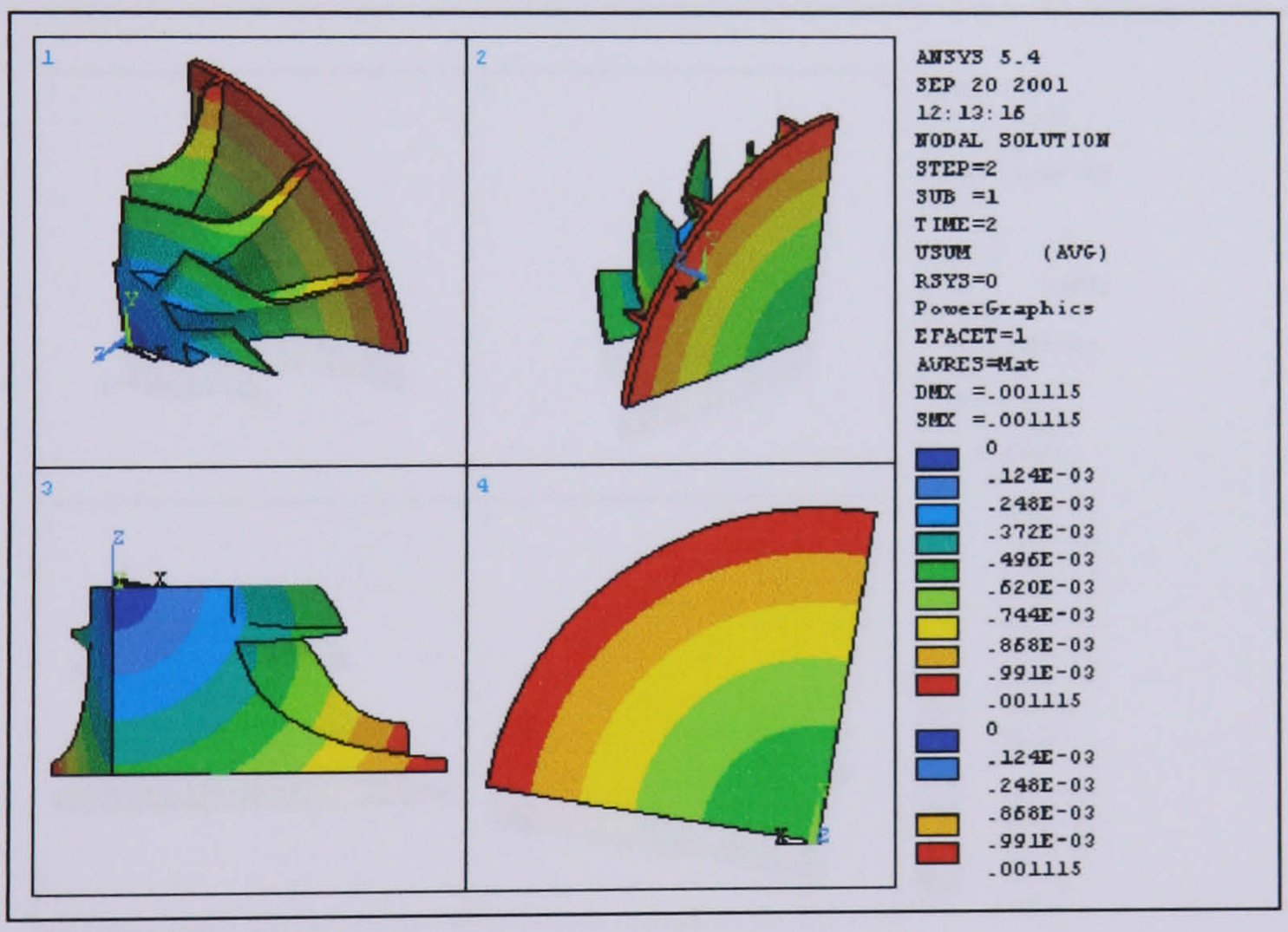

Load case 2: Thermal Displacement Analysis
Material : Inconel Alloy-718
Speed : 60000 rpm

Displacement unit (m)

FIG. 7.3 THERMAL ANALYSIS OF A SECTION OF A TURBINE ROTOR

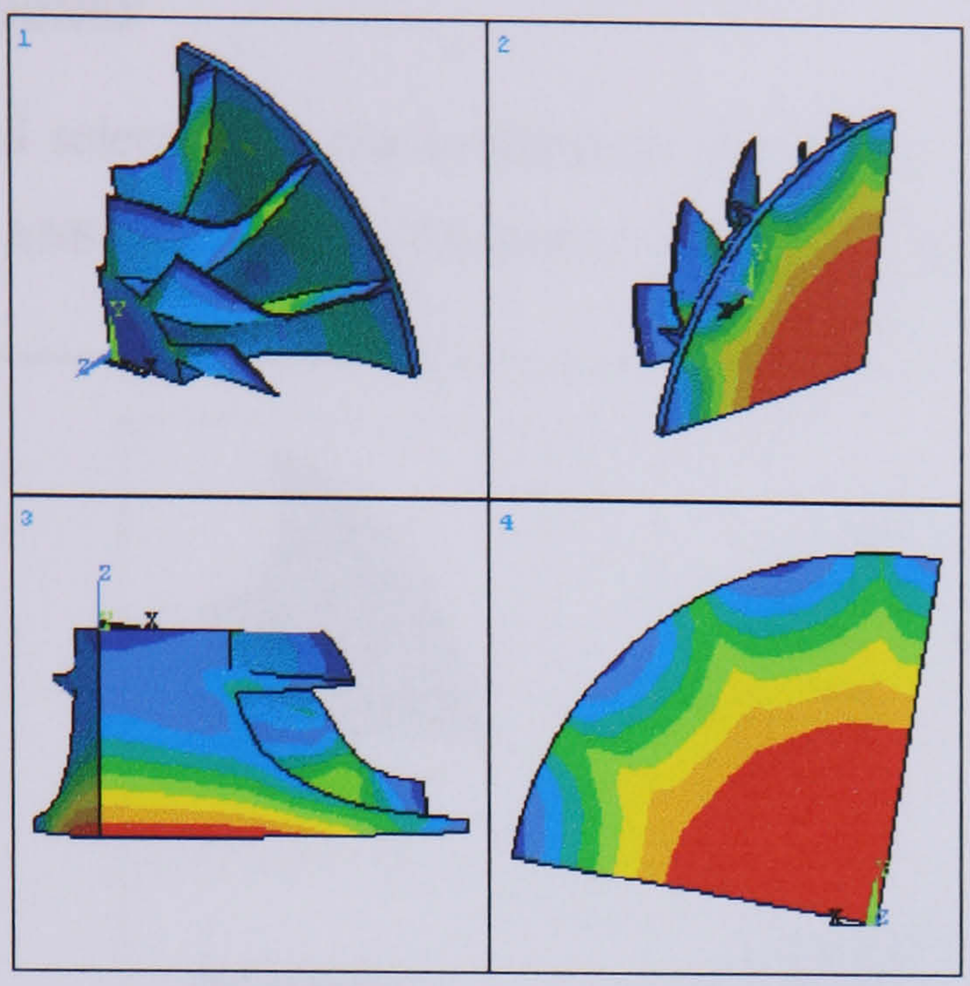

Load case 3: Combined Stress Analysis
Material : Inconel Alloy-718
Speed : 60000 rpm

Von Mises stresses (N/m^2)

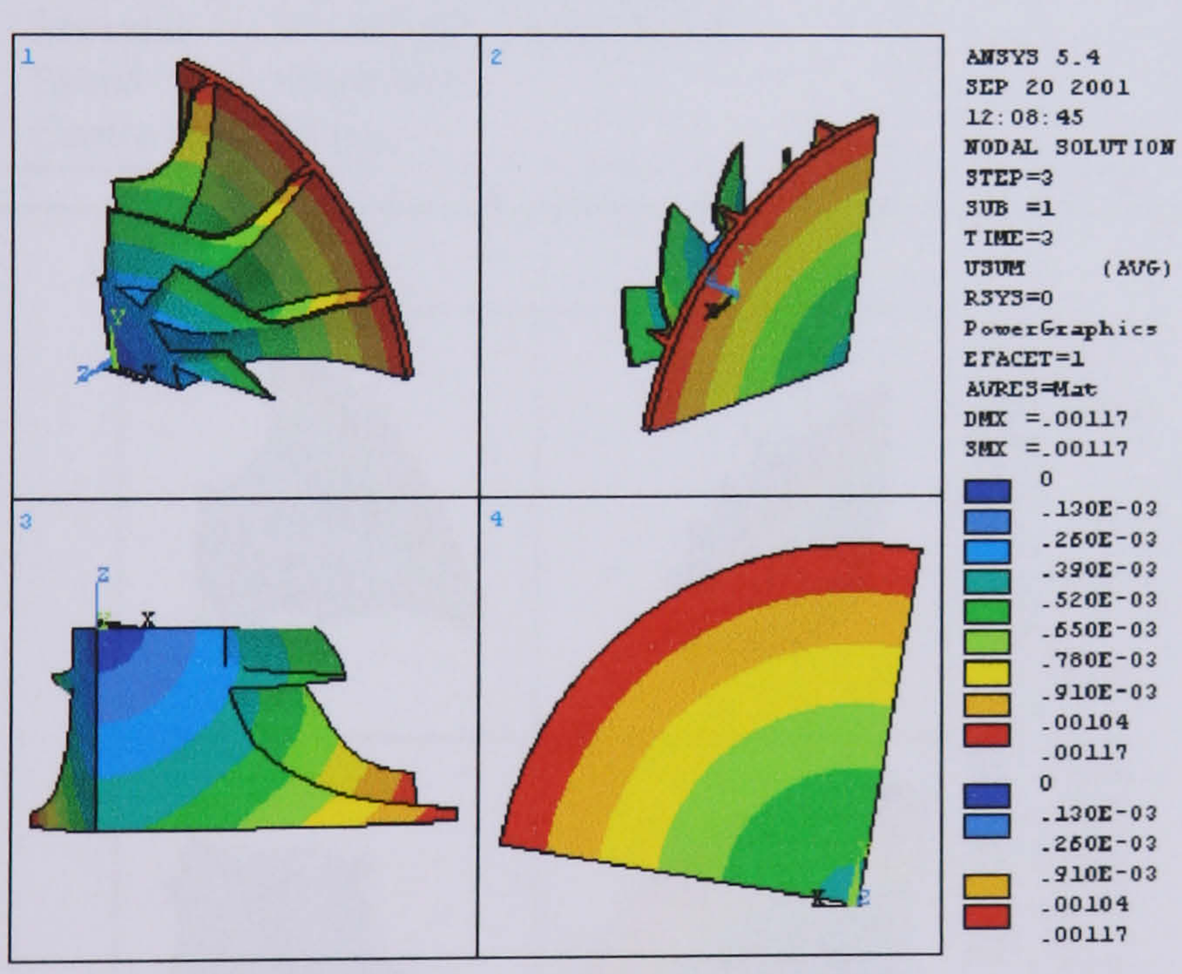

Load case 3: Combined Displacement Analysis
Material : Inconel Alloy-718
Speed : 60000 rpm

Displacement unit (m)

FIG 7.4 COMBINED STRUCTURE AND THERMAL ANALYSIS OF A SECTION OF A TURBINE ROTOR

7.4.2 Structure and Thermal Stress Anaylsis of a Compressor Impeller

The material selected for the compressor impeller is Titanium Ti-6AI-4V (Grade 5).

The output ANSYS results are illustrated in **Figs. 7.5 to 7.7**.

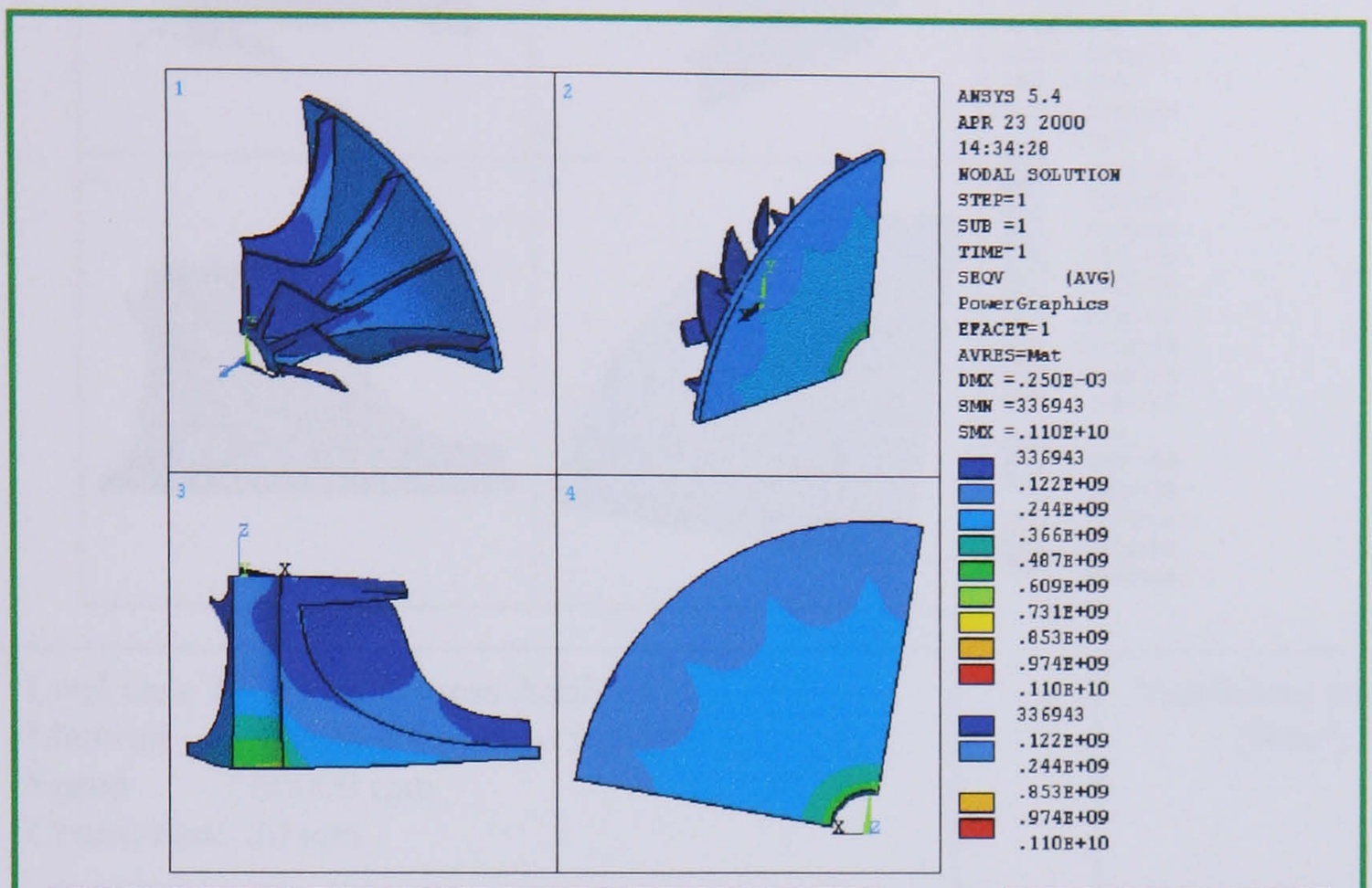

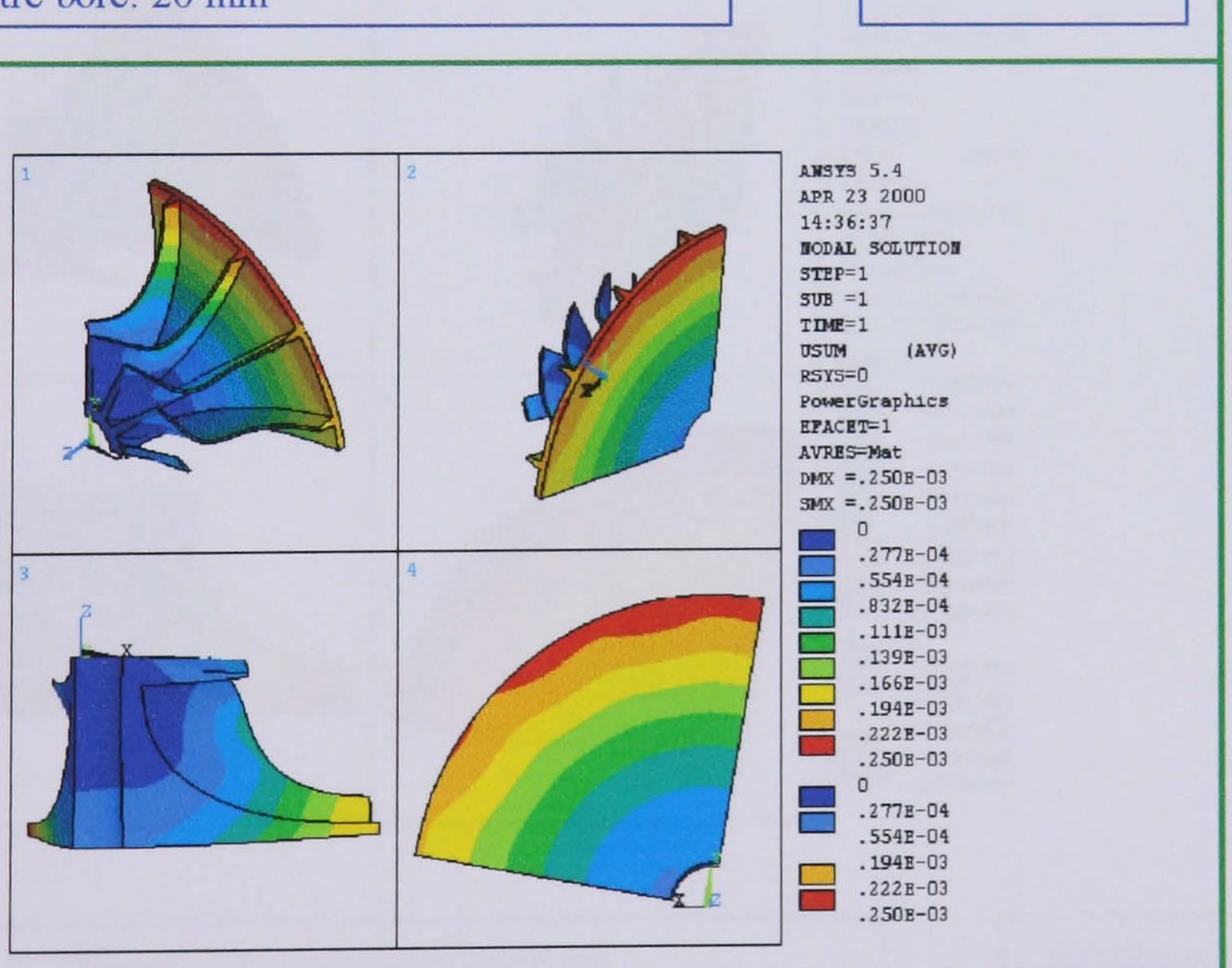

FIG. 7.5 STRUCTURE ANALYSIS OF A SECTION OF A COMPRESSOR IMPELLER

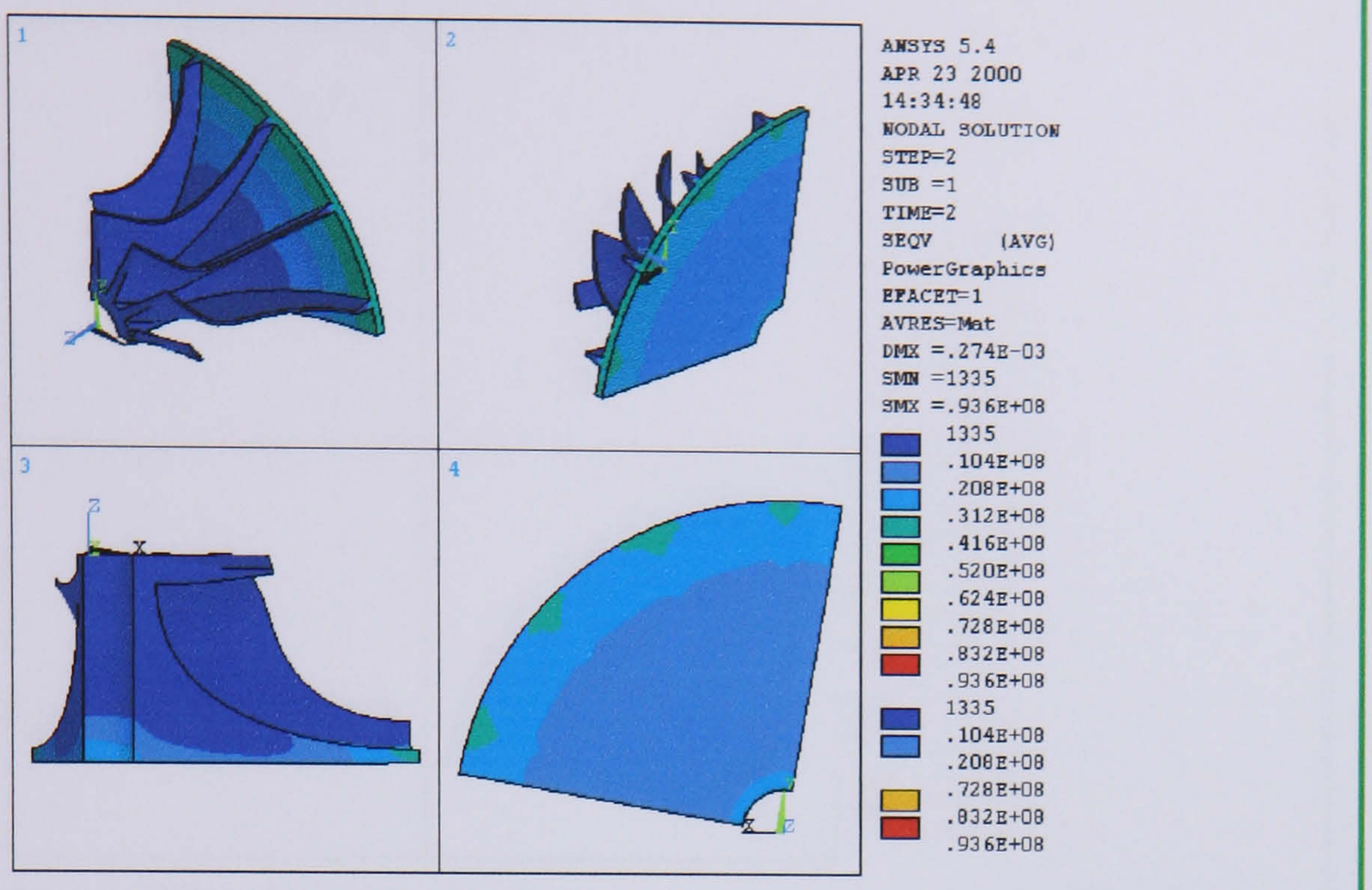

Load case 2: Thermal Stress Analysis
Material : Ti-6Al-4V (Grade 5),STA
Speed : 60000 rpm
Centre bore: 20 mm

Von Mises stresses (N/m^2)

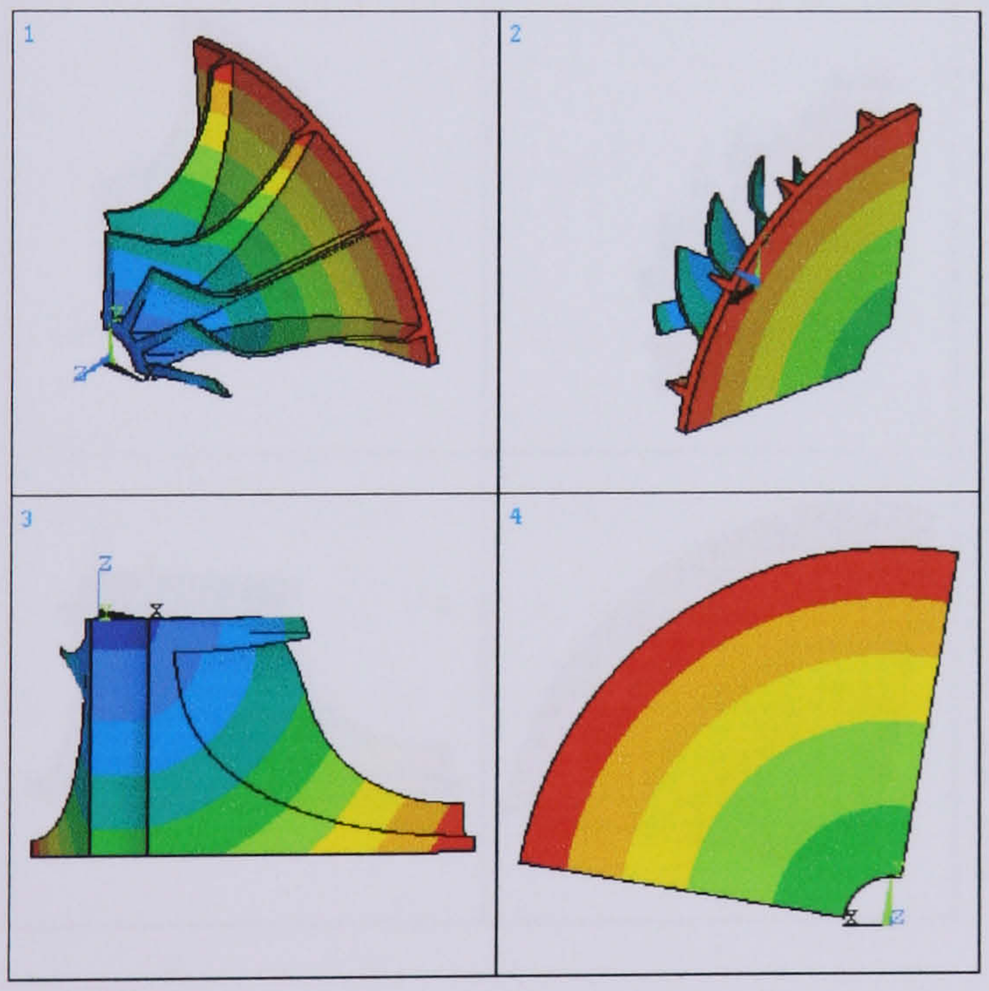

Load case 2: Thermal Displacement Analysis
Material : Ti-6Al-4V (Grade 5),STA
Speed : 60000 rpm
Centre bore: 20 mm

Displacement unit (m)

FIG. 7.6 THERMAL ANALYSIS OF A SECTION OF A COMPRESSOR IMPELLER

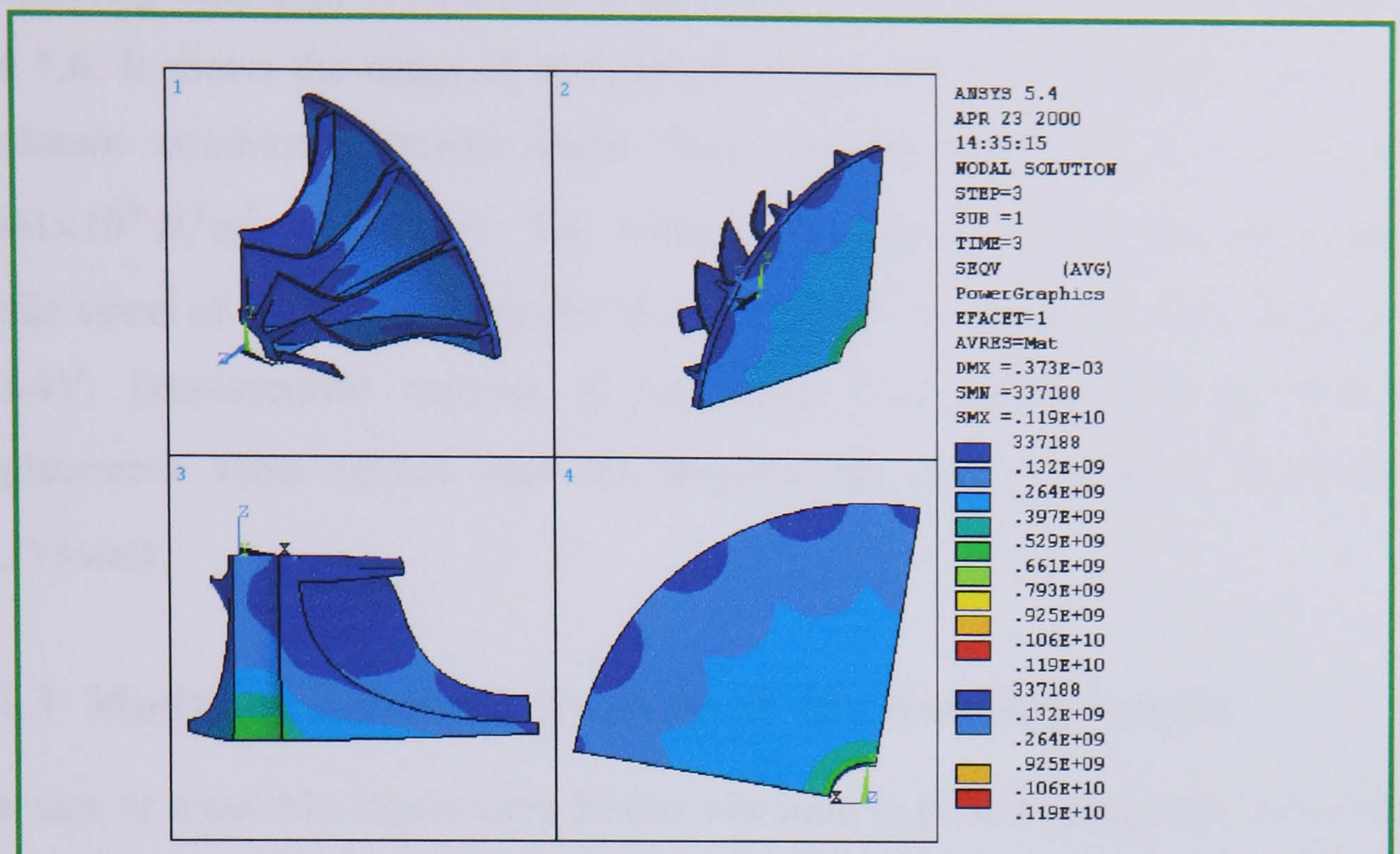

Load case 3: Combined Stress Analysis
Material : Ti-6Al-4V (Grade 5),STA
Speed : 60000 rpm
Centre bore: 20 mm

Von Mises stresses (N/m^2)

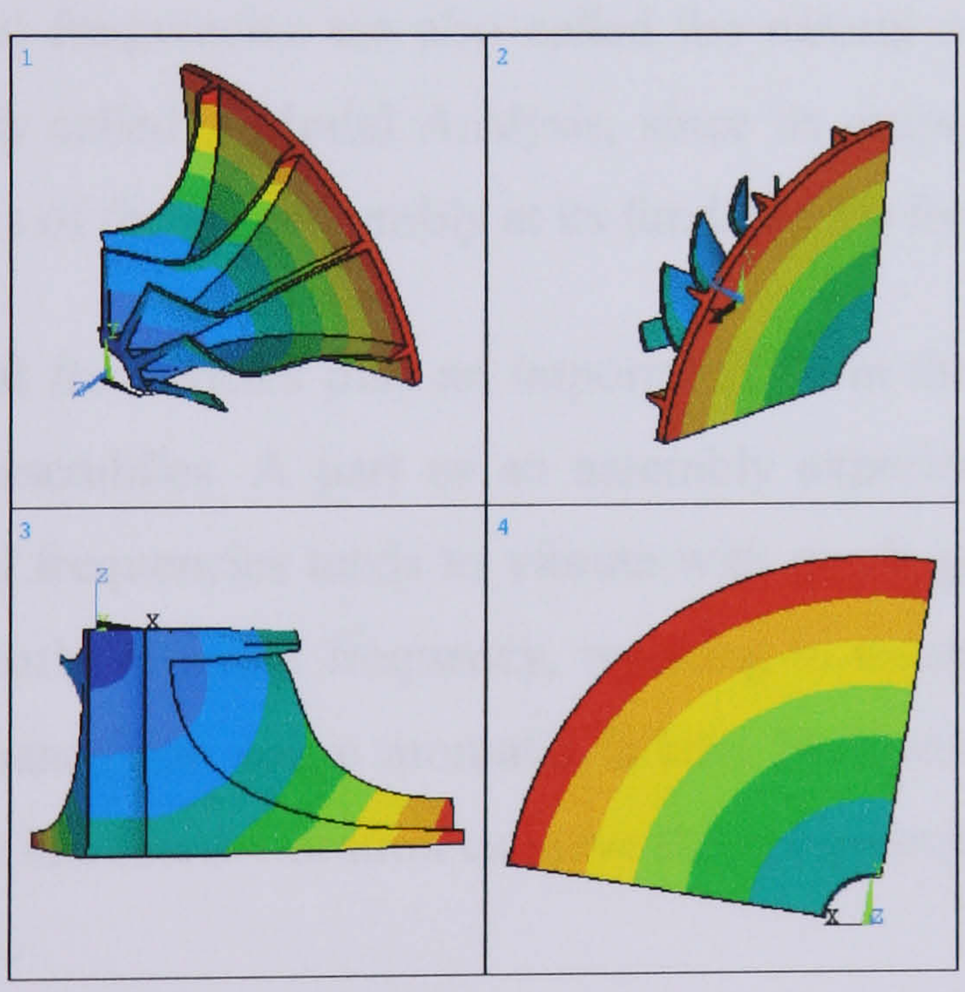

Load case 3: Combined Displacement Analysis
Material : Ti-6Al-4V (Grade 5),STA
Speed : 60000 rpm
Centre bore: 20 mm

Displacement unit (m)

FIG. 7.7 COMBINED STRUCTURE AND THERMAL ANALYSIS OF A SECTION OF A COMPRESSOR IMPELLER

Considering only **Fig. 7.7** because it represents the outcome of combining **Figs. 7.5 and 7.6**. It shows the range of stresses and their values in the impeller section. The maximum combined stresses occur near the impeller bore and its equal to $0.661\times10^{9}\ N/m^{2}$ $(661Mpa)$. The value of this stress is less than the maximum tensile stress of the material selected for the impeller which in this case Titanium Ti-6AI-4V. Displacement analysis of the same figure shows that the maximum displacement value occurs near the impeller tip and is equal to $0.373\times10^{3}\ m$ $(0.373mm)$.

7.4.3 Modal (Vibration) Analysis of the Rotating System.

If a part or assembly experiences forced vibration (e.g. as a component of a rotating machine), the designer should determine the ranges of operating frequencies. Simulation is often used to ensure that the part/assembly exhibits no fundamental frequencies near these ranges. This is done by finding the fundamental frequencies of a part or an assembly and comparing them to the ranges of operating frequencies. Fundamental frequencies are also called the natural or resonant frequencies. Such a simulation is called a Modal Analysis, since its output is usually in the form of the mode shapes of the part/assembly at its fundamental frequencies.

Fundamental frequencies play an important role in the design of dynamically loaded parts and assemblies. A part or an assembly experiencing forced vibration near its fundamental frequencies tends to vibrate with much greater amplitude than if excited at a sufficiently different frequency, resulting in resonance of the structure. In some cases, resonance can cause atomatic failure. However, even if resonance causes no damage, the increased vibration can give the appearance of low quality to an otherwise solid design.

7.4.3.1 Working frequency

The working frequency of the rotating system is calculated as follows:

Rotational Velocity (ω) = $N \times (2\pi/60)$ = 60,000 x (6.283/60) = 6283.18 rad/s

Frequency ((f) = ω / 2 π = 6283.18 / 6.283 = 1000 Hz

The output results obtained by the simulation were shown in **Figs. 7.8 to 7.10**. These figures show the mode shape associated with each particular fundamental frequency. The contours represent relative displacement of the assembly as it vibrates.

Mode Shapes & Fundamental Frequencies

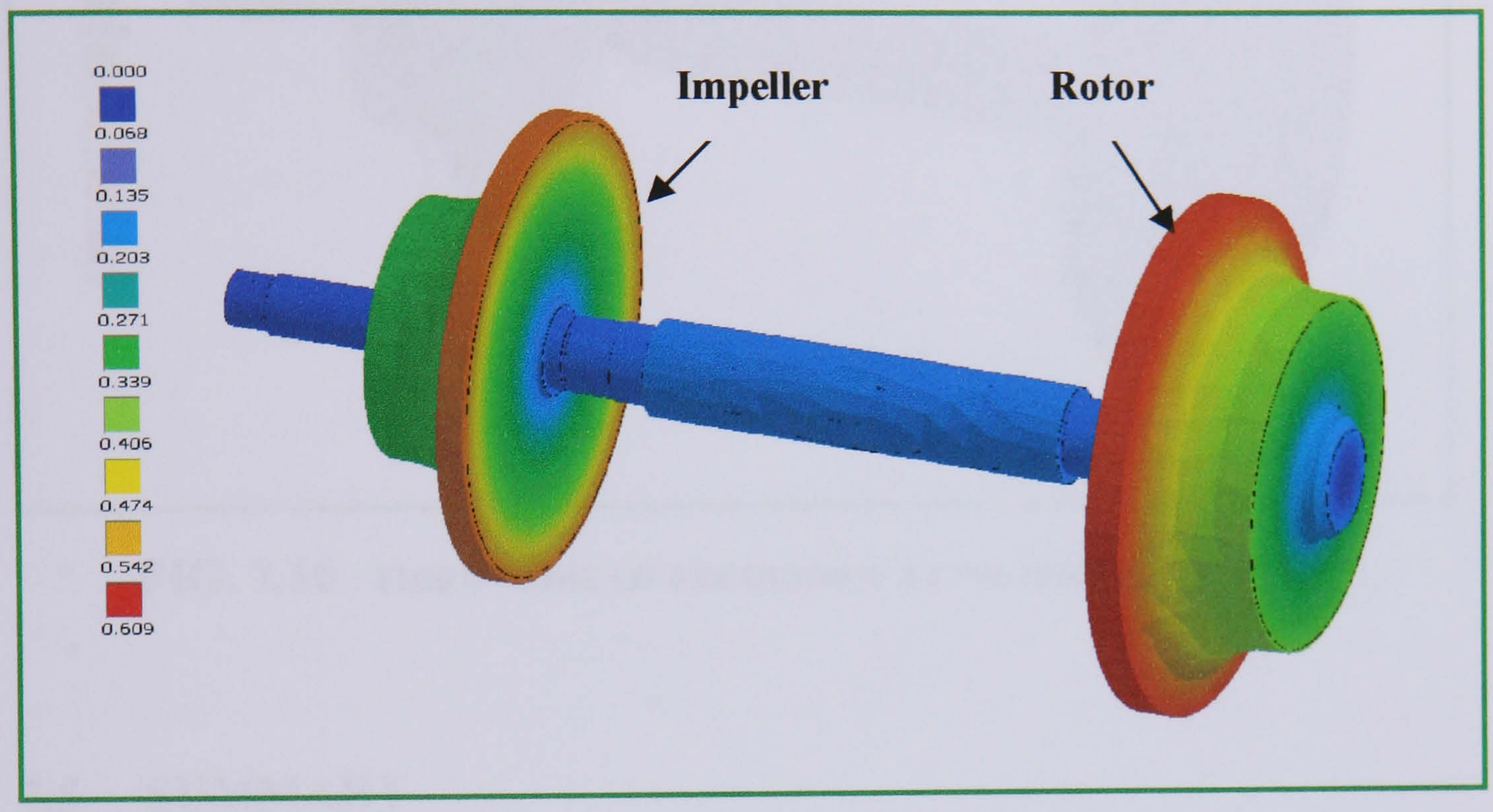

FIG. 7.8 FIRST MODE OF FREQUENCY AT 18.658 HZ (1119 RPM)

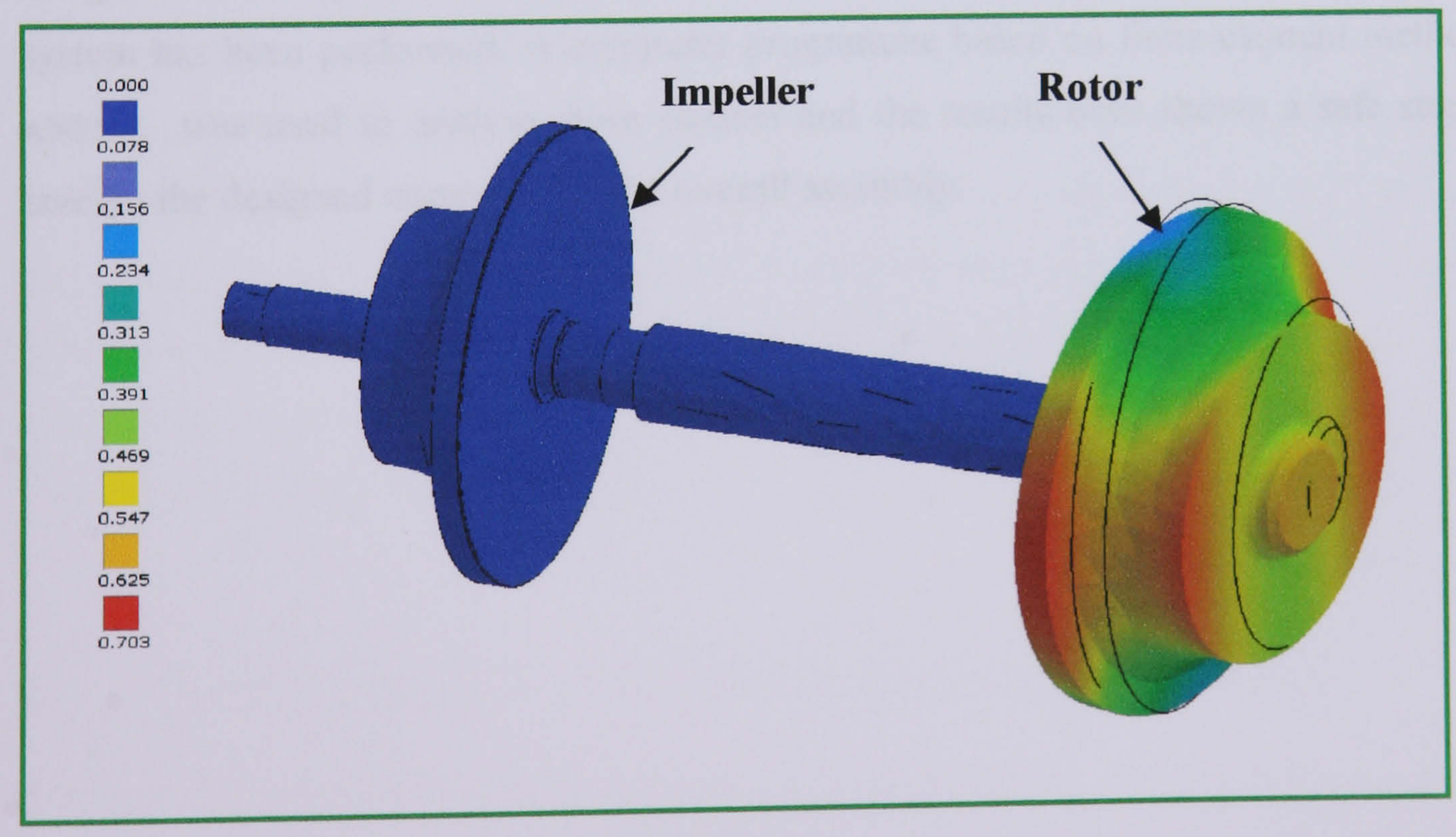

Fig. 7.9 SECOND MODE OF FREQUENCY AT 421.49 Hz (25,289 RPM)

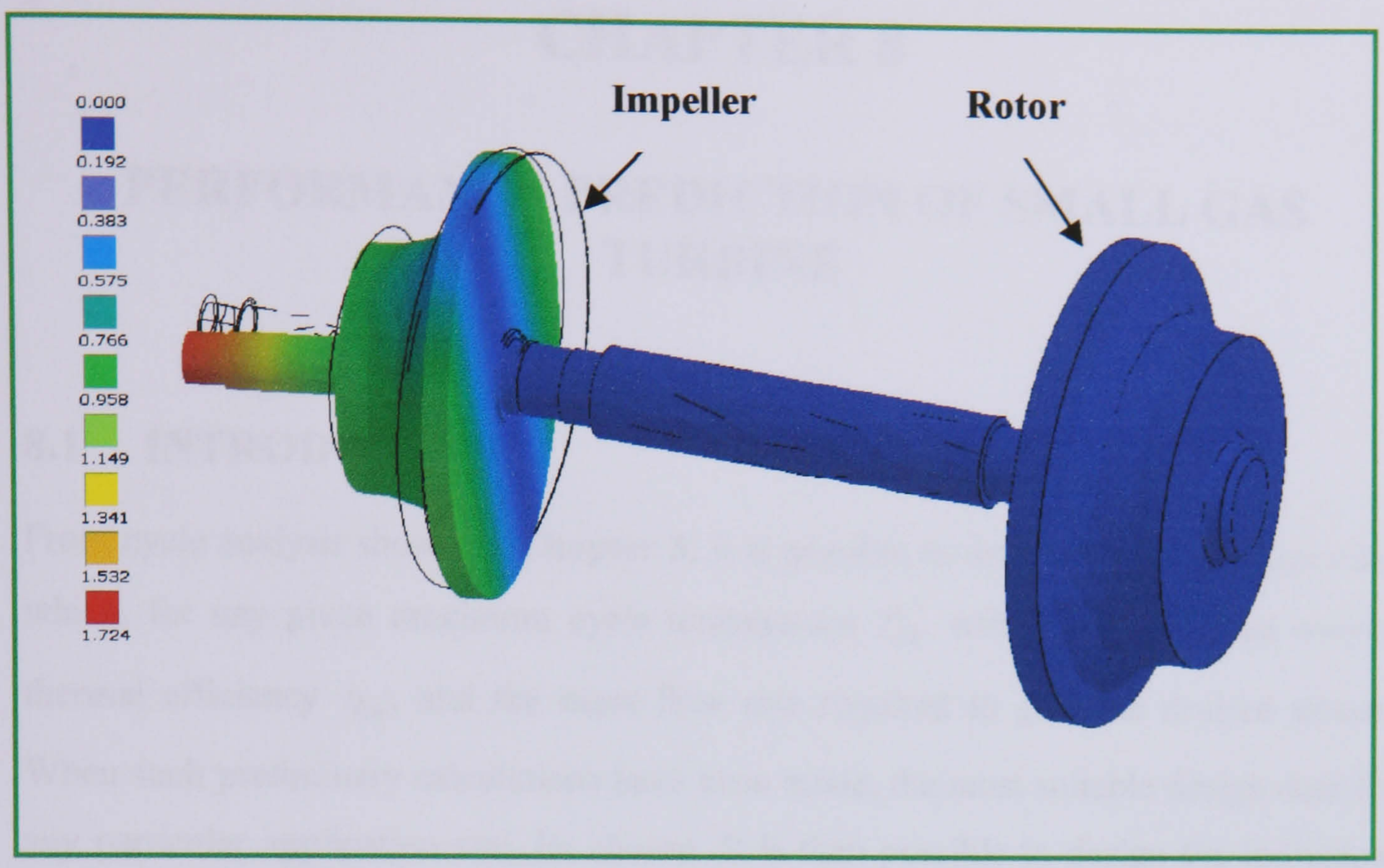

FIG. 7.10 THIRD MODE OF FREQUENCY AT 707.38 HZ (42,443 RPM)

7.5 SUMMARY

A complete anaylsis of the stresses and displacements in the individual components of the gas turbine engine have been undertaken. Also, a vibration anaylsis of the rotating system has been performed. A computer programme based on finite element method **ANSYS**, was used to analyse these stresses and the results have shown a safe stress level in the designed components and overall assembly.

CHAPTER 8

PERFORMANCE PREDICTION OF SMALL GAS TURBINE

8.1 INTRODUCTION

From cycle analysis shown in **Chapter 3**, it is possible to determine the pressure ratio which, for any given maximum cycle temperature T_{03}, will give the highest overall thermal efficiency η_{th}, and the mass flow rate required to give the desired power. When such preliminary calculations have been made, the most suitable design data for any particular application may be chosen. It is then possible to design the individual components of a gas turbine. The problem then is to find the variation of performance of the gas turbine over the complete operating range of power output and speed. Any point within the performance range other than the design point is referred to as **off-design point.**

The performance characteristics of the individual components may be calculated by means of analytical procedures, corrected by empirical coefficients or may be obtained by actual tests. When the components are linked together in an engine, the range of matching operating conditions for each component is considerably reduced. However, this range of operating conditions should satisfy the compatibility criteria, i.e mass flow rates, work output and rotational speed between the various components. Satisfying these criteria for multi shaft engines is considerably more involved than for single shaft engines. The prediction method developed as part of the current work is restricted to a single shaft engine only.

.

8.2 GAS TURBINE COMPONENT CHARACTERISTICS

The variation of mass flow rate, pressure ratio and efficiency with rotational speed of the compressor and of the turbine is obtained from the compressor and turbine characteristics. The constructions of these maps are described hereafter.

8.2.1 Compressor Characteristics

The performance characteristics of any compressor can be given in terms of these non-dimensional parameters:

$$\left(\frac{P_{02}}{P_{01}}, \eta_c, \frac{\dot{m}_a \sqrt{C_{pa} T_{01}}}{d_2{}^2 P_{01}}, \frac{d_2 N}{\sqrt{C_{pa} T_{01}}} \right)$$

The above parameters may be expressed graphically and the resulting plot would be the performance characteristics as shown in **Fig. 8.1 and Fig 8.2**. The data used in producing these plots were taken from actual test experiments on type 01 C.A.V compressor provided by **Bhinder [2]**.

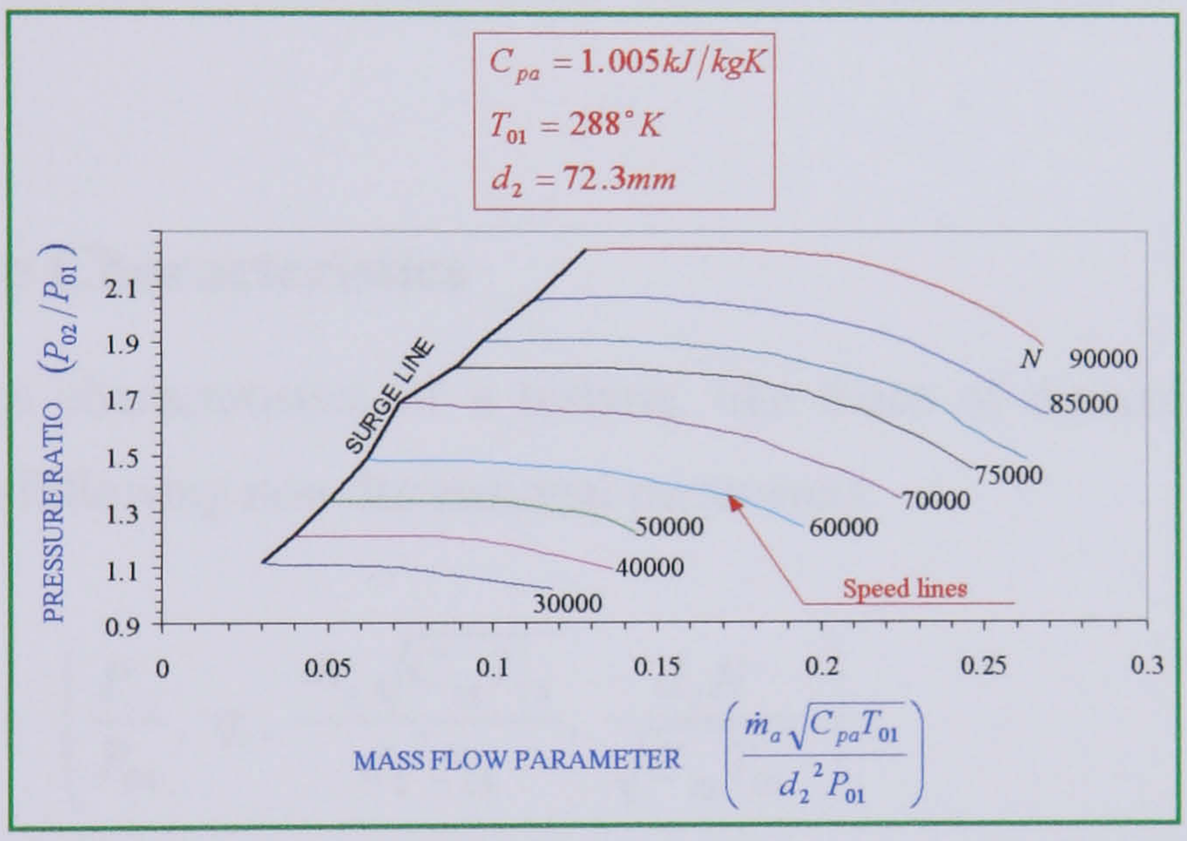

FIG. 8.1 PLOT OF PRESSURE RATIO AGAINST MASS FLOW OF A COMPRESSOR

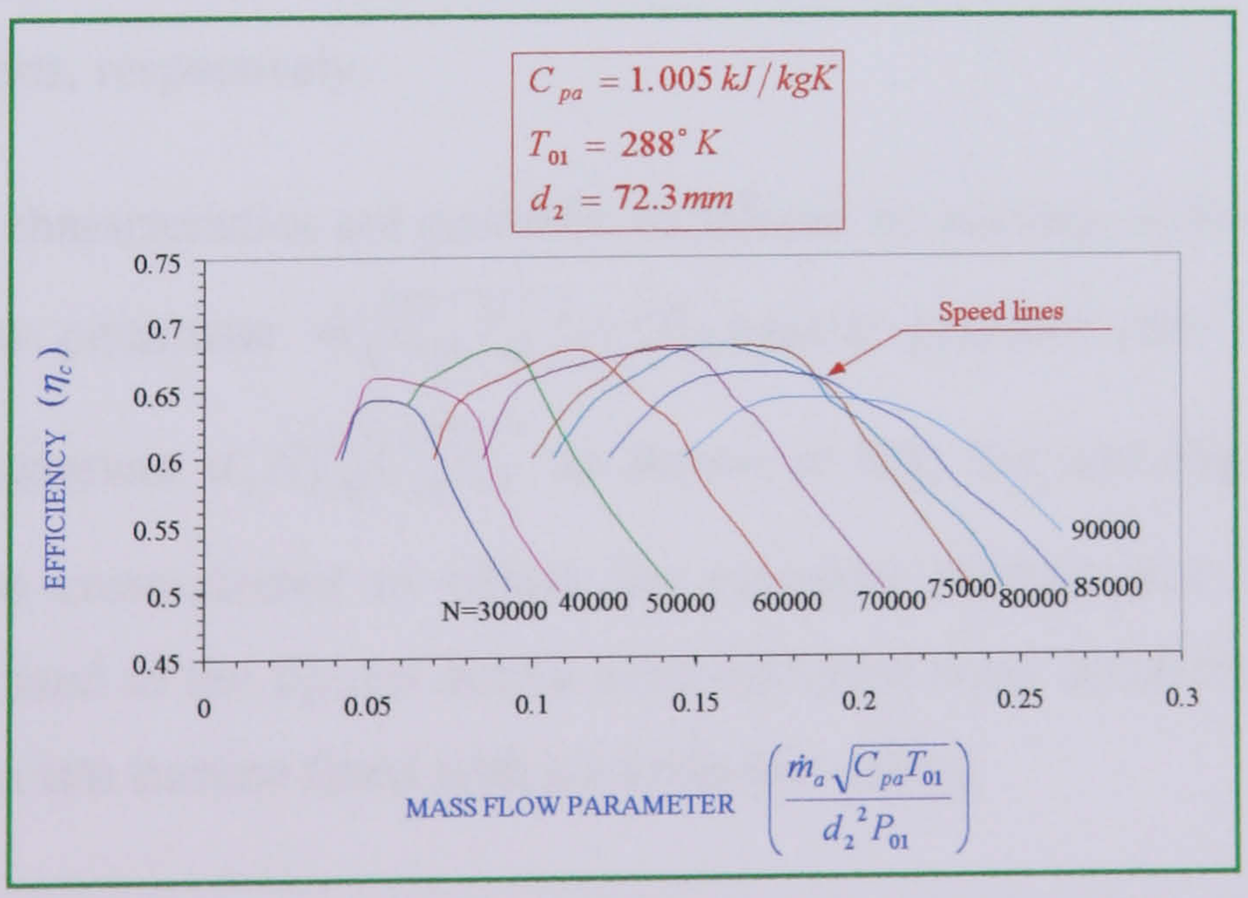

FIG. 8.2 PLOT OF EFFICIENCY AGAINST MASS FLOW OF A COMPRESSOR

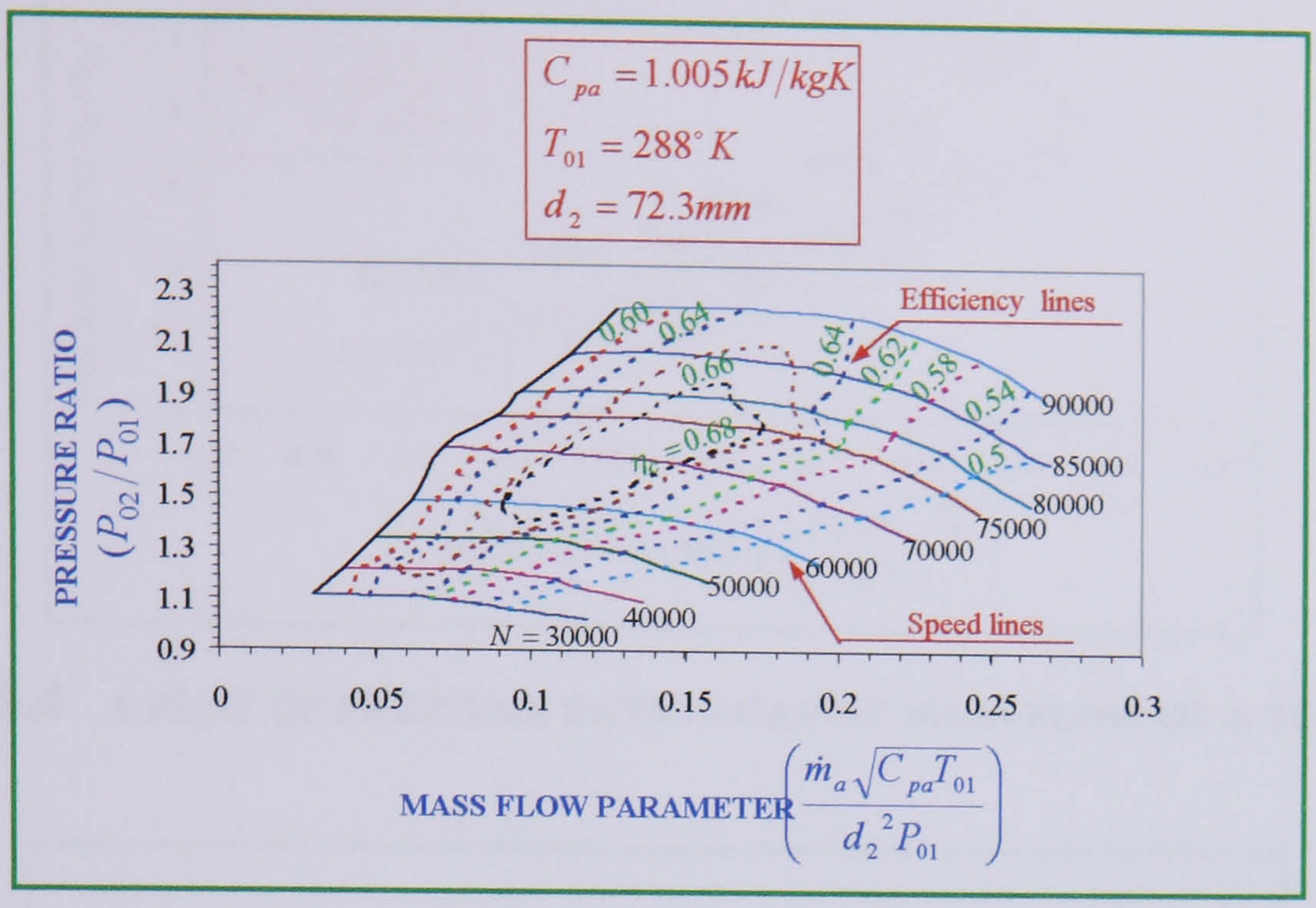

FIG. 8.3 COMPLETE PERFORMANCE CHARACTERISTICS OF A COMPRESSOR

8.2.2 Turbine Characteristics

The performance characteristics of a turbine, like those of the compressor can be described by the following non-dimensional parameters:

$$\left(\frac{P_{03}}{P_{04}},\ \eta_t,\ \frac{\dot{m}_g\sqrt{C_{pg}T_{03}}}{d_2{}^2P_{03}},\ \frac{d_2N}{\sqrt{C_{pg}T_{03}}}\right)$$

Here, the turbine cycle notation are used suffixes 3 and 4 and denote the turbine inlet and outlet conditions, respectively.

The performance characteristics are normally expressed by plotting turbine efficiency η_t and mass flow parameter $\dot{m}\sqrt{C_{pg}T_{03}}\,/\,d_2{}^2P_{03}$ against pressure ratio P_{03}/P_{04} for various speed parameters $d_2N/\sqrt{C_{pg}T_{03}}$ as shown in **Fig. 8.4** and **Fig. 8.5**. These parameters can be cross-plotted to obtain the complete performance map of this turbine. The data used in the figures above were extracted from actual tests provided by **Bhinder [2]** on **IFR** turbine fitted with a nozzle-less casing.

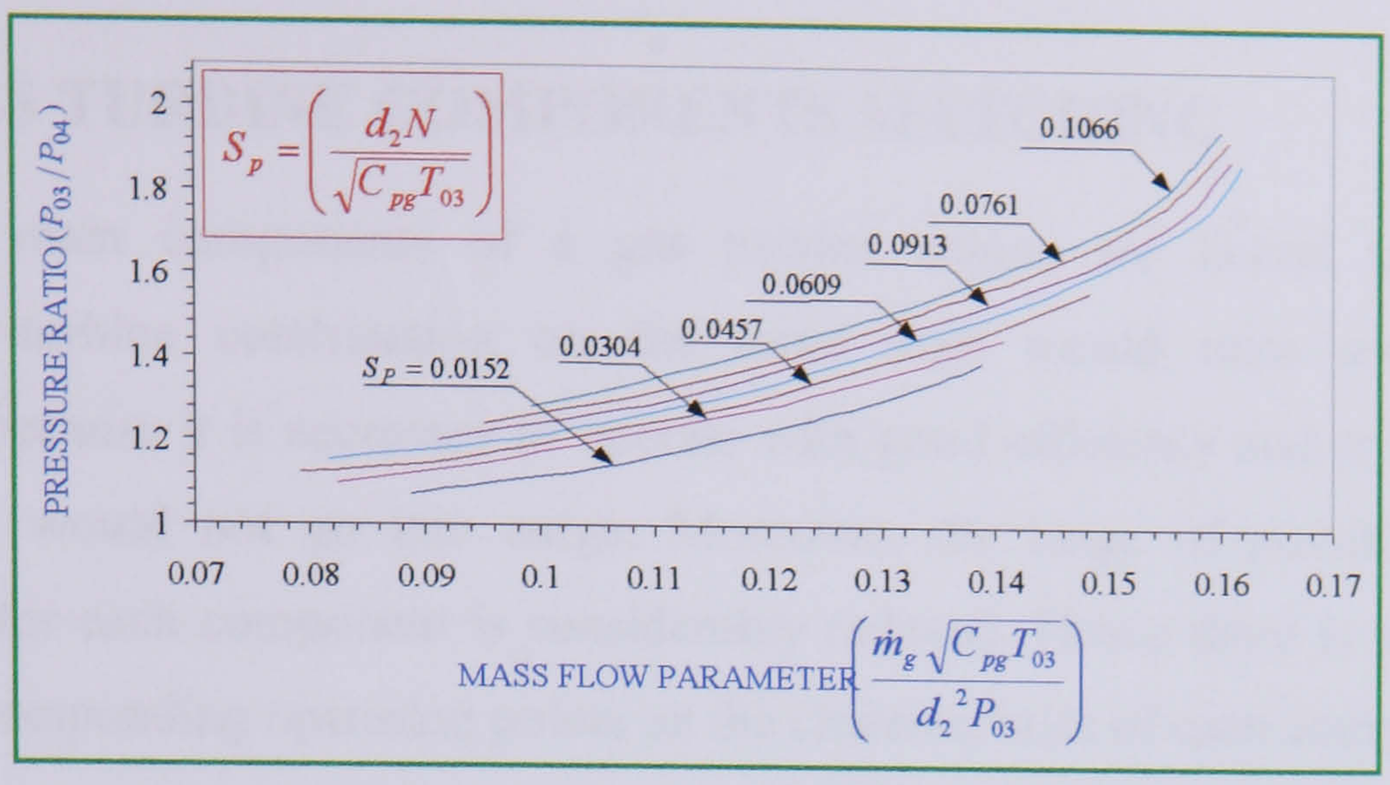

FIG. 8.4 A PLOT OF PRESSURE RATIO AGAINST MASS FLOW OF A TURBINE

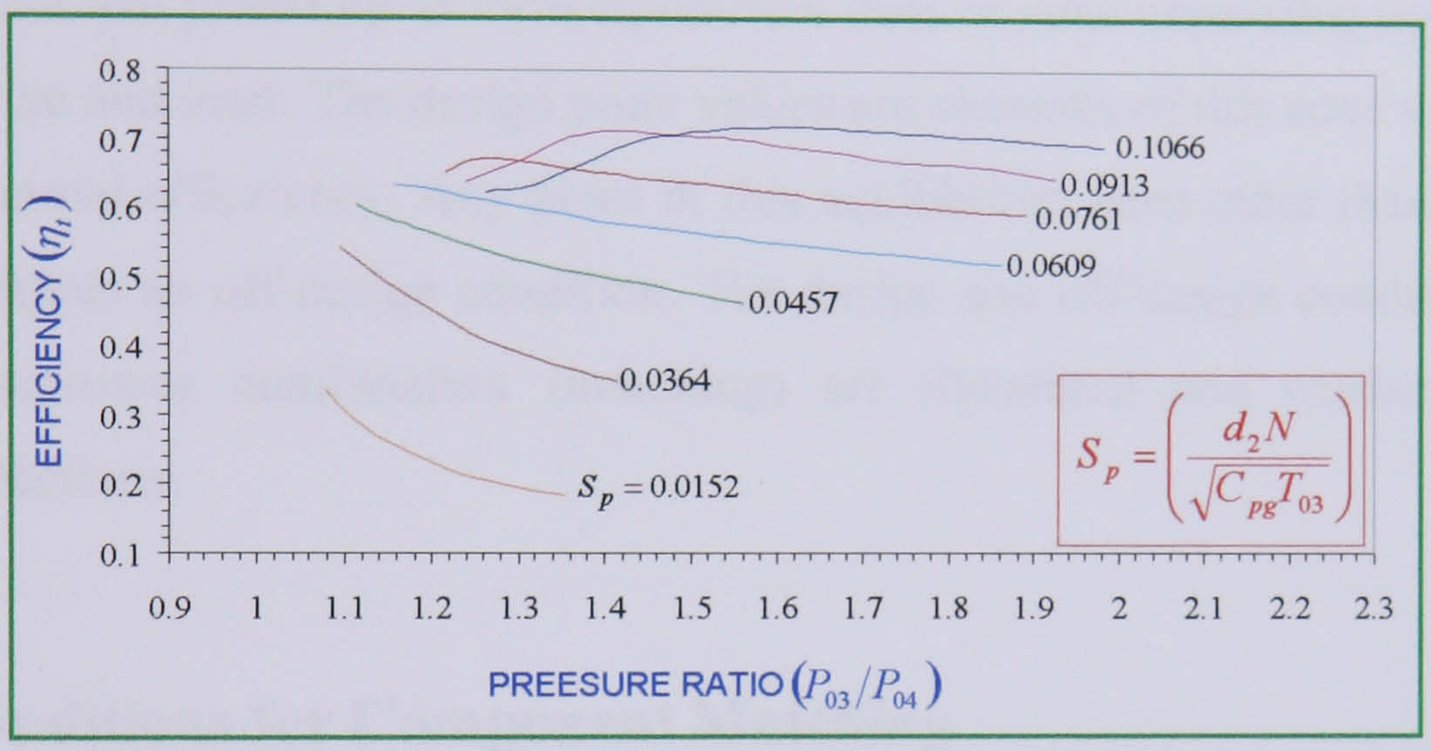

FIG. 8.5 A PLOT OF EFFICIENCY AGAINST PRESSURE RATIO OF A TURBINE

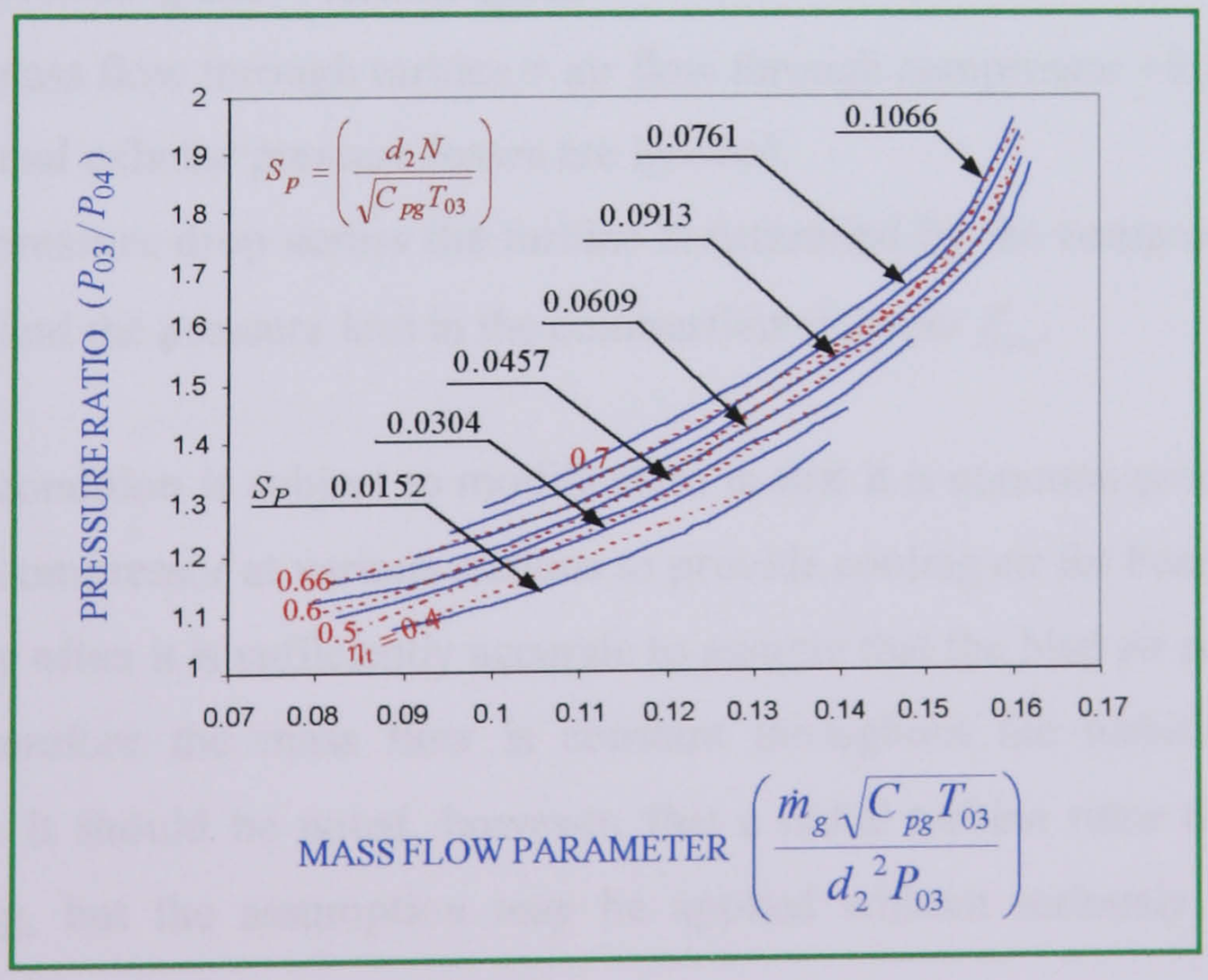

FIG. 8.6 COMPLETE PERFORMANCE CHARACTERISTICS OF A TURBINE

8.3 GAS TURBINE COMPONENTS MATCHING

When the main components of a gas turbine engine are linked together, the compressor-turbine combination on the same shaft would raise some difficult problems, because it is necessary to operate with good efficiency and ensure that the compressor would not go into surge. Moreover, the range of possible operating conditions for each component is considerably reduced. Hence there is a problem to find the corresponding operating points on the characteristics of each component when the engine is running at a steady speed, or in equilibrium as it is frequently termed. The equilbrium running points for a series of speeds may be plotted on the compressor characteristics and joined up to form equlibrium lines or zone depending upon the type of gas turbine and load. The design point values are elements of this zone which yeilds the best thermal effieciency. Any point in this equilibrium zone other than the design point represents an off-design condition. The design and off-design conditions of the turbine-compressor combination (matching) are illustrated and explained in the following sections.

8.3.1 Conditions for Component Matching

The following conditions must be satisfied for good turbine-compressor matching

i. Compressor speed = turbine speed

ii. Gas mass flow through turbine = air flow through compressor +fuel mass flow

iii. Inlet and exhuast pressure losses are ignored.

iv. The pressure drop across the turbine is determind by the compressor pressure ratio and the pressure loss in the combustion chamber ξ_{cc}.

The second condition is subject to modification in that it is common practice to bleed air from the compressor at various stations to provide cooling air for bearings and disc cooling. Very often it is sufficiently accurate to assume that the bled air equals the fuel flow and therefore the mass flow is constant throughout the turbine-compressor combination. It should be noted, however, that a radial turbine rotor does not have blade cooling, but the assumption may be applied without seriously affecting the

results. For the third condition, $P_{atm} = P_{01} = P_{04}$ and for the last condition $P_{03} = (1 - \xi_{cc}) P_{02}$.

8.3.2 Graphical Method of Components Matching

The steady state operation of gas turbine engine used for electrical power generation can be achieved by the matching of its compressor and turbine. In order to match the compressor and the turbine, that is, by superimosing the turbine performance map on the compressor map, it is necessary that the above conditions have to be met, and this is done by unifying the corresponding parameters of both axes, i.e the abscissa and the ordinate of both the compressor and the turbine maps to give the same parameters as described hereafter.

8.3.2.1 The compressor

For the mass flow parameter $\frac{\dot{m}_a \sqrt{C_{pa} T_{01}}}{d_{2C}{}^2 P_{01}}$, the abscissa axis of the compressor characteristics map for matching is transformed into:

$$\left[\frac{\dot{m}_a \sqrt{C_{pa} T_{01}}}{d_2{}^2 P_{01}}\right]\left[\frac{d_{2C} N}{\sqrt{C_{pa} T_{01}}}\right] = \left[\frac{\dot{m}_a N}{d_{2C} P_{01}}\right] \tag{8.1}$$

The resulting term $\left[\frac{\dot{m}_a N}{d_{2C} P_{01}}\right]$ is referred to as the mass flow matching parameter. For the pressure ratio parameter P_{02}/P_{01} , the ordinate axis remains the same. Once these tranformation are made, then the compressor characterisitics map is plotted again based on these new parameters as shown in **Fig. 8.7**.

8.3.2.2 The turbine

For the mass flow parameter $\frac{\dot{m}_g \sqrt{C_{pg} T_{03}}}{d_{2T}{}^2 P_{03}}$, the abscissa axis of the turbine characteristics map for matching is tranformed into:

$$\left[\frac{\dot{m}_g\sqrt{C_{pg}T_{03}}}{{d_{2T}}^2 P_{03}}\right]\left[\frac{d_{2T}N}{\sqrt{C_{pg}T_{03}}}\right]\left[\frac{P_{03}}{P_{04}}\right]\left[\frac{d_{2T}}{d_{2C}}\right]=\left[\frac{\dot{m}_g N}{d_{2C}P_{04}}\right] \tag{8.2}$$

By satisfying the conditions of matching, i.e, $\dot{m}_a = \dot{m}_g$ and $P_{01} = P_{04}$. Then the mass flow matching parameter of the turbine $\left[\frac{\dot{m}_g N}{d_{2C}P_{04}}\right]$ which is developed from equation 8.2 would be the same as the compressor matching parameter $\left[\frac{\dot{m}_a N}{d_{2C}P_{01}}\right]$.

For the pressure ratio P_{02}/P_{01}, the ordinate axis of the turbine characteristics map for matching is transformed into

$$\left[\frac{P_{03}}{P_{04}}\right]\left[\frac{1}{1-\xi_{cc}}\right]\left[\frac{P_{04}}{P_{01}}\right]=\left[\frac{P_{02}}{P_{01}}\right] \tag{8.3}$$

Note that $P_{03} = (1-\xi_{cc})P_{02}$ and $P_{04} = P_{01}$

Once these tranformations are made, then the turbine characterisitics map is plotted again based on these new parameters as shown in **Fig. 8.8**.

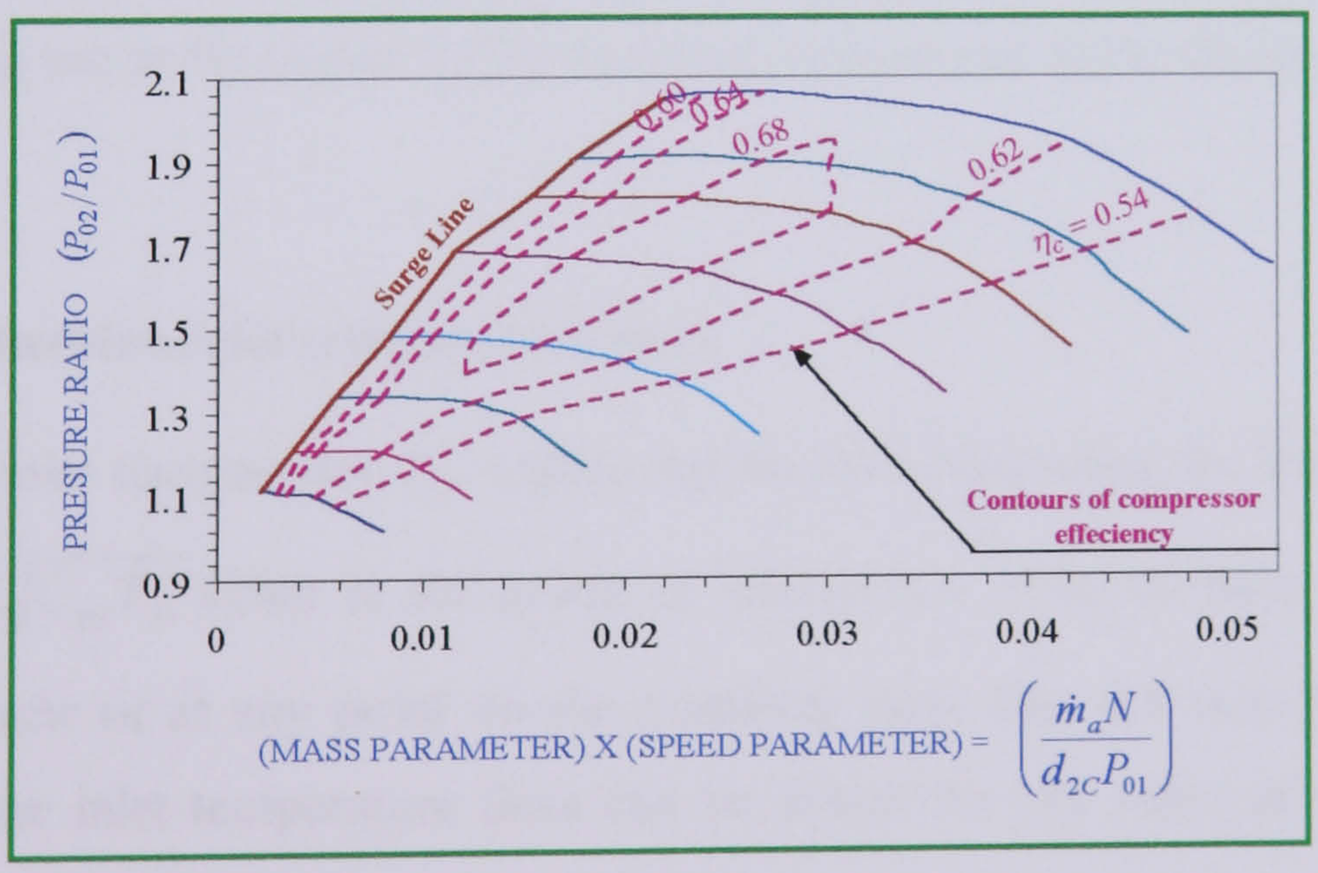

FIG. 8.7 PERFORMANCE MAP OF A COMPRESSOR BASED ON MATCHING PARAMETER

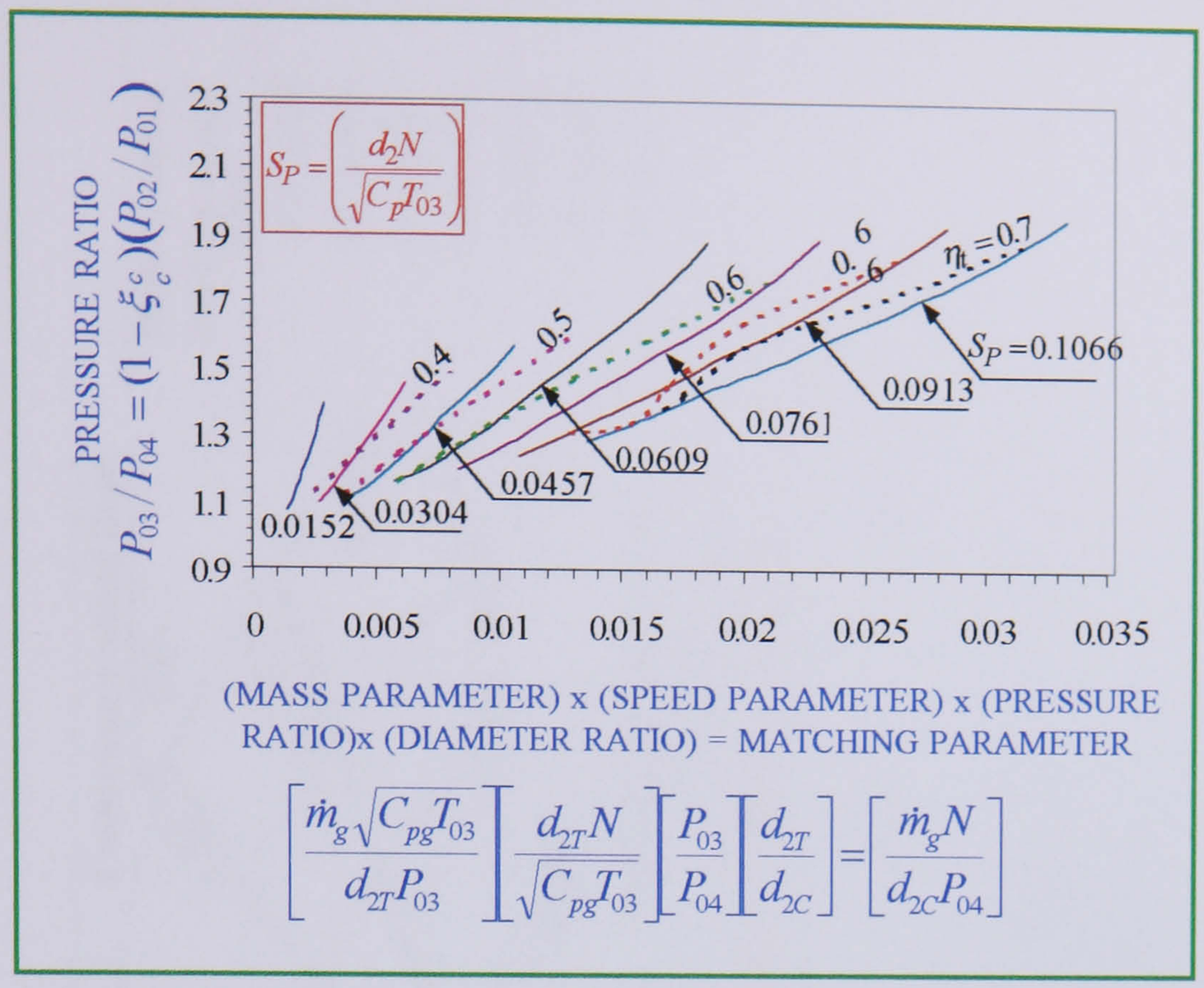

FIG. 8.8 PERFORMANCE MAP OF A TURBINE BASED ON MATCHING PARAMETER

It can be concluded from the graphical plot of the compressor and the turbine performance maps in **Fig. 8.7** and **Fig. 8.8** that the abscissa and the ordinate of these maps are the same. Therefore, the turbine map can now be superimposed on the compressor map to produce a complete matching map of the combination as shown in **Fig. 8.9**. It is important to know that this matching map will provide a quick method for predicting the performance of the matched components at the design and off-dsign conditions.

8.3.2.3 The turbine inlet temperature lines

The turbine inlet temperature T_{03} values can be calculated using the speed parameter, $S_P = d_{2T}N/\sqrt{C_{pg}T_{03}}$ either at the points of intersection of speed lines of the turbine and compressor or at any point on the matching map, **Fig. 8.9** over the full range. Hence, turbine inlet temperature lines can be drawn for any value as shown in **Fig. 8.10**.

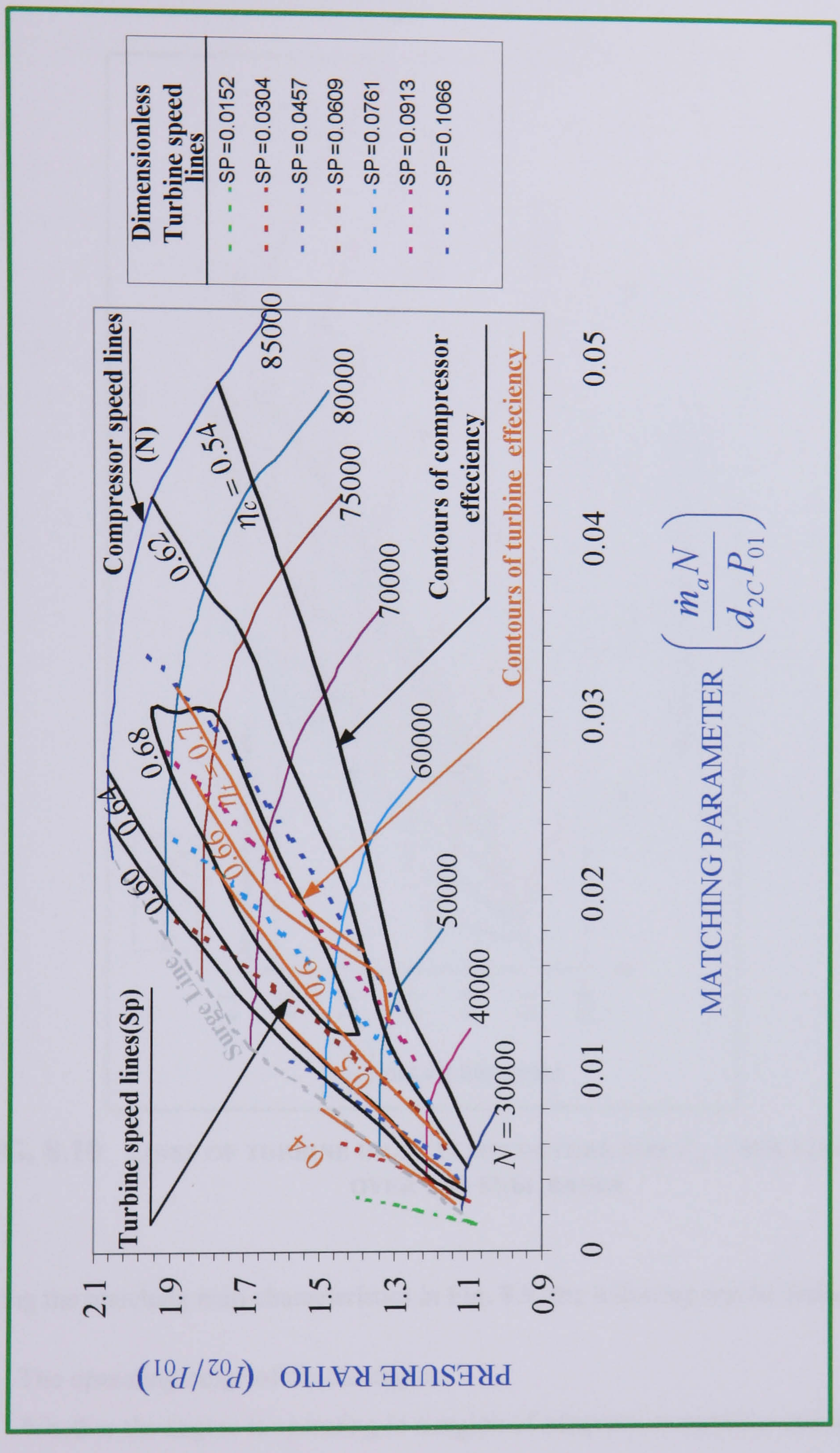

FIG. 8.9 COMPLETE PERFORMANCE MAP OF A COMPRESSOR AND TURBINE COMBINATION

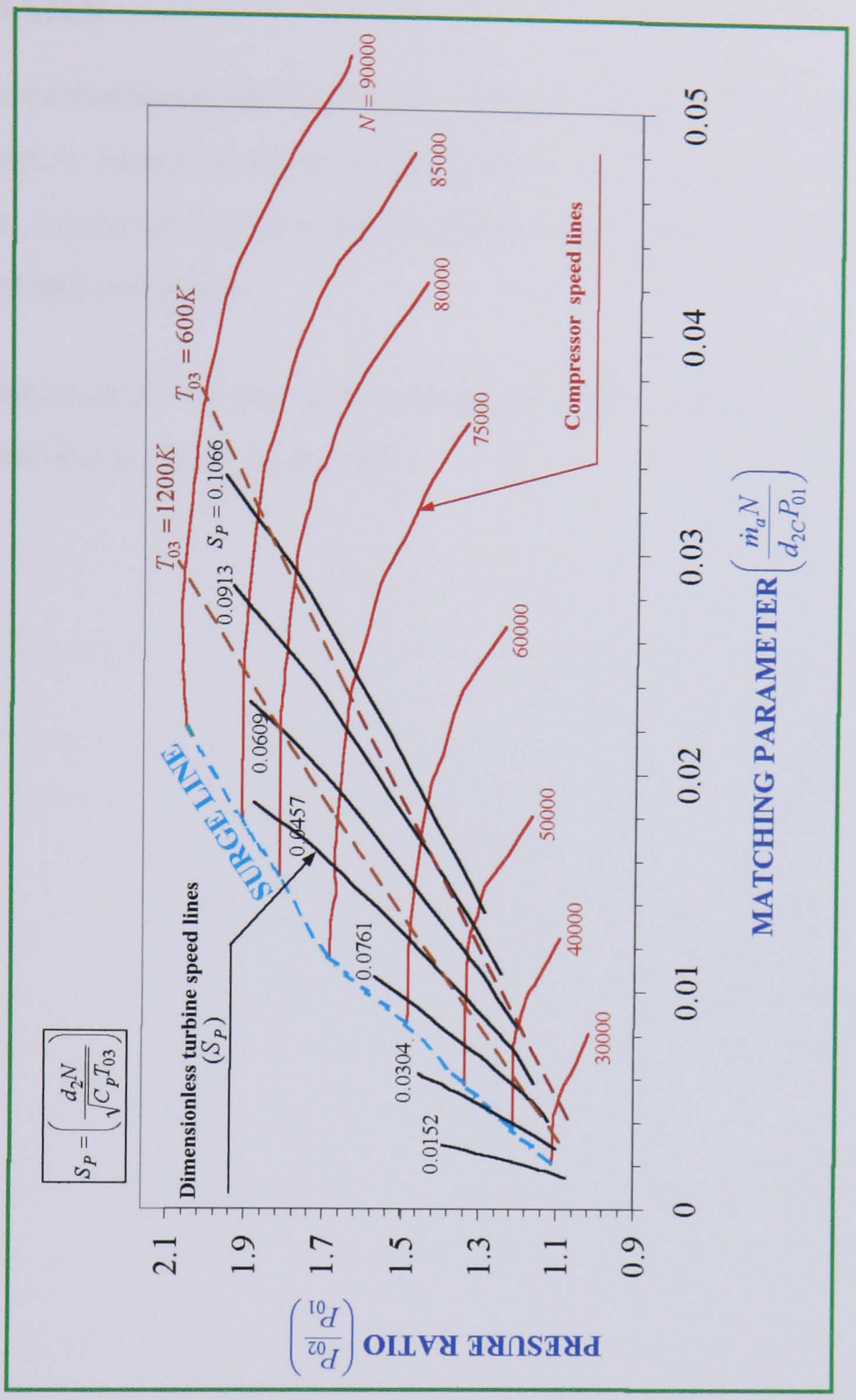

FIG. 8.10 LINES OF TURBINE INLET TEMPERATURE FOR $T_{03} = 600, 1200\,K$ OVER THE FULL RANGE

Studying the matching map characteristics in **Fig. 8.9**, the following can be deduced:

i. The operating range of the the engine.

ii. Whether the engine is operating in a region of adequate compressor and turbine efficiencies

iii. The proximity of the operating points to the compressor surge line.

iv. The maximum inlet temperature at the operating point of the turbine.

8.4 SUMMARY

Analysis of the performance prediction of small gas turbine unit has been presented in the current Chapter. Based on the individual performance map of both the compressor and the turbine, a complete performance matched characteristics map of the engine has been developed and presented.

It should be mentioned that the work carried out in this Chapter was a joint effort between the author and Qusai Al-hamdan.

CHAPTER 9

MANUFACTURE OF GAS TURBINE COMPONENTS, INSTRUMENTATION AND CONSTRUCTION OF THE EXPERIMENTAL FACILITY

9.1 MANUFACTURE OF GAS TURBINE COMPONENTS

9.1.1 Introduction

In the preceding chapters, the design details of gas turbine components including the compressor, combustion chamber, bearing assembly and power transmission shaft have been given. In order to verify the performance of these components, it was necessary to build a test cell facility comprising the gas turbine engine and the accessories to carry out the experimental work. To achieve that, the main components of the engine were manufactured apart from the combustion chamber liner and the fuel atomizer, both were adapted from an existing auxiliary power unit type **GTCP85**. In doing so, factors such as the selection of suitable materials, type and ease of manufacturing (cast or machined) were considered when preparing the final design.

In the following subsections, the material requirements and the type of manufacturing for each major component of the gas turbine engine are described.

9.1.2 The Manufacture of IFR Turbine Components

9.1.2.1 Turbine rotor

IFR turbines (the rotor and the casing) are normally exposed to high temperature approaching up to $1500K$. For the turbine rotor, the characteristics required for long life, high temperature services are high creep and rapture strength, resistance to hot corrosion, oxidation, good fatigue strength and low thermal expansion. To meet these requirements, materials currently used are almost exclusively **Nickel-base alloys** such

as Inconel (Nickle-Chromium alloys), Nimonic (Nickle-Chromium alloys and Nickle-Cobalt alloys), Incoloy (Nickle-Iron-Chromium alloys) and others. Detail specifications of these alloys are found in **Special metal product hand book [75]**. The results of the stress, thermal and vibration analyses, which have been carried out in **Chapter 7**, indicate that the selection of **Inconel alloy-718** material for the turbine rotor satisfies the design criteria of tensile strength and high temperature.

Method of manufacturing plays an important part in the design requirements. In the current work, there was an option for machining or casting the turbine rotor but machining was preferred to casting, because the latter will be more costly for one-off component. The turbine rotor was machined using five axes computerized numerically controlled (CNC) machines to do the work accurately. The rotor was manufactured by **Turbocam Company [76]** and the machined component is shown in **Fig. 9.1**.

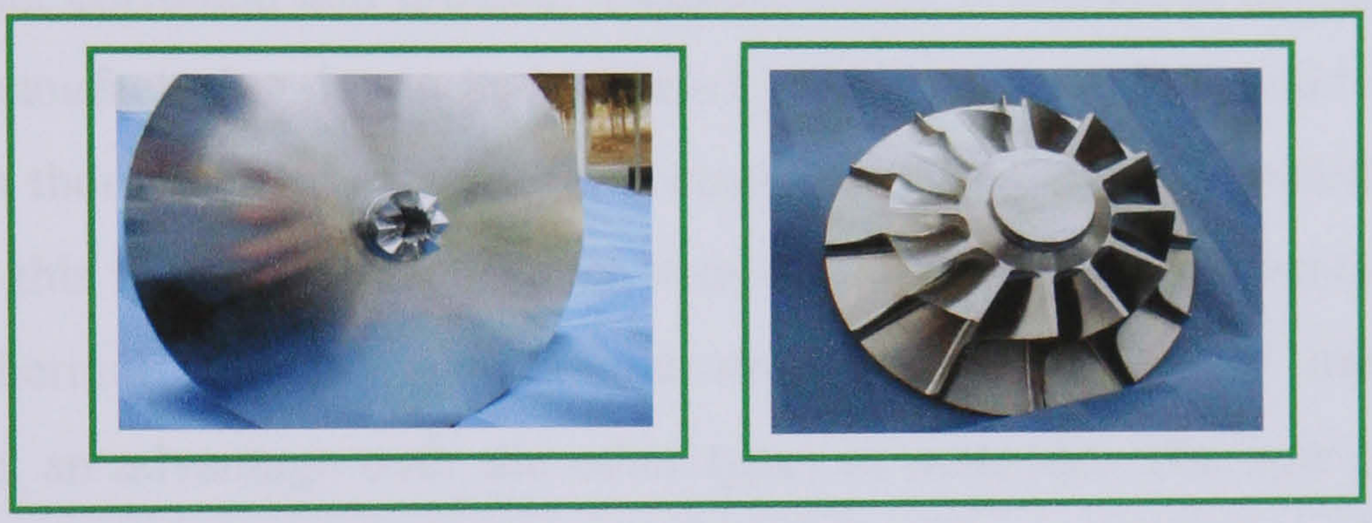

FIG. 9.1 TURBINE ROTOR MACHINED FROM INCONEL ALLOY-718

9.1.2.2 Turbine casing

The design of the turbine volute casing revealed that the casing is subjected to less tensile stress, thermal and vibration loading. Again, casting of the nozzle-less casing was considered to be too costly for one off component. Therefore, machining was considered as an alternative option. **Stainless steel alloys 304L** was selected for the manufacture of the casing. Once the decision was made to machine the casing, the design was altered to suit the manufacturing process, and to make it possible. To do that, the turbine casing was made into two parts; the volute and the casing cover. The casing was manufactured by the **Exact Engineering Ltd** [77] and the machined parts of the casing are shown in **Fig. 9.2**.

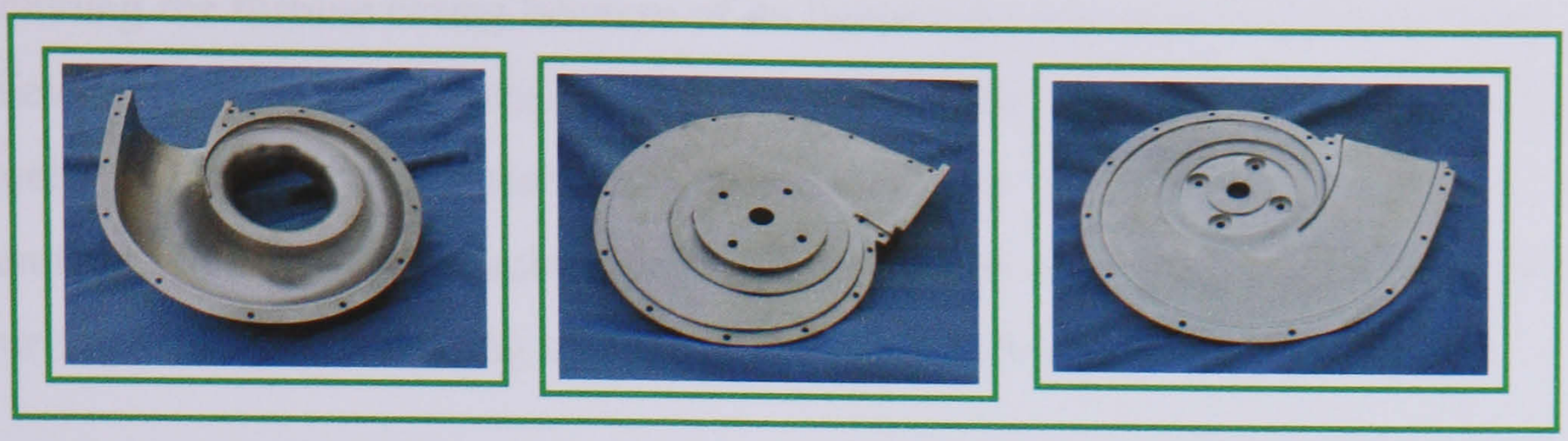

FIG. 9.2 NOZZLE-LESS CASING MACHINED FROM STAINLESS STEEL ALLOY, TYPE 304L

9.1.3 The Manufacture of the Centrifugal Compressor Components

9.1.3.1 Compressor impeller

Compressors are usually subjected to low temperatures as compared to turbines. The requirements for compressor impeller material are lightweight to reduce stresses, fatigue strength, corrosion and erosion. Titanium alloys is a material favourably used for impeller manufacturing due to its low density, which make it light and high fatigue strength. Even though Titanium material is costly compared to other materials, it was considered in this research work because it meets the design requirements regarding tensile and thermal stresses, high fatigue strength. Also, its good ductility and toughness was an advantage over the other types of materials. The type of material chosen was **Titanium Ti-6AI-4V**. The impeller was machined at **Turbocam Company [76]** as shown in **Fig. 9.3**.

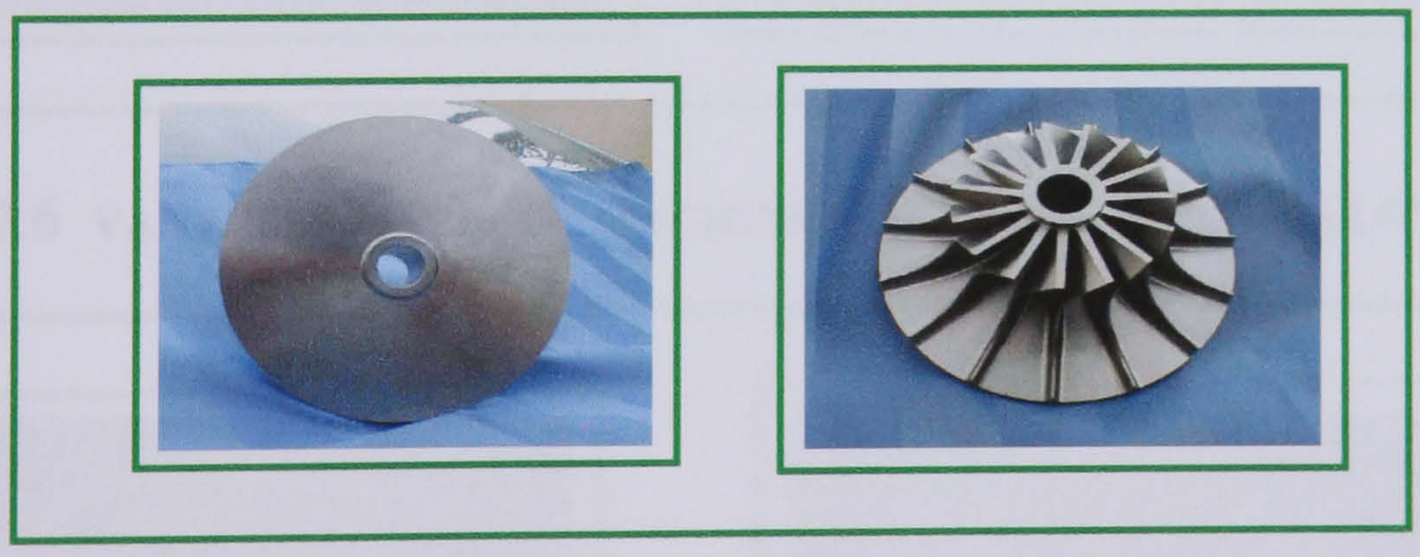

FIG. 9.3 COMPRESSOR IMPELLER MACHINED FROM TITANIUM TI-6AI-4V, GRADE 5

9.1.3.2 Compressor casing

For the compressor casing, it was decided to machine it to reduce the cost compared to casting for one off component. Therefore, Aluminum alloys, type 7075 was used for

machining the turbine casing because of its lightweight and ease of manufacturing. To achieve this purpose, the casing was designed to be manufactured of three parts, namely the vaneless diffuser, the volute and the casing cover. Again it was manufactured at **Exact Engineering Ltd** [77]. The machined components of the centrifugal compressor casing are shown in **Figs. 9.5, 9.6** and **9.7**, respectively.

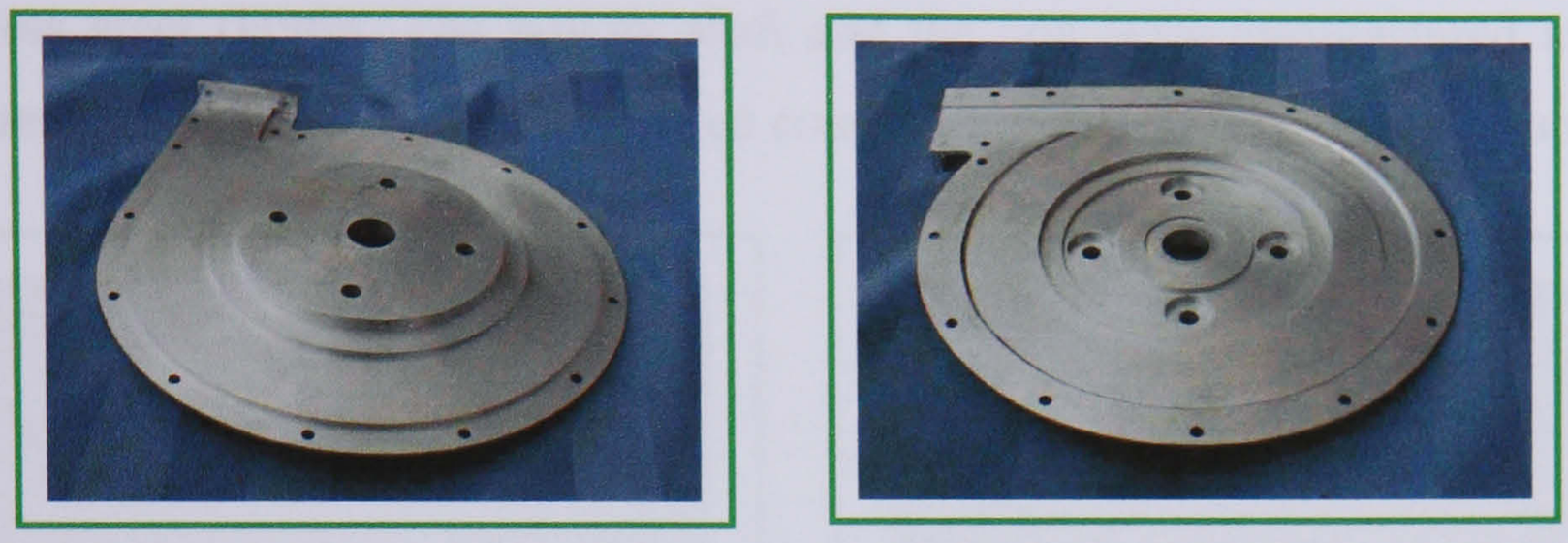

FIG. 9.5 COMPRESSOR CASING COVER MACHINED FROM ALUMINUM ALLOY-7075

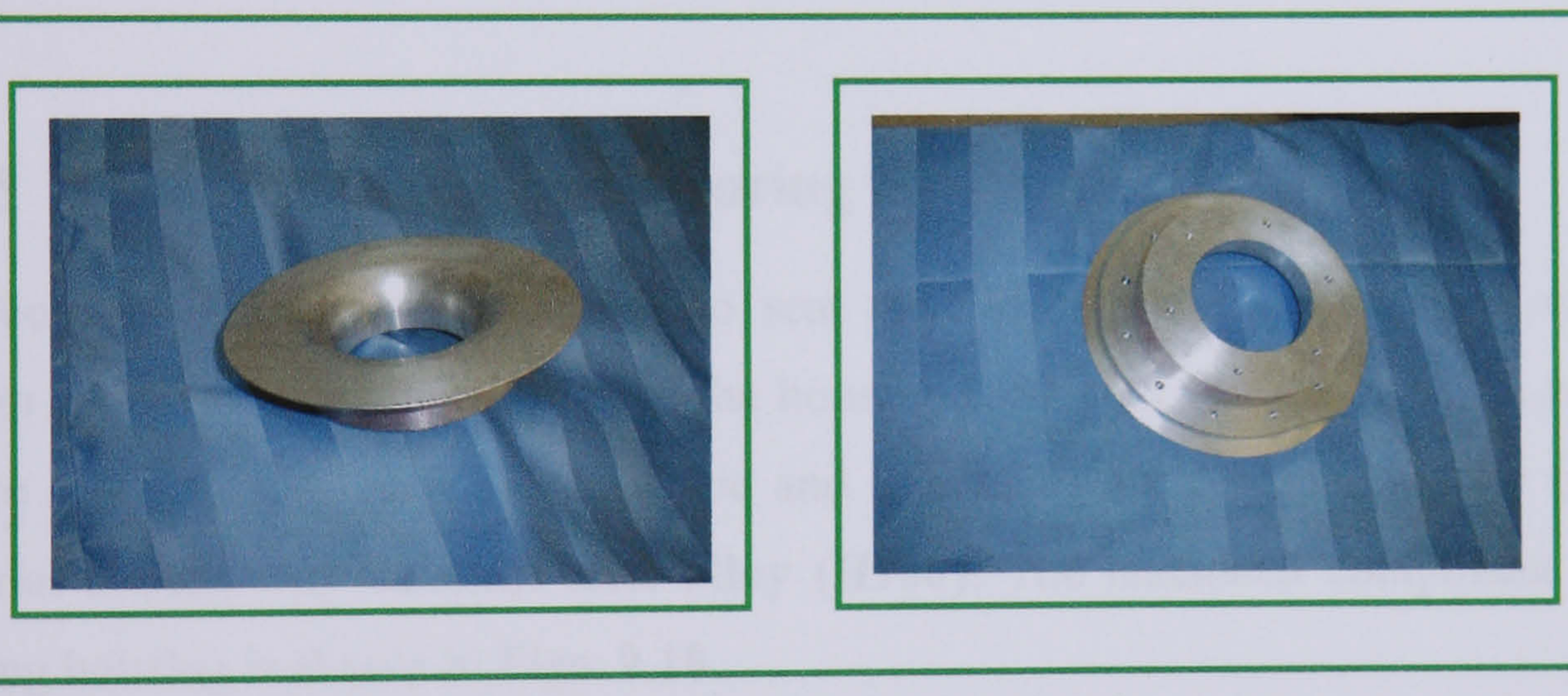

FIG. 9.6 VANELESS DIFFUSER MACHINED FROM ALUMINUM ALLOY-7075

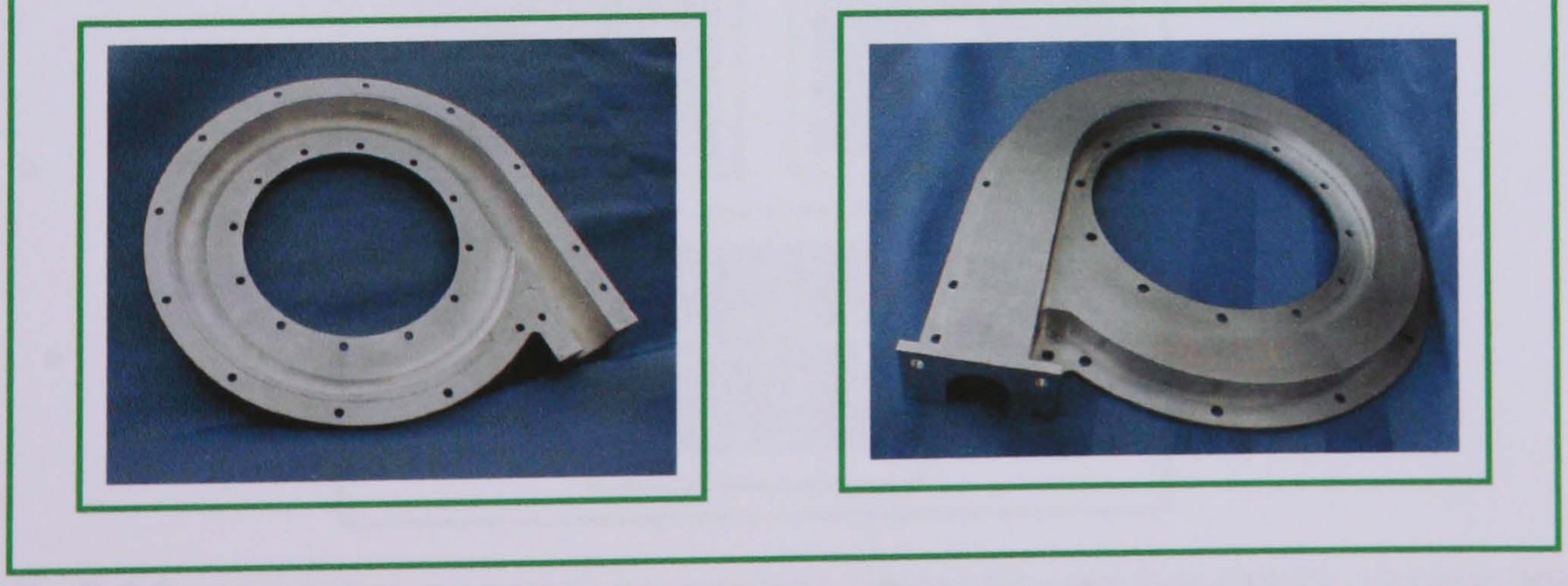

FIG. 9.7 COMPRESSOR VOLUTE MACHINED FROM ALUMINUM ALLOY-7075

9.1.4 The Manufacture of Power Transmission Shaft Assembly

The shaft-bolt assembly was designed as described previously in **Chapter 6** to connect the rotor and the impeller and to accommodate the selected bearings. The material chosen for the shaft and the bolt must be identical so that when both subjected to various loading conditions, similar effects would result. The chosen material was **stainless steel (H900**. The hollow shaft and the bolt were manufactured at **Exact Engineering Ltd [80]** and the machined components are shown in **Figs. 9.8** and **9.9**.

FIG. 9.8 HOLLOW SHAFT

FIG. 9.9 MAIN BOLT

9.1.5 The Manufacture of Bearing Housing

The bearing housing was designed to seat the bearings and lubricate the rotating system efficiently. Again, machining the housing compared to casting was a suitable choice when factors such as cost, time and tolerances are considered. The type of material chosen was **stainless steel alloy (H900)**. The machined component of the bearing housing is shown in **Figs. 9.10**.

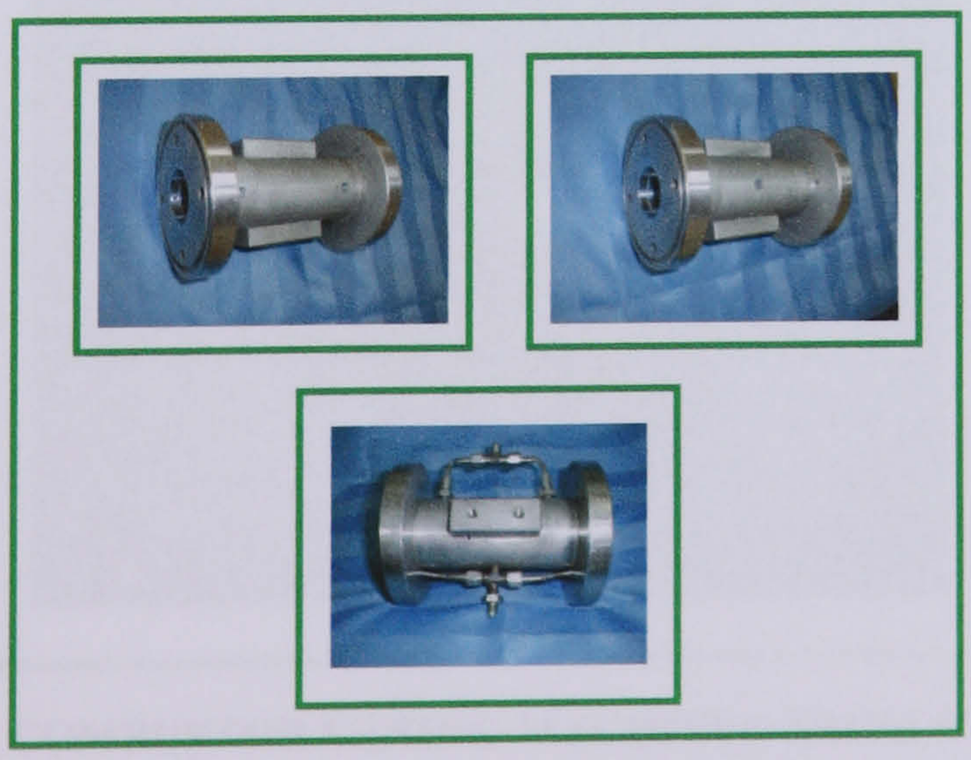

FIG. 9.10 BEARING HOUSING MACHINED FROM STAINLESS STEEL ALLOY, H900 INCLUDING THE OIL PORTS FOR LUBRICATIONS

9.1.6 The Manufacture of Combustion Chamber Casing

As mentioned earlier, the combustion chamber liner and the fuel atomizer excluding the casing were adapted from an existing auxiliary power unit type **GTCP85**. The combustor liner is shown in **Fig. 9.11**.

FIG. 9.11 SINGLE CAN COMBUSTOR LINER ADAPTED FROM AN EXISTING AUXILIARY POWER UNIT TYPE GTCP85

The combustion chamber casing has to be machined from **stainless steel alloy material (H900)** to resist the high temperature with high accuracy. The machined component of the combustor casing is shown in **Figs. 9.12**.

FIG. 9.12 COMBUSTOR CASING MACHINED FROM STAINLESS STEEL ALLOY, H900

The complete assembly of the combustion chamber is shown in **Fig. 9.13**.

FIG. 9.13 COMBUSTION CHAMBER ASSEMBLY

9.1.7 The Manufacture of the Air Duct

The air duct, which connects the compressor outlet and the combustion chamber inlet, was made of two parts. For compact design, the air duct is curved smoothly and designed of circular cross-section to fit the assembly and to reduce pressure losses. To achieve that, the air duct was machined from a **mild steel alloy material** that resists moderate temperatures of the pressurized air out of the compressor. This component was manufactured at the **Royal Scientific Society [78]** as shown in **Figs. 9.14**.

FIG. 9.14 VIEW OF AN AIR DUCT MACHINED FROM MILD STEEL ALLOY

9.1.8 The Manufacture of the IFR Turbine Outlet Duct

The outlet duct assembly was made of two parts, the first part was the interface flange, which was made of a steel type **42CD4 (AISI: 4140)** and fitted between the **IFR** turbine casing and the conical diffuser. The second part was the conical diffuser, which was selected from an existing auxiliary power unit **GTCP85** and fitted with straightners inside to direct the exhaust turbulent flow. The diffuser was made of steel sheet metal. The machined components of the outlet duct parts were manufactured at the main workshops at the **Jordan University for Science and Technology [79]**. The machined components are shown in **Figs. 9.15** and **9.16**.

FIG. 9.15 INTERFACE FLANGE MACHINED FROM STEEL TYPE 42CD4 (AISI: 4140)

FIG. 9.16 STRAIGHTNERS

FIG. 9.17 CONICAL DIFFUSER

The complete assembly of the outlet duct is shown in **Fig. 9.18.**

FIG. 9.18 COMPLETE ASSEMBLY OF THE IFR TURBINE OUTLET DUCT

9.1.9 The Manufacture of the Trailer Assembly

The trailer base as shown in **Fig. 9.19** was manufactured at **Al-Hussein Main workshop**. It was designed to carry out the gas turbine engine, to accommodate the oil and fuel systems, the ignition system with batteries.

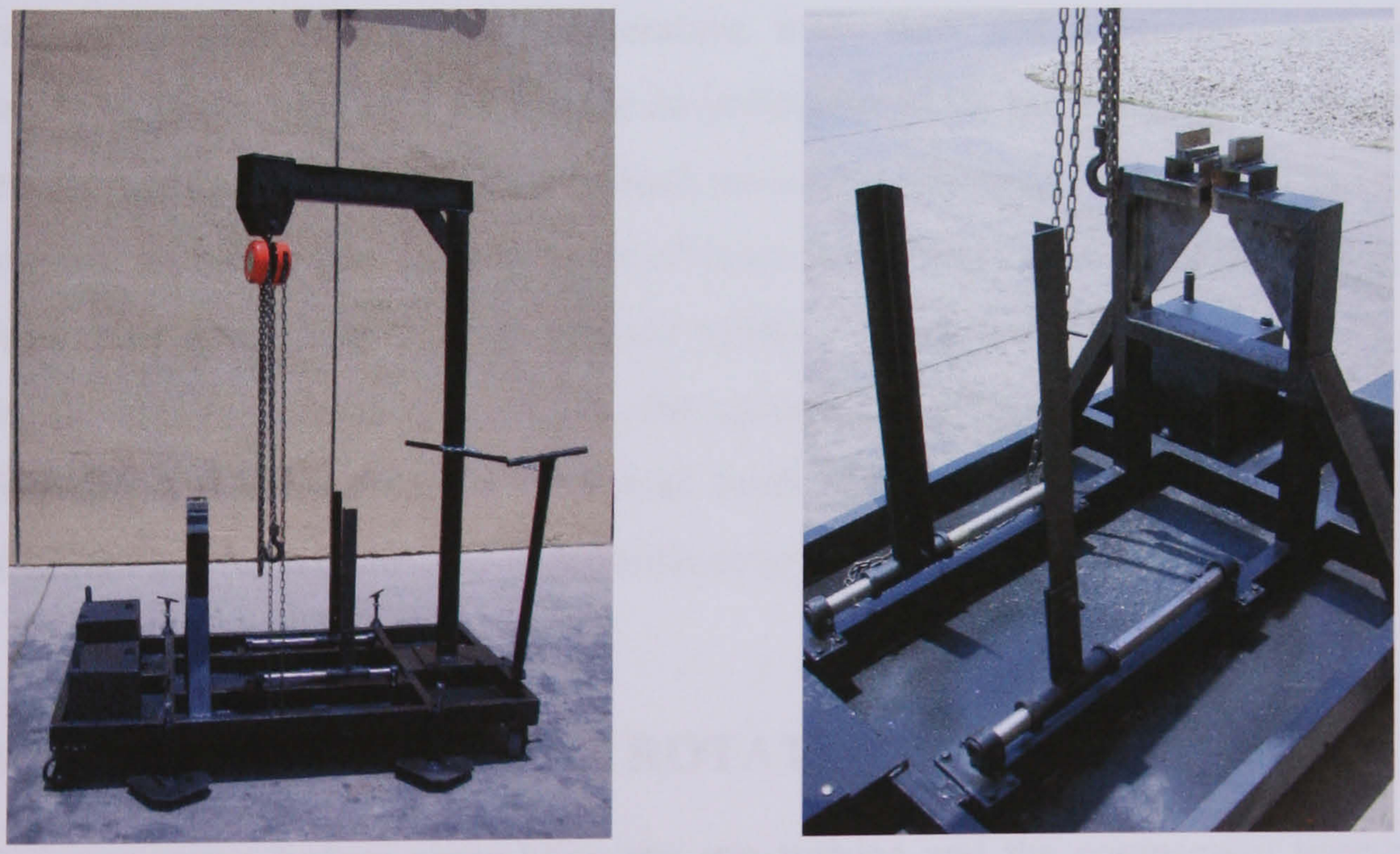

FIG. 9.19 TRAILER ASSEMBLY

9.1.10 Gas Turbine Assembly

The engine assembly was carried out at the workshops of the **Royal Air Force at Azraq base**. The complete engine is shown in **Fig. 9.20**.

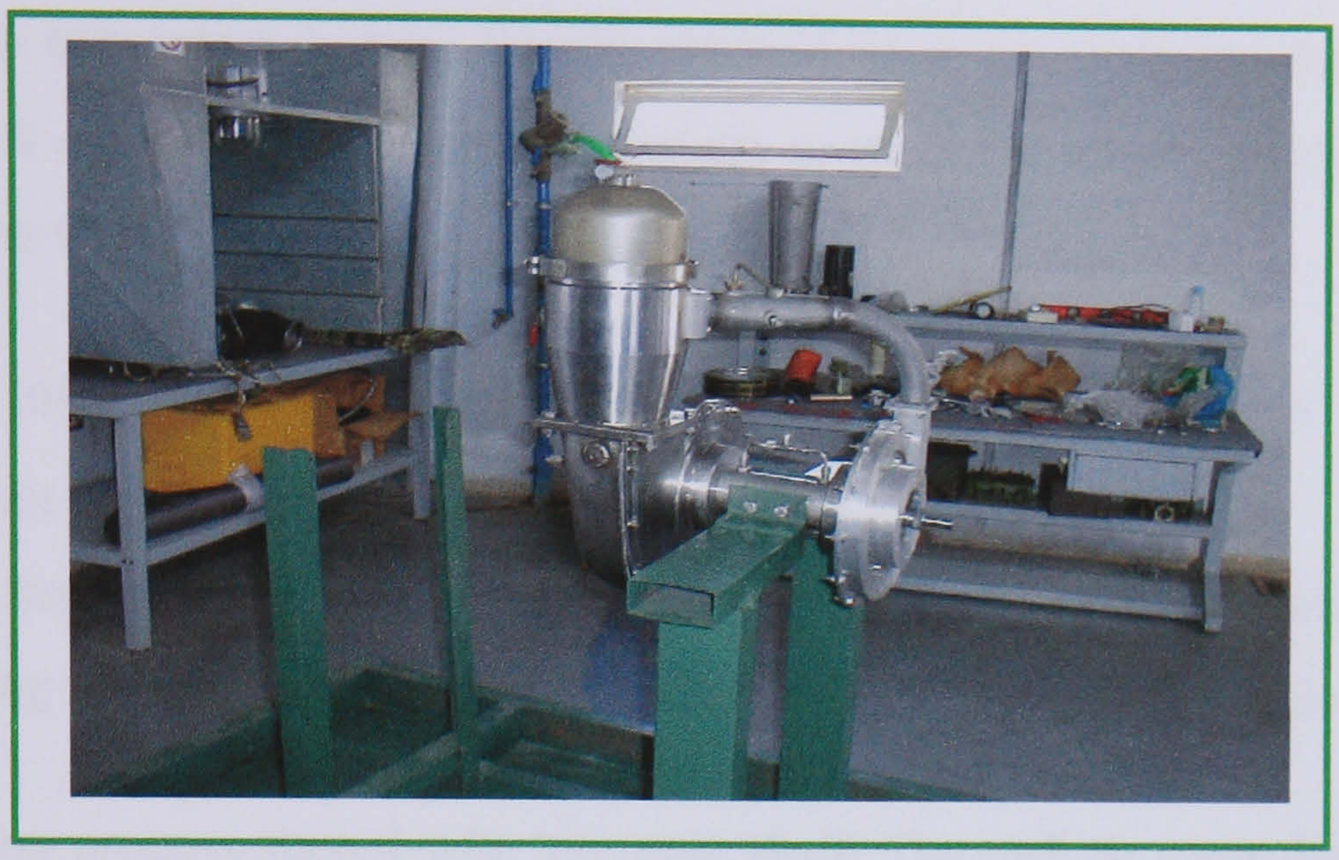

FIG. 9.20 SMALL GAS TURBINE ENGINE ASSEMBLY

9.2 INSTRUMENTATION OF THE TEST FACILITY

The function of the instrumentation system is to inform the operator of the events taking place inside the small gas turbine test rig. The internal functions of these components such as pressure, temperature, mass flow and rotational speed are of concern to the turbine user to provide an indication of the turbine performance and to keep the operator apprised of the critical measurements such as exhaust temperature, vibration. In this work, various types of instruments were used to measure pressure, temperature and mass flow at various locations of the experimental test rig. For accurate and reliable measurements, the specified instruments were calibrated. The calibration was carried out in the **Royal Jordanian Calibration Laboratory**. Each instrument has been calibrated in accordance to its specifications.

9.3 BALANCING OF THE ROTATING ASSEMBLY

It was necessary, before assembling the **IFR** turbine and the compressor together to balance the rotating assembly to ensure safe operation and to eliminate any serious

vibration effects. The balancing process was carried out at **Schenck Company [80]** and the balancing procedure is described below:

The primary process balancing of the individual components was carried out using wax material. This was to insure the tolerances based on balance quality grade **G2.5** according to **ISO 1940/1** is met. Results showed poor repeatability, therefore certain modifications on the components were made to meet the required tolerances. These modifications were:

i. The main bolt had to be reduced in length by $1\,mm$ to allow the turbine to tighten on the main shaft before bottoming in the turbine.
ii. The hearth coupling between the turbine and the main shaft was modified by adding flats to the main shaft to allow a higher torque to the main bolt.

The balancing process started with the main shaft. The turbine rotor then fitted to the main shaft with a torque of $40\,Nm$. Readings and repeatability checks were carried out for all positions of the turbine rotor relative to the main shaft. The position of the best repeatable reading was selected and the turbine rotor was dynamically balanced. It was then match marked relative to the main shaft as shown in **Fig. 9.21**.

The impeller was then fitted to the main shaft and index balanced in single plane on the back face. A single static correction was used, as there was no sacrificial material on the nose end of the impeller. Finally, the complete assembly was then trim balanced.

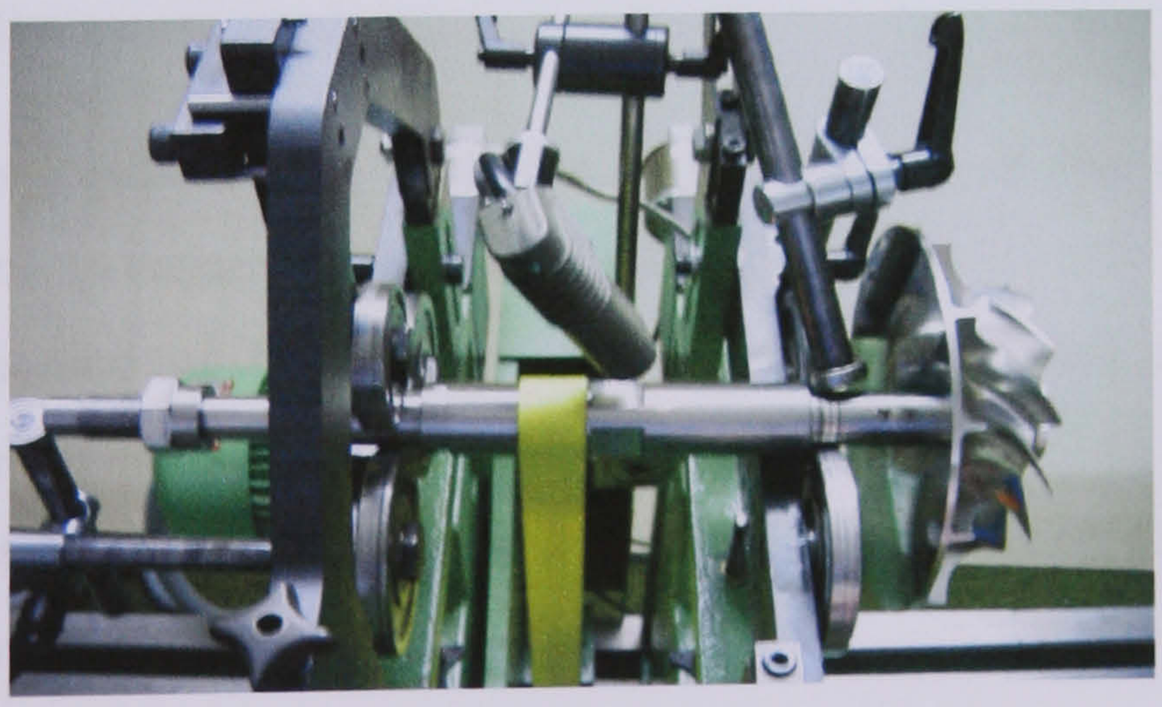

FIG. 9.21 BALANCING SETUP OF THE TURBINE ROTOR

9.4 CONSTRUCTION OF THE EXPERIMENTAL FACILITY

The construction of the experimental test facility was carried out at Al-Zaraq air force base. The work was divided into three sections:

i. The assembly of gas turbine engine. **Fig. 9.22** features the sequence of assembling the engine.
ii. The construction of the mechanical systems (fuel, oil and starting systems).
iii. The positioning of the measuring instruments.

The first part was completed. The second part was not completely constructed due to time limitation. However, It should be mentioned that both the fuel pump and the oil lubrication pump were selected from an existing auxiliary power unit type **GTCP85**. Both pumps were coupled together directly and tested by a driven an a.c motor running at $4000 rpm$ as shown in **Fig. 9.23**. For the third part, preparations for positioning the measuring devices were carried out and placed on the engine. The diagram given in **Fig. 9.24** shows the locations for measurements of pressure, temperature, mass flow rate, fuel flow and rotational speed.

9.5 EXPERIMENTAL WORK OF THE GAS TURBINE ENGINE

It was described in the preceding sections the manufacturing of the gas turbine components based on the design results given in **Chapters 4 and 5** and the construction of the test facility. The overall scope of the experimental work can be discussed under three main headings:

i. Preliminary tests dealing with the commissioning of the engine and fault rectification to ensure successful operation.
ii. Commissioning of the mechanical systems such as fuel and oil systems, starting and ignition systems.
iii. Final tests describing the measurements for obtaining the steady flow performance characteristics of the turbine.

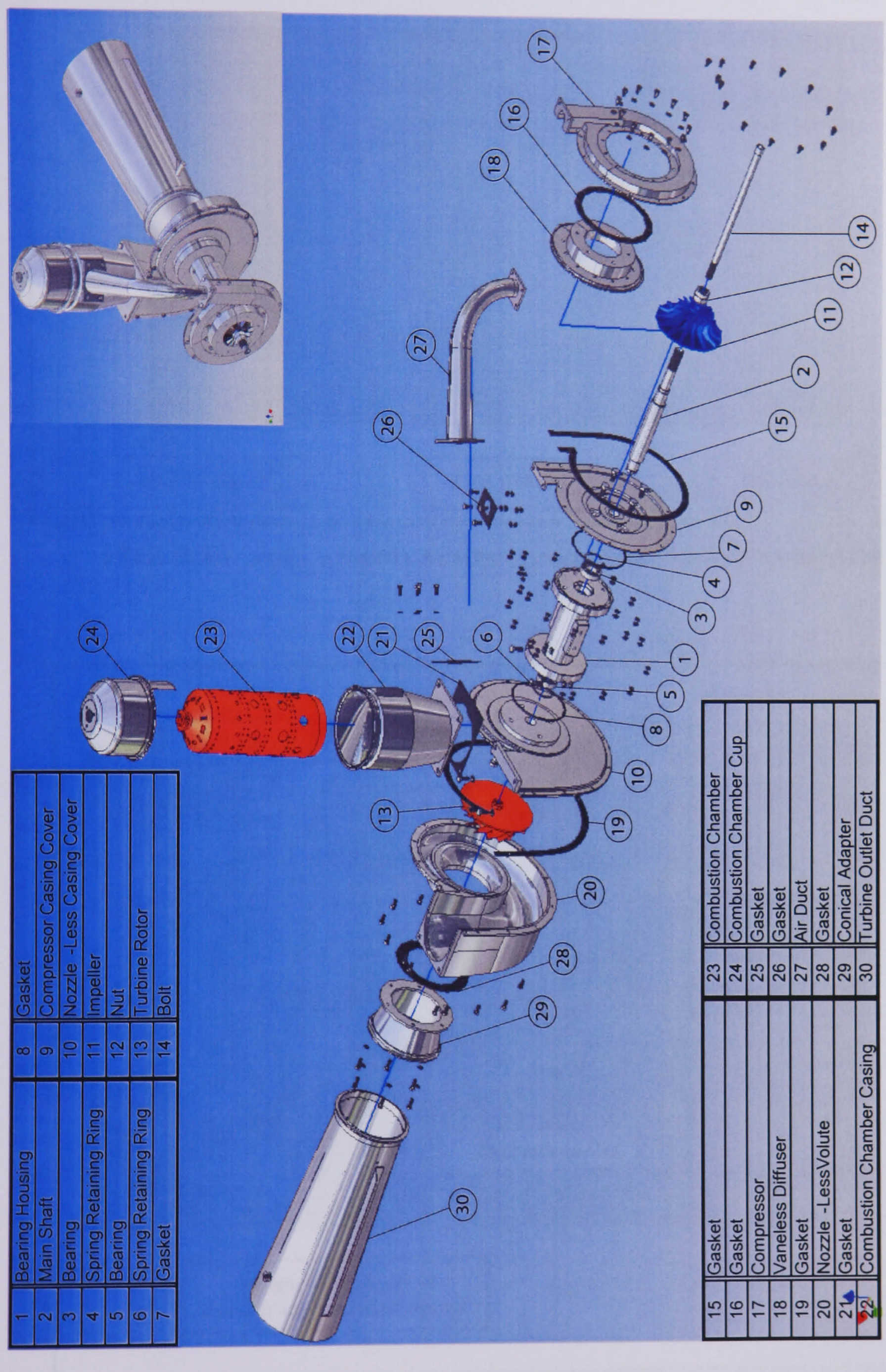

Fig. 9.22 DISASSEMBLY OF GAS TURBINE ENGINE

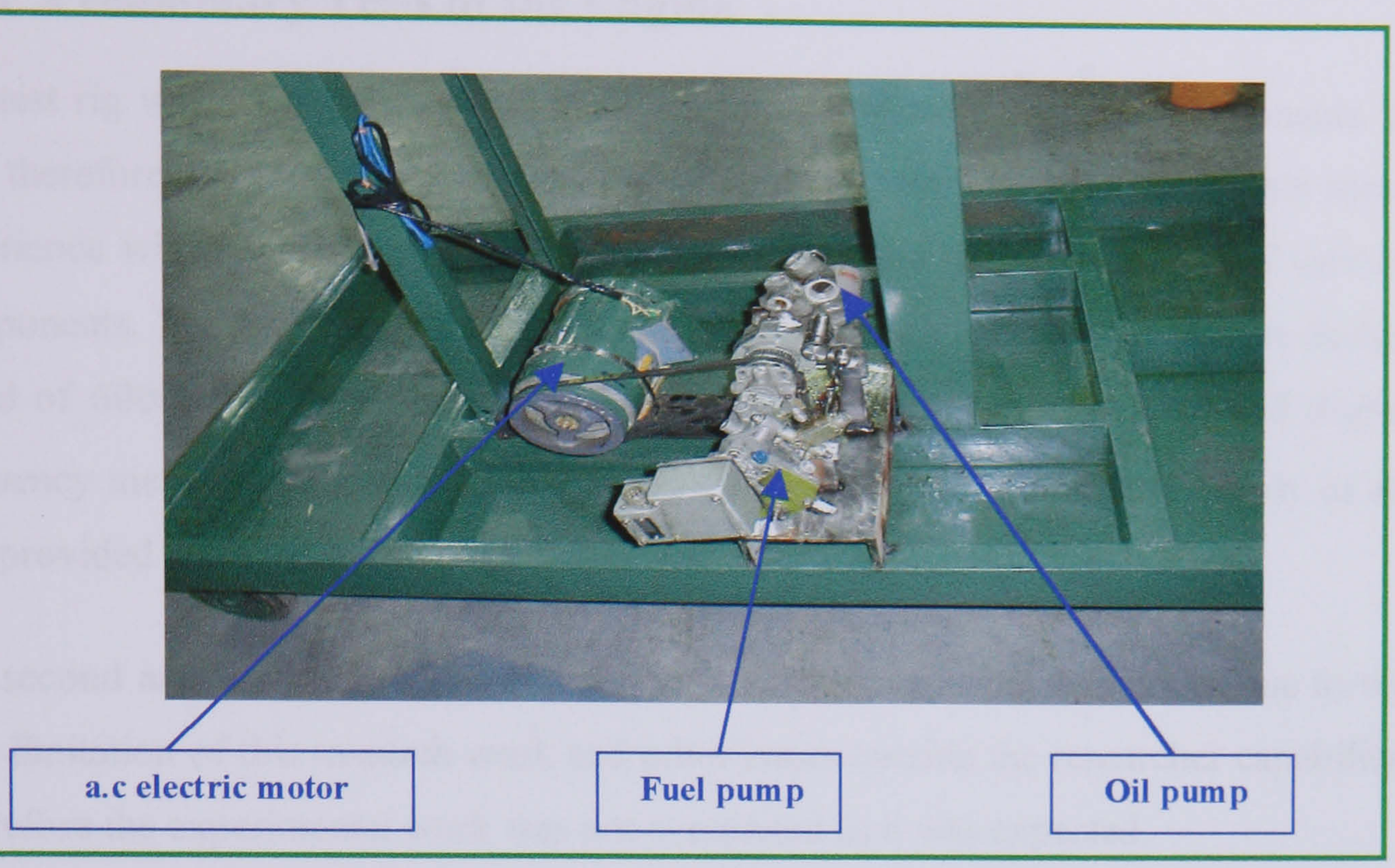

FIG. 9.23 FUEL AND OIL PUMPS CONNECTION TO THE A.C MOTOR

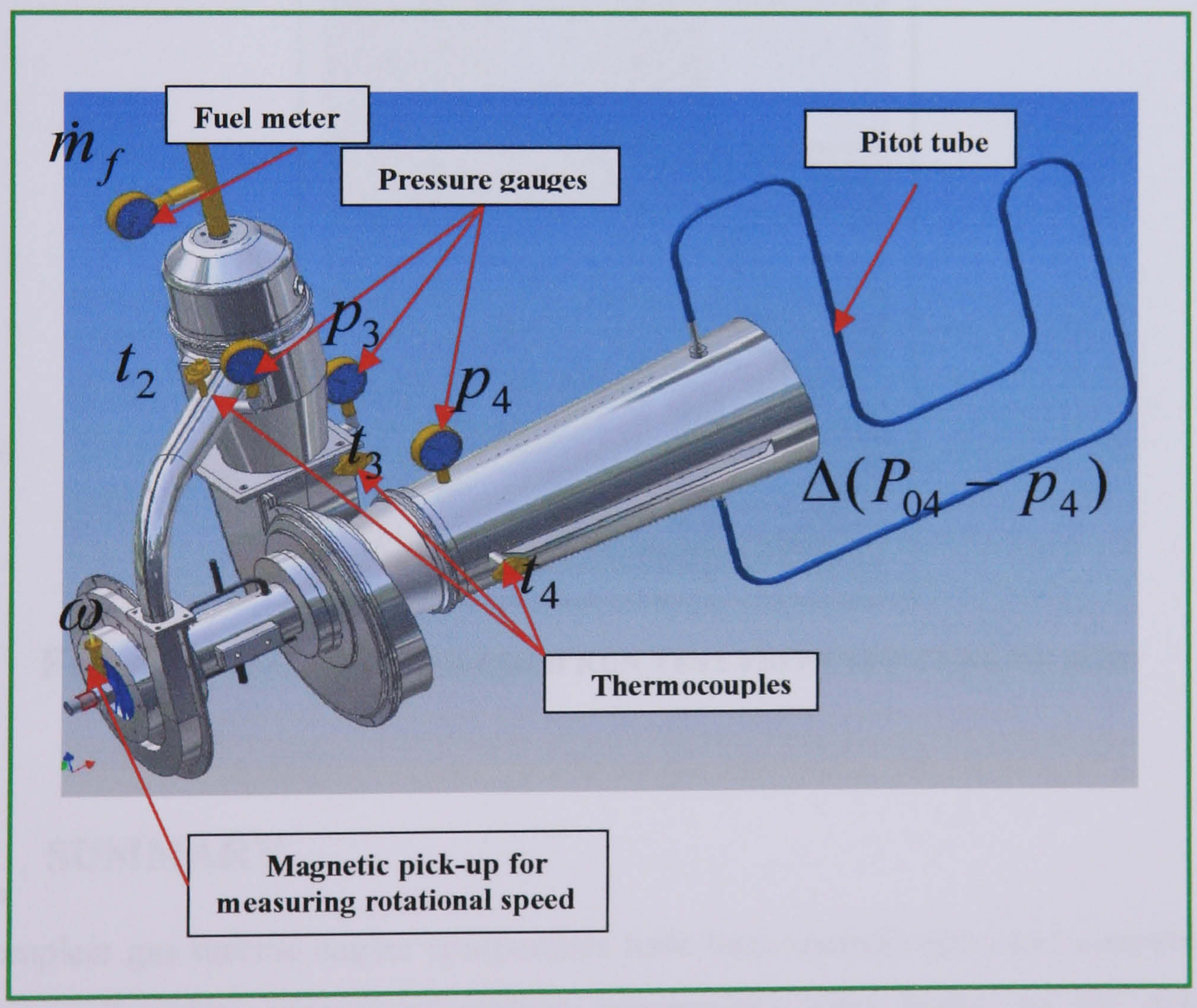

FIG. 9.24 THE LOCATION OF VARIOUS MEASURING DEVICES OF THE TEST RIG

9.5.1 Preliminary Tests of the Engine

The test rig was a complex system incorporating completely untested components. It was, therefore, very important to carry out preliminary tests of the engine to gain some experience with regard to operating sequence, safety and the performance of various components. The first test was to run the engine on cold air in order to reach the design speed of 60000*rpm*. The speed was measured using a magnetic pick-off and digital frequency meter. Several runs were carried out for a short time and the supply of air was provided from an existing auxiliary power unit as shown in **Figs. 9.25**.

The second and third part of the experimental work faced some difficulties due to the time limitation of this research work and other issues outside the researcher capability. Therefore the experimental work was not completed as it was expected.

Fig. 9.25 ENGINE UNDER COLD RUN TEST FROM THE TURBINE SIDE

9.6 SUMMARY

A complete gas turbine engine components have been manufactured and assembled. The manufacturing process of various components were based on the design procedures described in earlier Chapters. Balancing of the individual components of

the rotating system and the complete assembly has been carried out. The engine was fully instrumented on a test rig. Cold run has been successfully accomplished according to the specified design conditions and performance experiments were not completed due to time limitations.

CHAPTER 10

RESULTS AND DISCUSSION

10.1 INTRODUCTION

The aim of this research programme was to design, develop and test a small gas turbine to drive directly a permanent magnet alternator. Therefore, the work consisted of theoretical analysis and performance optimisation studies including the problems of turbine-compressor matching. The necessary practical work involved the construction of a complete gas turbine. The scope of the experimental work was to commission and run the engine under design conditions.

Based on this, theoretical investigation was undertaken and several technical and design issues regarding the components of the gas turbine were resolved. The author believes the successful outcome of the current study will make a significant contribution to the topic.

For the experimental part, the ambition was to carry out detail experimental work on the engine, but the outcome was not as expected due to the time limitation, techniacal and administration issues. Inspite of these limitations, the complete gas turbine was manufactured, assembled and commissioned for a cold run up to design speed.

In this chapter the final results of the theoretical and experimental work of this research programme are reported. The results and discussion have been divided into six main sections, namely:

i. The results of parametric studies of the gas turbine cycle, the design of IFR turbine and the centrifugal compressor.
ii. Optimisation of the geometric and aerodynamic parameters for the IFR turbine rotor and centrifugal impeller.

iii. Optimisation of the axial length and the design of the flow passage for the IFR turbine rotor and centrifugal impeller.

iv. Stress and vibration analysis.

iv. Turbine and compressor matching.

v. Experimental work.

10.2 DISCUSSION OF RESULTS OF PARAMETRIC STUDIES

Theoretical investigations of the effect of variable operating conditions on gas turbine performance and the study of geometric and aerodynamic variables on the design of inward flow radial turbine and centrifugal compressor were undertaken. In order to study the influence of these variables on the overall turbine's performance parameters and on each other, analytical models were developed as described in **Chapters 3 and 5**. These models demonstrated graphically the effects of the values of these variables over a wide range of turbine and compressor operating conditions. This information was used for the design of turbines and compressors by identifying important design parameters and their values. Studies based on developing and using analytical models are termed as parametric studies. The results of this parametric study for the following topics are discussed hereafter.

10.2.1 Parametric Results of Gas Turbine Cycle

The thermal efficiency, specific fuel consumption and the specific work output can be used to describe the gas turbine cycle performance. A computer program was written to solve equations 3.1 to 3.8 derived in **chapter 3** for each set of turbine inlet temperature and pressure ratio. A flow chart of the programme to calculate the specific fuel consumption and the thermal efficiencies is given in **Fig. A.1** of **Appendix [A].**

The results were used to plot **Figs. 10.1** and **10.2** to describe the performance parameters of a simple gas turbine cycle, i.e. specific fuel consumption SFC, cycle thermal efficiency η_{th} and the gas turbine net specific work output $\dot{W}_s$.

Figure 10.1 shows that *SFC* reduces with increased turbine inlet temperature and cycle pressure ratio simultaneously. The peak cycle greater than 1200 *K* would not be practical due to metallurgical limit of the turbine material.

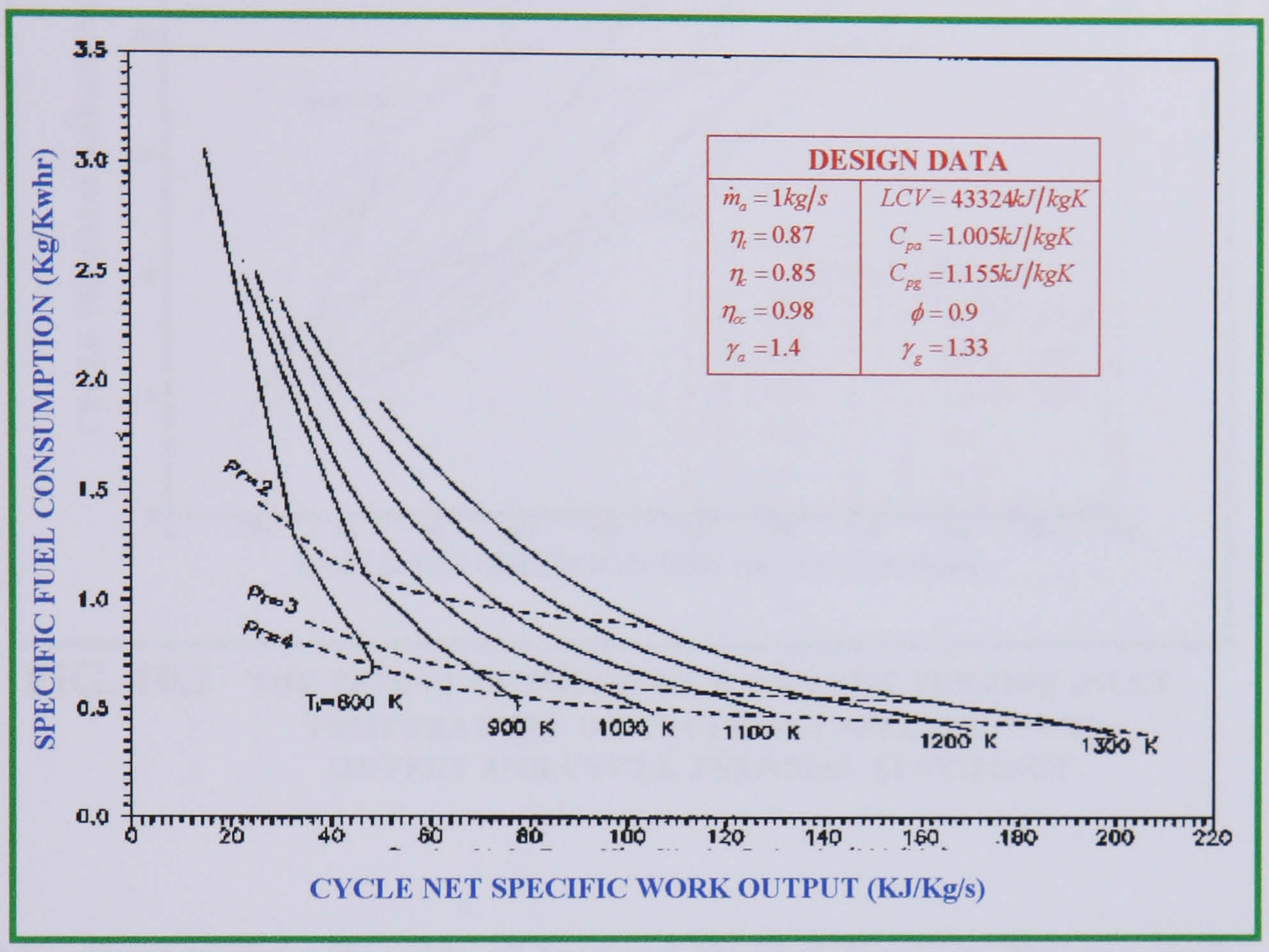

FIG. 10.1 THE EFFECT OF PRESSURE RATIO AND TURBINE INLET TEMPERATURE ON CYCLE NET SPECIFIC WORK OUTPUT AND SPECIFIC FUEL CONSUMPTION

Figure 10.2 shows that cycle thermal efficiency increases with increased turbine inlet temperature and cycle pressure ratio simultaneously. It also shows that the maximum efficiency point and the maximum specific work point, at each constant temperature or pressure ratio, are different, as clearly illustrated at $T_i = 800\ K$. The design choice can either favour the maximum efficiency (industrial applications with low operating cost) or maximum specific work (military applications with low capital cost) or any other point that may represent the optimum choice for a particular application.

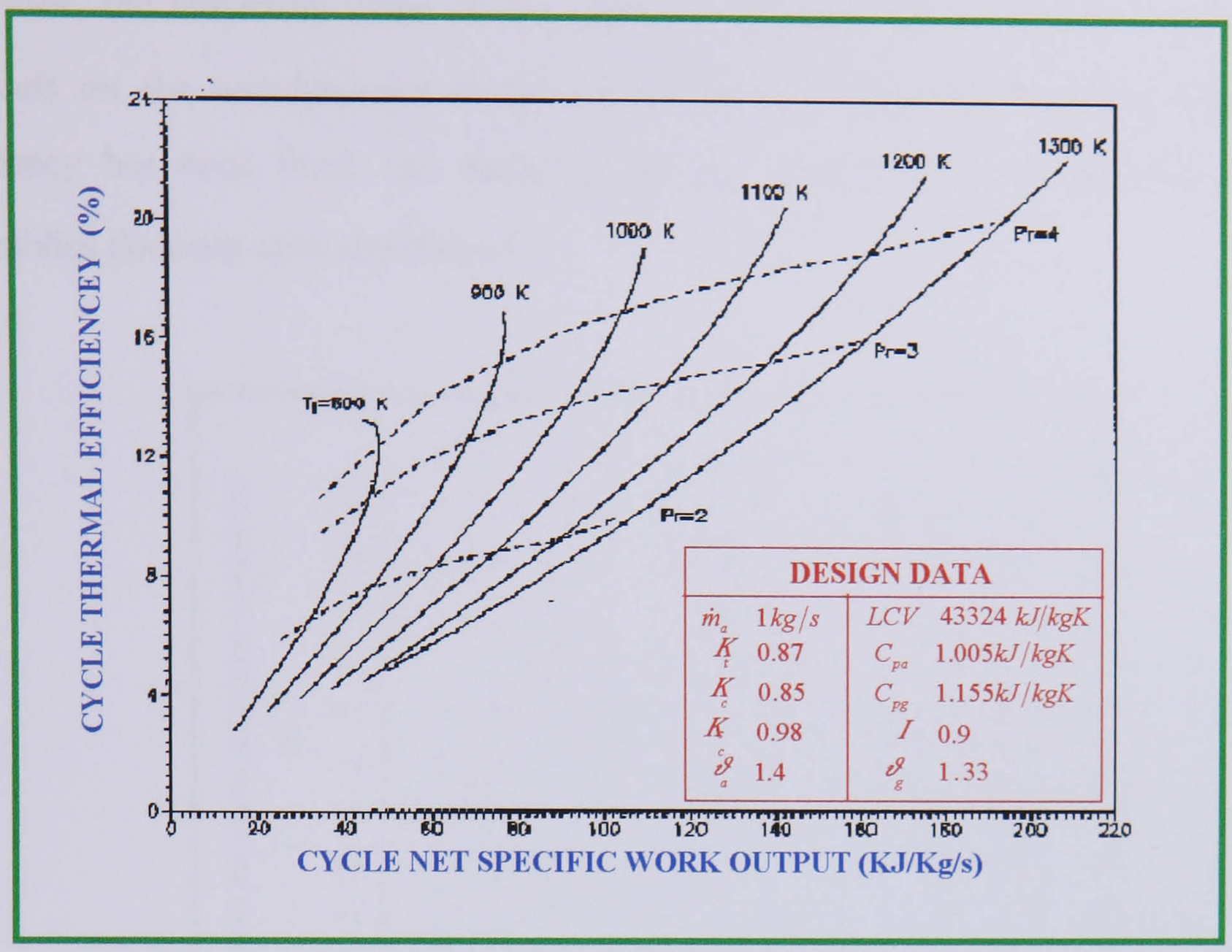

FIG. 10.2 THE EFFECT OF PRESSURE RATIO AND TURBINE INLET TEMPERATURE ON CYCLE NET SPECIFIC WORK OUTPUT AND CYCLE THERMAL EFFICIENCY

10.2.2 Parametric Results of Inward Radial Turbine Design and Performance

10.2.2.1 The effect of operating conditions on the performance of IFR turbine

The analytical model developed in equation 3.21 is quite important as it gives a simple relationship between the dimensionless specific torque ST, the velocity ratio u_2/c_s, the total-to-total efficiency η_{t-t} and the turbine pressure ratio P_i/P_e which is an important independent variable.

For moderate pressure ratio, the isentropic efficiency η_{t-t} is normally almost independent of the pressure ratio and can be assumed to be a unique function of the velocity ratio. **Hiett and Johnston [81]** and **Hiett and Palmer [82]**. A typical η_{t-t} versus u_2/c_s diagram is shown in **Fig. 10.3**.

However, the maximum value of η_{t-t} and the shape of the η_{t-t} versus u_2/c_s curve depends on the aerodynamics design of the turbine. However, once the maximum efficiency has been fixed, the shape of the η_{t-t} versus u_2/c_s for the **IFR** turbine assemblies does not alter significantly.

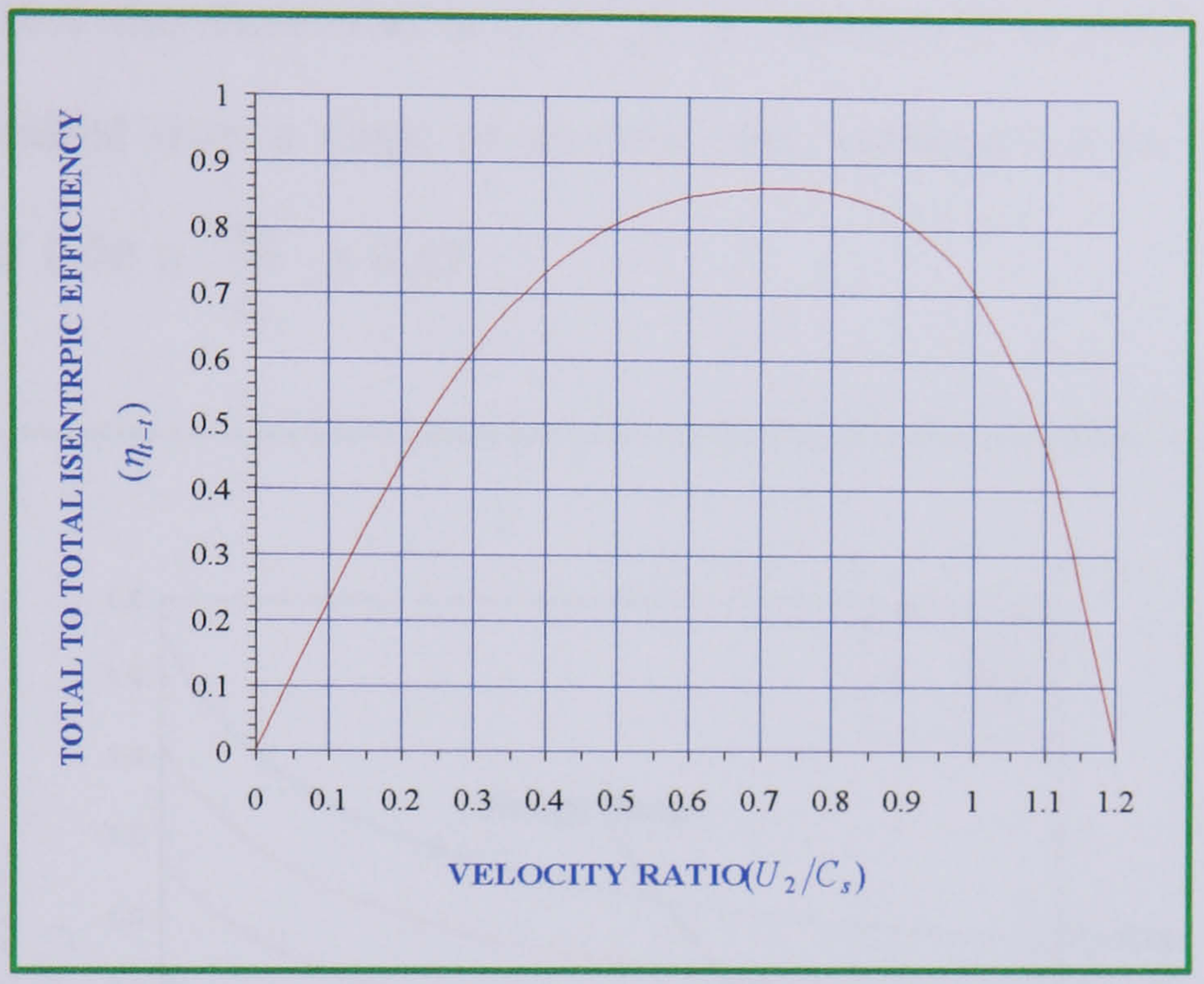

FIG. 10.3 A TYPICAL TOTAL-TO-TOTAL EFFICIENCY η_{t-t} VS. VELOCITY RATIO U_2/C_s CHARACTERISTICS FOR SMALL GAS TURBINES

Three computer programs were written to solve equations 3.17, 3.20 and 3.21 for each set of pressure ratio P_i/P_e, velocity ratio u_2/c_s, and speed parameter $d_2N/\sqrt{C_pT_i}$. Flow charts of these computer programmes were given in **Figs. A.2** to **A.4** of **Appendix [A]**. The output results were then used to plot **Figs. 10.4 to 10.6** from which the following observations were made:

i. **Figure 10.4**, (u_2/c_s versus P_i/P_e) shows that for pressure ratios less than 2:1 the lines of constant speed parameter $d_2N/\sqrt{C_pT_i}$ become very steep, consequently the range of pressure ratios for which $0.70 \geq \frac{u_2}{c_s} \geq 0.65$ is considerably reduced. Furthermore, for pressure ratios greater than 2:1, the lines

of constant speed parameter $d_2N/\sqrt{C_pT_i}$ become fairly flat. This implies that turbine can withstand large pressure fluctuations at constant speeds without loss in efficiency. This is because an accelerating flow can operate over a fairly wide range of incidence relative to the actual blade angles without significant flow disruption.

ii. **Figure 10.4** also shows that at $d_2N/\sqrt{C_pT_i}$ equal to 0.16, good efficiency can be maintained over a range of pressure ratio between 3.5 to 4.1 where the values of $0.70 \geq \frac{u_2}{c_s} \geq 0.67$.

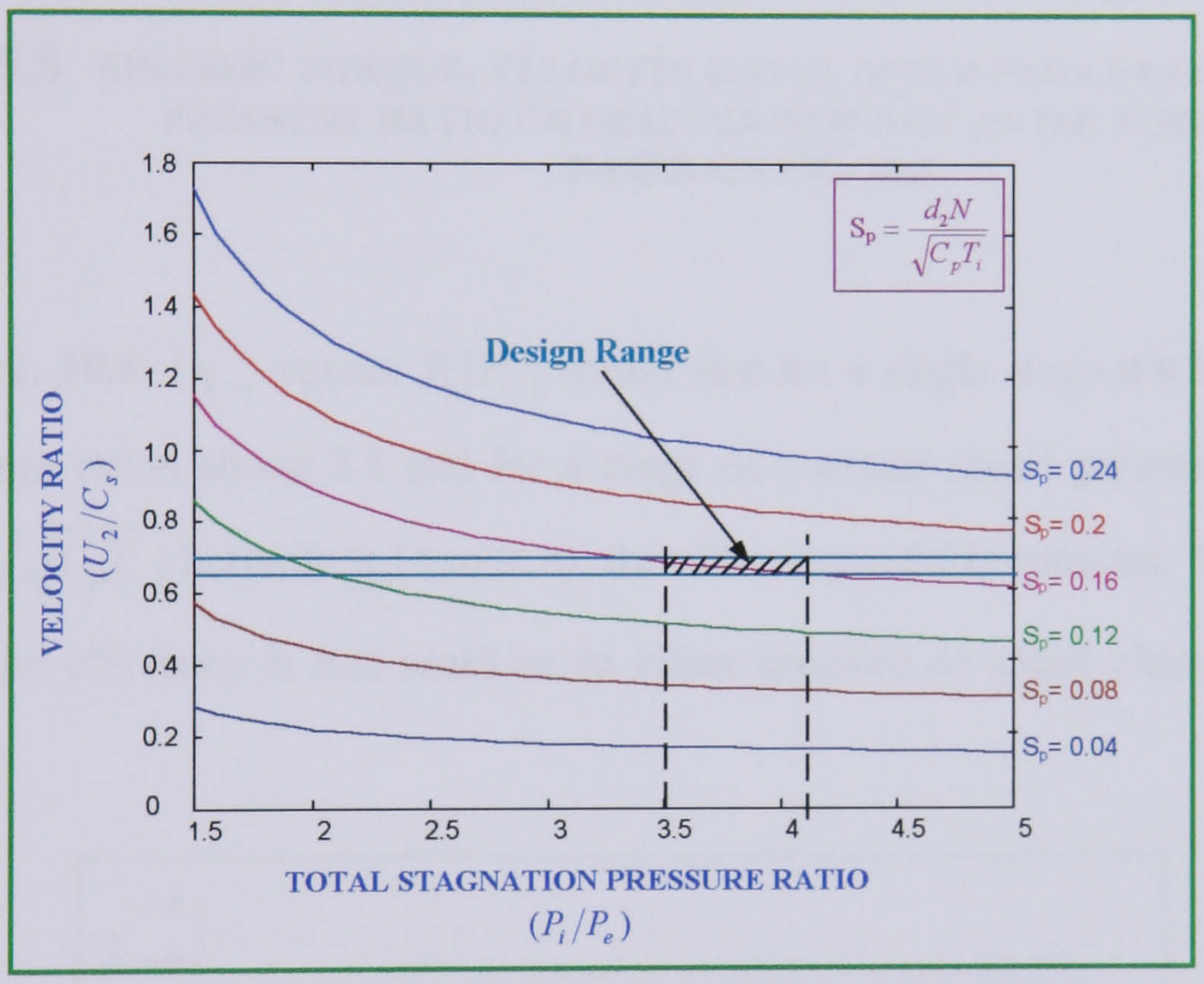

FIG. 10.4 THERMODYNAMIC RELATIONSHIPS BETWEEN PRESSURE RATIO VELOCITY RATIO AND DIMENSIONLESS SPEED PARAMETER

iii. **Figure 10.5**, $\tau/d_2\dot{m}\sqrt{C_pT_i}$ versus P_i/P_e reveals that the specific torque rises rapidly for pressure ratios less than 2.5, but as pressure ratios increase beyond 2.5, the slope of constant u_2/c_s and constant $d_2N/\sqrt{C_pT_i}$ curves decreases and become fairly flat. Also, it can be seen that specific torque (ST) reduces as the speed parameter and velocity ratio increased at constant pressure ratio.

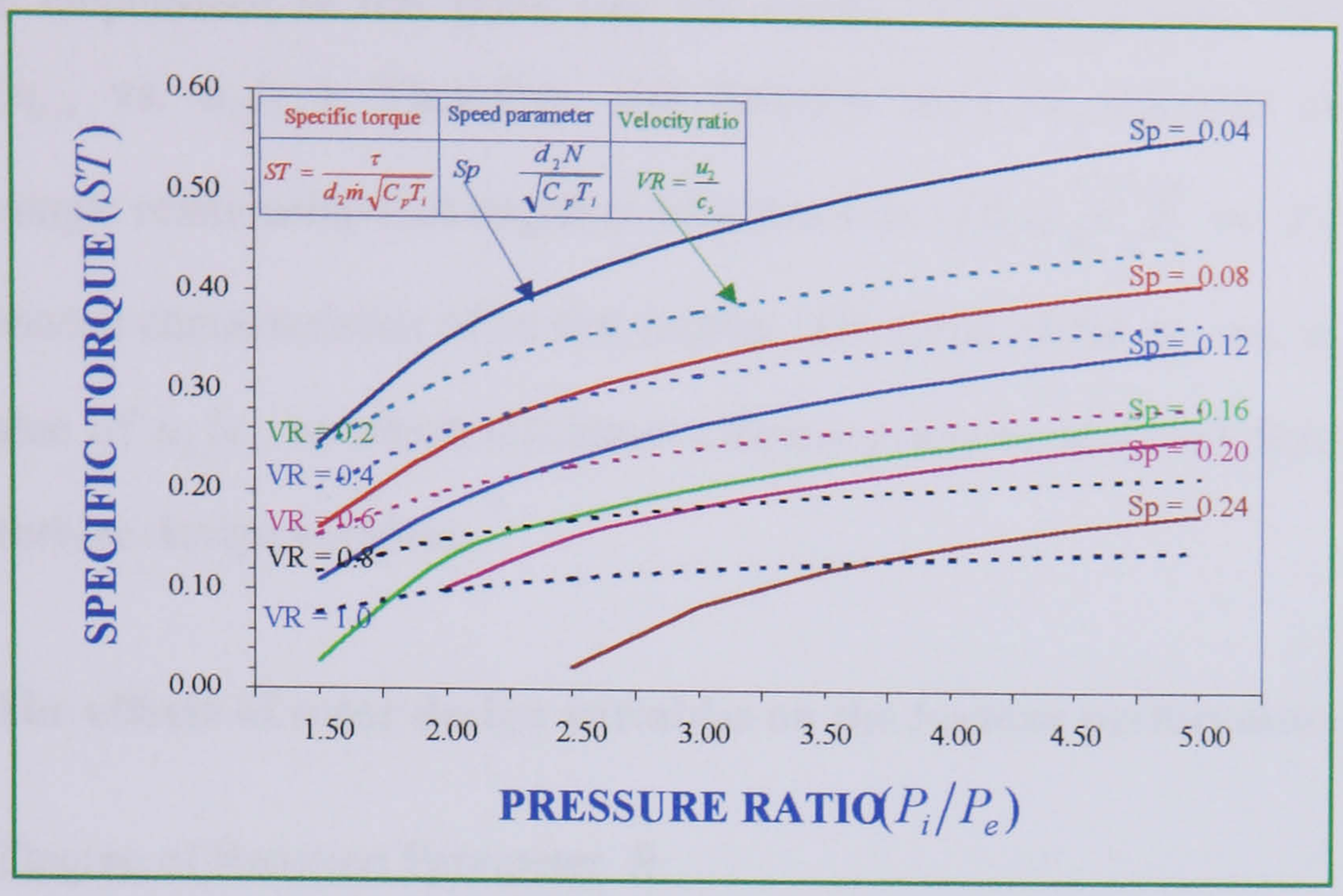

FIG. 10.5 SPECIFIC TORQUE, VELOCITY RATIO, SPEED PARAMETER AND PRESSURE RATIO CHARACTERISTICS OF AN IFR TURBINE BASED ON FIG. 10.3

iv. **Figure. 10.6**, (η_{t-t} versus P_i/P_e) shows that for a single stage **IFR** turbine for pressure ratios above 2.5 and for a range of constant speed parameter curves ($d_2N/\sqrt{C_pT_i}$) between 0.14 to 0.20, the efficiency is fairly constant. This means that the efficiency is less sensitive to either pressure or speed changes in this range.

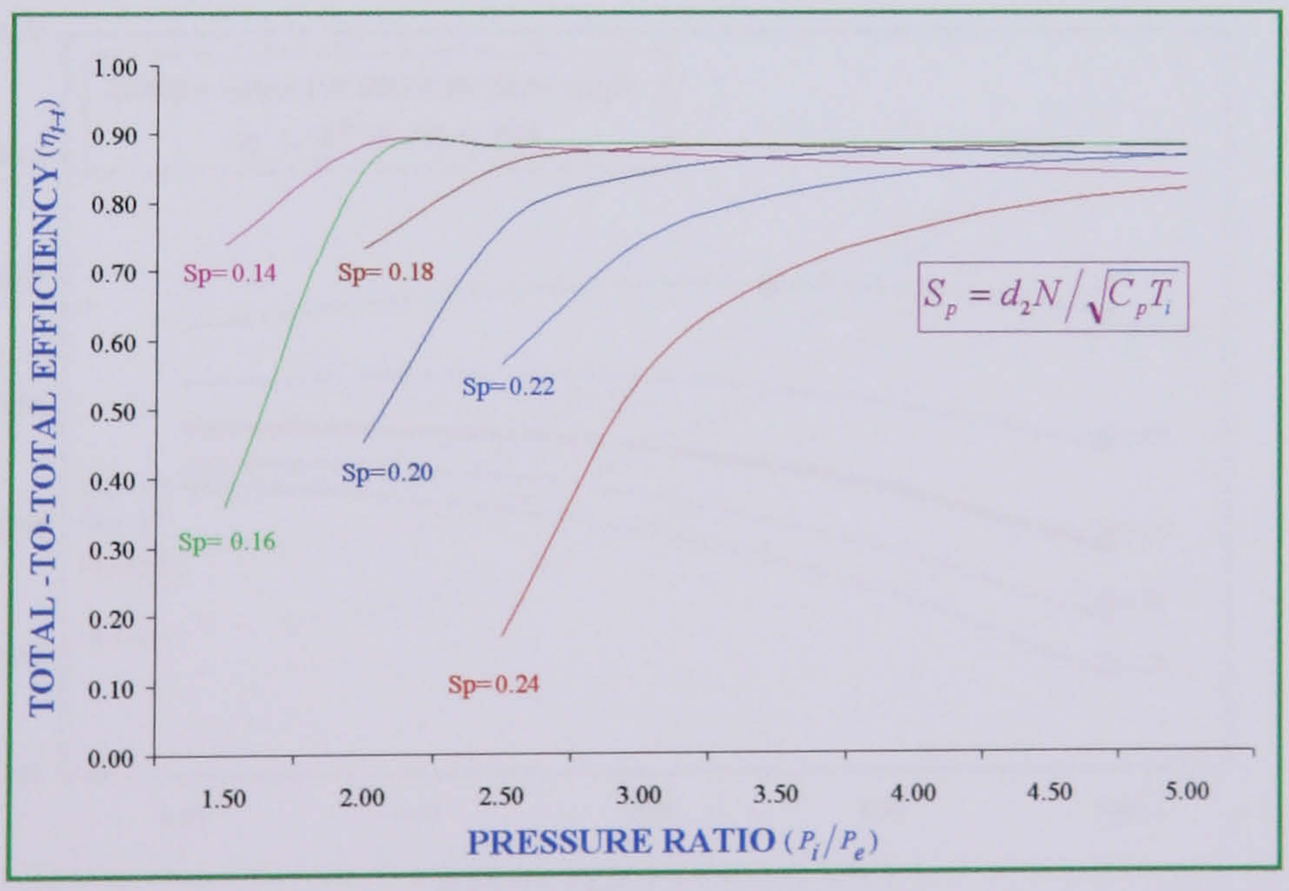

FIG. 10.6 EFFICIENCY, PRESSURE RATIO AND DIMENSIONLESS SPEED CHARACTERISTICS BASED ON FIG. 10.3

It must be emphasized at this point that the trends of these graphs depend on the function (η_{t-t} vs. u_2/c_s). Therefore, this function must be regarded as the most important single relationship that together with function $\tau/d_2\dot{m}\sqrt{C_pT_i}$ vs. P_i/P_e defines the performance characteristics of an **IFR** turbine. The trend of the η_{t-t} vs. u_2/c_s curve and the value of u_2/c_s at which maximum efficiency may be achieved depends on the choice of turbine design variables.

10.2.2.2 The effects of rotor design variables on the turbine performance

i. Degree of Reaction Parameter R

The solution to equation 3.29 was achieved with the aid of a written computer programme. The programme flow chart is shown in **Fig. A.5** of **Appendix [A]**. The graphical presentation of the output results is shown in **Figs. 10.7** and **10.8**. From these figures, the following observations can be made:

Figure 10.7 shows that as the values of diameter ratio d_1/d_2 vary from 0.4 to 0.6 and α_2 changes from 10° to 25°, the degree of reaction varies from 0.46 to 0.68. Similarly, the degree of reaction varies from 0.43 to 0.59 as β_1 changes from to 25° to 45°.

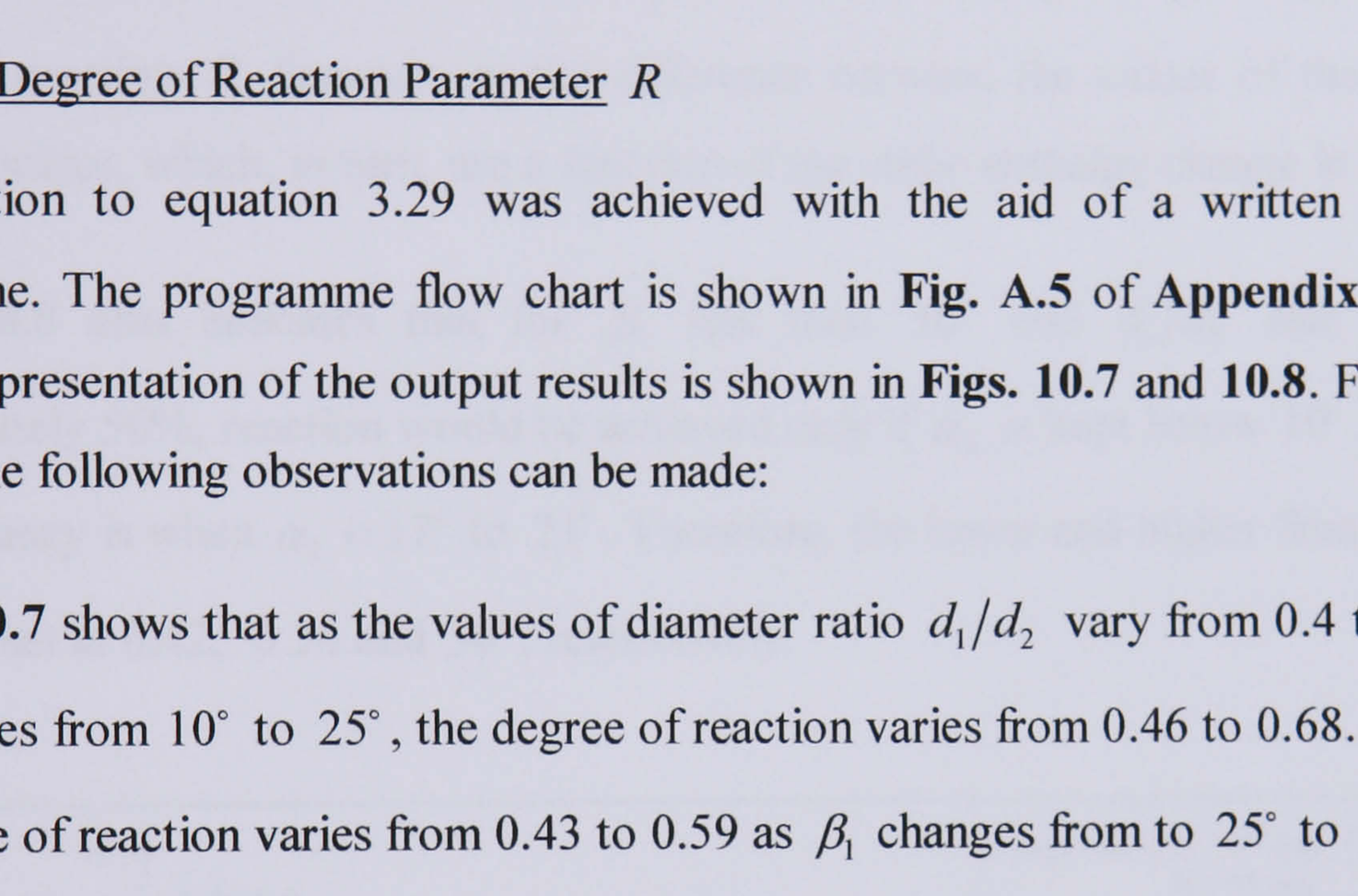

FIG. 10.7 RELATIONSHIP BETWEEN ROTOR GEOMETRIC DESIGN VARIABLES AND THE DEGREE OF REACTION

This is clearly contradiction of the widely believed theory that fixing the blade inlet angle β_{b-2} to 90° tantamount the degree of reaction. It also shows that for all values of α_2, the degree of reaction increases more rapidly with increasing d_1/d_2 for β_1 greater than 35°.

Figure 10.8 shows that for constant d_1/d_2 and β_1, the degree of reaction decreases as α_2 increased. Since with constant d_1/d_2 and β_1, the discharge velocity triangle would remain unchanged, therefore the difference between the inlet and outlet relative velocities would be reduced as a consequence of increasing the gas angle α_2. The degree of reaction R depends on the difference between the values of the inlet and outlet velocities, which, in turn, are a function of the static enthalpy change in the rotor.

Figure 10.8 also indicates that for β_1 less than 30° and d_1/d_2 less than 0.4, approximately 50%, reaction would be achieved only if α_2 is kept below 10°. Since for best efficiency is when $\alpha_2 = 17^\circ$ to 21°. Therefore, the lower and higher limit of d_1/d_2 and β_1 is set at 0.42, 0.56 and 30°, respectively.

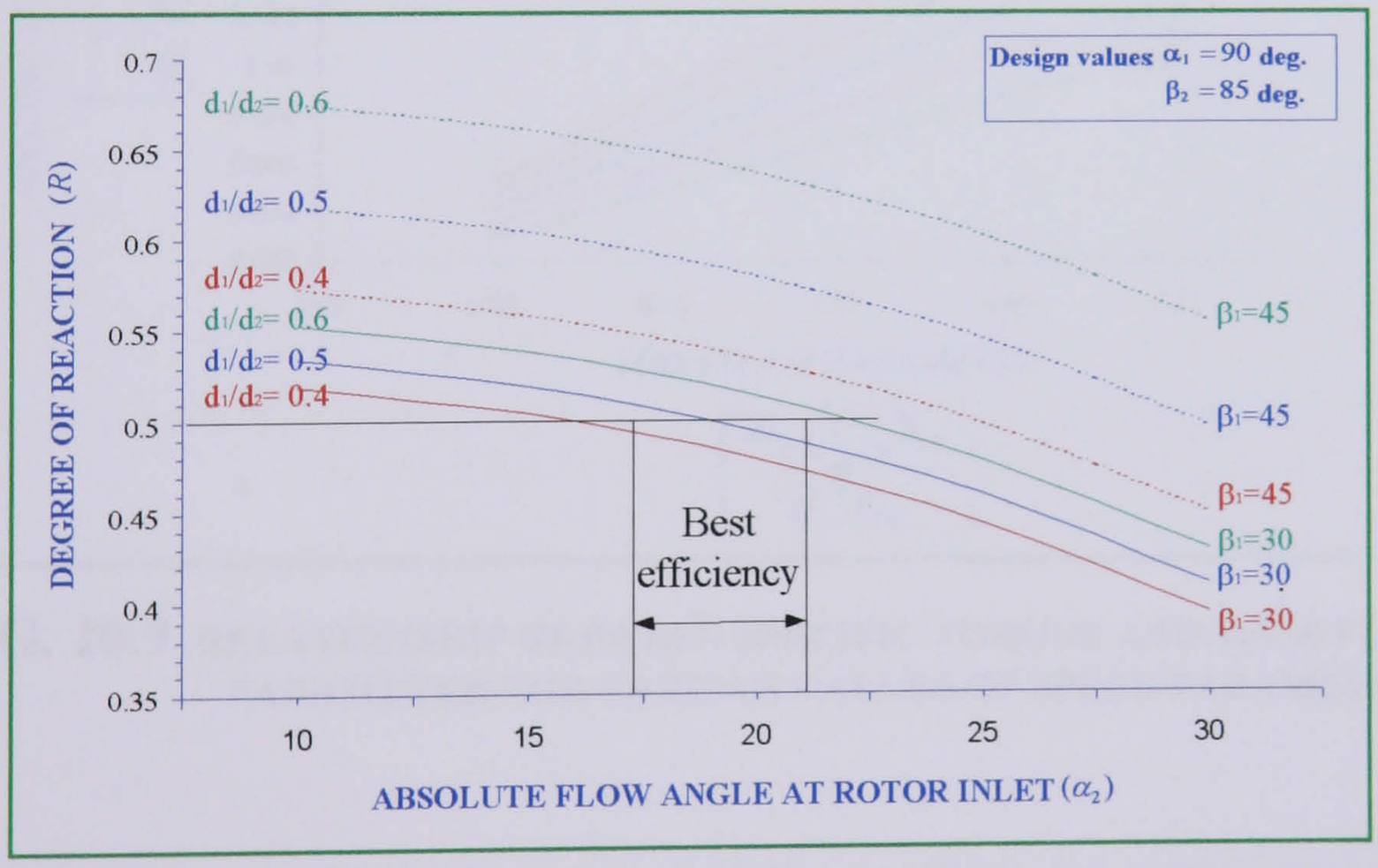

FIG. 10.8 EFFECT OF INLET GAS FLOW ANGLE, α_2 ON DEGREE OF REACTION R AT CONSTANT RELATIVE FLOW ANGLE, β_1 AND MEAN DIAMETER TO INLET DIAMETER RATIO, d_1/d_2

Increasing β_1 beyond 45°, unless accompanied by corresponding increase in α_2, would produce high reaction, excessive leaving loss, and consequently low efficiency. This result agrees well with the analytical work carried out by **Chen *et al* [18]**. They have reported that increasing β_1 beyond 45° would increase both relative and absolute flow velocities and hence internal and leaving loss and consequently produce low efficiencies.

ii. Torque parameter $(\tau/d_2^{\,3}P_i)$

Equation 3.41 shows that the design torque parameter is directly proportional to the product of dimensionless mass flow $\dot{m}\sqrt{C_pT_i}/d_2^{\,2}P_i$ and speed parameter $d_2N/\sqrt{C_pT_i}$, respectively, if only the relative flow velocity β_2 coincide with blade angle β_{2b} at rotor inlet, i.e. $\beta_2 = \beta_{2b} = 90^\circ$.

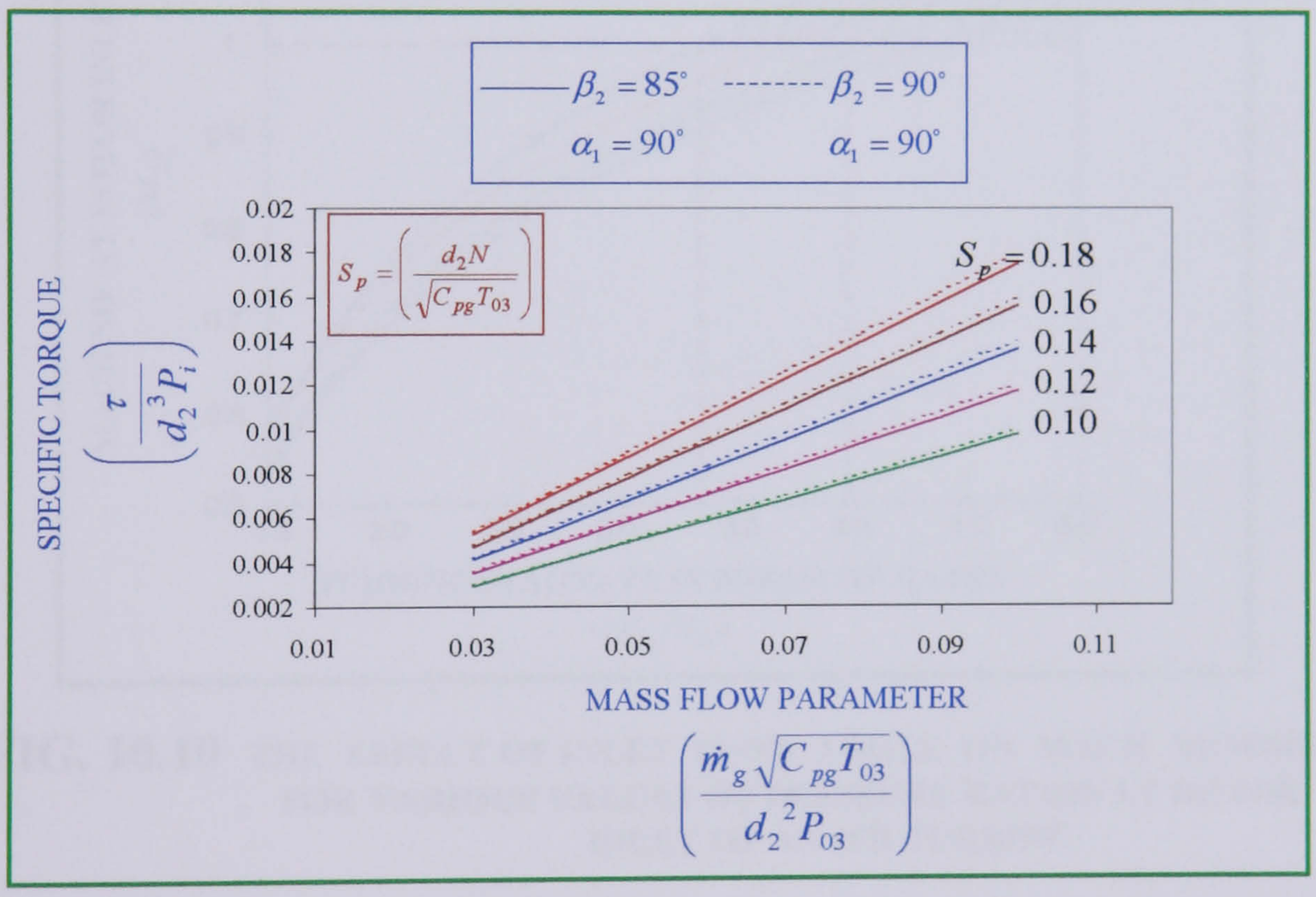

FIG. 10.9 RELATIONSHIP BETWEEN SPECIFIC TORQUE AND MASS FLOW PARAMETER FOR VARIOUS VALUES OF SPEED PARAMETERS

Therefore reducing the incidence loss to a minimum will produce higher power output as shown in **Fig. 10.9**. The permissible levels of mechanical and thermal stresses in the rotor, limit the value of blade tip speed u_2 and turbine inlet temperature T_i. Once these two values are specified, then the upper limit of $d_2N/\sqrt{C_pT_i}$ can be specified.

10.2.2.3 Relationship between rotor aerodynamics and geometric variables at various inlet design condition

i. The effect of absolute flow angle on absolute flow Mach number at various pressure ratios

The solution equation 3.55 to determine the value of M_2 for various values of P_i/P_e with α_2 as a parameter was achieved by runing a computer programme. The flow chart of the programme is presented in **Fig. A.6** of **Appendix [A]**. The output results are plotted as values of M_2 versus P_i/P_e for various values of α_2 as shown in **Fig. 10.10**.

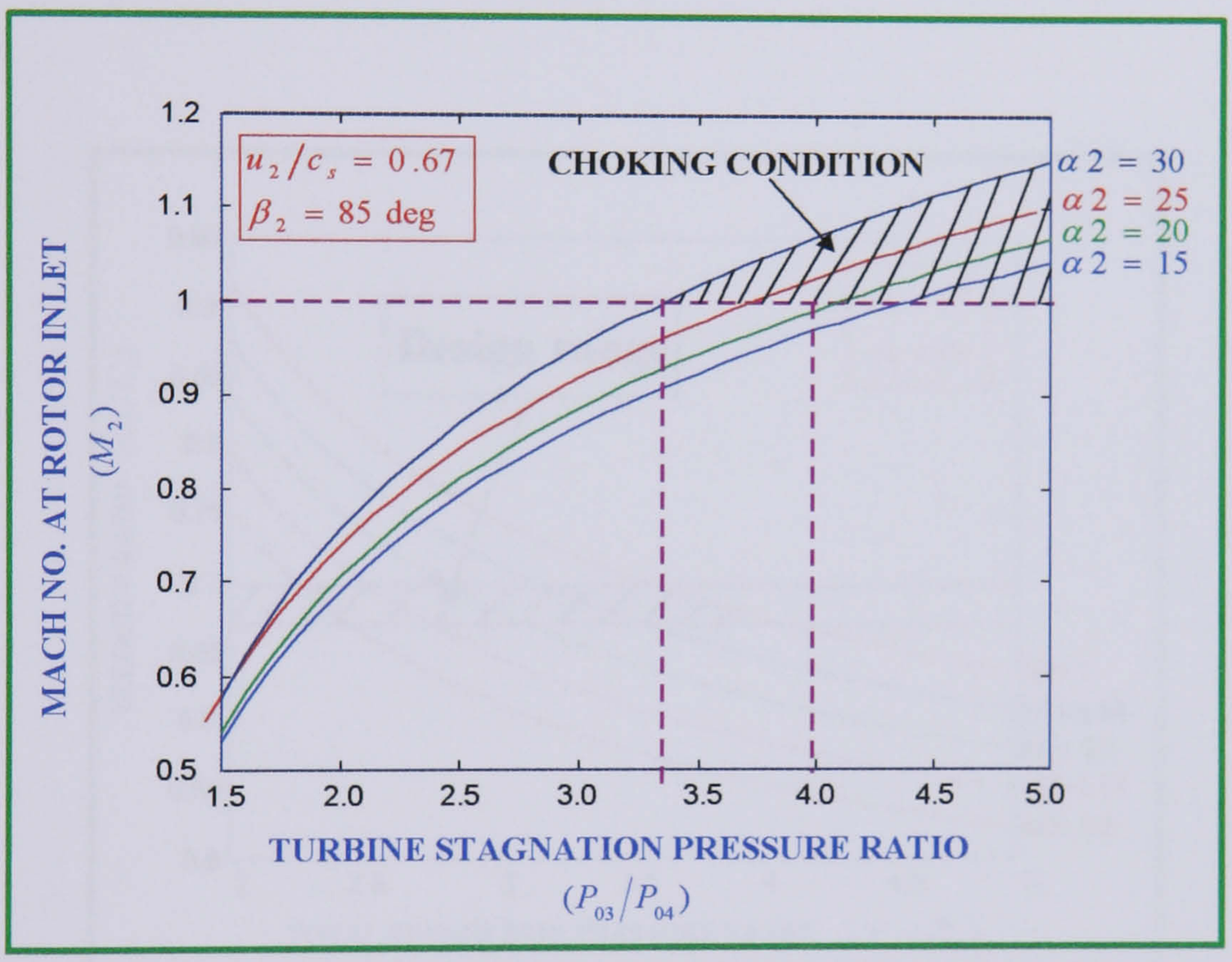

FIG. 10.10 THE EFFECT OF INLET FLOW ANGLE ON MACH NUMBER FOR VARIOUS VALUES OF PRESSURE RATIOS AT ROTOR INLET OF AN IFR TURBINE

For a given pressure ratio and relative flow angle at rotor inlet, the value of the absolute flow Mach number M_2 is controlled mainly by the blade tip velocity u_2 and the corresponding gas flow angle α_2. For a subsonic flow, the values of α_2 considered for any pressure ratio should be outside the shaded area to aviod choking conditions . Also, curves of constant α_2 rise steeply for a pressure ratio less 2.5 and rate of increase reduces for pressure ratio between 3.0 to 5.0. Increasing pressure ratio, unless

accompanied by a decrease in absolute flow angle α_2 would produce a supersonic flow in the stator part of the turbine and excessive losses. **Figure 10.10** shows that for a pressure ratio of 4.0, the value of α_2 must be less than 20°.

ii. Velocity ratio and pressure ratio relationship at various values of inlet flow Mach number

Equation 3.56 was solved for u_2/c_s, for different values of P_i/P_e with M_2 as a parameter using a computer programme of a flow chart given in **Fig. A.7** of **Appendix [A]**. In this solution, the constant relative and absolute flow angles β_2, α_2 were assumed.

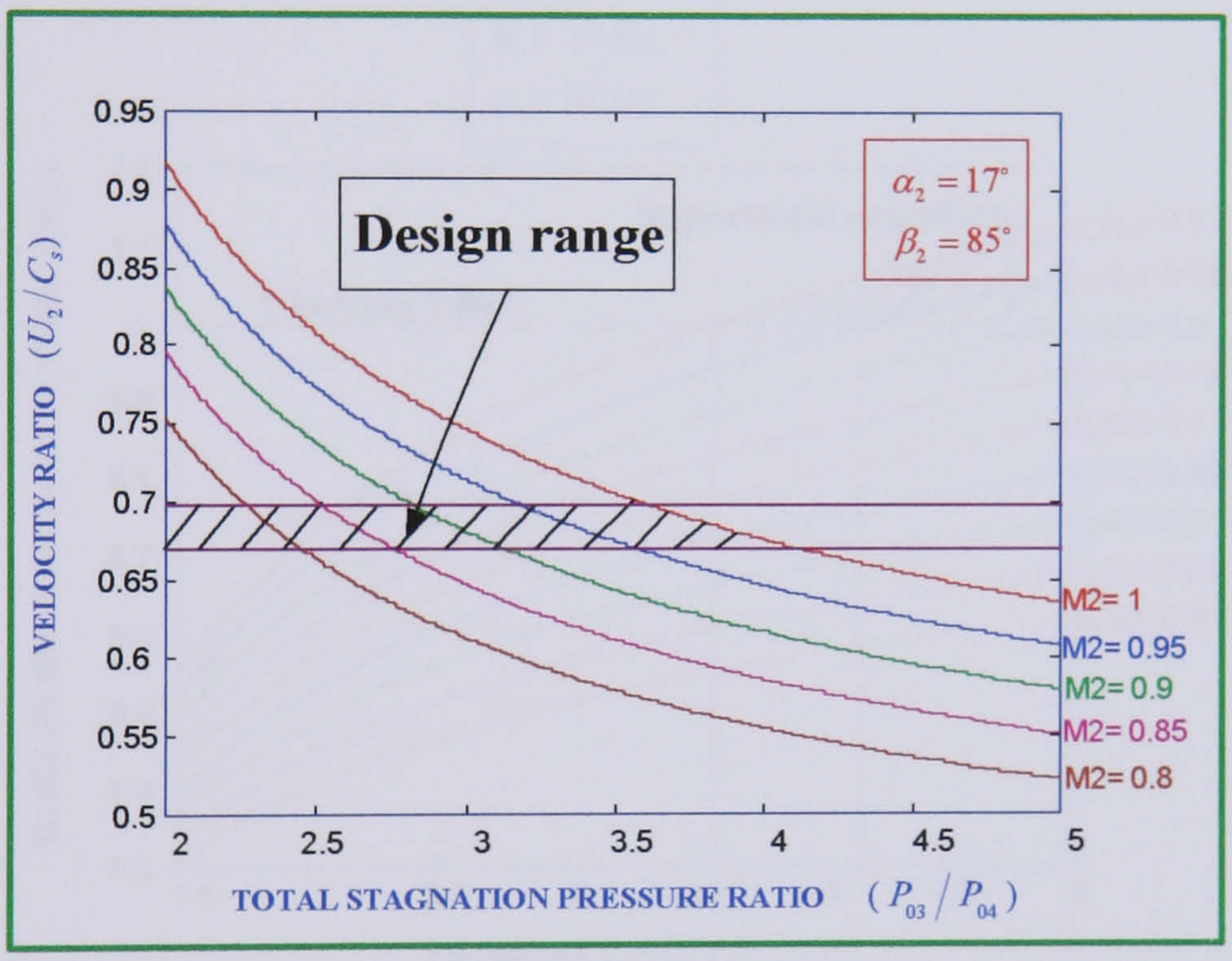

FIG. 10.11 THE EFFECT OF INLET MACH NUMBER ON VELOCITY RATIO AT ROTOR INLET

The output results are plotted in **Fig. 10.11**, in which the trend of the curves indicates that u_2/c_s decreases steeply at pressure ratio P_i/P_e less than 2.5. Also, it shows that for P_i/P_e higher than 3.0, the reduction in u_2/c_s becomes relatively small which means that the fluctuation of pressure ratio at this range will not have a large effect on u_2/c_s and hence on the efficiency of the turbine. The shaded area represents the design range for pressure ratio, Mach number combination to atchieve maximum efficiency.

It can be noted that for subsonic flow and for the design value of $u_2/c_s = 0.67$, the maximum attainable pressure ratio P_i/P_e would be less than 4.1:1

iii. Relative Mach number and pressure ratio relationship at various values of exducer to tip diameter ratio

The values of M_{er} and d_e/d_2 were obtained using a computer programme based on equation 3.60b, in which the value $\alpha_1 = 90^\circ$, i.e. $c_{we} = 0$ is considered. A flow chart of the computer programme is shown in **Fig. A.8** of **Appendix [A]**.

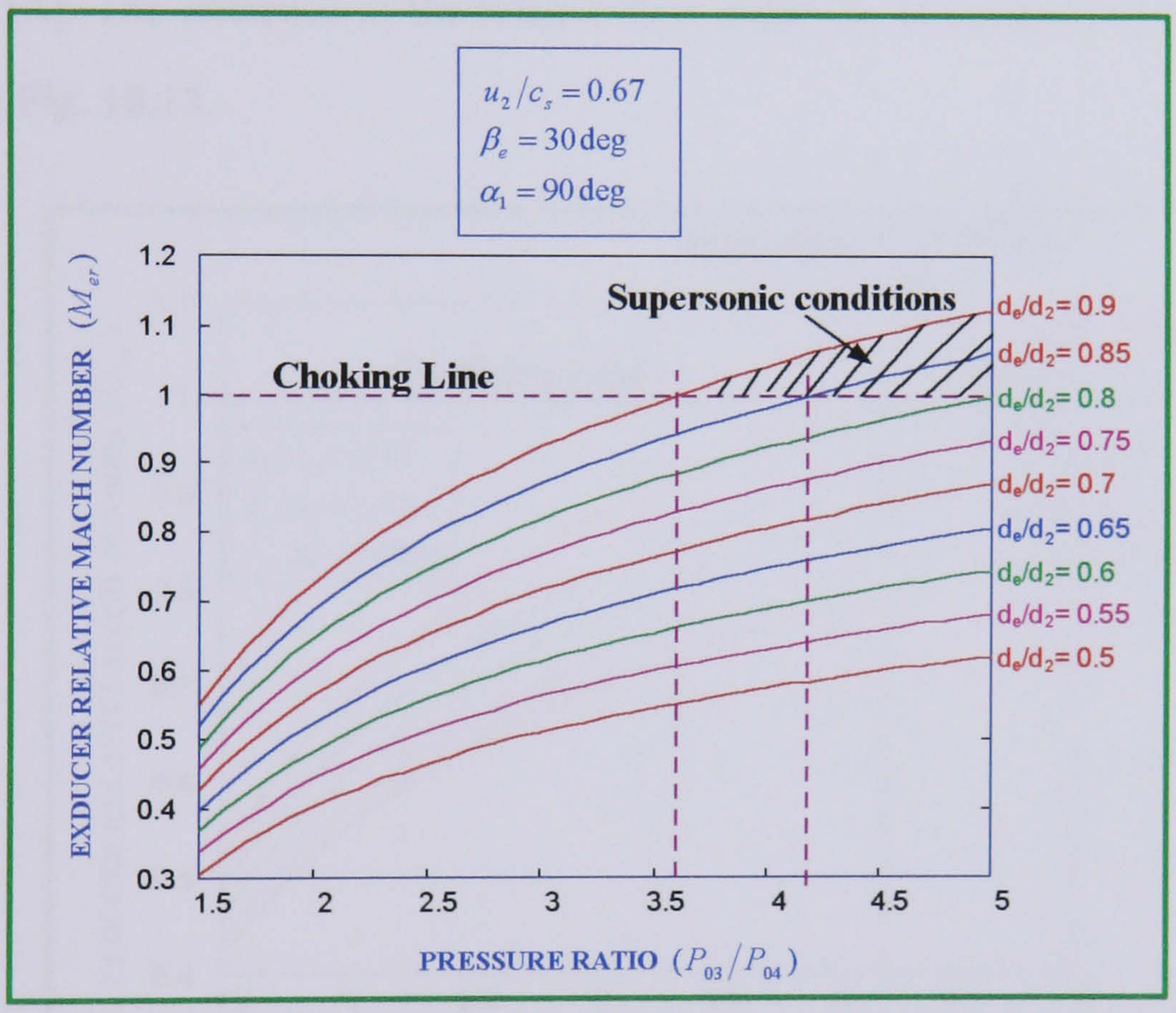

FIG. 10.12 THE EFFECT OF EXDUCER TIP/ INLET TIP DIAMETER RATIO d_e/d_2 ON RELATIVE FLOW MACH NUMBER M_{er} AT ROTOR EXIT

For a given pressure ratio, the value of the relative flow Mach number M_{er} is controlled mainly by the exducer to tip diameter ratio d_e/d_2 and the corresponding relative flow angle β_e. The relationship between M_{er} and P_i/P_e for various values d_e/d_2 is shown in **Fig. 10.12**. The pressure ratio, diameter ratio combination of the shaded area represents the supersonic condtions. Therefore, all the values within this

region are eliminated. For pressure ratio less than 3.6, values of d_e/d_2 should be less or equal to 0.9. For pressure higher than 5.0, values of d_e/d_2 should be less or equal to 0.8. Also, curves of constant d_e/d_2 rise steeply for a pressure ratio less 2.0 and become fairly flat for a pressure ratio between 3.0 and 5.0.

iv. Relative Mach number and pressure ratio relationship at various values of exducer tip blade angle

The values of β_e are obtained from equation 3.60b. The solution of this equation was based on a developed computer programme of a flow chart is shown in **Fig. A.9** of **Appendix [A]**. The influence of the relative flow angle β_e at the exducer tip diameter is shown in **Fig. 10.13**.

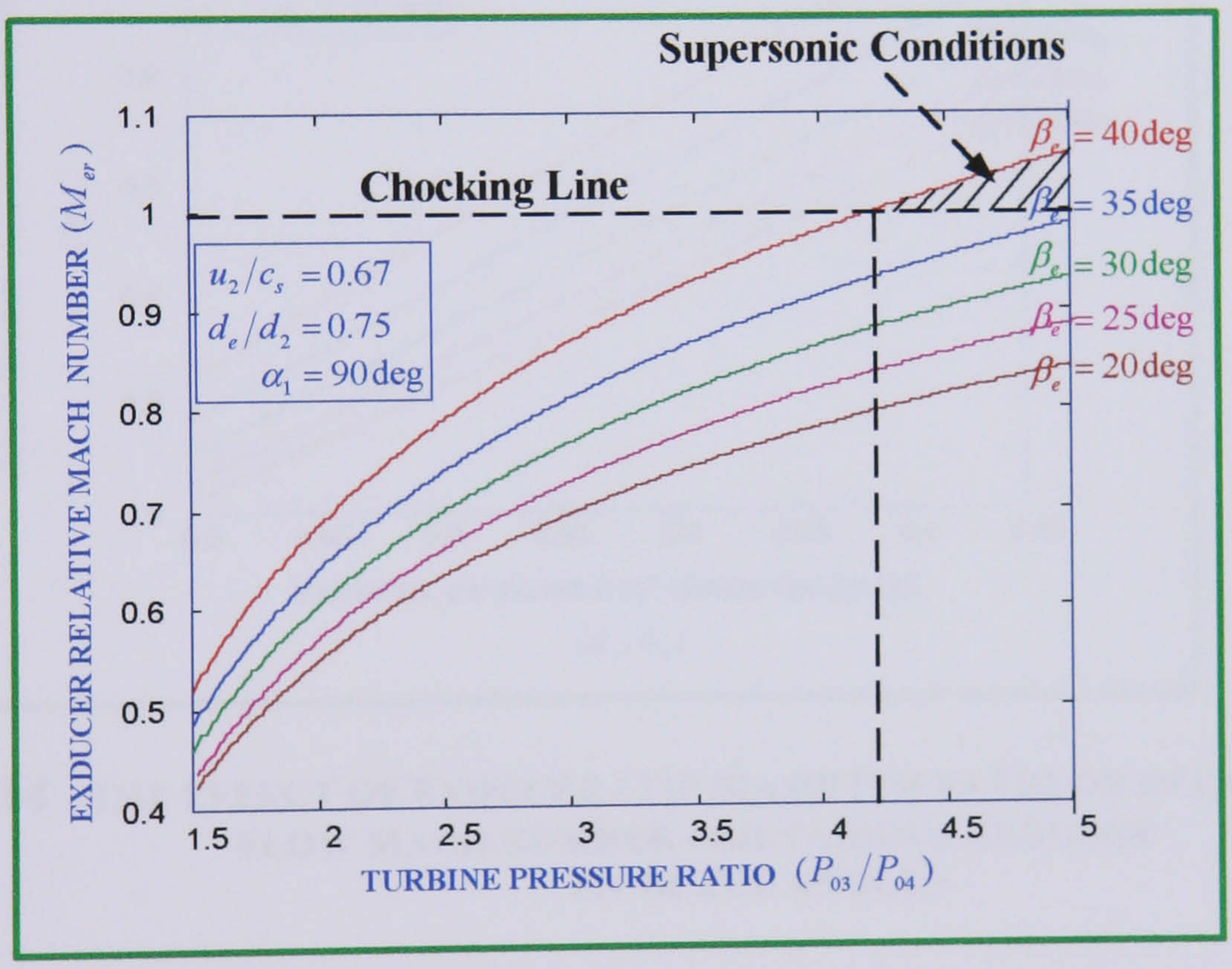

FIG. 10.13 THE EFFECT OF EXDUCER TIP BLADE ANGLE ON RELATIVE FLOW MACH NUMBER AT ROTOR EXIT

For a chosen value of $d_e/d_2 = 0.75$ for example, it is evident that, for a pressure ratio, blade tip angle angle combination within the shaded region would not be acceptable as it would exceeds the permissible upper limit for the relative Mach number M_{er} =1.0 and this will lead supersonic flow conditions.

v. Relative Mach number and exducer to tip diameter ratio relationship at various values of exducer tip blade angles

The relationship between the exducer Mach number M_{er} and tip diameter ratio is shown in **Fig. 10.14** which was based on the solution of equation 3.60b. A computer programme of a flow chart shown in **Fig. A.10** of **Appendix [A]** was written to achieve the solution. It can be noted that for a given pressure ratio and limiting exducer tip Mach number M_{er}, several combination of d_e/d_2 and β_e are possible, as indicated in **Fig. 10.14**.

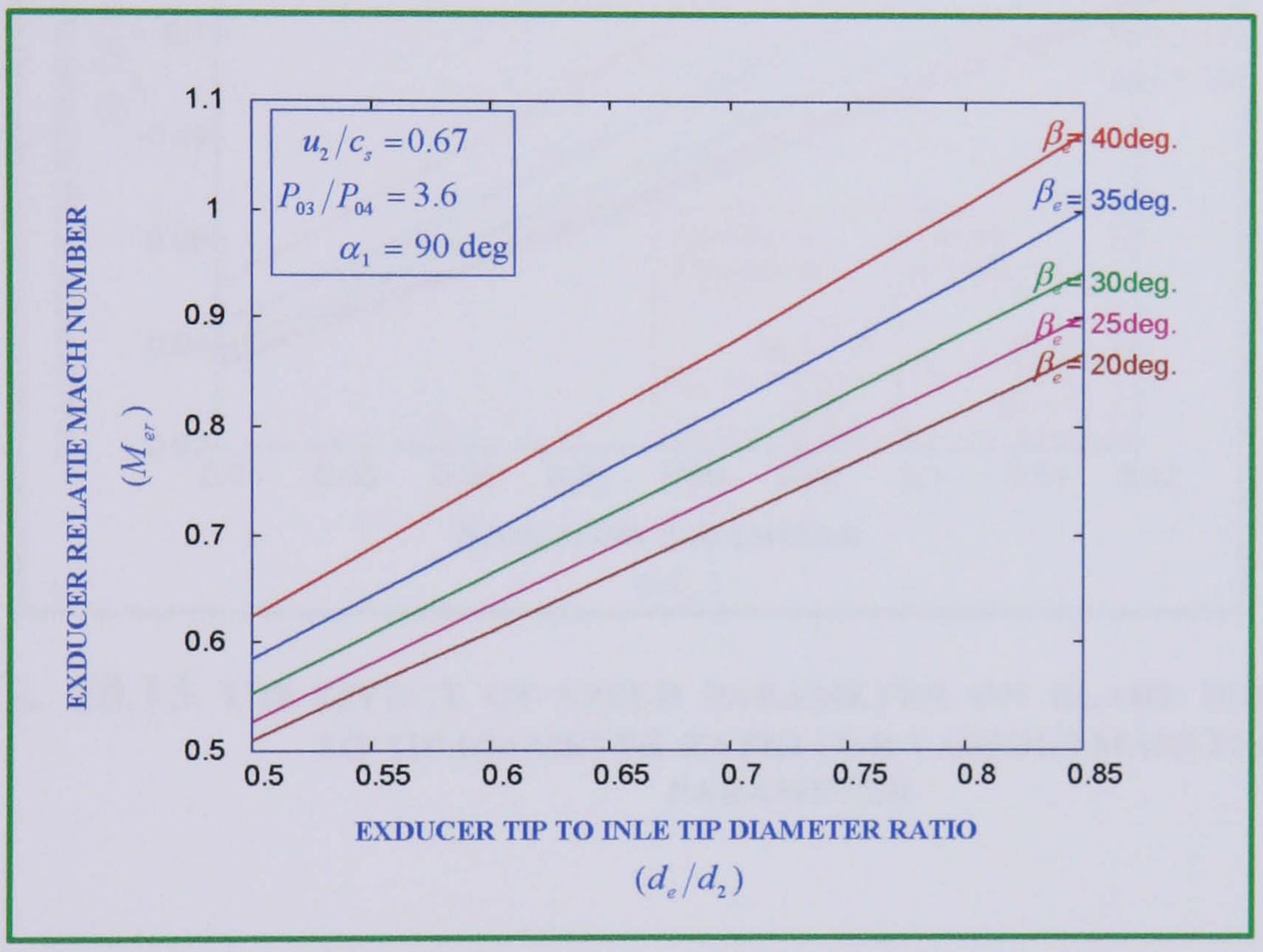

FIG. 10.14 THE EFFECT OF EXDUCER / TIP DIAMETER RATIO ON RELATIVE FLOW MACH NUMBER FOR VARIOUS EXDUCER TIP BLADE ANGLES

vi. Relationship between blade width to rotor tip diameter ratio and mass flow parameter at various speed parameter

Equation 3.83 was solved for b_2/d_2 by writing a computer programme of a flow chart shown in **Fig. A.11** of **Appendix [A]**. **Fig. 10.15** shows a plot of b_2/d_2 *vs.* mass flow parameter, $\dot{m}\sqrt{C_pT_i}\,/\,d_2{}^2P_i$ for a range of values of the speed parameter, $d_2N/\sqrt{C_pT_i}$.

It is evident that if the mass flow and speed were given to meet the design requirements the choice of b_2/d_2 is very limited. It also indicates that over the range of mass flow parameter M_p of 0.04 and 0.12 and for values of speed parameter S_p less than 0.14, the effect of speed parameter on b_2/d_2 ratio is quite significant.

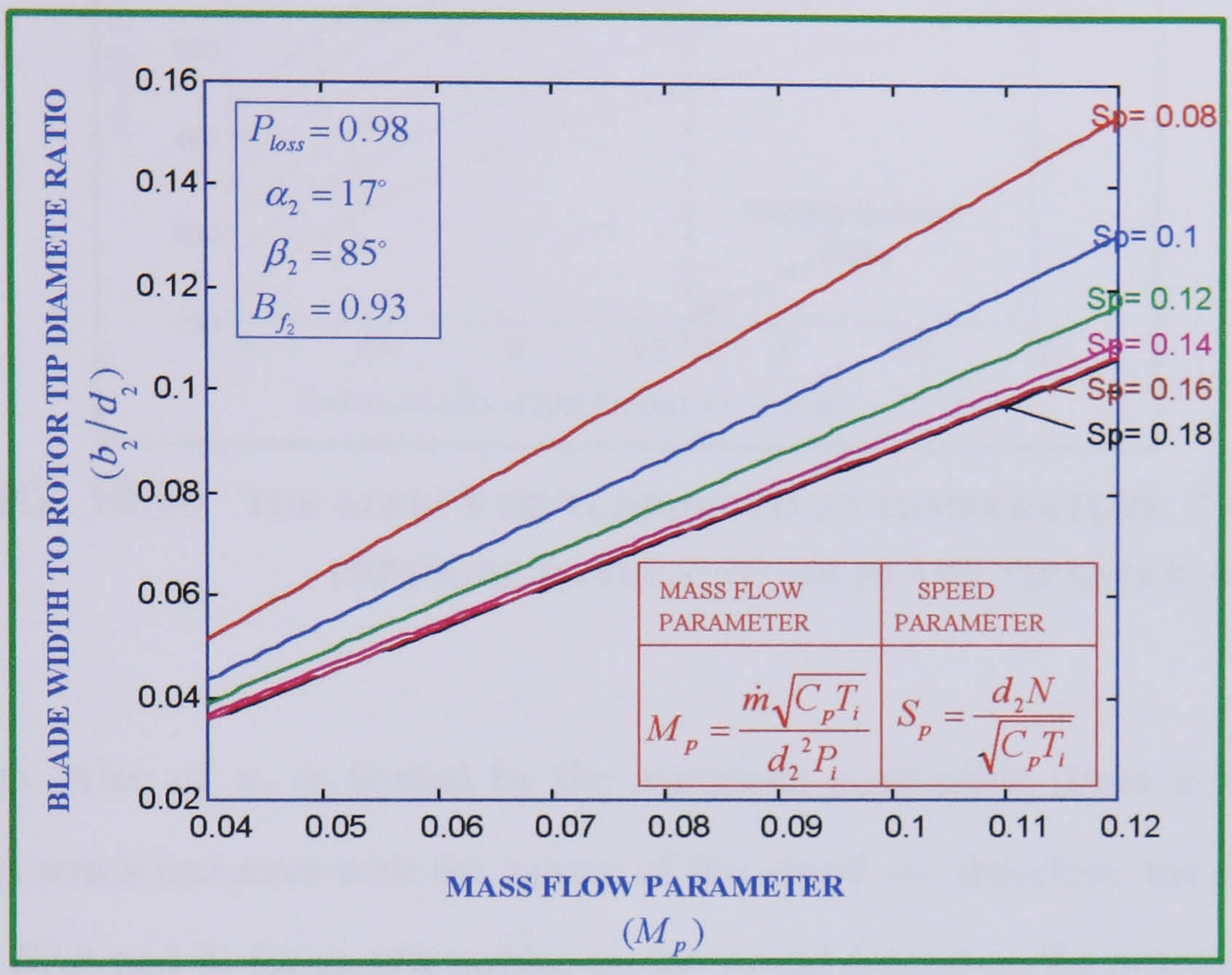

FIG. 10.15 THE EFFECT OF SPEED PARAMETER ON BLADE WIDTH TO TIP DIAMETER RATIO FOR VARIOUS MASS FLOW PARAMETER

For S_p higher than 0.14, the effect becomes relatively small and hardly noticeable. This means that at higher values of rotational speed, choking condition becomes apparent.

vii. Relationship between inlet tip speed and pressure ratio at various turbine inlet temperatures

Figure 10.16 was generated from equation 3.86 using a computer programme developed and depicted in **Fig. A.12** of **Appendix [A]**. **Fig. 10.16** shows that u_2 can be increased by either increasing the pressure ratio P_i/P_e or the turbine inlet temperature T_i.

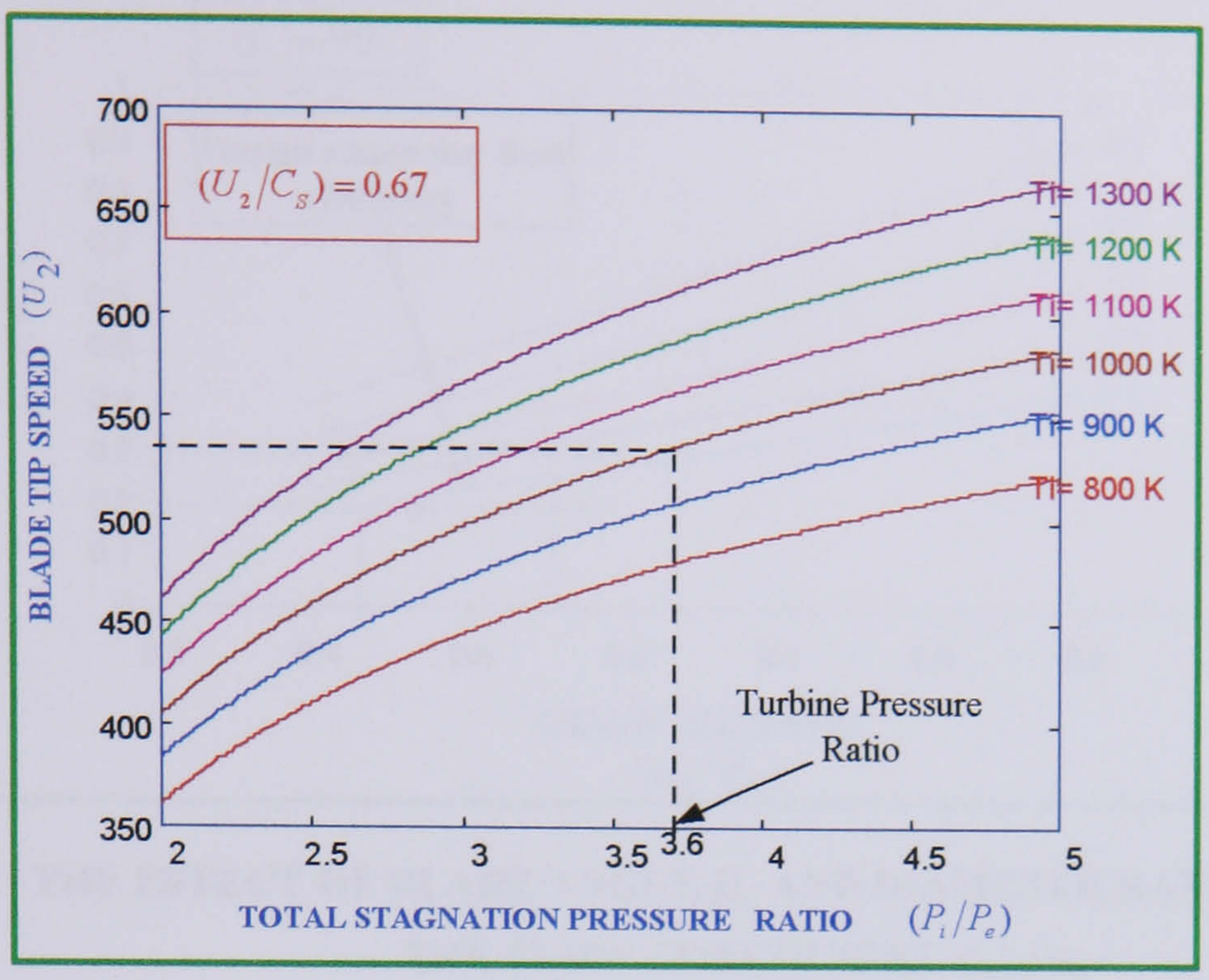

FIG. 10.16 THE EFFECT OF TURBINE INLET TEMPERATURE T_i AND PRESSURE RATIO P_i/P_e ON BLADE TIP SPEED U_2

The design value of u_2 is limited by the maximum permissible stress in the turbine rotor. This stress increases with the square of this speed u_2, therefore, the selection of values of P_i/P_e and T_i for an **IFR** turbine design would depend on the metrological limit of the material. Also, it can be seen that curves of constant T_i rises steeply for pressure ratio less than 3.0 and rate of increase reduces for P_i/P_e ratio greater than 3.0.

viii. <u>The relationship between flow coefficient and diameter ratio for various blade angles at rotor exit</u>

The solution to equation 3.42 is plotted in **Fig. 10.17**, which shows the relationship between the flow coefficient ϕ_{fc} and mean diameter ratio d_1/d_2 at various values of blade angle β_1. **Fig. 10.17** shows that flow coefficient c_{m1}/u_2 depends on the geometry of rotor angle β_1 and diameter ratio d_1/d_2 for zero swirl at exit. Also, for constant blade angles at rotor mean exit β_1, c_{m1}/u_2 increases linearly for increasing values of mean diameter to tip diameter ratio d_1/d_2 .

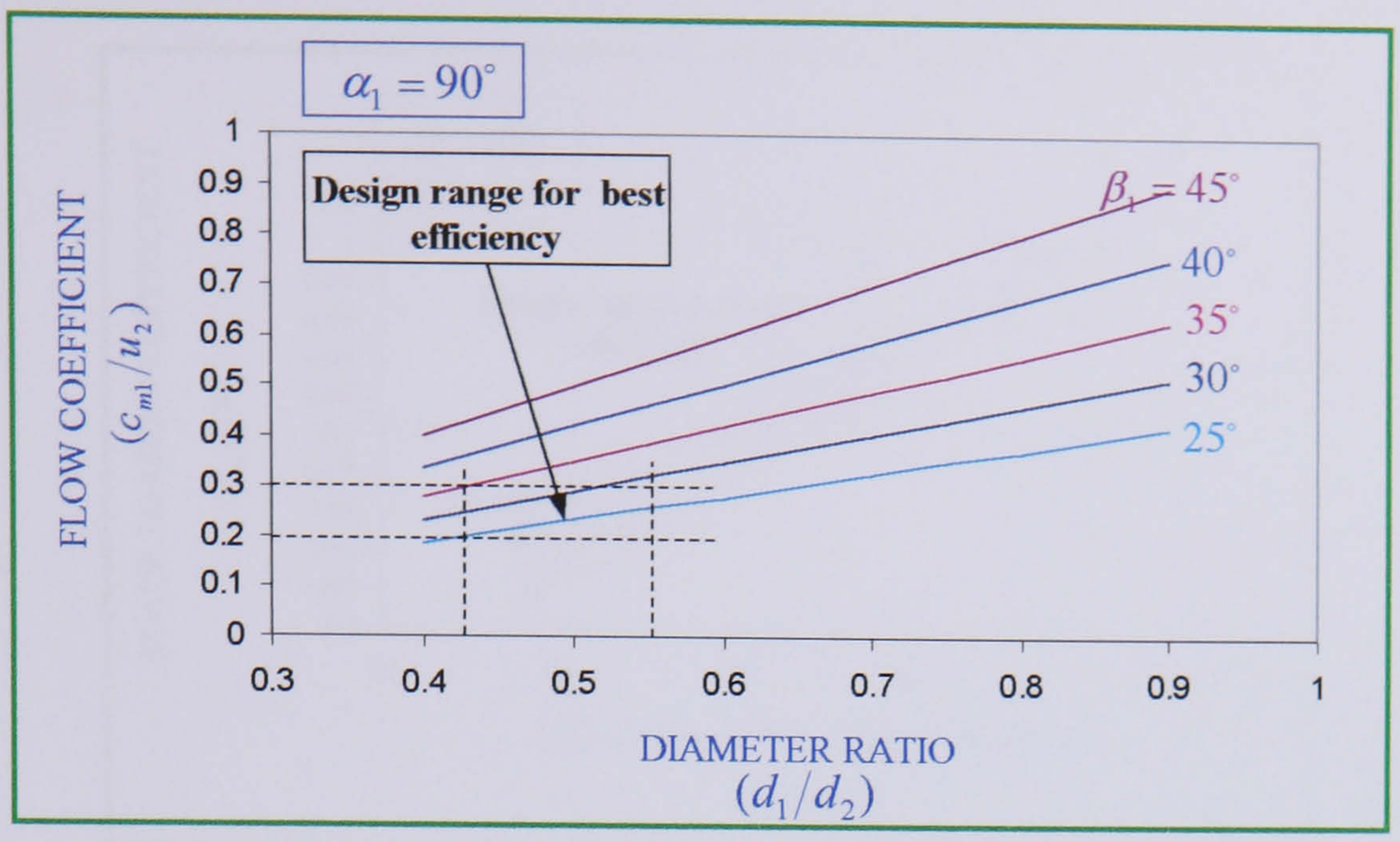

FIG. 10.17 THE EFFECT OF BLADE ANGLE β_1 AND DIAMETER RATIO d_1/d_2 ON THE FLOW COEFFICIENT c_{m1}/u_2

Rodgers [54] considers c_{m1}/u_2 being highly influential on turbine efficiency. By analysing performance data from some thirty radial turbine stages, **Rodgers** produced a chart as shown in **Fig. 10.24** and concluded that peak efficiencies are obtained with flow coefficients between 0.2 and 0.3. Therefore, for this range several combinations of β_1 and d_1/d_2 can be obtained. However, careful consideration for the selection of β_1 and d_1/d_2 should be made to achieve enough turning of the flow in the passage to avoid blockage.

viiii. <u>The relationship between blade loading and flow angles at rotor inlet</u>

Equation 3.43 shows that blade loading c_{w2}/u_2 is a function of rotor inlet flow angles α_2 and β_2, respectively, for zero swirl conditions. **Fig. 10.18** is plotted based on the solution of equation 3.43. It shows that blade loading coefficient c_{w2}/u_2 increases with increasing values of relative flow angle β_2 at constant absolute flow angle α_2. Also, it shows that the change in c_{w2}/u_2 at various values of α_2 becomes small at higher values of $\beta_2 > 80°$ and all the values merges to one at $\beta_2 = 90°$. It can be noticed that an increase in c_{w2}/u_2 should be accompanied by a decrease in α_2 at constant values of β_2.

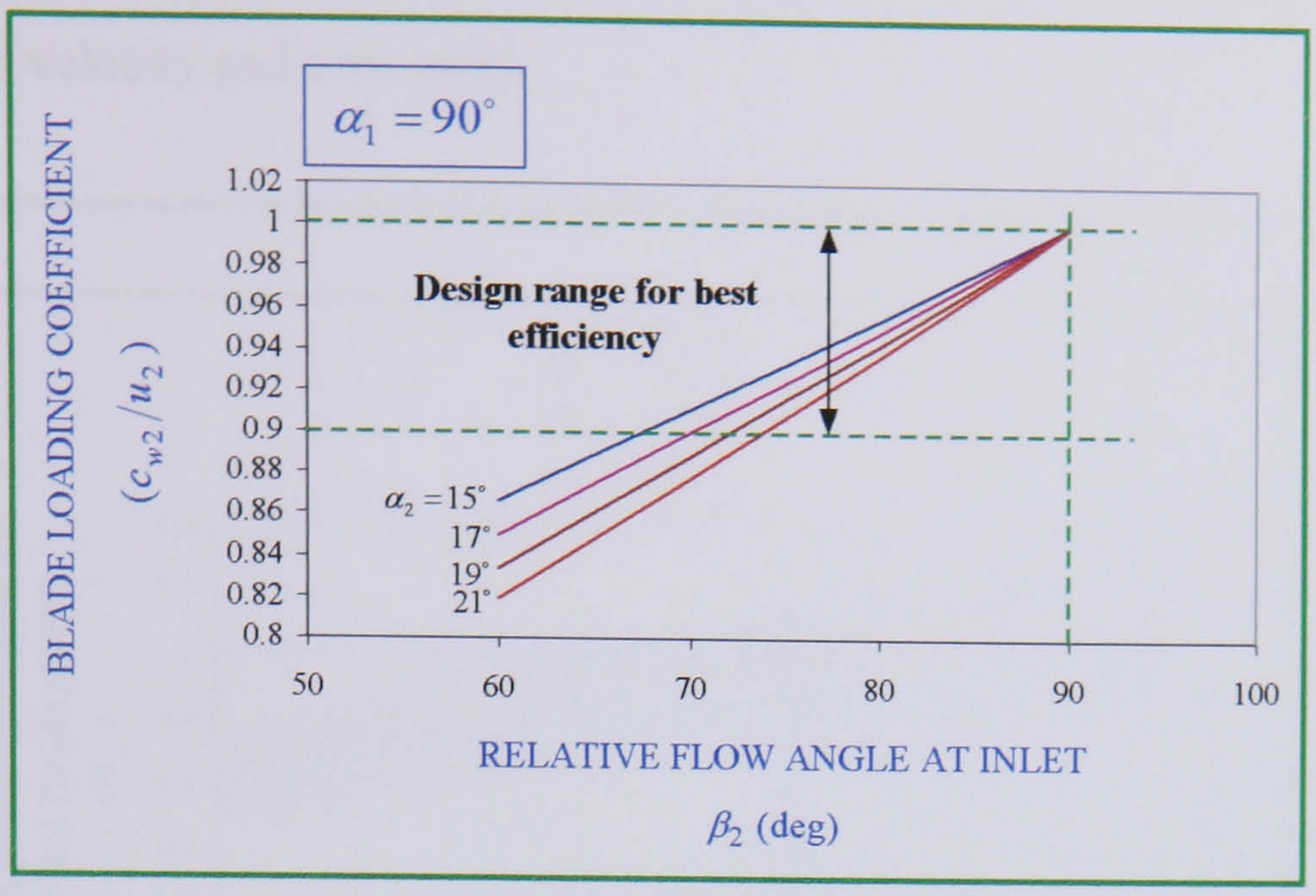

FIG. 10.18 THE EFFECT OF FLOW ANGLES α_2 AND β_2 ON BLADE LOADING COEFFICIENT c_{w2}/u_2

Baines [58] produced a chart based on the analysis of approximately forty different radial turbine stages, which correlates efficiency with c_{w2}/u_2. It shows that best performance is achieved with c_{w2}/u_2 in the range 0.9 to 1.0. This is not surprising since, for ideal flow with complete exhaust recovery (isentropic process), equation 3.36 is tranformed to: $\frac{c_{w2}}{u_2} = \frac{(\Delta H_{i-e})_{ideal}}{u_2^{\,2}} = \frac{1}{2}\frac{c_s^{\,2}}{u_2^{\,2}} = \frac{1}{2}\left(\sqrt{2}\right)^2 = 1.0$. Therefore, high efficiency designs must be based on a value of c_{w2}/u_2 close to unity by definition.

10.2.3 The Parametric Results of Centrifugal Compressor Design

10.2.3.1 Inducer tip to impeller tip diameter ratio (d_e/d_2)

Equations 5.9 and 5.11 derived in **Chapter 5** are combined and plotted graphically as shown in **Fig.10.19** to investigate the effects of inlet geometry d_e/d_2 and β_e on inlet design parameter M_{er} at different pressure ratios. **Fig. 10.19** shows that at design pressure ratio of 4:1 and for subsonic flow at different values of β_e, the inducer/tip diameter ratio d_e/d_2 must be less than 0.7. Also, it can be observed that the values of

M_{er} and d_e/d_2 are reduced as the blade tip angle β_e increases from 25° to 30° for constant axial velocity and zero swirl.

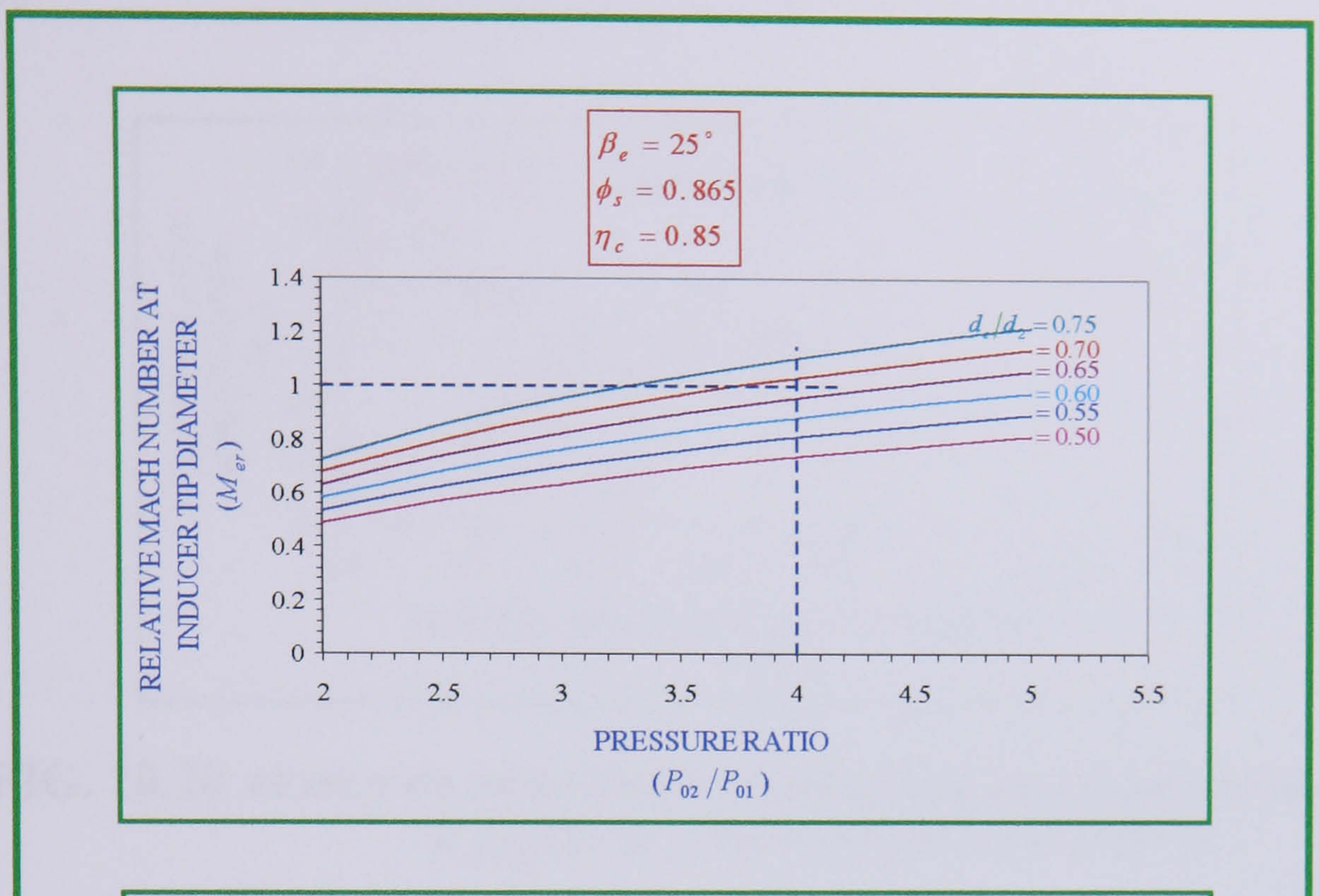

FIG. 10.19 THE EFFECT OF INDUCER/ TIP DIAMETER RATIO ON RELATIVE MACH NUMBER AT TWO VALUES OF BLADE TIP ANGLE $\beta_e = 25°$, $30°$ WITH ZERO SWIRL

Also, **Fig. 10.20** was plotted from solving equation 5.9 and 5.11. It showed that for a given design value of pressure ratio 4:1 and limiting the relative Mach number M_{er} to 1.0, several combinations of d_e/d_2 and β_e are possible. The best combination of M_{er},

d_e/d_2 and β_e can be found if any two values of these quantities are known and satisfy the design conditions. For example, for $\beta_e = 30^\circ$ and $M_{er} = 0.9$, d_e/d_2 should equal to 0.55.

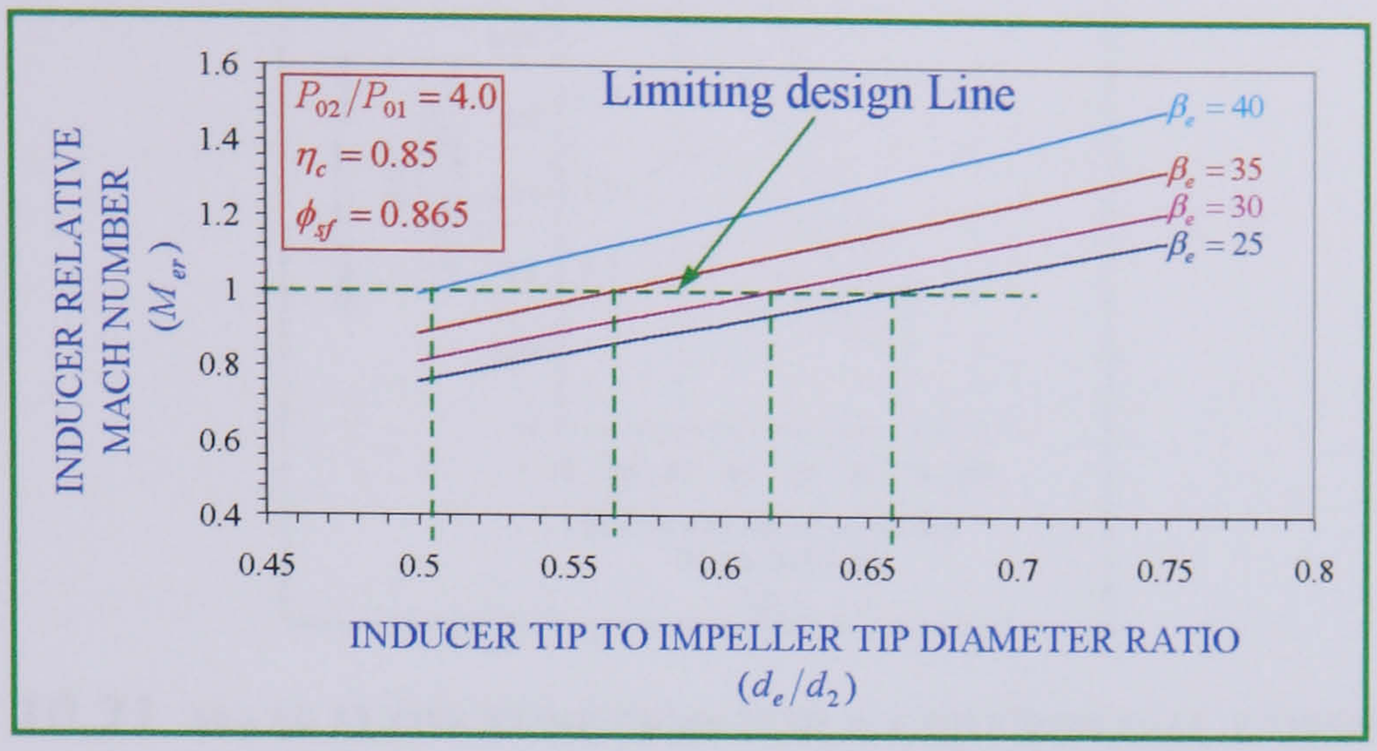

FIG. 10.20 EFFECT OF INDUCER TIP TO IMPELLER TIP DIAMETER RATIO d_e/d_2 ON M_{er} FOR VARIOUS VALUES OF β_e

10.2.3.2 Optimum design value of the blade angle at inducer tip diameter β_e

Equation 5.14 was extremely useful in determining the optimum design value of the blade angle at inducer tip diameter β_e. For a particular gas and known inlet design conditions, one can specify values of γ, R, P_{01}, N and T_{01} and substitute them in the RHS of equation 5.14, that is, $(\dfrac{\dot{m}N^2}{k_2 k_3 P_{01}\sqrt{\gamma R T_{01}}})$. By specifying several values of M_{er}, the optimum value of β_e for maximum mass flow rate can be found. Therefore, equation 5.14 is plotted as a function of β_e for several discrete values of M_{er} as shown in **Fig. 10.21**.

These curves are all seen to peak at approximately $\beta_e = 30^\circ$ at which condition $\dfrac{\dot{m}N^2}{k_2 k_3 P_{01}\sqrt{\gamma R T_{01}}}$ is a maximum. Therefore, $\beta_e = 30^\circ$ can be considered an optimum value for a zero swirl.

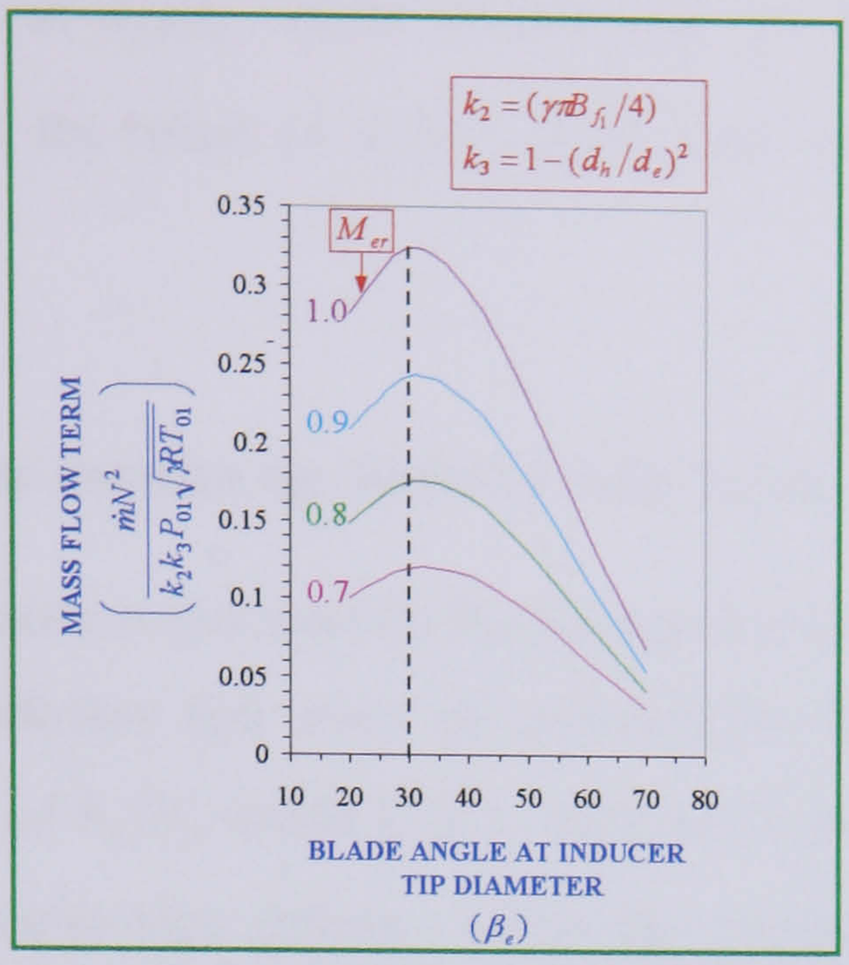

FIG. 10.21 MASS FLOW FUNCTION FOR A CENTRIFUGAL COMPRESSOR WITH ZERO ENTRY SWIRL

10.2.3.3 Inducer tip to impeller tip diameter ratio (d_e/d_2) and hub to impeller tip diameter ratio (d_h/d_2)

Equations 5.15 and 5.16 were plotted graphically as shown in **Fig. 10.22**. It can be observed that at $\beta_e > 25^\circ$, both d_e/d_2, d_h/d_2 values are reduced linearly for discrete values of M_{er}.

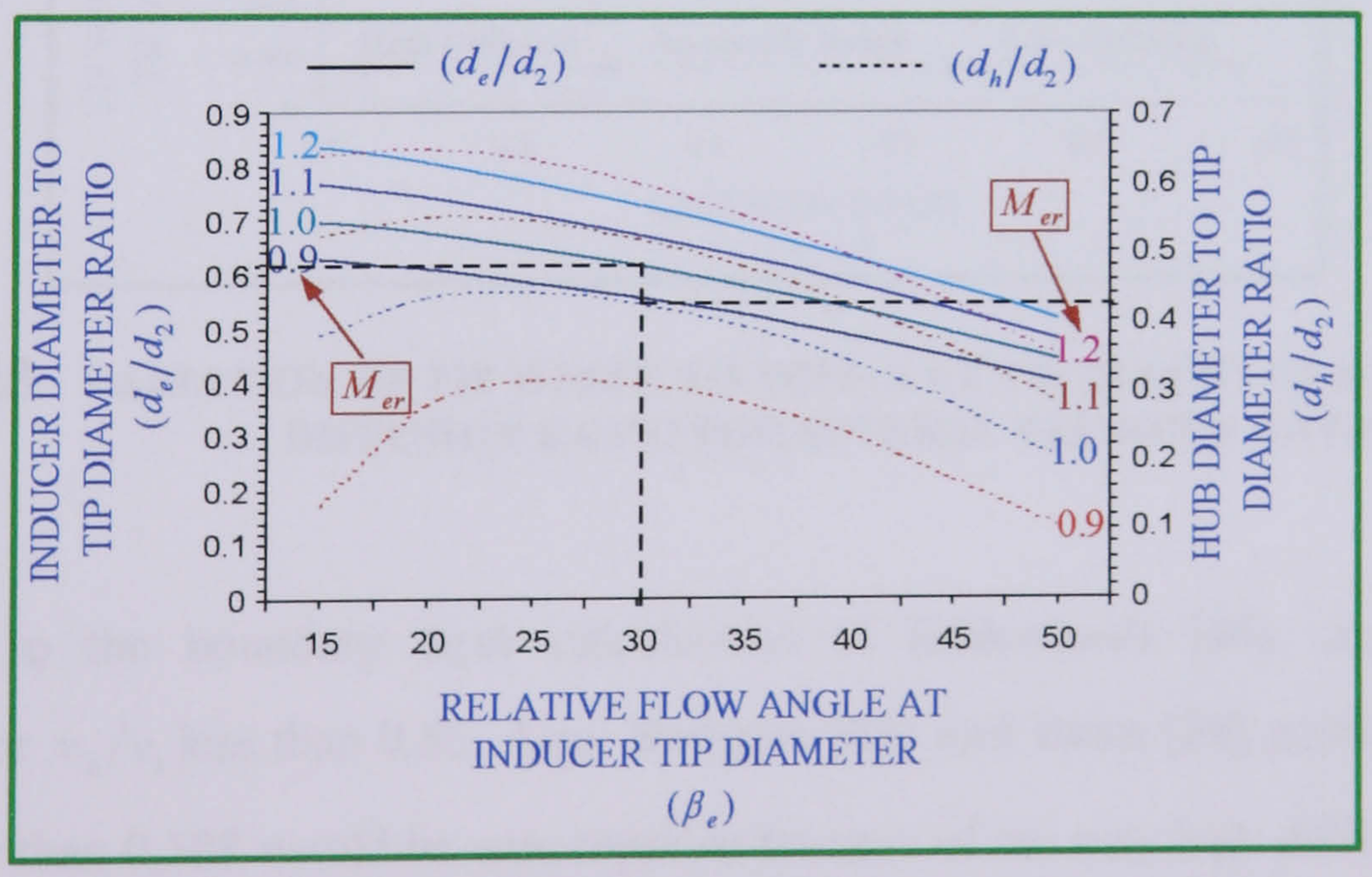

FIG. 10.22 THE EFFECT OF RELATIVE INDUCER TIP ANGLE β_e ON d_e/d_2 AND d_h/d_2 FOR VARIOUS OF M_{er} AT INDUCER TIP

At $\beta_e < 25^\circ$, the trends of d_e/d_2, d_h/d_2 are different. At optimum $\beta_e = 30^\circ$ and for subsonic flow $M_{er} < 1.0$, the values of d_e/d_2, d_h/d_2 must be less than 0.61 and 0.42, respectively.

10.2.3.4 Tip width to impeller tip diameter ratio (b_2/d_2)

The choice of this parameter is governed by the leakage loss consideration on one hand and the amount of diffusion that must be achieved on the other. Smaller than permissible lower value of b_2/d_2 would lead to increased leakage loss and large value would result in unacceptable high diffusion which may produce excessive loss due to flow separation. Equation 5.17 and 5.18 were solved and the results are plotted in **Fig. 10.23**. It can be seen that b_2/d_2 decreases as the diffusion ratio v_2/v_1 increases for various values of pressure ratio. Also, in **Fig. 10.23**, it was shown the upper and lower limits of v_2/v_1.

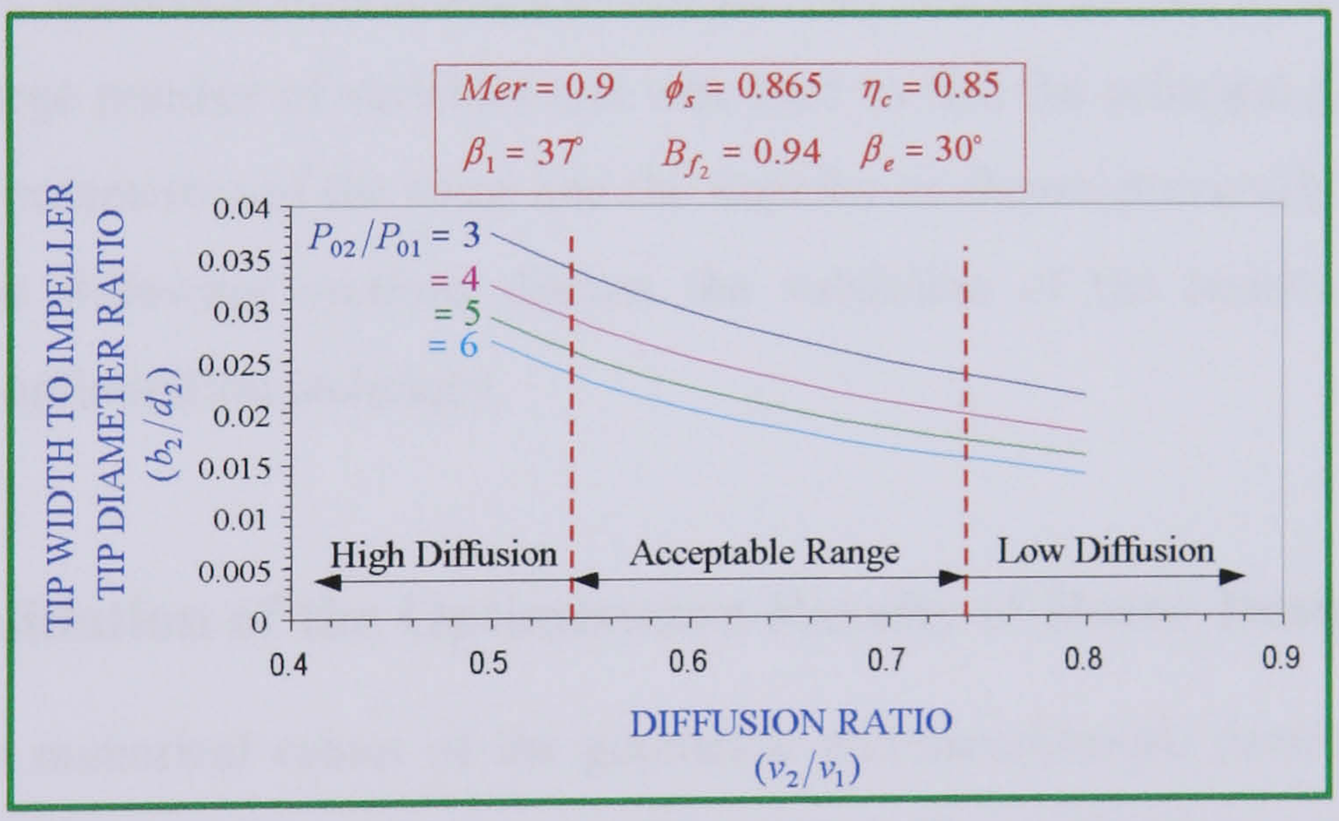

FIG. 10.23 VARIATION OF TIP WIDTH TO IMPELLER TIP DIAMETER RATIO AND DIFFUSION RATIO FOR SEVERAL PRESSURE RATIOS

According to the boundary layer calculations of **Dallenbach [44]**, separation is inevitable for v_2/v_1 less than 0.55. Also, **Rodgers [83] and Dean [84]** pointed out that v_2/v_1 lower than 0.588 would be unacceptable because of the very high diffusion within the impeller channels while values more than 0.72 would lead to higher leakage loss and hence loss in efficiency.

It should be mentioned here, that the solution for the equations used in **Sec. 10.2.3** of this Chapter, were all based on written computer programmes. The flow charts of these programmes were similar to those written for the turbine rotor, given in **Appendix [A]**. Therefore, in the interest of reducing the size of the thesis, these flow charts were not included.

10.3 OPTIMISATION OF GEOMETRIC AND AERODYNAMIC PARAMETERS OF THE IFR TURBINE ROTOR AND CENTRIFUGAL IMPELLER.

The parametric study of the effect of various geometric quantities on the aerodynamic variables was investigated and the results have been shown on a number of diagrams in the previous sections. The choice of the principal dimensions for a given set of a performance data on the basis of such diagrams is indeed difficult, and can be very time consuming, especially if the complete procedure has to be repeated for different cases. In view of this, numerical optimisation techniques can be a useful tool to solve problems involving a large number of variables and was used to find the principal geometric and aerodynamic parameters of the rotor and the impeller as shown previously in **Chapters 4** and **5**. The following sections discuss the validation of the results obtained by applying this optimisation technique.

10.3.1 Validation of the Optimisation Results of Rotor Design

The optimum numerical values of the geometric and aerodynamic parameters for the turbine rotor were found and given in **Chapter 4**. The validations of these results regarding the main design parameters are discussed in the following sections:.

10.3.1.1 Number of Blades

Several empirical formulae were cited in the open literature for calculating the number of blades. It should be noted here that the absolute flow angle α_2 notation used in this thesis is measured relative to tangential direction, therefore, a modification has been made to these formulae as their original notation was taken from the radial direction.

Several researchers reported these formulae for calculating the number of blades as described hereafter

i. Jamieson analysis

Jamieson [85] developed an empirical formula for calculating the number of blades. This formula is a function only of inlet flow angle at rotor inlet α_2 (degree) as shown below

$$N_b = 2\pi \tan(90 - \alpha_2) \tag{10.1}$$

ii. Wallace analysis

Wallace [4] analysis for calculating the number of blades was based on deriving an equation for the transverse pressure gradient of an isentropic flow in the rotor passage. Equation 10.2 represents the criterion for blade spacing where δ is the angle in radian subtended by the passage at the centre.

$$[\Delta P]_\delta = -\int_0^\delta \rho\left[\left(\frac{\partial v}{\partial r} v\cos\beta\sin\beta\right) - \left(\frac{\partial \beta}{\partial r} v^2 \sin^2\beta\right) + \left\{(v\sin\beta)\left(2\omega + (\frac{v\cos\beta}{r}\right)\right\}\right] d\theta \tag{10.2}$$

iii. Glassman empirical formula [86]

$$N_b = \left[\frac{\pi}{30}(20 + \alpha_2)\right]\tan(90 - \alpha_2) \tag{10.3}$$

iv. Whitfield and Baines empirical formula [12]

$$N_b = \frac{0.63\pi}{2\cos^2(90 - \alpha_2)} \tag{10.4}$$

v. Hiett and Johnston analysis [81]

Their analysis suggested that increasing the number of blades from 12 to 24 by introducing 12 intermediate stub blades for an absolute flow angle $\alpha_2 = 10^\circ$ resulted in a small gain in efficiency of 1%. It was also observed that the value of optimum u_2/c_s fell from 0.75 for the 12 bladed rotor to 0.68, thus indicating that the optimum

efficiency with 24 blades occurs at approximately zero incidence. In practical applications, however, it is probable that the increase in complexity and rotor inertia associated with the large number of blades would outweigh such a relatively small gain in performance. They presented a curve showing the optimum number of blades versus the absolute flow angle based on the criterion according to **Jamieson [85]** whereby the optimum blade number is the minimum required to prevent local flow reversal within the rotor passages. Therefore, for an absolute flow angle of $\alpha_2 = 17^\circ$, the optimum number of blades is 19.

vi. Mizumachi *et al* analysis [33]

Their analysis was based on experimental results of various turbine rotors with different number of blades. They found that the maximum efficiency was obtained using 17 blades. For the selected design value of $\alpha_2 = 17^\circ$, the number of blades calculated based on using these formulae are summarized in **Table 10.1**

EMPIRICAL FORMULA OR ANALYSIS	NUMBER OF BLADES FOR ROTORS
Jamieson empirical formula	21
Wallace analysis	12
Glassman empirical formula	12-13
Hiett and Johnston analysis	12-24
Mizumachi, *et al.* analysis	17
Whitfield empirical formula	12
Optimization technique	**12-20**

TABLE 10.1 NUMBER OF BLADES BASED ON USING VARIOUS EMPIRICAL FORMULAE AT $\alpha_2 = 17^\circ$

It can be deduced from **Table 10.1** that **Wallace [4], Glassman [86], Hiett and Johnston [81]** and **Whitfield and Baines [12]** analyses agree well with the results obtained by optimisation technique for predicting the number of blades of the turbine rotor.

10.3.1.2 Flow coefficient parameter ($c_1/u_2 = c_{m1}/u_2$)

Rodgers [54] specifies the key parameters upon which the turbine efficiency depends on:

i. Rotor tip speed, u_2
ii. Exit kinetic energy at mean diameter, $c_1 = c_{m1}$
iii. Tip clearance

Two important parameters ratios can be developed; these are the speed ratio u_2/c_s and the flow coefficient c_{m1}/u_2 ratios. These two coefficients were shown graphically in **Figs 10.4** and **10.17**. The optimisation design calculation gives the values of these ratios as 0.67 and 0.35, respectively. **Fig. 10.24** shows how the design point compares with the universal chart for small gas **IFR** turbines adapted from **Rodgers [54].** It can be seen from **Fig. 10.24** that the calculated design point is close to an efficiency of 0.86.

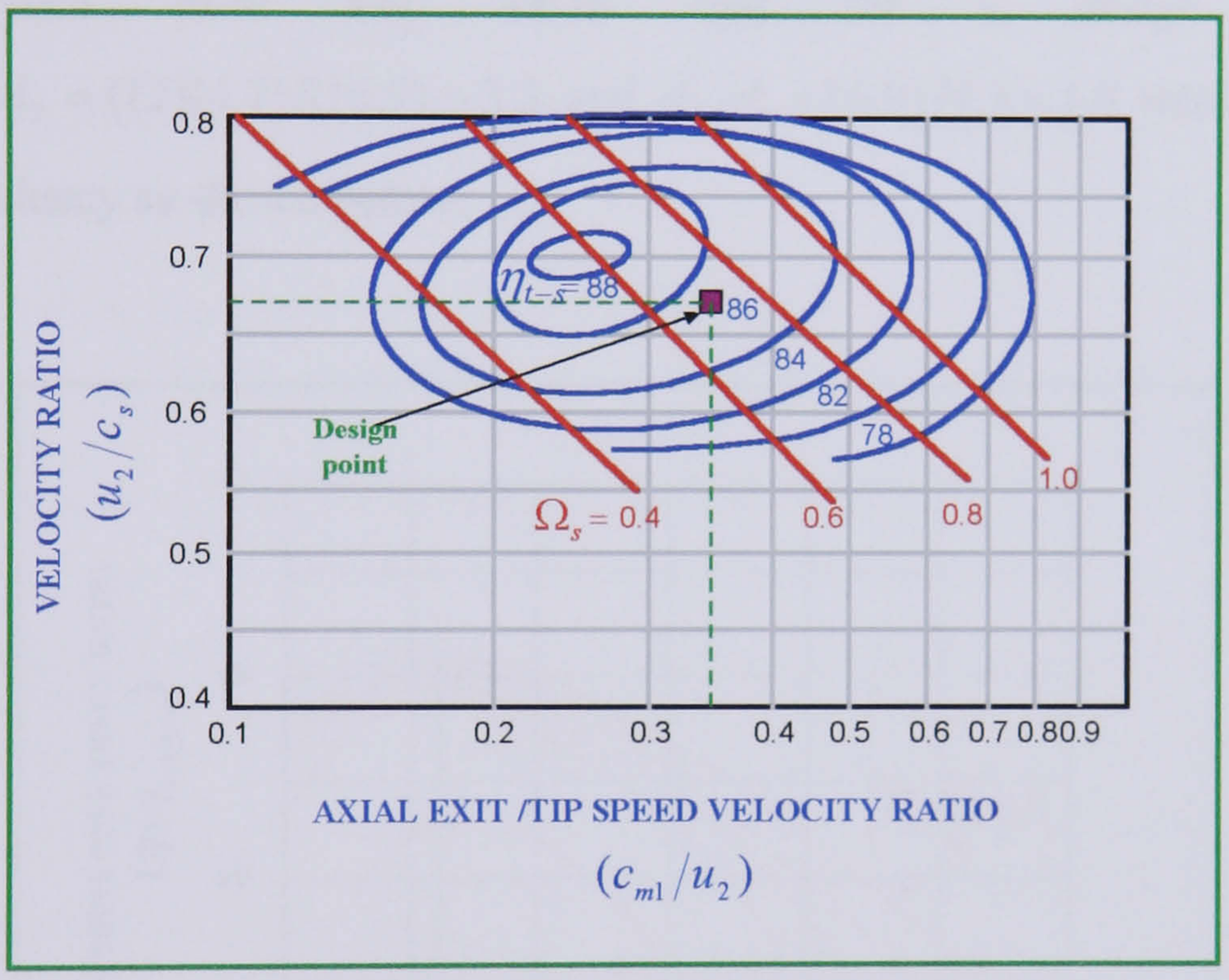

FIG. 10.24 CORRELATION OF ATTAINABLE RADIAL INFLOW TURBINE EFFICIENCIES WITH VELOCITY RATIOS

10.3.1.3 Mean exit to inlet tip diameter ratio parameter (d_1/d_2) and hub to inlet tip diameter ratio (d_h/d_2)

Rohilk [6] and Anon [87] research work recommended that d_1/d_2 ratio should not exceed 0.7 to avoid excessive curvature of the shroud. However, it must be acknowledged that it is often exceeded in applications where the designer desires to reduce the inlet tip diameter and hence the rotating mass.

This is very common in small turbocharger turbines and even the gas turbine applications cited by **Rodgers and Geiser [88]** who employed a diameter ratio in excess of 0.7. However, too small a diameter ratio d_1/d_2 will cause the blades to be crowded together at the exit hub and this may limit the available exit area. **Anon [87]** report suggested that the ratio of d_h/d_2 would not fall below 0.35 to aviod blockage. ($current\ work\ design\ value = 0.36$).

Rodgers and Geiser [88], presented a chart depicted in **Fig. 10.28**, which shows the variation of the efficiency as a function of the reciprocal diameter ratio d_1/d_2 and a blade number parameter $(N_b)(Z_{axial})/d_2$, where Z_{axial} is the axial length of the rotor. It can be seen from **Fig. 10.28** that for a design value of $(N_b)(Z_{axial})/d_2 = (12)(4.7)/(16.9) = 3.3$ and $d_2/d_1 = 16.91/9.3 = 1.8$ would result in an optimum efficiency as shown below.

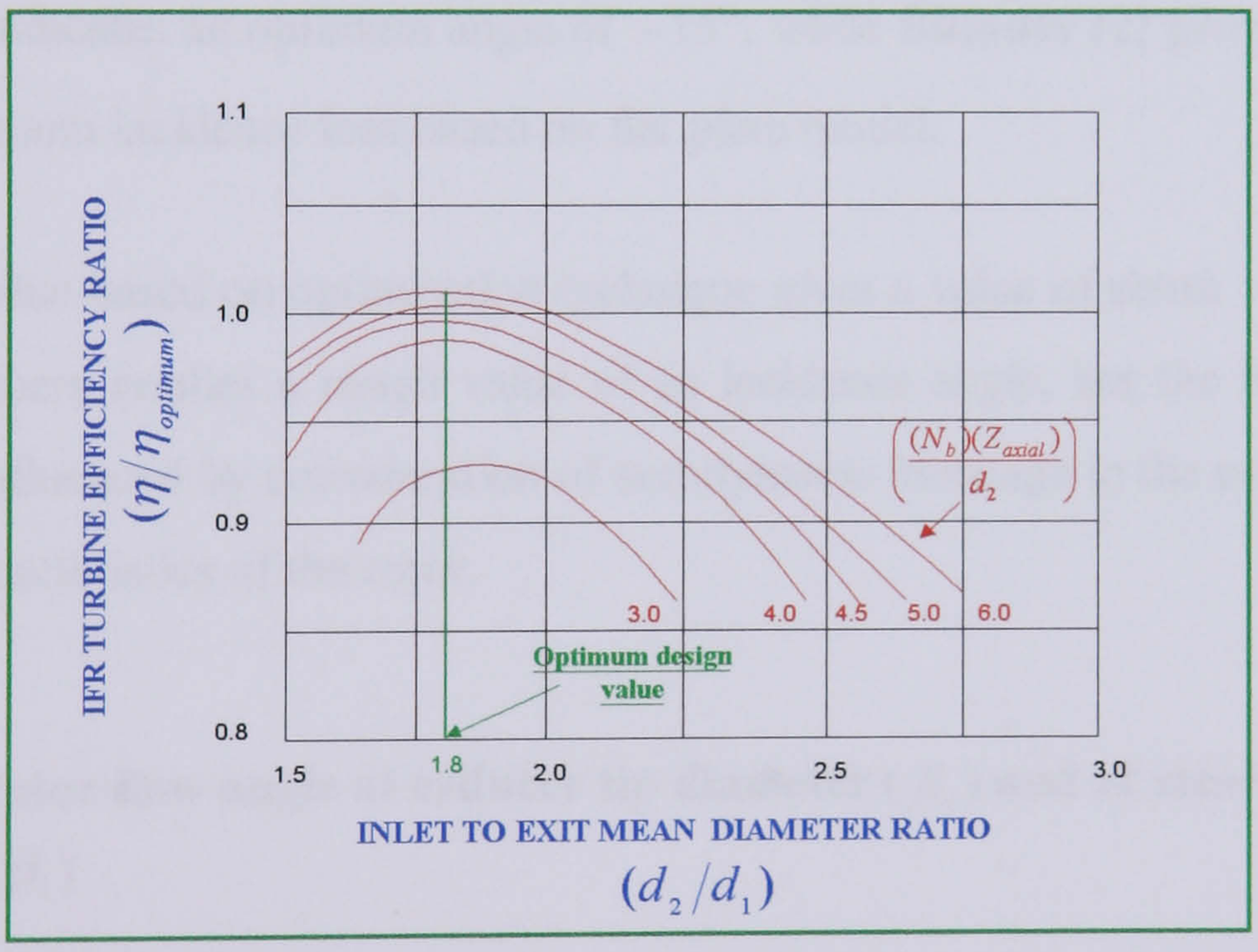

FIG. 10.28 THE EFFECT OF ROTOR DIAMETER RATIO AND BLADE SOLIDITY ON RADIAL TURBINE EFFICIENCY

10.3.1.4 Blade width to inlet tip diameter ratio parameter (b_2/d_2)

Hiett and Johnston [81] suggested in their experimental studies that a value of tip width / tip diameter of approximately 0.10 represents an optimum ratio.

Watanabe *et al* [89] reported that a value between 0.07-0.09 should be chosen. The turbine performance is probably not very sensitive to the values of this parameter in this range. The design value obtained from numerical optimisation is 0.051, which is relatively less compared with **Hiett and Johnston and Watanabe** values. The reason is due to the fact that the applied load and the rotational speed, given as design specifications, control the choice of the principal geometric ratio. Sometimes, as in the present case, these two requirements are not parallel. It is evident that if mass flow and speed are given to meet the design requirements, the choice of b_2/d_2 is very limited.

10.3.1.5 Incidence angle at rotor inlet (β_2)

The optimum incidence angle cannot be selected arbitrarily; rather it is a function of fluid dynamic conditions at the rotor inlet and geometric parameters, most notably the number of blades. **Rodger and Geiser [88]** quotes incidence angles of the order of -20° and **Rohlik [6]** gives values as high as -40°. Measurements by **Yeo and Baines [90]** indicates an optimum angle of -15°, while **Bhinder [2]** gives a value have -5° for minimum incidence loss based on flat plate model.

The design value based on optimisation technique gives a value of about -6°. A choice of blade numbers implies a rough value of an incidence angle, but the blade numbers will also be influenced by consideration of aerodynamic blockage in the exducer and the vibration characteristics of the rotor.

10.3.1.6 Rotor flow angle at exducer tip diameter (β_e) and at mean diameter (β_1)

Whitfield and Baines [12] reported that relative Mach number at exducer tip M_{er} is a minimum when the relative flow angle rotor flow angle β_e is about 30° was adopted based on minimum M_{er} which implies minimum internal losses in the rotor. However, the use of lower flow angles such as 20° cannot be dismissed as this leads to a reduction in the absolute Mach number at exit M_1. There is, a compromise to be made between a low relative Mach number to reduce the internal passage losses, and a low

absolute Mach number to reduce the exit kinetic energy. The design value reported in this work gives a value of $\beta_e = 27^\circ$. **Chen and Baines [91]** stated that the design criteria for the flow angle at mean diameter $\beta_1 \leq 45^\circ$. The design value reported in this work gives a value of $\beta_1 = 32.59^\circ$.

10.3.1.7 Rotor relative velocity ratio at mean diameter (v_1/v_2)

This parameter is a measure of the expansion drop in the rotor, and values substantially in excess of unity are required. **Ribaud and Mischel [5]** stated that Onera design code for velocity ratio is $2.0 < v_1/v_2 < 2.5$. The current design calculations based on optimisation technique provides a value of $v_2/v_1 = 2.13$

10.3.1.8 Specific speed parameter (Ω_s) and specific diameter (D_s)

Figure 10.29 shows the relationship between Ω_s, the exhaust energy factor $(c_1/c_s)^2$ and the area ratio A_1/A_d based on equation B.7 in **Appendix [B]**. According to **Wood [92],** the limits for the exhaust energy factor in gas turbine practice are $0.04 < (c_1/c_s)^2 < 0.3$. The calculated design value of $(c_1/c_s)^2 = 0.055$ for an area ratio $A_1/A_d = 0.30$. For these two values, it can be seen from **Fig. 10.29** that the value for Ω_s is 0.56. The numerical value of specific speed provides a general index of the flow capacity relative to work output. Low values of Ω_s are associated with relatively small flow passage area and visa versa.

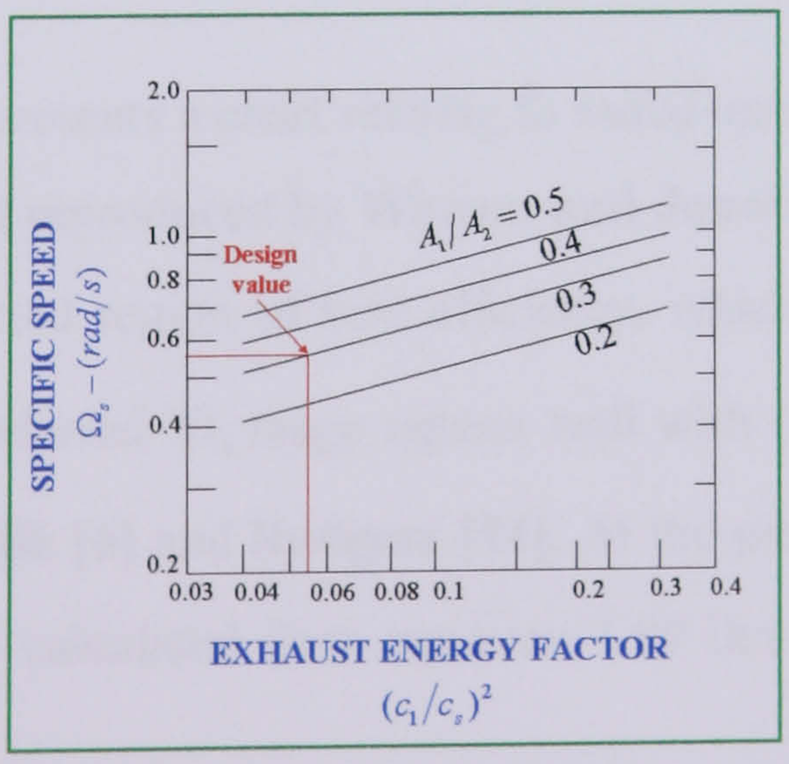

FIG. 10.29 SPECIFIC SPEED FUNCTION FOR IFR TURBINE "ADAPTED FROM WOOD[92]"

Specific speed has also been widely used as a general indication of achievable efficiency. **Fig. 10.30** presents a broad correlation of maximum efficiencies for hydraulic and compressible fluid turbines as functions of specific speed. Over the fairly limited range of specific speed, $0.3 < \Omega_s < 0.9$, the **IFR** turbine can produce a high efficiency. For $\Omega_s = 0.56$, the attainable efficiency gained from **Fig. 10.30** is $\eta_{tt} = 0.87$. In the present work, the value of $\Omega_s = 0.55$ was calculated from equation 3.95 of **Chapter 3**. This value agrees well with **Wood's** work.

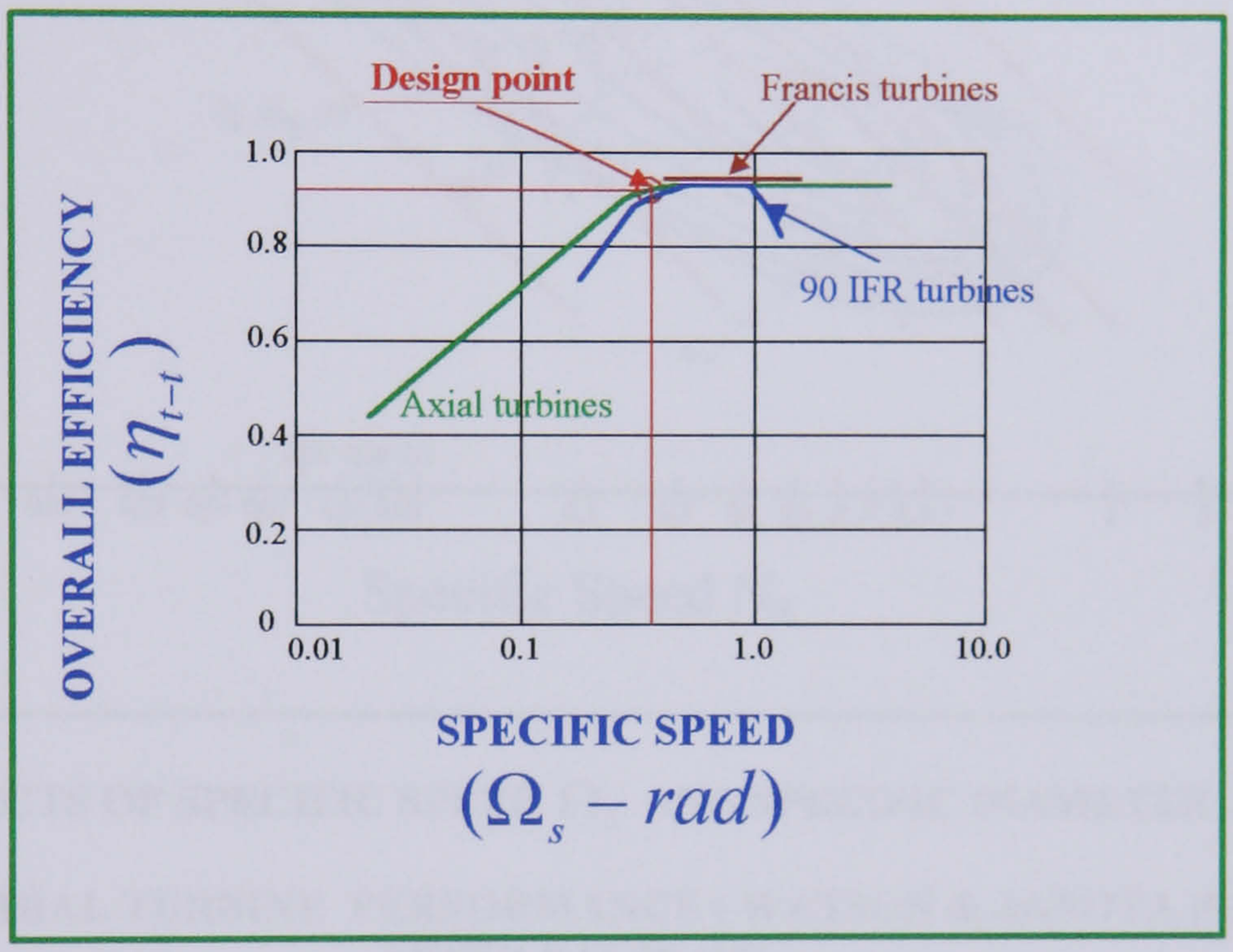

FIG. 10.30 SPECIFIC SPEED-EFFICIENCY CHARACTERISTICS FOR VARIOUS TURBINES "ADAPTED FROM WOOD [92]"

Furthermore, **Fig. 10.31** presents a chart relating to radial turbines, which was extracted from **Balje [10]** work and reproduced by **Watson and Janota [93]** using SI units. This chart indicates the predicted region of best efficiency, which suggests that Ω_s in the range 0.4 to 0.8. The preferred Ω_s range agrees well with the work of other authors such as **Wood [92], Rohlik [6]** and **Rodgers [94].** At the present work, the predicted design value of D_s=3.46 calculated from equation 3.99 lies within the range for high efficiency, see **Fig. 10.31**.

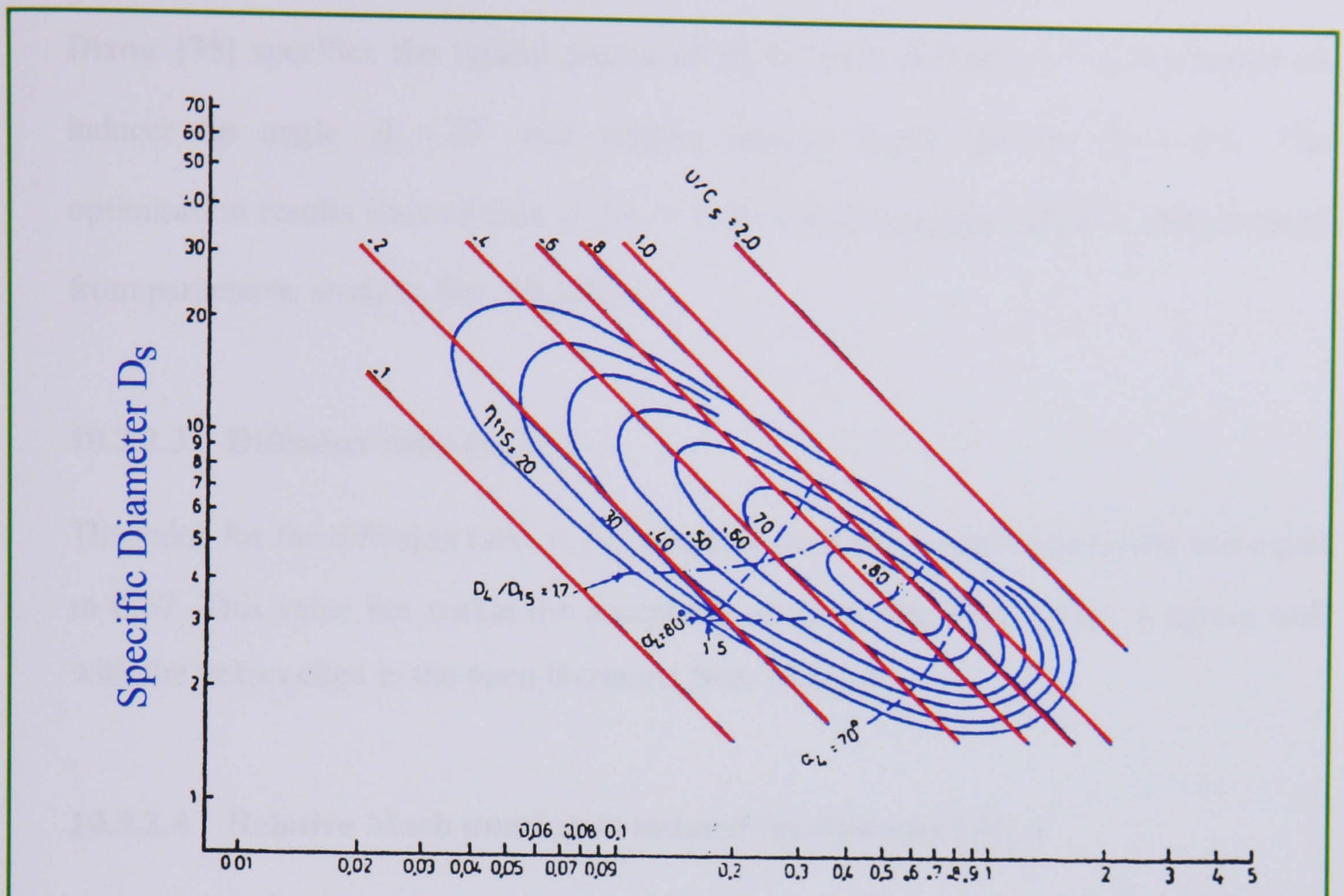

FIG. 10.31 EFFECTS OF SPECIFIC SPEED Ω_S AND SPECIFIC DIAMETER D_S ON RADIAL TURBINE PERFORMANCE (WATSON & JANOTA [92]) AFTER BALJE [10]

10.3.2 Validation of Optimisation Results of Impeller Design

The optimum numericl values of the geometric and aerodynamic parameters for the impeller were found and given in **Chapter 5**. The validations of these results regarding the most important design parametres are discussed in the following sections

10.3.2.1 Impeller flow angle at inducer tip diameter (β_e)

Parametric results in **Sec. 10.2.3.2** have shown that the optimum flow angle β_e is equal to 30° and this agrees exactly with the results for β_e obtained from numerical optimisation.

10.3.2.2 Hub to inducer tip diameter ratio (d_h/d_e)

Dixon [95] specifies the typical values of d_h/d_e ratio between 0.3 to 0.6 based on inducer tip angle $\beta_e = 30^\circ$ and relative inducer Mach number $M_{er} = 0.9$. The optimisation results showed that d_h/d_e = 0.36 and also agrees well with that obtained from parametric study in **Sec. 10.2.3.3**.

10.3.2.3 Diffusion ratio (v_2/v_1)

The value for the diffusion ratio v_2/v_1 obtained from the optimisation results was equal to 0.67. This value lies within the acceptable range in **Fig. 10.27**. Also, it agrees well with the values cited in the open literature, **Sec. 10.2.3.4**.

10.3.2.4 Relative Mach number at inducer tip diameter (M_{er})

The value for the relative Mach number at inducer tip diameter (M_{er}) obtained from the optimisation results was equal to 0.903. This value means that the flow will not be choked at the inducer section of the impeller.

10.3.2.5 Specific speed (Ω_s)

The calculation of specific speed based on the values of optimisation gives a value of 0.55. **Rodgers[54]** reported that for an impeller with radial blades, and for a flow coefficient of c_1/u_2 equal to 0.3, the value of specific speed for best efficiency was between 0.5 – 0.6 which agrees with the value from the optimisation results.

10.4 OPTIMISATION OF THE AXIAL LENGTH AND DESIGN OF FLOW PASSAGE FOR THE IFR TURBINE ROTOR AND CENTRIFUGAL IMPELLER.

The optimisation of the axial length of the rotor and the impeller was performed by **stage 2** of the programme as shown in **Fig. 10.32** below. The programme was based on

the theory of prescribed mean stream velocity distribution along the axial length and on the basis of rotor and impeller internal losses along the passage , respectively. **Stage 3** of the programme in **Fig. 10.32** was used to determine the hub and shroud contours.

The main features of this procedure are listed in the followings:

i. Once the velocity distribution and the constraints have been specified, the programme can be seen without any stops for decision inputs from the operator.

ii. The programme can justifably be claimed to offer a direct design method as it is not necessary to define an initial geometry of the rotor or impeller and then modify it progressively on the basis of the results from the detailed flow analysis programme. Therefore, both the time and the cost to produce a design can be considerably reduced.

iii. Extensive use is made of numerical optimisation algorithms which have been used very successfulully in many variable problems.

iv. The axial length of the rotor and the impeller, which has been shown in this thesis to be an important design variable was optimised and determind while most researcher choose the axial length quite arbitrarliy in their design work.

10.5 STRESS, THERMAL AND VIBRATION ANALYSIS

ANSYS finite element package was used to determine the stresses and displacements (structrural and thermal) for the rotor and the impeller operating under design conditions. Also, vibration (modal) analysis of the rotoating system was carried out under different operating condtion were given in **Chapter 7**. These output results were needed for the following reasons:

i. To ensure a safe design of the rotating components at the design conditions.

ii. To select a suitable material that withstand the stresses produced.

iii. To determine the clearances between the rotating components and the casing.

iv. To avoid failure due to resonance.

v. To modify the design of the components if necessary.

It should be noted that analytical methods cited in the open literature such those presented by **Swanson [73]** and **Schilhansh [74]** were not very accurate because of the complexity of the geometries of the rotating components , therefore employing packages such as **ANSYS** would produce a better design and would reduce the time and cost of the work.

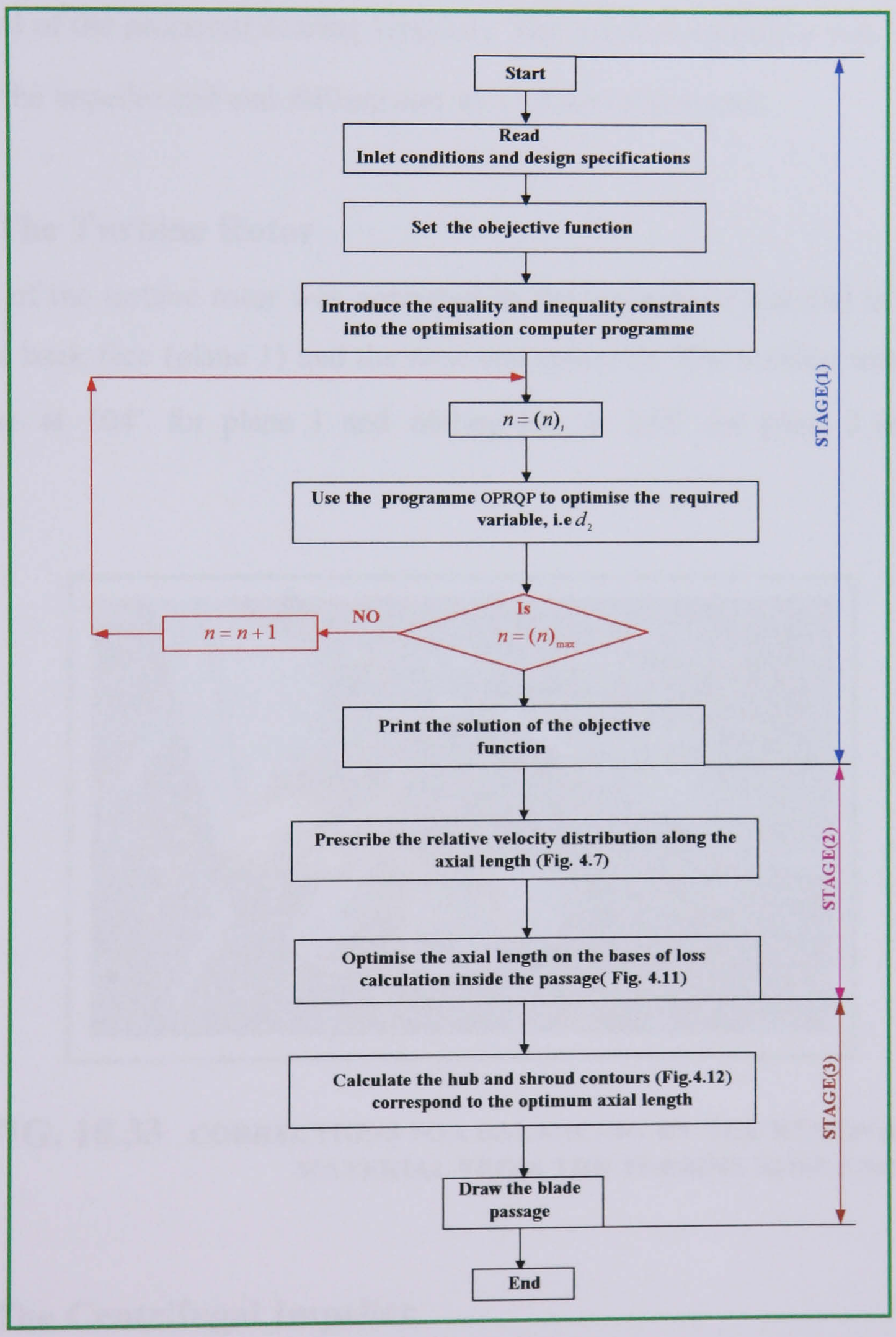

FIG. 10.32 FLOW CHART FOR THE COMPLETE DESIGN PROCESS OF THE ROTOR AND THE IMPELLER

10.6 BALANCING RESULTS

Balancing of the rotating components is important to ensure a safe operation of the small gas turbine engine. Procedure of balancing the components was undertaken as shown in **Chapter 9** and the results are given in the following .

10.6.1 The Main Shaft

The main shaft was dynamically balanced by removal of material from correction planes just inboard of the proposed bearing locations. The residual unbalance was $350\,mg\,mm$ at 220° at the impeller end and $640\,mg\,mm$ at 1° at the turbine end.

10.6.2 The Turbine Rotor

Balancing of the turbine rotor was corrected by the removal of material in two planes namely the back face (plane 1) and the nose end (plane 2). The residual unbalance was $960\,mg\,mm$ at 104° for plane 1 and $660\,mg\,mm$ at 358° for plane 2 as shown in **Fig.10.33**.

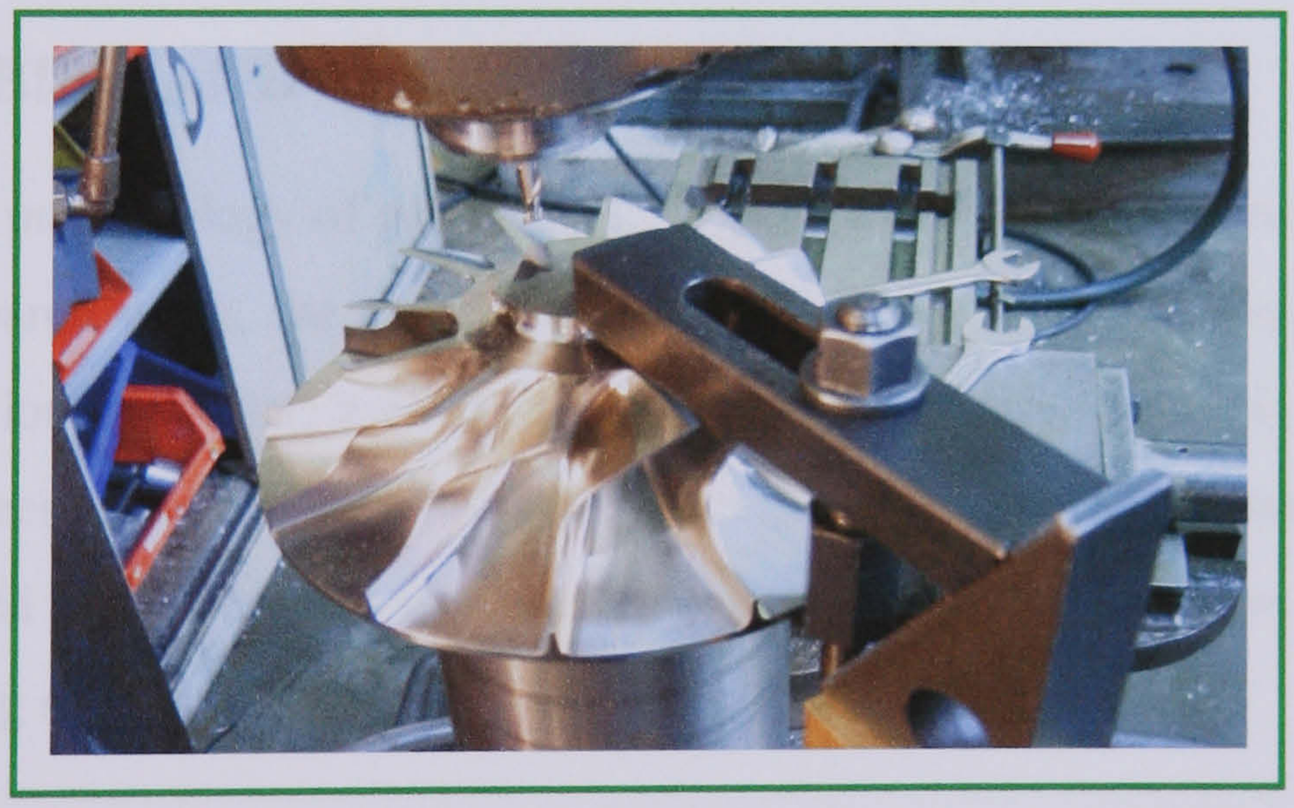

FIG. 10.33 CORRECTIONS FOR BALANCING BY THE REMOVAL OF MATERIAL FROM THE TURBINE NOSE END

10.6.3 The Centrifugal Impeller

the residual static unbalance on the impeller was $1.75\,mg\,mm$ at 276° as shown in **Fig. 10.34**.It should be noted that during re-assembly the match marks should be aligned and

the main bolt should be adjusted to a torque of $40\,Nm$. Any variation in the unbalance results is likely to be up to $1-1.5\,g\,mm$ at the turbine end due to the repeatability of the hearth coupling. Any auxiliary equipment, this rotating assembly may be coupled to, must also be precision balanced and accurately aligned.

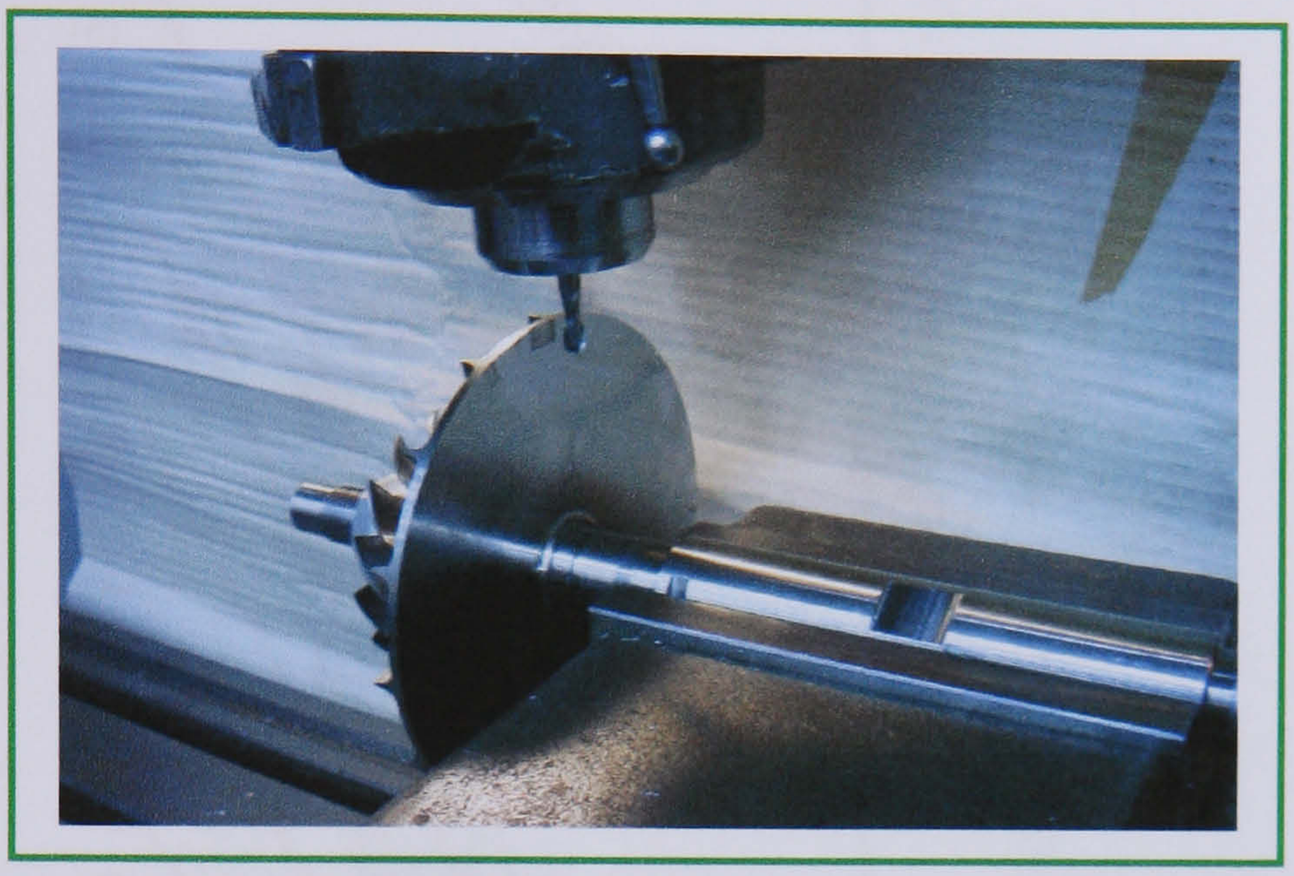

FIG. 10.34 CORRECTIONS FOR BALANCING BY THE REMOVAL OF MATERIAL FROM THE IMPELLER BACK FACE

10.7 TURBINE AND COMPRESSOR MATCHING

The matching methodology of gas turbine components has been explained in **Chapter 8**. In this research work, the method was restricted to a single shaft engine used for power generation. However, it can apply to other type of engines but this is outside the scope of this research. The results of performance prediction of the small gas turbine engine designed in this research work at design and off-design conditions are discussed in the following sections.

10.7.1 Turbine-Compressor Matching Map

Once the transformation maps of the turbine and the compressor have been produced, then the conditions for matching are achieved which can be superimposed to produce the matching prediction map of the designed gas turbine engine in the current work as shown in **Fig. 10.35**.

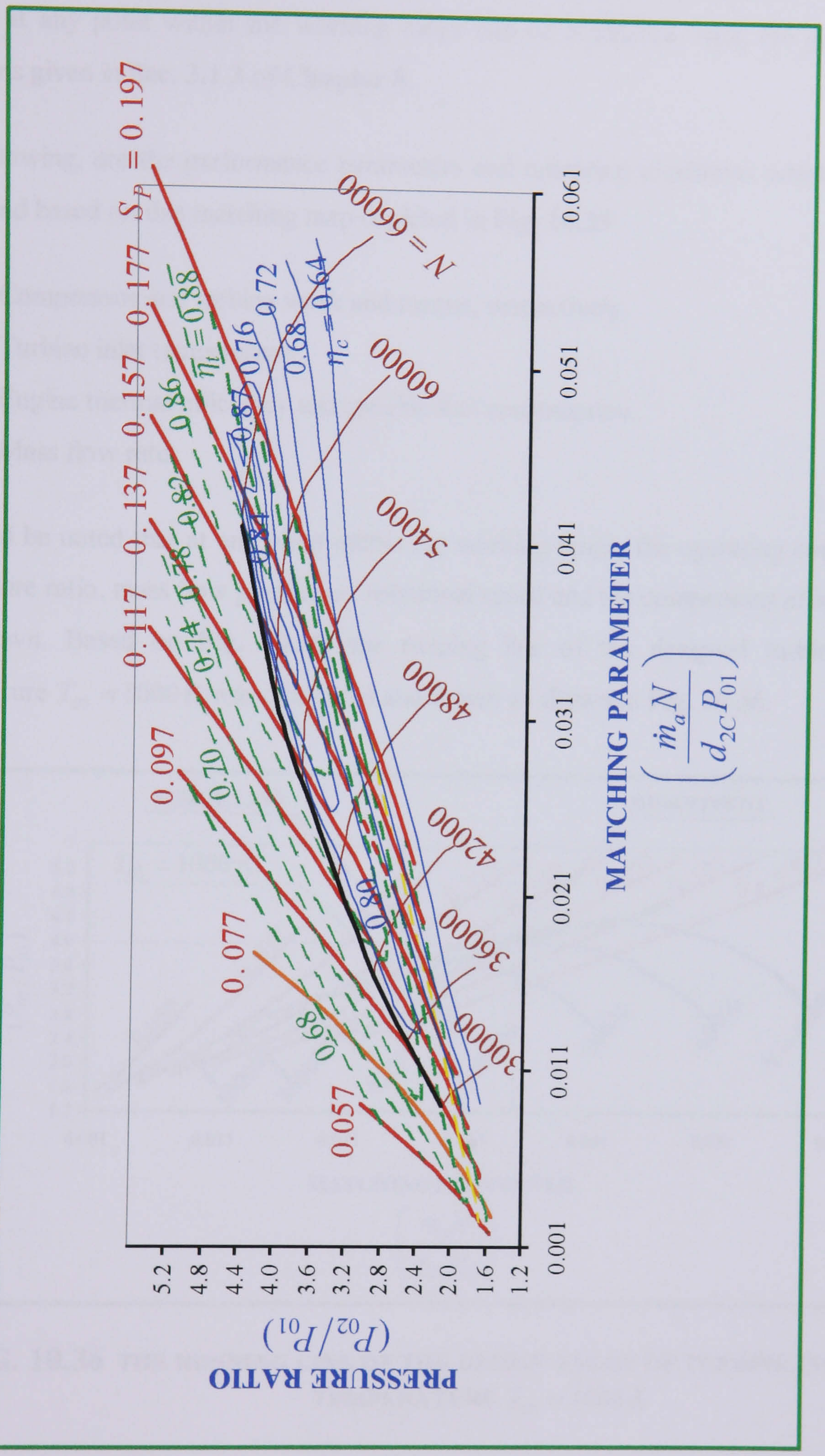

FIG. 10.35 MATCHING PREDICTION MAP OF THE DESIGNED GAS TURBINE ENGINE RUNNING AT 60000 *rpm*

This is a very useful map and the performance parameters of the compressor and the turbine at any point within the working range can be computed using the governing equations given in **Sec. 3.1.2** of **Chapter 8**.

The following, are the performance parameters and operating conditions which can be determind based on this matching map depicted in **Fig. 10.35**

i. Compressor and turbine work and torque, respectively.

ii. Turbine inlet temperature.

iii. Engine thermal efficiency and specific fuel consumption.

iv. Mass flow rate.

It should be noted that at any point within the working range, the operating conditions of pressure ratio, mass flow parameter, rotational speed and the components efficiencies are known. Based on **Fig. 10.35**, the running line of the designed turbine inlet temperature $T_{03} = 1000\,K$ was computed and drawn as shown in **Fig. 10.36**.

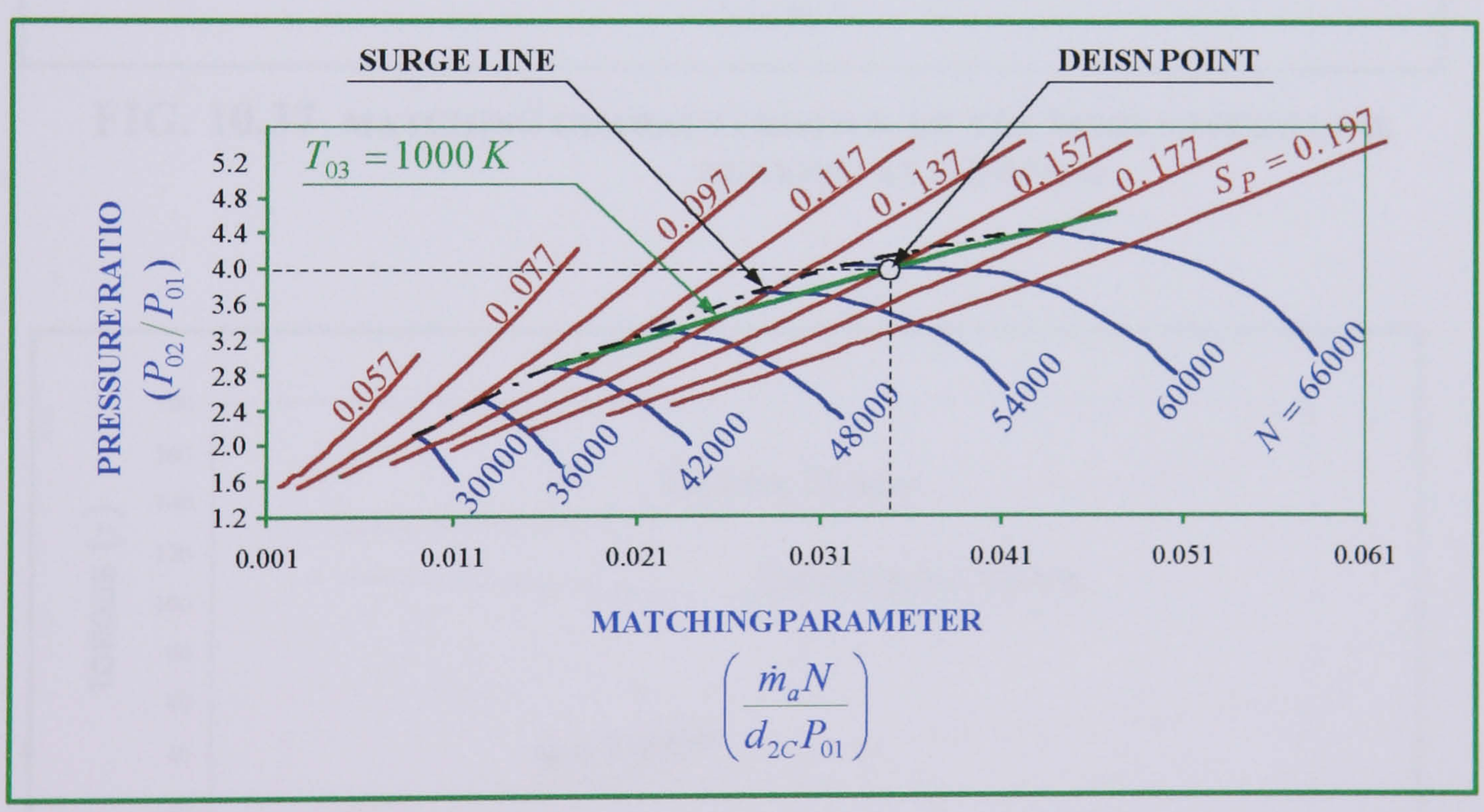

FIG. 10.36 THE RUNNING LINE OF THE DESIGN VALUE OF TURBINE INLET TEMPERATURE $T_{03} = 1000\,K$

The design speed line of the gas turbine engine under consideration is $60000\,rpm$. This speed line was extracted out from **Fig. 10.35** for clarity as shown in **Fig. 10.37**. It can

be seen from **Fig. 10.37** that all the matching values of the engine components at the design speed are known and they are used to predict the engine performance (thermal efficiency and specific fuel consumption) at design and off-design conditions. The output results are shown in **Figs. 10.38** and **10.39**.

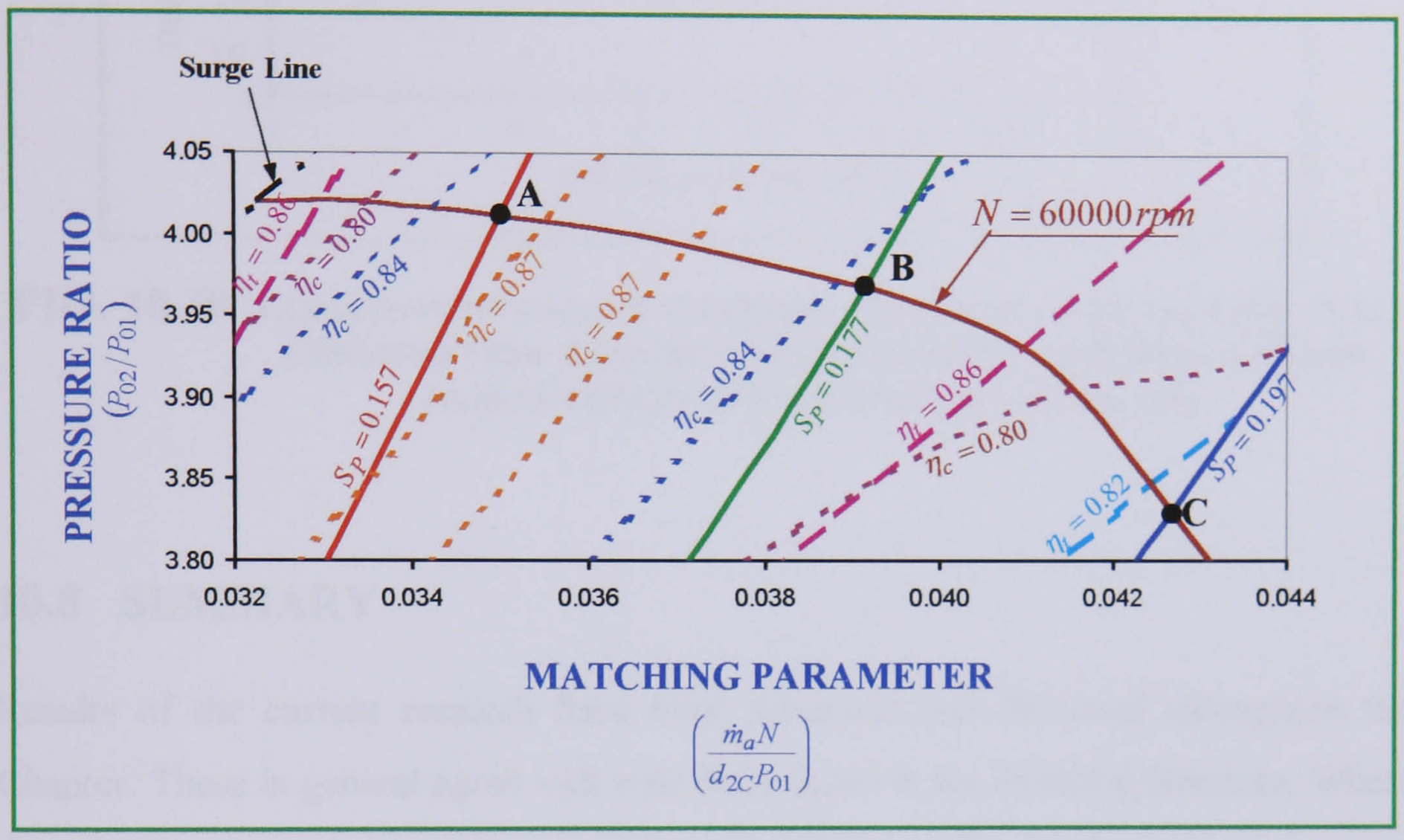

FIG. 10.37 MATCHING CHARACTERISTICS OF THE DESIGN SPEED LINE RUNNING AT $60000\,rpm$

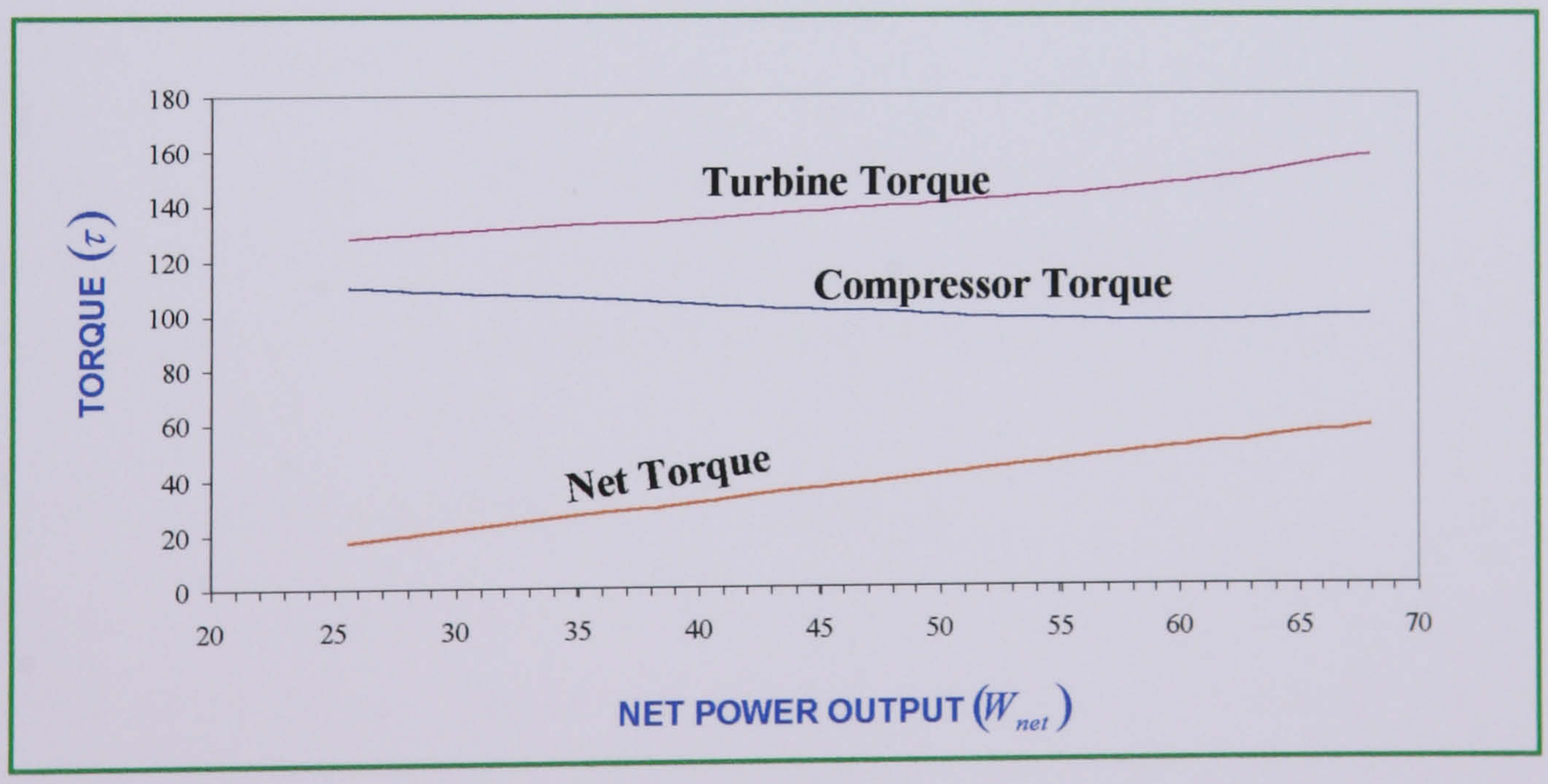

FIG. 10.38 VARIATION OF ENGINE TORQUE AT DESIGN AND OFF DESIGN CONDITIONS RUNNING AT $60000\,rpm$

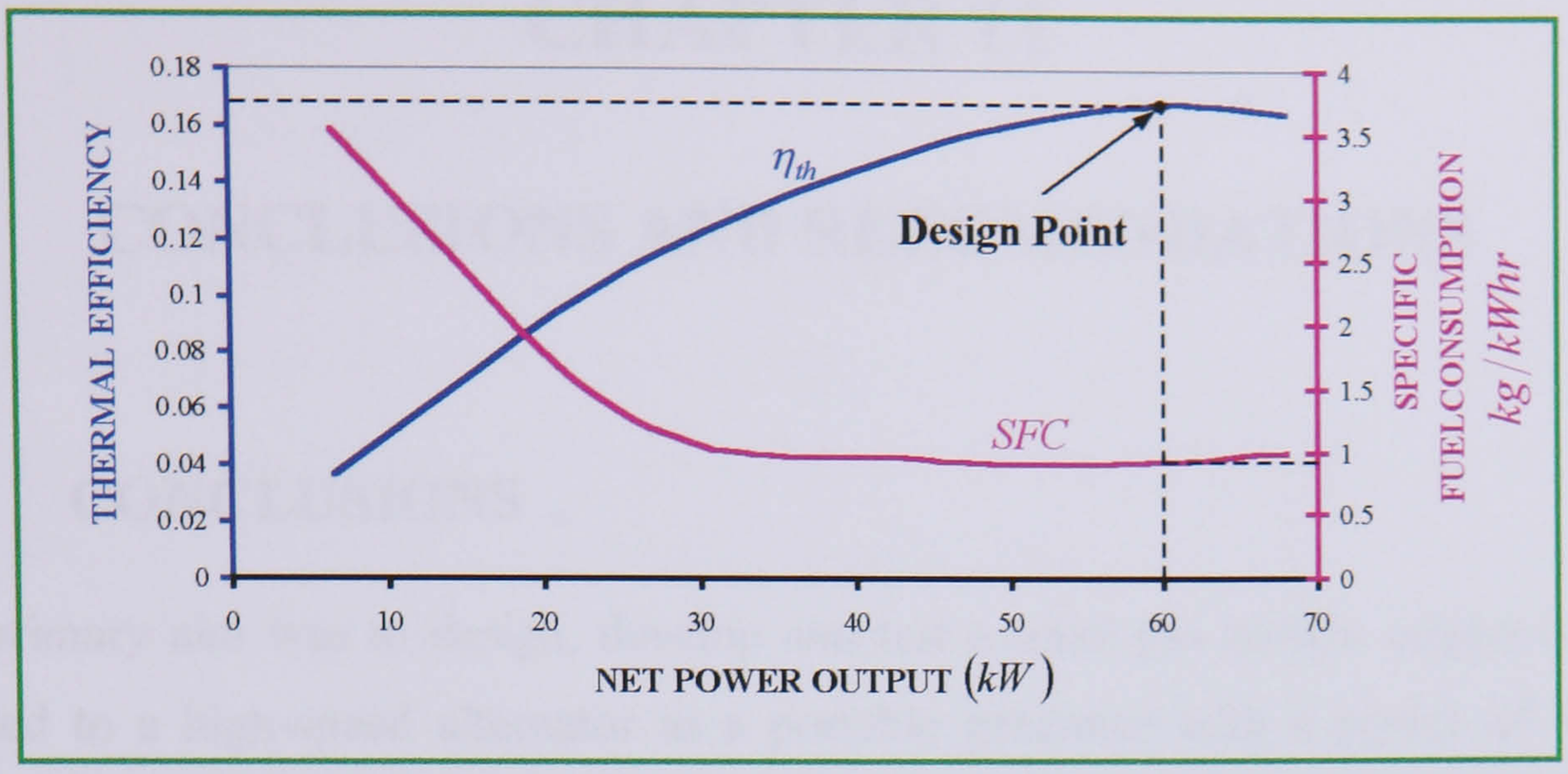

FIG. 10.39 VARIATION OF ENGINE THERMAL EFFICIENCY AND SPECIFIC FUEL CONSUMPTION WITH NET POWER OUTPUT AT DESIGN AND OFF DESIGN CONDITIONS RUNNING AT 60000 *rpm*

10.8 SUMMARY

Results of the current research have been presented and discussed throughout the Chapter. These in general agree well with those found in the technical literature. Where there is disagreement, the reasons have been provided and discussed.

CHAPTER 11

CONCLUSIONS AND RECOMENDATIONS

11.1 CONCLUSIONS

The primary aim was to design, develop and test a small gas turbine engine directly coupled to a high-speed alternator as a portable generator with a power of $60\,kW$ running at $60000\,rpm$. The motivation for producing such a device was the substantial reduction in weight and size of the generator in comparison to conventional low speed devices, such as those using a reciprocating engine as the prime mover.

The preferred end result of the project was to have a working demonstrator engine, which could be developed into a design suitable for low cost manufacture. Initially there was uncertainty as to how difficult it would be to achieve this target. Much of the uncertainty laid with the complete design and manufacture of the gas turbine components, that is, the turbine, the compressor and the power transmission shaft throughout the specified period of the project. However, an overall strategy was adopted to carry out theoretical and experimental research aimed at the goals of creating a technology base for the design of small gas turbine engine and of finally building the demonstrator engine.

In the next section, the achievements, to date, for the research programme are summarised. This is followed by a section giving details of further work required in order to achieve the final objective of building a demonstrator turbo-alternator.

11.1.1 Summary of Project Achievements

The list of achievements has been divided under headings of major component or subject areas. As it was explained in **Chapter 1**, it was necessary to undertake research in the areas of the turbine and compressor design, mechanical design of the power transmission shaft, selection of bearings and performance prediction of the engine.

11.1.1.1 Inward flow radial IFR turbine

A. Parametric study conclusions

The primary purpose of the parametric study was to show the influence of either the principal design variables and cycle configurations or the operating conditions on the performance of the **IFR** turbine to obtain the best design point. A parametric study was carried out and the results have been discussed in **Chapter 10**. The main conclusions are given in the followings:

i. The cycle thermal efficiency increases with increased turbine inlet temperature and cycle pressure ratio simultaneously. It was also shown that the maximum efficiency point and the maximum specific work point at each constant temperature or pressure ratio are different.

ii. At high-pressure ratio, the radial turbine can cope with large pressure fluctuations at constant speeds without loss in efficiency. This is because an accelerating flow can operate over a fairly wide range of incidence relative to the actual blade angles without significant flow disruption.

iii. Contrary to the general belief that fixing the blade angle $\beta_{2b} = 90^{\circ}$ at rotor inlet tantamount to fixing the degree of reaction R at 50%. It has been shown that if the values of diameter ratio d_1/d_2 vary from 0.4 to 0.6 and α_2 changes from 10° to 25°, the degree of reaction may be changed over a wide range from 0.46 to 0.68.

iv. The optimum choice of blade width to tip diameter ratio parameter b_2/d_2 would depend on the mass flow and speed. It was evident that if the mass flow and speed are to meet the design specifications set in the current research ($60\,kW$, $60000\,rpm$), the choice of b_2/d_2 is very limited. However, higher values of speed would be preferable as its effect on the b_2/d_2 ratio is hardly noticeable as shown in **Fig. 10.15**.

v. Increasing the blade angle at rotor mean exit β_1 beyond 45°, unless accompanied by corresponding increase in α_2, would produce high reaction. excessive leaving loss, and consequently low efficiency.

vi. If the maximum efficiency is less than 1.0 and it occurs when the inlet and outlet velocity triangles are right triangles, then the value of u_2/c_s at which the maximum efficiency is reached cannot be equal to 0.707.

vii. Increasing pressure ratio P_i/P_e in the radial turbine, unless accompanied by a decrease in absolute flow angle α_2 would produce a supersonic flow in the stator part of the turbine and high excessive losses.

viii. Flow coefficient c_{m1}/u_2 and blade loading coefficient ψ_{BL} depend entirely on the geometry of rotor. This thesis gives the basic equations, which may be used to obtain the desired values based on the choice of several combinations of the principle design variables. Expressing these performance parameters in terms of the geometric dimensions of the rotor will give a physical understanding of the shape of the rotor for best efficiency.

ix. The blade tip speed u_2 is increased by either increasing the pressure ratio P_i/P_e or the turbine inlet temperature T_i. Normally, the design value of u_2 is limited by the maximum permissible stress in the turbine rotor. This stress increases with the square of this speed u_2, therefore, the choice of the operating conditions P_i/P_e and T_i for an **IFR** turbine design would be, certainly, constrained by the metallurgical limit of the material.

x. An important parameter used for the design of the nozzle-less volute is the radius ratio at any azimuth angle $\bar{r}_\varphi/r_2$. The choice of $(\bar{r}_\varphi/r_2)_{\min}$ and $(\bar{r}_\varphi/r_2)_{\max}$ would normally be dictated by the tip diameter of the rotor d_2, the allowable overall size, the shape of the volute casing and the permissible absolute gas velocity in the volute.

B. Design methodology

The current research work presents the theoretical basis for a systematic approach to the design of the **IFR** turbine incorporating a nozzle-less volute casing. The sequence of operations can be given in the form of a design flow diagram as shown in **Fig. 11.1**

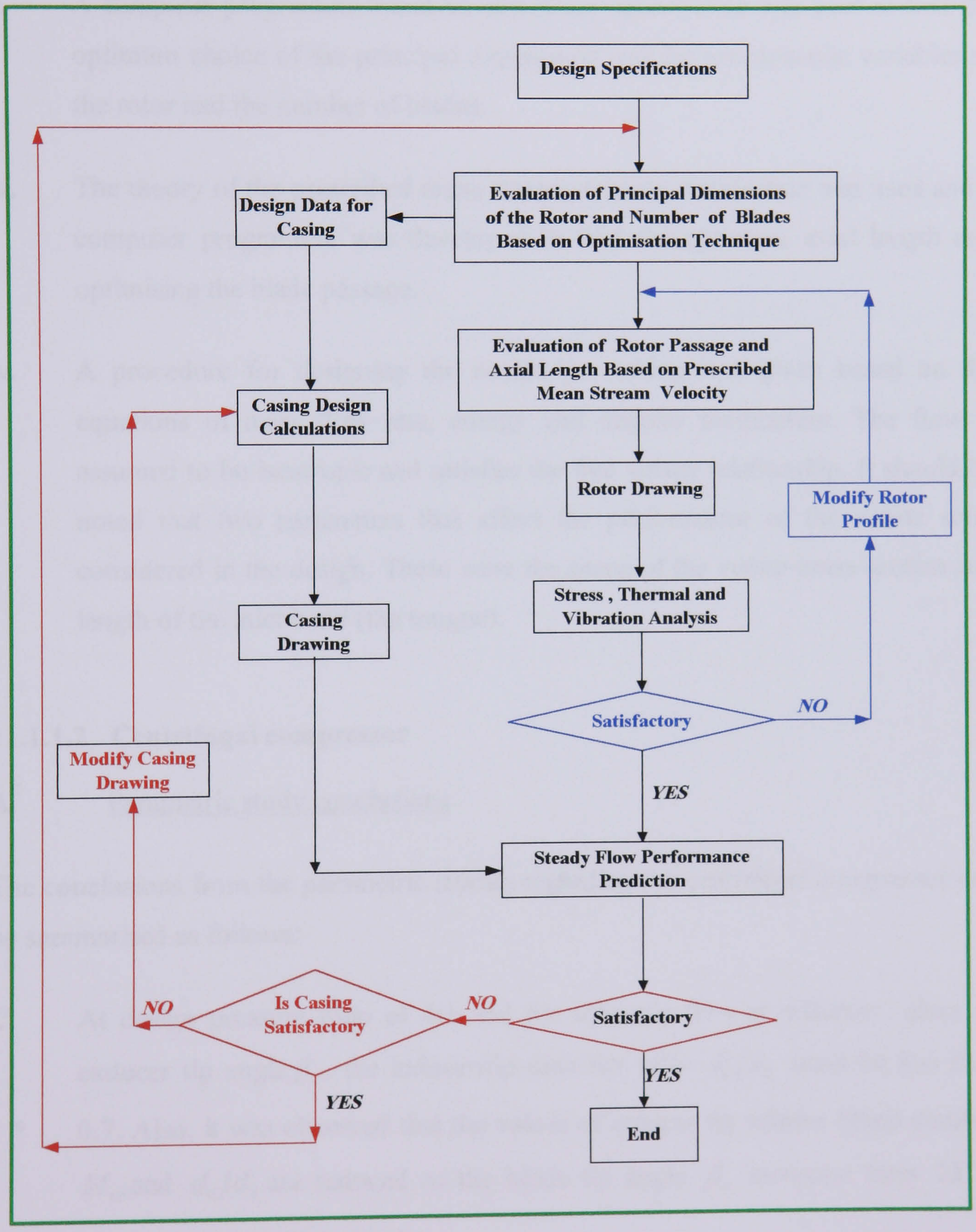

FIG. 11.1 FLOW DIAGRAM FOR A SYSTEMATIC APPROACH TO THE DESIGN OF IFR TURBINE

The concluding remarks can be summarised as follows:

i. A unified approach for designing a single stage inward flow radial turbine comprising a rotor and a nozzle-less casing has been described. The radial turbine has been designed to drive a direct-coupled permanent magnet high-speed alternator running at $60000\,rpm$ and developing $60\,kW$ electrical power.

ii. A computer programme based on non-linear optimisation was used to find the optimum choice of the principal dimensions and the aerodynamic variables of the rotor and the number of blades.

iii. The theory of the prescribed mean stream velocity distribution was used and a computer programme was developed to find the optimum axial length and optimising the blade passage.

iv. A procedure for designing the nozzle-less casing was given based on the equations of mass flow rate, energy and angular momentum. The flow is assumed to be isentropic and satisfies the free vortex relationship. It should be noted that two parameters that affect the performance of the volute were considered in the design. These were the shape of the volute cross-section and length of the inlet bend (the tongue).

11.1.1.2 Centrifugal compressor

A. Parametric study conclusions

The conclusions from the parametric studies regarding the centrifugal compressor can be summarised as follows:

i. At design pressure ratio of 4:1 and for subsonic flow at different values of exducer tip angle β_e, the inducer/tip diameter ratio d_e/d_2 must be less than 0.7. Also, it was observed that the values of inducer tip relative Mach number M_{er} and d_e/d_2 are reduced as the blade tip angle β_e increases from 25° to 40° for constant axial velocity.

ii. The optimum design value of the blade angle at inducer tip diameter β_e at several values of inducer tip relative Mach number M_{er} is always equal to 30°.

iii. At optimum $\beta_e = 30^\circ$ and for subsonic flow $M_{er} < 1.0$, the values of d_e/d_2 and d_h/d_2 must be less than 0.61 and 0.42, respectively.

iv. The choice of b_2/d_2 is governed by the leakage loss consideration on one hand and the amount of diffusion that must be achieved on the other. Smaller than permissible lower value of b_2/d_2 would lead to increased leakage loss and large value would result in unacceptable high diffusion which may produce excessive loss due to flow separation.

v. The diffusion ratio v_2/v_1 upper and lower limits were found to be 0.74 and 0.54. Separation is inevitable for v_2/v_1 less than 0.54, while values more than 0.74 would lead to higher leakage loss and hence loss in efficiency.

An optimisation programme was used to determine the principal dimensions of the impeller and the theory of prescribed mean stream velocity was used to determine the flow passage and the optimum axial length. The one-dimensional approach based on free vortex relationship was adopted for the design of the vaneless diffuser and the volute.

11.1.1.3 Mechanical Design

A. A finite element analysis package, **ANSYS**, was used to determine the combined maximum structural and thermal stresses due to the effect of centrifugal forces and elevated flow temperature for the rotor and the impeller, respectively. These analyses were necessary to select a suitable material for a safe design. Results showed that the selected materials, **Inconel alloy-718** for turbine rotor and **Titanium Ti-6AI-4V (Grade 5)** for the impeller in the design process were satisfactory and meet the design operating conditions.

ii. A displacement analysis was also carried out to find the maximum expansion in the rotor and impeller, respectively. This analysis would assist in determining

the clearances between the rotating and stator parts of the engine components.

iii. Vibration or model analysis was carried out for the rotating assembly. Since the rotating assembly reaches its operational rotational velocity from stand-still state initially, it is only natural to pass through rotational velocities corresponding to fundamental frequencies. Results showed that the rotating assembly structure's range of operating frequencies do not cross with its fundamental frequencies. Therefore, the structure is considered to be capable to safely withstand the intended working conditions, in regards to resonance.

It should be noted here that other loads including fluid flow, inertia effect due to rotation, weight effect and pre-stressing due to assembly were not included in the analysis due to the limitation ability of the software package. For such a simulation to be possible, an advanced dynamic & FEA simulation package is required.

iv. Balancing the rotor, the impeller and the shaft-bolt assembly was carried out separately and then the complete rotating assembly was balanced again and marked. The aim was to ensure safe operation during the experimental tests.

11.1.1.4 Performance prediction of the gas turbine engine

A new graphical approach for predicting the performance of the gas turbine engine at the design and off-design point was developed based on graphical matching between the turbine and the compressor. This was achieved by superimposing the turbine characteristics on the compressor characteristics with a suitable transformation of the co-ordinates. This was done by introducing a matching parameter ($\dot{m}N/d_{2C}P_{01}$) as discussed in **Chapter 8**. The end result was in developing a complete matching map characteristic for the turbine and the compressor from which the following conclusion can be deduced:-

i. The operating range of the engine and the design and off-design point performance at the design speed.

ii. Whether the engine is operating in a region of adequate compressor and turbine efficiencies.

iii. The proximity of the operating points to the compressor surge line.

iv. The maximum inlet temperature at the operating point of the turbine.

This method was applied only to a single shaft for power generation. Other engines are outside the scope of this research work.

11.1.1.5 Manufacture, construction and commission the gas turbine engine

Despite the difficulties and time limitations, the **IFR** turbine, the centrifugal compressor, the shaft assembly, the bearing housing, the combustion chamber casing, and ducting were designed and manufactured according to design specifications set by the current research. In addition to, the selection of bearings and the combustion chamber liner were also undertaken to suit the design requirements. These components were assembled together and were inspected for faults. The next step was to commission the engine to deal with any unforeseen faults in the components that may appear during the running trial. The assembly was tested/run normal air and without any combustion. The air was supplied from an existing power unit. The test/run was successful and the engine operated at $60000\,rpm$ without any problems.

11.1.1.6 Weight and size of turbine engine

The final measured weight of this engine was $45\,kg$ excluding other systems such as starting, ignition, fuel, oil lubrication and all other accessories. If theses were included, the engine weight may reach $70\,kg$. For the size consideration, the measured engine dimensions (length x width x height) were $955\times405\times656\,mm$, respectively

It is clear that two persons with out any problems can carry this engine, therefore the aim of this research of building an engine being portable has been achieved. A comparison between this engine and a conventional diesel engine driven alternators for a range of 10 to 100 kW, which are readily available in the commercial market are shown in **Figs. 11.2** and **11.3**.

It can be seen from **Figs. 11.2** and **11.3** the big difference in weight and size between this proposed gas turbine engine and the reciprocating diesel engine.

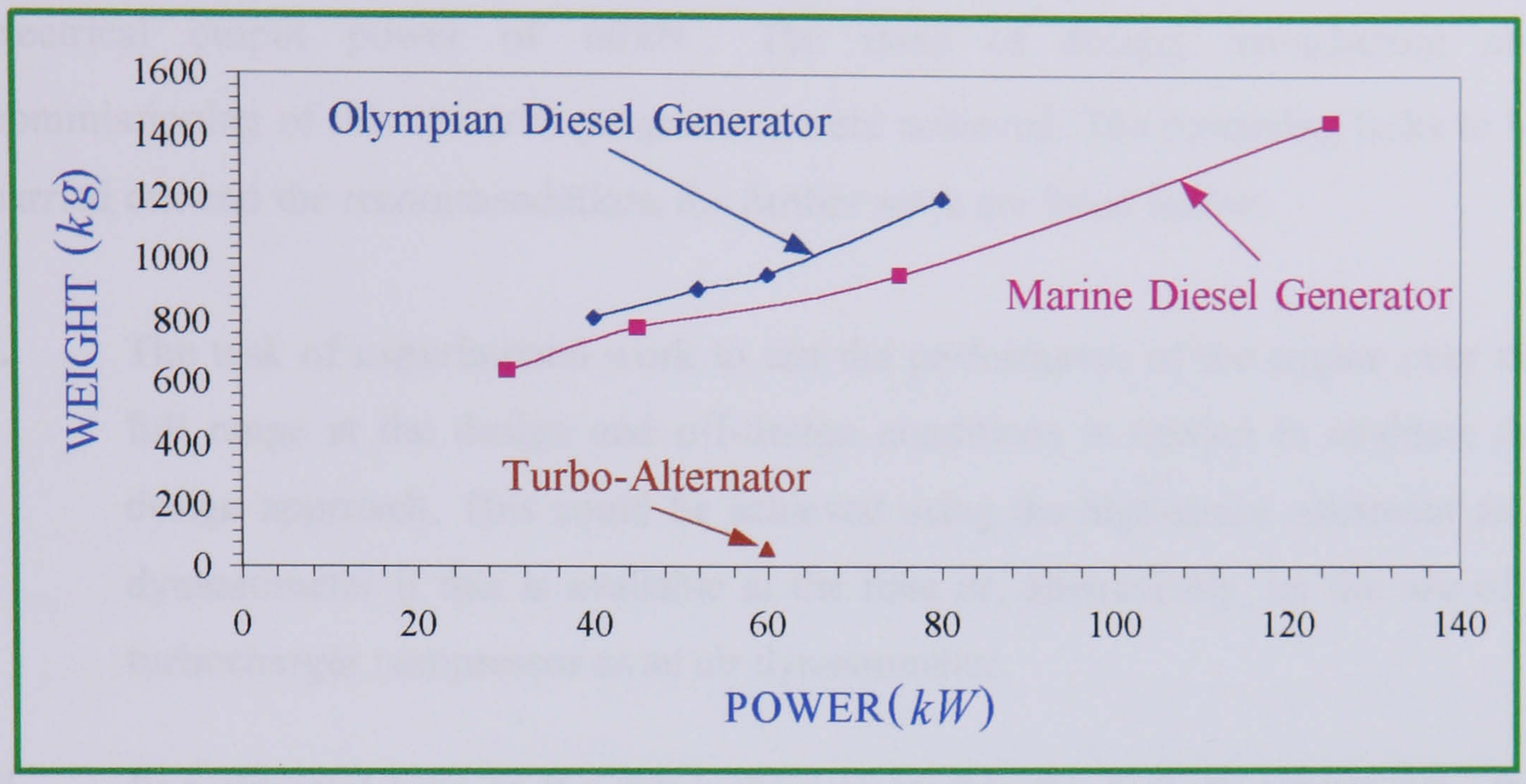

FIG 11.2 WEIGHT COMPARISON BETWEEN LOW SPEED AND HIGH-SPEED GENERATOR SETS

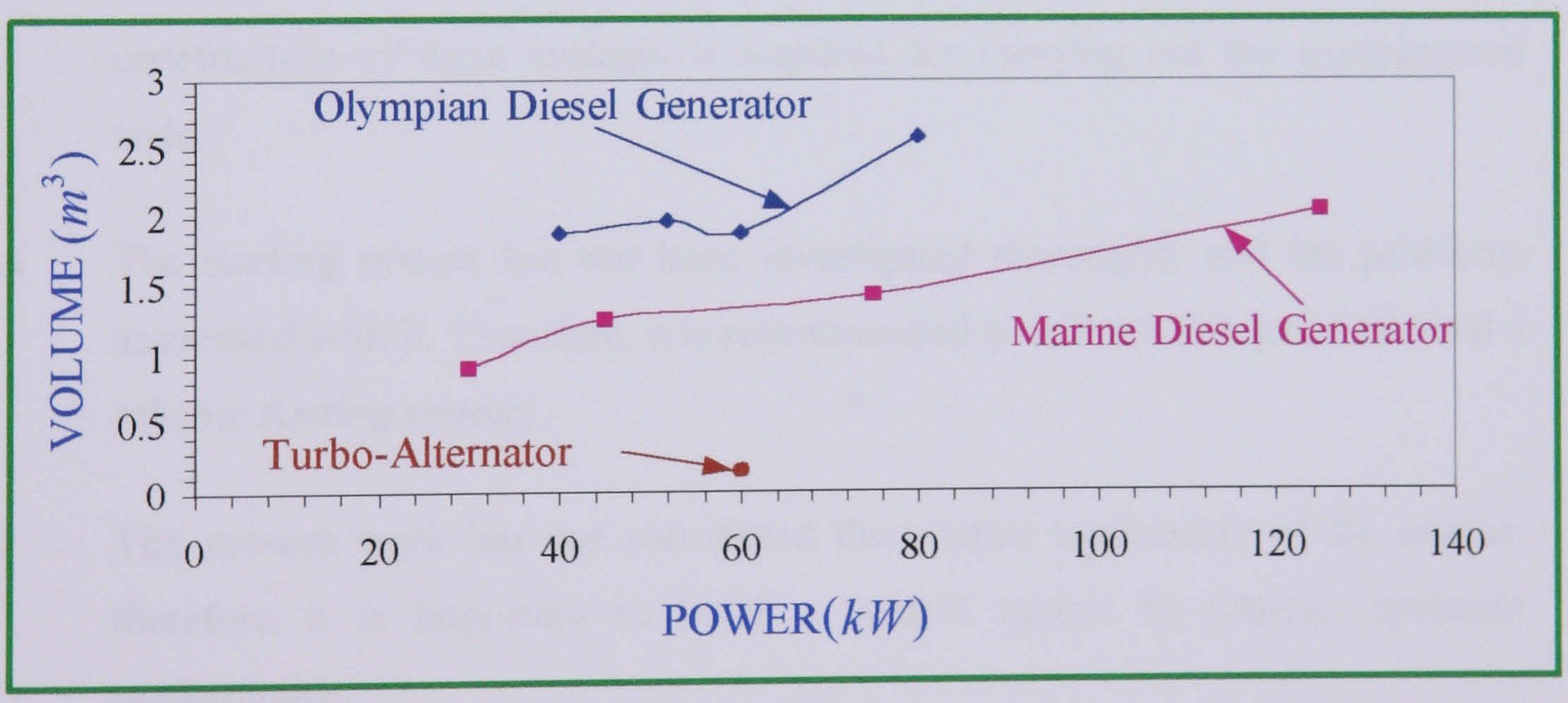

FIG. 11.3 SIZE COMPARISON BETWEEN LOW SPEED AND HIGH SPEED GENERATOR SETS

11.2 RECOMMENDATIONS FOR FURTHER WORK

It was stated before that the main objective of this research work was to design, manufacture and test a small gas turbine running at $60000\,rpm$ and developing an electrical output power of $60\,kW$. The tasks of design, manufacture and commissioning of this research programme were achieved. The remaining tasks to be carried out and the recommendations for further work are listed below:

i. The task of experimental work to test the performance of the engine over the full range at the design and off-design conditions is needed to evaluate the design approach. This could be achieved using the high-speed alternator as a dynamometer if this is available at the time or, alternatively, by the use of a turbocharger compressor as an air dynamometer.

ii. Experimental tests of the **IFR** turbine to investigate its performance over the full range and to generate the characteristics map. Similar work should be carried out for the compressor. This work is necessary to validate the matching concept proposed in the thesis.

iii. Fuel and oil lubrication systems were not completed. Therefore, a complete construction of these systems is required for carrying out the experimental tests.

iv. The starting system has not been investigated thoroughly and the problems associated with it. Therefore, it is recommended to address this area and build a reliable starting system.

v. The present work has not considered the control mechanism of the engine, therefore it is important to build a control system to achieve optimum performance.

vi. More analysis is needed to investigate the vibration, stress and thermal analysis of the complete rotating system under operating condition using advanced **ANSYS** package to ensure a safe and reliable design.

vii. The credibility of any design method stands or falls depending on the accuracy and applicability of the loss models it uses. In the procedure given in this thesis, available loss models have been adapted. Further work refining these models on the basis of more up to date data would be very useful. It should be remembered, however, that because of industrial confidentiality, reliable and detailed experimental data, from which new loss models may be derived, are very scarce.

It should be mentioned that the other research programme, the high-speed alternator, which was started at the same time likewise this research programme is progressing successfully. If both machines can be coupled directly and commissioned successfully, then this would mean reaching a significant milestone of proving the technical possibility of the device. Two very important questions, which will also be addressed in achieving this, it will be establishing the performance and the cost of the turbo-alternator. It will subsequently be possible to carry out detailed market research to determine the size of market and selling price. These parameters will decide whether large scale production is viable. It is envisaged that the turbo-alternator will not sell merely as an alternative to a diesel generator, but will create a new market in making it possible to have electrical power in situations previously not viable. Examples of this include areas affected by natural disasters such as earthquakes and floods, on board vehicles to drive motors, in rural areas with no road access.

REFERENCES AND BIBLIOGRAPHY

REFERENCES

[1] **Olympian Generator Sets.** *F. G. Wilson Engineering LTD, Church Road, Whitehouse, Newtownabbey, Belfast BT36 7LN, Northern Ireland, U.K.*

[2] **Bhinder, F. S.** " *Design parameters of centripetal turbine in non-steady flow* ". PhD thesis, King's college, London, March 1974.

[3] **Wosika, L. R.** *"Radial flow compressors and turbines for the simple small gas turbine* ". ASME, Paper No. 52-S-13, pp. 1337-1345, 1952.

[4] **Wallace, F. J.,** " *Theoretical assessment of the performance characteristics of inward radial flow turbine* ". Proceedings ImechE, pp. 931-942, 1958.

[5] **Ribaud, Y. and Mischel, C.** " *Study and experiments a small radial turbine for auxiliary power units* ". ASME, Paper No. 86-GT-23, 1986.

[6] **Rohlik, H. E.** " *Analytical determination of radial inflow turbine design geometry for maximum efficiency* ". NASA TN D-4384, 1968.

[7] **Bhinder, F. S.** " *A reappraisal of design methods for inward flow radial gas turbine* ". Israeli Journal of Technology, Vol. 10, No. 6, pp. 443-450, 1974.

[8] **Katsanis, T.** " *Use of arbitrary quasi-orthogonals for calculating flow distribution in the meridional plane of a turbo-machine* ". NASA, TN-D-2546, 1964.

[9] **Benson, R. S.** " *On - design performance characteristics of radial gas turbines* ". Israel Journal of Technology, Vol. 9, No. 4, pp 363-379, 1971.

[10] **Balje, O. E.** " *A study on design criteria and matching of turbo-machines: part A - Similarity relations and design criteria of turbines* ". T rans. ASME Journal Eng. Power, Vol. 84, No.1, 1962.

[11] **Baines, N. C.** " *The aerodynamic design of radial inflow turbines for compressible flow* ". Imperial college of science and technology, TPS/87.001, 1987.

[12] **Whitfield, A. and Baines, N. C.** " *Design of radial turbo-machines* ". Longman, Ist Edition, 44-45, 1990.

[13] **Watanabe, I. and Ando, T.** " *Experimental study on radial turbine with special reference to the influence of the number of impeller blades on the performance characteristics* ". Bulletin of JSME, Vol. 2, No. 7, pp.457-462, 1959.

[14] **Stantiz, J. D.** " *Some theoretical aerodynamic investigations of impellers in radial and mixed flow centrifugal compressors*". Transaction of ASME 74:374, 1952.

[15] **Ariga I., Watanabe, I. And Fujie, K.** " Investigation concerning flow patterns *within the impeller channels of radial inflow turbines, with some reference to the influence of the splitter vanes* ". Trans. ASME, Journal of Engineering for power, pp. 463-477, 1967.

[16] **Futral, S. M. and Wasserbauer, C. A.** " *Experimental performance evaluation of a 4.59-inch radial inflow turbine with and without splitter blades* ". NASA, TN-7015, 1970.

[17] **Takamura, T. and Nishiguchi, F.** " *Influence of blade aerodynamic loading on efficiency of radial inflow turbines* ". ASME paper, 92-GT-36, 1992.

[18] **Chen, H., Abidat, M., Baines, N. C. and Firth, M. R.** " *The effects of blade loading in radial and mixed flow turbines* ". ASME paper, 92-Gt-92, 1992.

[19] **Chen, H.** " *Design method of volute casings for turbochargers turbine applications* ". Proc.Instn.Imech Eng, Journal of power and energy, 1996.

[20] **Scrimshaw, K. H. and Williams, T. J.** " *Size effects in small radial turbine* ". ASME paper, 84-GT-215, 1984.

[21] **Whitfield, A. and Moh'd Noor, A. B.** " *A non-dimensional conceptual design procedure for the vaneless volutes of radial inflow turbines* ". ASME, Presented at the International Gas Turbine and Aeroengine Congress and Exposition, Orlando, Florida, June 3-6, 1991.

[22] **Whitfield, A. and Moh'd Noor, A. B.** " *Design and performance of vaneless volutes for radial inflow turbines* ". Part 1: non-dimensional conceptual design considerations ". Proc. ImechE, Vol. 208, pp. 199-211, 1994.

[23] **Owarish, H.** " *Design and performance of nozzle-less volute casings for inward flow radial turbine* ". PhD thesis, Hatfield Polytechnic, School of Engineering Division of Mechanical & Aeronautical Engineering, 1989.

[24] **Gaberav, A. V. and Fillipov, G. A.** " *Blade-less guide vane for centrifugal turbine* ". Translation from Russian, Foreign Technology Division, Air Force System Command, Ohio, FTD-TT/141/124, May 1961.

[25] **Hussian, M.** " *Investigation of flow in the nozzle-less volute casing of a centripetal gas turbine* ". PhD thesis, Hatfield Polytechnic, School of Engineering Division of Mechanical & Aeronautical Engineering, 1982.

[26] **Rogo, C.** " *Development of a high tip speed radial turbine system for small turbochargers* ". SAE Paper 710552, 1971.

[27] **Wislicensus, G.F.** " *Fluid mechanics of turbo-machinery* ". McGraw Hill, Book 6, New York, Vols. 1 and 2.

[28] **Kastner, L. J. and Bhinder, F. S.** " *A method for predicting the performance of a centripetal gas turbine fitted with a nozzle-less casing* ". ASME, Paper No 75- GT-65, 1975.

[29] **Benson, R. S., Cartwright, W. C. and Woollat, G.** " *Calculations of the low distribution within a radial turbine rotor* ". Thermodynamics and fluid mechanics Convention, Glasgow, 1970, Proc. I.Mech.E., Vol. 184, Pt.3G (II), 1969-1970.

[30] **Whitfield, A., MacGregor, S. A. and Mohd Noor, A. B.** " *Design and performance of vaneless volutes for radial inflow turbines; Part 2: Experimental investigation of the mean line performance-assessment of empirical design parameters* ". Proc. ImechE, Vol. 208, pp. 213-224, 1994.

[31] **Basset, R. W.** " *Pressure loss tests on a modal of a turbine volute* ". NRCC report No. MET-238, August, 1961.

[32] **Japaski, D.** " *turbocharger turbine design and development* ". Lecture B5, Lecture series on turbocharging I.C. engines, presented at the fluid dynamic Inst., Hanover, U.S.A.

[33] **Mizumachi, N., Endo, T., and Kitano, M.** " *A study of aerodynamic characteristics of rotating blades in a radial inflow turbine* ". Transaction JSMA, 1975.

[34] **Baines, N. C. and Lavy, M.** " *Flows in vaned and vaneless stators of radial inflow turbocharger turbines* ". C405/005 Turbocharging and Turbochargers, Proc. ImechE, 1990.

[35] **Balje, O. E. and Farmingdale, L. I.** " *A contribution to the problem of designing radial turbo-machines* ". Trans. ASME, May 1952.

[36] **Rodgers, C.** " *Typical performance characteristics of gas turbine radial compressors* ". Jour. Eng. Power, PP 161, April, 1964.

[37] **Ingham, D. R. and Bhinder, F. S.** " *The effect of inducer shape on the performance of high pressure ratio centrifugal compressors* ". ASME paper, No. 74-GT-122, 1974.

[38] **Stahler, A. F.** " *Transonic flow problems in centrifugal compressors* ". SAE, preprint No. 268C , Jan. 1961.

[39] **Came, P. M.** " *The development, application and experimental evaluation of a design procedure for centrifugal compressor* " I. Mech. E, Vol.192, No. 5. 1978.

[40] **Anderson, R. J, Ritter, W. K and Dildine, D. M.** " *An investigation of the effect of blade curvature on centrifugal impeller compressor* " National Advisory Committee for Aeronautics, Technical note, No. 1313, 1947.

[41] **Ingham, D. R.** " *An investigation into the effect of an inducer design on the performance of a centrifugal compressor impeller* ". PhD thesis, The Hatfield Polytechnic, July 1973.

[42] **Dean, R. C.** " *On the unresolved fluid dynamics of the centrifugal compressors* ". Presented at the Von Karman Institute, Lecture series 25, Advanced Radial Compressors, May 1970.

[43] **Lieblen, S and Johnson, I. A.** " *Resume of transonic compressor research at NASA Lewis Laboratory* ". Journal of Engineering for Power, pp 219, July 1961.

[44] **Dallenbach, Coppage *et al.*** " *Study of supersonic radial compressors for refrigeration and pressurization* ". WADC Technical Report 55-257, A.S.T.I.A document No. AD110467, Dec 1956.

[45] **Stiefel, W.** " *Experimental investigation on radial compressors to evaluate the parameters leading to a variation of the design point* ". Presented at the Von Karman Institute, March 1965. Reference VKI CN 53b.

[46] **Polikovsky, V. and Nevelson, M.** " *The performance of a vaneless diffuser fan* ". NACA. TM 1038, 1942.

[47] **Brown, W. B.** " *Friction coefficient in a vaneless diffuser* ". NACA. TN 1311,1947.

[48] **Dean, R. C. and Senoo, Y.** " *Rotating wakes in a radial vaneless diffuser* ". ASME., Series D, Sept. 1960.

[49] **Johnston, J. R. and Dean, R. C.** " *Losses in vaneless diffuser on centrifugal compressors and pumps* " Transaction ASME, Journal of engineering for power, Vol. 88, No. 1, Jan. 1966.

[50] **Anon.** " *Isuzu developing hybrid adiabatic engine* ". Japan Autotech Report, 27 Nov., pp. 52-54, 1986.

[51] **Cleland, D. L., Mcbride, G. and Tanner, R.** " *Development of an organic Rankine cycle expander for the 1-3 kW power range* ". Proc. 8th Biennial Congress of the International Solar Energy Society, pp. 1586-1591, Pergamon, 1983

[52] **Barber, R. E. and Boda, F. P.** " *Organic Rankin power conversion subsystem development for the small community solar thermal power system* ". Parabolic Dish Solar Thermal Power, Annual Program Review Proceedings, pp. 101-103, 1982.

[53] **Rodgers, C.** "*Small (10-200 kW) turbo-generator design considerations* ". ASME Cogen – Turbo, IGTI – Vol. 8, 1993.

[54] **Rodgers, C.** *"Performance development history – 10 kW Turbo-alternator* ". S.A.E, Paper No. 740849, 1974.)

[55] **Pullen, K. R.** " *The design and development of a small gas turbine and high speed generator*". PhD. Thesis, Imperial College, London University, 1991.

[56] **Mackay R. and Noe J. C.** "*High efficiency, low cost, small gas turbines* ". ASME, Cogen-Turbo IGTI-Vol. 6, 1991

[57] **Atkinson, M. J.** " *The design of efficient radial turbine for low power application*" PhD thesis, University of Sussex, school of Engineering, April 1998.

[58] **Baines, N. C.** " *New developments in radial turbine technology* " Concepts ETI, Inc. course notes, 1994a.

[59] **Biggs, M. C,** " *Recursive quadratic programming methods for non-linear constraints* ". In Powel, M. J. C., ed., " Nonlinear optimization ". 1981 (Academic press, London, 1982), pp. 213-221.

[60] **Numerical optimization centre.** " *Optima manual* ". School of Information sciences, Hatfield Polytechnic. Issue No.8, July 1989.

[61] **Biggs, M.C.,** " *Further methods for nonlinear optimization* ". Mathematics division, University of Hertfordshire, 1999.

[62] **Balje, O. E.** " *Loss and flow path studies on centrifugal compressors* ". Trans. ASME, Journal of Engineering for Power, pp 287-299, July 1970.

[63] **Johnston, J. P. and Eide, S. A.** " *Turbulent boundary layers on centrifugal compressors blades: prediction of the effects of surface curvature and rotation* ". Journal of fluid Eng., pp 374-381, Sept. 1976.

[64] **Ito, H.** " *Friction factors for turbulent flow in curved pipes* ". Trans. ASME, Journal of Basic Engineering, pp 123-133, June 1959.

[65] **Walshaw, A. C. and Jobson, D. A.** " *Mechanics of fluids* ". Third Edition Longman Group Limited, 1979.

[66] **Stodola, A.** " *Steam and gas turbine"*. Vols. I and II , McGraw-Hill, New york 1927. (Reprinted, Peter Smith, New York, 1945).

[67] **Wiesner, F. J.** " *A review of preliminary design and performance prediction techniques for centrifugal compressors. Part I: Preliminary design* ". Proceedings IME conference on development in industrial compressors, paper C390/001, 1967.

[68] **Stantiz, J. D.** " *Some theoretical aerodynamic investigations of impellers in radial and mixed flow centrifugal compressors*". Transaction of ASME 74:374, 1952.

[69] **Ferguson, T. B.** " *The centrifugal compressor stage* " . Butterwoth, London, 1963.

[70] **Fisher, F. B.** " *Development of vaned diffuser components for heavy duty diesel engine turbocharger* ". IMech.E, C108/86.

[71] **Herraty, A. G.** " *New method for the selection of rolling bearings* " . 7th Cheltenham bearing conference, 29th October 1986.

[72] **SNFA Bearing Limited.** " *Snfa general catalogue* ". Gloucestershire, England. 6th edition, 1998.

[73] **Swanson, N. S.** " *The stress analysis of a radial flow impeller* ". Australian defense scientific service note, ARL/ME 259.

[74] **Schilhansh, M. J.** " *Stress analysis of a radial flow rotor* ". Trans. ASME,series A, Vol. 84, No. 1, Jan. 1962.

[75] **Special Metals Wiggin Limited.** " *Product handbook* ", Holmer Road, Hereford, England.

[76] **Turbocam Europe,Ltd.** 23 The Apex Centre, Newgate Lane, Fareham, Hampshire, PO14 1TP, England.

[77] **Exact Engineering Company.** Kingsway South, Team Valley Trading Estate, Gateshead. Tyne & Wear, NE11 0JS, England.

[78] **Royal Scientific Society.** Al-jubaiha, P.O.Box 1438, Zip Code 11941,Amman-Jordan

[79] **University of Jordan for Science and Technology**, P.O. Box 3030, Zip Code 22110, Irbid, Jordan.

[80] **Schenck Company.** Balancing and diagnostic systems, Banbury, Oxfordshire, OX16 4TX

[81] **Hiett, G. F. and Johnston, I. H.** " *Experiments concerning the aerodynamic performance of inward radial flow turbine* ". Proc. Instn. Mech. Engrs. London, Vol. 178, Pt 3I (ii), pp. 28-42, 1964.

[82] **Hiett, G. F. and Palmer, R. M.,** " *D.I.G.T. Radial inflow turbine* ". Report No. 9-R-3, 15-R-5, 20-R-6, 1960.

[83] **Rodgers, C.** " *A diffusion factor correlation for centrifugal impeller stalling* " Jour. Eng. Power, Vol. 100, pp 592-603, Oct. 1978.

[84] **Dean, R. C.** " *The fluid dynamic of advanced centrifugal compressors* " . TN-153, Presented May 15-19 at Von Karman Institute, Brussels, Belgium, 1972.

[85] **Jamieson, A. W. H.** " *The radial turbine* ". Gas turbine principles and practice, edited by Sir H. Roxbee-Cox, chapter 9, George Newnes Ltd, London, 1955.

[86] **Glassman, A. J.,** " *Computer program for design and analysis of radial inflow turbines* ". NASA TN 8164, 1976.

[87] **Anon**. " *Conceptual design studies of a nuclear Brayton turbo alternator compressor* ". Contractor report, General Electric Company, NASA CR-113925, 1971.

[88] **Rodgers, C. and Gesier, R.** " *Performance of a high efficiency radial/axial turbine* ". Trans ASME, Journal of Turbo-machinery 109, 151-4, 1987.

[89] **Watenabi, I., Ariga, I. and Mashimo, T.** " *Effect of dimensional parameters of impellers on performance characteristics of a radial flow turbine* ". Trans. ASME, Journal of Engineering for Power, 93. pp. 81-102, Jan 1971.

[90] **Yeo, J. H. and Baines, N. C.** " *Pulsating flow behavior in a twin –entry vanleless radial inflow turbine* ". I.Mech. E., C405/004, pp 113-121, 1990.

[91] **Chen, H. and Baines, N. C.** " *Analytical optimization design of radial and mixed flow turbines* ". Proc. ImechE, Vol. 206, Part A: Journal of power and energy, pp. 177-187, 1992.

[92] **Wood, H. J.,** " *Current technology of radial inflow turbines for compressible fluids* ". Trans. ASME, Journal of Engineering for Power, Vol.85, No. 1, pp.72-83, 1963.

[93] **Watson, N. and Janota, M. S.** " *Turbocharging the internal combustion* ". Macmillan, 1982.

[94] **Rodgers, C.** " *High pressure ratio radial turbine design constraints* ". VKI Lecture series, 1987-07.

[95] **Dixon, S. L.** " *Fluid mechanics, thermodynamics of turbomachinery* ". 3rd Ed., Pergamon Press Ltd, 1978.

BIBLIOGRAPHY

[1] **Rodgers, C.** " *The performance of single shaft gas turbine load compressor auxiliary power units* ". AIAA, SAE, ASME, 19 th Joint Propulsion.

[2] **Swayer, J. W.** " *swayer's gas turbine engineering handbook* ". Second Edition, 1972.

[3] **Rodgers, C.** "*Thermo – Economics of a small 50 kW turbogenerator* ". Proceeding of 1997 the International Gas Turbine & Areo-engine Congress & Exhibition, Orlando,FL, USA. ASME. Paper No. 97–GT-260. 1997

[4] **Rodgers, C.** " *Review of mixed flow and radial turbine* ". AIAA/ SAE/ ASME/ ASEE. 26th Joint Propulsion Conference, July 16-18, Orlando, FL, 1990.

[5] **Napier, C. , Thompson , R. G. and Rodgers, C.** " *Development test status T – 100 multipurpose small power Unit* ". Gas Turbine & Aero-engine Congress & Eexposition, Toronto, Ontario, Canada, ASME, Paper No. 89-GT-117, June 4-8, 1989.

[6] **Rodgers. C.,** " *Fast start APU technology* ". SAE, Paper No. 861712, 1986. Conference, June 1983, Seattle, Washington. Paper No. AIAA-83-1159. 1983

[7] **Boyd, G. L., R. A, Kidwell and Kriener, R.** " *The AGT-101 advanced gas turbine technology update* ". ASME, Paper No. 86-GT-305, 1986.

[8] **Kidwell, J. R., Kriener, D. M. and Racey, R. A.** "*The AGT-101 advanced gas turbine technology update* ". ASME, Paper No. 84-GT-166, 1984.

[9] **Rackley, R. A. and Kidwell, J. R.** " *The AGT-101 advanced automotive gas turbine* ". ASME, Paper No. 82-GT-72, 1982

[10] **Birmann, R.** " *the elastic fluid centripetal turbine for high specific outputs* ". Trans. ASME, Feb., pp. 173-187, 1954.

[11] **Von der nuell, W. T.** " *Single stage radial turbines for gaseous substances with high rotative and low specific speed* ". Trans. ASME, pp. 499-515, 1952.

[12] **Balje, O. E.** " *A contribution to the problem of designing radial turbomachine* ". Trans. ASME, May, 1952.

[14] **Knoerschild, L.M.** " *the radial turbine for low specific speeds and low velocity factors* ". ASME, Journal of Engineering for Power, pp 1-8, 1961.

[15] **Von der nuell, W. T.** " *the radial turbine* ". High speed aerodynamics of jet propulsion, Vol. 10, ED. W. R Hawthrone, Oxford University Press, 1964.

[16] **Matsuo, E., Okazaki, N. and Nakazawa, N.** " *A development research of radial inflow turbines* ". International Gas Turbine Congress 62, Tokyo, Oct 23rd to 29th, 1983.

[17] **Wallace, F. G., Baines, N. C. and Whitfield, A.** " *A unified approach to the one-dimensional analysis and Design of radial and mixed flow turbines* ". ASME, Paper No. 76-Gt-100, 1976.

[18] **Sasaki, S., Takiazawa, N. and Mizumachi, N.** " *A development of advanced radial gas turbine for automobile* ". ASME, 1976.

[19] **Rodgers, C.** " *High pressure ratio radial turbine design constraints* ". VKI Lecture series, 1987-07.

[20] **Kofskey, M. G. and Wasserbauer, C. A.** " *Experimental evaluation of a 3.50-inch radial turbine designed for a 10-kW space power system* ". NASA TN D-3742, 1969.

[21] **Kofskey, M. G. and Holeski, D. E.** " *Cold performance evaluation of a 6.02-* inch radial inflow turbine designed for a 10- kW shaft output Brayton cycle space power generation system ". NASA TN D-2987, 1965.

[22] **Wasserbauer, C. A., Kofskey, M. G. and Nusbaum, W. J.** "*Cold performance evaluation of a 4.59-inch turbine designed for a Brayton cycle apace power system* ". NASA TN D-3260, 1966.

[23] **Futral, S. M. and Holeski, D. E.** " *Experimental performance evaluation of a 6.02 inch (15.29 cm) radial inflow turbine with an exit diffuser* ". NASA-TMX-1480, 1967.

[24] **Milton, G., Kofsky and Wasserbauer, C. A.** " *Experimental performance evaluation of a radial inflow turbine over a range of specific speed* ". NASA TN D-3742, 1966.

[25] **Bridle, E. A. and Boulter, R. A.** " *A simple theory for the prediction of losses in rotors of inward radial flow turbines* ". Proc. IMech.E, Vol. 182, Pt. 3H, pp. 393-405, 1968.

[26] **Benson, R. S., Cartwright, W. G. and Das, S. K.** " *an investigation of the losses in the rotor of a radial flow gas turbine at zero incidence under conditions of steady flow* ". Proc. IMech.E, Vol. 182, Pt. 3H, pp. 221-231.

[27] **Benson, R. S.** " *A review of methods for assessing loss coefficients in radial gas turbines* ". Int J. Mech Sci,Vol. 12, pp. 905-932, 1970.

[28] **Whitfield, A. and Wallace, F. J.** " *Study of incidence loss models in radial and mixed flow turbomachinery* ". IMech.E conference publication 3, C55/73, 1973.

[29] **Futral, S. M. and Wasserbauer, C. A.** " *Off-design performance predictions with experimental verification for a radial inflow turbine* ". NASA TN D-2621, 1965.

[30] **Watanabe, I., Ariga, I. and Fugie, K.** " *Investigations concerning flow patterns within the impeller channels of radial flow turbines, with some reference to the influence of the splitter vanes* ". ASME, Paper No. 66-WA-GT-2, 1967

[31] **Rodgers, C.** " *Efficiency and performance characteristics of radial turbines* ". SAE paper No. 660754, 1966.

[32] **Janson, W. and Qvale, E. B.** " *A rapid method for predicting the of design performance of radial inflow turbines* ". ASME paper, 67-WA/GT-3, 1967.

[33] **Mizmuachi, N.** " A *study of radial turbine* ". Report No. IP-476, Univeristy of Michicigan, 1960.

[34] **Todd, C. A and Futral, S. M.** " *A Fortran IV program to estimate the off design performance of radial inflow turbines* ". NASA TN D-5059, 1969.

[35] **Bhinder, F. S.** " *Investigation of flow in the nozzle-less spiral casing of a radial inward gas turbine* ". Thermodynamics and fluid mechanics Convention, Glasgow, Proc. IMech.E., 1969-1970, Vol. 184, Pt. 36(II).

[36] **Scholch, M.** " *A new approach to the description of the off design losses in radial inflow turbine rotors* ". ASME paper, 93-GT-105, 1992.

[37] **Dadone, A. and Pandolfi, M.** " *A method foe evaluating the off-design performance of a radial inflow turbine and comparison with experiments* ". Int. J. Mech. Science, Pergamon Press, Vol. 11, pp. 241-252, 1969.

[38] **Vavra, M. G.** " *Problems of fluid mechanics in radial turbomachines* ". Course note 55b, Von Karman Institute, 1965.

[39] **Futral, S. M. and Wasserbauer, C. A.** " *Off-design performance predictions with experimental verification for a radial inflow turbine* ". NASA, TN-2621, Feb.1965.

[40] **Nishiguchi, F., Sumi, Y. and Yamane, K.** " *Reduction in the polar moment of inertia of an automotive turbocharger by controlling aerodynamic blade loading* ". C43/82 IMech.E, 1982.

[41] **Rodgers, G. F. C. and Mayhew, Y. R.** " *Engineering thermodynamics work and heat transfer* ". Second Edition, pp 33-35, 1967.

[42] **John, C. and Chilver, A. H.** " *Strength of materials and structures* ". Second Addition, pp 278-180, 1971.

[43] **Wasserbauer, C. A. and Glassman, A. J.** " *Fortran programme for predicting off-design performance of radial flow turbines* ". NASA report TN D-8063, 1975.

[44] **Massey, B. C.** " Mechanics of fluids ". 4th Edition, 1979.

[45] **Bhinder, F. S.** "*A contribution to designing a radial flow gas turbine stage* ". ASME, Paper No, 90-GT-187, 1990.

[46] **Jawed, S. N. M.** " *Computer aided design of rotors for radial flow compressors* ". PhD thesis, The Hatfield Polytechnic, 1982.

[47] **Polikovsky, V. and Nevelson, M.** " *The performance of a vaneless diffuser fan* ". NACA. TM 1038, 1942.

[48] **Brown, W. B.** " *Friction coefficient in a vaneless diffuser* ". NACA. TN 1311,1947.

[49] **Brown, W. B. and Bradshaw, G. R.** " *Methods of designing vaneless diffusers and experimental investigation of certain undetermined parameters* ".NACA. TN 1426, 1947.

[50] **Dean, R. C. and Senoo, Y.** " *Rotating wakes in a radial vaneless diffuser* ". ASME., Series D, Sept. 1960.

[51] **Johnston, J. R. and Dean, R. C.** " *Losses in vaneless diffuser on centrifugal compressors and pumps* " Transaction ASME, Journal of engineering for power, Vol. 88, No. 1, Jan. 1966.

[52] **Ingham, D. R. and Watson, N.** " *Compressible flow in a radial vaneless diffuser* ". Symposium on internal flows, University of Salford, 1971.

[53] **Cartwright, W. G. and Lam, C. K. G.** " *The analytical design of centrifugal compressors for maximum efficiency* ". Conference on scaling for performance prediction in rotodynamic machines, IMech.E, C 189/77, 6-8 Sept 1977.

[54] **Jansen, W.** " *Rotating stall in a radial vaneless diffuser* ". Trans. ASME J. Eng. Vol. 86, pp. 750-758, New York, NY, 1964.

[55] **Roberson, J. A, and Crowe, C. T.** " *Engineering fluid mechanics* ". Sixth edition, John Wiley & Sons, Inc., 1997.

[56] **Ellison, L. F. and Partridge, J. M.** " *Van vibration in radial flow turbochargers* ". I. Mech.E. , C67/78, 1978.

[57] **Watson, N. and Janota, M. S.** " *Turbocharging the internal combustion* ". Macmillan, 1982.

[58] **Dale, A., Watson, N.** " *Vaneless radial turbocharger turbine performance* ". Turbocharging and turbochargers, I.Mech.Eng. Paper C110/86, London, 1986

[59] **Rohlik, H. E.** " *Radial inflow turbines* ". In A J (ed) Turbine design and appli cation. NASA SP 290, Vol. 3, 1975.

[60] **Japaski, D.** " *Fluid dynamic performance of turbocharger turbines* ". Course Notes, Concepts ETI, Nowrich, Connecticut, 1989.

[61] Holowenko, A. R, and Laughlin, H. G. " *Theory and problems of machine design* ". Schaum's outline series, McG-hill book, Allen S. Hall, . 1961.

[62] Kurzke, J. " *How to get component maps for aircraft gas turbine performance calculations* ". ASME paper 96-GT-164, 1996.

[63] Schlichting, H. " *Boundary layer theory* ". McGraw Hill, New York, 1955.

[64] Spannhake, W. " *Centrifugal pumps, Turbines and propellers* ". The technology Press, MIT, 1934.

[65] Shepherd, D.G. " *Principles of turbo-machinery* ". Macmillan publishing Co. INC. New York, 1659.

[66] Joned, L.D, and Dhin, A. F. " *Electric instruments and measurements* ". Second Edition, Prentice Hall International, inc, 1991.

[67] Lode, B. " *Organic Rankine cycles for waste heat recovery from diesel engines* ". Marine Engineers Review, Dec, pp. 5-12, 1982

[68] Chapple, P. M., Flynn, P. F. and Mulloy, J. M. " *Aerodynamic design of fixed geometry nozzle-less turbine casings* ". Trans. ASME, Journal for engineering and Power, Vol. 102, Jan.1980.

[69] Hussian, M., Ilyas, M. and Bhinder, F. S. " *A contribution to designing a nozzle-less volute casing for the inward flow radial gas turbine* ". I.Mech.E. Conference on Turbocharging and Turbochargers, London, , Paper C35/82, pp. 49-54, 26-28 April, 1982.

[70] Benson, R. S. " *An analysis of the losses in a radial gas turbine* ". Proc. ImechE, Vol. 180, Pt.3J, pp. 41-53, 1966.

[71] Benson, R. S. " *Prediction of performance of radial gas turbine in automotive turbochargers* ". ASME, Paper 71-GT-66, NewYork, 1976.

PUBLICATIONS

ASME PAPER

Unified Approach for Designing a Radial Flow Gas Turbine

ASME Turbo Expo Land, Sea & Air, Amsterdam, 3-6 June 2002.

Recommended for publications in either **Journal of Eng. for the gas turbines and power** or in the **Journal of Turbomachinery.**

A UNIFIED APPROACH FOR DESIGNING A RADIAL FLOW GAS TURBINE

M. S. Y Ebaid, F. S Bhinder, G. H. Khdairi and T. S. El-Hasan

ABSTRACT

Radial flow turbo machines have been used for a long time in a variety of applications such as turbochargers, cryogenics, auxiliary power units, and air conditioning of aircraft cabins. Hence numerous papers have been written on the design and performance of these machines. The only justification for yet another paper is that it would describe a unified approach for designing a single stage inward flow radial turbine comprising a rotor and the casing. The current turbine is designed to drive a direct-coupled permanent magnet high-speed alternator running at 60000 rpm and developing a maximum of 60 kW electrical power.

The freedom of choice of the tip diameter and the tip width of the rotor that would be necessary for optimum isentropic efficiency of the turbine stage was restricted by the specified rotational speed and power output. Hence, an optimisation procedure was developed to determine the principal dimension of the rotor.

The mean relative velocity in the rotor passages in the direction of the flow would be accelerated but flow velocity on the blade surfaces experiences a significant space rate of deceleration. The rate of deceleration can be controlled by means of a proper choice of the axial length of the rotor. A prescribed mean stream velocity distribution procedure was used to spread the rate of deceleration of the mean flow velocity along the meridional length of the flow passages.

The nozzle-less volute casing was designed to satisfy the mass flow rate, energy and angular momentum equations simultaneously.

This paper describes the work undertaken to design both the rotor and the casing. The work was motivated by the growing interest in developing gas turbine based hybrid power plant for road vehicles.

The authors believe that the paper would lead to a stimulating discussion.

NOTATION

A	Area normal to mean flow direction (m^2)
b	Blade width (m)
B_f	Blockage factor
C	Absolute flow velocity of gas (m/s)
C_p	Specific heat capacity at constant pressure for gas (kJ/kgK)
d	Diameter (m)
f_c	Friction factor
M	Absolute Mach number
M_r	Relative Mach number
$\dot{m}$	Mass flow rate (kg/s)
N	Rotational speed (rpm)
N_s	Specific speed
n_b	Number of blades
P	Stagnation pressure (N/m^2 , bar)
R	Degree of reaction
R_e	Reynolds number
r_c	Radius of curvature (m)
S_p	Speed parameter
S_T	Specific Torque
T	Stagnation temperature (K)
t	Blade thickness (m)
u	Rotor tip velocity (m/s)
v	Relative velocity (m/s)

W Work output (kJ)
z Axial length (m)

Greek symbols

α Absolute flow angle relative to axial direction (degree), angle between meridional streamline and axis
β Relative flow angle relative to axial direction (degree), angle between relative velocity vector and meridional plane
β_b Blade angle
θ Relative angular co-ordinate
γ Ratio of specific heats
η Efficiency of a process
ρ Gas density (kg/m^3)
ψ Blade loading
ϕ Pressure loss coefficient
φ Centroid
ω Angular velocity (rad/s)
Δ Small increment of

Subscripts

0 Stagnation conditions
3 Turbine station
2 Rotor inlet station
1 Rotor outlet station at mean
a Air
av Average
c Compressor
e Exit condition, exducer
h Hub
i Inlet condition
m Mean
s Spouting velocity, shroud
SFL Skin friction loss
t Turbine
tt Total to total
w Tangential direction
rms Root mean square
r Radial direction
x Any station inside the rotor passage

INTRODUCTION

Inward flow radial turbines have established their place in industrial applications, especially in the field of small turbo-machinery because of their simplicity, reliability, low emissions, multi-fuel capabilities and fast response. These attractive features have made them ideal prime movers for many applications, particularly for producing small electrical power, typically in the range of 10-100 kW.

Research programmes regarding the design of these machines have been cited in the open literature. For the rotor design, both **Von der Nuell [1] and Balje [2,3]** suggested that the choice of the principal dimensions might be based on specific speed and specific diameter. **Rohlik [4]** developed a relationship between specific speed and a number of important design ratio. He argued that for the same specific speed, it was possible to produce a large number of rotor shapes by choosing different combination of these ratios. Therefore, the problem was to determine specific speed that would result in maximum efficiency.

Wallace *et al.* [5] used one-dimensional analysis together with empirical loss models to determine the principal dimensions of the rotor. Further studies on one-dimensional design analysis procedures have been described also by other authors, **Rodgers [6], Whitfield and Baines [7] and Wasserbauer and Glassman [8].** The common features of these studies are that the user has to specify the geometry of the turbine, together with any assumptions about losses from which to calculate efficiency values. Since most of the turbine geometry is likely to be undefined and many different assumptions about losses are possible, a large combinations are possible and must be investigated. This is time consuming therefore, there is a great incentive to reduce the time taken and the number of cases to be investigated. **Whitfield [9]** proposed a method based on maximizing efficiency by minimizing the energy losses of the fluid which are considered to be a function of the square of the velocity and expressed at inlet and outlet conditions in terms of Mach numbers. The procedure is largely non–dimensional and it is based on an initial power ratio and an estimate of the total to static efficiency. The later in particular can cause problems, because the designer has still to decide on the likely magnitude of the efficiency that can be achieved.

In recent years, a number of computer aided design procedures have been developed for turbine rotors. **Benson and Fisher [10] and Baines *et al.* [11]** in their work assumed a preliminary shape, which would be improved progressively through analysis. This work is an indirect mode and the main draw back of this approach is that a decision on whether or not a particular step produces a satisfactory result tends to be made quite arbitrarily. Furthermore, it is not a simple matter to determine what changes in the geometry would produce the desired results.

The turbine casing design is often based on the assumptions of an adiabatic incompressible flow, together with a free vortex distribution about the rotor. The passage design is specified in terms of area to radius ratio at the centroid as described by **Bhinder [12], Chapple *et al* [13], Hussian *et al* [14]**. **Whitfield and Noor [15]** extended the work further by considering the flow to be viscous and compressible.

From the foregoing introduction, several limitations to these procedures can be identified which deserve attention:

(1) Most of the design methodologies were based on iterative procedures involving successive modifications to the hub, shroud and blade profiles to arrive at an acceptable and efficient design.

(2) For a given set of performance requirements such as power output, pressure ratio and rotational speed or mass flow parameter, several rotor shapes may be drawn which would appear to meet the specifications. The choice of optimum shape is by no means simple.

(3) The choice of number of rotor blades was based on empirical formulae given in the open literature and the choice of axial length was made arbitrarily based on known engineering practice.

(4) Papers describing the whole design of the rotor and the casing were scarce for a specific rotational speed and power intended for the current design.

This paper provides a unified approach for designing radial flow gas turbines, which, it is claimed, does not suffer from the above limitations.

PROPOSED DESIGN PROCEDURE

The design procedure of an inward flow radial (IFR) turbine was divided into the following two stages:

(1) The design of the turbine rotor for which the design methodology consists of two main procedures: Firstly, the determination of the optimum principal dimensions and number of blades of the turbine rotor. Secondly, the optimisation of axial length and passage geometry for a prescribed or assumed mean-stream velocity.

(2) The design of the nozzle-less volute casing for which the mass flow rate, energy and angular momentum equations must be satisfied simultaneously.

ROTOR DESIGN

The choice of the principal dimensions of the rotor.

The geometrical shape of a typical IFR turbine rotor is shown in Fig.1. The inlet and outlet velocity diagrams and the thermodynamics of the expansion process are illustrated in Figs. 2 and 3, respectively.

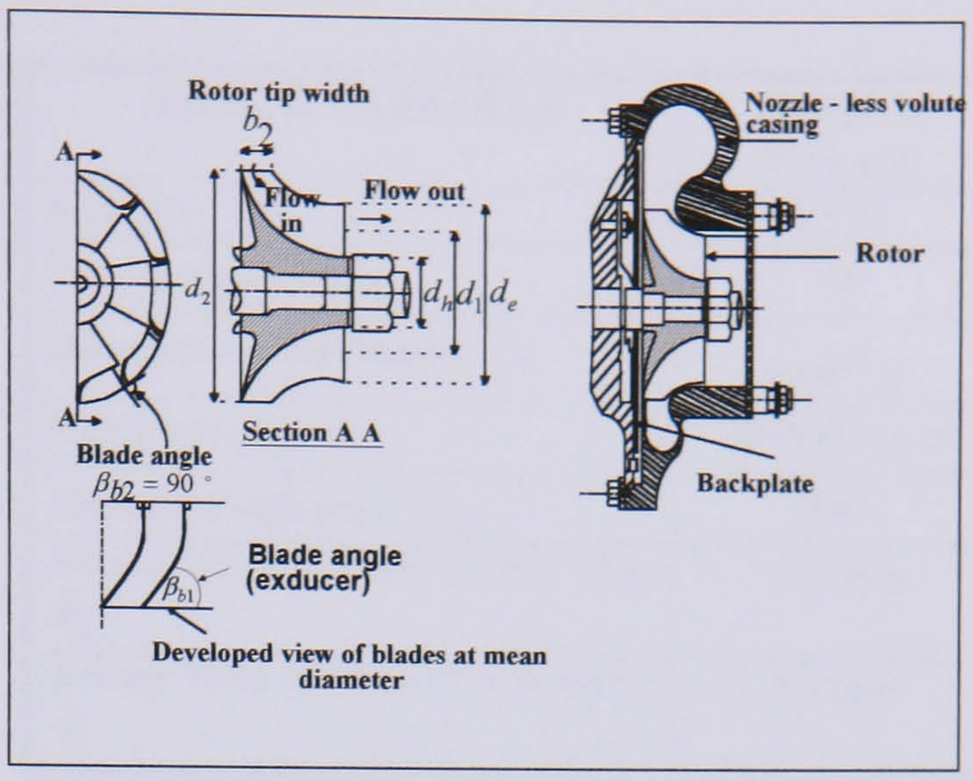

Fig.1 The geometrical shape and the principal dimensions of the IFR gas turbine

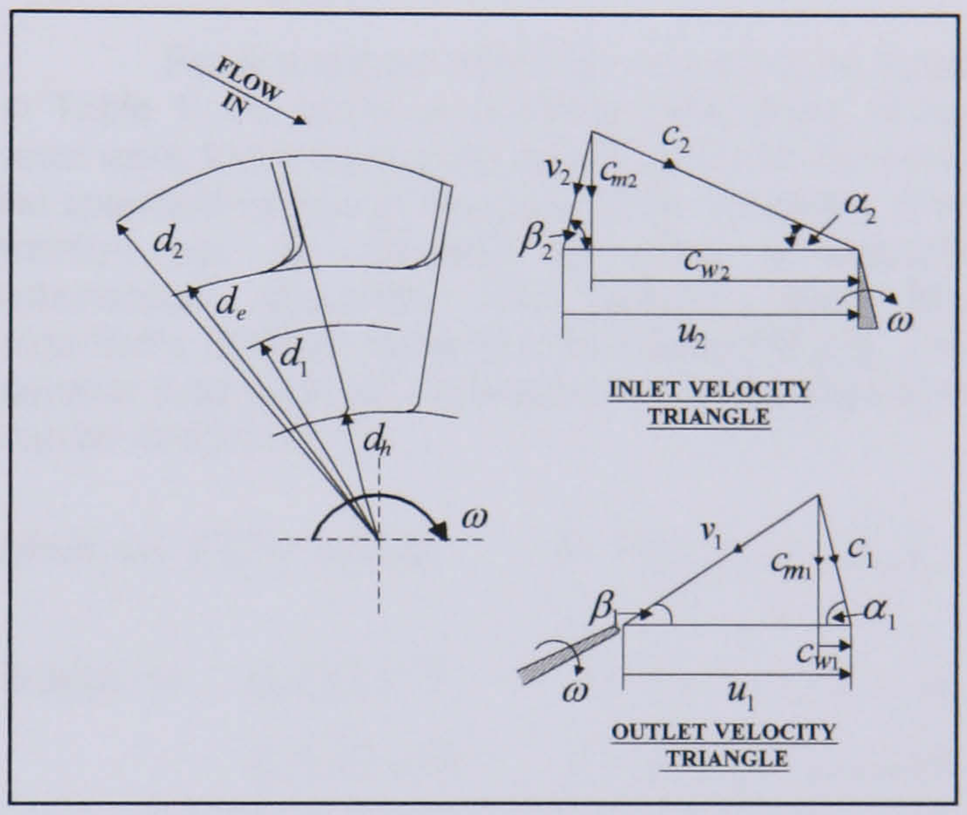

Fig.2 Velocity triangles of an inward flow radial gas turbine

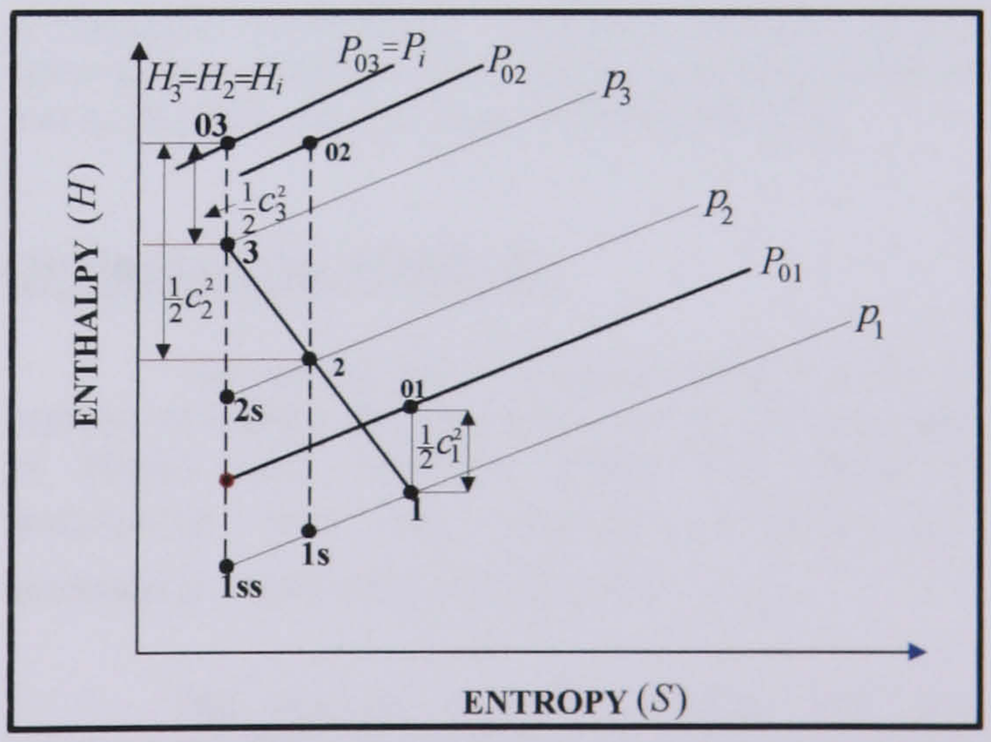

Fig. 3 Enthalpy – entropy diagram for a turbine stage

The momentum, continuity and energy equations can be combined to produce the following principal equations:

(1) Speed parameter

$$\frac{d_2 N}{\sqrt{C_p T_i}} = \left(\frac{60\sqrt{2}}{\pi}\right)\cdot\left(\frac{u_2}{c_s}\right)\cdot\left[\sqrt{1-\left(\frac{P_e}{P_i}\right)^{\gamma-1/\gamma}}\right] \quad (1)$$

(2) Absoluter flow angle at rotor inlet

$$\cos\alpha_2 = \left(\frac{c_{w2}}{u_2}\right)\cdot\left(\frac{\pi}{60}\right)\cdot\left(\frac{d_2 N}{\sqrt{C_p T_i}}\right)\cdot\left(\sqrt{\frac{1+\frac{\gamma-1}{2}M_2^{\,2}}{(\gamma-1)M_2^{\,2}}}\right) \quad (2)$$

(3) Blade width to tip diameter ratio

$$\left(\frac{b_2}{d_2}\right) = \frac{\dot{m}\sqrt{C_p T_i}}{d_2^{\,2} P_i}\left[\frac{1}{\pi B_{f_2}}\left(\frac{\sqrt{\gamma-1}}{\gamma}\right)\right]\left[\frac{\left(1+\frac{\gamma-1}{2}M_2^{\,2}\right)^{\gamma+1/2(\gamma-1)}}{M_2\sin\alpha_2}\right] \quad (3)$$

(4) Mass flow parameter

$$\frac{\dot{m}\sqrt{C_p T_i}}{d_2^{\,2} P_i} = \left(\frac{P_e}{P_i}\right)\cdot\left[\frac{1}{\left\{1-\eta_{tt}\left(1-\left(\frac{P_e}{P_i}\right)^{\gamma-1/\gamma}\right)\right\}}\right]^{1/2} x \quad (4)$$

$$\left[B_f\left(\frac{\pi}{4}\right)\left(\frac{\gamma}{\sqrt{\gamma-1}}\right)\cdot\left(\left(\frac{d_e}{d_2}\right)^2-\left(\frac{d_h}{d_2}\right)^2\right)\right] x$$

$$\left[\frac{M_{er}\sin\beta_e}{\left(1+\left(\frac{\gamma-1}{2}\right)(M_{er}\sin\beta_e)^2\right)^{\gamma+1/2(\gamma-1)}}\right]$$

$$B_{f_2} = 1-\frac{1}{\pi}\left[n\left(\frac{\bar{t}_2}{d_2}\right)\right] \quad (5)$$

$$B_{f_1} = \frac{2}{\pi}\frac{n(\bar{t}_1/d_2)}{\left[(d_e/d_2)+(d_h/d_2)\right]} \quad (6)$$

DESIGN VARIABLE	DESIGN VALUE
Mass flow, $\dot{m}$	0.572
Pressure ratio, P_i/P_e	3.6
Inlet stagnation temperature, T_i	$1000^\circ K$
Rotational speed, N	60,000 $r.p.m$
Total to total efficiency, η_{tt}	0.87
Average blade thickness at rotor inlet, $\bar{t}_2$	2.5 mm
Average blade thickness at rotor outlet, $\bar{t}_1$	1.5 mm

Table 1 Input data at design point

For a given set of design condtions as listed in Table 1, the optimum principal dimensions of the rotor were found by solving equations (1) to (6) within the specified ranges of the constraints variables. The solution can be obtained by using a suitable optimisation algorithm. The authors used the algorthims OPRQP developed by **Biggs [16,17]**. The general mathematical representation of the algorithm can be described as:

Minimise $F(\bar{x})$, where $\bar{x} = [x_1, \ldots\ldots x_n]^t$

Subject to: $g_i(\bar{x}) = 0 \qquad i = 1, \ldots\ldots q$

$g_j(\bar{x}) \geq 0 \qquad j = q+1, \ldots\ldots m$

Where $F(\bar{x})$ represents the objective function, in this case is the inlet tip diameter d_2 and the functions $g_i(\bar{x})$ and $g_j(\bar{x})$ are sets of equality and inequality constraints, respectively. Providing detailes of the optimisation program used are beyond the scope of this paper, but may be found in **Refs. [16,17]**.

OPTIMIZATION RESULTS

The optimization program was run for a number of blades ranging from 12 to 20. The number of blades was specified within this range in accordance with the assumed efficiency η_{tt}, blockage B_f and blade loading factor c_{w2}/u_2.

The results indicated clearly that the optimum number of blades lies in the range between 12 and 20. Consequently, any blade number in this range would be acceptable provided it satisfies the other design criteria and specifications set by the designer. The design velocity diagrams based on optimization technique and the complete design data are shown in Fig. 4 Table 2 and Table 3, respectively.

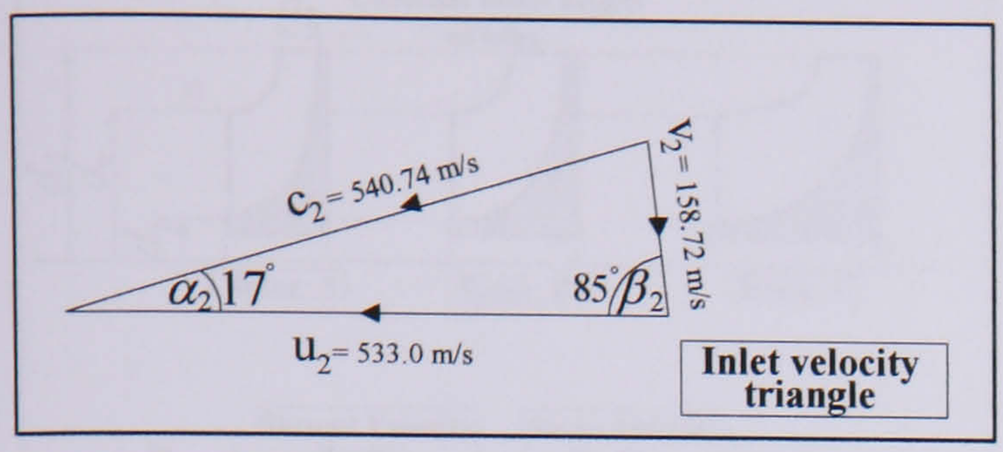

Fig. 4 Velocity triangle based on numerical Optimization program

DESIGN SPECIFICATIONS	GEOMETRICAL DIMENSIONS
$W_{net} = 60\,kW$	$d_2 = 16.91\,cm$
$N = 60000\,r.p.m$	$b_2 = 0.87\,cm$
$P_i/P_e = 4.0$	$\bar{t}_2 = 0.25\,cm$
$T_i = 1000\,K$	$d_1 = 9.30\,cm$
$u_2/c_S = 0.67$	$d_h = 6.09\,cm$
	$d_e = 11.67\,cm$
	$\bar{t}_1 = 0.15\,cm$
FLOW ANGLES AT ROTOR INLET AND EXIT	**MACH NUMBERS AT ROTOR INLET AND EXIT**
$\alpha_2 = 17.0°$	$M_2 = 0.93$
$\beta_2 = 84.2°$	$M_1 = 0.35$
$\alpha_1 = 90°$	$M_{hr} = 0.50$
$\alpha_h = 90°$	$M_{1r} = 0.65$
$\alpha_e = 90°$	$M_{er} = 0.8$
$\beta_h = 44.32°$	
$\beta_1 = 32.59°$	
$\beta_e = 27.0°$	

TABLE 3 Design data (2) for the turbine rotor based on numerical optimization

FLOW VELOCITIES AT ROTOR INLET	FLOW VELOCITIES AT ROTOR EXIT
$c_2 = 538.82\,m/s$	$c_1 = 186.77\,m/s$
$v_2 = 158.13\,m/s$	$c_{w2} = 0.0\,m/s$
$c_{m2} = 157.34\,m/s$	$c_h = 186.77\,m/s$
$c_{w2} = 515.11\,m/s$	$c_e = 186.77\,m/s$
	$v_1 = 346.77\,m/s$
	$v_h = 267.32\,m/s$
	$v_e = 411.39\,m/s$
ROTOR SPEED AT ROTOR INLET AND EXIT	**PERFORMANCE PARAMETERS**
$u_2 = 531.24\,m/s$	$\dot{m} = 0.574$
$u_1 = 292.18\,m/s$	$S_P = 0.157$
$u_h = 191.25\,m/s$	$S_T = 0.24$
$u_e = 366.55\,m/s$	$\eta_{tt} = 0.87$
	$R = 0.56$
	$c_{m1}/u_2 = 0.32$
	$N_s = 0.56$

TABLE 2 Design data (1) for the turbine rotor based on numerical optimization

Optimization of passage geometry and the choice of axial length

The choice of a suitable axial length is almost a pre-requisite for completely defining the passage geometry. The effect of the axial length on velocity distribution is shown qualitatively in Fig. 5. It can be seen that the shortest channel length of rotor (A) should produce minimum friction loss, but the flow would separate due to high deceleration rate in the exducer section. In contrast, rotor (C), which has the longest channel, would be expected to produce highest friction loss, but flow separation would be delayed due to the gradual deceleration rate in the exducer.

Following this, a prescribed mean stream velocity distribution approach was used to optimize the passage geometry and the axial length of the rotor.

The relative velocity vector $\overline{V}$ at any point inside the turbine rotor passage, as shown in Fig. 6, can be resolved into three basic components along the axial, radial and tangential directions, $\overline{V}_z$, $\overline{V}_r$ $\overline{V}_w$,... Here $\overline{V}_m$ is the velocity vector along the mean streamline in the hub-to-shroud plane, hence:

$$\overline{V} = \overline{V}_z + \overline{V}_r + \overline{V}_w \qquad (7)$$

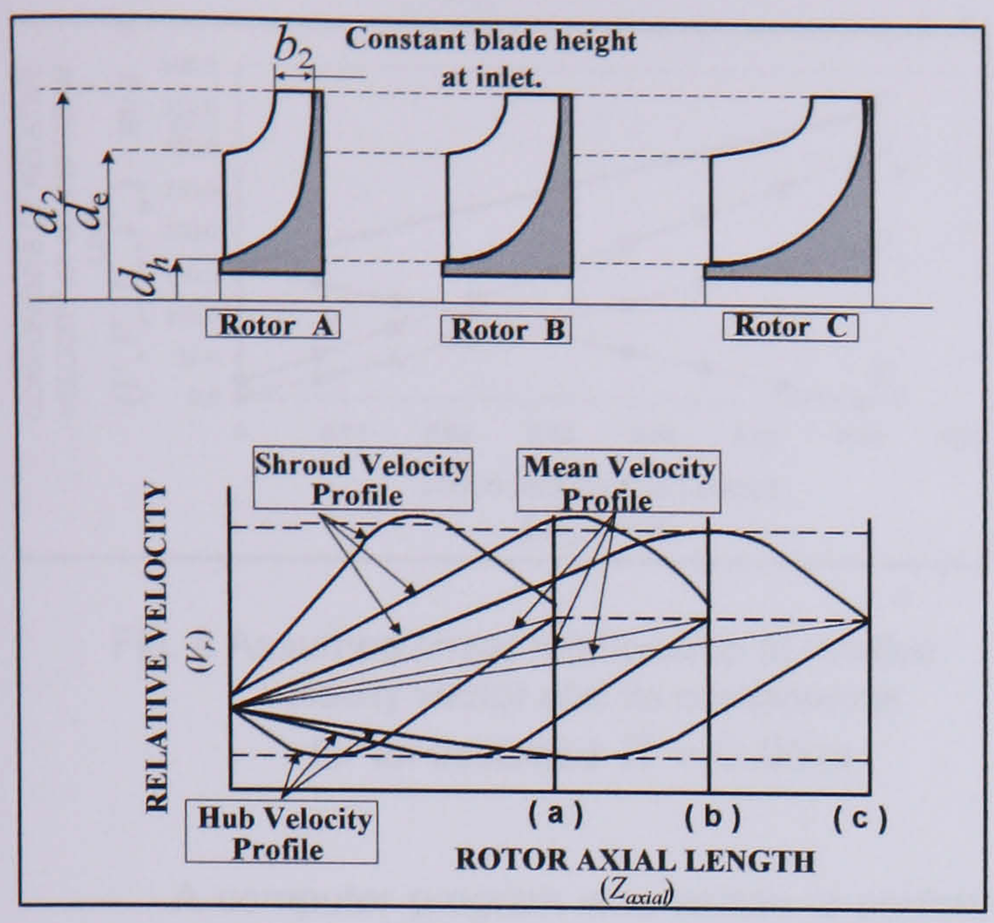

Fig 5 Qualitative description of the effect of axial length on velocity distribution

The boundary values of the components of the relative velocity are known from the inlet and outlet velocity triangles, which resulted from the previous optimisation as shown in Fig. 6.:

At rotor inlet: $V_z = 0$,

$V_r = (V_r)_{\max}$ and $V_w = (1-\psi)U_2$

At rotor outlet: $V_z = (V_z)_{\max}$, $V_r = 0$ and

$V_w = V_2 \sin\beta_1$

The angles shown in Fig. 6 can be expressed in terms of the velocities as shown below:

$$\beta = \sin^{-1}\sqrt{1 - V_m^{\,2}/V}\ ,\ \tan\theta = \frac{V_z}{V_w} \text{ and } \cos\alpha = \frac{V_z}{V_w}$$

By combining the above relationships, the angles (α, β and θ) are related to each other by the following relationship:

$$\tan\beta = \tan\theta\cos\alpha \qquad (8)$$

The spatial description of the mean streamline can be found iteratively by assuming a starting value for the meridional length z_m, and the distributions of the relative velocity vector.

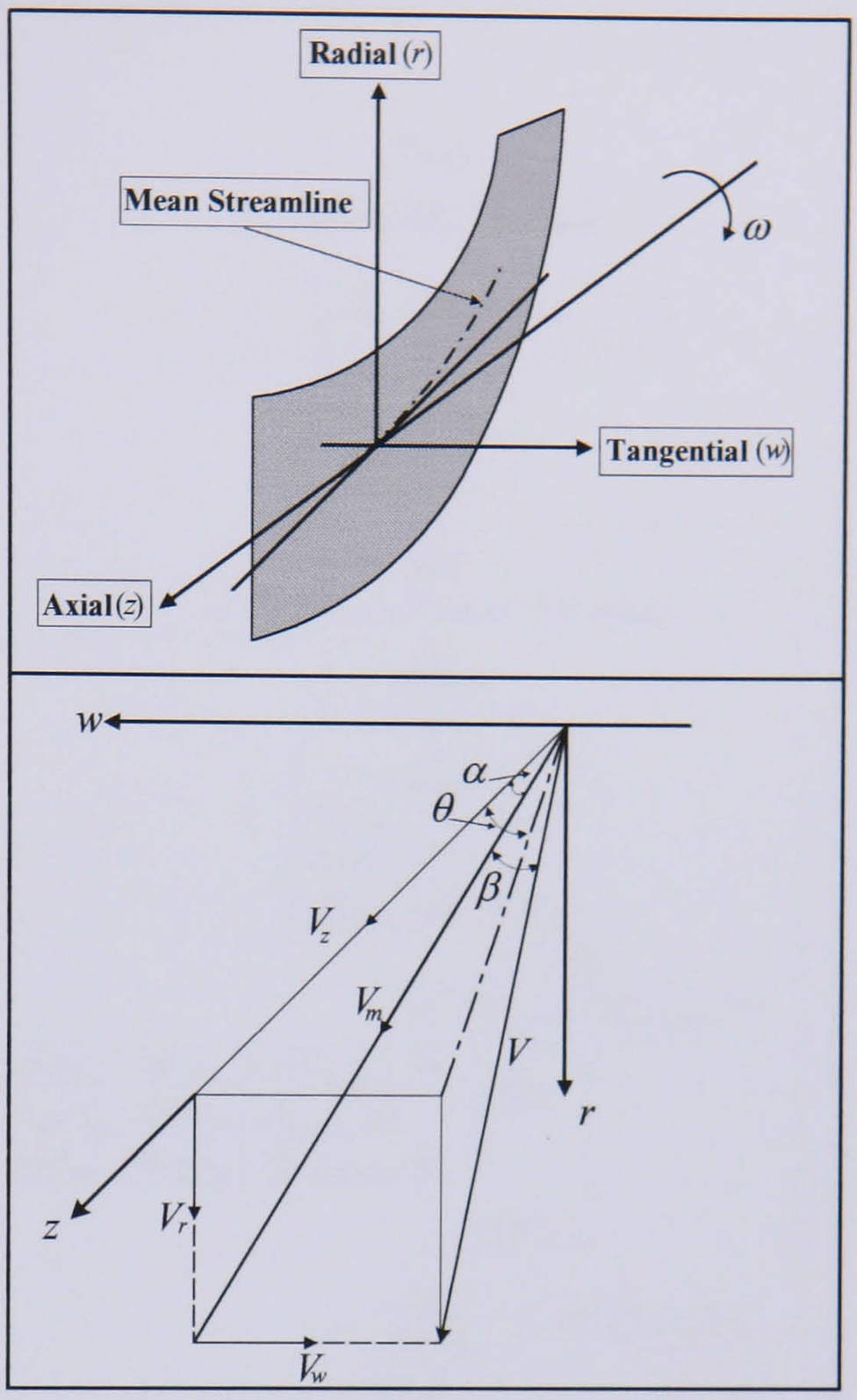

Fig. 6 Notation for the relative velocity vector and its components

Figure 7 shows three meridional lengths $0.02, 0.04$ and 0.06 of the turbine rotor. Fig. 8 describes the velocity components V_r, V_z and V_w for one assumed value of Z. At the start, all these figures are based on the assumption that the variation of the relative velocity vector (V) is linear.

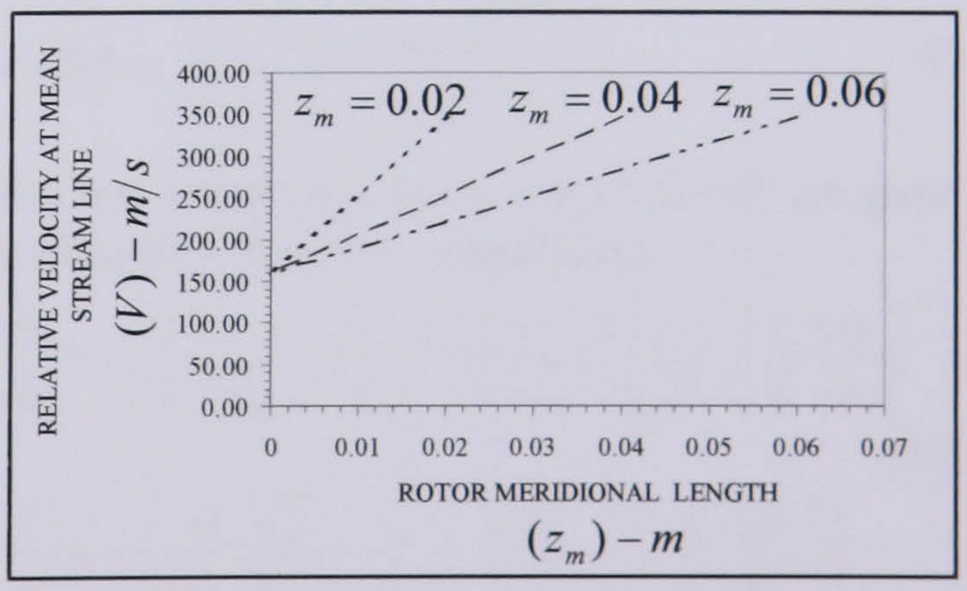

Fig. 7 Assumed variation of the relative velocity vector at various meridional lengths for the same boundary conditions

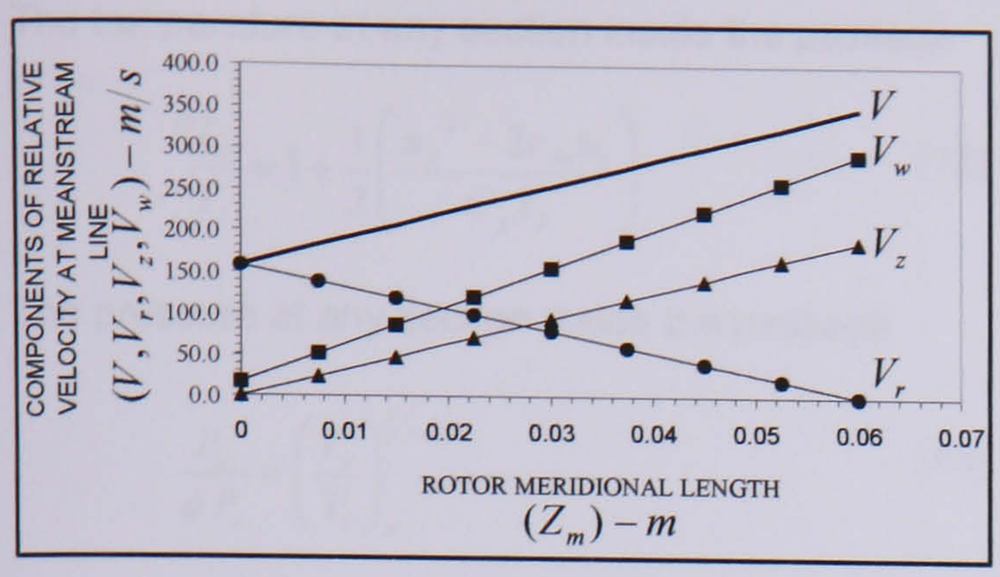

Fig. 8 Assumed linear relationship of relative velocity vector and its components for an assumed $Z = 0.06m$

A computer program was written to perform the iterative calculations to check this linear relationship variation of relative velocity vector along the mean streamline. The output results are plotted in Fig. 9 and a flow chart based on this program is shown in Fig. 10.

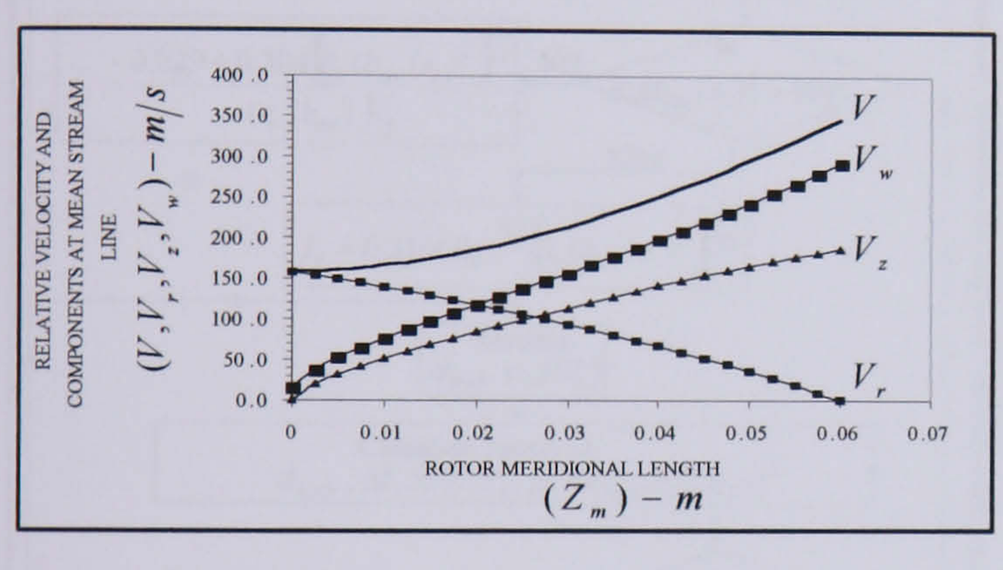

Fig. 9 Prescribed relative velocity distribution along mean streamline for an assumed meridianal length of $0.06\,m$

The next step was to optimize the axial length (Z) by minimizing the loss of stagnation pressure in the flow channels. For this purpose, the losses were expressed as functions of the resultant velocity (V), the length of the channel, and the radius of curvature r_c.

Several models are available in the published literature **Dallenbach [18] and Rodgers [19]** which take account of the losses. These loss models were adopted for the turbine rotor. A detailed review of these loss models is outside the scope of this paper, but it should be mentioned that any loss models might be integrated into the program as sub-routine. A computer program was written to optimize the axial length and the flow passage based on the relations listed here.

Here the radius r of the mean streamline in the meridional plane can be represented using Lame' ovals relationship as:

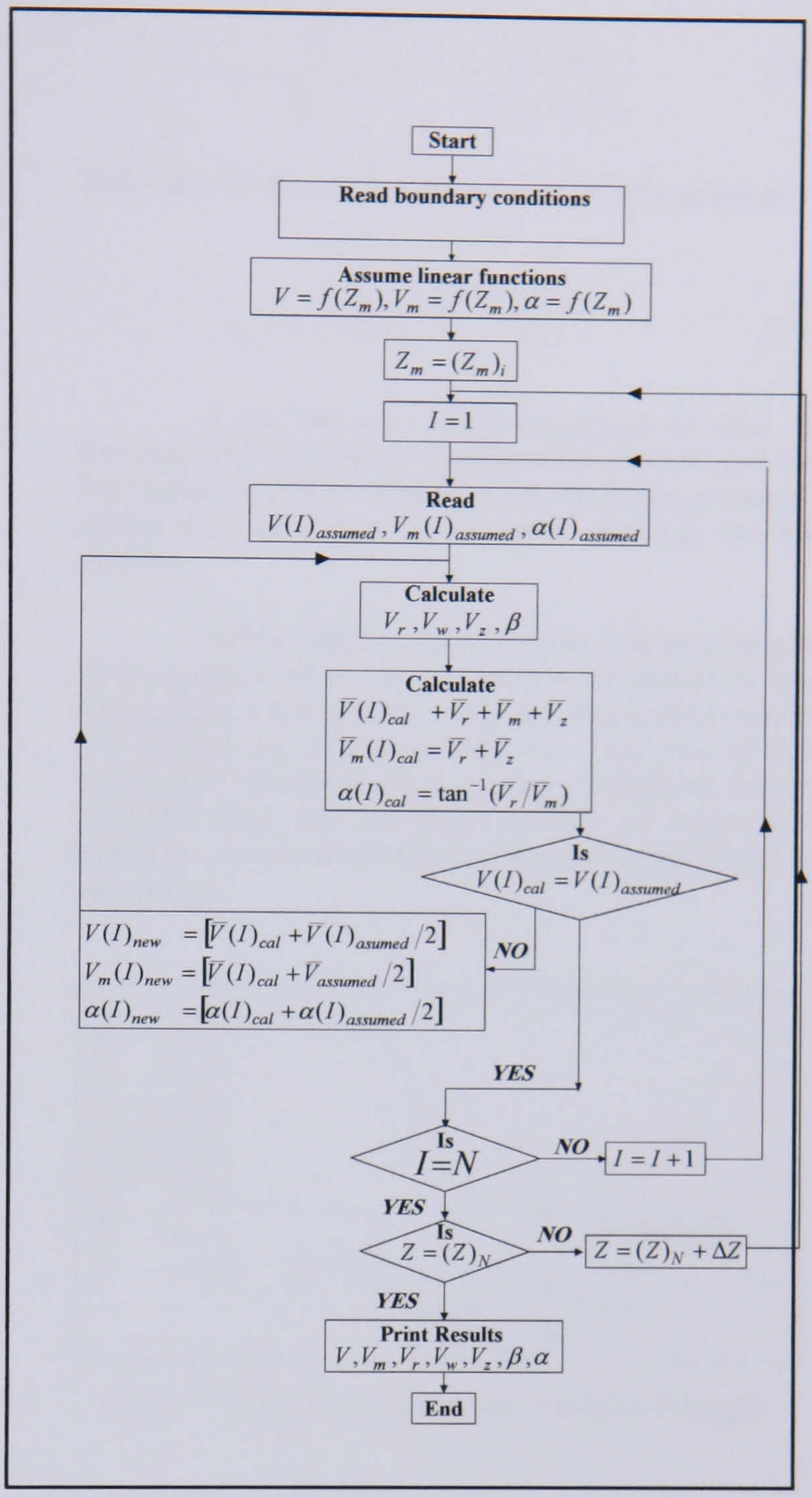

Fig. 10 Flow chart for relative velocity vector variation along mean streamline

$$r = (r - r_2)\left[1 - \left(\frac{z_m - z_{m1}}{z_{m2} - z_{m1}}\right)^3\right]^{1/2} + r_2 \tag{9}$$

The first and second derivatives of dr/dz are given in equations 10 and 11, respectively:

$$\frac{dr}{dz} = -\left[\frac{3}{2}\right]\left(\frac{r_1 - r_2}{z_{m2} - z_{m1}}\right)\frac{l}{j}\left(\frac{z_m - z_{m1}}{z_{m2} - z_{m1}}\right)^2\left(\frac{r - r_2}{r_1 - r_2}\right)^{-1} \tag{10}$$

$$\frac{d^2 r}{dz_m^{\,2}} = \left[\frac{dr}{dz_m}\right]\left[\left(\frac{2}{z_m - z_{m1}}\right) + \left(\frac{-1}{r - r_2}\right)\left(\frac{dr}{dz_m}\right)\right] \tag{11}$$

The length of the streamline is given by:

$$L = \int_{z_{m1}}^{z_{m2}} \left(1 + \frac{dr}{dz_m}\right) dz_m \tag{12}$$

The temperature at any section inside the passage

$$\frac{T_x}{T_i} = 1 + \frac{1}{2}\left(\frac{u_x{}^2 - 2c_{wi}u_i}{C_p T_i}\right) \tag{13}$$

The pressure at any section inside the passage

$$\frac{P_x}{\phi P_i} = \left(\frac{T_x}{T_i}\right)_s^{\gamma/\gamma-1} \tag{14}$$

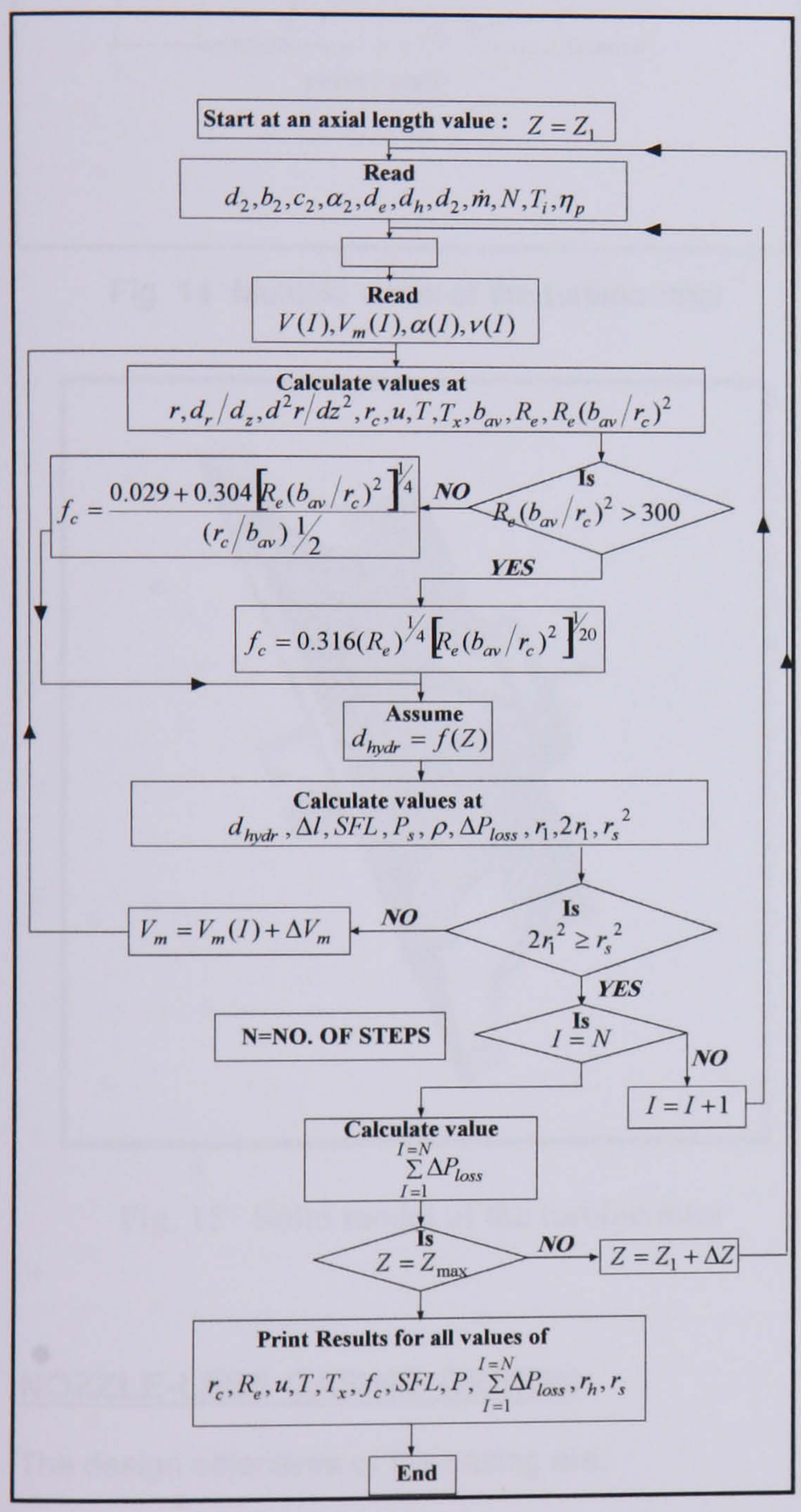

Fig. 11 Flow chart for the design of the flow passage and the optimization of the meridional length

The density at any section inside the passage

$$\rho_x = \left(1 - \frac{v_x{}^2}{2C_p T_x}\right)^{1/\gamma-1}\left(\frac{P_x}{RT_x}\right) \tag{15}$$

The shroud contours at any section inside the passage

$$r_{sx} = \sqrt{(r_{rms}{}^2)_x + \frac{1}{2}\frac{\dot{m}\cos\alpha_x}{\pi\rho_x v_{mx} B_{fx}}} \tag{16}$$

The hub contours at any section inside the passage

$$r_{hx} = \sqrt{(2r_{rms}{}^2)_x - r_{sx}{}^2} \tag{17}$$

It can be seen from Equations 16 and 17 that they can be used to calculate the shroud and the hub contours at any section inside the blade passage, hence the final shape of the blade passage can be defined.

A flow diagram for optimising the axial length of the turbine rotor and the optimised design of the flow passage are shown in Fig. 11. The output results are plotted as shown in Fig. 12. The plot of the stagnation pressure loss vs. the meridional length indicates that the minimum losses of stagnation pressure occurs when the meridional length equal to $40.0\,mm$.

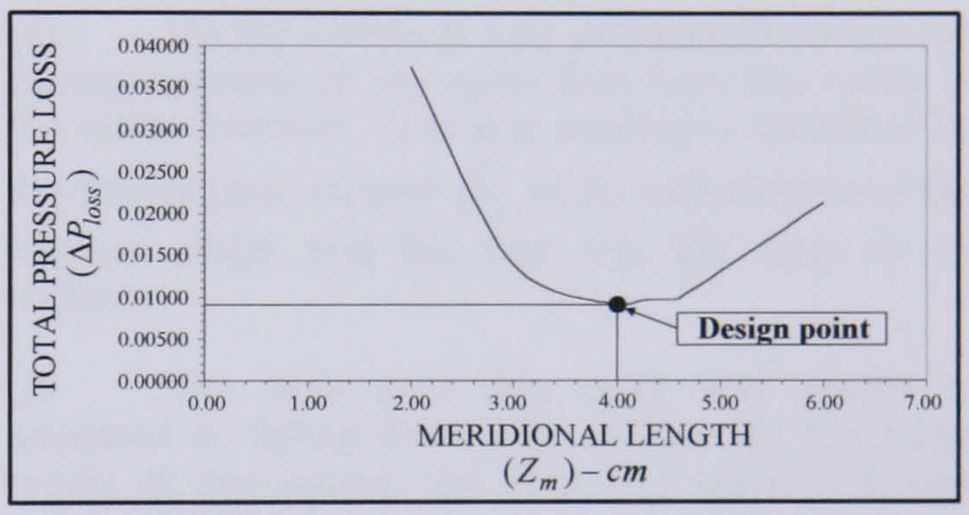

Fig.12 Total pressure loss vs. meridional length

The final design drawings of the turbine rotor are shown in Figs. 13 to 15, respectively.

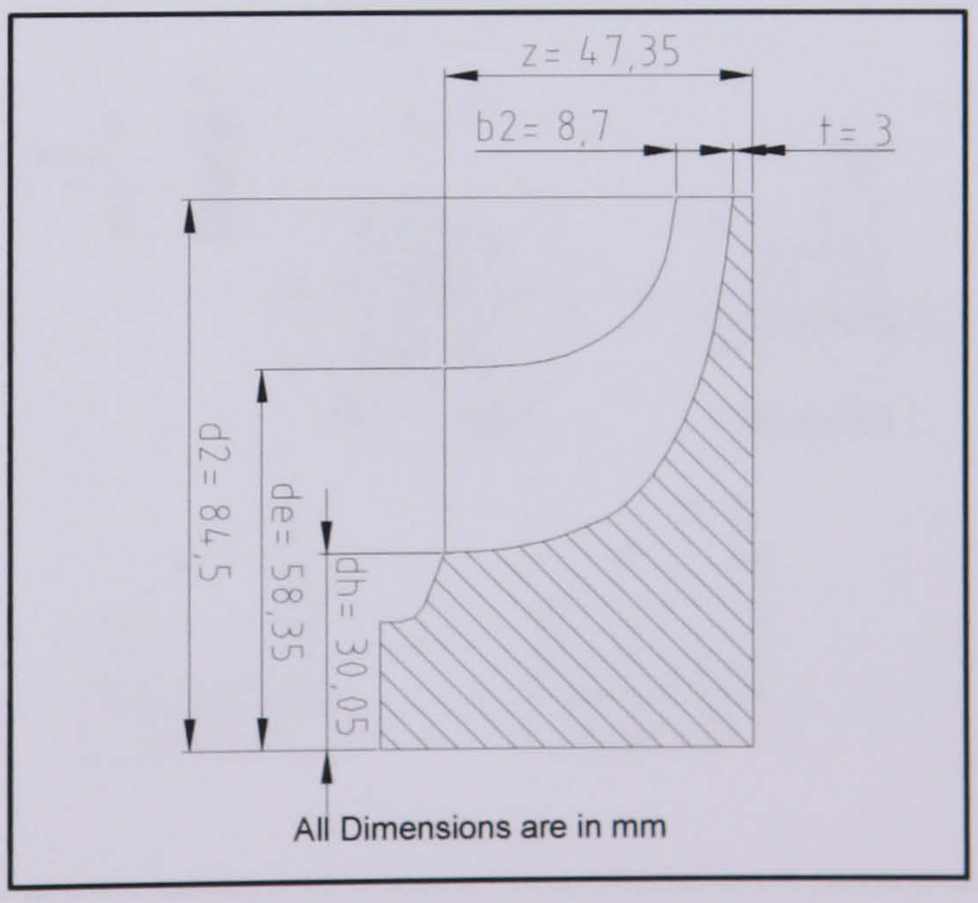

Fig. 13 Meridional section of the turbine rotor

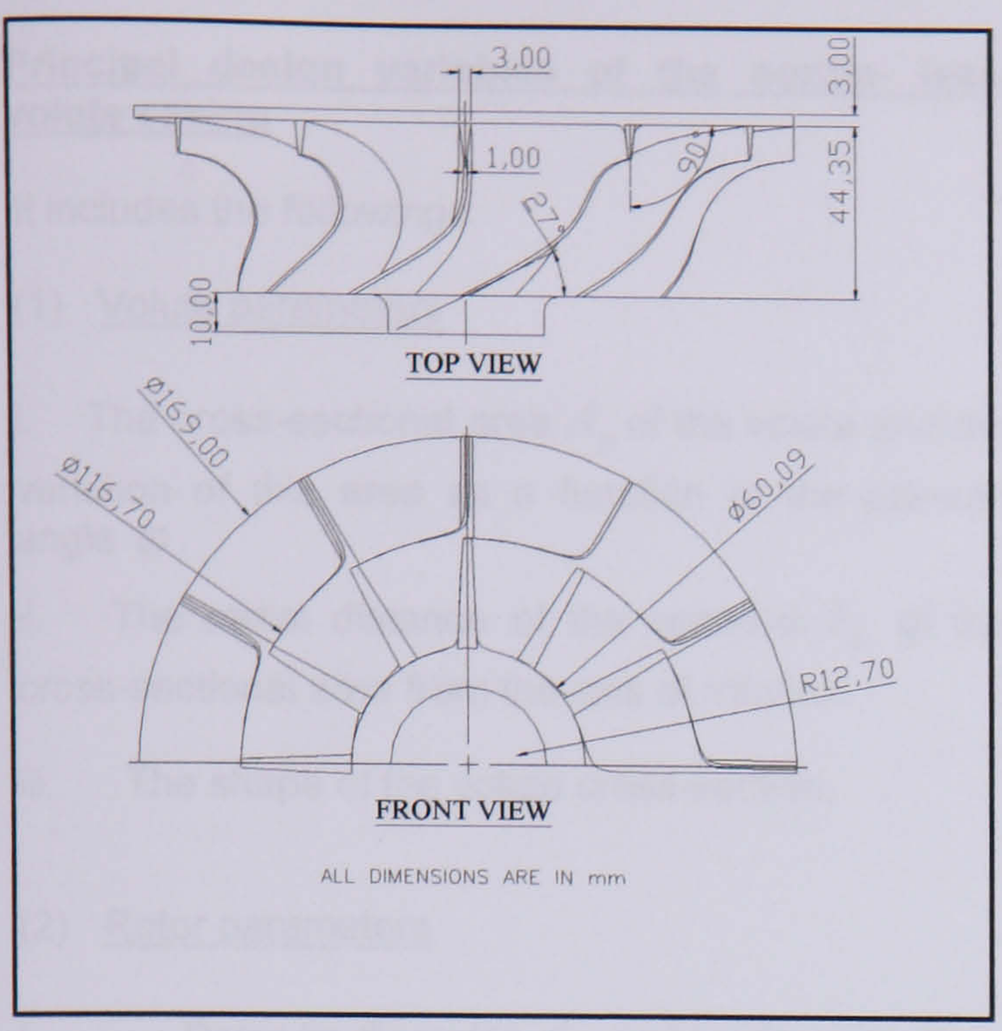

Fig. 14 Multiple views of the turbine rotor

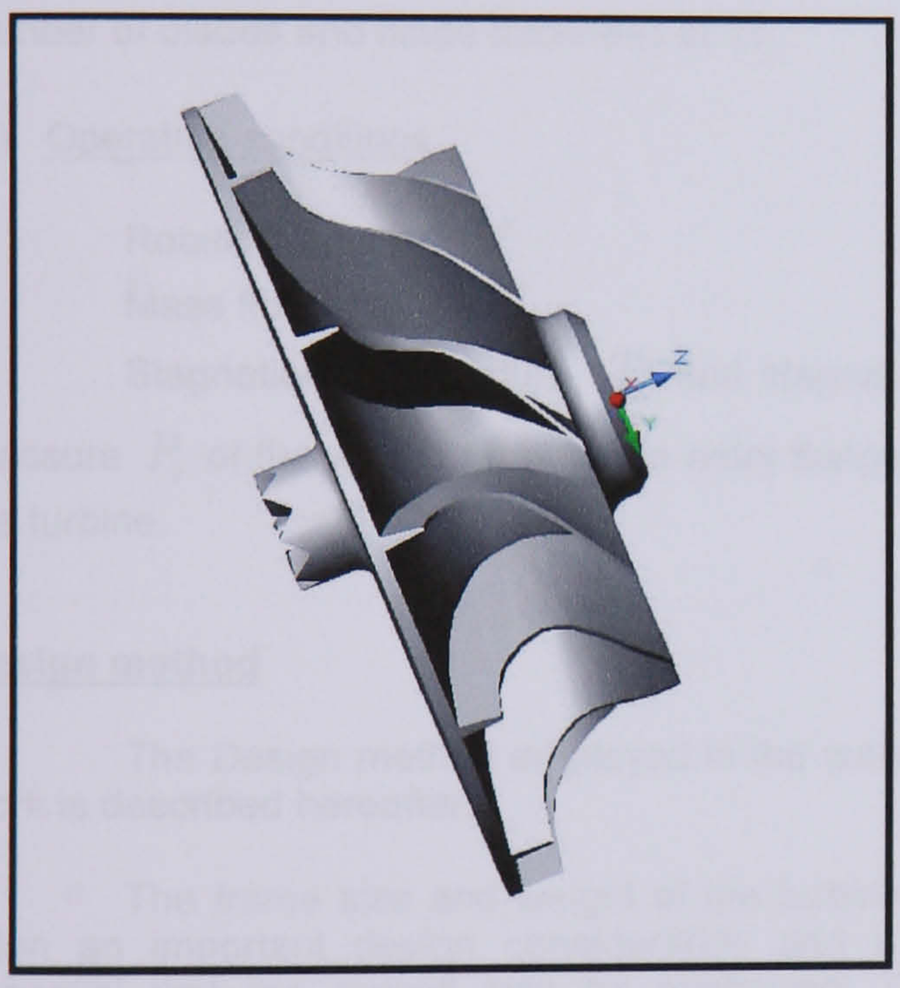

Fig. 15 Solid model of the turbine rotor

NOZZLE-LESS CASING DESIGN

The design objectives of the casing are:

(1) Accelerate the working fluid to the leading edge of the rotor and generate the desired rotor inlet conditions in terms of the magnitude and direction of the absolute velocity vector.

(2) Distribute the working fluid uniformly around the rotor periphery.

(3) Achieve these requirements as efficiently as possible that is with minimum loss in stagnation pressure.

The required inlet conditions must be derived from the desired turbine performance, e.g. the desired rotational speed and power output. The nozzle-less volute must be designed to provide these rotor inlet conditions peripherally uniform. The preliminary design of the volute is often based on the assumptions of an isentropic flow, together with a free vortex distribution about the rotor.

The passage design is often specified in the form of the variation, with azimuth angle, of cross-sectional area, casing width or parameter $A_\varphi / \bar{r}_\varphi$. The desired rotor inlet condition is one of a uniform distribution of angular momentum about the rotor periphery, whilst the volute inlet conditions at the tongue are those of a fully developed turbulent flow.

THEORY OF VOLUTE DESIGN PROCEDURE

Assumptions

The following assumptions were used in the design procedure

(1) Steady, one-dimensional, isentropic flow, constant angular momentum, energy and linear distribution of mass along the volute length.

(2) Vortex motion is fully established before the commencement of any outer flow from the volute in the radial direction. This is a necessary condition for the flow angles α_2 and β_2 to be independent of the azimuth angle and the flow into the rotor to be uniform.

(3) The flow near the outer wall profile is assumed to follow the same contour as the outer profile of the casing, the boundary layer thickness being negligible.

A diagrammatic sketch of a centripetal turbine fitted with a nozzle-less casing is shown in Fig. 16.

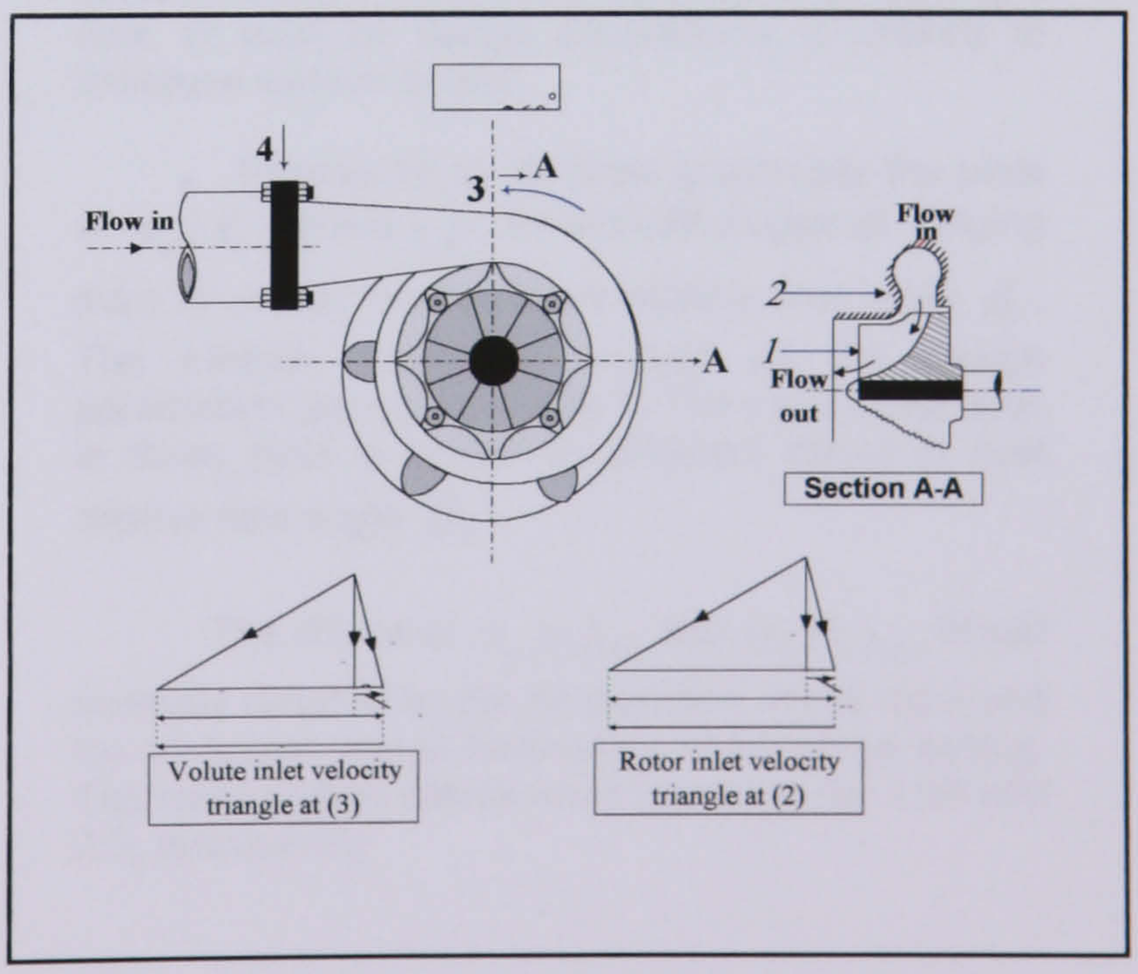

Fig. 16 IFR turbine fitted with a single nozzle-less volute casing

Principal design variables of the nozzle- less volute casing

It includes the followings:

(1) Volute parameters

i. The cross-sectional area A_φ of the volute and the variation of this area as a function of the azimuth angle φ.

ii. The radial distance of the centriod $\bar{r}_\varphi$ of the cross-sectional area from the axis of rotation.

iii. The shape of the volute cross-section.

(2) Rotor parameters

i. Rotor tip diameter d_2 and blade width b_2.

ii. Effective peripheral flow area A_2 or the number of blades and blade thickness at d_2.

(3) Operating conditions

i. Rotational speed, N

ii. Mass flow rate, $\dot{m}$

iii. Stagnation temperature, T_i and stagnation pressure P_i of the working gas at the entry flange of the turbine.

Design method

The Design method employed in the current work is described hereafter.

The frame size and weight of the turbine is often an important design consideration and it is essential that the overall size be minimized. The design procedure first assesses the overall size in terms of the volute radius ratio $\bar{r}_3/r_2$, and area ratio A_3/A_2 and consider the parameters, which must be varied in order to adjust the overall size.

Using the equations of mass flow, energy and angular momentum and based on the assumption of free vortex relationship, the following expression defining the interconnection of the design parameters of the casing:

$$\frac{A_\varphi}{\bar{r}_\varphi} = (B_{f_2})(\tan\alpha_2)\left(\frac{\varphi}{360}\right)\left(\frac{A_2}{r_2}\right)\left[\frac{1-\left(\frac{\pi}{\sqrt{2}}\cdot\frac{d_2N}{\sqrt{C_pT_i}}\cdot\frac{\sin\beta_2}{\sin(\alpha_2+\beta_2)}\right)^2}{1-\left(\frac{\pi}{\sqrt{2}}\cdot\frac{r_2}{\bar{r}_\varphi}\frac{d_2N}{\sqrt{C_pT_i}}\cdot\frac{\sin\beta_2\cos\alpha_2}{\sin(\alpha_2+\beta_2)}\right)^2}\right]^{1/\gamma-1} \quad (18)$$

Where B_{f_2} is the blockage factor corresponding to rotor entry and is given as:

$$B_{f_2} = \frac{Total\ flow\ area\ of\ the\ passage}{Peripheral\ area}$$

$$B_{f_2} = \frac{Peripheral\ flow\ area - Blockage\ due\ to\ blades}{Peripheral\ area}$$

$$B_{f_2} = 1-\left(\frac{n_b\, t_2 b_2}{\pi\, d_2 b_2}\right) \quad (19)$$

Where n_b : Number of blades

t_2 : Thickness of inlet rotor blades

Equation 18 represents a fundamental design formula linking the main design parameter $A_\varphi/\bar{r}_\varphi$ of the volute with relevant principal dimensions of the rotor and the operating conditions as shown below

$$\frac{A_\varphi}{\bar{r}_\varphi} = f\left[\left(\frac{\dot{m}\sqrt{T_i}}{A_2P_i}\right),\left(\frac{b_2}{d_2}\right),(\alpha_2),(\varphi),(N)\right]$$

i.e. $\frac{A_\varphi}{\bar{r}_\varphi} = f(A_2, d_2, b_2, \alpha_2)$ - these variables represent rotor parameters.

And $\frac{A_\varphi}{\bar{r}_\varphi} = f(\dot{m}, P_i, T_i, N, \alpha_2)$ - these variables represent operating conditions.

The losses may be included in equation 18. However experiments have shown **[20,21]** that, in general, stator losses are a small fraction of the overall losses, therefore the assumption of isentropic flow, at least for design calculations, is unlikely to introduce serious errors.

Figures 17 to 19 show graphically the plots of A_φ/A_2 versus $\bar{r}_\varphi/r_2$ for azimuth angles φ ranging from 0° *to* 360° and different relative flow angle β_2. The plotted graphs are based on the design parameters depicted in Table 3. The trend of the lines in these plots is similar for different values of inlet relative flow angle β_2.

The choice of $(\bar{r}_\varphi/r_2)_{\min}$ and $(\bar{r}_\varphi/r_2)_{\max}$ would normally dictated by the tip diameter of the rotor and the allowable overall dimensions of the volute casing. The initial design values were chosen to be 1.06 and 2.5, respectively.

DESIGN PARAMETER	VALUES
Speed parameter, $d_2N/\sqrt{C_pT_i}$	0.157
Inlet absolute flow angle, α_2	17°
Inlet relative flow angle, β_2	73°, 85°, 90°
Blockage factor, B_{f_2}	0.93

Table 3 Constant design parameters

Therefore, The corresponding pairs of values of the dimensionless parameters A_φ/A_2 and $\bar{r}_\varphi/r_2$ can be directly read from such a plot by joining $(\bar{r}_\varphi/r_2)_{\min}$ and $(\bar{r}_\varphi/r_2)_{\max}$ by a straight line as shown in Figs. 18 to 20

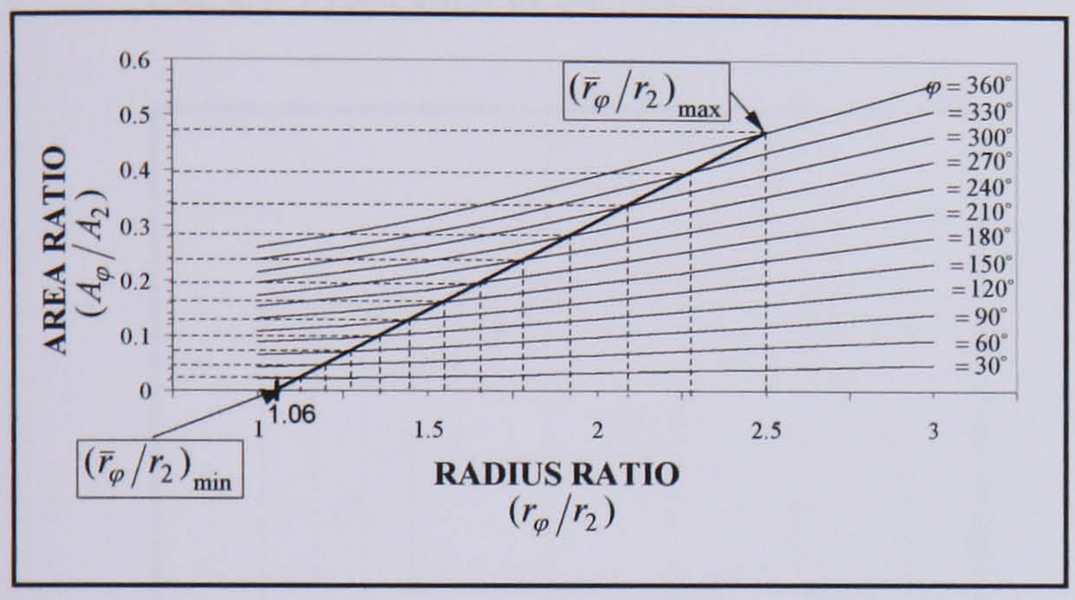

Fig. 17 Relationship between area ratio, radius ratio and azimuth angle $\beta_2 = 85°$

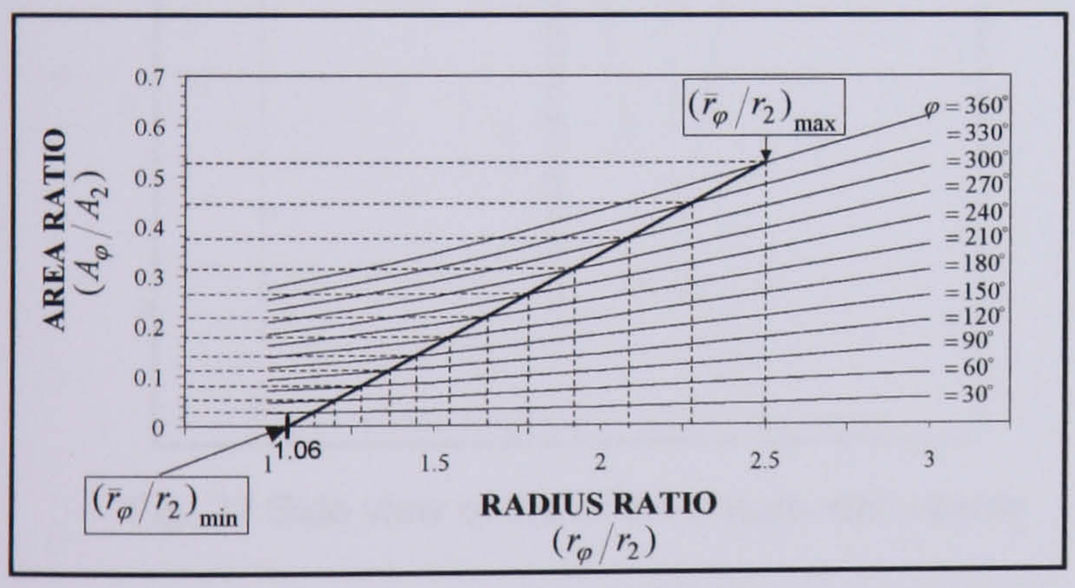

Fig. 18 Relationship between area ratio, radius ratio and azimuth angle for $\beta_2 = 73°$

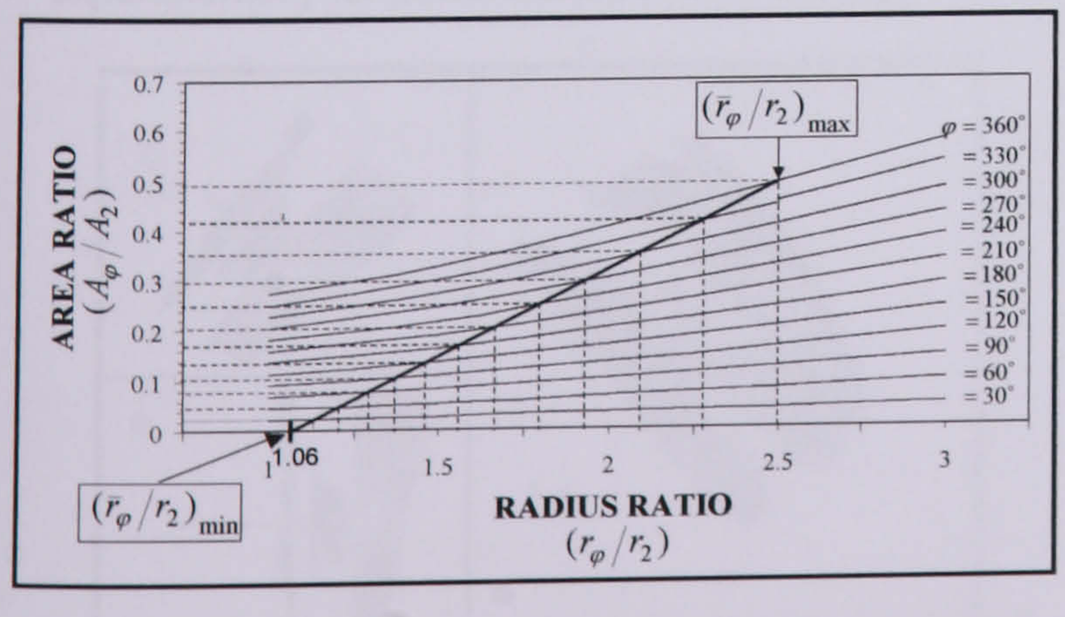

Fig. 19 Relationship between area ratio, radius ratio and azimuth angle for $\beta_2 = 90°$

Since $(A_\varphi/\bar{r}_\varphi) \propto \left[(A_\varphi/A_2) \div (\bar{r}_\varphi/r_2)\right]$, Then

$$\left(\frac{A_\varphi}{\bar{r}_\varphi}\right) = K\left(\frac{A_\varphi}{A_2}\right)\left(\frac{r_2}{\bar{r}_\varphi}\right)$$

Where $K = A_2/r_2$ to satisfy the expression above. The final design graph of $A_\varphi/\bar{r}_\varphi$ versus φ can be obtained from the corresponding values of A_φ/A_2, $\bar{r}_\varphi/r_2$ and φ which can be read either from Figs. 17 to 19. Such a graph is shown in Fig. 20.

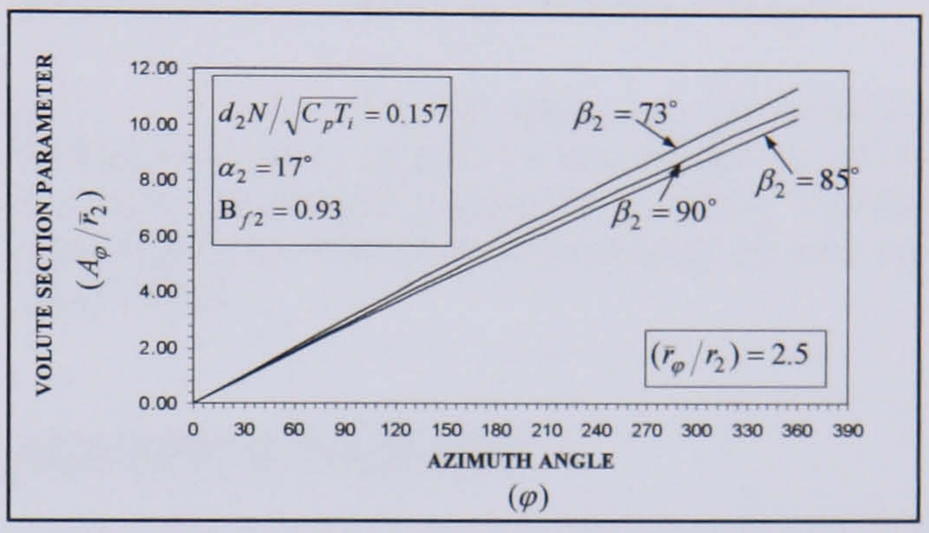

Fig. 20 Design graph for nozzle-less volute casing for various incidence angles

It should be noted that the shape of the graph above depends on the shape of the line joining the minimum and maximum values of $(\bar{r}_\varphi/r_2)$ chosen by the designer. Once the shape of cross-section, i.e $b = f(r)$ has been decided, in the current work, a circular cross-section was chosen, its dimensions can be found from the following equation

$$\left(\frac{A_\varphi}{r_\varphi}\right) = \int_{r_2}^{r_1}\left(\frac{b}{r}\right)_x . dr \qquad (20)$$

The final design dimensions and drawings for the nozzle-less casing are shown in Table 4 and in Figs. 21 and 22.

Position of Points	Azimuth angle (Degree)	Radius of Centroid(mm)	Elevation- z - (mm)	Radius of Casing Cross Section(mm)
1	0	85.65	-53	3.00
2	30	90.26	-51.53	4.47
3	60	94.87	-50.93	5.07
4	90	99.49	-48.23	7.77
5	120	104.10	-44.62	11.38
6	150	108.71	-40.6	15.40
7	180	113.32	-36.27	19.73
8	210	117.94	-31.67	24.29
9	240	122.55	-26.91	29.09
10	270	127.16	-21.89	34.11
11	300	131.77	-16.64	39.36
12	330	136.39	-11.16	44.84
13	360	141.00	-5.43	50.57
14	383	144.54	-5.43	50.57

Table 4 Design values of turbine nozzle-less casing

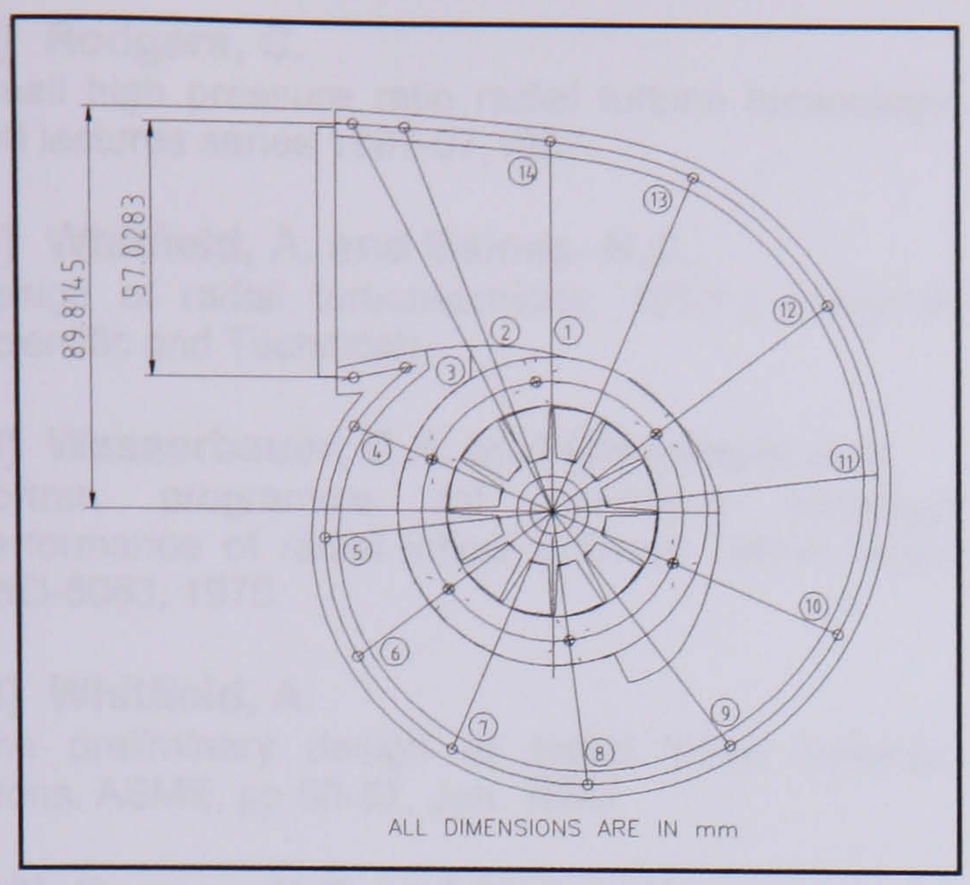

Fig. 21 Front view of the nozzle-less casing

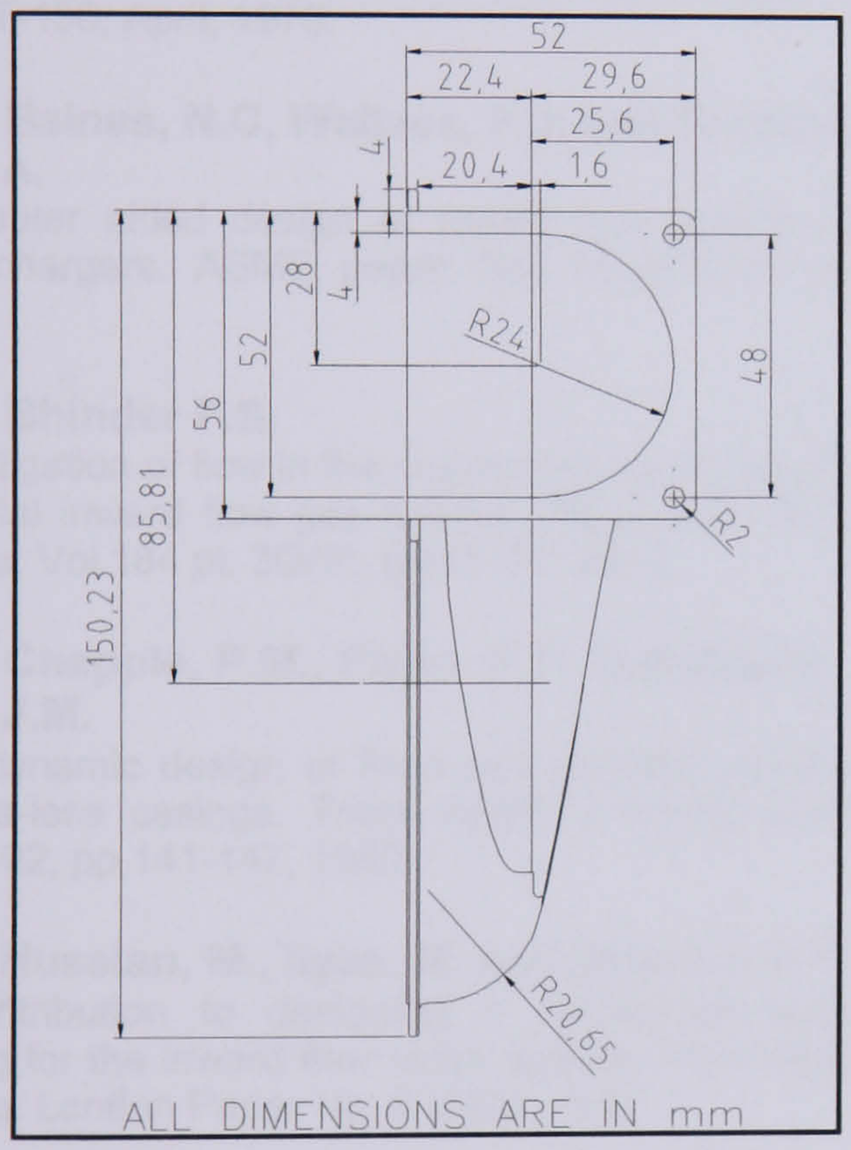

Fig. 22 Side view of the of the nozzle-less casing

The final design of the IFR turbine assembly is shown in Fig. 23. This assembly has been processed for manufacturing so that it can be tested experimentally for performance and efficiency.

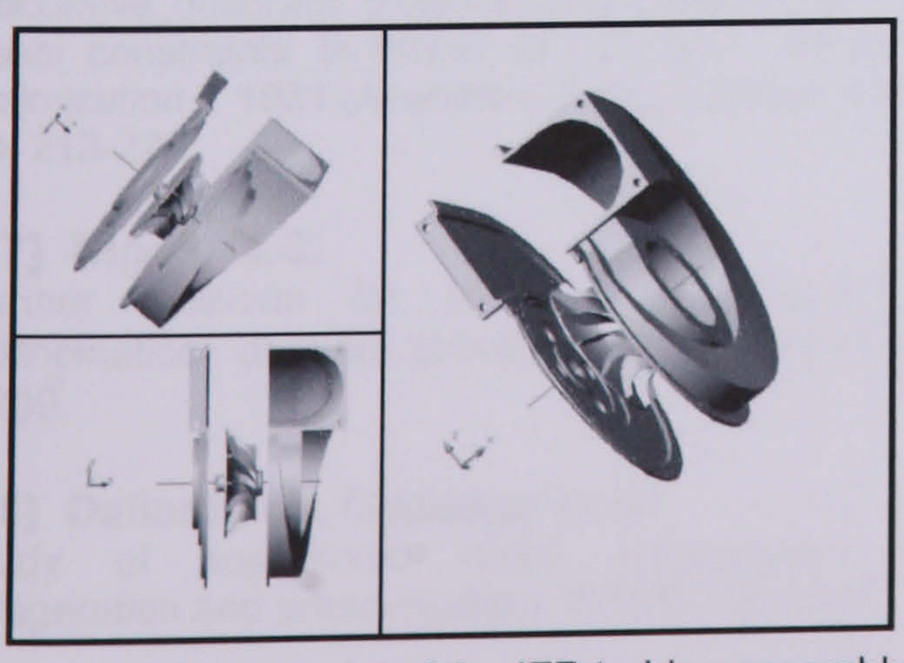

Fig. 23 Solid model of the IFR turbine assembly

CONCLUDING REMARKS

(1) A unified approach for designing a single stage inward flow radial turbine comprising a rotor and a nozzle-less casing has been described. The radial turbine has been designed to drive a direct-coupled permanent magnet high-speed alternator running at $60000\,rpm$ and developing $60\,kW$ electrical power.

(2) A computer program was developed to find the optimum choice of the principal dimensions of the rotor and the number of blades.

(3) The theory of the prescribed mean stream velocity distribution was used to find the optimum axial length and optimizing the blade passage.

(4) A procedure for designing the nozzle-less casing was given based on the equations of mass flow rate, energy and angular momentum. The flow is assumed to be isentropic and satisfies the free vortex relationship.

ACKNOWLEDGEMENTS

The authors wish to thank king Abdullah II Design & Development Bureau for their endless support and encouragements. Also, would like to thank the University of Hertfordshire for their cooperation and help throughout this research programme.

REFERENCES

[1] Von Der nuell
Single stage radial turbines for gaseous substances with high rotative and low specific speed ASME paper 51-f-16, Fall meeting. Minneapolis, Sept 1951.

[2] Balje, O.E.
A contribution to the problem of designing radial turbomachines. ASME paper 51-F-12, Fall meeting, Minneapolis, Sept.1951

[3] Balje, O.E.
A study of design criteria and matching of turbomachines. Part A-similarity relations and design criteria of turbines. ASME paper No. 60-Wa-230 winter annual meeting. New York, Nov-Dec, 1960.

[4] Rohlik, H.E.
Analytical determination of radial inflow turbine design geometry for maximum efficiency. NASA- TN D 4384, Oct 1970.

[5] Wallace, F.J., Baines, N.C and Whitfield, A.
A unified approach to one dimensional analysis and design of radial and mixed flow turbines. ASME paper No. 76-GT-100, March, 1976.

[6] Rodgers, C.
Small high pressure ratio radial turbine technology. VKI lectures series 1987-07,1987.

[7] Whitfield, A. and Baines, N.C.
Design of radial turbomachines, 1990 (Longman Scientific and Technical)

[8] Wasserbauer, C.A. and Glassman, A.J.
Fortran programme for predicting of-design performance of radial inflow turbines. NASA report TND-8063, 1975.

[9] Whitfield, A.
The preliminary design of radial inflow turbines. Trans. ASME, pp 50-57, Jan. 1990

[10] Benson, R.S. and Fisher, U.
A proposal scheme for computer aiaded design and manufacture of radial turbine rotors. ASME paper No. 78-GT-156, April, 1978.

[11] Baines, N.C, Wallace, F.J. and Whitfield, A.
Computer aided design of mixed flow turbines for turbochargers. ASME paper No. 78-GT-191, April 1978.

[12] Bhinder F.S.
Investigation of flow in the nozzle-less spiral casing of a radial inward flow gas turbine, Proc. Instn. Mech. Engns, Vol.184 pt. 3G(II), pp 66-77, 1969.

[13] Chapple, P.M., Flynn, P.F. and Mulloy, J.M.
Aerodynamic design of fixed and variable geometry nozzle-less casings. Trans ASME J engng power, Vol. 102, pp 141-147, 1980.

[14] Hussian, M., Ilyas, M. and Bhinder, F.S.
A contribution to designing a nozzle-less volute casing for the inward flow radial turbine. Instn. Mech. Engns. London Paper No. C35/82, 1982.

[15] Whitfield, A. and Noor, A.B.
A non-dimensional conceptual design procedure for the vaneless volute of radial inflow turbines. ASME, 1991.

[16] Biggs, M. C.
Recursive quadratic programming methods for non-linear constraints. In Powel, M.J.C., ed., " Nonlinear optimization ". 1981 (Academic press, London, 1982), pp. 213-221.

[17] Biggs, M.C.
Further methods for nonlinear optimization ". Mathematics division, University of Hertford shire, 1999.

[18] Dallenbach, Coppage *et al.*
Study of supersonic radial compressors for refrigeration and pressurization. WADC Technical Report 55-257, A.S.T.I.A document No. AD110467. Dec 1956.

[19] Rodgers.C
A diffusion factor correlation for centrifugal impeller stalling, Trans. ASME. Jr. of Eng. For Power, Vol. 100.Oct,1978

[20] Hiett, G. F. and Johnston, I. H.
Experiments concerning the aerodynamic performance of inward radial flow turbine ". Proc. Instn. Mech. Engrs. London, 178, Pt 3I (II), 1964.

[21] Benson, R. S.
An analysis to the losses in a radial gas turbine. Paper No. 16, I.Mech.E. Thermodynamics and Fluid Mechanics Convention, April 1966.

This paper was submitted to the ASME Turbo Expo Land, Sea & Air. Amsterdam, 3-6 June 2002. It was sponsored by International Gas Turbine Institute with the support of these participating organization: Dutch Gas Turbine Association (VGT), Institution of Mechanical Engineers (ImechE), German Aerospace Centre (DLR) and The von Karman Institute for fluid Dynamics.

This paper was accepted and has been recommended for publication in the TRANSACTIONS of the ASME in either the Journal of Engineering for the Gas Turbines and power or in the Journal of Turbomachinery.

APPENDICES

APPENDIX A: FLOW CHARTS.

APPENDIX B: SPECIFIC SPEED FUNCTION DEVELOPED BY WOOD [92].

APPENDIX A

FLOW CHARTS

The flow charts presented here are based on written computer programmes to solve the equations (3.1 to 3.8, 3.17, 3.20, 3.21, 3.29, 3.55, 3.56, 3.60b, 3.83, 3.86). The results were shown graphically in **sect. 10.2 of Chapter 10**. It should be noted that other graphs presented in **Chapter 10** were based on similar written computer programmes, but for the sack of brevity, it was not included.

These flow charts are listed as follows:

Fig. A.1 Flow chart based on equations 3.1 to 3.8 for calculating gas turbine cycle parameters SFC and η_{th} for various values of pressure ratios P_i/P_e and turbine inlet temperatures T_i.

Fig. A.2 Flow chart for calculating velocity ratio U_2/C_s based on equation (3.20) for various values of pressure ratios P_i/P_e and speed parameter S_p.

Fig. A.3 Flow chart for calculating specific torque $\tau/d_2\dot{m}\sqrt{C_pT_i}$ based on equation (3.17) for various values of pressure ratios P_i/P_e and speed parameter $d_2N/\sqrt{C_pT_i}$.

Fig. A.4 Flow chart for calculating specific torque parameter $\tau/d_2\dot{m}\sqrt{C_pT_i}$ based on equation (3.21) for various values of pressure ratios P_i/P_e and velocity ratio U_2/C_s.

Fig. A.5 Flow chart based on equation 3.29 for calculating degree of reaction R for different values of d_1/d_2, α_2 and β_2.

Fig. A.6 Flow chart based on equation (3.55) for calculating M_2 for various values of P_i/P_e and α_2.

Fig. A.7 Flow chart based on equation (3.56) for calculating U_2/C_s for various values of P_i/P_e and M_2.

Fig. A.8 Flow chart based on equation (3.60b) for calculating M_{er} for various values of P_i/P_e and d_e/d_2.

Fig. A.9 Flow chart based on equation (3.60b) for calculating M_{er} for various values of P_i/P_e and β_e.

Fig. A.10 Flow chart based on equation (3.60b) for calculating M_{er} for various values of d_e/d_2 and β_e.

Fig. A.11 Flow chart based on equation (3.83) for calculating b_2/d_2 for various values of $\dot{m}\sqrt{C_pT_i}/d_2{}^2P_i$ and $d_2N/\sqrt{C_pT_i}$.

Fig. A.12 Flow chart based on equation (3.86) for calculating blade tip speed U_2 for various values of P_i/P_e and T_i.

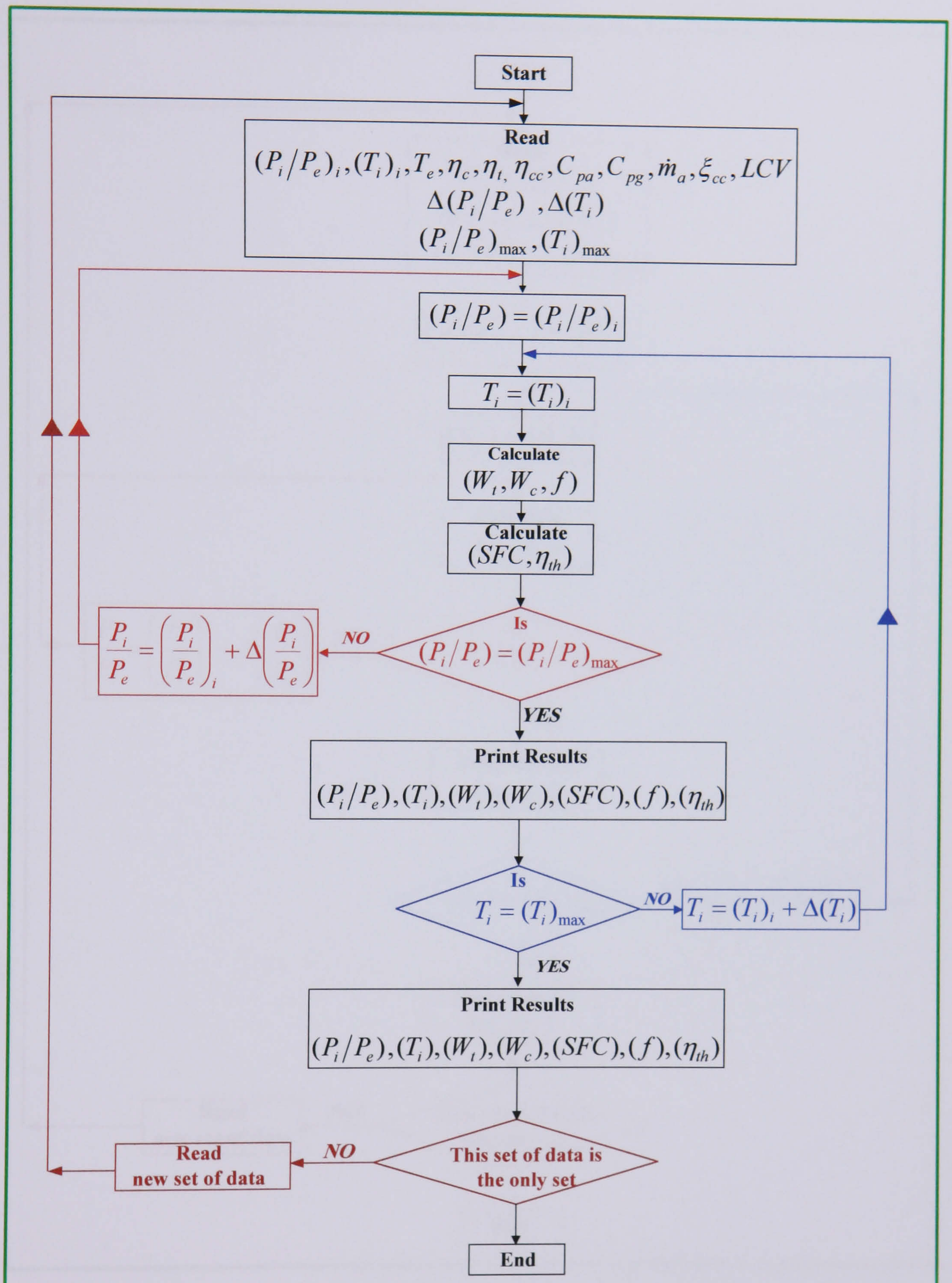

FIG. A.1 FLOW CHART FOR CALCULATING SPECIFIC FUEL CONSUMPTION SFC AND THERMAL EFFICIENCY η_{TH} BASED ON EQUATIONS 3.1 TO 3.8 FOR VARIOUS VALUES OF PRESSURE RATIOS P_i/P_e AND TUREINE INLET TEMPERATURES T_i

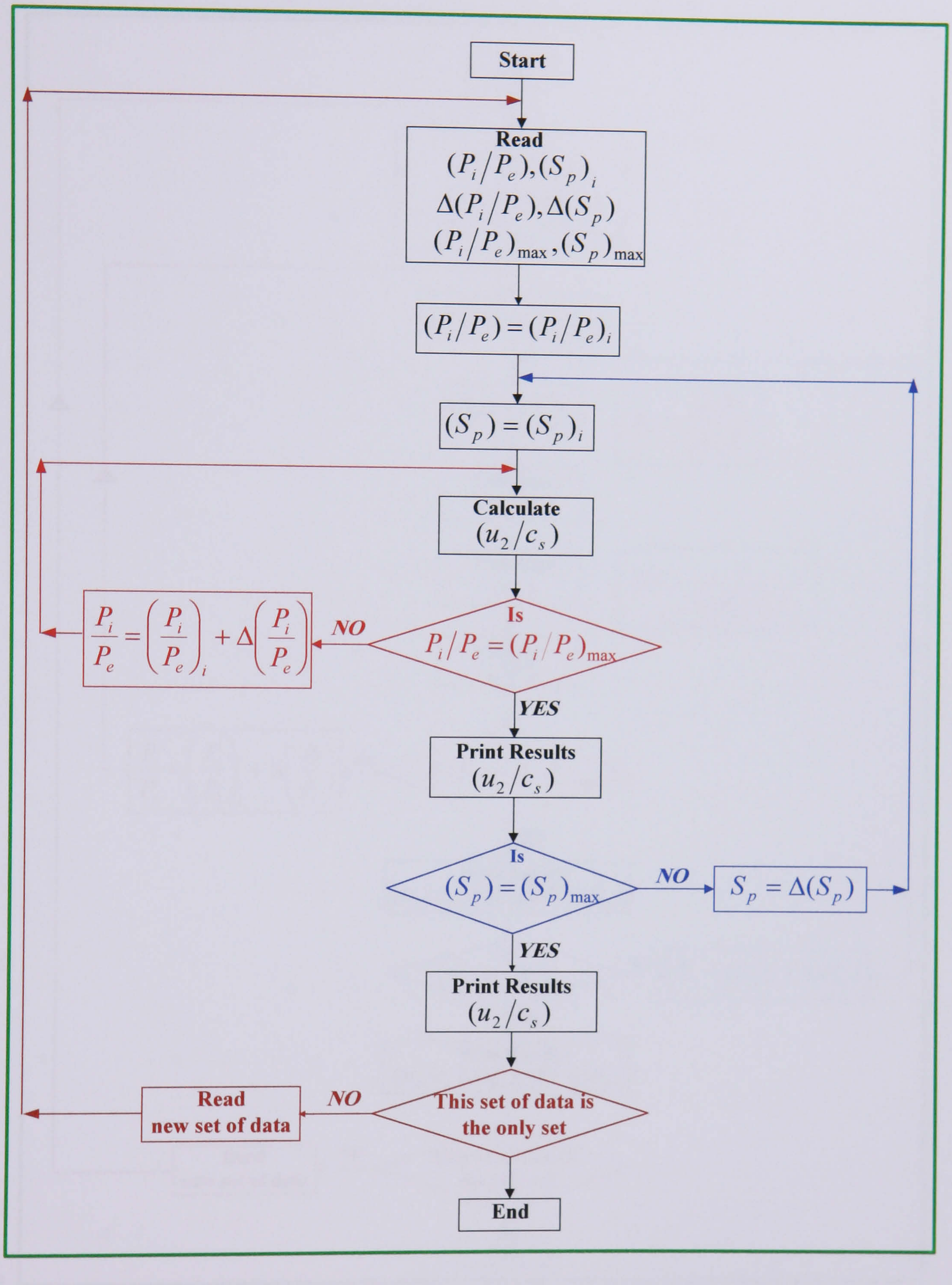

FIG. A.2 FLOW CHART FOR CALCULATING VELOCITY RATIO U_2/C_s BASED ON EQUATION (3.20) FOR VARIOUS VALUES OF PRESSURE RATIOS P_i/P_e AND SPEED PARAMETER S_p

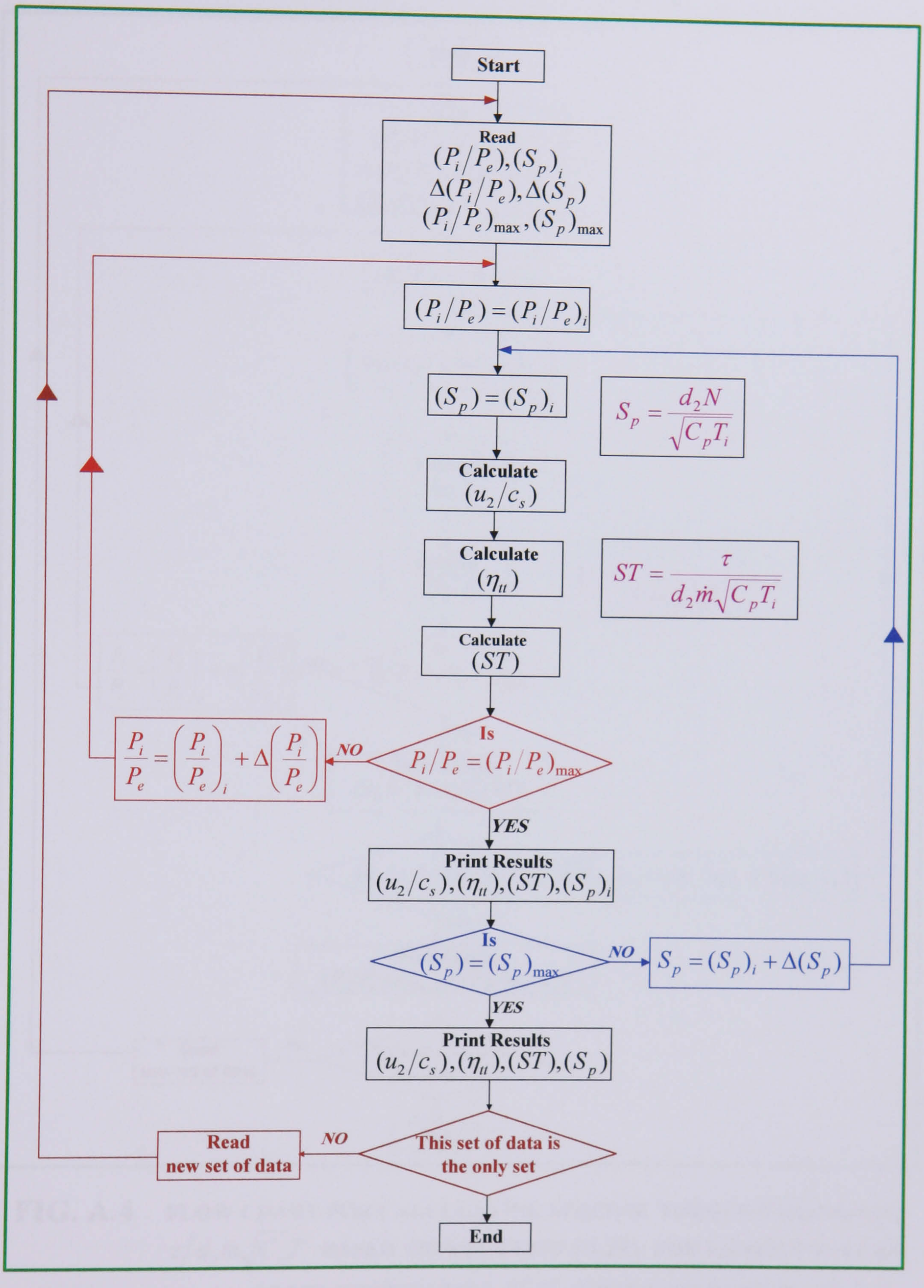

FIG. A.3 FLOW CHART FOR CALCULATING SPECIFIC TORQUE $\tau/d_2\dot{m}\sqrt{C_pT_i}$ BASED ON EQUATION (3.17) FOR VARIOUS VALUES OF PRESSURE RATIOS P_i/P_e AND SPEED PARAMETER $d_2N/\sqrt{C_pT_i}$

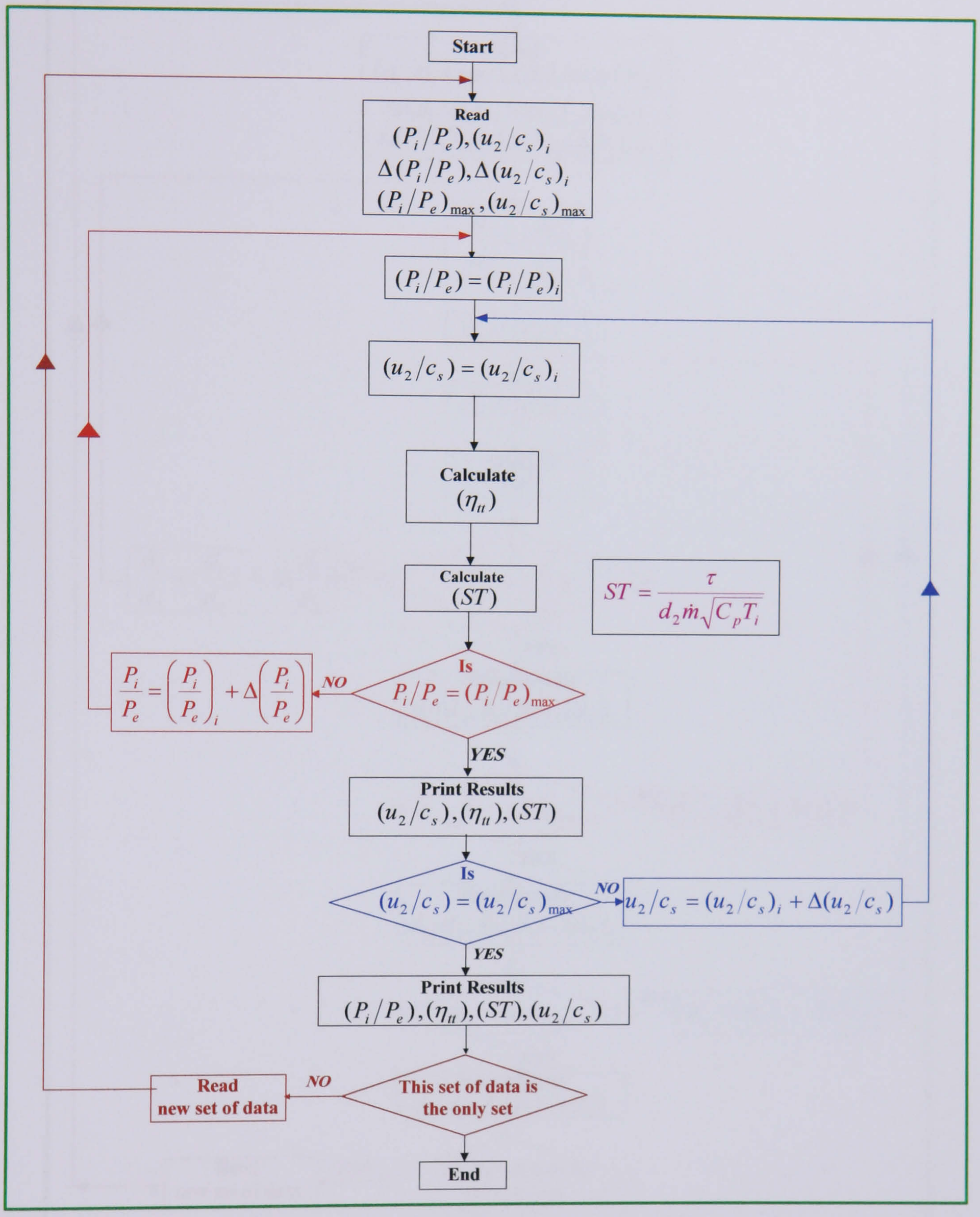

FIG. A.4 FLOW CHART FOR CALCULATING SPECIFIC TORQUE PARAMETER $\tau/d_2\dot{m}\sqrt{C_pT_i}$ BASED ON EQUATION (3.21) FOR VARIOUS VALUES OF PRESSURE RATIOS P_i/P_e AND VELOCITY RATIO U_2/C_s

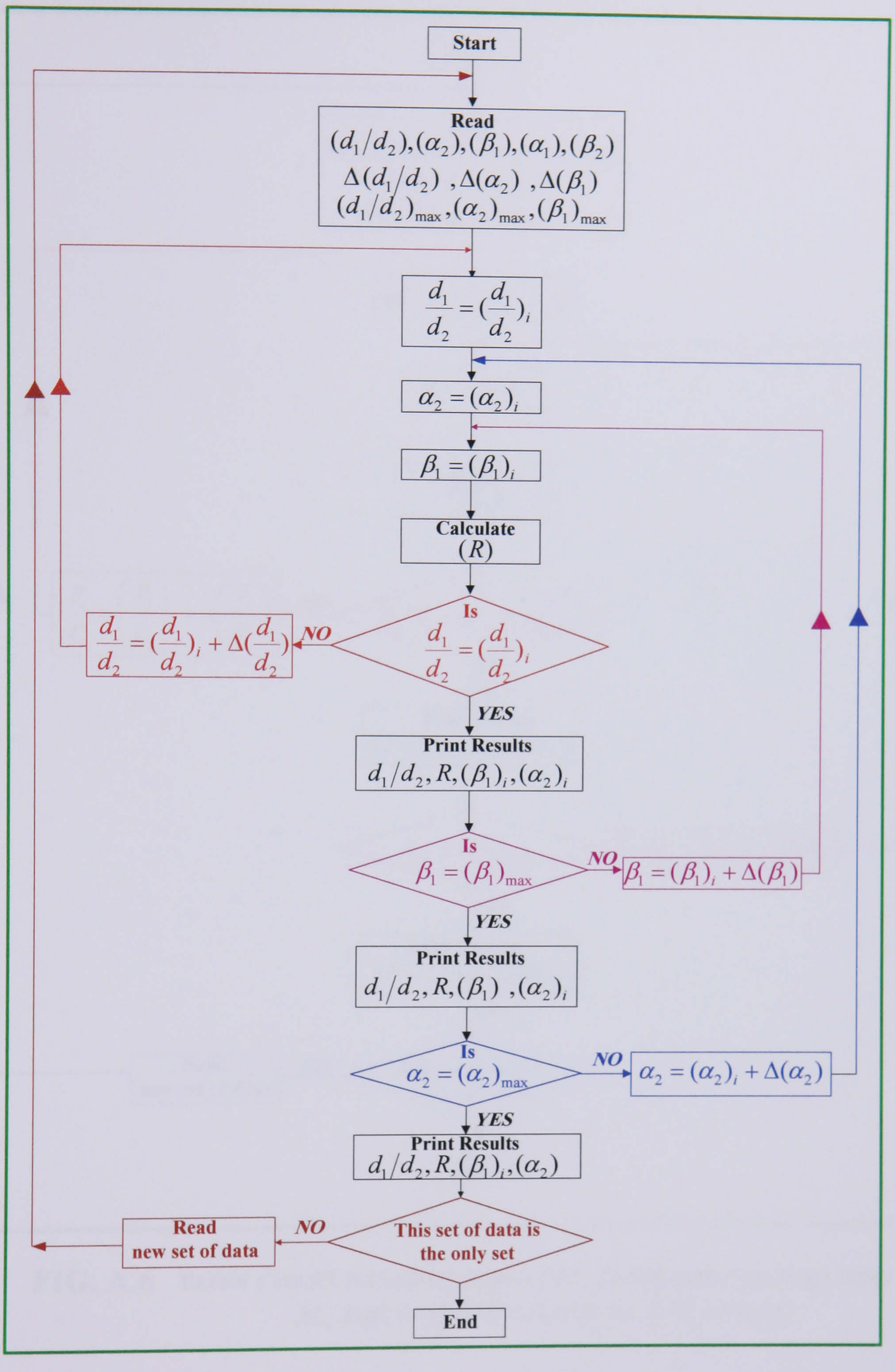

FIG. A.5 FLOW CHART BASED ON EQUATION (3.29) FOR CALCULATING DEGREE OF REACTION R FOR DIFFERENT VALUES OF d_1/d_2 α_2 AND β_2

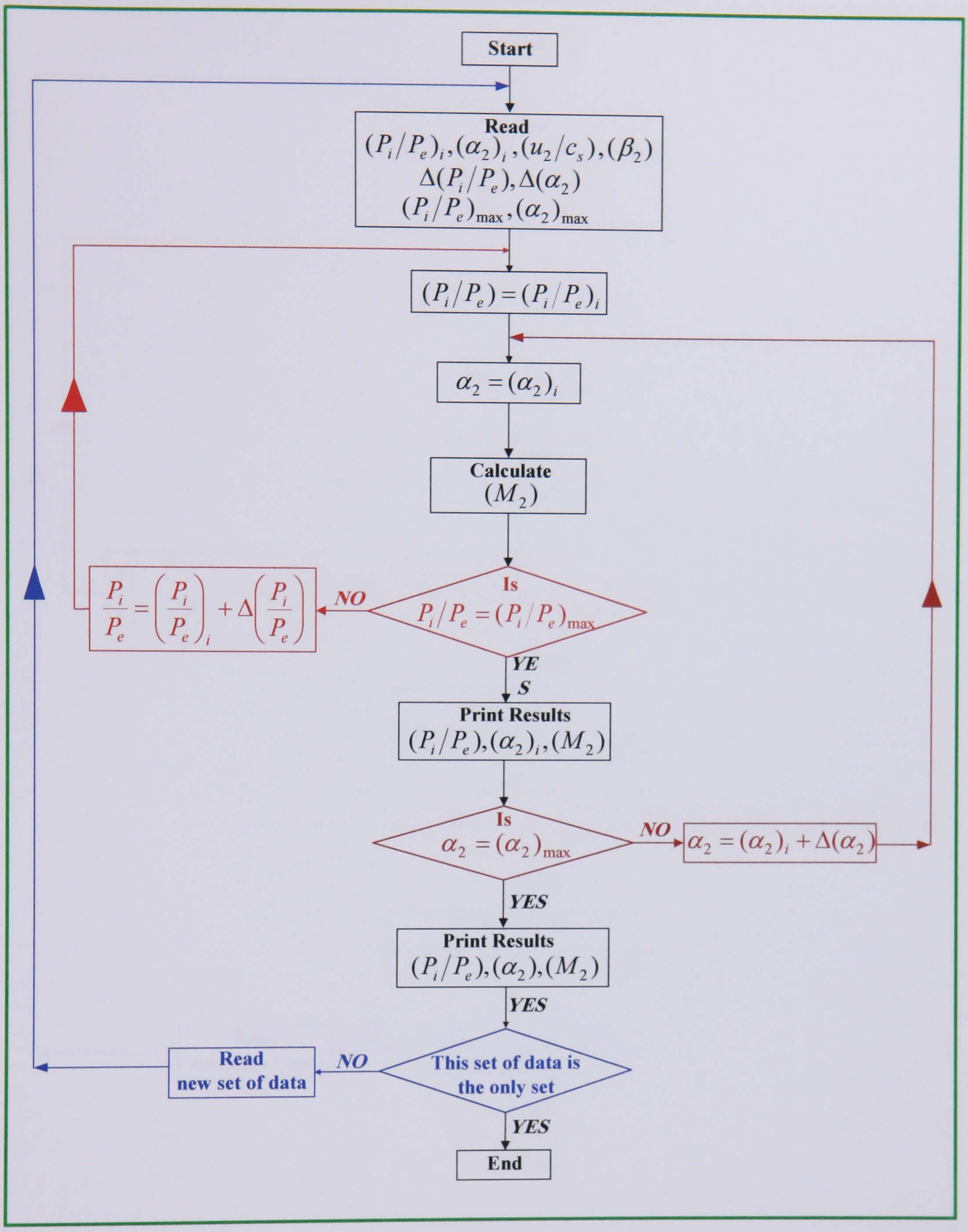

FIG. A.6 FLOW CHART BASED ON EQUATION (3.55) FOR CALCULATING M_2 FOR VARIOUS VALUES OF P_i/P_e AND α_2

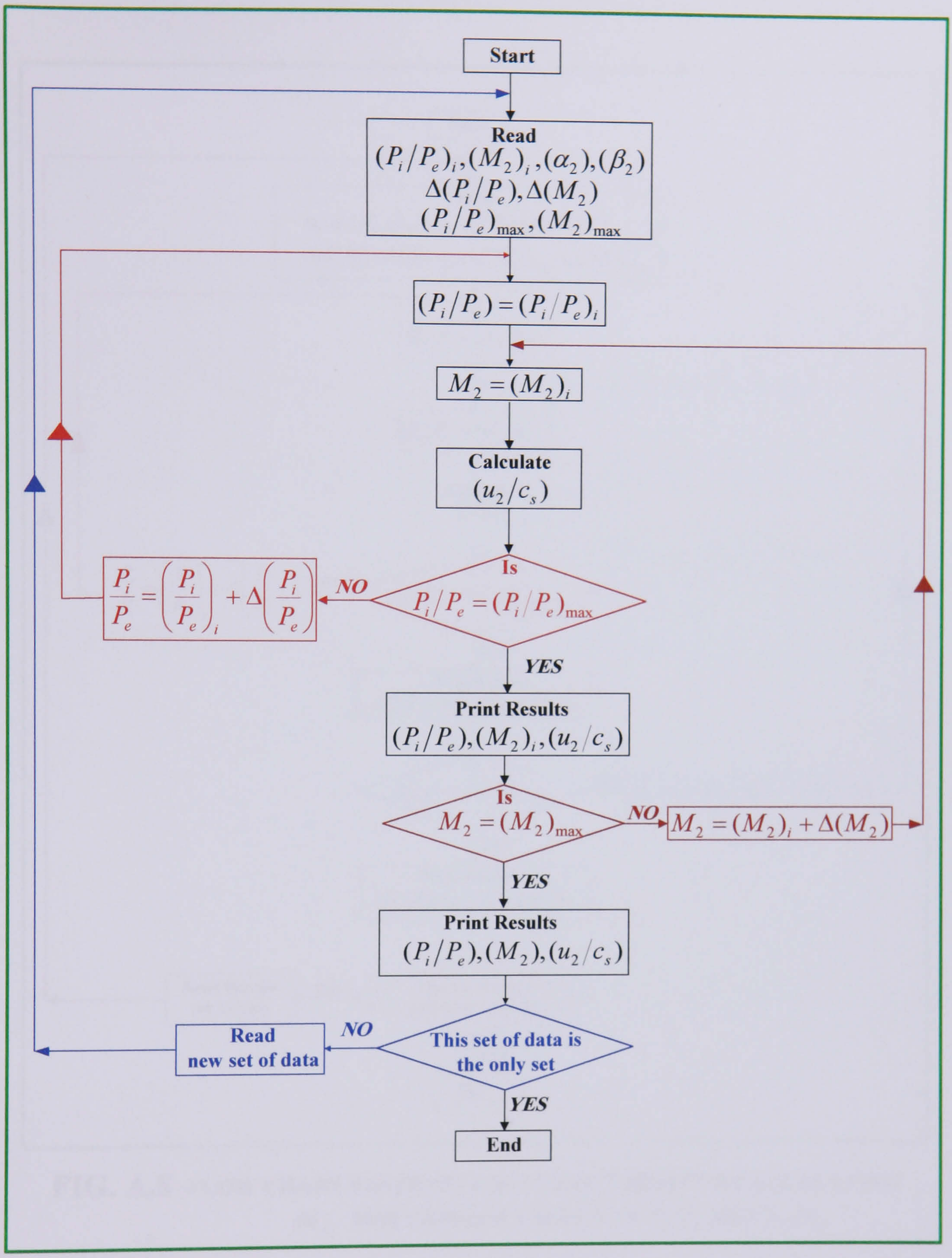

FIG. A.7 FLOW CHART BASED ON EQUATION (3.56) FOR CALCULATING U_2/C_s FOR VARIOUS VALUES OF P_i/P_e AND M_2

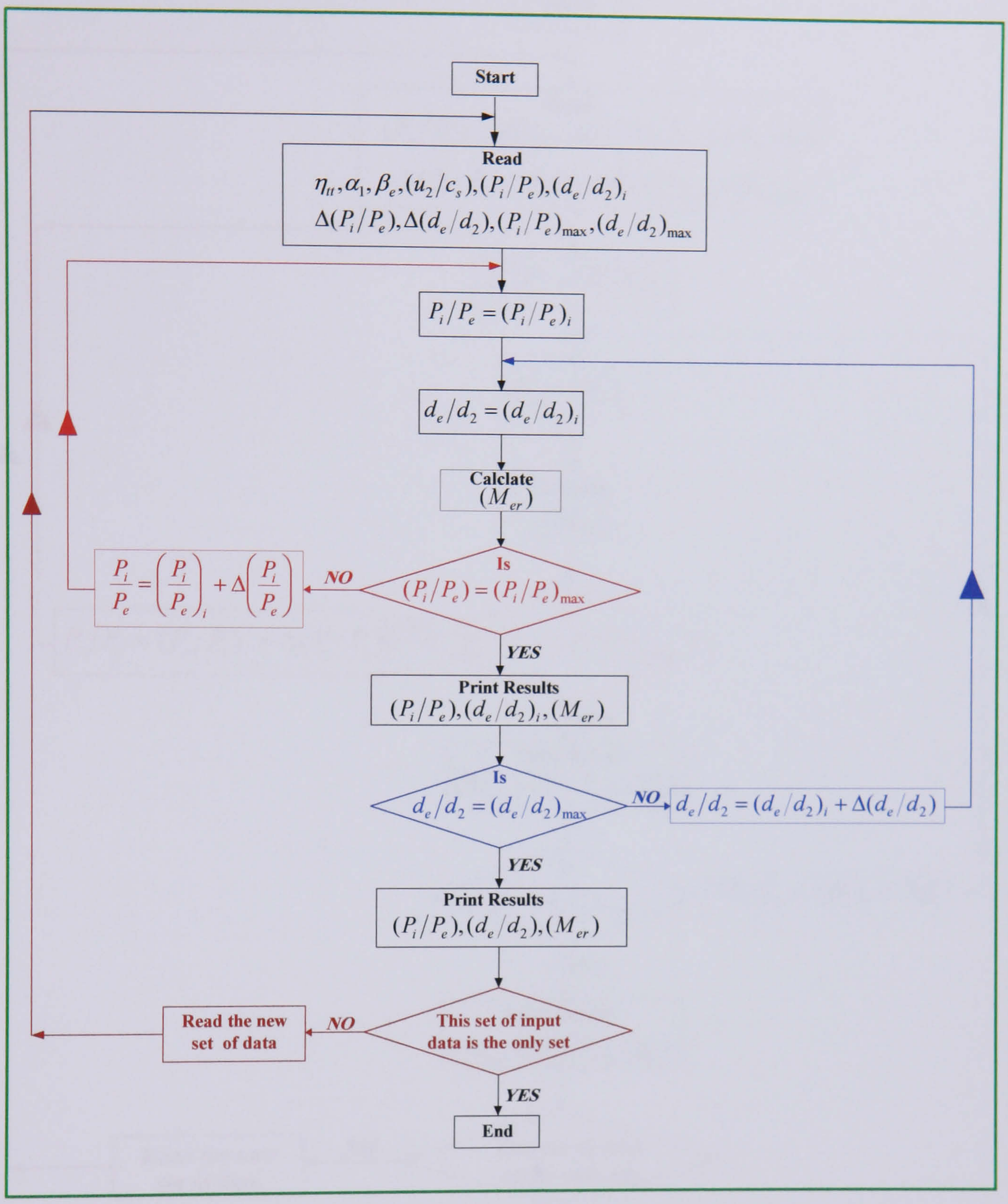

FIG. A.8 FLOW CHART BASED ON EQUATION (3.60b) FOR CALCULATING M_{er} FOR VARIOUS VALUES OF P_i/P_e AND d_e/d_2

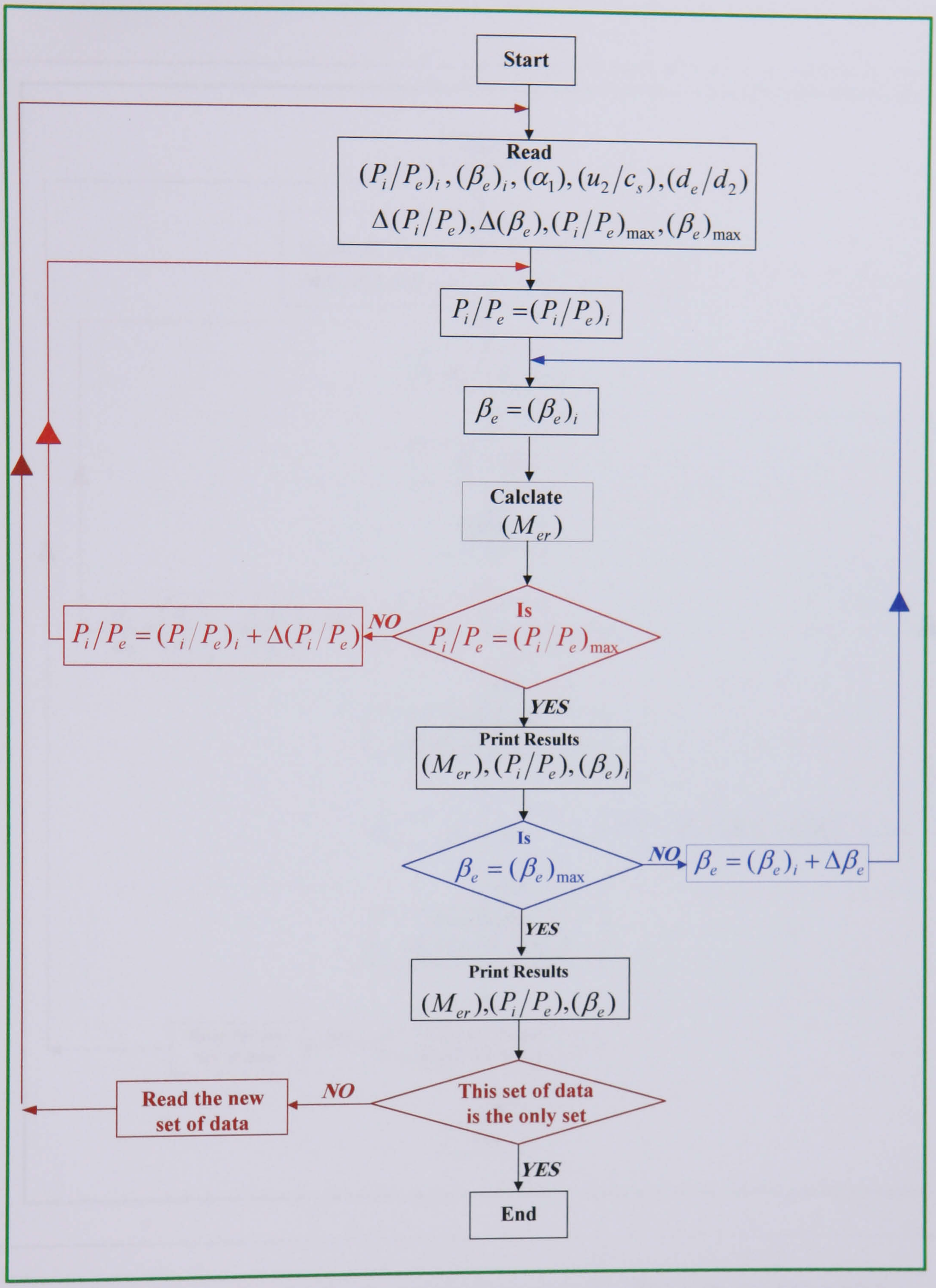

FIG. A.9 FLOW CHART BASED ON EQUATION (3.60b) FOR CALCULATING M_{er} FOR VARIOUS VALUES OF P_i/P_e AND β_e

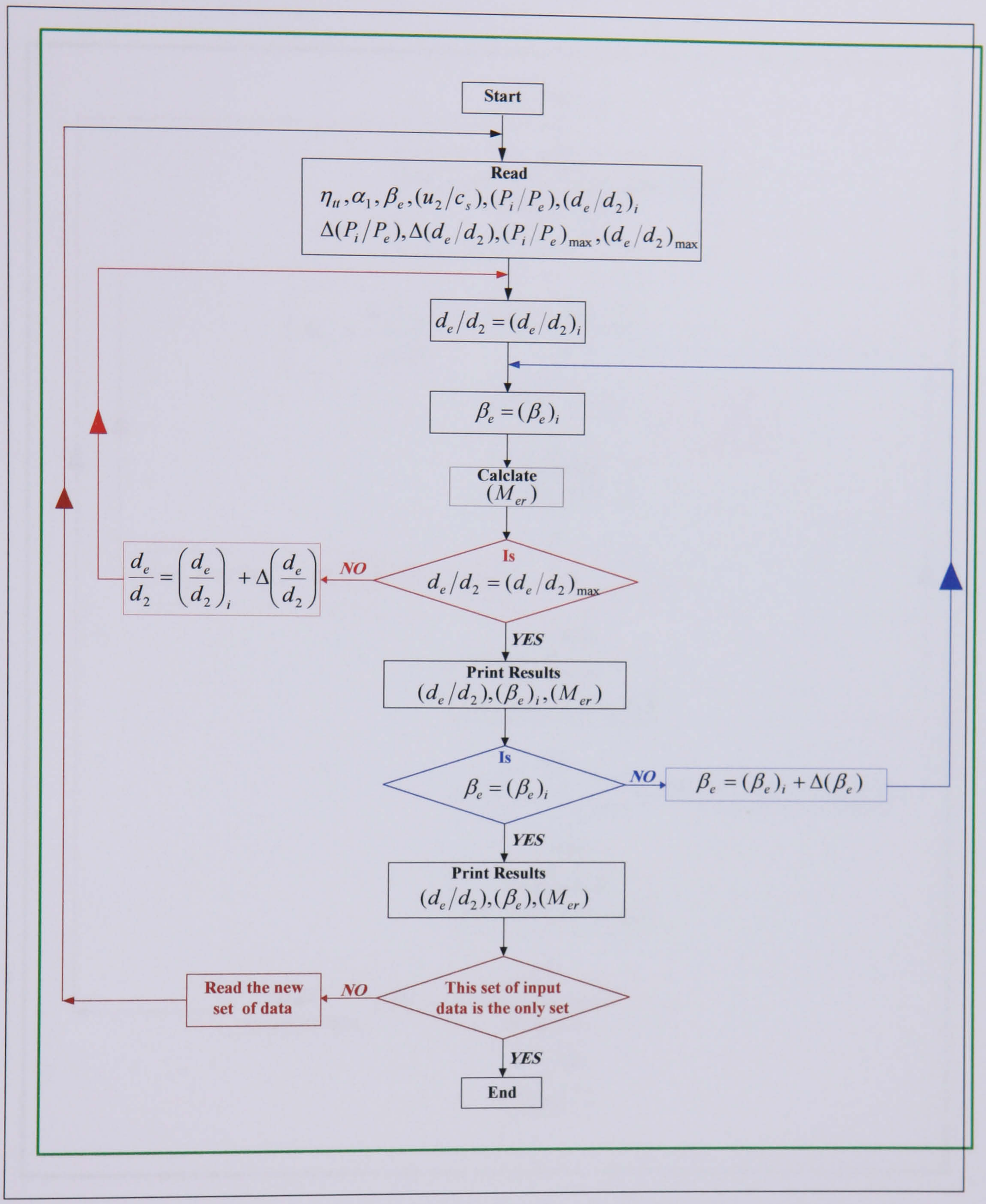

FIG. A.10 FLOW CHART BASED ON EQUATION (3.60b) FOR CALCULATING M_{er} FOR VARIOUS VALUES OF d_e/d_2 AND β_e

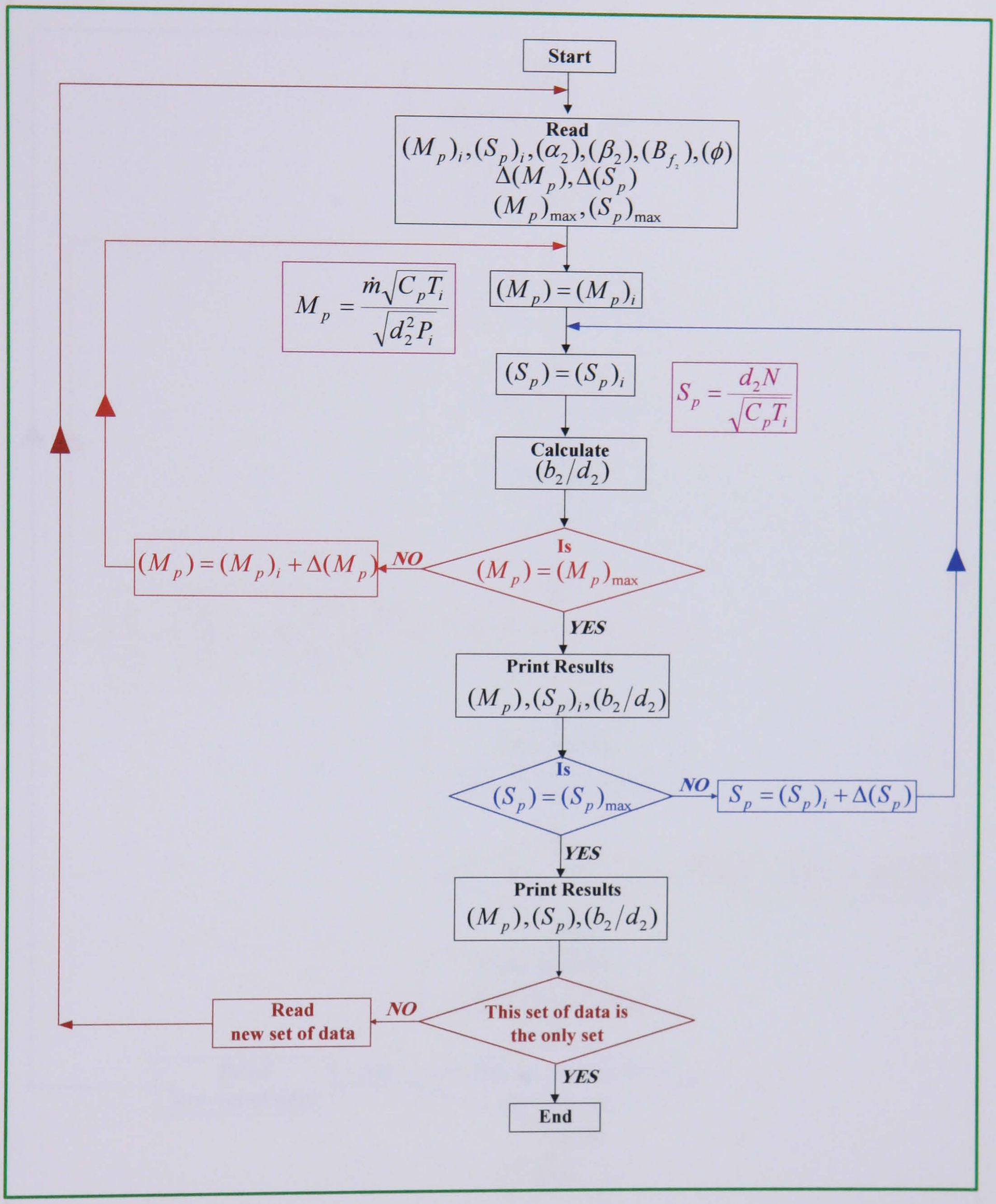

FIG. A.11 FLOW CHART BASED ON EQUATION (3.83) FOR CALCULATING b_2/d_2 FOR VARIOUS VALUES OF $\dot{m}\sqrt{C_pT_i}/d_2{}^2P_i$ AND $d_2N/\sqrt{C_pT_i}$

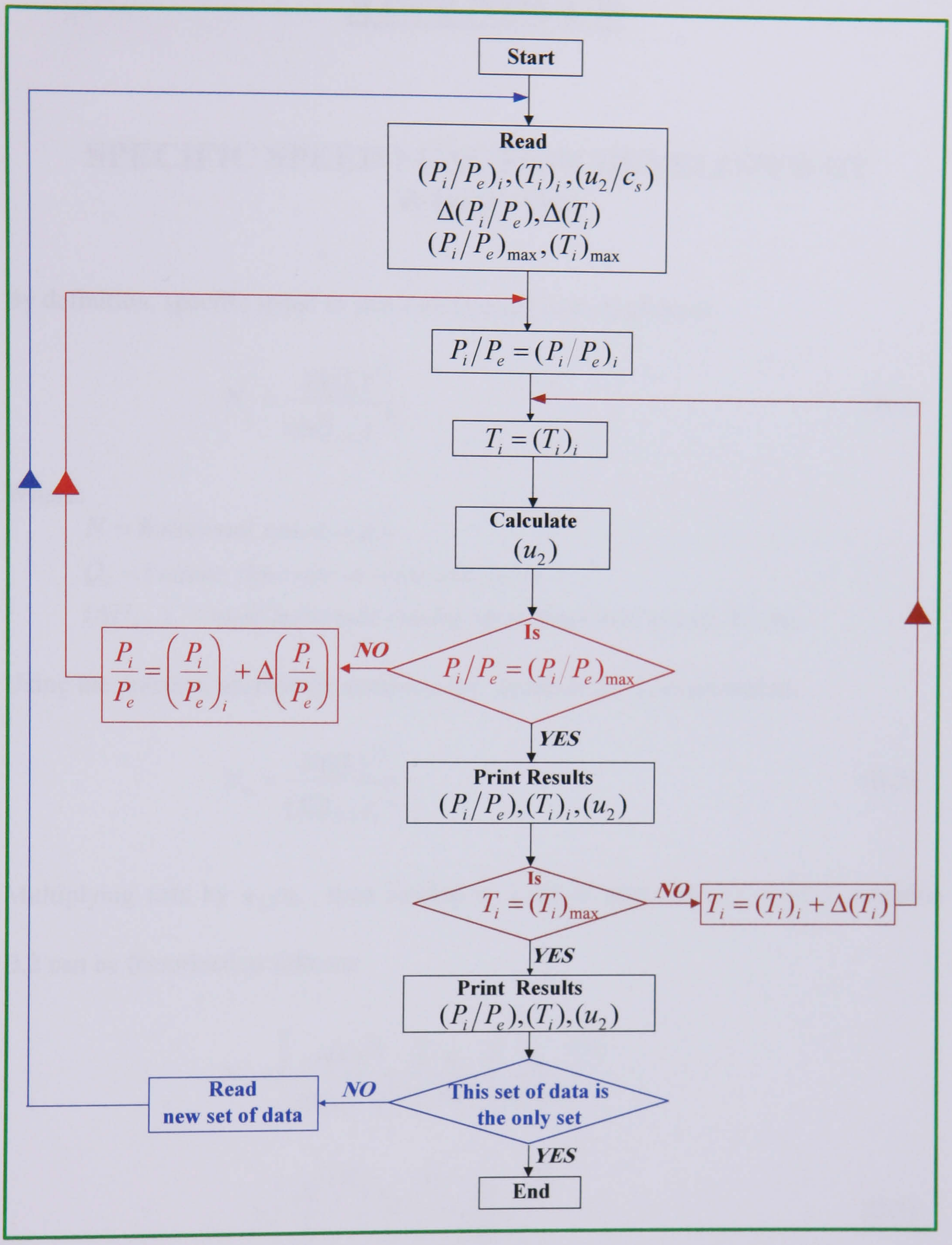

FIG. A.12 FLOW CHART BASED ON EQUATION (3.86) FOR CALCULATING BLADE TIP SPEED U_2 FOR VARIOUS VALUES OF P_i/P_e AND T_i

APPENDIX B

SPECIFIC SPEED FUNCTION DEVELOPED BY WOOD [92]

By definition, specific speed in non-dimensional form is given as:

$$N_s = \frac{N(\dot{Q}_e)^{1/2}}{(\Delta H_{i-e})_s^{3/4}} \tag{B.1}$$

Where:

$N = Rotational\ speed, r.p.s$

$\dot{Q}_e = Volume\ flow\ rate\ at\ rotor\ exit, m^3/s$

$(\Delta H_{i-e})_s = total\ Isentropic\ entalpy\ drop\ from\ inlet\ to\ exit, kJ/kg$

Using the notation adopted for turbine rotor, equation B.1 is expressed as:

$$N_s = \frac{N(\dot{Q}_1)^{1/2}}{(\Delta H_{3-1})_s^{3/4}} \tag{B.2}$$

Multiplying **LHS** by u_2/u_2, then writing $u_2 = \pi d_2 N$ and $(\Delta H_{3-1})_s = \frac{1}{2}c_s^{\,2}$, equation B.2 can be factorized as follows:

$$N_s = \left(\frac{(\dot{Q}_1)^{1/2}}{(0.5c_s^{\,2})^{3/4}}\right)\left(\frac{u_2}{\pi d_2}\right)\left(\frac{u_2}{\pi N d_2}\right)^{1/2}$$

$$= \left(\frac{\sqrt{2}}{\pi}\right)^{3/2}\left(\frac{u_2}{c_s}\right)^{3/2}\left(\frac{\dot{Q}_1}{N d_2^{\,3}}\right)^{1/2} \tag{B.3}$$

For the ideal **IFR** turbine, the velocity ratio $u_2/c_s = 1/\sqrt{2} = 0.707$. Substituting this value into equation B.3 will give:

$$N_s = 0.18\left(\frac{\dot{Q}_1}{Nd_2{}^3}\right)^{1/2} \tag{B.4}$$

To obtain some physical significance from equation B.4, define a rotor disc area $A_d = \pi d_2{}^2/4$ and assume a uniform rotor exit velocity at mean diameter c_{m1} so that $Q_1 = A_1 c_{m1}$, then as

$$N = \frac{u_2}{\pi d_2} = \frac{c_s\sqrt{2}}{2\pi d_2}$$

$$\frac{\dot{Q}_1}{Nd_2{}^3} = \frac{A_1 c_{m1} 2\pi}{\sqrt{2}c_s d_2{}^2} = \left(\frac{A_1}{A_d}\right)\left(\frac{c_{m1}}{c_s}\right)\left(\frac{\pi^2}{2\sqrt{2}}\right) \tag{B.5}$$

Substituting equation B.5 into equation B.4

$$N_s = (0.336)\left(\frac{c_{m1}}{c_s}\right)^{1/2}\left(\frac{A_1}{A_d}\right)^{1/2} \tag{B.6}$$

Equation B.6 expressed in $r.p.s$ and in rad/s as $\Omega_s = 2\pi N_s$, would result into:

$$\Omega_s = (2.11)\left(\frac{c_{m1}}{c_s}\right)^{1/2}\left(\frac{A_1}{A_d}\right)^{1/2} \tag{B.7}$$

Where:

$\Omega_s = rotational\ speed, rad/s$

$\frac{c_{m1}}{c_s} = Exhaust\ energy\ factor$

$\frac{A_1}{A_d} = Ratio\ of\ exit\ flow\ area\ at\ mean\ diameter\ to\ rotor\ disc\ area$

Referring to design values obtained to calculate, c_1/u_2 and A_1/A_d as shown below:

$$\frac{c_1}{c_s} = \left(\frac{c_1}{u_2}\right)\left(\frac{u_2}{c_s}\right) = \left(\frac{c_1}{u_2}\right)(0.67) = \frac{186.77\times 0.67}{531.24} = 0.236$$

$$\left(\frac{c_1}{c_s}\right)^2 = (0.236)^2 = 0.055$$

and $$\frac{A_1}{A_d} = \left(\frac{d_1}{d_2}\right)^2 = \left(\frac{9.30}{16.91}\right)^2 = 0.30$$